

6-9-2020

Metabolic Network Analysis of Filamentous Cyanobacteria

Daniel Alexis Norena-Caro

Louisiana State University and Agricultural and Mechanical College

Follow this and additional works at: https://digitalcommons.lsu.edu/gradschool_dissertations



Part of the [Biochemical and Biomolecular Engineering Commons](#), [Bioinformatics Commons](#), [Biotechnology Commons](#), [Cell Biology Commons](#), [Computational Biology Commons](#), [Environmental Microbiology and Microbial Ecology Commons](#), and the [Systems Biology Commons](#)

Recommended Citation

Norena-Caro, Daniel Alexis, "Metabolic Network Analysis of Filamentous Cyanobacteria" (2020). *LSU Doctoral Dissertations*. 5293.

https://digitalcommons.lsu.edu/gradschool_dissertations/5293

This Dissertation is brought to you for free and open access by the Graduate School at LSU Digital Commons. It has been accepted for inclusion in LSU Doctoral Dissertations by an authorized graduate school editor of LSU Digital Commons. For more information, please contact gradetd@lsu.edu.

METABOLIC NETWORK ANALYSIS OF FILAMENTOUS CYANOBACTERIA

A Dissertation

Submitted to the Graduate Faculty of the
Louisiana State University and
Agricultural and Mechanical College
in partial fulfillment of the
requirements for the degree of
Doctor of Philosophy

in

The Gordon A. and Mary Cain Department of Chemical Engineering

by
Daniel Alexis Noreña Caro
B.S., Universidad EAFIT, 2011
M.Eng., Universidad EAFIT, 2015
August 2020

© [2020]

[Daniel Alexis Norena Caro]

I dedicate this dissertation to my parents, Mery and Gustavo, my siblings, Yeraldin, David, and Vanesa, and my grandmother Maria de los Angeles. I complete this experience of personal and professional growth thanks to their infinite love, patience and support.

ACKNOWLEDGEMENTS

I want to thank all the people, programs and organizations that supported my doctoral education in the United States. I thank the Fulbright program, the Colombian Ministry of Science (Colciencias), and Louisiana State University for their professional, logistic, and financial support. Furthermore, I want to thank the current and former members of the Fulbright Colombia commission, LASPAU, and Dr. John Flake for their essential administrative role in different stages of this long-term project.

My gratitude also goes to the professional network of scientists and engineers that I created in LSU. Most importantly, I am grateful with my mentor, Dr. Michael G. Benton, for showing me a different perspective as chemical engineer and helping me develop unimagined professional faculties in the field of biotechnology. I will always thank him for trusting in my scientific abilities, nurturing my leadership skills, and giving me freedom to develop my own path in biotechnological research. I thank the members of my dissertation committee, Dr. Adam Melvin, Dr. Naohiro Kato, and Dr. Juan Martinez, for their time, constructive suggestions and thoughtful comments. I thank the wonderful teachers and colleagues that I met throughout this research and learning experience, specially to Dr. Eric Achberger, Dr. Cristal Zuniga, Dr. Teresa Gutierrez-Wing, Dr. Laura Sanchez, and Dr. Mario Rivera. Moreover, I want to thank my fellow graduate students and friends from the Cain department of chemical engineering for helping me realize unexpected connections among our research topics, specially to Natalia da Silva Moura, Behnam Safavinia, Amber Pete and Benjamin Peterson. I will always be thankful with Andres Vodopivec and Sara Stofela for their vital support at the beginning of this journey, which was significantly difficult. I also want to thank the undergraduate researchers, who

worked with me in Benton's lab, specially to Sven Saemundsson, Morgan Donaldson, and Tara Malone for their commitment, work ethics, and clever questions.

Finally, I want to acknowledge the outstanding moral and emotional support that I received while living in Baton Rouge. Most importantly, to my family in Colombia, for accepting this challenging and beautiful international experience with me. Despite being thousands of kilometers away, they always found a way to make me feel their presence and support in every possible way. I thank all my life-long friends from Medellin for their kind words and messages of motivation before and during this intense period of concentration, specially to Juliana Lasprilla, Monica Poveda, Janeth Rios, Lina Serna, Diana Gallego, Ivan Santa and Alejandro Herrera. I thank all my friends from the LSU School of Music for showing me a beautiful world away from science and engineering, especially to Guillermo Salas and Monica Muñoz. I am also extremely grateful with Dr. Tiffany McCaughey and Dr. Melinda Le for helping me develop better habits of mental health, mindfulness and self-care. Furthermore, I want to thank my dear friends Rosi Stutzenstein-McGowan, Carmen Zapata, Dr. James Board, and Paola Mosquera for becoming my family away from home. Overall, I thank God, in any of her/his multiple identities, for giving me the strength and courage to keep moving forward.

TABLE OF CONTENTS

CHAPTER 1. INTRODUCTION.....	1
1.1 Preamble.....	1
1.2 Justification and significance.....	1
1.3 Specific Objectives.....	4
CHAPTER 2. CYANOBACTERIA AS PHOTOAUTOTROPHIC BIOFACTORIES OF HIGH-VALUE CHEMICALS	6
2.1 Preamble.....	6
2.2 The Biology of Cyanobacteria	6
2.3 Carbon dioxide and Nitrogen fixation capabilities.....	17
2.4 Primary metabolism	38
2.5 Secondary metabolism.....	56
2.6 Synthetic biology of Cyanobacteria	63
2.7 Large-scale cultivation of cyanobacteria	90
2.8 Chapter conclusion	96
CHAPTER 3. STRAIN SELECTION AND CHARACTERIZATION METHODS	100
3.1 Preamble.....	100
3.2 The filamentous strain <i>Anabaena</i> sp. UTEX 2576	100
3.3 Laboratory-scale cultivation of <i>Anabaena</i>	102
3.4 Measurement of cellular growth and biomass generation	104
3.5 Extraction and quantification of pigments.....	107
3.6 Quantification of total protein and cyanophycin.....	110
3.7 Quantification of total carbohydrates.....	111
3.8 Determination of lipid composition and fatty acid methyl esters	113
3.9 Quantification of nucleic acids.....	115
3.10 Scanning-electron microscopy and analysis of cell diameter	116
3.11 Determination of N-source concentration and urease activity	117
3.12 Quantification of total organic carbon (TOC)	121
3.13 Determination of mineral element composition in growth media	122
3.14 Chapter conclusion	124
CHAPTER 4. MATHEMATICAL MODELLING OF METABOLIC NETWORKS.....	125
4.1 Preamble.....	125
4.2 Simulation and analysis of metabolic networks	125
4.3 Bioinformatic tools used for developing microbial GSMMs	130
4.4 Chapter conclusion	131
CHAPTER 5. DEVELOPMENT OF iDN1004, A PRECISE GENOME-SCALE METABOLIC RECONSTRUCTION OF <i>ANABAENA</i>	133
5.1 Preamble.....	133

5.2	Introduction to <i>DN1004</i>	133
5.3	Reconstruction model of the <i>Anabaena</i> metabolism	138
5.4	Model simulations	139
5.5	Results and Discussion	142
5.6	Chapter conclusion	181
CHAPTER 6. NITROGEN METABOLISM AND IRON AVAILABILITY AFFECT PIGMENT BIOSYNTHESIS AND NUTRIENT CONSUMPTION IN <i>ANABAENA</i>		183
6.1	Preamble.....	183
6.2	Introduction to inorganic interactions in cyanobacteria.....	183
6.3	Methodology.....	188
6.4	Results	190
6.5	Discussion.....	222
6.6	Chapter conclusion	226
CONCLUSIONS AND RECOMMENDATIONS		228
APPENDIX A. PUBLISHING AGREEMENTS		233
APPENDIX B. GENOME-SCALE METABOLIC MODEL.....		234
B.1	List of <i>DN1004</i> Reactions.....	234
B.2	Biomass equations for <i>Anabaena</i> sp. UTEX 2576	279
B.3	List of <i>DN1004</i> Metabolites	281
APPENDIX C. MATLAB CODE		310
C.1	FBA Algorithm called from MATLAB CobraToolbox.....	310
C.2	FVA Algorithm called from MATLAB CobraToolbox.....	315
APPENDIX D. REGRESSION EQUATIONS FOR MINERAL CONSUMPTION		318
LIST OF REFERENCES		320
VITA		361

LIST OF TABLES

2.1. CO ₂ bio-fixation rates of cyanobacteria at different conditions	22
2.2. CO ₂ bio-fixation rates of microalgae at different conditions	23
2.3. CO ₂ bio-fixation rates of C ₃ and C ₄ plants	24
2.4. Average rates of chemical production in microorganisms	71
3.1. Retention times and calibration curves for <i>Anabaena</i> FAMES.	115
3.2. Element concentrations of calibrations standards for ICP-OES.	124
5.1. Properties of iDN1004 compared to reference GSMMs.	144
5.2. Two-Way ANOVA factors for biomass composition analysis	155
5.3. Growth rate parameters and model constraints.....	159
5.4. Comparison of experimental and simulated metabolic flux values.	170
6.1. Growth and biomass generation of <i>Anabaena</i> in different media	193
6.2. Properties of fresh mineral media.....	194
6.3. Concentration of mineral elements in growth media.....	195
6.4. Rate constants for N and C-source consumption.	208
B.1. List of Reactions in iDN1004.....	234
B.2. List of metabolites in iDN1004	281
C.1. List of reactions for FVA	316
D.1. Regression equations for mineral consumption.....	318

LIST OF FIGURES

2.1. Cellular organization in cyanobacteria.....	9
2.2. Structure of phycobilisomes attached to photosystem II.	15
2.3. Structure of carboxysomes in α - and β -cyanobacteria	28
2.4. Biochemical reactions in cyanobacterial metabolism	40
2.5. Glycolysis pathway in cyanobacteria.....	42
2.6. Amino-acid production pathways in cyanobacteria.....	48
2.7. Cyanobacterial secondary metabolites.....	60
2.8. Downstream processing of cyanobacterial biomass.....	94
3.1. Correlation for estimating <i>Anabaena</i> biomass concentration	105
3.2. Correlation for estimating <i>Anabaena</i> cell density	107
3.3. FL4 fluorescent signal of <i>Anabaena</i> cells.....	108
3.4. Calibration curve for quantification of β -Carotene	111
3.5. Glucose calibration curve for carbohydrate estimation.....	112
3.6. GC-FID chromatograms of <i>Anabaena</i> FAME.....	114
3.7. SEM image of diazotrophic <i>Anabaena</i> filaments.....	118
3.8. Calibration curve for NO_3 quantification	119
3.9. Calibration curve for urea quantification	121
3.10. ICP-OES Calibration for elemental analysis of BG11x.	123
4.1. Mathematical modelling of metabolic reaction networks	127
5.1. Photodiazotrophic and photoautotrophic filaments of <i>Anabaena</i>	143
5.2. General properties of the <i>Anabaena</i> GSMM, <i>DN1004</i>	147
5.3. Whole-cell biomass composition of <i>Anabaena</i>	149

5.4. Stacked chart of standardized effects for composition data	157
5.5. Growth kinetics of <i>Anabaena</i> cultures.....	161
5.6. NO ₃ consumption, N ₂ -fixation and CPC production rates.....	162
5.7. Amino acid production sub-network of <i>Anabaena</i>	173
5.8. Amino acid production ranking predicted by FBA and FVA.....	178
6.1. Growth kinetics of <i>Anabaena</i> sp. in BG11 _o , BG11 and BG11 _u	192
6.2. Growth constants of <i>Anabaena</i> sp. in different media.	194
6.3. Pigmentation of <i>Anabaena</i> sp. cultures.....	196
6.4. Concentration of PBPs in media with different N-sources.....	197
6.5. Abundance of phycobiliproteins (PBPs) per cell over time.	199
6.6. Relative abundance of ChlA and CaroT per cell.	202
6.7. Concentration of ChlA and CaroT in different growth media.	202
6.8. MS-TOF analysis of methanol extracts.	203
6.9. Cellular abundance and oxidation of β-Carotene.	205
6.10. TOC formation profiles.	208
6.11. <i>Anabaena</i> sp. urease activity in different media.....	209
6.12. Consumption profiles of N-sources.	209
6.13. Fe consumption profiles in growth media.....	210
6.14. Consumption profiles of P, Ca, Mg and Mn.....	211
6.15. Consumption profiles of B, Mo, Zn and Cu.....	212
6.16. Concentration profiles of Na, K, Ni and Co.....	213
6.17. Consumption profiles of P, Ca, Mg and Mn per cell.	215
6.18. Consumption profiles of B, Mo, Zn and Cu per cell.	216

6.19. Ranking of mineral element demands per cell.	220
---------------------------------------------------------	-----

ABSTRACT

Cyanobacteria were the first organisms to use oxygenic photosynthesis, converting CO₂ into useful organic chemicals. However, the chemical industry has historically relied on fossil raw materials to produce organic precursors, which has contributed to global warming. Thus, cyanobacteria have emerged as sustainable stakeholders for biotechnological production. The filamentous cyanobacterium *Anabaena* sp. UTEX 2576 can metabolize multiple sources of Nitrogen and was studied as a platform for biotechnological production of high-value chemicals (i.e., pigments, antioxidants, vitamins and secondary metabolites). From a Chemical engineering perspective, the biomass generation in this organism was thoroughly studied by interpreting the cell as a microbial bio-factory. Nutrient consumption kinetics was studied to analyze raw material requirements from the growth medium. Transformation operations were analyzed with a Genome-Scale Metabolic Model, as a robust metabolic network of biochemical reactions. Production of valuable compounds was assessed through chemical characterization of the cyanobacterial biomass, generating biomass equations of cellular growth. Here, systemic interpretations of cellular processes are discussed with the aim of optimizing photosynthetic chemical production, by controlling stress biology and environmental conditions. This work demonstrates that the sophisticated metabolic network of *Anabaena* sp. UTEX 2576 is highly dependent on their biological interactions with organic and inorganic nutrients. In addition, this work brings up new strategies for studying the utilization of metallic and mineral elements in cyanobacteria for biotechnological and environmental purposes, going beyond Carbon and Nitrogen.

CHAPTER 1. INTRODUCTION

1.1 Preamble

This chapter describes the significance of this research project and introduces fundamental topics discussed throughout this document. This introduction summarizes essential scientific findings that have led to consider the meaningful role of cyanobacteria in the development of new biotechnological applications and sustainable chemical processes. Additional details will be provided within this dissertation.

1.2 Justification and significance

Photosynthesis is a biological and physicochemical process sustaining different forms of life on Earth. Although the ability to transform sunlight into chemical energy may be overlooked, this phenomenon is essential to sustain current human activities. More than 2.5 billion years ago, ancient prokaryotes were the first organisms to transform light, carbon dioxide (CO_2) and water into organic molecules to produce their own food [1, 2]. The main byproduct of this natural process was molecular oxygen (O_2). Hence, cyanobacterial ancestors were not only involved in the development of biological CO_2 fixation, but also for the great oxygenation event allowing the emergence of aerobic life and the formation of the Ozone layer [3]. In a series of evolutionary events, ancient cyanobacteria became not only modern species inhabiting most terrestrial and aquatic ecosystems, but also the chloroplasts of algae and plants, enabling photosynthesis in eukaryotes [4].

Nowadays, phytosequestration (i.e., CO₂ fixation by photosynthetic organisms) sustains agricultural activities and is the primary driver of the global carbon cycle. While terrestrial plants (e.g. forests and crops) are responsible for 50% of the CO₂ reintroduced to the carbon cycle, marine and freshwater algae and cyanobacteria are responsible for the remaining CO₂ that is recycled [5, 6]. Among these, cyanobacteria alone account for 20 to 30% of global CO₂ phytosequestration [7, 8]. Considering the currently alarming levels of atmospheric CO₂ (ca. 410 ppm in April of 2020), and the fact that only 57% of anthropogenic carbon emissions is recycled, there is a dire need to implement carbon sequestration technologies aiming to minimize the effects of climate change [9, 10]. In this case, cyanobacteria not only represent an alternative for CO₂ capture, but also for sustainable production of chemicals and waste-water bioremediation.

A global understanding of phytosequestration, bioremediation and biochemical production capabilities in cyanobacteria requires a deep evaluation of the metabolic processes that produce biomass. Photosynthesis and CO₂ fixation only represent the starting point for biosynthesis of essential metabolites in cyanobacteria, but the analysis of their metabolic network elucidates how these compounds are used and transformed to sustain growth, specially under the influence of different nitrogen sources and metalloregulators. In general terms, cyanobacteria use light to produce Adenosine triphosphate (ATP) and Nicotinamide adenine dinucleotide phosphate (NADPH). Then, this chemical energy fuels the Calvin-Benson-Bassham (CBB) cycle pathway by which inorganic CO₂ is converted into sugars and other organic compounds [11, 12]. This sophisticated biosynthesis process is not complete without the introduction of Nitrogen (N) and other essential elements. N makes up more than 10% w/w of the total cellular

biomass, and is necessary for the synthesis of amino acids, nucleic acids, amino sugars, pigments, coenzymes, vitamins, and secondary metabolites [13]. Therefore, the N-bioavailability has a significant impact on the biosynthetic capabilities of cyanobacteria, which can metabolize different N-sources. Among these, cyanobacteria are able to assimilate nitrates, nitrites, cyanates, urea, glutamine, and arginine [14–16]. Some cyanobacteria are also diazotrophs and can couple photosynthesis and CO₂ bio-sequestration with atmospheric dinitrogen (N₂) fixation [17]. Ultimately, all these N-substrates are transformed into ammonium (NH₄⁺) to fuel downstream biosynthesis reactions.

Apart from Carbon (C) and N, other elements play a crucial role in the generation of cyanobacterial biomass. Among these, Phosphorous (P) and Iron (Fe) are essential for the synthesis of energy carriers (i.e., ATP and NADPH) and Iron-sulfur proteins involved in key energy transformation processes [18]. The Fe-role is more relevant in cyanobacteria than in other non-photosynthetic bacteria because this element is indispensable for photosynthesis and N-metabolism [19]. Based on this, a thorough understanding of the C/N/Fe relationships within the cyanobacterial metabolic network is significant for the design of bioremediation and bioproduction operations using these photosynthetic microorganisms.

The central goal of this dissertation is providing a deeper understanding of the metabolic network of *Anabaena* sp. UTEX 2576 (a.k.a., *Nostoc* sp. PCC 7120, henceforth *Anabaena*). This strain is a model filamentous cyanobacterium that relies on a tightly regulated C/N/Fe balance to perform metabolic activities [20]. Specifically, this work describes how the metabolism of *Anabaena* is affected by the C/N/Fe status to produce

phycobiliproteins and β -Carotene, which have commercial applications as pigments and antioxidants. Since chemical production relies on the transformation of raw materials, nutrient consumption is also substantially covered. The studies presented in this document are intended to advance the current understanding on the biochemistry of *Anabaena*, aiming to develop this organism as a photosynthetic micro-factory of valuable chemicals. Furthermore, these experiments provide new information on the implications of coupling bioremediation and biotechnological production by means of biological CO₂ fixation. In general, this work is intended to advance the development of cleaner and more sustainable chemical production operations, which is one of the central roles for chemical engineers in the 21st century.

1.3 Specific Objectives

Objective 1: Identify the challenges and opportunities for large-scale cultivation of cyanobacteria by reviewing their potential role as photoautotrophic bio-factories of high-value chemicals.

- i) Understand the importance of cyanobacterial metabolism for production of commodity and specialty chemicals
- ii) Analyze the utilization of Synthetic biology approaches to enhance metabolite production in cyanobacteria
- iii) Discuss current large-scale cultivation of cyanobacteria

Objective 2: Develop a precise mathematical model of *Anabaena* cells for comprehensive analysis of the metabolic network using systems biology and bioinformatic tools.

- i) Reconstruct a genome-scale metabolic model (GSMM) from the *Anabaena* genome sequence
- ii) Determine experimental biomass equations for diazotrophic and non-diazotrophic growth
- iii) Define linear programming constraints using nutrient consumption and pigment production rates
- iv) Implement Flux Balance Analysis (FBA) and Flux Variability analysis (FBA) to analyze amino acid production

Objective 3: Investigate the effect of different N-substrates and Fe-availability on pigment production and nutrient consumption via rational reformulation of mineral growth media.

- i) Design an efficient chemical analysis method for cyanobacterial growth medium using Inductively Coupled Plasma Optical Emission Spectrometry (ICP-OES)
- ii) Compare the production levels of phycobiliproteins and β -Carotene in growth media with different N-sources (N_2 , sodium nitrate and urea) and Fe-levels
- iii) Analyze the effect of Fe-availability and N-substrate on the consumption levels of CO_2 , P and metallic elements from the growth medium

CHAPTER 2. CYANOBACTERIA AS PHOTOAUTOTROPHIC BIOFACTORIES OF HIGH-VALUE CHEMICALS¹

2.1 Preamble

This chapter constitutes the main literature review section of this dissertation. It is written from a Chemical engineer's perspective, starting from fundamental concepts and analyzing the transformation of raw materials into products. The subsections are organized to respond to specific objective 1. Here, the biology of cyanobacteria, as well as their primary and secondary metabolism, are discussed in detail. The Carbon concentration mechanism (CCM) is sufficiently described to explain the differences in CO₂ fixation potential among plants, algae and cyanobacteria. Synthetic biology strategies recently used to enhance commodity chemical production in cyanobacteria are also covered. The final part of this chapter summarizes industrial-scale cultivation experiences with cyanobacteria.

2.2 The Biology of Cyanobacteria

2.2.1 Cyanobacteria and Earth's Atmosphere

Cyanobacteria are among the oldest organisms living on earth (more than 2.5 billion years old). These prokaryotes can be found in oceans, lakes, estuaries, rivers, swamps, deserts, tropical rainforests, hot springs, and Antarctic dry valleys [1, 2]. Remarkably, cyanobacteria developed carbon fixation when the atmospheric

¹ This chapter was previously included in the review paper published as Noreña-Caro, D. and Benton, MG (2018). Cyanobacteria as photoautotrophic biofactories of high-value chemicals. J. CO₂ Util. 28, 335–366. Reprinted by permission of Elsevier.

concentration of CO₂ was 10 to 100 times its current value [21, 22]. Cyanobacteria were the first organisms to develop oxygenic photosynthesis and are deemed responsible for the great oxygenation event that raised the atmospheric oxygen concentration. Because of this, ancient cyanobacteria were also indirectly involved in the formation of the ozone layer [3].

Cyanobacteria are primarily aerobic photoautotrophs but can also perform anaerobic photosynthesis. Some of them can also grow as photoheterotrophs or chemoheterotrophs [23]. The main catalyzer for carbon fixation in cyanobacteria and other aerobic photosynthetic organisms is the ribulose-1,5-biphosphate carboxylase (RuBisCo) enzyme [2]. Many species of cyanobacteria are also diazotrophs playing a remarkable role in the fixation of molecular Nitrogen (N₂), where nitrogenase catalyzes the reduction of N₂ to ammonium (NH₄⁺) [11]. Because this enzyme is inhibited by molecular oxygen, N₂ fixation must be separated from oxygenic photosynthesis. Cyanobacteria have evolved temporal and spatial separation of N₂ reduction to overcome this problem. During temporal separation, photosynthesis and nitrogen fixation take place at different times. For spatial separation, cyanobacteria have differentiated cells [24].

2.2.2 Cellular structure

Cyanobacteria are prokaryotes and less complex than eukaryotes. However, their cell configuration is also different from simpler bacteria and archaea [24]. The general cyanobacterial cell organization is presented in Figure 2.1. The cyanobacterial cell wall is formed by an outer protective membrane rich in lipopolysaccharide (LPS) and one inner layer of peptidoglycan separated by periplasm. In contrast with other Gram-negative

bacteria, the cyanobacterial peptidoglycan layer is at least five times thicker and their LPS lacks bound phosphate, heptoses, and keto-deoxyoctonate [25, 26]. Other exclusive components of the outer membrane are carotenoids, hydroxylated fatty acids, and Toc75 homologue porins responsible for protein translocation in photo- synthetic organisms [26–29]. Cyanobacteria are also surrounded by sheaths, capsules, and slimes. These biofilms are formed by the release of exocellular polysaccharides (EPS) through the junctional pore complex (JPC) connecting the cytoplasm with the exterior. Capsules and sheaths play a protective role under extreme environmental conditions and extruded slime is necessary for gliding movement [3].

The cell wall is separated from the cell membrane by the inner periplasmic space. The thylakoids are intracellular membranes that occupy most of the cytoplasm and are arranged in a series of concentric cylinders aligned with the long axis of the cell [12]. The thylakoids are organized as lipid bilayers made of monogalactosylglycerol (MGDG) (~40%), digalactosyldiacylglycerol (DGDG) (~32%), sulfoquinovo- syldiacylglycerol (SQDG) (~15%), and phosphatidylglycerol (PG) (~13%) [30]. The space inside the thylakoids is the lumen and the space outside them is a prolongation of the cytoplasm [12]. The thylakoids are the centers for light reactions in photosynthesis, but are not present in some cyanobacteria (e.g., *Gloeobacter violaceus*). In those cases, light reactions are directly associated to the cytoplasmic membrane [11, 12]. One of the main morphological differences between cyanobacterial thylakoids and chloroplast thylakoids of higher plants is the lack of membrane stacking or formation of grana [3].

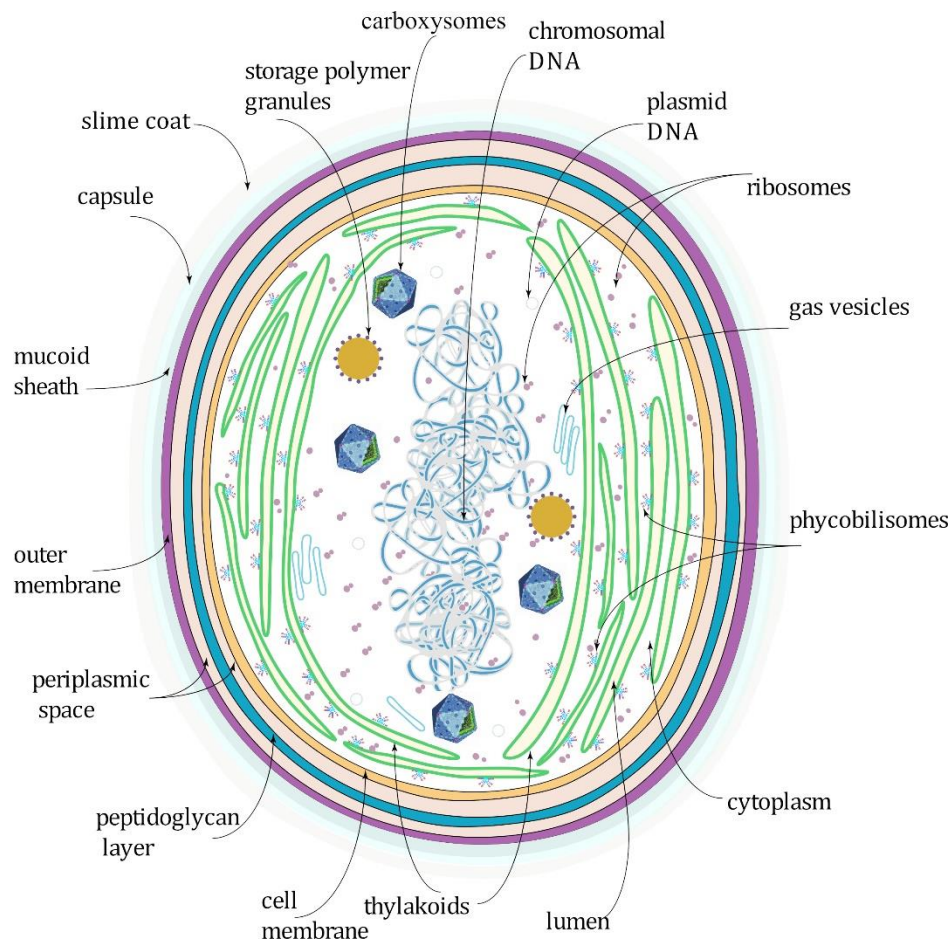


Figure 2.1. Cellular organization in cyanobacteria

The cyanobacterial cytoplasm contains carboxysomes and genetic material [31]. Carboxysomes are bacterial organelles formed by polyhedral proteins housing RuBisCO and involved in carbon concentration mechanisms [32]. The DNA of most cyanobacteria is organized in circular chromosomes with wide range of ploidy levels. Cyanobacterial chromosomes are commonly single or double copies in monoploid and diploid marine species, but highly polyploid organisms also exist. As an example, the model cyanobacterium *Synechocystis* sp. PCC 6803 may have up to 218 chromosome copies per cell. On the other hand, cyanobacterial plasmids may be completely absent (in

Prochlorococcus and *Synechococcus*) or present as multiple copies with sizes reaching hundreds of kilobases [33]. The cytoplasm of cyanobacteria also contains polymer granules and gas vesicles. Granules are used as reserves of storage polymers (i.e., cyanophycin and polyhydroxyalkanoates) and gas vesicles are used for buoyant movements [3, 34, 35].

2.2.3 Morphology

Cyanobacteria are among the most diverse groups of prokaryotes, showing unique cell morphologies, variable size, and different colors. They can be unicellular organisms or complex filamentous groups of cells with a high level of differentiation. Unicellular cyanobacteria can be spherical, rod-like shaped, or aggregated. Filamentous cyanobacteria are organized in the form of branched or linear chains of cells called trichomes that resemble smooth threads surrounded by a slimy sheath [36]. While unicellular *Prochlorococcus* are the smallest cyanobacteria (0.7 μm cell diameter), cells of filamentous *Oscillatoria princeps* (55 μm cell width) are the largest [37].

Morphology is used to classify cyanobacteria. There are five subsections closely representing five orders of cyanobacteria. Subsection I includes unicellular species reproducing by binary fusion (order *Chroococcales*). Subsection II includes the order *Pleurocapsales*, unicellular organisms reproducing by multiple division with daughter cells called baeocytes. Filamentous and mostly undifferentiated cyanobacteria belonging to the order *Oscillatoriales* compose Subsection III. Subsections IV and V include members of the orders *Nostocales* and *Stigonematales*. Both subgroups include filamentous cyanobacteria capable of cellular differentiation but only members of subsection V

present true branching and division in more than one plane. Branched cyanobacteria have the most advanced structure among prokaryotes [11, 24].

Cellular differentiation in filamentous cyanobacteria yields formation of heterocysts, diazocytes, akinetes, and hormogonia [24, 36]. Heterocysts are specialized cells responsible for N₂ fixation in most species of subsections IV and V [11]. They are thick-walled cells within filaments that lack photosystem II, do not perform water splitting and do not produce Oxygen. However, they have photosystem I and produce the necessary ATP for N₂ fixation. The primary assimilation of ammonium derived from N₂ fixation is performed by glutamine synthase enzymes [24, 38]. Heterocysts cannot fix CO₂ and rely on adjacent vegetative cells for carbon supply [17]. These cells have thick polysaccharide layers around their cell walls blocking gas diffusion and protecting nitrogenase from oxygen inactivation. Heterocysts represent the main example of spatial separation for N₂ fixation because they provide a suitable micro-anaerobic environment [3]. Heterocyst forming cyanobacteria can be found in symbiotic associations with eukaryotic organisms [17, 23], and around 8% of the 17,000 lichen species comprise associations between heterocyst cyanobacteria and fungi. Because of this, cyanobacteria also play an important role as biofertilizers [11].

Diazocytes are unique Nitrogen-fixing cells found in cyanobacteria from subsection III (genus *Trichodesmium* in the order *Oscillatoriales*) [3, 11]. These cells are more homogeneous and transparent than their vegetative counterparts because of their prominent gas vacuoles and lower content of storage compounds [3, 38]. Diazocytes have retained complete photosynthetic machinery and can temporarily downregulate oxygenic photosynthesis to enhance N₂ fixation [38]. Moreover, diazocytes may

reproduce and revert into non-nitrogen fixating vegetative cells. Since they are not permanently differentiated cells, diazocytes illustrate temporal separation of Nitrogen fixation in cyanobacteria [11, 38].

Akinetes are brown thick-walled cyanobacterial spores found in species from subsections IV and V. They are produced under light limitation or phosphate deprivation and can germinate once the environmental conditions improve [3, 11, 17]. They are larger than vegetative cells, contain reserve materials and are resistant to cold and dry conditions [24]. Hormogonia are reproductive trichomes made of small vegetative cells derived from terminal points of cyanobacteria from subsections IV and V. Hormogonia glide away from their parental colony and are useful for relocation [24, 36, 39].

2.2.4 Photosynthesis

Photosynthesis is an electron transport process that converts light energy into chemical energy. Photosynthesis reactions are divided in light and dark phases. Light reactions occur in the thylakoids and dark reactions take place in the cytoplasm [12, 40]. In general, light reaction centers working in series capture photons to oxidize water and reduce nicotinamide adenine dinucleotide phosphate (NADP) to NADPH. During the process, molecular oxygen (O_2) is produced and adenosine diphosphate (ADP) is transformed into adenosine triphosphate (ATP). The chemical energy, stored in the form of NADPH and ATP, is subsequently used to power light-independent reactions to produce organic compounds [11, 12]. In cyanobacteria, ATP is also used to power N_2 -fixation in diazotrophic species [17]. An extensive description of light reactions and the

structure of photosystems I and II is beyond the scope of this literature review, but the reader is referred to the following materials for further details [3, 11, 12, 30, 40–42].

2.2.5 Cyanobacterial pigments

Cyanobacteria are widespread organisms that evolved chromatic adaptation to dominate diverse illuminated environments [24, 43]. The main photosynthetic pigments in cyanobacteria are chlorophylls and phycobilins [12, 43]. Akin to higher plants, cyanobacteria also contain carotenoids supporting light absorption and protecting cells from light damage [44]. Chlorophyll a is widespread among photosynthetic organisms, but some cyanobacterial species contain alternative chlorophylls in their photosystems [11, 24, 45]. Phycobilins, on the other hand, are a family of auxiliary pigments, which are exclusive to cyanobacteria, red algae and cryptomonads [46].

Green cyanobacteria, or *Prochlorophytes*, demonstrate the evolution of alternative photosynthetic pigments in cyanobacteria. This group is an independent lineage lacking phycobilins and formed by *Prochlorococcus*, *Prochlorothrix*, and *Prochloron* [24, 47, 48]. *Prochlorococcus* are major constituents of ocean surface picoplankton, which use divinyl-chlorophyll a and divinyl-chlorophyll b as photosynthetic pigments [11]. On the other hand, *Prochlorothrix* and *Prochloron* are rarer cyanobacteria living in brackish waters of Northern Europe and coral reefs, respectively [48, 49]. These cyanobacteria are the only prokaryotes using chlorophyll b for photosynthesis [3].

Depending on their pigment type and concentration, cyanobacteria may be green, blue-green, brown, purple, red, and even black [11, 24]. The diversity in cyanobacterial pigmentation allows for a better utilization of visible light (400–700 nm) as compared to

plants and most algae, which only have chlorophylls and carotenoids in their photosystems. In cyanobacteria, chlorophylls absorb blue ($400 < \lambda < 500$ nm) and red light ($600 < \lambda < 700$ nm), and carotenoids aid chlorophylls at harvesting blue and blue-green wavelengths. In addition, phycobilins absorb yellow-green, yellow and orange radiations ($480 < \lambda < 600$ nm) that chlorophylls alone would otherwise emit [11, 12, 31, 44]. In some cases, cyanobacteria can even expand the range of usable radiation for photosynthesis. Some examples are the chlorophyll d containing species *Acaryochloris marina* and the Chlorophyll f containing genera *Halomichronema*, *Aphanocapsa*, and *Chlorogloeopsis*. The presence of chlorophyll d and f in the photosystems enables using near infrared radiations ($710 < \lambda < 740$ nm) as energy sources [11, 24, 43, 45].

2.2.6 Phycobilisomes

The phycobilisomes (PBSs) are multidimensional extraneous antennae located on the cytoplasmic side of the thylakoids. These light-harvesting complexes are larger in size than the photosystems and consist of core horizontal cylindrical protein structures anchoring six, eight, or ten peripheral rods formed by stacked disc-shaped proteins [12]. The general structure of a phycocyanin rich phycobilisome is presented in Figure 2.2. Each disc in the PBSs is constituted by phycobiliproteins (PBPs) attached via thioester bonds to open chain tetrapyrrole prosthetic groups called phycobilins [12, 50]. The phycobilins are a group of chromophores constituted by phycocyanobilin (PCB), phycoerythrobilin (PEB), phycourobilin (PUB), and phycoviolobilin (PVB), which are blue, red, yellow, and purple, respectively [46]. Depending on their composition and content of

chromophores, PBPs may be classified as phycocyanins (PCs), phycoerythrins (PEs), and allophycocyanins (APCs) [50].

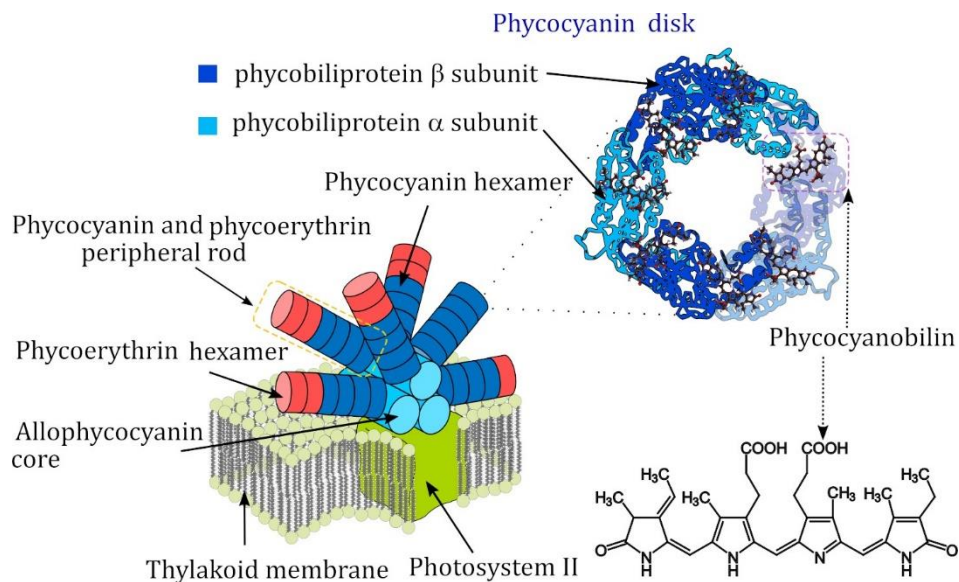


Figure 2.2. Structure of phycobilisomes attached to photosystem II.

PCs are deep blue or blue purple PBPs with maximum absorption wavelengths between 615 and 640 nm. The most common PBP in cyanobacteria is C-phycocyanin (CPC) with $\lambda_{\text{max}} \sim 615\text{-}620$ nm, but some species may also produce another PC called phycoerythrocyanin (PEC), with $\lambda_{\text{max}} \sim 575$ nm. A third kind of PCs (i.e. R-phycocyanin, $\lambda_{\text{max}} \sim 615$ nm) is less common [46]. The most common chromophore in CPC is the blue PCB, which may be transformed into PVB, PEB or PUB in response to the variation of light and nutrient conditions. PCs are organized as trimers of two-subunit polypeptide monomers ($\alpha\beta$) forming disk-shaped hexamers [46, 50]. The main components of peripheral rods in the PBSs are PCs (see Figure 2.2).

PEs are red PBPs with strong absorption capabilities of green light and λ_{max} between 480 and 570 nm. PEs may be further classified as B-phycoerythrin (λ_{max} ~540-560 nm), R-phycoerythrin (λ_{max} ~565, 545 and 495 nm) and C-phycoerythrin (λ_{max} ~563, 543 and 492 nm). The latter is the most common PE and can be found in red marine cyanobacteria *Trichodesmium erythraeum* [3, 46]. PEs have an important role in chromatic adaptation of marine cyanobacteria living at ocean depths where green light is most abundant [12]. The organization of PEs in the PBSs is similar to the structure of PCs (stacked discs), but PEs contain PEB instead of PCB chromophores [46].

APCs are blue green PBPs with absorption maxima between 650 and 670 nm. There are three kinds of APCs: allophycocyanin (APC, λ_{max} ~650-655 nm), allophycocyanin-B (APC-B, λ_{max} ~670 nm), and allophycocyanin core – membrane linker complex (APC-LCM). APC exists in most cyanobacteria inside the PBS core. Within the PBS, APCs also exist as trimers of $\alpha\beta$ -polypeptide monomers. However, the stacked disks of APC form three horizontal rods. While APC-B and APC-LM exist only as constituents of the two bottom rods, APC is the main PBP in the three cylinders. APC-B and APC-LCM connect phycobilisomes with internal antenna subunits of photosystem II [12, 46, 50].

Phycobilisomes enhance adaptability of cyanobacteria under varying light conditions as their size changes to control the flow of energy. PCs and PEs in the periphery absorb energy from more energetic radiations and APCs in the core are excited with less energetic radiations. Because of this, the photo excitation is efficiently transferred from high energy to low energy points within the PBS. When the light intensity is low, more PCs and PEs are produced making the peripheral rods grow. On the contrary,

as the light intensity increases, the peripheral rods shrink, leaving only core APCs under extreme illumination [12]. Despite their fundamental role, PBSs are absent in some cyanobacterial species, such as *Prochlorococcus marinus*, *Acaryochloris marina*, and *Gloeobacter violaceus* [3, 12, 51].

2.3 Carbon dioxide and Nitrogen fixation capabilities

2.3.1 Carbon dioxide fixation

Light independent or “dark phase” reactions in photosynthetic organisms utilize ATP and NADPH to power biochemical reactions of CO₂ fixation. Despite the name, these reactions only occur when there is light. The metabolic pathway is the Calvin-Benson-Bassham cycle (CBB) and it involves 13 reactions catalyzed by 11 different enzymes. The CBB cycle, or reductive pentose phosphate cycle, is essential for the metabolism of Carbon in oxygenic photosynthesis, as it connects light reactions with subsequent metabolic pathways that produce carbohydrates and other organic compounds [2, 52]. The biochemical reactions occurring in the CBB cycle convert high energy compounds of intermediate stability into more stable organic molecules that can be used for building biomass or for long-term storage [53].

The overall CBB cycle can be divided into three phases (i.e., carboxylation, reduction, and regeneration). During carboxylation, three molecules of CO₂ are combined with three molecules of ribulose 1,5-bisphosphate (RuBP) to produce six molecules of 3-phosphoglycerate (PGA). In the reduction phase, NADPH and ATP are used to reduce PGA to triose phosphate, which is a collective term grouping the isomers 3-phosphoglyceraldehyde (PGAL) and dihydroxyacetone phosphate (DHAP). In the final

phase, five molecules of PGAL are used to regenerate three molecules of RuBP. The regeneration of RuBP is a series of biochemical reactions that starts with the production of fructose 1,6-bisphosphate (FBP) from PGAL. FBP is subsequently converted to fructose 6-phosphate (F6P) and combined with PGAL to yield erythrose 4-phosphate (E4P) and xylulose 5-phosphate (X5P). E4P and DHAP are fused to obtain sedoheptulose 1,7-bisphosphate (SBP), which is later transformed into sedoheptulose 7-phosphate (S7P). RuBP five carbon sugars are produced by combining S7P with PGAL. The latter reaction yields ribose 5-phosphate (R5P) and X5P. These sugars are isomerized to ribulose 5-phosphate (Ru5P), which is next phosphorylated to produce RuBP. The molecule of triose phosphate (DHAP) that skips the RuBP regeneration reactions enters subsequent metabolic pathways, where it is combined and rearranged to produce glucose [52, 53]. The main product of the CBB cycle is DHAP and the overall stoichiometry of this process is described by Equation 2.1.

Equation 2.1

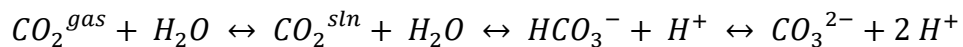


The most important enzyme in the CBB cycle is RuBisCO, which is also the most abundant protein on Earth. This enzyme catalyzes the carboxylation reaction that combines CO₂ and RuBP to form PGA [53, 54]. The essential role of photoautotrophs as producers of biomass relies on the ability to incorporate inorganic carbon in their metabolism through photosynthesis. Nevertheless, this potential is limited by the inverse relationship between activity and selectivity in RuBisCO. In the first place, the specific

activity of an average RuBisCO, measured in terms of the turnover number (*kcat*), is between one and two orders of magnitude below the specific activity of other enzymes involved in central carbon metabolism [55]. Secondly, RuBisCO also catalyzes a side reaction where one molecule of RuBP interacts with one molecule of O₂, forming PGA and 2-phosphoglycolate (G2P) [2]. G2P is toxic and it is transformed to glycolate by spending additional energy, reducing power, and fixated CO₂. This side reaction is called photorespiration and accounts for around 30% loss of photosynthetic efficiency [55]. Whereas RuBisCO enzymes with higher catalytic activity have lower selectivity towards carboxylation, photorespiration is reduced only when the activity of the enzyme is also reduced [55, 56].

The concentration of O₂ in the atmosphere is around 500 times higher than the concentration of CO₂ (21% vs 0.04% v/v). This relatively low concentration of CO₂ restricts the productivity of terrestrial photosynthetic organisms [5]. The O₂ to CO₂ concentration ratio in aquatic environments is different due to the chemical equilibrium established by carbon dioxide, bicarbonate ions (HCO₃⁻), and carbonate ions (CO₃²⁻) when CO₂ is dissolved (see Equation 2.2). Because of this equilibrium, the solubility of CO₂ in water is higher than the solubility of O₂, and water bodies, specially oceans, act as large natural sinks of atmospheric carbon [57].

Equation 2.2



Using Henry's law for the dissolution of atmospheric CO₂ and O₂ in water at 20°C and the atmospheric partial pressures of each gas, it can be estimated that equilibrium concentrations of Oxygen and Carbon dioxide in freshwater are roughly 300 µM and 16 µM (20:1 ratio), respectively [58, 59]. These values are representative for the euphotic zone of most lakes and rivers [60], but the actual concentration of dissolved CO₂ depends on water pH, temperature and salinity. In seawater, the total concentration of inorganic carbon (Ci) in equilibrium with the atmospheric CO₂ is 2 mM, but most of the Ci exists as bicarbonate [60]. For example, at pH 8.08 - 8.33 (average 8.195 for seawater with 3.5% w/w salt) and 25°C, around 90% of dissolved CO₂ in seawater is present as HCO₃⁻, while 10% exists as CO₃²⁻ [2, 5, 61].

Photosynthetic organisms have evolved different mechanisms to grow in habitats with low concentrations of CO₂ relative to O₂. These strategies depend on expressing high amounts of RuBisCO, producing RuBisCO with high CO₂ affinity, and developing mechanisms for increased intracellular concentration of CO₂ [2]. The latter strategy is preferred by cyanobacteria, and they have evolved an efficient CCM for the uptake of Ci. The CCM is necessary because Ci exists mainly as bicarbonate in neutral to slightly alkaline water, and because the diffusion rate of CO₂ in water is 1x10⁴ times slower than it is in air [60]. This concentrating mechanism is integrated by the carboxysomes and the transporters of CO₂ and HCO₃⁻ [3]. The operation of the CCM in cyanobacteria actively brings Ci into the cell, converts bicarbonate ions back to CO₂, and creates an intracellular CO₂-enriched environment around RuBisCO. The CBB cycle in cyanobacteria is continuously fed with CO₂ through the CCM during photosynthesis [5, 11]. This

mechanism is analogous to the C₄ and CAM pathways in some terrestrial plants, which have also evolved strategies to improve their carbon fixation rate.

Table 2.1 presents CO₂ bio-fixation rates (CFR) of selected cyanobacteria. These rates can be compared with CO₂ uptake rates of microalgae and plants included in Table 2.2 and Table 2.3. Reported CFR values are listed in descending order to facilitate comparison among photosynthetic organisms. The following observations can be supported based on the different carbon fixation rates of photosynthetic organisms. First, CO₂ uptake rates increase as environmental CO₂ concentration and illumination increase. Optimal CO₂ concentration for cyanobacteria and microalgae generally lies between the 5 and 10% v/v range [62], but the maximum tolerable CO₂ and photosynthetic photon flux density (PPFD) are species-specific. Second, photo-bioreactor design influences the CFR, as bigger and more sophisticated culture vessels tend to promote higher uptake rates across species. This makes sense considering that photo-bioreactors are designed to maximize illumination and CO₂ diffusion in the liquid [63]. Although reported CFR for cyanobacteria are generally higher than microalgal CFR (implying differences in photosynthetic efficiency), both groups of microorganisms have similar carbon sequestration capabilities greatly affected by culture conditions. Third, direct comparison between cyanobacterial, microalgal, and plant CO₂ uptake rates would require converting CFR values in g m⁻³ h⁻¹ to g m⁻² h⁻¹ based on photo-bioreactor working volume, surface to volume ratio, and land area occupied by each photo- bioreactor. Considering, the relatively low CFR numbers for plants in Table 2.3, and the land limitations associated with expanding cultivated areas of terrestrial plants, cyanobacteria and microalgae are more attractive for large-scale photosynthetic sequestration of CO₂. Furthermore,

photosynthetic microorganisms can be grown in liquid medium and this facilitates their utilization at industrial level.

Table 2.1. CO₂ bio-fixation rates of cyanobacteria at different conditions

Organism	[CO ₂] in air	PPFD ($\mu\text{mol m}^{-2} \text{s}^{-1}$)	PP (Hours) ^a	T (°C)	Net CFR ^b	Culture vessel	Ref
<i>Aphanothece microscopica</i>	15% v/v	150	24	30	330-1122	Bubble column photo- bioreactor, 2L	[64]
<i>Na⁺geli</i>	15% v/v	150	12	30	105-414		
<i>Synechocystis aquatilis</i>	10% v/v	450	12	40	138.9	Vertical flat plate photo- bioreactor, 17L	[65]
<i>Synechocystis</i> sp.	10% v/v	1200-2272	16	25-40	31.3-79.2	Bubble column photo- bioreactor, 1L	[66]
<i>Anabaena</i> sp. ATCC 33047	n.r. ^c	900	12	27	60.4	Bubble column photo- bioreactor, 9L	[67]
<i>Spirulina platensis</i>	2-15% v/v	132 ^d	24	20	38.3-60.1	Bench hollow fiber membrane photobioreactor	[68]
<i>Anabaena</i> sp.	10% v/v	250	24	32	42.1	Bubble column photo- bioreactor, 5L	[69]
<i>Nostoc</i> sp. PCC 7120	5% v/v	120	24 ^e	30	28.2	Airlift photobioreactor, 1.4L	[70]
<i>Synechococcus elongatus</i> PCC 7942	5% v/v	132 ^d	24 ^e	30	25	Illuminated airlift column chemostat, 1.1L	[71]
<i>Microcystis ichthyoblabe</i>	10% v/v	200	24 ^e	27	21.7	Conical photobioreactor, 1L	[72]
<i>Microcystis aeruginosa</i>	10% v/v	200	24 ^e	27	20.4	Conical photobioreactor, 1L	[72]
<i>Spirulina platensis</i>	5% v/v	58 ^d	12	30	13.3	Illuminated BioFlo fermentor, 8L	[73]
<i>Synechocystis salina</i>	0.04-10% v/v	163.5	24	23.4	2.3-5.7	Erlenmeyer flasks, 0.4L	[62]

a. PP: Photoperiod, b. CFR: CO₂ Fixation Rate in g m⁻³ h⁻¹

c. n.r.: not reported [CO₂] varied to keep pH at 8.5, d. Converted from original value in lux

e. Not specified, time assumed considering experimental conditions

Table 2.1. CO₂ bio-fixation rates of microalgae at different conditions

Organism	[CO ₂] in air	PPFD ($\mu\text{mol m}^{-2} \text{s}^{-1}$)	PP (Hours) ^a	T (°C)	Net CFR ^b	Culture vessel	Ref
<i>Phaeodactylum tricornutum</i>	40% n/n	1200	10	20	396.1	Tubular airlift photo-bioreactor, 50L	[74]
<i>Chlorella vulgaris</i>	1% v/v	178.2 ^c	24	25	221-275	Membrane photobioreactor, 5.6L	[75]
<i>Chlorella vulgaris</i>	0.04-12% v/v	350	24	26	1.3-46.7	Bubble column photo-bioreactor, 1.4L	[76]
<i>Scenedesmus sp.</i>	5% v/v	300	16	30	29.2	Bubble column photo-bioreactor, 0.5L	[77]
<i>Chlorella sorokiniana</i>	5% v/v	300	16	30	25.8	Bubble column photo-bioreactor, 0.5L	[77]
<i>Scenedesmus sp.</i>	10% v/v	200	24 ^d	27	25.5	Conical photobioreactor, 1L	[72]
<i>Chlorogonium sp.</i>	5% v/v	300	16	30	25.4	Bubble column photo-bioreactor, 0.5L	[77]
<i>Scenedesmus obliquus</i>	10% v/v	60	24	28	22.9	Column photobioreactor, 1L	[78]
<i>Dunaliella tertiolecta</i>	0.04-12% v/v	350	24	26	0.8-21.3	Bubble column photo-bioreactor, 1.4L	[76]
<i>Botryococcus braunii</i>	5% v/v	58 ^c	12	25	20.7	Illuminated BioFlo fermentor, 8L	[73]
<i>Chlorella vulgaris</i>	10% v/v	200	24 ^d	27	19.2	Conical photobioreactor, 1L	[72]
<i>Chlorella pyrenoidosa</i>	10% v/v	180	24 ^d	25	10.8	Erlenmeyer flasks, 0.8L	[79]

a. PP: Photoperiod, b. CFR: CO₂ Fixation Rate in g m⁻³ h⁻¹

c. Converted from original value in lux

d. Not specified, time assumed considering experimental conditions

Table 2.2. CO₂ bio-fixation rates of C₃ and C₄ plants

Organism	[CO ₂] in air	PPFD ($\mu\text{mol m}^{-2} \text{s}^{-1}$)	PP (Hours) ^a	T (°C)	Net CFR ^b	Growth space	Ref
<i>Zea mays</i> (corn) ^c	550 ppm 370 ppm	1900-2175 1900-2175	14 14	27-33 27-33	3.8-7.6 3.5-6.3	Open area. Summer and fall	[80]
<i>Sorghum halepense</i> (Johnsongrass) ^c	330 ppm ^f	184-1472 ^e	10	35	1.2-6	Greenhouse. Winter and spring	[75]
<i>Triticum aestivum</i> (wheat) ^d	350 ppm ^f	1000	10	-	1.8-3.5	Greenhouse. Fall, winter, and spring	[81]
<i>Festuca arundinacea</i> (tall fescue) ^d	330 ppm ^f	184-1472 ^e	10	25	1.2-2.5	Greenhouse. Winter and spring	[82]
<i>Glycine max</i> (Soy bean) ^d	350 ppm ^f	500	14	25	1.84- 2.19	Greenhouse	[83]
<i>Hordeum vulgare</i> (barley) ^d	330 ppm ^f	400	14	27	1.4-1.9	Grown in pots for 11 days	[84]
<i>Vicia faba</i> (bell bean) ^d	330 ppm ^f	400	14	27	1.4-1.7	Grown in pots for 11 days	[86]
<i>Solanum lycopersicum</i> (tomato) ^d	400 ppm ^f	500	12	24	1.4	Hydroponic culture, grown for two weeks	[85]
<i>Euphorbia forbesii</i> (tree) ^c	300-400 ppm	500	24 ^g	22	1.2-1.3	Greenhouse	[86]
<i>Claoxylon sandwicense</i> (tree) ^d	300-400 ppm	500	24 ^g	22	0.8-1.0	Greenhouse	[86]
<i>Oryza sativa</i> (rice) ^d	370 ppm ^f	800	14 ^g	27	0.3	Hydroponic culture, grown for 45 days	[87]

a. PP: Photoperiod, b. CFR: CO₂ Fixation Rate in g m⁻² h⁻¹, c. C₄ plant, d. C₃ plant
e. Converted from original value in fc, f. Approximate [CO₂] in atmosphere,
g. Not specified, time assumed considering experimental conditions

2.3.2 Carbon concentrating mechanism (CCM)

Dissolved CO₂ may enter the cyanobacterial cell by diffusion or through CO₂–uptake complexes [40]. On the other hand, negatively charged bicarbonate ions (HCO₃[–]) are only introduced by specialized energy-driven transporters. Bringing Ci inside the cell requires ATP, NADPH, and electrochemical gradients of sodium ions (Na⁺) and protons [5]. Genes encoding the production of Ci transporters are mainly expressed under high illumination and their transcription also depends on cyclic electron flow around photosystem I [2]. Five Ci transporters have been identified in cyanobacteria: *BCT1*, *SbtA*, and *BicA* (specific HCO₃[–] transporters), as well as *NDH-I3* and *NDH-I4*, which are specific for CO₂ [2, 5, 40]. Based on their CCM features, cyanobacteria may be classified as α-cyanobacteria (marine species with α-carboxysomes) and β-cyanobacteria (freshwater and estuarine species with β-carboxysomes) [54, 88]. Not all cyanobacteria produce the five transporters, and the presence of each Ci transporter is associated to the type of carboxysome in the cell.

Bicarbonate transporters can be found in the plasma membrane of cyanobacteria. *BCT1* is encoded by the *cmpABCD* operon. It is an ATP-binding cassette transporter, commonly found in β-cyanobacteria and some α-cyanobacteria (e.g., *Synechococcus* sp. WH 5701), that may be acquired by horizontal gene transfer. This transporter has a high affinity for HCO₃[–] and is induced under high illumination and low concentrations of Ci. *SbtA* transporter is a symporter of HCO₃[–] and Na⁺ with medium-high affinity for bicarbonate ions. *SbtA* is induced at low HCO₃[–] concentrations and can be found only in β-cyanobacteria. *BicA* transporter is also a Na⁺/ HCO₃[–] symporter that can be found in

both α and β -cyanobacteria. This transporter has low affinity for bicarbonate and can be constitutively expressed (not induced) [2, 5, 40, 88].

CO₂ transporters in cyanobacteria are located in the thylakoids and their main function is hydration of carbon dioxide entering the cell by diffusion. They are not true transporters but facilitate the absorption of CO₂ and are needed to prevent it from leaking out of the cell. These transporters also recycle CO₂ escaping from carboxysomes and are used to maintain a bicarbonate pool inside cyanobacteria. *NDH-13* has higher affinity for CO₂, it contains the *ChpY* protein as reaction center for hydration and is induced under low levels of Ci. *NDH-14* has lower CO₂ affinity, it is constitutively expressed in the plasma membrane and in the thylakoids, and its hydration reaction center is located in the *ChpX* protein. *NDH-13* and *NDH-14* may be found in β -cyanobacteria at the same time, but only one of them can be found in α -cyanobacteria [2, 5, 40, 88]. Other important complexes involved in the CCM of cyanobacteria are *PxcA*, *Mnh*, and *NhaS3*. These complexes are necessary to balance the interchange of ions proper of Na⁺ dependent transporters *SbtA* and *BicA*. While *PxcA* is responsible for H⁺ extrusion and pH regulation, *Mnh* also transports Na⁺ ions out of the cell and *NhaS3* acts as a Na⁺/H⁺ symporter [5].

The cyanobacterial CCM creates a pool of bicarbonate inside the cell (internal pH ~7.4), with a peak cytoplasmic concentration of HCO₃⁻ between 20 mM and 40 mM [60]. Bicarbonate ions stay inside the cell because their cell membrane permeability is 1000 times lower than that of uncharged CO₂ [5]. Bicarbonate is transported into the carboxysomes, which constitute the core component of the CCM. Carboxysomes are polyhedral bacterial microcompartments (BMC) composed by a thin selectively permeable shell encapsulating RuBisCO and carbon anhydrase enzymes. The

carboxysome shell allows free movement of protons, and experiments suggest that there is no pH difference between the cytoplasm and the carboxysomal interior [89, 90]. In addition, it has been estimated that RuBisCO carboxylation activity is maximum at pH~7.5 [91]. Once inside the carboxysome, carbon anhydrase enzyme dehydrates HCO_3^- back to CO_2 and the CBB cycle proceeds. The carboxysome shell is also permeable to RuBP, PGA, Mg^{2+} , and HCO_3^- , but constitutes a diffusion barrier preventing CO_2 escape and O_2 introduction. Carboxysomes are rich in CO_2 and are essential to enhance RuBisCO activity and minimize photorespiration [2, 5, 60, 88, 92].

2.3.3 Carboxysomes

The α -cyanobacteria have α -carboxysomes, β -cyanobacteria have β -carboxysomes, and this division is based on RuBisCO enzyme. RuBisCO appears in nature in up to four different forms, and cyanobacteria have type I RuBisCO. The enzyme is organized as a hexadecamer of eight large subunits (LSU, ~55 kDa) and eight small subunits (SSU, ~15 kDa). Type I RuBisCO may be further subdivided into type IA and type IB depending on the amino acid sequence of the large subunit [2, 5]. The core of α -carboxysomes is RuBisCO type IA and the core of β -carboxysomes is RuBisCO type IB. These carboxysomes perform the same function, but their structure is different. A common feature shared by carboxysomes, regardless of the type, is the content of RuBisCO, which is ~70% of the total protein. Apart from the structure of RuBisCO, the differences between α - and β -carboxysomes are related to size, protein composition, and internal organization [2, 54, 88]. The carboxysomal organization in α - and β -cyanobacteria is presented in Figure 2.3.

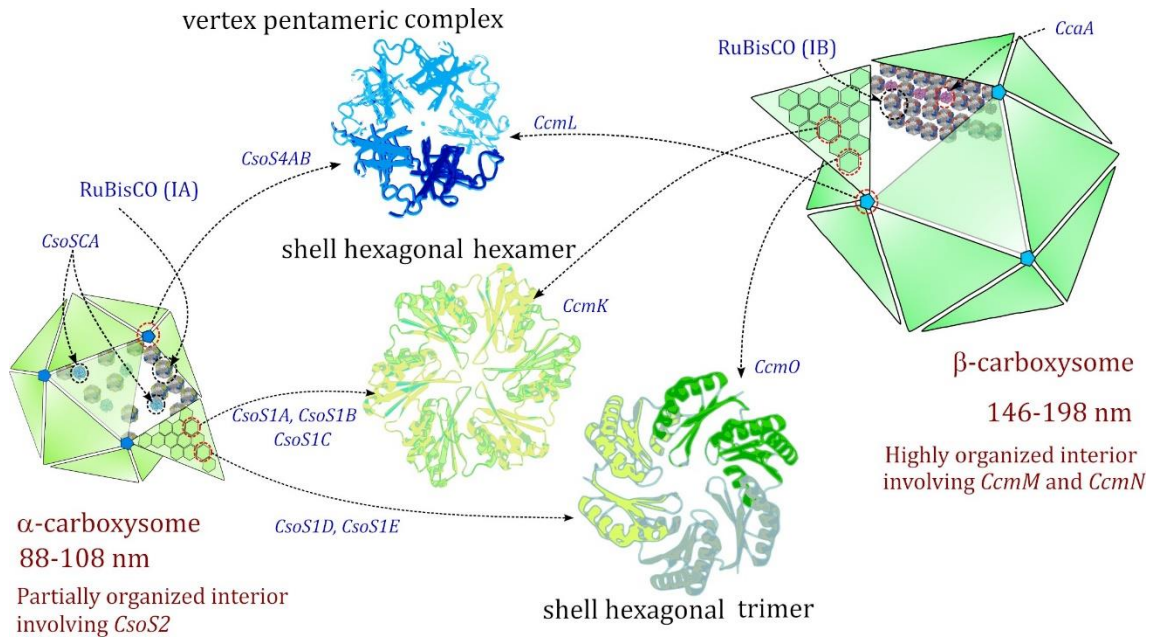


Figure 2.3. Structure of carboxysomes in α- and β-cyanobacteria (adapted from [88])

The α-carboxysomes are regular icosahedra whose diameter varies between 88 and 108 nm (measured in marine *Synechococcus* sp. WH8102) [54]. The shell of α-carboxysomes is 3 to 4 nm thick and is composed by small 10 to 11 kDa proteins (*CsoS1A*, *CsoS1B*, *CsoS1C*, *CsoS1D*, *CsoS1E*, *CsoS4A*, and *CsoS4B*) forming flattened hexagonal hexamers or trimers. These protein groups interact closely with each other forming the faces of the icosahedral structure. In addition, each hexamer has a central pore allowing the preferential transit of charged molecules (RuBP , HCO_3^- , and Mg^{2+}). Proteins of the *CsoS1* family are the main constituents of the shell, and *CsoS4* proteins fit in the gaps and vertices of the carboxysome. Proteins of the *CsoS2* and *CsoSCA* families are attached to the shell of α-carboxysomes. *CsoS2* proteins are possibly responsible for organizing the subshell structure by linking RuBisCO to the inner side of the carboxysome. On the other hand, *CsoSCA* proteins (also known as *CsoS3*) are

carbon anhydrase enzymes (57 kDa homodimers) responsible for the reversible dehydration of bicarbonate. Regarding organization, α -carboxysomes are shell-centered structures, in which RuBisCO type IA is partially organized in the form of packed spheres. RuBisCO proteins adjacent to the shell form organized layers, but they are randomly arranged inside the carboxysome [54, 88].

Carboxysomes in β -cyanoabacteria are also polyhedral structures (possibly icosahedra) with diameters in the 146-198 nm range (measured in *Synechococcus* sp. PCC 7942) [54]. In general, the structure of β -carboxysomes is more complex than that of α -carboxysomes. The shell is 5 to 6 nm thick, and is formed by two protein layers containing *CcmK*, *CcmL*, and *CcmO* proteins outside, and *CcmN* and *CcmM* proteins inside. *CcmK* proteins are organized as hexamers and form the flat faces of the polyhedral shell. These proteins also contain the central pores, which are used for the transit of charged molecules in and out of the carboxysome. *CcmO* proteins form trimers and are also involved in the construction of flat shell faces. *CcmL* proteins are analogue to *CsoS4* proteins in α -carboxysomes, as they fit in the vertices of the shell. Although *CcmN* proteins may connect the inner and outer layers of the shell, *CcmM* proteins are the most important structural proteins in the carboxysome. There are two essential *CcmM* proteins, *CcmM*-58 (58 kDa) and *CcmM*-35 (35 kDa). *CcmM*-58 simultaneously interconnects adjacent RuBisCo type IB, carbonic anhydrase enzymes, and outer shell proteins. The distinct carbon anhydrase enzyme in β -carboxysomes is called *CcaA*, but it has been proposed that freshwater species lacking this enzyme (e.g., *Thermosynechococcus elongatus*) may use *CcmM* proteins for bicarbonate dehydration inside the carboxysome [93]. The structural enzyme *CcmM*-35 is confined inside the

carboxysome and arranges RuBisCO into crystalline arrays. Because of this, the β -carboxysomes are more organized than α -carboxysomes and are considered lumen-centric compartments [54, 88].

2.3.4 Regulation of CO₂ uptake

It is only possible to present a partial description of CO₂ uptake regulation mechanisms in cyanobacteria because carbon transport has been better characterized in β -cyanobacteria than in α -cyanobacteria. Considering that Ci (CO₂ and HCO₃⁻) concentrations in freshwater bodies and estuaries are more variable than in the ocean, β -cyanobacteria require more diverse mechanisms to deal with limited inorganic carbon availability [94]. In addition, it is likely that CO₂ uptake in α -cyanobacteria is less regulated because most marine species lack inducible high affinity Ci transporters [62, 97]. Most of the previously described transporters of CO₂ and HCO₃⁻ in the CCM have been characterized in β -cyanobacteria (*Synechocystis* sp. PCC 6803, *Synechococcus elongatus* PCC 7942, and *Synechococcus* sp. PCC 7002). Therefore, it is also possible that α -cyanobacteria make use of other Ci transporters, which cannot be identified by sequence homology [95].

The concentration of extracellular Ci influences the activity of CCM in β -cyanobacteria. Therefore, it is possible to distinguish between a basal or constitutive CCM and a fully induced CCM. The basal CCM involves expression of genes coding only for RuBisCO, carboxysomal peptides, and low affinity Ci transporters, like *NDH-I₄* or *BicA*, which are necessary for survival in aquatic environments, regardless of the external Ci levels [62]. When external Ci is in excess ($\sim 2\%$ v/v CO₂), the maximum

concentration of intracellular Ci (carbon pool of HCO_3^-) reaches ~ 20 mM. In this case, the affinity for Ci is lower because only the basal CCM is active. Besides, the overall Michaelis constant (K_M) for carboxylation falls between 200 and 300 μM . When the external Ci concentration is low (e.g., ~ 20 ppm of CO_2), the affinity of β -cyanobacteria for Ci is increased to maintain a cytoplasmic carbon pool with maximum Ci concentrations reaching ~ 40 mM. In that sense, β -cyanobacteria are able to maintain intracellular HCO_3^- concentrations above the thermodynamic equilibrium. To do this, the high affinity CO_2 and HCO_3^- uptake systems are activated (fully induced CCM) and additional carboxysomes are produced to bring the global carboxylation K_M between 10 and 15 μM [60, 96].

Transcriptional control of the CCM relies on two LysR-type transcriptional regulators (LTTR): the *CmpR* activator and the *CcmR* repressor. When the intracellular Ci concentration is low, cyanobacteria accumulate RuBP and G2P as the CBB cycle slows down and photorespiration increases. RuBP and G2P are considered signaling metabolites promoting the binding of the *CmpR* activator to the operator region of *cmpABCD* operon [97]. The expression of high affinity HCO_3^- transporter *BCT1* is activated once G2P concentration exceeds a threshold value, that has yet to be determined [95]. *CmpR* activator was originally studied in *Synechocystis* sp. PCC 6803, but homologue sequences of the *cmpR* gene have been found in other β -cyanobacteria, like *Synechococcus elongatus* PCC 7942, *Nostoc* sp. PCC 7120, and *Nostoc punctiforme* [98]. Expression of *BCT1* transporter is also induced under high illumination, but additional experimental evidence is necessary to fully describe the relationship between

inducible bicarbonate uptake systems and response mechanisms to changing illumination conditions [96, 99].

The *CcmR* repressor is critical for regulating carbon uptake in β -cyanobacteria. In general, this LTTR represses most high affinity Ci uptake systems, except for the *BCT1* transporter [60]. When Ci availability is low, nicotinamide adenine dinucleotide phosphate (NADP) is converted to NADPH through photosynthesis, but no longer regenerated through the CBB cycle. Furthermore, as the Ci pool shrinks, oxo-glutarate (OG) concentration is expected to decrease because of the lack of carbon sources feeding the tricarboxylic acid cycle (TCA) [95]. NADP and OG are necessary to stabilize the binding of *CcmR* to its target DNA [100]. As NADP and OG levels go down, binding of *CcmR* to DNA is disturbed and gene repression stops. Hence, expression of higher affinity transporters is enhanced to bring in additional CO_2 and HCO_3^- . In *Synechocystis sp.* PCC 6803, *CcmR* represses the genes coding for *SbTA* and *NDH-I₃* transporters when Ci concentration is high. In addition, *CcmR* also represses the *mnh* operon, that codes for an auxiliary Na^+ extrusion system required by the *SbTA* transporter [96, 101]. In *Synechococcus sp.* PCC 7002, *CcmR* represses *SbTA* and *NDH-I₃* transporters, but also blocks the production of *BicA* and HCO_3^- porin *PorB* at Ci -repleted conditions [102].

Other transcriptional and post-transcriptional regulators have been discovered in model organism *Synechocystis sp.* PCC 6803. For example, a second repressor protein *CyAbrB2* was found to block the expression of *SbTA* and *NDH-I₃* transporters along with *CcmR* under Ci -repleted conditions [103]. In addition, transcriptome analysis lead to the discovery of the carbon stress induced RNA1 *CsiR1*, a small non-coding RNA fragment (sRNA) overly produced under Ci limitation. Although the functions of this sRNA are not

clear, it could be involved in translational control of CCM proteins [104, 105]. The carbon uptake regulation mechanism in cyanobacteria is more complex than the description provided in this document. Please refer to the following scientific reviews for further information [60, 95, 105].

2.3.5 Nitrogen assimilation and fixation

Sources of inorganic carbon are crucial to keep cyanobacteria and other photosynthetic organisms alive. However, macro-nutrients containing nitrogen and phosphorous are also essential. While total phosphorous content in cyanobacterial biomass is less than 1% w/w, elemental nitrogen makes up more than 10% w/w of the total weight, and is necessary for the synthesis of peptides, nucleic acids, pigments, co-enzymes, vitamins and other metabolites [13, 106]. Hence, Nitrogen availability becomes a major factor influencing growth and maintenance of the metabolic network. Besides free NH_4^+ , suitable Nitrogen sources include nitrates (NO_3^-), nitrites (NO_2^-), cyanates (OCN^-), urea, glutamine, arginine, and even atmospheric N_2 . Remarkably, NO_3 , NO_2 and OCN uptake genes are expressed only at low NH_4^+ levels because ammonium ions repress their intracellular conversion [14–17]. Regardless of the Nitrogen source used, intracellular NH_4^+ and glutamate are the definitive products of external nitrogen assimilation.

Nitrogen compounds should be imported and converted to intracellular NH_4^+ to fuel bio-synthetic pathways [14, 16]. Import of NH_4^+ is accomplished by means of secondary permeases of the Amt family, which possibly bring in ions using a membrane potential-driven transport mechanism [14]. Free NH_4^+ is the preferred source of Nitrogen

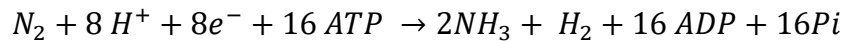
when present in the external medium at low concentrations around 1 μM [15]. However, higher levels of external NH_4^+ become detrimental because most ammonium is converted to free ammonia (NH_3) as the concentration rises and the pH goes above 9.25. Although free ammonia is toxic for cyanobacteria, some species like *Spirulina platensis* can tolerate up to 10 μM NH_4^+ concentrations and survive at pH 10 or higher [106, 107]. The incorporation of NO_3 , NO_2 , OCN , urea, glutamine and arginine is possible by the action of multicomponent ABC-type transporters attached to the cytoplasmic membrane of cyanobacteria. This is a light-driven process because permeases make use of ATP to power active and concentrative transport of specific substrates into the cell [15].

Once inside the cell, nitrogenous compounds are converted to NH_4^+ using different enzymes. Nitrate ions are reduced to nitrite by ferredoxin-nitrate reductase (*NarB*) enzyme, and nitrites are ultimately reduced to NH_4 by ferredoxin-nitrite reductase (*NirA*). Cyanate conversion into CO_2 and NH_4^+ is catalyzed by the cyanase enzyme (*CynS*). Urea is decomposed to CO_2 and NH_4^+ by a Ni^{2+} dependent urease enzyme and arginine is catabolized by longer metabolic routes involving production of urea and activation of the arginase pathway. Finally, glutamine is used directly in the glutamine synthase-glutamate synthase pathway, that produces precursor metabolites for further production of amino-acids [14–16, 108]. Considering that cyanobacteria can assimilate Nitrogen from different sources, they have also gained recent attention for treatment of agro-industrial wastewater with high levels of nitrogen-containing compounds [107].

Readily available atmospheric N_2 is a very important Nitrogen source for diazotrophic cyanobacteria. The ability to fixate N_2 is exclusive of prokaryotes, and this constitutes a powerful biological advantage. In that sense, diazotrophic cyanobacterial

metabolism becomes even more interesting because these organisms can use oxygenic photosynthesis and anaerobic N₂ fixation to sustain their rich metabolic network [17, 109]. Nitrogenase 1 enzyme is necessary for N₂ fixation. Since this enzyme is inhibited by oxygen, some unicellular and heterocyst-forming filamentous cyanobacteria make use of spatial and temporal separation mechanisms to reduce N₂ and produce NH₄⁺ (See subsection 2.2.3). Nitrogenase 1 is a molybdenum dependent ATP-hydrolyzing complex capable of reducing diffused N₂ into two molecules of NH₃ and producing H₂ as a byproduct. As presented in Equation 2.3, this process requires a considerable amount of energy (16 ATP) to break the stable triple bond formed between nitrogen atoms in N₂. Once NH₃ is produced, it is hydrated to form NH₄⁺. Photosynthetic production of ATP is the main energy source for N₂-fixation in cyanobacteria. Hence, this is also a light-driven process [15, 17, 109].

Equation 2.3



Diazotrophic cyanobacteria play a fundamental role in the global Nitrogen cycle. Recent estimations suggest that 413 Tg of reactive elemental Nitrogen are fixated every year through natural (203 Tg-N) and anthropogenic processes (210 Tg-N). From these, around 140 Tg-N (~34%) are biologically fixated by marine prokaryotes [110]. Interestingly, marine cyanobacteria from the genus *Trichodesmium* are responsible for the fixation of ~100 Tg-N, becoming the most important nitrogen supplier for ocean life [109–111]. Freshwater diazotrophic cyanobacteria are also important bio-fertilizers of wet

rice crops, supporting the cultivation of one of the most important staple foods worldwide. Notably, the maximum nitrogen fixation potential of cyanobacteria commonly found in rice fields (genera *Nostoc*, *Fischerella*, *Anabaena*, and *Calothrix*) ranges from 50 to 75.5 kg-N $ha^{-1} year^{-1}$ [17]. Considering that ~ 120 Tg-N are fixated every year by the Haber-Bosch reaction [110], diazotrophic cyanobacteria are more important than any industrial process for the global Nitrogen supply. In addition, replacement of synthetic fertilizers by cyanobacterial bio-fertilizers could potentially reduce the eutrophication caused by agro-industrial wastewater.

Unlike plants and microalgae, which naturally require symbiotic associations with bacteria to use N_2 for biosynthesis, axenic cultures of diazotrophic cyanobacteria could potentially be used to transform sunlight, carbon dioxide, and atmospheric Nitrogen into high value chemical products. Cyanobacteria belonging to *Anabaena* and *Nostoc* are candidates for the development of diazotrophic photosynthetic bio-factories [17]. When grown in photo-autotrophic mode and in liquid medium without Nitrogen sources, each filament of these cyanobacteria becomes a multicellular bacterial community of vegetative cells fixing CO_2 and heterocysts fixing N_2 . The outer membrane of each filament is continuous, and the cells therein contained share a common periplasmic space, where they exchange metabolites [112]. Because of this, *Anabaena* and *Nostoc* can sustain their metabolic network using light and fewer nutrients. Nitrates and other sources of Nitrogen are major components of common liquid media used to grow cyanobacteria [13, 113]. Hence, the reduction or complete elimination of nitrates in the formulation of culture medium is also economically beneficial for massive cultivation of these organisms.

Two specific heterocyst forming cyanobacteria are good examples of diazotrophic organisms able to produce high-value chemicals from light. First, *Nostoc sp.* PCC 7120 has been widely studied as model for heterocyst differentiation, but also produces high quantities of C-phycoerythrin (CPC), a natural blue pigment used in foods and cosmetics [114]. Other uses of CPC include fluorescent markers for biomedical applications, dietary supplements, and pharmaceuticals [17, 115]. Interestingly, anticancer properties have also been attributed to CPC [116, 117]. In recent studies, synthetic biology has been used for heterologous production of non-ribosomal peptide Lyngbyatoxin A in *Nostoc sp.* PCC 7120 [118]. This toxin is a proteinase kinase C activator naturally produced by marine cyanobacterium *Moorea producens* and could be used for drug discovery applications [119, 120]. Furthermore, heterologous production of marine secondary metabolites in *Nostoc sp.* PCC 7120 opens the door to develop enhanced bio-factories producing powerful therapeutic agents from marine cyanobacteria. The second organism showing interesting properties for commercial use of photosynthetic diazotrophs is *Anabaena sp.* ATCC 33047. These cyanobacteria have a relatively high CO₂ fixation rate at high illumination (see Table 2.1) and has been proposed for large scale carbon sequestration from air and flue gases [67, 121]. Carbon and Nitrogen assimilation constitute only the starting point for photoautotrophic biosynthesis of high value chemicals in cyanobacteria. The metabolic reactions leading to these valuable compounds will be described in section 2.4 and section 2.5.

2.4 Primary metabolism

The most important mechanisms of ATP production in cyanobacteria are the light phase of photosynthesis and cellular respiration. Both processes converge in the thylakoids and are essential to power primary metabolism. Light reactions and carbon fixation processes are the starting biochemical processes for the synthesis of sugars in photoautotrophic organisms. After carbon fixation by the CBB cycle, glucose can be produced from the triose phosphate pool. Two molecules of triose phosphate (PGAL and DHAP) are fused and converted into one molecule of FBP by means of fructose-bisphosphate aldolase enzyme. Subsequently, enzyme fructose 1,6-bisphosphate phosphatase transforms FBP into F6P. Then, F6P is isomerized to glucose 6-phosphate (G6P) by enzyme hexose phosphate isomerase. G6P is further modified by phosphoglucomutase enzyme to produce glucose 1-phosphate (G1P). In the form of G1P, glucose is ready to be processed for longer term storage as glycogen [53].

The main biochemical reactions taking place in the cytoplasm of cyanobacteria are the CBB cycle and the tricarboxylic acid cycle (TCA). Both cycles are connected by glycolysis/glycogenolysis and oxidative pentose phosphate (OPP) catabolic pathways [122]. Primary metabolism also includes synthesis of lipids, porphyrin metabolism, and production of amino-acids and nucleotides [123–125]. Another important biosynthetic pathway that takes place in cyanobacteria is the methyl-erythritol-4-phosphate (MEP) pathway, which is responsible for the synthesis of terpenoids [126–129]. The products of primary metabolism are necessary for cellular growth. Under ideal culture conditions, the global composition of cyanobacteria derived from the primary biosynthetic pathways is 10 to 30% w/w carbohydrates, 5 to 10% w/w intermediate lipids, and 40 to 79% w/w

proteins. In contrast, algae can be much richer in lipids (up to 40% w/w), and plants are much richer in carbohydrates (70-80% w/w) [130]. The biochemical reactions of the primary metabolism of cyanobacteria are represented in Figure 2.4.

2.4.1 Glycogen production

The main carbon storage molecules (carbon sinks) of prokaryote and eukaryote photosynthetic organisms are different. Algae and plants store glucose in the form of starch and use it to build their cellulose-based cell walls. In contrast, cyanobacteria use glycogen as the main glucose reservoir and invest their carbohydrate resources to build their EPS layers [130]. Glycogen is a branched polyglucose composed by glucose monomers linked by α -1,4-glycosidic bonds (~90%) and α -1,6-glycosidic bonds (~10%) [131]. Although glucose is the most abundant monosaccharide in the EPS layers, twelve other monosaccharides (mainly hexoses, pentoses, and deoxyhexoses) have also been identified as constituents of the external sugar matrix of cyanobacteria [132]. Except for photosynthesis, glycogen production features, and some differences in oxidative phosphorylation, the primary metabolism in cyanobacteria is fairly similar to that of heterotrophic bacteria [125].

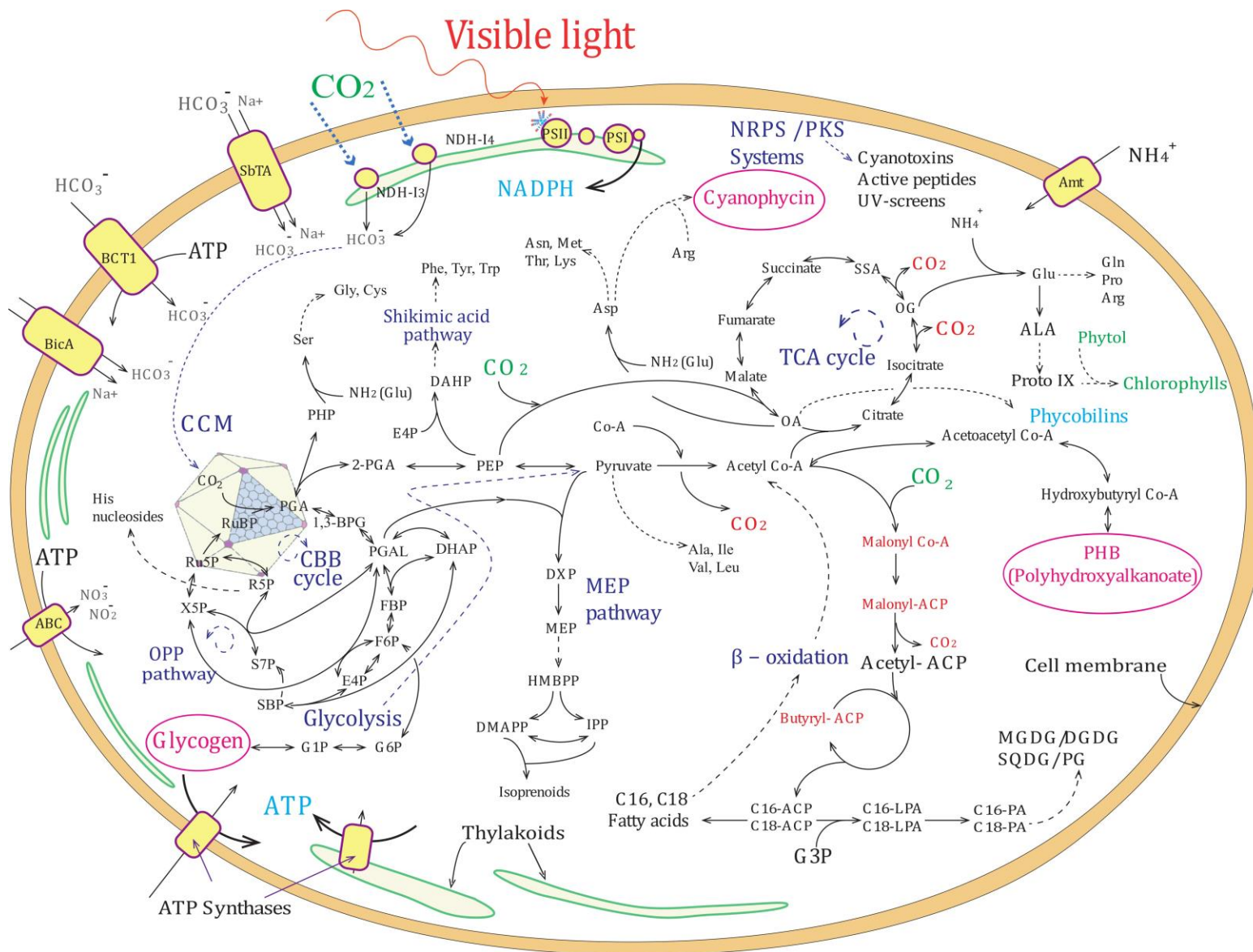


Figure 2.4. Biochemical reactions in cyanobacterial metabolism

2.4.2 Glycolysis and oxidative pentose phosphate pathways

Glycolysis and OPP catabolic pathways are mainly activated under dark conditions, when cyanobacteria make use of the glucose accumulated under illumination [133]. The glycolytic pathway is necessary to produce ATP and pyruvate from stored glucose. This process is summarized in Figure 2.5. First, glycogen phosphorylase enzyme catalyzes the breakdown of glycogen to G6P, which is later converted into F6P. ATP mediated phosphorylation of F6P yields FBP, which can be broken into two fragments of triose phosphate (PGAL and DHAP). Phosphoglyceraldehyde dehydrogenase catalyzes the oxidation of PGAL to 1,3-bisphosphoglycerate (1,3-BPG) using nicotinamide adenine dinucleotide (NAD) and phosphate. Next, enzyme phosphoglycerate kinase uses 1,3-BPG and ADP to generate PGA and ATP. PGA mutase enzyme converts PGA into 2-phosphoglycerate (2-PGA). Later, enolase catalyzes the dehydration of 2-PGA to form phosphoenolpyruvate (PEP). Pyruvate is then produced after pyruvate kinase dephosphorylates PEP. In this process, one molecule of ATP is formed for every molecule of pyruvate produced [134]. The OPP pathway is used during aerobic dark respiration, it is divided into oxidative and non-oxidative phases, and essentially consists of the reverse reactions of the CBB cycle (see CBB cycle in Figure). First, the oxidative phase produces NADPH by converting G6P into R5P and releasing CO₂. In the second phase (non-oxidative interconversion), three-, four-, five-, six-, and seven-carbon sugar are also converted into five carbon sugars (mainly R5P). Five carbon sugar R5P and its derivatives may be further used in the synthesis of nucleosides, which

can be further used to produce nucleotides, nucleic acids, ADP, NAD, flavin adenine dinucleotide (FAD), and coenzyme A [135].

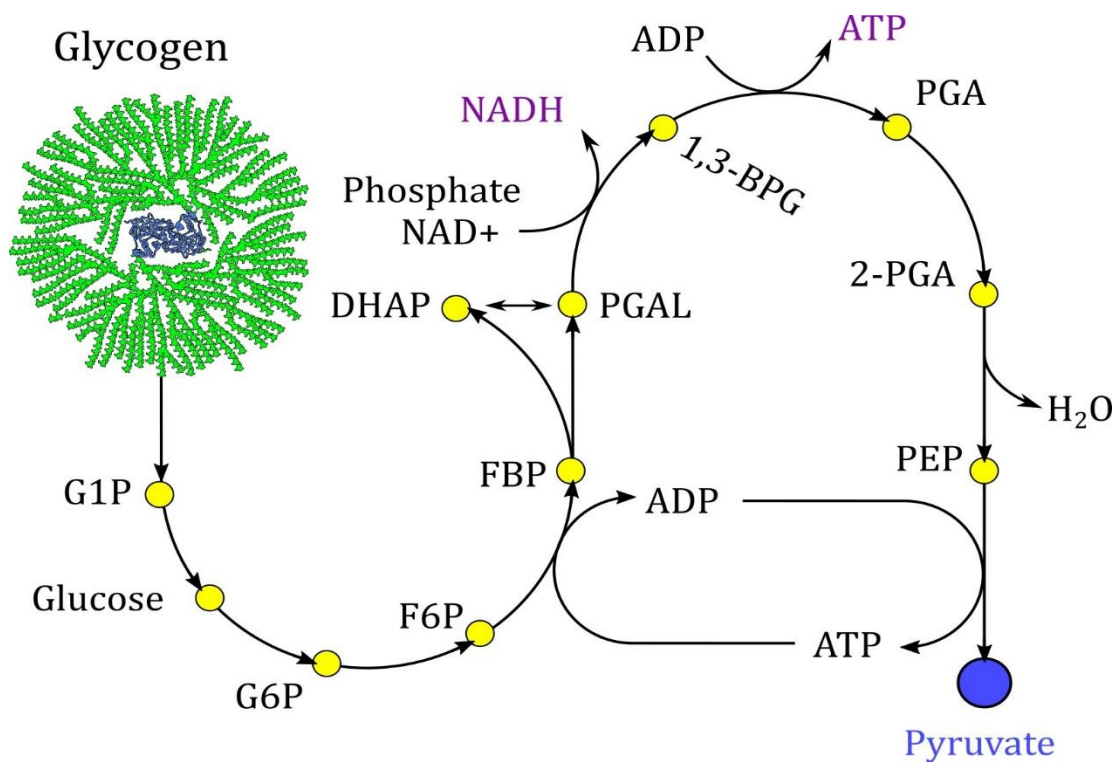


Figure 2.5. Glycolysis pathway in cyanobacteria

Glycogen is degraded to produce ATP, NADPH and pyruvate

2.4.3 Tricarboxylic acid cycle and oxidative phosphorylation

The TCA cycle is the first stage of cellular respiration. The main function of the cycle is the oxidation of carbon fuels to produce reductive power in the form of NADH and FADH₂ (reduced forms of NAD and FAD) [136]. In addition, the TCA cycle provides precursor metabolites for the biosynthesis of building blocks (e.g., amino-acids, nucleotide bases, cholesterol, and porphyrin) [137]. Carbohydrates, fatty acids, and amino acids are the carbon fuels used in the TCA cycle for the extraction of energy.

However, these fuel molecules should be transformed into acetyl coenzyme A (acetyl Co-A) before they enter the cycle. When carbohydrates are used as fuel for the TCA cycle, acetyl Co-A is formed after pyruvate from glycolysis is decarboxylated (CO_2 released) and the resulting acetyl is fused with coenzyme A. In the TCA cycle, acetyl Co-A is condensed with oxaloacetate (OA) to yield citrate (six-carbon tricarboxylic acid), which is then isomerized and decarboxylated to produce five-carbon oxo-glutarate (OG) [136]. In *Synechococcus* sp. PCC 7002 cyanobacteria, OG is converted by 2-oxoglutarate decarboxylase enzyme to succinic semialdehyde (SSA) (CO_2 released again), which is later transformed into succinate by succinic semialdehyde dehydrogenase. The remaining reactions in the TCA cycle convert succinate to fumarate and malate to regenerate OA, restarting the cycle [137]. During decarboxylation and OA regeneration, NAD^+ and FAD^{2+} coenzymes are reduced. Overall, the TCA cycle oxidizes two carbon units coming from acetyl Co-A, produces two molecules of CO_2 , and transfers high energy electrons to NADH and FADH_2 , which are further used in the oxidative phosphorylation pathway [136–138].

The oxidative phosphorylation pathway is the final stage of cellular respiration initiated with the TCA cycle [139]. Along with the protein complexes that transport electrons during the light phase of photosynthesis, the thylakoid membranes also contain complexes involved in respiration. In cyanobacteria, NADH , FADH_2 , and succinate are first oxidized by complex-I (NADH : ubiquinone-oxidoreductase) or complex-II (succinate: ubiquinone-oxidoreductase). Next, the reduced ubiquinol cofactor interacts with complex-III (ubiquinol: cytochrome c oxidoreductase) and transfers its electrons to cytochrome c (Cyt c). The final complex in the oxidative phosphorylation chain is Cyt c oxidase (COX),

which catalyzes the reduction of molecular O_2 to water. Four protons are used by COX to reduce one oxygen molecule. At the same time, four protons from the cytoplasm are translocated across the thylakoids. Inside the thylakoid lumen, these hydrogen ions contribute to the proton motive force (PMF) needed to synthesize ATP by ATP synthase enzyme [41, 140].

2.4.4 Production of lipids

The synthesis of lipids depends on the conversion of acetyl Co-A to malonyl Co-A [133]. In this reaction, one molecule of CO_2 and one molecule of acetyl Co-A are combined by means of acetyl Co-A carboxylase enzyme. Next, malonyl Co-A is converted into lipid precursors by fatty acid synthase (FAS) enzyme. Cyanobacteria produce type II FAS, an acyl-carrier protein (ACP) composed of several subunits that catalyze individual reactions in the biosynthesis of fatty acids. Cyanobacterial FAS differs from eukaryote type I FAS in which the latter is a multi-functional enzyme instead of a multi-subunit complex. In order to synthesize fatty acids, malonyl Co-A is converted to malonyl-ACP by malonyl-CoA:ACP transacylase, which is a subunit of the FAS complex. Later, malonyl-ACP goes through a sequence of cyclic elongation reactions involving other FAS subunits that first produce butyryl-ACP. The FAS subunits involved in this pathway are 3-ketoacyl-ACP synthase, 3-ketoacyl-ACP reductase, 3-hydroxyacyl-ACP dehydrase, and enoyl-ACP reductase. To close the cycle, butyryl-ACP is combined with the acetyl unit of one malonyl-ACP. The cycle is repeated until palmitoyl-ACP (sixteen carbon chain) or stearyl-ACP (eighteen carbons) are synthesized. C_{16} and C_{18} acyl precursors (palmitoyl-ACP and stearyl-ACP) donate their acyl moiety to glycerol 3-

phosphate (G3P) to produce phosphatidic acid (PA) in a two-step process. First, G3P acyltransferase catalyzes the conversion to lysophosphatidic acid (LPA) and then LPA acyltransferase transforms LPA into palmitic and stearic phosphatidic acids [146]. In the form of C₁₆ and C₁₈ PAs, the lipids can be used to synthesize MGDG, DGDG, SQDG, and PG, which are the main components of the cellular and thylakoid membranes [31, 138, 146]. For additional details, refer to the work by Sato and Wada [141].

Fatty acyl-ACP thioesterase enzyme uncouples fatty acids from lipid synthesis by hydrolyzing the ACP fragments from fatty acyl-ACP molecules. As a result, free fatty acids are produced. Free fatty acids may be further combined with coenzyme A by means of acyl-CoA synthase. This reaction is the precursor of the β -oxidation pathway, which can be used by cyanobacteria to obtain energy from the catabolism of lipids. Co-A fatty acids need to be transformed first to acetyl co-A, so they can be used as fuel in the TCA cycle. When there is an excess of energy, but also under phosphate and nitrogen depletion conditions, cyanobacteria can produce polyhydroxyalkanoates (PHA) for the storage of carbon [133]. Production of PHA is directly linked to the metabolism of lipids as it can be synthesized starting from acetyl Co-A or through β -oxidation of fatty acids [142].

2.4.5 Synthesis of polyhydroxyalkanoates

PHAs are polymer storage substances naturally produced by heterotrophic and autotrophic bacteria. Among these, cyanobacteria are unique in that they produce PHAs directly from sunlight and CO₂ using oxygenic photosynthesis [143, 144]. The dominant PHA produced by cyanobacteria is polyhydroxybutyrate (PHB), which is synthesized from

the polymerization of hydroxybutyryl Co-A monomers under nitrogen and phosphate depletion. These monomers are obtained after acetylation and reduction of acetyl Co-A by β -ketothiolase and acetoacetyl Co-A reductase enzymes respectively. The synthesis of medium chain length PHB is also possible using products of the fatty acid β -oxidation process that degrades C₁₆ and C₁₈ free fatty acids. In both cases, polymerization of hydroxyacyl Co-A thioester monomers is catalyzed by PHA synthase enzyme [142]. Accumulation of PHB may be thought of as a buffering pathway using excess acetyl Co-A and NADH. In darkness and under stressful fermentation conditions, PHA is the second storage compound to be degraded for energy production in the TCA cycle (after glycogen) [145]. Recently, a PCR based methodology was developed to identify potential PHA producing cyanobacteria [142]. Moreover, it has been reported that cyanobacteria of the order *Nostocales* (subsection IV), especially *Nostoc muscorum*, have the highest accumulation potentials of PHA under photoautotrophic and mixotrophic conditions, ranging from 21 to 78% dry cell weight (DCW) [35]. Other producers of high amounts of PHA could be the filamentous cyanobacteria of the genera *Leptolyngbya* and *Calothrix*, which are easy to harvest and whose rate of biomass production is comparable to commercially exploited strains of *Arthrospira* and *Spirulina* [143, 146].

2.4.6 Production of amino acids

As photoautotrophic organisms, cyanobacteria can synthesize the 20 standard proteinogenic amino acids [3, 11, 147]. This section provides a general description of amino-acid production pathways in cyanobacteria. However, amino acids can be synthesized through different metabolic reactions involving ATP and NADPH dependent

enzymes or spontaneous processes. Variations can occur depending on the genome of specific cyanobacterial species. For details on species specific amino acid production pathways, the reader is referred to specialized databases like the pathway collection of the Kyoto Encyclopedia of Genes and Genomes (KEGG) [148, 149]. Figure 2.6 shows a qualitative metabolic network to produce amino acids in cyanobacteria. The names of important intermediates are included, and the number of steps involved in each biosynthesis route is also represented. Figure 2.6 also depicts dependency relations and interactions among amino-acid production pathways. Larger icons are used for glutamate and glutamine to represent their higher importance in the synthesis of other amino acids.

The essential carbon skeleton for the biosynthesis of amino acids is OA, which is also the pivotal reagent in the TCA cycle [150]. In the TCA cycle, OA is first fused with acetyl Co-A to form citrate and the subsequent decarboxylation of citrate produces OG. The synthesis of glutamate, the most abundant amino acid in cyanobacteria, is catalyzed by the NADPH dependent enzyme glutamate dehydrogenase, which combines OG with ammonium to form glutamate and water. The role of glutamate in the biosynthesis of other amino acids becomes clear from Figure 2.6 because it is the direct or indirect amino group donor in most pathways.

Glutamine is exclusively synthesized by means of glutamine synthase enzyme, which adds ammonium to glutamate. Glutamine and glutamate are involved in the synthesis of the remaining amino acids acting as amino group donors. In addition, the amide group of glutamines is necessary for the biosynthesis of purines (guanine and adenine) and pyrimidines (thymine, cytosine, and uracil). Proline and arginine are also

directly derived from glutamate. Proline is obtained in a three-enzyme pathway comprising glutamic- γ -semialdehyde production and dehydration. On the other hand, arginine is synthesized by an eight-enzyme pathway within the urea cycle, where acetyl Co-A is first combined with glutamic acid [147, 151, 152].

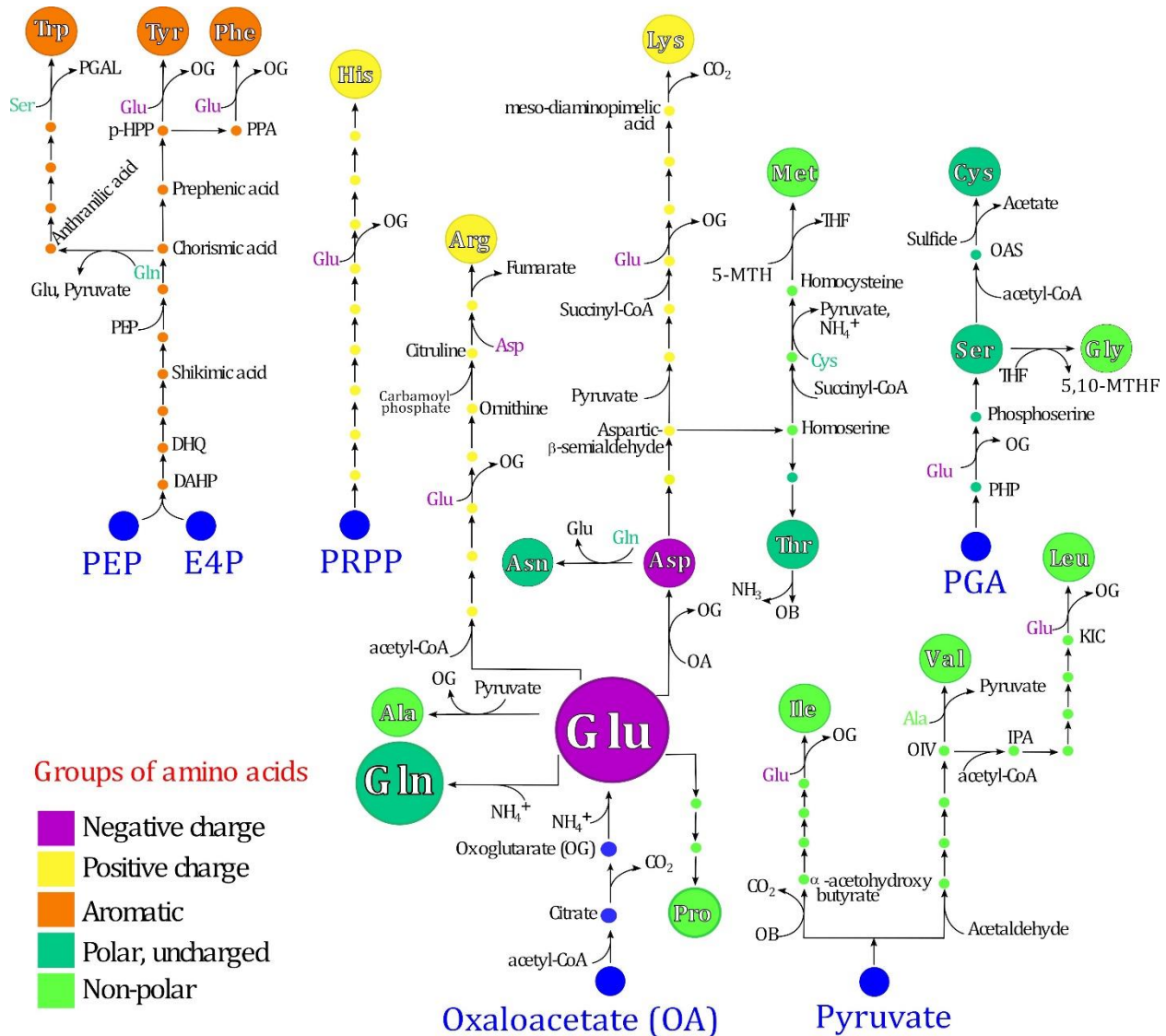


Figure 2.6. Amino-acid production pathways in cyanobacteria

Aspartate (aspartic acid) is another important precursor in the synthesis of cyanobacterial amino acids. The production of asparagine, methionine, threonine, and lysine directly depends on the availability of aspartate (see Figure 2.6). Aspartate biosynthesis is mediated by an aminotransferase enzyme that transfers the amino group from glutamate to OA. The amidation of aspartate with glutamine yields asparagine, and the process is mediated by asparagine synthase enzyme. Aspartate is also transformed into aspartic- β -semialdehyde and homoserine. These derivatives constitute two important branch intermediates, from which amino acids belonging to the aspartate family are produced. Aspartic- β -semialdehyde and pyruvate are needed for the synthesis of lysine. After a series of aldol condensation and dehydration reactions that also involve succinyl Co-A and oxoglutarate, these precursors are converted to meso-diaminopimelic acid. The decarboxylation of the latter meso-diaminopimelic acid yields lysine. Homoserine is necessary for the synthesis of methionine and threonine. In order to synthesize methionine, homoserine is sequentially combined with succinyl Co-A and cysteine yielding homocysteine, pyruvate, and NH_4^+ . Later, vitamin B₁₂ aided methylation of homocysteine produces methionine. The biosynthesis of threonine is biochemically simpler, as it can be produced by the direct isomerization of homoserine [149, 151].

Pyruvate is the starting point in the synthesis of alanine, isoleucine, valine, and leucine. Direct production of alanine is catalyzed by the aminotransferase enzyme that transfers the amino group from glutamate to pyruvate. For synthesizing isoleucine, acetaldehyde derived from the decarboxylation of pyruvate is first combined with oxobutyrate (OB) to produce α -aceto-hydroxybutyrate. OB is obtained via deamination of threonine. Isoleucine is obtained after four enzymatic reactions comprising acetyl group

migration, dehydration, and amino group transfer from glutamate. The synthesis of valine and isoleucine are biochemically similar. First, acetaldehyde is combined with pyruvate to produce α -aceto-lactate. Next, four biochemical reactions involving methyl group migration, dehydration, and amino group transfer are necessary to obtain valine. The synthesis of leucine from pyruvate requires a longer biosynthetic pathway. First, 2-oxoisovalerate (OIV), an intermediate in the valine pathway, is condensed with acetyl Co-A to yield 2-isopropylmalic acid (IPA). This acid is further transformed into 3-isopropylmalic acid, which is decarboxylated to produce 4-methyl-2-oxopentanoate, also known as α -ketoisocaproate (KIC). In a final step, the amino group from glutamate is transferred to KIC to form leucine [149, 151].

The synthesis of aromatic amino acids (i.e., phenylalanine, tyrosine, and tryptophan) starts with the condensation of PEP with E4P. The latter is one of the four-carbon sugars produced through the OPP pathway. The products of condensation are inorganic phosphate and 3-deoxy-D-arabino-heptulosonate-7-phosphate (DAHP). This reaction is catalyzed by the DAHP synthase enzyme. DAHP is next cyclized to yield 5-dehydroquinic acid (DHQ), which is latter converted into shikimic acid. After phosphorylation reactions involving ATP and PEP, shikimic acid is transformed into chorismic acid. This is the branching point from which the three aromatic amino acids originate. For the synthesis of tryptophan, chorismic acid reacts with glutamine to form anthranilic acid. Tryptophan is produced after four additional biochemical reactions comprising phosphorylation, decarboxylation, dehydration, and amine transfer from serine. The production of tyrosine and phenylalanine depends on the conversion of chorismic acid to prephenic acid. In the first case, prephenic acid is dehydrogenated and

decarboxylated to form p-hydroxyphenylpyruvic acid (p-HPP), which is later converted into tyrosine by transferring the amino group from glutamate. In the second case, the dehydration and decarboxylation of prephenic acid yields phenylpyruvic acid (PPA). The latter is then transformed into phenylalanine by means of aminotransferase enzyme that incorporates an amino group from glutamate [149, 151].

Serine and glycine can be produced as a result of glycolate metabolism derived from photorespiration. However, it was demonstrated that most serine in cyanobacteria is produced through the phosphorylated pathway [153]. In this pathway, PGA is first transformed into phosphohydroxypyruvate (PHP). Next, aminotransferase uses glutamate to convert PHP into phosphoserine, which is later hydrated and dephosphorylated to obtain serine. Glycine can be directly derived from serine by means of hydroxymethyltransferase enzymes. This enzyme simultaneously converts serine into glycine and tetrahydrofolate (THF) into 5,10—methylentetrahydrofolate (5,10-MTHF) [153, 154]. Serine is also used in a two-step pathway that produces cysteine. First, serine acetyltransferase enzyme catalyzes the reaction between serine and acetyl Co-A to produce O-acetyl-L-serine (OAS). In the second step, OAS-sulfhydrylase enzyme catalyzes the reaction between OAS and sulfide (S^{2-}) or thiosulfate ($S_2O_3^{2-}$) ions to produce cysteine and acetate [155].

The biosynthesis of histidine is an energy expensive process and this amino acid is one of the least abundant in cyanobacteria [138, 152, 156, 157]. Histidine is the only amino acid that can act as proton donor or proton acceptor in neutral pH conditions because it has an imidazole ring side chain with basic aromatic properties ($pK_a = 6.0$). The biosynthesis of histidine is an unbranched pathway that seems to be conserved

among archaea, bacteria, lower eukaryotes, and plants. The pathway has ten enzymatic reactions that convert phosphoribosyl pyrophosphate (PRPP) into histidine. Since PRPP is produced from R5P during the OPP pathway, the production of histidine is also related to the biosynthesis of purines, pyrimidines, and folates [138, 158].

2.4.7 The role of phosphoenolpyruvate carboxylase

The replenishment of oxaloacetate is necessary to maintain a balance between cellular respiration and amino acid biosynthesis [2, 133]. Phosphoenolpyruvate produced during glycolysis can be converted to OA by means of phosphoenolpyruvate carboxylase (PEPc) enzyme. PEPc is a very efficient CO₂ fixation enzyme that catalyzes the irreversible β -carboxylation of PEP in the presence of Mg²⁺ and Mn²⁺ cofactors [159]. The regulatory mechanism of PEPc in cyanobacteria is not fully understood. However, it is known that this enzyme is not active in darkness. The reduction of PEPc activity has been attributed to the increase in the concentrations of malate, aspartate, and citrate, which occurs when, in the absence of light, only cellular respiration is active. These acid ions lower the cytoplasmic pH and may inhibit cyanobacterial PEPc. The enzyme is activated again when photosynthesis, CO₂ fixation, and transport of bicarbonate (HCO₃⁻) ions into the cell raise the pH [2].

After RuBisCO, PEPc is the most important carbon fixation enzyme in cyanobacteria, being responsible for up to 25% of the total incorporation of inorganic carbon [2, 7]. This enzyme has a high affinity for HCO₃⁻ ions and, unlike RuBisCO, its performance is not affected by O₂ [159]. These characteristics of PEPc could explain why the final allocation of carbon in cyanobacteria is preferentially oriented towards the

synthesis of amino-acids and proteins [133]. Recently, PEPc played a key role in the design of the malonyl Co-A oxaloacetate-glyoxylate (MOG) biosynthetic pathway for increased carbon fixation [2, 32, 56]. Based on experiments with *Synechocystis* sp. PCC 6803, the overexpression of PEPc in cyanobacteria could also enhance the cellular growth under limited light conditions [160]. PEPc carboxylation is also required in the production of cytochromes, chlorophyll a, phycobilins, and cyanophycin [159].

2.4.8 Synthesis of cyanophycin

Akin to other prokaryotes, cyanobacteria can store energy in the form of glycogen or PHA. However, cyanobacteria can also store amino acids in the form of cyanophycin granule (CPG) polypeptides [161]. Cyanophycin (multi L-arginyl–poly–L-aspartate) is a highly charged and net-neutral structure formed by multiple zwitterionic monomers, which can have a molecular weight ranging between 25 and 100 kDa [34]. This peptide-like biopolymer is water insoluble and is formed by an equimolar poly aspartate backbone with arginine branches. These amino-acids are connected by amide bonds between the α -amino group of arginine and the β -carboxyl groups in the aspartate chain [162]. CPG may be thought as a dynamic fluctuating reservoir in the assimilation of nitrogen, where aspartate and arginine accumulate before they are used in the synthesis of other amino acids [163]. Arginine can be transformed to glutamate, the most important donor of amino groups in the synthesis of other amino acids. On the other hand, aspartate can be converted into OA, and is also directly involved in the synthesis of asparagine, methionine, threonine, and lysine. Cyanophycin is non-ribosomally synthesized by cyanophycin synthase enzyme during the transition from exponential to stationary phase,

under low concentration of essential nutrients [161, 163]. As an example, the CPG content in *Synechocystis* sp. PCC 6803 can vary from 1% dry cell weight (DCW) during the exponential phase to 18% DCW under phosphate or sulfate starvation conditions [162]. Although it is not strictly necessary for survival, heterocysts from filamentous diazotrophic cyanobacteria can also accumulate cyanophycin close to their junctions with adjacent vegetative cells [164]. When observed under the microscope, CPGs are opaque granules, with size changing over time depending on the nitrogen availability [34].

The solubility properties of cyanophycin are important for dynamic accumulation of nitrogen reserves in cyanobacteria. This polypeptide reserve can only be solubilized under acidic ($\text{pH} < 2$) or alkaline conditions ($\text{pH} > 9$) [165]. Because of this, cyanophycin can be compartmentalized in the form of CGPs to control its consumption as Nitrogen availability varies. Loss of valuable amino-acid reserves through competing cytoplasmic reactions is minimized because cyanophycin is insoluble at cytoplasmic pH [166]. In addition, the storage of aspartate and arginine in CPGs does not affect the osmotic pressure, maintaining cell homeostasis [165]. On the other hand, insoluble cyanophycin inclusions produced by heterocysts act as nitrogen buffers mediating in the transference of fixated nitrogen to vegetative cells [164]. Intracellular cyanophycin degradation is mediated by cyanophycinase (*CphB*) and isoaspartyl dipeptidase enzymes. Extracellularly, cyanophycin is decomposed by the catalytic action of cyanophycin hydrolase (*CphE*) [162, 163].

2.4.9 Production of terpenoids

Isoprene (C_5H_8) is a short chain volatile hydrocarbon acting as the structural unit of terpenoids or isoprenoids. Terpenoids play a key role in the growth and survival of photosynthetic organisms because they form the basic structure of carotenoids, tocopherols, phytol, sterols, and hormones [126]. In addition, isoprenoids constitute the side chains of chlorophylls, ubiquinones, and plastoquinones, which are essential in photosynthesis and oxidative phosphorylation. Isoprenoids are also used as defense molecules produced in response to stressful conditions [127]. Cyanobacteria biosynthesize terpenoids using the MEP pathway, which is a seven-step biochemical route [129]. First, PGAL and pyruvate condensate to form 1-deoxy-D-xylulose-5 phosphate (DXP) in a reaction catalyzed by DXP synthase enzyme. DXP is later reductively isomerized to form MEP. Next, MEP is sequentially coupled with cytidine triphosphate (CTP), phosphorylated, cyclated, and reductively dehydrated by the action of ferredoxin to form hydroxy-2-methyl-2-butenyl-4-diphosphate (HMBPP) [126, 167]. The latter intermediate is the common precursor of dimethylallyl pyrophosphate (DMAPP) and isopentenyl pyrophosphate (IPP), which are the isoprenoid precursors in cyanobacteria. Intracellularly, DMAPP and IPP can be interconverted by means of enzyme IPP isomerase [168]. Other substrates derived from the OPP pathway may enter the MEP pathway in later steps, and they can also be used to synthesize DMAPP and IPP [126]. DMAPP and IPP can be sequentially combined to form geranyl pyrophosphate (GPP), farnesyl pyrophosphate (FPP), and geranylgeranyl pyrophosphate (GGPP). These metabolites can be converted into monoterpenes, sesquiterpenes, triterpenes, and tetraterpenes by the action of dedicated cytochrome P450 systems [127].

2.4.10 Production of Chlorophyll A

Chlorophylls are the most important pigments in photosynthetic organisms. Chlorophyll A (ChlA) is a macrocycle of Mg^{2+} chelated tetrapyrrole with an adjacent isocyclic pentanone ring (a fifth ring). ChlA also has a conjugated phytol side chain (a terpenoid) at the C₇ position [169]. In plants and cyanobacteria, the synthesis of ChlA consists of a biochemical pathway comprising at least 15 enzymatic steps divided into three sections. First, glutamate is converted into 5-aminolevulinate (ALA) by means of ALA synthase enzyme. Later, ALA is used to build the structure of protoporphirin IX (Proto IX), a porphyrin compound with a tetrapyrrole macrocycle structure. In the last stage, Mg^{2+} ion is inserted into the Proto IX group, the fifth ring is added, and the isoprenoid (phytol) chain is attached. Proto IX is the precursor of protoheme, which is necessary for the synthesis of biliverdin and phycobilins [149, 169, 170].

2.5 Secondary metabolism

Secondary metabolites are organic molecules, which are not essential for normal growth, reproduction, and development of organisms. These compounds are frequently called natural products and provide the cells with defense mechanisms under stressful conditions, facilitate reproduction, and grant survival advantages in aquatic environments inhabited by diverse macrograzers [171–174]. Overall, cyanobacteria produce three kinds of secondary metabolites i.e., cyanotoxins, bioactive compounds, and UV protectants [175–177]. This classification is a simple way to categorize the copious number of natural products derived from the secondary metabolism of cyanobacteria. Cyanotoxins are mostly produced by freshwater species and can cause serious health

problems in humans and animals. Therefore, most research on secondary metabolism of cyanobacteria has historically been focused on harmful freshwater cyanobacterial blooms [178]. Cyanobacteria from the genera *Microcystis*, *Pseudoanabaena*, *Anabaena*, *Dolichospermum*, *Nodularia*, *Cylindrospermopsis*, and *Oscillatoria* are frequently associated to the production of toxins in freshwater bodies [179–182].

Marine cyanobacteria have gained recent recognition as prolific producers of bioactive compounds with a wide range of pharmaceutical applications [172, 174, 175, 177, 183–188]. As of 2015, more than 550 cyanobacterial secondary metabolites had been reported as bioactive natural products with potential medical applications acting as antibiotics, antifungal, antiviral, anticancer, and anti-inflammatory compounds [172, 186, 188–190]. The production of bioactive secondary metabolites has been reported for 39 genera of cyanobacteria but around 66% of these natural products have been identified in organisms belonging to the *Lyngbya*, *Microcystis*, *Nostoc*, and *Hapalosiphon* genera [176]. Among these, filamentous cyanobacteria of the genus *Lyngbya* are the most active producers and around 30% of all marine cyanobacterial metabolites have been obtained from *Lyngbya majuscula* (a.k.a *Moorea producens*) [188].

Cyanobacteria are continuously exposed to radiation in the photosynthetically active (400–700 nm) and ultraviolet (280–400 nm) regions. Therefore, they can also produce sunscreens to be protected against harmful UV rays. Mycosporine like aminoacids (MAAs) and scytonemin (SCY) are useful secondary metabolites that absorb high energy UV radiations to avoid photodamage [177, 191]. The complete list of UV absorbents produced by cyanobacteria is still under construction but is in the spotlight of current research [191–193]. While the synthesis of MAAs, has been identified in members

of the genera *Calothrix*, *Chlorogloeopsis*, *Gloeocapsa*, *Synechococcus*, *Nostoc* and *Anabaena*, the production of SCY has been associated to cyanobacteria belonging to *Lyngbya*, *Anabaena*, *Nodularia* and *Scytonema* [177, 191].

Detailed description of biochemical pathways leading to the synthesis of secondary metabolites is out of the scope of this review. However, all the secondary metabolites are derived from organic compounds produced through primary metabolism (see subsection 2.4). Chemically speaking, secondary metabolites can be polyketides, non-ribosomal and ribosomal peptides, alkaloids, terpenoids, amino-acid and fatty acid derivatives, shikimate-derived molecules, and amino glycosides [172, 174, 177, 179]. Most cyanobacterial secondary metabolites are polyketides and peptides produced by type I polyketide synthases (PKSs) and non-ribosomal peptide synthases (NRPSs), respectively. Hybrid pathways involving different combinations of PKSs and NRPSs are also common in cyanobacteria [176, 184, 185]. Recently, it was realized that ribosomally synthesized peptides also contribute in the production of secondary metabolites. In this case, precursor peptides are first synthesized in the ribosomes to be later processed by means of post-translational modifications [172, 179]. Such modifications include heterocyclization, oxidation, or prenylation of amino acids [194]. By analyzing whole genome sequences of cyanobacteria, it has become clear that the synthesis of some secondary metabolites usually requires a complex integration of the NRPS and PKS systems. Although these secondary biosynthetic pathways still remain enigmatic, gene clusters (8 to 64 kb long) encoding NRPS/PKS assembly systems have been identified in cyanobacteria belonging to *Anabaena*, *Microcystis*, *Nostoc*, *Nodularia*, *Scytonema*,

Tolypothrix, *Gloeobacter*, *Leptolyngbya*, *Lyngbya*, *Microcoleus*, *Planktothrix*, *Oscillatoria*, and *Plectonema* [176, 184].

The list of cyanobacterial secondary metabolites has been growing for three decades, and new compounds are constantly discovered using techniques like genome mining and mass spectrometry [195]. For more information regarding secondary metabolites, the reader is remitted to recent detailed reviews covering the potential pharmaceutical applications of cyanobacteria [175, 186–188, 190]. Figure 2.7 presents examples of selected cyanobacterial secondary metabolites classified by biological function and route of production. The name of the producer cyanobacteria is also indicated in parenthesis. Among these, curacin A, desmethoxymajusculamide C (DMMC), cryptophycin, and dolastatin 10 are remarkable examples of cyanobacterial metabolites in different stages of clinical trial [196]. Note that scytonemin is listed as a ribosomal peptide, but it is synthesized from tryptophan using ribosomally translated enzymes [192].

2.5.1 Type I polyketide synthases

Type I polyketide synthases are multifunctional enzyme complexes with different modules, and each module catalyzes one cycle of chain elongation. Instead of peptides, these enzymes produce macrolides, which are large macrocyclic lactone rings produced from acyl Co-A moieties [172]. There are three types of PKS enzymes, but only type I are commonly found in cyanobacterial species [184]. The order of PKSs modules dictates the polyketide chain sequence and the different domains in each module are responsible for specific enzymatic reactions [190].

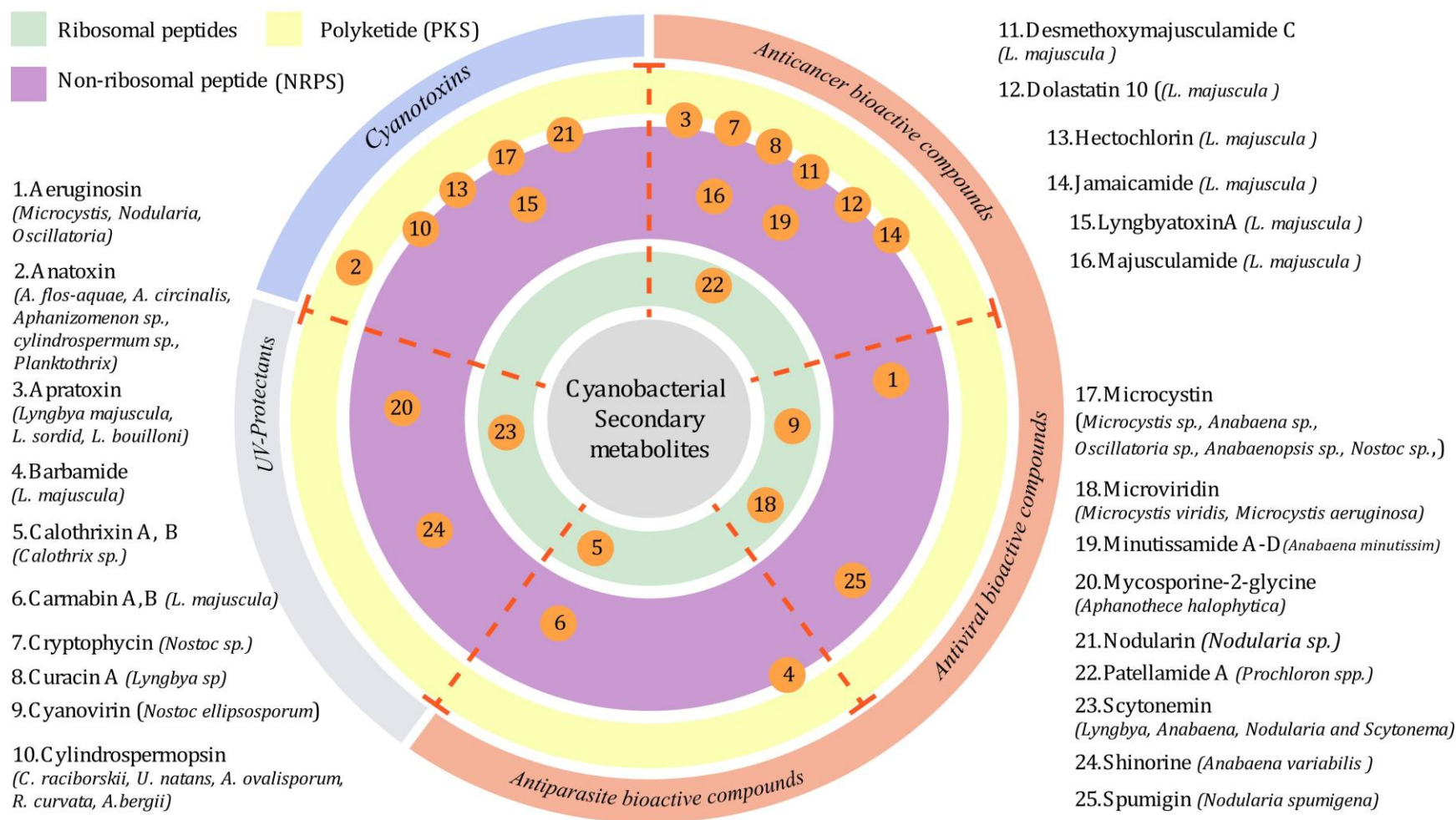


Figure 2.7. Cyanobacterial secondary metabolites
Constructed based on [175, 176, 188]

Each module of cyanobacterial PKS contains at least three domains: a β -ketosynthase domain, an acyltransferase domain, and an acyl carrier protein. These domains select, activate and catalyze a decarboxylative Claisen condensation between the substrate and the growing polyketide chain (a β -ketoacyl-S-ACP intermediate) [184]. The PKS modules may also have ketoreductase, dehydratase, and enoyl reductase domains, which can carry out additional modifications before the next PKS module adds another molecule to the macrolide precursor. One PKS module is similar to the FAS enzyme, and both systems contain the exact same domains when a PKS module has all the six domains previously described [172, 184, 190].

2.5.2 Non-ribosomal peptide synthases

Non-ribosomal peptide synthases are also multifunctional enzyme complexes composed by many modules. Each module incorporates either a proteinogenic or a non-proteinogenic amino acid into the final product following a collinearity rule similar to a linear assembly line. The order of the modules in the enzyme complex determines the order of the components in the final non-ribosomal peptide. The modules in the NRPS enzymatic complex typically contain an adenylation domain A, a peptide carrier protein (PCP), and a condensation domain C. The A domain is responsible for substrate selection and amino acid activation, the PCP (also called thiolation domain) is in charge of thioesterification of the activated amino acid to tether the substrate to the complex, and the C domain catalyzes peptide formation and chain elongation [172, 184, 190]. NRPSs complexes can accept about 300 different substrates and grant cyanobacteria with the ability of synthesizing diverse peptides. Therefore, non-ribosomal peptide synthesis is

beyond the limits of ribosomal protein translation, which generally uses 20 proteinogenic amino acids [172]. After producing non-ribosomal peptide backbones, additional NRPS domains can further modify the base structure by N-methylation, epimerization, and heterocyclation [176].

2.5.3 Ribosomal synthesis of metabolites

The most important ribosomally synthesized secondary metabolites are cyanobactins [176]. These are small cyclic peptides produced by freshwater and marine cyanobacteria living in symbiosis. Cyanobactin is a general term grouping cyclic peptides consisting of proteinogenic amino acids, oxazolines, oxazoles, thiazolines, and thiazoles. In addition to heterocyclized amino acids, cyanobactins also contain isoprenoid amino acid derivatives [194]. The production of cyanobactins is encoded in gene clusters (~10 kb in size), which are composed of 7 to 12 genes. The clusters encode the production of two proteases, the peptide precursor, and the proteins in charge of cyanobactin maturation (post-translational modifications). After translation, the precursor peptide is cleaved by the proteases, and the resulting pieces undergo head-to-tail cyclization by forming new amide linkages between the α -carbonyl of a C-terminal amino acid and the α -amino group of an N-terminal amino acid. The post-translational modifications occur only on specific amino acids recognized by the cyanobactin maturation proteins. Production capabilities of patellamides, tenuecyclamide, trichamide, lyngbyabactin, and microcyclamide cyanobactins have been reported in *Prochloron spp.*, *Nostoc spongiaeforme*, *Trichodesmium erythraeum*, *Lyngbya aestuarii*, and *Microcystis aeruginosa*, respectively [194, 197].

2.6 Synthetic biology of Cyanobacteria

Synthetic biology (SB) is a growing interdisciplinary field combining techniques of systems biology and genetic, metabolic, molecular, and computational science and engineering. Such combination of biology and engineering tools is useful to design, construct and characterize improved or novel biological systems [198]. In other words, synthetic biology aims to engineer the metabolic pathways of an organism to produce a given biological molecule, a metabolic product, or a completely new organism [199]. This approach can be applied to develop a photosynthetic bio-factory of chemical compounds. Genetic engineering tools for model cyanobacteria are available and complete compilations have been published [1, 200]. On the other hand, one example of molecular engineering is the manipulation of carboxylases (e.g., RuBisCO and PEPc) in model cyanobacteria as a leading alternative to study potential improvements in the carbon fixation capabilities of photosynthetic organisms [40, 55, 56, 160, 160]. Regarding systems biology and computational engineering, the coupling of genome-scale metabolic reconstructions with mathematical optimization is gaining attention as a powerful methodology to predict the effect of genetic modifications on the metabolic network of cyanobacteria [125, 201–203]. Although the development of genome scale metabolic models has been focused on unicellular cyanobacteria [204–211], it can also be applied to analyze filamentous species [212–214]. Considering this background, the application of SB methodologies opens a door to enhance cyanobacteria as photoautotrophic bio-factories of high-value chemicals.

Biotechnological industry has relied on the heterotrophic metabolism of microorganisms like *Escherichia coli* and *Saccharomyces cerevisiae* to convert

carbohydrates into value-added compounds [130]. However, the potential application of cyanobacteria for the photosynthetic production of chemicals has been recently explored [8, 32, 122, 129, 130, 215, 216]. In most cases, metabolic engineering of unicellular cyanobacteria *Synechocystis* sp. PCC 6803 (freshwater), *Synechococcus elongatus* PCC 7942 (freshwater), and *Synechococcus* sp. 7002 (estuarine) has been chosen as the preferred strategy to develop photoautotrophic chemical bio-factories. Metabolic engineering is an important component of SB as it focuses on the design and implementation of new biosynthetic pathways in genetically modified cells [129]. Following this strategy, the two most important microorganisms in the field of microbial biotechnology (i.e., *S. cerevisiae* and *E. coli*) have been converted into powerful heterotrophic bio-factories of pharmaceuticals and chemicals.

Since cyanobacteria can fixate CO₂ and are already native producers of diverse chemical compounds, the introduction of exogenous biosynthetic pathways is emerging as a promising methodology to convert cyanobacterial metabolites into carbon-based specialty or commodity chemicals, biofuels, and biopolymer precursors [122]. The potential exploitation of photosynthetic microorganisms is enhanced by the inexpensive raw materials needed to fuel the cyanobacterial metabolism, i.e., sunlight, water, CO₂, and some minerals [32]. Being aquatic organisms, cyanobacteria do not require arable land to grow, and massive cultures would not compete for land with traditional food crops [55, 130, 215]. On top of these attractive features, the application of synthetic biology in diazotrophic cyanobacteria could boost the development of solar cell bio-factories using readily available raw materials: sunlight and atmospheric Nitrogen.

The role of SB in the development of photoautotrophic cyanobacterial biofactories involves efficient harvesting of light for photosynthesis, increased CO₂ fixation, control of the gene regulatory network, improvement of production titers of target compounds, removal of metabolic bottlenecks, and design of alternative biosynthetic pathways [215]. Among these, the last three objectives are covered by metabolic engineering. In metabolic engineering, the concept of carbon partitioning is essential as it indicates how incorporated CO₂ is invested throughout the photoautotrophic metabolism (see Figure). Metabolic redesign of cyanobacteria should aim for establishing an equilibrium between native metabolism (needed for growth and survival) and chemical production [129, 215, 216]. In that sense, cyanobacteria should be able to utilize more than 50% of the energy and CO₂ income in order to be called cellular bio-factories. This becomes clear considering that highly productive cell factories are often directly linked with increased carbon partitioning towards the production of chemicals of interest or carbon sinks. Because of this partitioning, it is important to notice that highly productive cellular factories also have lower growth rates than their non-modified counterparts [122].

Increased carbon partitioning in redesigned metabolic networks is enhanced by strong driving forces, use of stable enzymes, production of low-toxicity carbon derivatives, efficient removal of chemical products, and abundant sources of inorganic carbon [129]. A strong driving force in a biochemical reaction is achieved by using highly active enzymes that catalyze irreversible reactions (i.e., decarboxylation). In these reactions, the equilibrium “pulls” towards the desired product, enforcing the fixation of additional CO₂ to replenish this reactant [215]. Engineered metabolic networks may require the introduction of exogenous enzymes. The stability of these enzymes depends

on how active they are in the photosynthetic environment. In order to maximize the enzymatic activity and stability, introduced biosynthetic pathways should ideally depend on NADPH, which is the most abundant reductive cofactor produced by cyanobacteria [122, 217]. If NADH dependent enzymes are required, NADPH can be converted to NADH by introducing non-native transhydrogenase enzymes in cyanobacteria [8].

The toxicity of target products should be considered in metabolic engineering because the yield of cytotoxic derivatives needs to be low to assure survival. If production of organic compounds that negatively affect the cellular activity of cyanobacteria is still desired, the tolerance of microorganisms can be increased by laboratory-based adaptation or by introducing non-native transporters, that take these toxic products out of the cell [122, 218]. Removing intracellular non-toxic chemical products also increases the carbon partitioning. Although cyanobacteria can release exocellular polysaccharides through their JPC, they generally lack transporters for other hydrophilic organic molecules. Therefore, the introduction of new metabolic pathways producing non-hydrophobic compounds should be accompanied by the expression of non-native transporters like those belonging to the major facilitator superfamily (MFS). In the case of hydrophobic products, the excretion is facilitated because these compounds can more easily diffuse out through the cell membrane [3, 32].

The availability of abundant carbon sources is related to the number of enzymatic steps that separate the fixation of CO₂ in the carboxysomes and the starting point of the metabolic route of interest. In cyanobacteria, the different metabolic pathways compete for carbon and the yield of a given metabolite will be lower as the starting point of the production pathway is further from the CBB cycle fixation step [122, 215]. Therefore,

highly productive heterologous pathways should start from a primary metabolite as close as possible to the carboxysomal carbon pool to minimize competing metabolic reactions [129]. As an example, pyruvate is the starting metabolite for most non-native biosynthetic pathways introduced in cyanobacteria so far. In those cases, higher yields and carbon partitioning are possible because the central pyruvate metabolite is only three steps away from PGA production in the CBB cycle (see Figure 2.4) [122]. In the same way, the low titers of isoprenoids are related to the longer metabolic route described by the MEP pathway [126, 127, 129]. Other strategies used in metabolic engineering to increase the carbon partitioning include overexpressing carbon fixation steps (i.e., overexpression of PEPc) [2, 56, 160], blocking the production of storage polymers (glycogen and PHB) [8, 215], and increasing the osmotic stress in cyanobacterial cultures to promote the production of sucrose and trehalose, which act as additional carbon sinks [130]. As mentioned earlier, molecular engineering of RuBisCO has not proven to be a viable option to increase carbon fixation because it is possible that this enzyme has already been optimized through evolution [2, 55].

Metabolic engineering of cyanobacteria is still under development, and there are underexplored non-native metabolic pathways starting from other central metabolites like acetyl Co-A, phosphoenolpyruvate, and oxaloacetate [2, 122, 216, 219]. Since sugars are exclusively produced by photosynthesis, metabolic engineering and SB approaches are still required to take maximum advantage of cyanobacterial sugars for producing green chemicals [130]. Another feature of cyanobacterial metabolism that requires more attention is their natural predilection to use most fixated CO₂ in the synthesis of amino acids, peptides, and proteins. Considering this, metabolic engineering and SB can be

used to increase the production of high value chemicals such as phycobiliproteins, cyanophycin and peptide-based secondary metabolites, which can be used as precursors of nutrition supplements, specialty chemicals and potent bioactive pharmaceutical products [34, 161, 175, 176, 188].

Cyanobacterial production of chemicals still requires major improvements to be viable in bio-based economies, however different strategies can be evaluated to advance this field in the following years. First, using genome scale metabolic reconstruction, mathematical optimization, and dynamic metabolic flux analysis would be useful to better quantify and understand carbon partitioning in cyanobacteria under photoautotrophic growth conditions. To do this, detailed knowledge of the cellular chemical composition and species-specific biomass equations will also be necessary. One step forward would also include transcriptomics and metabolomics information on metabolic reconstructions. Detailed knowledge of the carbon partitioning in cyanobacteria would allow to propose non-obvious gene editing strategies for increasing the yield of a compound of interest. Such genome-edition plans should make use of high-throughput genetic engineering techniques involving CRISPR-Cas9 or CRISPR-Cpf1 systems, which have been recently tested in cyanobacteria [220–222]. Secondly, increasing the number of fully sequenced cyanobacterial genomes would allow to compare different species at genome scale and design improved metabolic pathways by transferring genes within cyanobacteria. After looking for cyanobacterial genomes in the National Center for Biotechnology Information (NCBI) [223], and the Pathosystems Resource Integration Center (PATRIC) [224] databases, it was found that most available genomes are incomplete . As of April of 2018, only 118 (15.6%) out of 756 cyanobacterial genomes found in NCBI, and 151 (12.5%)

out of 1206 cyanobacterial genomes found in PATRIC had been completed. Given that around 2700 species of cyanobacteria have been described, and the total number of cyanobacterial species could reach 6280 [225], it is still required to elucidate additional genomic features controlling the production capabilities of cyanobacteria.

A third strategy to improve the role of cyanobacteria in solar-based economies involves their nitrogen fixation capabilities. Diazotrophic cyanobacteria need to be further studied to understand how dark-light cycles and light availability affect the gene regulatory network that controls the development of heterocysts and diazocytes. Apart from CO₂ fixation, Nitrogen fixation is essential in the development of solar cell bio-factories because this would represent a sustainable alternative to the energy intensive Haber-Bosch process, which is the most important process to produce ammonia (NH₃) and fertilizers in the chemical industry. Evaluation of chemical production capabilities of nitrogen fixing cyanobacteria, or co-cultures of N₂-fixing species with non-fixing species could also enhance the development of biotechnological processes with low-nutrient requirements. All these strategies are important to optimize the production levels of valuable nitrogen containing cyanobacterial chemicals like phycobilins, cyanophycin, and secondary metabolites.

In the following subsections, current applications of metabolic engineering for increased production of some commodity and specialty chemicals will be presented. This information is summarized in Table 2.4, where average production rates, in g L⁻¹ day⁻¹, are compared among microbial producers. These rates were calculated using the titers obtained after culturing genetically engineered organisms during specific times under optimized conditions. In most cases, chemical production in *E. coli* from glucose was the

benchmark used to assess the photoautotrophic production. Producing chemicals in cyanobacteria using only light and CO₂ is a slow process. However, this can be acceptable due to low nutrient requirements, and reduced CO₂ emissions. In addition, the processes for growing *E. coli* and *S. cerevisiae* are well developed and continuously optimized. Because of this, the development of cyanobacteria as solar cell bio-factories will depend on optimizing the carbon partitioning towards products of interest using synthetic biology and designing photobioreactors that optimize space and light availability.

2.6.1 Alcohols, diols and polyhydric alcohols

Cyanobacteria have been engineered to produce ethanol [226–228], isopropanol [229], 1-butanol [230], 1,3-propanediol [231], 2,3-butanediol [232], and mannitol [233]. The metabolic engineering strategies for producing ethanol, isopropanol, 2,3-butanediol, and mannitol will be further described. Metabolic engineering of freshwater cyanobacteria *Synechocystis* sp. PCC 6803 (*SynPCC6803*) was used to increase the native production of ethanol. Industrial production of ethanol is essential in the field of biofuels and important advances have been achieved by companies like Algenol Biofuels and Joule Unlimited [227]. The genes to produce pyruvate decarboxylase (*Pdc*) and alcohol dehydrogenase II (*Adh*) enzymes from *Zymomonas mobilis* were transferred to the *SynPCC6803* chromosome using a double homologous recombination strategy. These genes were under the control of the *psbAII* promoter, which is a strong native light driven promoter in *SynPCC6803*. Pyruvate was first converted to acetaldehyde by *Pdc*, and acetaldehyde was later transformed into ethanol by *Adh*.

Table 2.3. Average rates of chemical production in microorganisms

Compound	Organism	Genes involved	GE technique ^{a,b}	Starting compound	Titer ^c mg L ⁻¹	Time (h)	Carbon source	PPFD ^d	APR ^e g L ⁻¹ day ⁻¹	Ref	
Ethanol	<i>SynPCC6803</i>	<i>psbAII, pdc, adh</i>	H.Recomb	Pyruvate	460	144	CO ₂	400 ppm	1000	0.08	[226]
	<i>PCC6803</i>	<i>rbc, pdc, adh</i>	H.Recomb	Pyruvate	5500	624	CO ₂	5% v/v	100	0.21	[227]
	<i>E. coli</i>	<i>pflB, idhA</i>	Mutagenesis	Pyruvate	20700	96	Glucose	50 g/L	-	5.18	[234]
	<i>S. cerevisiae</i>	<i>pdc2, adh1</i>	Immobilized cells	Pyruvate	10000	24	Glucose	50 g/L	-	10	[235]
	<i>S. cerevisiae</i>	<i>pdc2, adh1</i>	Immobilized cells	Pyruvate	130120 ^f	65	Glucose	280 g/L	-	48.04	[236]
	<i>S. cerevisiae</i>	<i>pdc2, adh1</i>	Immobilized cells	Pyruvate	69680	16	Glucose	200 g/L	-	104.52	[237, 238]
Isopropanol	<i>SynEPCC7942</i>	<i>thl, atoAD, adc, adh</i>	H.Recomb	Acetyl-CoA	21.7	168	CO ₂	5% v/v	50	3.10E-03	[229]
	<i>SynEPCC7942</i>	<i>thl, atoAD, adc, adh, pta</i>	H.Recomb	Acetyl-CoA	33.1	336	CO ₂	5% v/v	100	2.40E-03	[231]
	<i>E. coli</i>	<i>thl, atoAD, adc, adh</i>	Expr. plasmid	Acetyl - CoA	4904.2	31	Glucose	20 g/L	-	3.86	[239]
	<i>E. coli</i>	<i>thl, atoAD, ctfAB, adc, adh</i>	CRISPR/Cas9	Acetyl-CoA	7100	24	Glucose	60 g/L	-	7.1	[240]
	<i>E. coli</i>	<i>thl, atoAD, adc, adh</i>	Expr. plasmid	Acetyl-CoA	143000 ^g	240	Glucose	20 g/L	-	14.3	[241]
2,3-Butanediol	<i>SynEPCC7942</i>	<i>alsS, alsD, adh</i>	H.Recomb	Pyruvate	2380	480	NaHCO ₃	50 mM	55	0.12	[232]
	<i>E. coli</i>	<i>lysR, budA, budB, budC</i>	Expr. plasmid	Pyruvate	2200	25	Glucose	40 g/L	-	2.11	[242]
	<i>E. coli</i>	<i>alsS, alsD, budB, adh</i>	Expr. plasmid	Pyruvate	9200	56	Glucose	215 g/L	-	3.94	[243]
	<i>E. coli</i>	<i>lysR, budA, budB, budC</i>	Expr. plasmid	Pyruvate	73800	62	Glucose	160 g/L	-	28.57	[244]

Table 2.4. Average rates of chemical production in microorganisms (Continued)

Compound	Organism	Genes involved	GE technique _{a,b}	Starting compound	Titer ^c mg L ⁻¹	Time (h)	Carbon source	PPFD ^d	APR ^e g L ⁻¹ day ⁻¹	Ref	
Mannitol	<i>SynPCC7002</i>	<i>mtlD, mlp</i>	H.Recomb	F6P	1100	288	CO ₂	5% v/v	250	0.09	[233]
	<i>E. coli</i>	<i>mtlD, ptxD</i>	Expr. plasmid	Glucose	8956	24	Glucose	10 g/L	-	8.2	[245]
Succinic acid	<i>SynEPCC7942</i>	<i>ppc, gltA, kgd, gabD</i>	H.Recomb/ overexp.	OG	430	192	NaHCO ₃	50 mM	30	0.05	[246]
	<i>E. coli</i>	<i>ptsG, pykF, pykA</i>	Gene KO	PEP	17350	80	Glucose	9 g/L	-	5.21	[247]
	<i>E. coli</i>	<i>cra, aceA, aceB, iclR, ppc, mdh, gltA</i>	Random mutagenesis	PEP	79800 ^h	84	Glucose	40 g/L	-	22.8	[248]
	<i>SynEPCC7942</i>	<i>mcr, msr</i>	H.Recomb	Malonyl-CoA	665	288	NaHCO ₃	50 mM	50	0.06	[249]
3-Hydroxy-propionic acid	<i>S. cerevisiae</i>	<i>mcr, acc1, acs, pdc1, ald6, gapdh, dhaB, dhaR, aldH, gpd1, gpp2, ptsG, glpK, yqhD, xylR</i>	H.Recomb/ overexp.	Pyruvate	9800 ⁱ	100	Glucose	27.5 g/L	-	2.35	[250, 251]
	<i>E. coli</i>		H.Recomb/ gene KO/ overexp.	Glucose glycerol	29400 ^j	55	Glucose Xylose	500 g/L 250 g/L	-	12.95	[251, 252]
	<i>E. coli</i>	<i>ppc, fum, sdh, ptsG, iclR, aspA, panD, pa0132, ydfG, ynfI</i>	H.Recomb/ gene KO/ overexp.	Fumarate	31100 ^k	49	Glucose	700 g/L	-	15.23	[253]

Table 2.4. Average rates of chemical production in microorganisms (Continued)

Compound	Organism	Genes involved	GE technique ^{a,b}	Starting compound	Titer ^c mg L ⁻¹	Time (h)	Carbon source		PPFD ^d	APR ^e g L ⁻¹ day ⁻¹	Ref
3-Hydroxy-butyric acid	<i>SynPCC6803</i>	<i>thil, hbd, tesB, phaA, phaB, phaE, phaC</i>	H.Recomb/ gene KO	Acetyl - CoA	533	504	CO ₂	400 ppm	120	0.03	[144]
	<i>E. coli</i>	<i>pdc, phbA, phbB, tesB</i>	Expr. plasmid	Acetyl - CoA	4000 ^l	24	Glucose	20 g/L	-	4	[254]
	<i>E. coli</i>	<i>phaA, phaB, phaC, pta</i>	H.Recomb	Acetyl-CoA	9900 ^m	36	Glucose	20 g/L	-	6.6	[255]
Fatty alcohols	<i>SynPCC6803</i>	<i>maqu2220, sll0208, sll0209</i>	H.Recomb/ gene KO	Acyl-CoA	3.6	384	CO ₂	400 ppm	40	2.20E-04	[256, 257]
	<i>S. cerevisiae</i>	<i>acc1, fas1, fas2, far</i>	H.Recomb	Acyl-CoA	100	168	Glucose	20 g/L	-	0.01	[258]
	<i>E. coli</i>	<i>tesA, fadD, maqu2220</i>	Expr. plasmid/ overexp.	Acyl-CoA	1725 ⁿ	110	Glucose	30 g/L	-	0.38	[259]
Fatty acid ethyl esters (FAEE)	<i>SynEPCC7942</i>	<i>atfA, xpkA, pta, pdc, adh</i>	H.Recomb	Pyruvate and acyl-CoA	27	240	CO ₂	5% v/v	100	2.70E-03	[260]
	<i>S. cerevisiae</i>	<i>ws2, adh2, ald6, acs, acc1, acb1</i>	H.Recomb/ gene KO/overexp.	Pyruvate and acyl-CoA	4.4	100	Glucose	20 g/L	-	1.1 E-03	[261]
	<i>E. coli</i>	<i>pdc, adhB, tesA, atfA, faa2, fadD</i>	Expr. plasmid	Pyruvate and acyl-CoA	674	48	Glucose	20 g/L	-	0.34	[262]
	<i>E. coli</i>	<i>pdc, adhB, atfA</i>	Expr. plasmid	Pyruvate and acyl-CoA	1280 ^o	72	Glucose	20 g/L	-	0.43	[263]

Table 2.4. Average rates of chemical production in microorganisms (Continued)

Compound	Organism	Genes involved	GE technique ^{a,b}	Starting compound	Titer ^c mg L ⁻¹	Time (h)	Carbon source		PPFD ^d	APR ^e g L ⁻¹ day ⁻¹	Ref
Hydrocarbons	<i>SynPCC6803</i>	<i>aar, ado, lipA, aas, ddh</i>	H.Recomb/ overexp.	Acyl-ACP	6.5 ^p	240	CO ₂	5% v/v	100	6.50E-04	[264]
	<i>E. coli</i>	<i>zwf, aar, ado, edd, ppsA, idhA, aceA, poxB, plsX</i>	Transduction/ gene KO	Acyl-ACP	425	48	Glucose	20 g/L	-	0.21	[265]
Isoprene	<i>SynEPCC7942</i>	<i>ispS, dxs, idi</i>	H.Recomb/ overexp.	IPP DMAPP	15	72	NaHCO ₃	100 mM	55	0.01	[168]
	<i>SynEPCC7942</i>	<i>ispS, dxs, idi</i>	H.Recomb/ overexp.	IPP DMAPP	1260 ^p	504	CO ₂	5% v/v	100	0.06	[168]
	<i>E. coli</i>	<i>mvaE, mvaS, oleT, ohyA</i>	Expr. plasmid/ overexp.	Acetyl- CoA	620 ^q	72	Glucose	20 g/L	-	0.21	[266]
	<i>E. coli</i>	<i>ispS, ackA-pta, poxB, ldhA, dld, adhE, pps, atoDA</i>	Expr. plasmid/ gene KO	Acetyl-CoA	1832	72	Glycerol	20 g/L	-	0.61	[267]
Farnesene	<i>NosPCC7120</i>	<i>aFS, nir, psbA1</i>	Expr. plasmid	FPP	0.31	360	CO ₂	1% v/v	50	2.04E-05	[268]
	<i>E. coli</i>	<i>aFS, ispA, mvaE, mvaS, mvaD, idi</i>	Expr. plasmid	Acetyl-CoA	380	48	Glycerol	40 g/L	-	0.19	[269]
	<i>S. cerevisiae</i>	<i>aFS, xpk, pta, ada, acs1, acs2, ald6, rhr2</i>	H.Recomb/ gene KO	Acetyl-CoA	105000 ^r	144	Sucrose	40 g/L	-	17.5	[270]

Table 2.4. Average rates of chemical production in microorganisms (Continued)

Compound	Organism	Genes involved	GE technique _{a,b}	Starting compound	Titer ^c mg L ⁻¹	Time (h)	Carbon source	PPFD ^d	APR ^e g L ⁻¹ day ⁻¹	Ref
Limonene	<i>SynPCC6803</i>	<i>lms, dxs, crtE, ipi</i>	H.Recomb/overexp.	GPP	1	712	CO ₂	1% v/v	100	3.40E-05 [271]
	<i>E. coli</i>	<i>mevT operon, lms, gpps</i>	Expr. plasmid	Acetyl-CoA	430	72	Glucose	10 g/L	-	0.14 [272]
Polyhydroxybutyrate	<i>SynPCC6803</i>	<i>sigE, phaA, phaB, phaC, phaE, glgX, glgP, zwf</i>	H.Recomb/overexp./N-depletion	Acetyl-CoA	9.1	72	CO ₂	1% v/v	70	3.00E-03 [257, 273]
	<i>SynPCC6803</i>	<i>phaC, nphT7, phaB, phaA</i>	H.Recomb/N-depletion	Acetyl-CoA	226.8	168	CO ₂	3% v/v	100	0.03 [257, 274]
	<i>C. necator</i>	<i>phaC1</i>	Expr. plasmid	Acetyl-CoA	912	72	Fructose	20 g/L	-	0.3 [275]
	<i>E. coli</i>	<i>phaC1</i>	Expr. plasmid	Acetyl-CoA	2500 ^s	60	Sucrose	10 g/L	-	1 [276]
	<i>C. necator</i>	<i>phaCAB operon</i>	Glycerol excess	Acetyl-CoA	44250 ^t	60	Glucose Glycerol	40 g/L 50 g/L	-	17.7 [277]

Table 2.4. Average rates of chemical production in microorganisms (Continued)

Compound	Organism	Genes involved	GE technique ^{a,b}	Starting compound	Titer ^c mg L ⁻¹	Time (h)	Carbon source	PPFD ^d	APR ^e g L ⁻¹ day ⁻¹	Ref.	
Cyanophycin	<i>SynPCC6803</i>	<i>glnB</i> , <i>cphA</i>	H.Recomb/ point mutation	Glutamate Arginine Aspartate	648	288	CO ₂ NaHCO ₃	2% v/v 5 mM	50	0.05	[257, 278]
	<i>E. coli</i>	<i>cphA</i>	Expr. plasmid	Arginine, Aspartate Lysine	1720	48	Glucose Arginine Aspartate Lysine	20 g/L 10mM 9mM 1mM	-	0.86	[279]

a: Genetic engineering technique

b: H.Recomb: homologous recombination with integration in chromosome, Expr. plasmid: gene expression from plasmid without integration in chromosome, Overexp.: Gene overexpression, Gene KO: gene knockout.

c: Production in laboratory flasks, unless otherwise stated, d: PPFD in $\mu\text{mol}/(\text{m}^2\text{ s})$, e: APR: Average production rate.

f: Cells grown in multistage 1.5L continuous fermentation reactor, g: Fed-batch fermentation with gas stripping recovery conducted in 0.3L flasks.

h: Cells grown in dual-phase fed-batch 7.5L. bioreactor. i: Fed-batch fermentation conducted in 0.5L bioreactor.

j: Fed-batch fermentation conducted in 2.5L bioreactor. k: Cells grown in 6.6L fed-batch fermentor, l: Cells grown in 6L fed-batch fermentor.

m: Cells grown in 2.5L jar fermentor, n: Cells grown in 5L fermentor, o: Cells grown in 2L fed-batch bio-reactor, p: Cells grown in bubble column photo-bioreactor.

q: Cells grown in 5L fed-batch fermentor, r: Cells grown in 0.5L continuous fermentor, s: Cells grown in 3.5L fermentor, t: Cells grown in 7.5L bio-reactor.

Following this strategy, 0.46 g/L of ethanol were produced in batch culture after 6 days of incubation [226]. Following a similar strategy, but under the control of the *rbc* promoter, the production of ethanol in *SynPCC6803* was further increased to 5.5 g/L after 26 days of incubation [228]. In both cases, cyanobacterial cultures were kept at 30°C with continuous illumination (24-hour light regimes) at photosynthetic photon flux density (PPFD) ranging from 50 to 200 $\mu\text{mol}/(\text{m}^2 \text{ s})$ [122, 226].

Isopropanol is a secondary alcohol that can be dehydrated to obtain propylene, which is the precursor of widely used polypropylene. The isopropanol production pathway in freshwater cyanobacteria *Synechococcus elongatus* PCC 7942 (*SynEPCC7942*) was constructed using enzymes from *Clostridium acetobutylicum* ATCC 824, *Escherichia coli* K-12 MG1655 and *Clostridium beijerinckii*. Genes to produce acetyl Co-A acetyl transferase (*Thl*), acetoacetyl Co-A transferase (*AtoAD*), acetoacetate decarboxylase (*Adc*), and secondary alcohol dehydrogenase (*Adh*) enzymes were integrated into the cyanobacterial chromosome by homologous recombination of different plasmids containing the *lac* promoter of *E. coli*. In this pathway, isopropanol was produced from acetyl Co-A after four biochemical reactions. Under optimized conditions, involving aerobic and anaerobic, as well as illuminated and dark stages, *SynEPCC7942* produced 26.5 mg/L of isopropanol after 9 days of incubation under a continuous flow of air (250 ml/min) with 5%v/v CO₂ at 30°C and PPFD ranging from 0 to 100 $\mu\text{mol}/(\text{m}^2 \text{ s})$ [229]. In a similar recent work, isopropanol production in *SynEPCC7942* was further increased to 33.1 mg/L after 14 days of incubation [231].

In the chemical industry, 2,3-butanediol (23BD) is an important raw material to produce solvents (methyl-ethyl ketone), polymers (1,3-butadiene), plasticizers, inks, and

fumigants [232]. *SynEPCC7942* was engineered to enhance the production of 23BD introducing genes for the production and conversion of acetoin. The starting point of this recombinant biosynthetic pathway was pyruvate, and three exogenous enzymes (i.e., acetolactate synthase, acetolactate decarboxylase, and alcohol dehydrogenase) were involved in this metabolic route. First, acetolactate synthase catalyzed the production of acetolactate from two molecules of pyruvate. Then acetolactate was turned into acetoin by means of acetolactate decarboxylase. In the final reaction, acetoin was reduced to 23BD by the secondary alcohol dehydrogenase. Genes encoding the production of these enzymes were under the control of the *lac* promoter from *E. coli*, but it was demonstrated that this promoter had a narrow expression range in *SynEPCC7942*. The concentration of 23BD reached 2.38 g/L after incubating the engineered cyanobacteria during 20 days at 30°C and 55 $\mu\text{mol}/(\text{m}^2 \text{ s})$ PPFD. In this work, the inorganic carbon source was sodium bicarbonate (NaHCO_3), with an initial concentration of 50 mM [215, 232]

Polyhydric alcohol D-mannitol is used in the production of processed food, pharmaceuticals, and chemicals [280]. The metabolism of marine cyanobacteria *Synechococcus* sp. PCC 7002 (*SynPCC7002*) was redesigned to photosynthetically produce D-mannitol. The non-native biosynthetic pathway was constructed using F6P as the starting point. In this recombinant metabolic route, F6P was converted into mannitol 1-phosphate (M1P) by means of enzyme mannitol-1-phosphate dehydrogenase (M1PDH). Later, M1P was dephosphorylated using the enzyme mannitol-1-phosphatase (M1Pase). The genes to produce M1PDH were taken from *E. coli* and M1Pase was translated from the genes of protozoan chicken parasite *Eimeria tenella*. The expression system of these genes was based on a synthetic cassette with the *psbA* promoter from

the chloroplast of *Amaranthus hybridus*. The single synthetic operon was inserted into the chromosome of *SynPCC7002* by homologous recombination. This study also involved genetic inactivation of the glycogen production pathway to increase the accumulation of intracellular and extracellular mannitol. Under optimal conditions, the concentration of mannitol reached 1.1 g/L after 12 days of incubation under an atmosphere with 1%v/v CO₂ at 30°C and continuous illumination of 250 μmol/(m² s) PPFD [233].

2.6.2 Organic acids

Cyanobacteria have been engineered for increased photosynthetic production of succinic acid, 3-hydroxypropionic acid and 3-hydroxybutyric acid. Four carbon 1,4-diacids like succinic acid have important applications in the food, pharmaceutical, and chemical industries. In addition, the U.S Department of Energy has included these organic acids in the list of top 12 value added chemicals from biomass [281]. The production of succinic acid (succinate) in model cyanobacteria *SynEPCC7942* was enhanced using an alternative pathway, where OG from the TCA cycle was the starting metabolite. In this non-native pathway, genes for producing the enzymes OG-decarboxylase (*kgd* from *SynPCC7002*), succinic semialdehyde dehydrogenase (*gabD* from *E. coli*), PEP carboxylase (*ppc*), and citrate synthase (*gltA*) were introduced in *SynEPCC7942* using homologous recombination of plasmids (the *ppc* and *gltA* genes were cloned from *Cornebacterium glutamicum*). First, OG was converted into succinic semialdehyde by (*Kgd*) and then transformed into succinate (*GabD*). Enzymes encoded from *ppc* and *gltA* were introduced to replenish the spent OG by increasing the

conversion of PEP into citrate in two steps. The concentration of succinate reached 430 mg/L after 8 days in a liquid culture at 30°C, 30 $\mu\text{mol}/(\text{m}^2 \text{ s})$ PPFD, and with CO_2 provided as NaHCO_3 (50 mM initial concentration) [246].

3-hydroxypropionic acid (3HP) can be used as precursor of acrylic acid and other polymers in the plastic industry. This organic compound is also included in the list of top 12 biomass-derived chemicals published by the U.S Department of Energy [281]. The photoautotrophic production of 3HP in cyanobacteria was enhanced by means of metabolic engineering. Two non-native metabolic pathways depending on malonyl Co-A and β -alanine were constructed in *SynEPCC7942*. In the first heterologous pathway, genes to produce malonyl Co-A reductase (*Mcr*) and malonate semialdehyde dehydrogenase (*Msr*) from *Sulfolobus tokodaii* and *Metallosphaera sedulawere* were introduced in *SynEPCC7942*. While *Mcr* catalyzed the conversion of malonyl Co-A into malonate semialdehyde (MSA), *Msr* transformed the latter compound into 3HP. In order to increase the yield of 3HP, a second pathway starting from PEP was attached. In the second pathway, genes to produce PEP carboxylase (*ppc*) and aspartate transaminase (*aspC*) were transferred from *E. coli*. In addition, aspartate decarboxylase (*PanD*) from *Corynebacterium glutamicum*, and β -alanine transaminase (*SkPYD4*) from *Saccharomyces kluyveri* were introduced to *SynEPCC7942*. In the alanine dependent pathway, *Ppc* converted PEP into Oxaloacetate (OA), then OA was transaminated to form aspartate by means of *AspC*. Enzyme *PanD* catalyzed the production of β -alanine from aspartate and *SkPYD4* turned β -alanine into MSA. This second pathway was added to increase the pool of MSA, which was originally derived from a primary metabolite that is further from the central carbon fixation. In this work, all the chromosomal modifications

were conducted by homologous recombination of plasmids. The maximum production of 3HP reported was 665 mg/L after 12 days of incubation in a liquid medium containing an initial concentration of 50 mM NaHCO₃. The cultures were kept at 30°C, under continuous illumination of 50 $\mu\text{mol}/(\text{m}^2 \text{ s})$ PPFD [249].

Precursor chemical 3-hydroxybutyrate (3HB) is used to produce polyhydroxyalkanoate (PHA) polymers. Some cyanobacteria are natural producers of PHB, which is the most common PHA. However, improving the physical properties of PHB for engineering applications requires additional copolymerization with 4-hydroxybutyrate or 3-hydroxyvalerate monomers, and this process is difficult to control in living organisms [144, 282]. Therefore, one strategy to produce plastics using cyanobacterial metabolism is to synthesize monomeric units, which are further polymerized using heterogeneous catalysis. The photosynthetic production of 3HB was studied in model cyanobacteria *SynPCC6803*, which naturally accumulates PHB during nitrogen and phosphate starvation. In order to boost the production of 3HB, the metabolism of *SynPCC6803* was modified by homologous recombination introducing the genes *phaA* (β -ketothiolase) and *phaB* (acetoacetyl Co-A reductase) from *Ralstonia eutropha*, *tesB* (thioesterase) from *E. coli*, and *thil* (β -ketothiolase) and *hbd* (acetoacetyl Co-A reductase) from *Clostridium acetobutylicum*. In addition, the native *phaC* and *phaE* genes encoding the translation of PHA synthase enzyme were deleted to avoid intracellular polymerization of 3HB. In this engineered pathway, the β -ketothiolases promoted the conversion of acetyl Co-A to acetoacetyl Co-A, and the acetoacetyl Co-A reductases converted the latter intermediate into 3-hydroxybutyryl Co-A. In a final step, the thioesterase cleaved the coenzyme A portion, producing free 3HB. It was reported

that overproduced 3HB could be exported out of the cell without introducing specialized transporters. The concentration of 3HB produced in liquid medium reached a maximum of 533.4 mg/L after 21 days of incubation. The photosynthetic production of 3HB in *SynPCC6803* was conducted at 30°C with continuous illumination of 120 $\mu\text{mol}/(\text{m}^2 \text{ s})$ PPFD. The CO_2 was continuously provided from atmospheric air flowing into the culture (~ 400 ppm of CO_2) [144].

2.6.3 Fatty acid derivatives

Cyanobacteria have been engineered to produce fatty alcohols, fatty acid ethyl esters, and hydrocarbons by altering the metabolic route that synthesizes fatty acids. These compounds can be used as chemical precursors, or more importantly, as biofuels [283]. The photoautotrophic production of fatty alcohols in *SynPCC6803* was improved by introducing the fatty acyl Co-A reductase enzyme from *Marinobacter aquaeolei*, which converted fatty acyl-ACPs (palmitoyl-ACP and stearyl-ACP) into their respective fatty alcohols. The initial yield was further increased by knocking out the genes encoding native enzymes aldehyde-deformylating oxygenase, and acyl-ACP reductase. The liquid cultures were supplied with continuous aeration and remained under PPFD levels ranging from 30 to 50 $\mu\text{mol}/(\text{m}^2 \text{ s})$. After 16 days, the maximum yield of fatty alcohols was 2.87 mg/g dry weight [256].

Fatty acid ethyl esters (FAEEs) are components of biodiesel. The production of FAEEs from CO_2 and sunlight in *SynEPCC7942* was enhanced by introducing a non-native phosphoketolase (PHK) pathway replenishing the pool of intracellular acetyl Co-A. The production of ethanol from pyruvate was facilitated by the enzymes *Pdc* (pyruvate

decarboxylase) and *Adh* (alcohol dehydrogenase II) from *Z. mobilis*. Ethanol and acyl Co-A from the lipid metabolism were combined to produce FAEEs. The latter reaction was catalyzed by enzyme diacylglycerol acyltransferase from *Acinetobacter baylyi*. The liquid cyanobacterial cultures were grown at 30°C under an atmosphere with 5% v/v CO₂ and continuous fluorescent light of 100 $\mu\text{mol}/(\text{m}^2 \text{ s})$ PPFD. The maximum concentration of FAEEs was 10 mg/L/OD₇₃₀ after 10 days using hexadecane to reduce the toxic effect of FAEE on *SynEPCC7942* [260].

The production of hydrocarbons in cyanobacteria is closely related to the production of fatty alcohols [283]. By means of metabolic engineering in *SynPCC6803*, it was demonstrated that the overexpression of acyl-acyl carrier protein reductases (*Aar*) and aldehyde-deformylating oxygenases (*Ado*) from different species of cyanobacteria could enhance the production of alkanes and alkenes. In this heterologous metabolic route, the fatty acyl-ACPs were reduced to the corresponding aldehydes by *Aar*, and then converted into hydrocarbons by the catalytic activity of *Ado*. The maximum concentration of combined alkanes and alkenes (heptadecane and heptadecene) was 26 mg/L after 10 days of incubation at 30°C under continuous flow of air with 5% v/v CO₂. The illumination levels ranged from 50 to 100 $\mu\text{mol}/(\text{m}^2 \text{ s})$ PPFD [264].

2.6.4 Isoprenoids

Isoprenoids or terpenoids are the major components of essential oils, steroids, and carotenoids. These compounds are commonly used in the production of flavors, perfumes, medicines, and cosmetics [268, 271, 284]. Cyanobacterial isoprenoids are derived from DMAPP and IPP, which are produced following the MEP pathway. Metabolic

engineering has been used to enhance the production of non-native isoprene, farnesene, and limonene in cyanobacteria [126, 268, 271]. The production of isoprene in *SynEPCC7942* was achieved by introducing the genes encoding the production of isoprene synthase enzyme (*IspS*) from *Eucalyptus globulus*. The genetic modification was achieved by double homologous recombination and isoprene was directly produced from DMAPP reaching a maximum concentration of 1260 mg/L after 21 days. Liquid cultures of cyanobacteria were grown in a photo-bioreactor at 30°C, with constant illumination of 100 $\mu\text{mol}/(\text{m}^2 \text{ s})$ PPFD and using air with 5% v/v CO_2 as the only source of carbon [168].

Farnesene is a volatile sesquiterpene that can be used to produce lubricants, cosmetics, fragrances, and biofuels. Following the MEP pathway, DMPP and IPP are condensed in a reaction catalyzed by geranyl pyrophosphate synthase. The product of this reaction, geranyl pyrophosphate (GPP), is the precursor of all isoprenoids containing 10 carbon atoms. In a second condensation, GPP and IPP are combined to form farnesyl pyrophosphate (FPP), which is the precursor of the C_{15} sesquiterpenes. The production of farnesene in *Nostoc sp.* PCC 7120 (*NosPCC7120*) was achieved by introducing a codon-optimized farnesene synthase (*aFS*) from *Picea abies* (Norway spruce). The cyanobacterial culture was kept at 30°C under constant illumination of 50 $\mu\text{mol}/(\text{m}^2.\text{s})$ PPFD. The sole carbon source used was filtered air with 1%v/v CO_2 . After 15 days of growth, the liquid culture of *NosPCC7120* produced an average of 305.4 $\mu\text{g}/\text{L}$ of farnesene. The highest rate of production of farnesene was observed during the first 3 days and corresponded to $\sim 69.1 \mu\text{g}/[(\text{L})(\text{OD})(\text{day})]$ [268].

Limonene, a popular fragrance used in different cleaning products, is a C₁₀ isoprenoid derived from GPP. The production of limonene was enhanced in *SynPCC6803* by introducing the genes encoding the limonene synthase *lms* enzyme from *Schizonepeta tenuifolia*. These genes were incorporated in the chromosomes of *SynPCC6803* by double homologous recombination of plasmids. The cyanobacteria were illuminated with 50-100 $\mu\text{mol}/(\text{m}^2 \text{ s})$ PPFD and grown at 30°C with bubbling of 1%v/v CO₂. The maximum production of limonene was 1 mg/L after 1 month of continuous growth [271].

2.6.5 Polyhydroxyalkanoates

The use of cyanobacterial PHAs to produce bioplastics has called the attention of the scientific community for a long time [285, 286]. The production of PHA in wild type cyanobacteria is around 13 mg/L/h. However, there is still a large gap that separates native cyanobacterial metabolism from highly productive microbial factories of PHB and other PHAs with production rates on the order of 3.2 g/L/h (250 times faster) [35]. Despite the slow production rate, wild type cyanobacteria can accumulate considerable fractions of carbon in the form of PHA under photoautotrophic conditions. Some examples of this are *Spirulina platensis* (6% DCW of PHB), *Gloeotheca* sp. (6% DCW of PHB), *Synechococcus* sp. MA19 (~30% DCW of PHB), and *Oscillatoria limnosa* (6% DCW of poly- β -hydroxyvalerate) [285]. Significant fractions of PHB accumulation have been reached in *SynPCC6803* (~38% DCW), *Nostoc muscorum* (~78% DCW), and *Aulosira fertilissima* (~85% DCW) by modifying the culture conditions and making use of stressful conditions such as phosphate and nitrogen starvation. However, most of these

alternatives comprise mixotrophic metabolism that makes use of photosynthesis and additional carbon sources (i.e., acetate, citrate, sugar) [35, 145, 287]. In order to favor the economic feasibility of cyanobacterial bioplastics against petroleum derived polymers, exclusive photoautotrophic metabolism should be considered, and the addition of costly external carbon sources should be disregarded. In this respect, the application of synthetic biology represents an underexplored alternative to speed up the photosynthetic production of polymers in cyanobacteria.

Metabolic redesigns for the photosynthetic production of PHA in cyanobacteria have focused on reinforcing the native PHB biosynthesis pathway using enzymes of other PHA producing bacteria [35, 287]. Native photoautotrophic production of PHB in *SynPCC6803* was enhanced by introducing genes encoding an acetoacetyl Co-A synthase enzyme from *Streptomyces sp.*, an acetoacetyl Co-A reductase from *Ralstonia eutropha*, and a highly active PHA synthase from *Chromobacterium sp.* These genes were introduced using homologous recombination and remained under the control of the light-inducible *psbAII* promoter. Using this approach, the maximum autotrophic production of PHB in *SynPCC6803* reached 14% DCW after 7 days of incubation in a liquid medium bubbled with 2-3%v/v CO₂. The cultures were kept at 30°C under continuous illumination of 100 $\mu\text{mol}/(\text{m}^2 \text{ s})$ PPFD [274].

The PHB accumulation in *SynPCC6803* was increased by introducing the enzymes catalyzing the production of PHA in *Alcaligenes eutrophus* (*Ralstonia metallidurans*). The PHB production pathway was further enhanced by overexpressing the *SigE* sigma factors of RNA polymerase during nitrogen starvation. The maximum accumulation of the modified *SynPCC6803* reached only 1.4% DCW after 3 days of

incubation at 30°C and 50-70 $\mu\text{mol}/(\text{m}^2 \text{ s})$ PPFD in a liquid medium bubbled with 1%v/v CO_2 [273]. The photoautotrophic production of PHB polymer and poly 3-hydroxybutyrate-co-4-hydroxybutyrate (P3HB-co-4HB) copolymer was studied in *SynPCC7002*. This copolymer is thought to have improved thermal and mechanical properties as compared to the native PHB. The production of both polymers in marine *SynPCC7002* was enhanced by the introduction of the complete gene cluster encoding the production pathway of PHB from *Chlorogloeopsis fritschii*. Moreover, the synthesis of 4-hydroxybutyryl-CoA was supported by the genes encoding the enzymes 4-hydroxybutyrate dehydrogenase and 4-hydroxybutyryl-Co-A transferase from *Porphyromonas gingivalis*. These enzymes catalyzed the conversion of SSA (a metabolite from the TCA cycle) to 4-hydroxybutyrate (4HB). After culturing the cyanobacteria at 38°C, continuous bubbling of 1%v/v CO_2 , and high intensity illumination of 250 $\mu\text{mol}/(\text{m}^2 \text{ s})$ PPFD, modified *SynPCC7002* accumulated 4.5% DCW of the P3HB-co-4HB copolymer. The latter contained 88% 3HB and 12% 4HB monomers [282].

2.6.6 Cyanophycin

The accumulation of carbon in the form of cyanophycin is more prevalent than the accumulation of PHB in most cyanobacteria [288]. Cyanophycin is economically important because it is a precursor of low arginine poly aspartic acid polymers (poly-Asp), which represent a biodegradable alternative to polyacrylates. Based on this, poly-Asp can be used in the production of wastewater treatment chemicals, super absorbents, or additives for the paper, paint, and oil industries. Cyanophycin is also attractive in the polymer industry as a material for biomedical applications or as precursor of traditional

polymers [165]. The decarboxylation of poly-Asp produces β -Alanine, which can be further converted into acrylonitrile and acrylamide. These last two compounds are used as raw materials in the production of polyacrylonitrile (PAN) and polyacrylamide (PAM) polymers [161]. The content of cyanophycin in cyanobacteria is less than 1% DCW during exponential growth phase and the polymer usually accumulates during stressful conditions different from nitrogen depletion. When the cells reach stationary phase or experience sulfate or phosphate starvation, light stress, or low temperatures, the content of cyanophycin may reach 18% DCW [163, 165, 278]. Due to their relatively slow growth rate, cyanobacteria are not used as massive producers of cyanophycin. Instead, some genetic engineering strategies for increased productivity comprise the transfer of cyanophycin synthesis genes from cyanobacteria to heterotrophic microorganisms like *E. coli*, *C. glutamicum*, *R. eutropha*, *Rhizopus oryzae*, *Saccharomyces cerevisiae*, *Pseudomonas putida*, or *Pichia pastoris* [161, 289–291].

The field of synthetic biology for increased photosynthetic production of cyanophycin in cyanobacteria is underexplored. However, an evaluation of the material properties of cyanophycin produced by *SynPCC6803* was recently presented [34]. In a different study, the accumulation of cyanophycin in *SynPCC6803* was enhanced after increasing the activity of N-acetylglutamine kinase (NAGK) enzyme, which is important in the arginine production pathway. A single point mutation in the P_{II} signaling protein was responsible for increasing the activity of NAGK enzyme under nitrogen starvation. Cultures of *SynPCC6803* were grown at 50 $\mu\text{mol}/(\text{m}^2 \text{ s})$ PPFD, under a 2% v/v CO_2 atmosphere supplemented with 5 mM NaHCO_3 in the liquid. The average maximum fraction of cyanophycin reached 40% DCW after 12 days of incubation [278].

2.6.7 Carbohydrates

Being photosynthetic organisms, cyanobacteria naturally produce sugars and carbohydrates directly from CO₂, water, and sunlight. These carbohydrates are normally stored in the form of glycogen or exported through the JPC, forming complex extracellular polymeric layers [132]. In response to osmotic stress, cyanobacteria are also able to produce glucosylglycerol, glucosylglycerate, glycine betaine, trehalose, and sucrose by using their glycogen reserves [130]. One example of the use of metabolic engineering for increased production of carbohydrate derivatives (mannitol) was presented before [233]. However, additional efforts involving synthetic biology are needed to take better advantage of cyanobacterial sugars [130]. In general, cyanobacteria lack transporters facilitating the export of hydrophilic metabolites (e.g., glucose, fructose, and lactose) across the cellular membrane. Therefore, synthetic biology can also be used to introduce sugar transporters allowing extracellular accumulation of carbohydrates for further conversion outside the cell [292]. Recently, cyanobacteria have been explored as a source of biomass to feed the production of ethanol by yeast fermentation. Following this strategy, *SynPCC7002* was cultured under Nitrogen-limiting conditions to reach a carbohydrate content of 60% DCW after 2 days of incubation at 38°C, 250 μmol/(m² s) PPFD, and bubbling of 1%v/v CO₂. Next, *Saccharomyces cerevisiae* produced ethanol by fermentation of hydrolyzed cyanobacterial biomass obtained from the digestion of *SynPCC7002* cultures with lysozyme and α-glucanases [293]. Considering these findings, cyanobacteria have yet to be engineered to produce and secrete high-value products directly derived from sugars, which are closer to the central carbon fixation.

2.7 Large-scale cultivation of cyanobacteria

2.7.1 Commercialization of *Spirulina* and *Nostoc*

Large-scale cultivation of *Spirulina* sp., a.k.a., *Arthrospira*, is the most significant example of commercial exploitation of cyanobacteria. Because of their harmlessness and high protein content (60% - 70% DCW), nourishing *Spirulina* filaments have been incorporated in human and animal diets. Consumption of *Spirulina* has been popular in Asia, Mesoamerica, and central Africa for at least 400 years [294–296]. The French Petroleum Institute pioneered the studies on mass cultivation of *Spirulina* from Lake Chad in 1963, and the Sosa Texcoco company started industrial production of *Spirulina platensis* near Mexico City in 1973 [13, 114, 294]. Nowadays, *Spirulina* is not only known as a rich source of amino-acids, but also for its content of health-beneficial C-phycocyanin (CPC) and γ -linolenic acid [295, 297, 298]. Mass cultivation of *Spirulina* takes place in more than 23 countries, with a global production between 5000 and 15000 metric tons DCW every year [295, 299]. *Spirulina* powders, flakes, tablets, and capsules are mainly sold as dietary supplements, but there is also a growing interest on high purity CPC. In 2015, the global production of CPC reached 110 metric tons and a total market size of 1.9 billion USD. However, this market is expected to grow 30% by 2020 due to the increasing demand of natural blue pigments in the food and cosmetic industries [114, 297]. Some of the largest farms of *Spirulina* belong to DIC Lifetec corporation, with presence in Japan, China, and California, or Cyanotech corporation from Hawaii [114, 300, 301]. Other companies in the *Spirulina* business are Boonsom (Thailand) [302], Parry Nutraceuticals (India) [303], IGV Biotech GmbH (Germany) [304], and Algae Biotecnologia (Brazil) [305]. Although not as widespread as *Spirulina*, *Nostoc commune*,

Nostoc flagelliforme, and *Nostoc sphaericum* are also edible cyanobacteria. Commercial exploitation of *Nostoc* started in China in 2008, and Algaen Corporation from North Carolina has sold *Nostoc* as a delicacy since 2011 [295, 306].

2.7.2 Cultivation systems

Cultivation of cyanobacteria can take place in cost-effective open-pond systems or in more expensive and elaborate closed photo-bioreactors. The choice of a suitable farming system is mostly influenced by the species of cyanobacteria and the commercial value of the product [13]. Raceway ponds with paddlewheels and surface areas from 300 to 5000 m² are the most common open systems for industrial cultivation of *Spirulina*. Although the risk of contamination in raceway ponds is higher than in closed photo-bioreactors, mass farming of *Spirulina* in open systems is possible because they thrive at high levels of bicarbonate (pH 9.5 - 11.0), that are not tolerated by potential contaminants [114, 294]. Other types of open systems used for mass production of cyanobacterial biomass are natural ponds and lakes, thin layer inclined systems, and circular ponds with rotating arms [295]. Closed photo-bioreactors with capacities between 100 and 1000 L are used for improved control of processing conditions (e.g., light penetration, gas exchange, pH, and temperature) and to maintain axenic conditions. Since they are more expensive, closed systems are only used to cultivate specialized cyanobacterial species capable of producing biochemicals, biopolymers and higher-value products like pharmaceuticals and secondary metabolites. Different types of closed systems have been designed to maximize light and space utilization, but the most popular are tubular photo-bioreactors. These systems can be arranged as flat tubular circuits

sitting on the ground, vertical structures with horizontal parallel tubes, or frame supported helical loops. Other closed systems include cylindrical and flat-panel photo-bioreactors. A thorough description of large-scale cultivation systems for cyanobacteria is outside of the scope of this review, but additional details have been compiled elsewhere [13, 295, 307] [109, 298, 310]. Independent of the farming system, mass cultivation of cyanobacteria is limited by the self-shading effect that arises as cultures become denser. While heterotrophic microorganisms grown in fermentation systems reach cell densities of 50 g/L or more, the maximum cell density of photoautotrophically grown cyanobacteria is only 5 to 10 g/L DCW, even under optimal growing conditions [113]. Considering this difference in biomass concentration, economically feasible mass production of cyanobacterial derivatives is highly dependent on downstream processing operations.

2.7.3 Downstream processing

A general process flow diagram for downstream processing of cyanobacteria is presented in Figure 2.8. Once optimal cell density is reached, cyanobacterial biomass from ponds and photo-bioreactors needs to be transformed. From there, downstream operations involve harvesting, drying, extraction, and purification. The purpose of harvesting operations is to separate cells from the liquid medium, bringing the biomass percent from around 1% to 8-15 % w/w [294, 295]. Proper selection of harvesting techniques is essential because the operation of this equipment accounts for 20 to 30% of the total production cost. Suitable harvesting operations depend on cell size, morphology, and density. Screening, filtration and gravity sedimentation are cost-effective operations for concentrating larger filamentous cyanobacteria (>70 μm), but

centrifugation, and dissolved air flotation are preferred to separate smaller unicellular species (<30 µm). Although microfiltration and ultrafiltration can be used to concentrate unicellular species with particle size under 10 µm, these harvesting techniques can be more expensive [298, 308, 309]. The efficiency of harvesting operations can be improved through flocculation with aluminum sulfate, ferric sulfate, cationic polymers, or chitosan [308], but addition of chemical aids should be carefully evaluated to avoid contamination or increased purification costs. Ideally, cyanobacterial production of chemicals should take place in fast-growing and filament-forming species [298].

After biomass harvesting, removal of excess water content is necessary, either to enhance further extraction operations, or to prevent degradation. Drying operations are energy intensive processes needed to bring the biomass concentration to 90-95% w/w (~7% w/w moisture). Again, the selection of suitable dehydration systems is critical for large-scale processing because their operation represents up to 30% of the total production cost [13]. On top of efficient energy use, fast drying of biomass is also required to avoid degradation of heat-sensitive compounds [295]. Among different technologies, spray drying, drum drying, cross-flow-drying, and lyophilization can be used for large-scale processing of cyanobacteria. While spray drying is preferred at industrial-level production of cyanobacterial derivatives (e.g., *Spirulina* supplements, biofuels or biopolymers), lyophilization may be a better option for high-value chemicals like pigments and pharmaceuticals [295, 308].

The last steps in downstream processing of cyanobacterial products are extraction and purification. In order to extract intracellular metabolites, mechanical and chemical treatments can be used to disrupt the cyanobacterial cell wall. While mechanical

operations include ultrasound disruption, high-pressure homogenization, and bead beating, chemical treatments involve enzymatic treatments and liquid and supercritical fluid extraction. In addition, pulse electric field disintegration is a promising method to alter the cell membrane permeability [308].

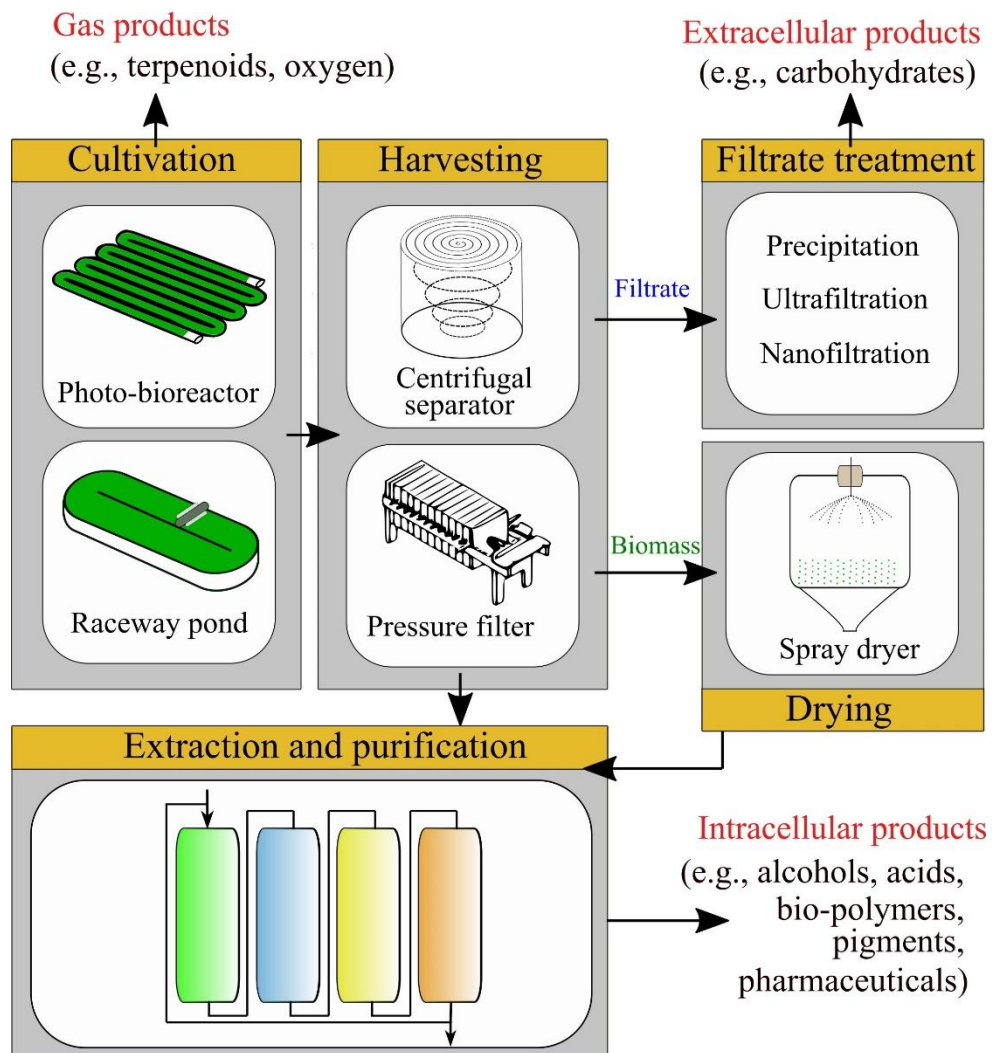


Figure 2.8. Downstream processing of cyanobacterial biomass

Integration of cell disruption methods in large-scale processing is a challenging task because some of these methods are expensive and their efficiency is influenced by biological and morphological properties of cyanobacteria [298, 308]. Liquid extraction is the most common operation to recover cyanobacterial metabolites and the type of solvent depends on the product of interest. While extraction of biopolymers and biofuels is conducted with organic solvents, pigments can be extracted with aqueous buffers. Once the crude extract has been obtained, industrial chromatography can be used to purify chemical compounds. Given that solvent recovery and chromatography are expensive operations, extraction and purification costs should be leveraged with the production of valuable metabolites [299, 308]

Different operation sequences and additional technologies may be necessary for the exploitation of specific metabolites. Since cyanobacteria can release valuable exopolysaccharides with potential applications in cosmetic industries, filtrates or supernatants from harvesting operations can be further processed through alcoholic precipitation or nanofiltration [310]. Provided that genetically modified cyanobacteria can also release terpenoids in gas phase (e.g., isoprene, limonene or farnesene) [168, 268, 271, 311], coupling gas absorption columns to cultivation systems might be another alternative to obtain valuable chemical products from cyanobacterial bio-factories.

2.7.4 Prospects and ventures

Increased product recovery and profitability of cyanobacteria mass cultivation will be influenced by future improvements on cultivation, harvesting, drying, cell disruption, extraction, and purification technologies. For improved cultivation, optimization of

individual strains and optimization of medium formulation are necessary. In addition, increased light availability in new photo-bioreactors will require more efficient light-emitted diode (LED) or fluorescent lamps supplying optimal wavelengths for cyanobacterial growth [296, 312, 313]. Provided that chemical production in cyanobacteria starts with photosynthesis, and large-scale operations are greatly influenced by concentration and drying technologies, adopting good manufacturing practices from traditional agro-industrial facilities (e.g., pulp and paper plants) might be beneficial to develop cyanobacterial bio-factories. In that sense, profitability could be enhanced by sustainable management of cyanobacterial farms or improved solid-liquid separation technologies. On the other end, the high cost of purification operations could be absorbed with the commercialization of cyanobacterial secondary metabolites with pharmaceutical applications like dolastatin, cryptophycin, and curacin, that might soon be approved [298]. Overall, future efforts will require the transformation of cyanobacterial bio-factories into biorefineries. Currently, good examples of venture companies aiming to use cyanobacteria as bio-factories are Algenol (ethanol production in Florida [314]), HelioBioSys (polysaccharide production in California [315, 316]), Phytonix (n-butanol production in North Carolina [317]), CyanoBiotech GmbH (drug discovery in Germany [318]), and Photanol (organic acid production in the Netherlands [319]).

2.8 Chapter conclusion

Cyanobacteria are a diverse group of photosynthetic prokaryotes with the potential to be developed as solar cell factories of value-added chemicals. Since they are photoautotrophic organisms, intracellular cyanobacterial biochemistry can be powered by

solar energy and inorganic carbon in the form of carbon dioxide and bicarbonate ions. Through evolution, cyanobacteria have developed concentrating mechanisms to increase carbon availability, which is used for sustained growth and production of essential metabolites. The native cyanobacterial metabolism comprises the production of diverse primary metabolites that can be used as precursors of industrial organic compounds of all kinds. Among these, metabolic engineering has been used to enhance the production of alcohols, diols, polyhydric alcohols, organic acids, fatty acid derivatives, and isoprenoids in cyanobacteria. In addition, cyanobacteria can also produce a vast set of peptide-like secondary metabolites, with potential applications in the pharmaceutical industry. Although these features convert cyanobacteria into ideal systems for biotechnological production, the productivity of these microorganisms under photoautotrophic growth conditions is still too slow to assure economic feasibility of massive cyanobacterial bio-factories.

In order to overcome these limitations, the use of synthetic biology tools (systems biology, metabolic engineering, bioinformatics, and genetic engineering) is recommended to optimize the carbon partitioning towards organic compounds of interest within the entire photosynthetic metabolic network. In addition, further improvements are required on large-scale cultivation, harvesting, drying, extraction, and purification of cyanobacterial biomass. Optimization of individual strains, as well as design of photobioreactors equipped with improved LED and fluorescent lamps, will be useful to maximize biomass production rates and to enhance light utilization. Implementation of cost-effective solid-liquid separations (i.e., filtration or centrifugation) to concentrate biomass will depend on accurate understanding of the morphology of individual species.

The high cost of dehydration, extraction, and purification operations may be currently restrictive for the exploitation of cyanobacteria. However, technological improvements on drying, cell disruption, and solvent extraction technologies, will be beneficial for large-scale processing. Furthermore, increased cost of downstream processing operations may be absorbed if high-value compounds (i.e., pigments and pharmaceuticals) can be successfully commercialized. Purification of high-value compounds produced by cyanobacteria and released to the liquid medium or the atmosphere (e.g., exopolysaccharides and isoprenoids) will also leverage production costs.

Biotechnological production in cyanobacteria has focused on producing chemicals derived from pyruvate and increasing the production of polyhydroxyalkanoate polymers using model unicellular freshwater cyanobacteria *Synechocystis elongatus* PCC 7942, *Synechocystis* sp. PCC 6803, and marine *Synechococcus* sp. PCC 7002. However, a highly unexplored field is the use of synthetic biology for enhancing photoautotrophic production of cyanophycin, and peptide like secondary metabolites with higher market value. Other research opportunities include the exploitation of filamentous cyanobacteria, which could be more productive and easier to process than unicellular cyanobacteria. A variety of high-value chemicals can be obtained from amino-based metabolites [320], and diazotrophic cyanobacteria have access to a vast reserve of atmospheric nitrogen that can be used to produce ammonium. The carbon partitioning in cyanobacteria is naturally oriented towards the production of peptides and sugars. Therefore, converting cyanobacteria into high yield photoautotrophic biofactories of valuable chemicals will require the design of new metabolic pathways reinforcing the utilization of amino-acids and carbohydrates. In this regard, the integration of multiple technologies, like synthetic

biology and biochemical engineering, will help accelerate the development of cyanobacteria as solar cell biofactories. Although industrial production of *Spirulina* started almost 50 years ago, different venture companies are now willing to develop the next generation of chemical factories using the power of cyanobacterial metabolism.

CHAPTER 3. STRAIN SELECTION AND CHARACTERIZATION METHODS

3.1 Preamble

After an exhaustive revision of current biotechnological applications of cyanobacteria, the filamentous strain *Anabaena* sp. UTEX 2576 was chosen as a model for metabolic network analysis. This Chapter describes characterization methods used to analyze biological and chemical properties of the cyanobacterial biomass. Growth media analysis methods are also presented.

3.2 The filamentous strain *Anabaena* sp. UTEX 2576

Choosing a cyanobacterial strain for studying their CO₂ fixation and bio-production capabilities at large scale requires the consideration of multiple factors like nutrient requirements, growth rate, biomass productivity, ease of separation, and biosynthesis capacities encoded in the genome [294, 295]. In first place, it is desirable to cultivate strains with low nutrient requirements and the ability to use different Carbon and Nitrogen substrates [13, 321]. Secondly, fast-growing cyanobacteria are preferable from an industrial production standpoint because they could be more easily used in large-scale biotechnological operations already dominated by well-understood species like *Escherichia coli* and *Saccharomyces cerevisiae* [205, 322]. The biomass productivity is critical to develop financially viable operations aiming to harvest cyanobacteria at industrial scale. Currently, the most important example of commercial exploitation of cyanobacteria is the *Spirulina* business due to the high yield and nutritional values of strains like *Arthrospira platensis* and *Arthrospira maxima* [294, 295]. Therefore, new

biotechnological processes based on cyanobacteria should exhibit similar productivity levels compared to the *Spirulina* benchmark. Some limitations for mass-cultivation of cyanobacteria are the difficulty to recover the biomass and the high energy demanded for separation. This happens because photoautotrophically grown cyanobacterial cultures reach maximum concentrations that are 5 to 10 times lower than the maximum cell densities of heterotrophically grown *E. coli* and *S. cerevisiae* [113]. In addition, the energy needed to separate cyanobacterial biomass through filtration or centrifugation operations also increases when working with small unicellular cyanobacterial strains with less than 30 μm of cell diameter [308]. One last factor to consider are the genetic features of the strain. In this case, it is important to pick non-toxic strains producing high-value chemicals that can be easily commercialized. Moreover, selecting a strain that can be genetically engineered is also important to investigate targeted genetic manipulations aiming to improve the productivity [1, 322].

The filamentous cyanobacterial strain *Anabaena* sp. UTEX 2576 (a.k.a., *Nostoc* or *Anabaena* sp. PCC 7120 and henceforth, *Anabaena*) meets most of the previously described recommendations. Although this species grows significantly slower than *Synechococcus elongatus* UTEX 2973, the fastest growing cyanobacterium reported for biotechnological applications so far [322], it is non-toxic, grows forming long filaments (longer than 70 μm) of multiple cells, is able to use multiple sources of nitrogen (including N_2 , sodium nitrate and urea), and exhibits biomass productivity and metabolic traits resembling *Spirulina*. Among the different laboratory cultivable cyanobacterial species, *Anabaena* also exhibits the highest production of blue phycobiliproteins, which are light-harvesting pigment-protein complexes and nitrogen reserves with potential applications

as natural colorants for foods, cosmetics, and pharmaceuticals [50]. In nature, members of the *Anabaena* genus act as bio-fertilizers forming symbiotic relationships with aquatic *Azolla* ferns and can be found in rice paddies [17]. Interestingly, studies on paleoclimatology suggested that *Azolla* blooms had a fundamental role on reducing the temperature and CO₂ levels in the Arctic around 50 million years ago [323]. From a biotechnological production standpoint, *Anabaena* has been studied to produce valuable chemical compounds like cyanophycin, a precursor of poly-aspartate [165, 288, 324], farnesene, a versatile building block for chemical additives [268], and marine secondary metabolites with potential pharmaceutical applications [118, 172, 186, 188].

3.3 Laboratory-scale cultivation of *Anabaena*

Strain *Anabaena* sp. UTEX 2576, from the culture collection of the University of Texas at Austin, grew autotrophically inside an illuminated New Brunswick Innova 4340 incubator shaker at 130 RPM using atmospheric CO₂ (409 ppm) and sodium carbonate (0.19 mM) from mineral medium as the main sources of Carbon. The incubation temperature was 28°C and four 20-Watt white fluorescent light bulbs provided a constant photosynthetic photon flux density (PPFD) of $100 \pm 10 \mu\text{mol m}^{-2} \text{s}^{-1}$. Cyanobacterial cultures grew inside sterile Erlenmeyer flasks covered with foam plugs. For most experiments, 500-ml flasks were used to maintain up to 260 ml of actual culture volume, keeping consistent void fractions between 48% and 75% to ensure proper aeration. Depending on the number of replicates or incubator space, 250-ml flasks filled with up to 125 ml of cyanobacterial culture were also frequent.

Batch cultures of *Anabaena* sp. were routinely grown for at least two weeks in three types of growth media (i.e., BG11_o, BG11 and BG11_u) using N₂, NaNO₃ and urea as N-sources, respectively. While N₂ is the most abundant component of the atmosphere, nitrates are the most abundant form of dissolved inorganic N in surface and deep-water bodies. Urea, a typical component of the urine of mammals, is often used as fertilizer and is abundant in agro-industrial wastewaters. Ammonium (NH₄⁺) was not considered because it is rapidly metabolized by multiple microorganisms and it is notably less abundant in water than nitrates [325]. The formulation of these liquid media was based on the composition of the standard mineral medium BG-11 [326]. However, some modifications were introduced to ensure sustained cellular growth with different N-substrates. Fresh BG11 contained NaNO₃ (17.7 mM), BG11_u contained urea (3.0 mM) and BG11_o lacked any N-source to force development of heterocysts for N₂ fixation [327, 328]. The urea concentration in BG11_u media was limited to 3.0 mM because higher levels led to rapid chlorosis (bleaching) and cellular death within the first two-days of cultivation, regardless of pH control. This observation was consistent with previous observations setting the urea toxicity threshold level for *Anabaena* sp. under 5.0 mM [329, 330]. The nominal starting pH of fresh media was adjusted to 8.0 with NaOH or HCl 0.5 N. Buffer addition was not necessary for sustained growth of *Anabaena* sp. in BG11_o nor BG11 media, but TES buffer (10 mM) was needed for long term growth in BG11_u medium because the liquid becomes more acidic as urease degrades urea into NH₄⁺ and carbonic acid over time [331, 332]. Soluble Fe was supplied in the form of Ammonium ferric citrate (Fe³⁺ as C₆H₈FeNO₇).

3.4 Measurement of cellular growth and biomass generation

Cellular abundance in liquid cultures was monitored by tracking the absorbance at 730 nm (optical density, OD₇₃₀) over the entire duration of growth experiments. OD₇₃₀ was routinely measured with a Beckman Coulter DU730 Life science UV-visible spectrophotometer. Given the filamentous nature of *Anabaena*, short 10-W sonication pulses (2 to 5 seconds) were used to homogenize 1-1.5-ml culture samples prior to any OD₇₃₀ measurement. A Fischer Scientific sonic dismembrator model 500 was used to sonicate the liquid samples. Biomass generation was monitored using OD₇₃₀ measurements, cell densities, and dry biomass readings. Ultimately, cell densities and dry biomass were correlated with the OD₇₃₀ of the culture, which was the main indicator of cellular population (*N*). The OD₇₃₀ at the beginning of every growth experiment was standardized at 0.1 to ensure starting cellular populations (*N*₀) between 8x10⁵ and 1.2x10⁶ cells ml⁻¹. Cellular growth rates and generation times were determined after fitting OD₇₃₀ data to a saturation kinetic model (See Equation 3.1), where age (time, *t*) was normally given in days [333]. This saturation model involved two parameters: the intrinsic growth rate constant (μ_{max} , day⁻¹), and the normalized ratio between final and initial populations (*y*_∞). Since bacterial reproduction implies bipartition, the experimental growth rate was calculated as $\mu_{max}/\text{Ln}(2)$ and generation times were calculated as $\text{Ln}(2)/\mu_{max}$.

Equation 3.1

$$\text{Ln}\left(\frac{N}{N_0}\right) = \text{Ln}\left(\frac{OD_{730}}{OD_{730_{t=0}}}\right) = y_{\infty} \cdot \left(1 - \exp\left(\frac{-\mu_{max} \cdot t}{y_{\infty}}\right)\right)$$

3.4.1 Estimation of biomass dry weight

The empirical relationship between dry *Anabaena* biomass and OD₇₃₀ of the liquid culture was constructed using 35 data pairs (see Figure 3.1). For each pair, the optical density of *Anabaena* cultures in regular BG11 medium was measured and then 10 ml of culture were filtered through a Whatman 0.22 µm cellulose nitrate filter carefully placed on a filter funnel attached to a vacuum pump. Filter circles with cyanobacterial biomass dried out for 12 hours inside an oven at 90°C and 20 in Hg of vacuum pressure.

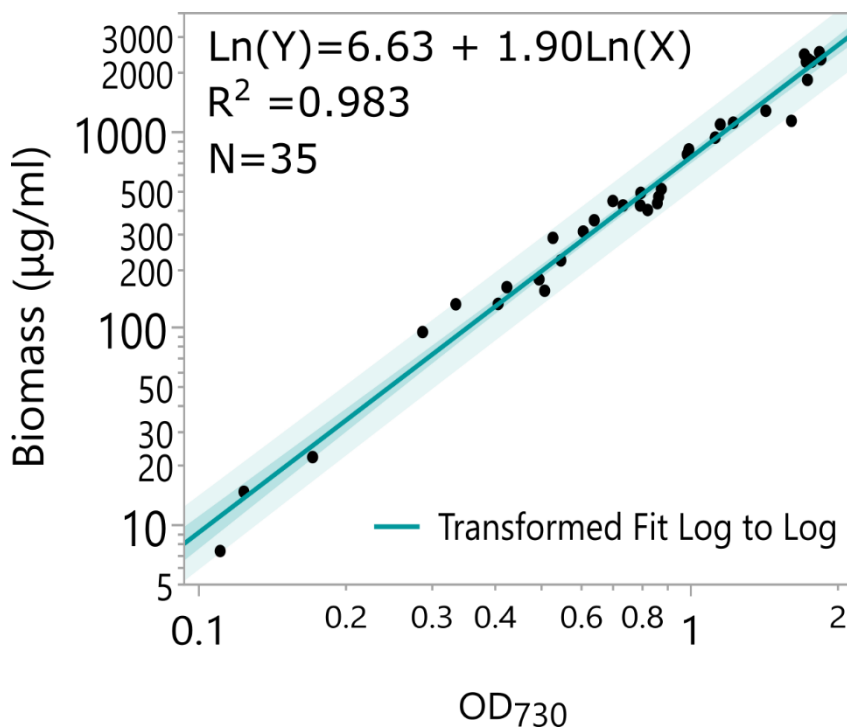


Figure 3.1. Correlation for estimating *Anabaena* biomass concentration

Biomass weight grows exponentially with increasing OD₇₃₀, which can be used as a predictor of biomass generation. Shaded areas represent the confidence interval of the predicted values, with significance level $\alpha=0.05$. Biomass vs OD₇₃₀ plot was generated with N=35 data pairs.

3.4.2 Estimation of cell density with flow cytometry

An empirical relationship between cell density (cell count in liquid) and OD₇₃₀ was determined with 21 data pairs (see Figure 3.2). For each pair, the optical density of the culture was measured and then the cell density was measured using a BD Accuri C6flow cytometer using a modified protocol for filamentous cyanobacteria [334]. In order to have individual cells before the flow cytometry, the sonic dismembrator was used to disrupt *Anabaena* filaments. Before the sonication, 500 µl of filament suspension and 1000 µl of isolation solution (0.5% v/v Triton-X 100 in deionized water) were mixed and incubated at room temperature for 10 minutes. After the incubation, filaments were disrupted by applying six 30-second pulses of 40-W on the cyanobacterial suspensions immersed on ice. Each pulse was separated by a 30-second wait time and the total sonication time was 3 minutes per sample.

A different protocol was used to isolate heterocysts from photodiazotrophic *Anabaena* cultures in BG11_o [335]. This was necessary to identify heterocyst-specific fluorescence signals and to differentiate them from vegetative cells in samples containing both types of cells (See Figure 3.3). Individual cells obtained through filament disruption or heterocyst isolation were diluted and run in the flow cytometer. While cell counts were directly determined from the number of events recorded in a 40 µl volume of diluted sample, heterocyst and vegetative cells groups were identified based on the fluorescent signal produced after exciting the cells with a red 640 nm laser and filtering through a 670 long pass filter to use the FL4 detector. FL4 channel was used in this case because phycobilisomes, and allophycocyanin (APC), are absent in the heterocysts. The Cflow sampler software (BD Biosciences) was used to analyze the cell counts and determine

the correlation with the optical density. Spherotech RCP-30-5 (6 peaks) and RCP-30-5A (8 peaks) were used for routine validation checks of the fluorescent channels. Flow cytometry plots were generated using the flowCore cytometry package in R version 1.48.1 [336].

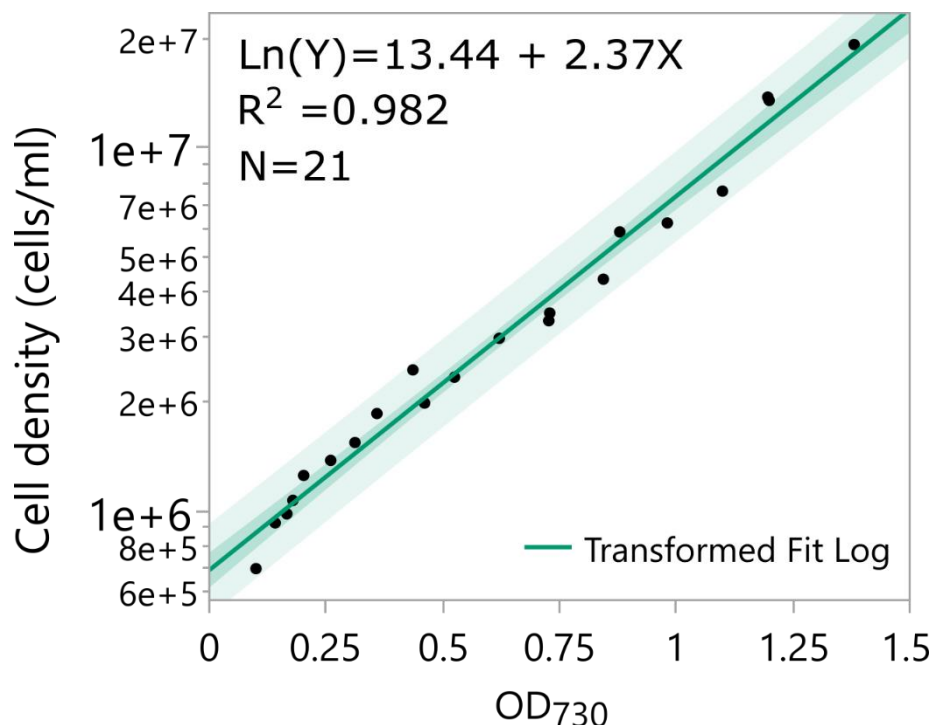


Figure 3.2. Correlation for estimating *Anabaena* cell density

Cell density grows exponentially with increasing OD₇₃₀, which can be used as a predictor of cellular abundance. Shaded areas represent the confidence interval of the predicted values, with significance level $\alpha=0.05$. Cell density vs OD₇₃₀ plot was generated with N=21 data pairs.

3.5 Extraction and quantification of pigments

3.5.1 Quantification of phycobiliproteins (PBPs)

PBPs were extracted from the cells by lysozyme digestion. Briefly, a 1.5 ml-sample of cyanobacterial culture was centrifuged for 15 minutes at 15000 RCF. The resulting pellet was resuspended in 1 ml of lysozyme solution (2.7 mg/ml in TE buffer at pH 8.0)

and sonicated for 10 seconds at 40 W. The cyanobacterial pellet was digested at 37 °C overnight in a dry block incubator. During the digestion reaction, PBPs were released from the cells forming a blue extract. Lysed cells were separated from the extract after a second centrifugation step at 15000 RCF for 15 minutes. The concentration of PBPs in the blue extract was estimated from spectrophotometric readings at 570 nm for PEC, 620 nm for CPC, and 650 nm for APC using specific equations for *Anabaena* [337]. Total concentration of PBPs was calculated as the sum of PEC, CPC and APC concentrations.

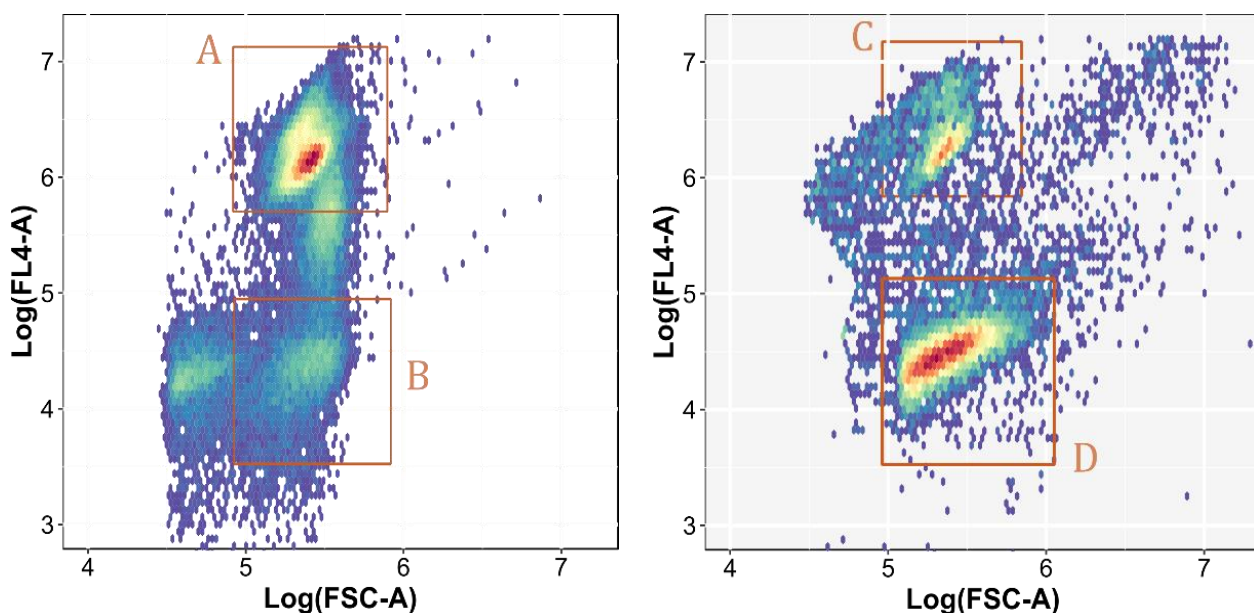


Figure 3.3. FL4 fluorescent signal of *Anabaena* cells.

FL4 detector is specific for allophycocyanin fluorescence signal, which is higher for vegetative cells that contain phycobilisomes (region A). Lower fluorescence FL4 signals indicate degradation of phycobilisomes (region B). Lower region (D) corresponds to isolated heterocysts. Region C represents vegetative cells remaining after the heterocyst isolation procedure. The percent of heterocysts in photodiazotrophic cultures was determined using gated cell counts around B region using CFlow sampler software.

3.5.2 Quantification of Chlorophyll A and total carotenoids

Chlorophyll A (ChlA) and total carotenoids (CaroT) concentrations were determined after solvent extraction with cold acetone. Samples of *Anabaena* cultures (1.5 ml) were centrifuged for 15 minutes at 15000 RCF to isolate the cells from their medium. The supernatant was separated from the cell pellet and replaced by 1 ml of 90% v/v acetone. The mixture was homogenized for 10 seconds at 40 W with a sonic dismembrator and stored in darkness at 4°C for 4 hours. The resulting yellow extract was separated from spent cells by a second round of centrifugation at 15000 RCF for 15 minutes. The concentration of ChlA was calculated from the absorbance of the extract at 664 nm using Beer's law and an extinction coefficient of $87.67 \text{ l g}^{-1} \text{ cm}^{-1}$ [338]. The same extract was analyzed to determine the concentration of CaroT (xanthophylls and carotenes) by measuring the absorbance at 470 nm and using an extinction coefficient of $250 \text{ l g}^{-1} \text{ cm}^{-1}$ [339, 340].

3.5.3 Quantification of β -Carotene

The concentration of β -Carotene and the ion abundances of other photosynthetic pigments (e.g., Echinenone, Pheophytin A, and Chlorophyll A) were determined after cold methanol extractions. The extraction method was like the cold acetone extraction process, but the supernatant from the first centrifugal separation was replaced by 1.5 ml of pure cold methanol to minimize headspace in 1.5-ml microcentrifuge tubes. Carotenoids can be degraded, and the presence of air should be minimized for highest quantification accuracy. After sonic homogenization, samples were extracted in darkness at 4°C for 2 hours. Extraction samples were always kept cold, either on ice or at 4°C, to

minimize degradation. Carotene extracts from lyophilized pellets of *Anabaena* did not present apparent differences in concentration, compared to extracts from pellets that were not subject to freeze drying. Green extracts were separated from spent cells by centrifugation (15 minutes at 15000 RCF and 4 °C) and immediately analyzed with an ESI-TOF Agilent 6230 Mass spectrometry analyzer. A 0.2 µL- aliquot of methanol extract was injected to the MS analyzer and combined with a continuous stream (0.4 mL/min) of 70% v/v acetonitrile and 30% v/v aqueous solution (0.1% v/v formic acid in water) at 30°C. Mass acquisition in positive mode covered a range from 100 to 3200 m/z, keeping a fragmentor voltage of 150 V. The ion abundance of β-Carotene was measured following the signal of the molecular ion ($[C_{40}H_{56}]^+$, m/z = 536.4382) [341]. A calibration curve relating β-Carotene concentration in methanol extracts with the abundance of the molecular ion is presented in Figure 3.4. Ion abundance for Echinenone was determined by observing the peak of the protonated molecule ($[C_{40}H_{54}O + H]^+$, m/z = 551.4253). Pheophytin A ChlA ion abundances were related to the signals of their protonated molecules: $[C_{55}H_{74}N_4O_5 + H]^+$, m/z = 871.5737 for Pheophytin A and $[C_{55}H_{74}MgN_4O_5 + H]^+$, m/z = 893.5431 for ChlA. MS signals for pure methanol were subtracted from MS data recorded for methanolic extracts.

3.6 Quantification of total protein and cyanophycin

A commercial Pierce BCA protein kit was used to measure protein content through Biuret reduction with bicinchonic acid [342]. Protein concentration was determined from absorbance readings at 562 nm, using a calibration curve constructed with bovine serum standards. Cyanophycin was extracted by cell disruption and isolation based on granule

size, density and solubility in 0.1 N HCl [343]. Cyanophycin concentration was quantified with the modified Sakaguchi method, measuring the absorbance of the extract at 506 nm [344].

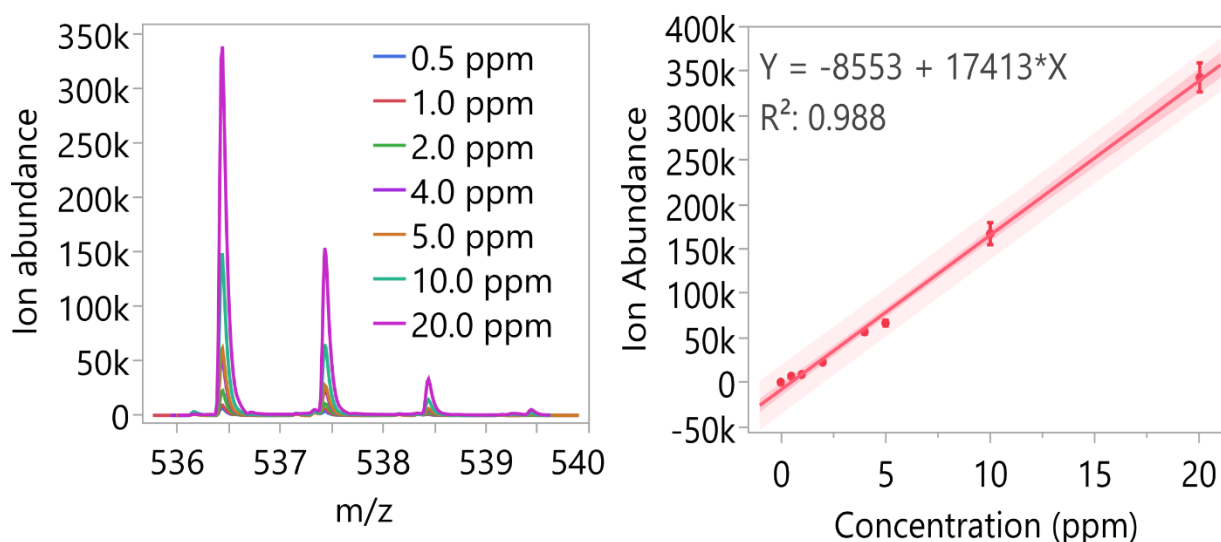


Figure 3.4. Calibration curve for quantification of β -Carotene

The ion abundance of β -Carotene changes with its concentration in the methanolic extract. A linear calibration curve was determined for the β -Carotene concentration range between 0 and 20 $\mu\text{g ml}^{-1}$. Shaded area represents the confidence interval of the predicted values, with significance level $\alpha=0.05$. Error bars were constructed using one standard error from the mean. Three independent measurements per calibration point were used for the regression.

3.7 Quantification of total carbohydrates

Total carbohydrate concentration was measured with the Phenol-Sulfuric acid method [345]. Absorbance readings at 490 nm (gold color) helped determine the carbohydrate concentration with a glucose calibration standard (See Figure 3.5). The fraction of carbohydrates stored as glycogen was approximated from a study on *Synechocystis* sp. PCC 6803 [346]. Total carbohydrate concentration was measured with the Phenol-Sulfuric acid method [345]. Absorbance readings at 490 nm (gold color) helped determine the carbohydrate concentration with a glucose calibration standard

(See Figure 3.5). The fraction of carbohydrates stored as glycogen was approximated from a study on *Synechocystis* sp. PCC 6803 [346]. The peptidoglycan fraction within the total carbohydrate value was estimated using a reference peptidoglycan to total carbohydrate ratio reported for the cyanobacterium *Arthrospira platensis* [347]. The contribution of lipopolysaccharides to the total carbohydrate value was derived from a fraction reported for *Escherichia coli* [348].

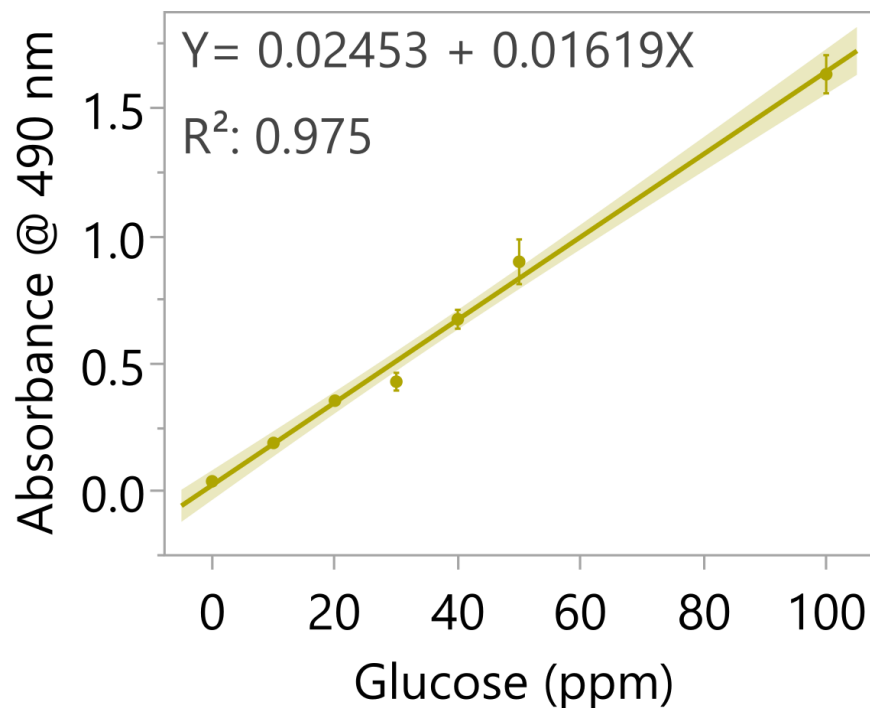


Figure 3.5. Glucose calibration curve for carbohydrate estimation

Total carbohydrate content is estimated by the Phenol-Sulfuric acid method. Shaded area represents the confidence interval of the predicted values, with significance level $\alpha=0.05$. Error bars are constructed one standard error from the mean of three measurements per glucose concentration

3.8 Determination of lipid composition and fatty acid methyl esters

Lipid fractions were measured on cell pellets by transforming cell membrane and thylakoid lipids into fatty acid methyl esters (FAME). Fatty acids were converted into FAME to determine the lipid profile using a Hewlett Packard HP 5890 Series II Gas Chromatograph with a flame ionization detector (GC-FID). Lipids were extracted from the cell membranes and the thylakoids using the Bligh-Dyer method and transformed into FAME through saponification with NaOH in methanol (6 N) and methylation with methanol and HCl 6 N (1:1.2 volume ratio) [349, 350]. After saponification of cyanobacterial biomass, FAME were extracted with a mixture of hexane and methyl ter-butyl ether (1:1 volume ratio), which was also used as the solvent for the chromatography. FAME separation was accomplished in a SP-2380 fused silica column (60 m, 0.25 mm ID, 0.2 μ m df), using Argon as the mobile phase (2 ml/min). A volume of 2.5 μ l of sample was injected at 270°C, and the column temperature was kept between 170°C and 250°C, with a gradient of 5°C/min. The total hold time per sample was 19 minutes, including three minutes at a constant temperature of 250°C for total elution of FAME. Detection was accomplished with the FID detector at 270°C [351]. Palmitic (C16:0), palmitoleic (C16:1), stearic (C18:0), oleic (C18:1), linoleic (C18:2), and γ -linolenic (C18:3) acid standards (\geq 95% purity) were used for the quantification of the most abundant fatty acids in *Anabaena* [352]. Extra pure commercial coconut oil with 5% w/w hexanoic acid (C6:0), 3% w/w octanoic (C8:0) acid, 4% w/w decanoic acid (C10:0), 38% w/w lauric acid (C12:0), and 20% w/w myristic acid (C14:0) was used for the quantification of less abundant fatty acids. Figure shows typical chromatograms of the FAME profiles for photoautotrophic and photodiazotrophic *Anabaena* filaments. Table 3.1 summarizes the retention times

and the calibration curves determined for each type of FAME. FAME standards were prepared from fatty acids following the saponification method as previously described. Total fatty acid concentrations in the standards varied from 0.2 to 50 mg/ml.

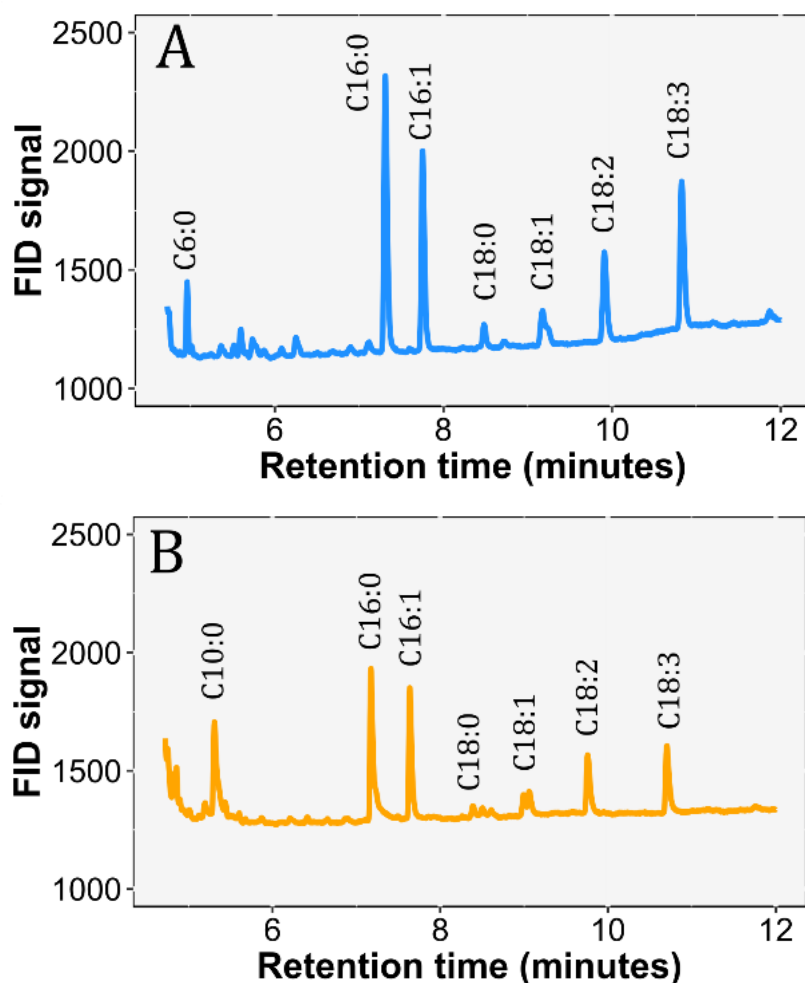


Figure 3.6. GC-FID chromatograms of *Anabaena* FAME

Plot A represents FAME profile of photoautotrophic cells (BG11 medium). Plot B represents FAME profile of photodiazotrophic cells (BG11_o medium). The main fractions (peaks) correspond to palmitic (C16:0), palmitoleic (C16:1), linoleic (C18:2) and linolenic (C18:3) acid residues. Lipids derived from hexanoic acid (C6:0) were identified as the main component of short-chain lipids in photoautotrophic filaments. In that regard, a higher fraction of lipids derived from decanoic acid (C10:0) was found in photodiazotrophic cultures.

3.9 Quantification of nucleic acids

DNA and RNA were extracted with DNeasy and RNeasy (Qiagen) high-purity isolation kits. The absorbance of nucleic acid extracts at 260 and 280 nm was determined with a 0.2 mm path NanoVette cuvette in a Beckman Coulter DU730 Life science UV-visible spectrophotometer. Concentrations of double strand DNA and single strand RNA were calculated using Beer's law and extinction coefficients of $20 \text{ l g}^{-1} \text{ cm}^{-1}$ and $25 \text{ l g}^{-1} \text{ cm}^{-1}$, respectively [353]. High purity nucleic acid extracts were verified by ensuring 260 to 280 absorbance ratios of at least 1.8.

Table 3.1. Retention times and calibration curves for *Anabaena* FAMES.

FAMES concentrations in hexane extracts (mg/ml) were measured by GC-FID. Average retention times and standard errors were calculated from 3 independent measurements for each FAME standard. The variation (R^2) is better explained for FAME derived from longer fatty acids because high purity standards were used for C16:0, C16:1, C18:0, C18:1, C18:2 and C18:3. X represents peak area.

FAME type	Retention time (min)	Calibration equation FAME (mg ml ⁻¹)	R ²
C6:0	4.87 ± 0.01	114441x + 1095.30	0.981
C8:0	5.14 ± 0.01	71434x + 54.29	0.974
C10:0	5.35 ± 0.01	42825x + 16188	0.935
C12:0	5.56 ± 0.01	52324x - 3058.60	0.955
C14:0	6.21 ± 0.05	152600x - 5162	0.988
C16:0	7.19 ± 0.04	119475x - 2812.10	0.995
C16:1	7.65 ± 0.05	122378x - 1248.70	0.997
C18:0	8.52 ± 0.04	176958x + 902.26	0.990
C18:1	9.01 ± 0.05	154927x + 1032.91	0.990
C18:2	9.78 ± 0.05	126822x - 3733.60	0.998
C18:3	10.71 ± 0.06	147716x - 17866	0.996

3.10 Scanning-electron microscopy and analysis of cell diameter

Anabaena cells were fixed and dried for observation with a JSM-6610 scanning electron microscope (SEM). The method was adapted from a standard protocol used for *Chlamydomonas reinhardtii* at the Louisiana State University shared instrumentation facility (SIF) [354, 355]. Filaments from cultures in BG11 and BG11_o media were mixed with a solution of 1%v/v osmium tetroxide (OsO₄), 2% v/v formaldehyde and 2% v/v glutaraldehyde. The mixture was drawn through a 13 mm-diameter, 0.2 µm pore-size polycarbonate filter using a 10-ml syringe with a Swinney filter holder. Filtered cells rested for 2 hours to promote fixation onto the filter. Then, cells were rinsed twice with deionized (5 minutes per wash), *en bloc* stained with 0.5% uranyl acetate for 30 minutes in the dark and rinsed again with deionized water twice. Dehydration of the samples was performed with sequential ethanol wash, rinsing first with 50%v/v ethanol for 15 minutes, then with 67% v/v ethanol for 15 minutes, and twice with 100% ethanol at the end of the series. Hexamethyldisilazane (HMDS) was used for critical point drying of the biological specimens. Cells were first rinsed with 50% v/v HMDS and 50% v/v ethanol for 15 minutes, then with 67% v/v HMDS and 33% v/v ethanol for another 15 minutes, and finally twice with 100% HMDS for 15 minutes. After this, cells rested in the syringe for one extra hour. Filters with fixed and dried cells were withdrawn from the syringe and mounted on aluminum SEM stubs. Specimens were coated with gold for 4 minutes at 0.1 mBar vacuum and 25 mA using an Edwards S150 sputter coater. SEM pictures of *Anabaena* filaments were obtained with acceleration voltage of 15 kV and working distance of 12 mm.

The cell diameter distribution of vegetative cells and heterocysts was estimated from *Anabaena* SEM pictures. The diameter of 165 vegetative cells (V) and 193 heterocysts was determined using the reference bar and the size estimation tool from Image J software. Heterocysts could be easily identified in *Anabaena* filaments because they were larger than vegetative cells and occurred every 10 to 20 cells [356]. The average diameter of heterocysts and vegetative cells was estimated from the distribution. Figure 3.7 presents a typical SEM picture of diazotrophic *Anabaena* filaments grown in BG11_o medium. While the mean diameter of vegetative cells was $2.84 \pm 0.44 \mu\text{m}$, the average diameter of heterocysts was $4.40 \pm 0.61 \mu\text{m}$. The larger size of heterocysts is due to the heterocyst glycolipid layer (HGL) and the heterocyst envelope polysaccharide (HEP) [328].

3.11 Determination of N-source concentration and urease activity

The concentrations of nitrate and urea were measured for cell-free supernatants and growth media to determine consumption profiles of these nutrients in BG11 and BG11_u media. Total Nitrogen content was measured on samples of diazotrophic cultures grown in BG11_o medium to determine N₂-fixation rates. NO₃ was measured by two equivalent methods. The first method was based on the nitrate reduction test with sulfanilic acid [357]. NO₃ levels of fresh media were measured after diluting the sample 20 times. Samples with cyanobacterial biomass were centrifuged for 10 minutes at 15000 RCF to separate cells from the liquid. The supernatant was diluted with deionized water (1 part of supernatant for 19 parts of water) before running nitrate reduction tests to measure NO₃ concentration. 1 ml of the diluted liquid was mixed with 20 μl of a solution

containing 8 mg/l of sulfanilic acid in 5 N acetic acid. Then, 10 mg of fine Zinc powder were added and mixed vigorously for 1 minute with a vortex mixer. After this, the sample was mixed with 20 μ l of a solution with 6 mg/l of N,N-Dimethyl-1-naphthylamine in 5 N acetic acid and vortexed for another minute. The samples stood in the dark for 10 minutes, waiting for color development. The absorbance of the resulting pink liquid was determined at 525 nm to estimate NO_3 concentration with a calibration curve (See Figure 3.8).

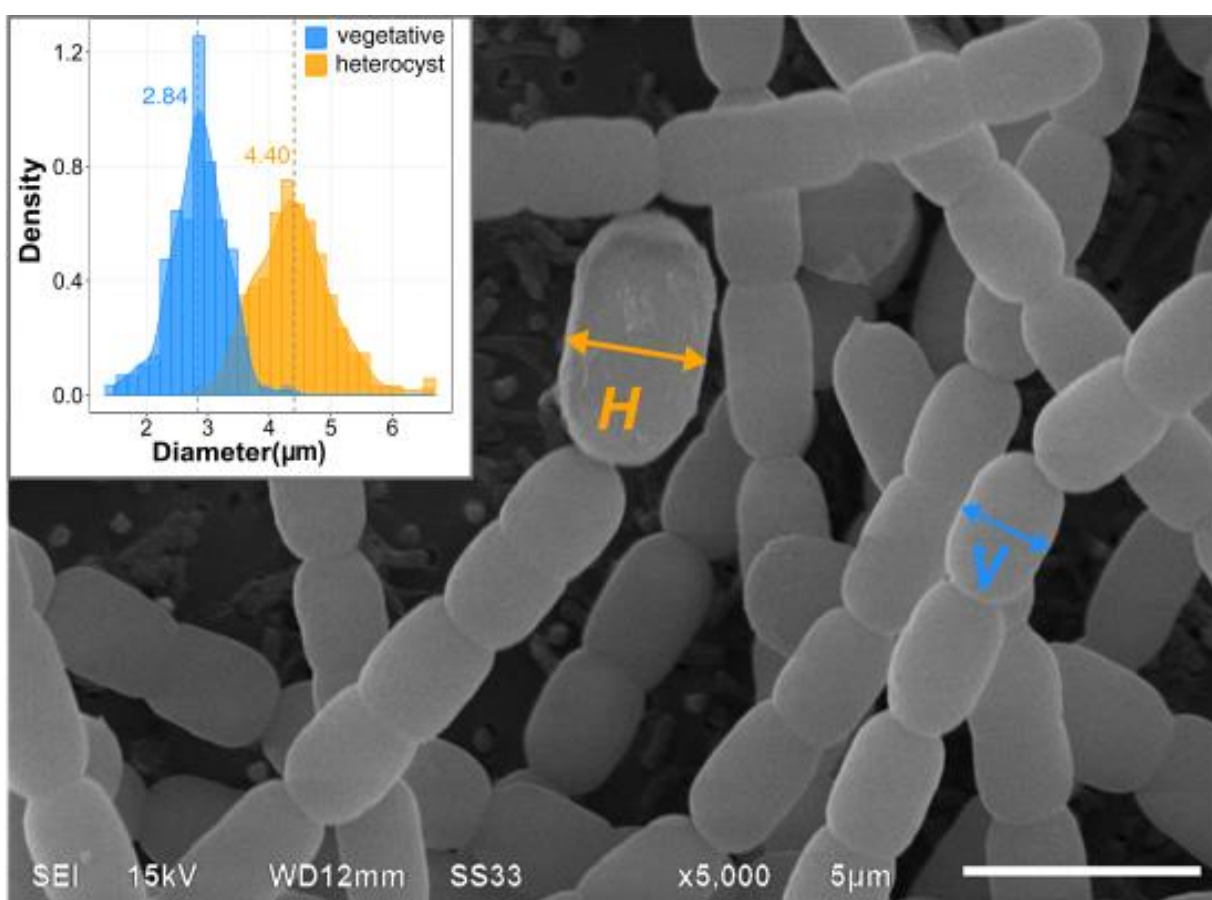


Figure 3.7. SEM image of diazotrophic *Anabaena* filaments

Average cell diameters and standard deviations of the size distributions were determined from at least 165 measurements. Heterocysts (H) are larger than vegetative cells (V) due to the protective layers that block the entrance of oxygen. Reference bar (bottom right) represents 5 μ m. The image was magnified 5000 times.

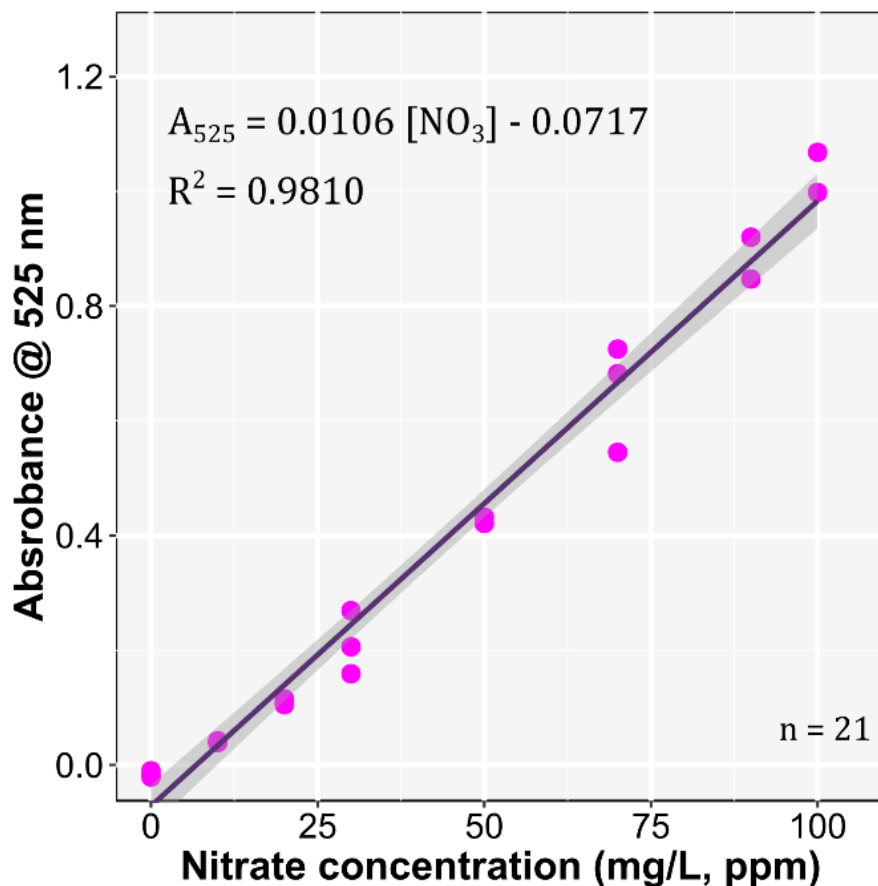


Figure 3.8. Calibration curve for NO_3 quantification

NO_3 was determined using a UV-visible spectrophotometry method based on the nitrate reduction test with sulfanilic acid. Twenty-one nitrate standards were employed to build this curve. Shaded area represents the confidence interval of the prediction with a significance level $\alpha=0.05$. Standards were prepared in triplicate.

NO_3 levels were also determined through the Cadmium reduction method using NitraVer 5 Nitrate Reagent powder pillows (HACH product# 2106169). NO_3 was measured with a DR300 Pocket colorimeter (HACH# LPV445.97.02110), following manufacturer's instructions after diluting the liquid sample 100 times. Both methods yielded similar results. NO_3 readings were conducted in triplicate for each sample, using deionized water as blank.

Total nitrogen content (N_T) for diazotrophic cultures in BG11_o medium was measured by adapting a method based on persulfate digestion (Test 'N tube, HACH method 10072 [358]). Persulfate digestion reagent was prepared in deionized water with potassium persulfate ($K_2S_2O_8$, 50g/L), NaOH (16.8 g/L) and boric acid (H_3BO_4 , 30 g/L). Equal volumes of persulfate reagent and diazotrophic culture sample were mixed in a glass vial and placed inside an autoclave at 121°C for 1 hour to oxidize the organic matter and transform nitrogen containing compounds into NO_3 . The resulting NO_3 content of the digested sample was analyzed either by the sulfanilic acid or the cadmium reduction tests. Nitrate concentrations were converted to N_2 and N_T equivalents using stoichiometric relations. The Nitrogen oxidation efficiency of the persulfate digestion reaction was determined with glycine and serine standards. The minimum conversion of these amino acids into nitrates after digestion was 96%. Hence, the stoichiometric transformation to N_2 (and N_T equivalents) did not involve correction factors.

Urea concentration in cell-free liquids was quantified through the O-phthalaldehyde (OPA) reaction with Naphtylethylenediamine (NED) [359]. Briefly, 500 μ l of OPA reagent were mixed with 25 μ l of sample and 250 μ l of deionized water and thoroughly mixed. Then, 500 μ l of NED reagent were added to the mixture. The liquid samples were placed in a water bath at 37°C for 4 minutes and the absorbance at 480 nm was immediately measured. A reagent blank prepared with DI water instead of sample was used as blank. The Urea calibration curve is presented in Figure 3.9. The urease activity was measured with a BioVision Urease activity kit (product # K378-100) following manufacturer's instructions after sample homogenization with sonic dismembration at 40 W (three cycles of 30 seconds on ice). Urease concentration in the lysed sample was

determined with a Pierce BCA kit and results were measured with a BioTek Epoch 2 microplate spectrophotometer.

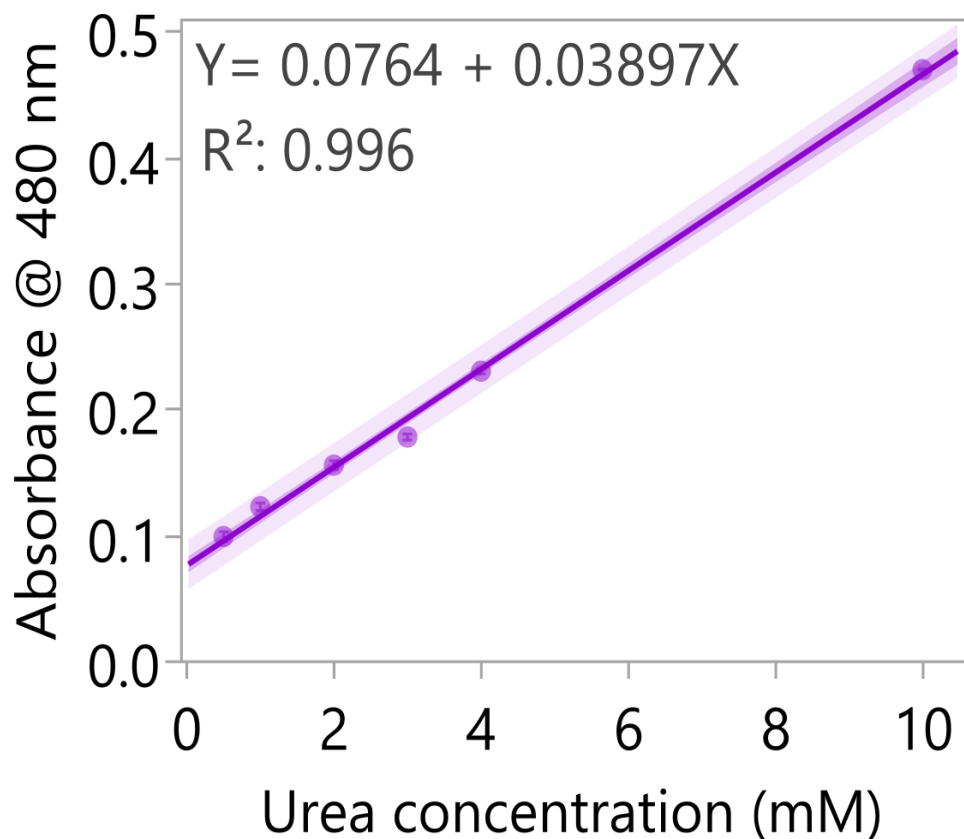


Figure 3.9. Calibration curve for urea quantification

Urea was determined using a UV-visible spectrophotometry method based on the O-phthalaldehyde method. Eighteen urea standards were employed to build this curve. Shaded area represents the confidence interval of the prediction with a significance level $\alpha=0.05$. Standards were prepared in triplicate.

3.12 Quantification of total organic carbon (TOC)

TOC was measured with a HACH high range total organic Carbon reagent set (product #2760445). Manufacturer's instructions were followed to measure TOC in a HACH DR 6000 spectrophotometer (Program 426). Standards with 200 and 500 ppm of

organic Carbon were used for quality control. Blanks were prepared with organic-carbon free HPLC grade water. Samples of cells grown in BG11_u medium were diluted four times before TOC analysis. Samples from BG11 and BG11_o cultures did not require prior dilution.

3.13 Determination of mineral element composition in growth media

Inductively coupled plasma optical emission spectroscopy (ICP-OES) was used for growth medium quality control and to track changes in the concentration of mineral elements in liquid media during cellular growth. A multielement ICP-OES detection method based on the EPA 200.7 protocol was developed for efficient quantification of B, Na, Mg, P, K, Ca, Mn, Fe, Co, Ni, Cu, Zn in fresh media and supernatants [360]. The minimum sample volume required for this analysis was 4 ml. Atomic emission was measured with a PerkinElmer Optima 8000 ICP-OES spectrometer. Radio frequency power was 1500 W and plasma viewing was set to axial mode. Plasma, auxiliary gas and nebulizer gas flow rates were set to 8 L/min, 0.2 L/min and 0.7 L/min, respectively. Samples were analyzed at a flow rate of 1 ml/min, using HNO₃ 5% v/v as washing fluid. Detection wavelengths were iterated to minimize spectral interference. The concentrations of the calibration standards were adjusted considering the composition of standard mineral BG-11 medium [361]. Initial measurements conducted on liquid samples digested with HNO₃ 2% v/v at 85 °C demonstrated that acid digestion of cyanobacterial growth media was not necessary. Calibration curves and detection wavelengths for each element are summarized in Figure 3.10. Concentrations of calibration standards are presented in Table 3.2.

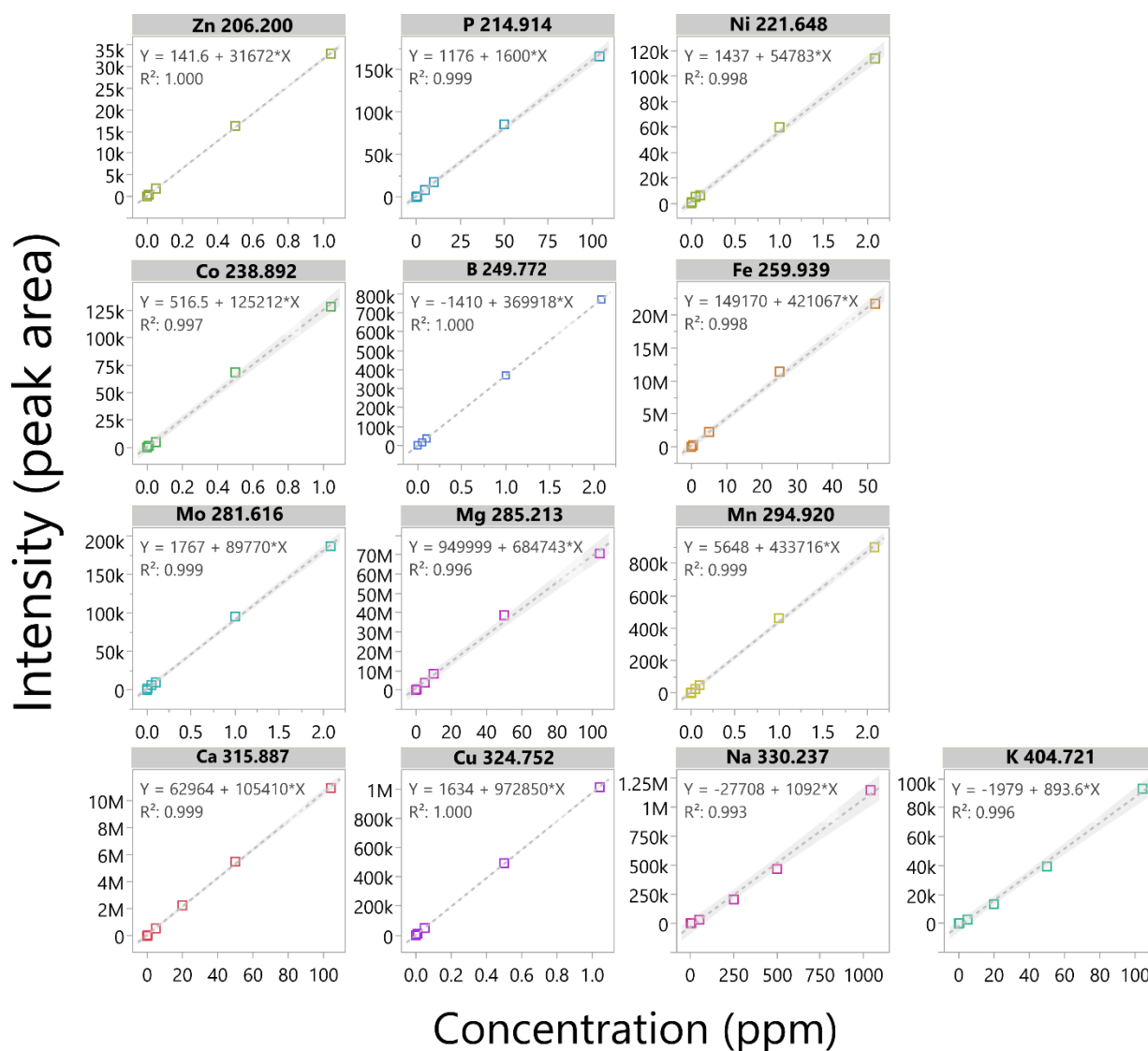


Figure 3.10. ICP-OES Calibration for elemental analysis of BG11x.

Simultaneous quantification of Zn, P, Ni, Co, B, Fe, Mo, Mg, Mn, Ca, Cu, Na, and K levels in cyanobacterial media was conducted using an atomic emission technique. The calibration curves and detection wavelengths (in nm) for each element are presented. Standards were prepared twice. Shaded regions represent the confidence interval of the predictions with a significance level $\alpha=0.05$.

Table 3.2. Element concentrations of calibrations standards for ICP-OES.

These concentration levels were defined considering typical element levels in standard BG-11 medium. Standards were prepared in HNO₃ 2% v/v from commercial standards for ICP-OES.

Element	ST1	ST2	ST3	ST4	ST5
Na (ppm)	5	50	250	500	1042
K (ppm)	0.5	5	20	50	104.2
Ca (ppm)	0.5	5	20	50	104.2
Mg (ppm)	0.5	5	10	50	104.2
Fe (ppm)	0.05	0.5	5	25	52.1
P (ppm)	0.5	5	10	50	104.2
B (ppm)	0.005	0.05	0.1	1	2.084
Ni (ppm)	0.005	0.05	0.1	1	2.084
Mo (ppm)	0.005	0.05	0.1	1	2.084
Cu (ppm)	0.001	0.01	0.05	0.5	1.042
Co (ppm)	0.001	0.01	0.05	0.5	1.042
Mn (ppm)	0.005	0.05	0.1	1	2.084
Zn (ppm)	0.001	0.01	0.05	0.5	1.042

3.14 Chapter conclusion

This chapter presented all the chemical composition and biological characterization methods used in this research project. Significant outcomes of these section are: the definition of a method to quantify heterocysts abundance using flow cytometry, the definition of a quick method for quantification of β -Carotene that does not require column separation, and the development of a protocol for quality control and monitoring of elemental composition in cyanobacterial growth media. The methodologies presented in this section were used to quantify nutrient demands and the effect of different N-sources and Fe-levels on the chemical composition and reproduction of *Anabaena*. This is important to compare the bioproduction potential of valuable pigments and biomass generation in different growth media.

CHAPTER 4. MATHEMATICAL MODELLING OF METABOLIC NETWORKS

4.1 Preamble

This chapter presents the basic concepts on mathematical modeling of cellular metabolism using a Genome-Scale mathematical reconstruction (GSMM). This method for simulation of metabolic networks was selected to gain a global understanding of the biosynthetic pathways in microorganisms. Most importantly, the construction of a GSMM is useful to simulate metabolic fluxes through biochemical reactions in microbial biofactories.

4.2 Simulation and analysis of metabolic networks

Understanding the metabolic network of any organism is a difficult task because of the complex relationships and regulatory mechanisms at cellular level. However, it is necessary to provide a detailed description of the metabolic reactions happening inside *Anabaena* to enhance their utilization for biotechnological production. Production rates in *Anabaena* are still a limiting factor and metabolic optimization is required to improve product titers. The development of *in silico* mathematical models has been proposed to predict changes in productivity after targeted genetic modifications. In that sense, Systems Biology computational tools represent a significant step forward towards improving biological production processes. Unfortunately, metabolic modeling and experimental characterization of diazotrophic cyanobacteria remain a challenge and currently represent a bottleneck to improve the understanding of these biological systems.

A genome-scale metabolic reconstruction model (GSMM) is an *in silico* mathematical model describing the entire metabolic network of a microorganism. Such a model can be constructed in a bottom-up fashion from the whole-genome sequence, the genome annotation, and the biochemical information deposited in databases. Therefore, a GSMM is an organized collection of known biochemical reactions happening inside an organism [362, 363]. GSMMs also include Information about coding genes for enzymes and proteins that catalyze those reactions [364]. This kind of models can be used to visualize metabolic networks and simulate the transformation of nutrients into biomass and metabolites. Figure 4.1 presents a graphical summary of the mathematical modelling of metabolic networks.

Given that a mathematical description of the full metabolic network requires a large set of ordinary differential equations, the analysis of a GSMM makes use of the Flux-balance (FBA) and Flux-variability analysis (FVA) algorithms [362, 365]. FBA is a constraint-based linear optimization technique that calculates the flux of metabolites through the biochemical reactions in the metabolic network, thus predicting cellular phenotypes [362, 364]. FVA relies on FBA results to calculate the flux variability through reactions of interest as a result of metabolic redundancies [366]. In a GSMM, the biochemical reactions are tabulated showing the transformation from substrates to products and this information is used to generate a numerical matrix of stoichiometric coefficients. A given compound (i.e., rows) may participate in different reactions (i.e., columns) and the stoichiometric matrix also represents constraints on how each compound flows through the metabolic network.

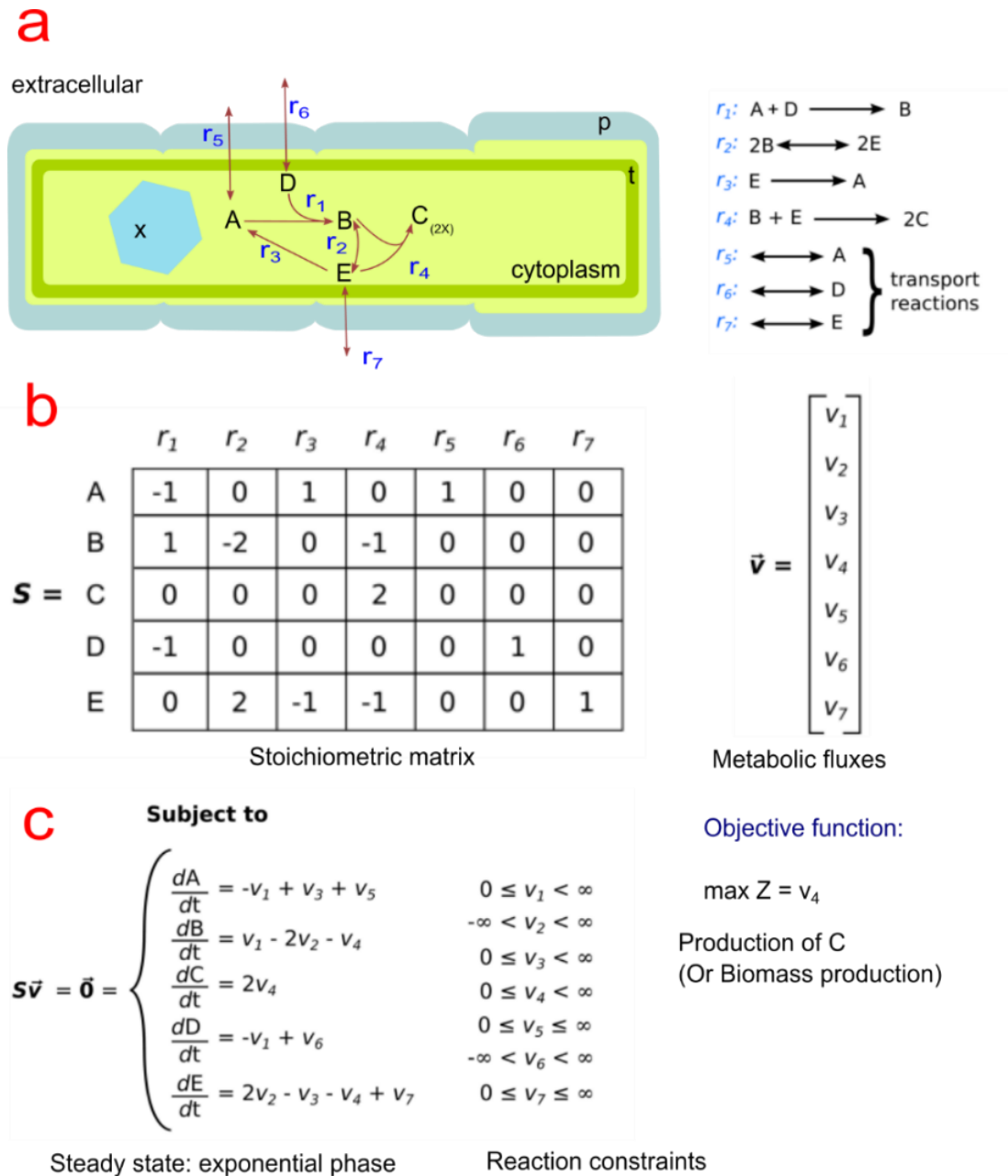


Figure 4.1. Mathematical modelling of metabolic reaction networks

The cellular metabolism is represented by a network of metabolic, transport and exchange reactions. (a) Cells are divided in compartments, where different metabolic reactions take place. (b) A Stoichiometric matrix is used to represent the stoichiometric coefficients of metabolites (rows) through the metabolic reactions (columns). A solution vector represents the metabolic fluxes through the biochemical reactions in the GSMM. (c) The steady state approximation and flux constraints are used to solve the GSMM using FBA. The objective function of the resulting linear programming problem is normally defined in terms of biomass production or metabolite production. Adapted from [362].

Respecting the law of mass conservation, the definition of a stoichiometric matrix ensures that the total amount of any metabolite being produced is equal to the total amount of metabolite being consumed at steady state [364]. In other words, the stoichiometric matrix becomes the essential information used to solve the mass balance of the system. Thiele and Palsson, Orth et al, and Mahadevan and Schilling previously described the protocols to develop high-quality GSMM models and the mathematical fundamentals of the FBA and FVA algorithms [362–364, 366].

One of the most important equations in the GSMM is the biomass equation. The biomass reaction is derived from the chemical composition of the microorganism, quantifying the metabolic sinks that give rise to cell biomass [367]. Normally, this equation is used as the objective function for the FBA analysis when maximization of cellular growth is intended. When defining the biomass equation of a GSMM, it is imperative to check that the biomass has a molecular weight of 1 g mmol^{-1} . This is necessary to ensure complete mass balance [368]. The biomass equation may also be understood as the main constraint for the model when the objective is to maximize the production rate (i.e., metabolic flux) through a biochemical reaction of interest. In these cases, the mathematical solution will try to satisfy the biomass generation equation before attempting to maximize the target metabolic fluxes. In most cases, the biomass equation is calculated using publicly available information on the chemical composition of the organism. However, since the biomass defines the identity of a GSMM, an accurate formulation of the metabolic model requires experimental determination of the biomass composition of the cell culture under controlled growth conditions [213]. One additional component of the biomass equation is the energy (i.e., ATP) required for biosynthesis

and for sustaining other metabolic functions like motility, formation of macromolecules, maintenance of transmembrane gradients, and cellular homeostasis [369]. Given that these energetic requirements are difficult to measure experimentally, those values are normally taken from reference organisms like *E. coli* [369], or *Synechocystis* for cyanobacteria [370, 371].

The GSMM also contains other equations representing exchange and transport of metabolites through different cellular compartments, which are used to define subsystems within the cell, roughly representing cellular organization. For example, the organelles of eukaryotes and the bacterial micro-compartments (BMCs) of prokaryotes are normally defined as compartments because only specific chemical reactions occur in those subsystems. The definition of compartments in a GSMM also allows for a better mathematical and biological description for the FBA problem. Exchange reactions describe source or demands (i.e., sinks) of metabolites (chemical compounds) involved in the metabolic network. In other words, an exchange reaction may describe the uptake of a nutrient from the growth medium (source) or the total evacuation of a cellular byproduct from the system (sink). Finally, a transport reaction is a representation of the movements of metabolites across different compartments. While most metabolic reactions used to construct the stoichiometric matrix involve gene-enzyme associations, the transport reactions are usually defined by the presence of specific transporters encoded in the DNA, or by metabolic processes like photosynthesis and oxidative phosphorylation, which require movement of protons across cellular membranes [363, 372].

Genomic reconstructions almost always have more reactions than compounds and are mathematically underdetermined. Hence, the resolution of an FBA analysis requires the definition of constraints. In general, these constraints represent the limits or bounds of the metabolic fluxes (v_n) through different chemical reactions [362]. When specific constraints are experimentally determined (e.g., nutrient uptake or chemical production rates), these bounds may be described by single numbers or narrow ranges. When constraint limits are unknown, the bounds are normally defined based on the reaction thermodynamic equilibrium. For reversible reactions, constraints are unbounded ($-\infty < v_n < \infty$), and for irreversible reactions, constraints are bounded ($0 \leq v_n < \infty$). In practical terms, infinite metabolic fluxes are defined as $\pm 1000 \text{ mmol h}^{-1} \text{ gDW}^{-1}$. One final consideration for the resolution of an FBA problem is the steady state approximation (See Figure 4.1). This approximation means that the metabolites within the network are consumed as soon as they are produced, maintaining a constant concentration. Because of this, the FBA analysis for the GSMM proceeds without any species-specific kinetic parameters, which are scarce for most cyanobacteria. Although the FBA is unable to predict concentrations of metabolites, the metabolic fluxes through the different reactions can be used for strain optimization [362–364]. Since the increase in bacterial populations takes place at reproducible rates during the exponential phase, consumption and production rates in the logarithmic phase are normally used to define FBA constraints [213, 348, 362].

4.3 Bioinformatic tools used for developing microbial GSMMs

Developing a high quality GSMM is a labor and time-consuming task. The process can take anywhere between six months to two years depending on the information

available for the organism of interest [363]. The minimum information needed to start a GSMM is the genome sequence, which is only fully available for 10 to 15% of the cyanobacterial species listed in specialized databases [373]. Although there are some tools for semi-automatic development of reconstruction models, creating the mathematical model still requires manual curation and gap filling. In this case, building a GSMM uses bioinformatics to go from DNA sequences to functional roles of enzymes and biochemical reactions [362].

Specifically, the reconstruction process requires the use of databases and tools like BiGG [374] (Biochemical, genetic, and genomic database), NCBI Genomes [375] (National center for biotechnology information), BRENDA [376] (the comprehensive enzyme information system), UniProt [377] (Universal protein resource), KEGG [378] (Kyoto encyclopedia of genes and genomes), PATRIC [379] (Pathosystems resource integration center), MetaCyc [380] (the Metabolic pathway database), and ModelSEED [381]. In addition, a high-quality GSMM needs constant literature review to obtain updated information regarding metabolic features of the organism under study. Even for well-studied microorganisms like *E. coli*, the genomic reconstruction is an iterative process that can be refined for decades [363].

4.4 Chapter conclusion

This chapter introduced basic concepts on mathematical modelling of metabolic networks. A deeper mathematical description of the techniques is presented by authors referenced in this chapter [362–364, 366]. The first and only GSMM model for *Anabaena* was published in 2017 [382]. However, this model was mainly used to study the transit of

nitrogenous metabolites between vegetative cells and heterocysts. Moreover, this model used biomass composition data for *Synechocystis* sp. PCC 6803 to define the objective function of the FBA problem. Chapter 5 will describe the integration of concepts from Chapters 2, 3 and 4 to develop *i*DN1004, a precise genome-scale metabolic reconstruction of *Anabaena* sp. UTEX 2576. The most significant aspect *i*DN1004 is the definition of biomass equations using chemical composition and nutrient consumption data for diazotrophic and non-diazotrophic cultures of *Anabaena*.

CHAPTER 5. DEVELOPMENT OF *DN1004*, A PRECISE GENOME-SCALE METABOLIC RECONSTRUCTION OF *ANABAENA*

5.1 Preamble

This chapter integrates chemical characterization techniques and simulation of microbial metabolic networks to analyze the potential of *Anabaena* as a photosynthetic bio-factory of specialty chemicals. The subsections are organized to respond to specific objective 2. The GSMM model *DN1004* was used to analyze the subnetwork of amino-acid biosynthesis to define potential applications of *Anabaena* as a platform to produce secondary metabolites. The model was named using the initials of its creator and the number of genes involved, as is customary in the metabolic modelling field. This chapter was being prepared for publication when this dissertation was presented. This part of the project is the result of a collaboration between the LSU Cain Department of Chemical Engineering and the University of California San Diego (UCSD) Department of Pediatrics. Daniel A. Norena-Caro was listed as first author of this study. Cristal Zuñiga, Amber J. Pete, Sven A. Saemundsson, Morgan R. Donaldson, Alexandria J. Adams, Kerry M. Dooley and Karsten Zengler were listed as co-authors. Michael G. Benton was listed as corresponding author.

5.2 Introduction to *DN1004*

Cyanobacterial metabolism encompasses key biochemical pathways that enable light-based production of valuable compounds from CO₂ fixation. On top of their CO₂-fixation ability, cyanobacterial species from the genera *Anabaena* and *Nostoc* can also fix dinitrogen (N₂), becoming potential photoauto- and photodiazotrophic bioenergy

platforms [17, 373]. N₂-fixation in *Anabaena* takes place in specialized cells referred to as heterocysts, which arise under photodiazotrophic growth. Additionally, *Anabaena* is a model organism to study cellular differentiation of filamentous cyanobacteria, useful in several developmental studies [115]. In nature, *Anabaena* serve as symbiotic partners of *Azolla*, metabolizing N₂ inside leaf cavities of water ferns commonly found in rice paddies [337]. The main biotechnological application of *Anabaena* is as natural fertilizer [17] and as potential decontaminant of nitrogen-containing pollutants of agro-industrial wastewaters [107]. Industrial-scale cultivation of *Anabaena* in association with wastewater bioremediation can potentially produce specialty chemicals simultaneously.

N₂-assimilation is an essential process thoroughly coupled with the central carbon metabolism [15, 383]. In *Anabaena*, starvation and oversupply of Nitrogen in the growth medium also have a significant impact on the regulation of biosynthetic pathways linked to phosphoglyceraldehyde, glucose-6-phosphate, or oxaloacetate [383]. *Anabaena* stores surplus nitrogen in the form of phycobiliproteins (PBPs) and cyanophycin, while dynamically consuming glycogen (main reserve of glucose-6-phosphate). Accumulation of cyanophycin depends on the intracellular availability of L-aspartate and L-arginine [288, 384, 385]. Some cyanobacterial species are able to accumulate polyhydroxybutyrate under soluble nitrogen starvation, but the main consequence of nitrogen starvation in *Anabaena* is the development of heterocysts [35, 115, 285, 287, 288].

Nitrogen metabolism has been overlooked in most metabolic engineering initiatives for cyanobacteria despite being a central component of the metabolic network [32, 122]. Common engineering efforts aim to overexpress genes or introduce exogenous biosynthetic pathways to produce biofuels and commodity chemicals from carbon

skeletons closely derived from the carboxysomal carbon fixation pool [373]. Because filamentous cyanobacteria are also a potential source of valuable specialty chemicals derived from amino-acids and other Nitrogen-containing metabolites (e.g., natural products, bioactive compounds and pigments) [50, 190, 386], it is still desired to enhance or introduce biosynthetic pathways using amino-acid pathways as branching points. Some examples of metabolites derived from amino acids in *Anabaena* are the chromophore phycocyanobilin (PCB) and the cyanophycin polymer granule. The tetrapyrrole PCB is synthesized from heme following a pathway that starts with the formation of 5-aminolevulinate (ALA) from L-glutamate [387–389]. On the other hand, the cyanophycin polypeptide is non-ribosomally synthesized from L-aspartate and L-arginine in an ATP-dependent elongation reaction [278]. While cyanophycin could be used as a precursor of polyaspartic acid (PASP) to replace non-biodegradable polyacrylates [34, 165], PCB finds application as a dyeing and nutraceutical additive for foods and cosmetics, because of its natural blue color and antioxidant and radical-scavenging properties [50, 114, 297]. Another example of an amino-acid derived metabolite is schizokinen, a hydroxamate-based siderophore involved in iron uptake and copper ion chelation mechanisms [390, 391]. Although siderophores can stem from L-aspartate 4-semialdehyde [392], lysine and L-ornithine (from the L-arginine biosynthesis pathway) are the most likely primary metabolic precursors for the production of cyanobacterial schizokinen [393, 394]. The importance of schizokinen and other cyanobacterial siderophores arises as a new generation of targeted antimicrobial delivery drugs based on siderophore-conjugated β -lactam antibiotics are being developed for the treatment of drug resistant bacterial infections [395, 396].

Although *Anabaena* is not a native producer of important bioactive compounds, it represents an alternative to speed up the biosynthesis of marine secondary metabolites, which are important for pharmaceutical applications. Because marine cyanobacteria grow slowly, their large-scale cultivation remains a technical challenge that could be circumvented in *Anabaena*. Videau *et al* studied the strain as a general heterologous expression host for secondary metabolites because it recognizes native promoters of marine cyanobacterial gene clusters [118]. Many of these secondary metabolites have been discovered in the marine cyanobacterium *Moorea producens*, which produces anti-cancer and anti-inflammatory compounds [174, 386]. Some examples are barbamide, a molluscicidal agent, and lyngbyatoxin A, an inflammatory agent with possible uses in anticancer therapy [397, 398]. While the barbamide biosynthesis pathway starts with L-leucine, lyngbyatoxin A is derived from L-valine and L-tryptophan [118, 398, 399]. Another natural product that could be produced in *Anabaena* through metabolic engineering is the ultraviolet sunscreen shinorine [190, 400] (from sedoheptulose 7-phosphate, glycine, and L-serine), which has found application in cosmetic products like Helioguard 365™ [401].

Considering the central role of amino acids in the biosynthesis of specialty chemicals, there is interest in estimating the abundance of these primary metabolites under different growth conditions, to quantify the metabolic capacity of autotrophic *Anabaena* cultures [118, 190, 386, 402]. Such estimation is useful to rank metabolic engineering efforts aiming to produce high-value nitrogen compounds in cyanobacteria. Hypothetically, higher bio-product yields result from pathways using abundant precursor amino acids (e.g., with large metabolic fluxes). Although there are protocols to determine

the amino-acid composition of biological samples using liquid and gas chromatography [403], these analytical methods do not provide information on how amino acids are used as precursors within the metabolic network. In this regard, comprehensive genome-scale metabolic models (GSMM) coupled with flux balance analysis (FBA) [364], flux variability analysis (FVA) [366] or ^{13}C metabolic flux analysis (MFA) have emerged as alternatives to analyze the metabolic pathways used by cyanobacteria to transform nutrients into biomass and bio-products [404]. While models analyzed through FBA and FVA are valuable predictive tools to estimate theoretical metabolic flux distributions, stoichiometric and genome-scale models analyzed by isotopically nonstationary MFA (INST-MFA) can measure those fluxes experimentally in autotrophic cultures of cyanobacteria [210, 405–407]. Although each of these methods has limitations, their results taken collectively help clarify the metabolic map of potentially productive cyanobacteria like *Anabaena*.

This work estimates the metabolic fluxes through amino-acid producing biochemical pathways in *Anabaena* sp. UTEX 2576 growing under photoauto- or photodiazotrophic conditions in BG11 or BG11_o media, respectively. To do this, the GSMM *DN1004* was developed with specific reactions for this organism and analyzed using FBA and FVA. Considering that phycocyanobilin is one of the most representative bio-products derived from the *Anabaena* amino-acid metabolism, the model was useful to predict production rates of this chromophore and to compare with experimental information on PCB biosynthesis. Experimentally determined biomass equations for photoautotrophic and photodiazotrophic filaments improved the prediction ability of *DN1004*, as presented for the N_2 -fixing cyanobacteria *Trichodesmium erythraeum* [213].

In addition, *i*DN1004 contains metabolic flux constraints derived from the experimental determination of nitrate uptake, nitrogen fixation, biomass generation, and photon flux for the cyanobacterial cultures. Compared with a previously published *Anabaena* GSMM [382], *i*DN1004 improves the accuracy of the metabolic flux predictions because it includes *Anabaena* specific biomass objective functions and phycobiliprotein biosynthesis equations. Considering that *i*DN1004 provides a detailed description of the *Anabaena* metabolic network, it was designed to become a benchmark to analyze promising biotechnological applications of filamentous cyanobacteria. To the authors' knowledge, this is the first work using simulation of metabolic networks to analyze the potential of filamentous cyanobacteria to produce valuable nitrogen-containing metabolites beyond the central carbon metabolism.

5.3 Reconstruction model of the *Anabaena* metabolism

*i*DN1004, the *Anabaena* GSMM, was generated in a bottom-up fashion from the whole-genome sequence [408], genome annotation, and biochemical information deposited in databases, following the recommendations for a high-quality metabolic model reconstruction [362, 363]. PATRIC database provided the genome sequence annotation of *Anabaena* (NCBI taxonomy ID 103690) [409]. The genome annotation specified location and identity of *Anabaena* genes, including the Enzyme Commission (EC) numbers of enzyme coding genes. PATRIC metabolic reconstruction tool based on SEED generated a draft metabolic reconstruction [381]. This draft reconstruction was our starting point and included specific metabolic reactions for *Anabaena* and cyanobacteria. The manual curation of the model was accomplished using KEGG [148], BiGG [374],

MetaCyc [410], and UniProt [411] databases as well as primary literature. In general, the construction of *i*DN1004 relied on biochemical information for the heterotypic synonym strains *Anabaena* sp. PCC 7120, *Anabaena* sp. UTEX 2576, *Nostoc* sp. PCC 7120, *Nostoc* sp. ATCC 27893, and *Nostoc* sp. SAG 25.82. Electron-transfer reactions through photosystem II, cytochrome b6f complex, photosystem I, and ferredoxin were incorporated based on the *i*JN678 GSMM of *Synechocystis* [204, 208]. The light usage was described by spectral decomposition reactions based on the visible-light spectrum template of photosynthetic microorganisms [367, 404]. Spectral bandwidth reactions specific for cyanobacterial photosystems and phycobilisomes were defined by allowing only indigo/blue (406 to 454 nm), violet/blue (378 to 482 nm), red (659 to 691 nm), and red/orange (608 to 666 nm) radiations to participate in photosynthesis. *i*DN1004 was initially constructed in MS Excel 2016 and transferred to MATLAB (The MathWorks Inc) using COBRA Toolbox [412]. Model properties were evaluated with Memote test suite [413]. Quality control tests for mass and charge balances proceeded in COBRA Toolbox. The constrained model is available in mat (Matlab) and json (JavaScript) formats. COBRApy [414] and Escher web application v 1.7.0 [415] were utilized to represent portions of the amino-acid metabolism within the metabolic network.

5.4 Model simulations

*i*DN1004 describes the global metabolic behavior of *Anabaena*. Metabolic fluxes through the biochemical reactions in *i*DN1004 were calculated with FBA [364] implemented in MATLAB Cobra Toolbox 2.19.1 [412]. Appendix B presents the main components of the GSMM, e.g., metabolites, reactions and biomass equations. Appendix

C presents the MATLAB codes for calling FBA and FVA routines in CobraToolbox. Additional datasets may be provided upon request. For the FBA analysis, the biomass equations “BOF_ANA_AUTO” and “BOF_ANA_DIAZO” were used as objective functions to maximize growth of photoautotrophic and photodiazotrophic filaments, respectively. The remaining reactions in *DN1004* were used as constraints for the FBA problem and their default constraint limits are included in Table B.1. Specific constraint limits were derived from experimental measurements of Nitrate consumption, N₂-fixation, and CPC production. FVA was implemented to verify the solution space for the amino-acid production fluxes. To do this, the 70 amino acid producing reactions from *DN1004* were used as objective functions for FVA simulations. As defined by the FVA algorithm [365, 366], the metabolic flux through each of the 70 amino-acid producing reactions was first maximized and then minimized to obtain a range of feasible amino-acid production fluxes. For each of these maximization and minimization steps, the model constraints were the same as the ones listed for the initial FBA problem. In addition, the FVA problem was solved keeping at least 95% of the original growth rate predicted by FBA. Thus, the photoautotrophic and photodiazotrophic growth rates calculated by FBA were used to calculate additional growth rate constraints for the FVA problem. The FBA and FVA linear programming (LP) problems were resolved with Gurobi 7.0.2 solver running on Intel Core i5 3.20 GHz and Intel Kaby Lake dual-core i5-7200U processors.

In the simulations, the standard units of the metabolic fluxes were mmol g_{DW}⁻¹ h⁻¹ and mmol g_{DW}⁻¹ for metabolite coefficients in the biomass equations. Using this standard, *DN1004* predicted *Anabaena* growth rates in h⁻¹ by considering a nominal biomass molecular weight of 1000 mg mmol⁻¹ [364, 368]. Differences in biomass composition of

photoauto- and photodiazotrophic cultures were accounted in the form of biomass equations. These equations resulted from biomass fractions (in $\text{g g}_{\text{DW}}^{-1}$) taken during the exponential and stationary phases. A two-way ANOVA statistical analysis with data from cultures of different age and nitrogen source supported the construction of biomass equations (see subsection 0). Biomass fractions were transformed into molar coefficients ($\text{mmol g}_{\text{DW}}^{-1}$) of metabolites included in *DN1004* considering the molecular weights and protein, DNA, RNA, pigment, glycerolipid, and carbohydrate composition values from reference studies on *Anabaena*. Metabolic flux values for NO_3 uptake, N_2 fixation, and CPC production resulted from experimentally determined kinetic constants. First-order rate constants (in day^{-1}) resulted from measuring the change on NO_3 and N_T concentration over time. Metabolic flux values of NO_3 uptake and N_2 fixation were calculated after multiplying the rate constants by the cumulative ratios of Nitrogen source consumed per biomass unit ($\text{mg g}_{\text{DW}}^{-1}$) at a given point of cellular growth. Molecular weights of 85 mg mmol^{-1} and 28 mg mmol^{-1} for NaNO_3 and N_2 , respectively, were considered. Zero-order rate constants (in $\text{mg L}^{-1} \text{ day}^{-1}$) resulted from measuring the change of CPC concentration over time. The metabolic flux through the CPC producing reaction was computed after dividing these rate constants by the biomass concentration (in $\text{g}_{\text{DW}} \text{ L}^{-1}$) at a given point of cellular growth. Calculations involved a nominal molecular weight of $35900 \text{ mg mmol}^{-1}$ for *Anabaena* CPC, which is constituted by α and β subunits [416]. The maximum theoretical flux of photons entering the cells was determined by converting PPFD in $\mu\text{mol m}^{-2} \text{ s}^{-1}$ to $\text{mmol g}_{\text{DW}}^{-1} \text{ h}^{-1}$, using mass and surface area estimates of *Anabaena* cells. The experimental values of NO_3 uptake flux, N_2 fixation flux, CPC production flux, and maximum photon flux were used to calculate modelling constraints

for *i*DN1004. FBA calculated the metabolic flux values of the reactions in *i*DN1004, including amino acid and PCB producing pathways. Then, total amino-acid production fluxes were calculated as the sum of the predicted fluxes through the amino-acid producing reactions. The ranges of the total amino-acid production fluxes were derived from the FVA analyses. Given that FVA predictions can result in highly variable fluxes (i.e., cycles carrying any flux) [364], only physiologically relevant results were considered to estimate the solution space for amino-acid production fluxes.

5.5 Results and Discussion

5.5.1 Properties of the *Anabaena* Genome-scale metabolic model

The GSMM of *Anabaena* sp. UTEX 2576, *i*DN1004, encompasses 1073 total reactions, 858 metabolites, and 1004 unique genes, distributed across cellular compartments. Given that *Anabaena* filaments present a continuous outer membrane and a continuous periplasmic space, where cells exchange nutrients [417], the whole cellular community was simulated as a single unit with five compartments: extracellular space ([e]), periplasmic space ([p]), cytoplasm ([c]), carboxysome ([cx]), and thylakoid ([u]). Figure 5.1 represents the key biological features of photoauto- and photodiazotrophic filaments of *Anabaena* represented in *i*DN1004. This model includes 155 genes not considered in the previous *Anabaena* model [382] and provides a more detailed representation of unique cyanobacterial processes. Instead of describing the metabolite exchange between vegetative cells and heterocysts within the filament, *i*DN1004 is useful to understand the biochemical production potential of *Anabaena*.

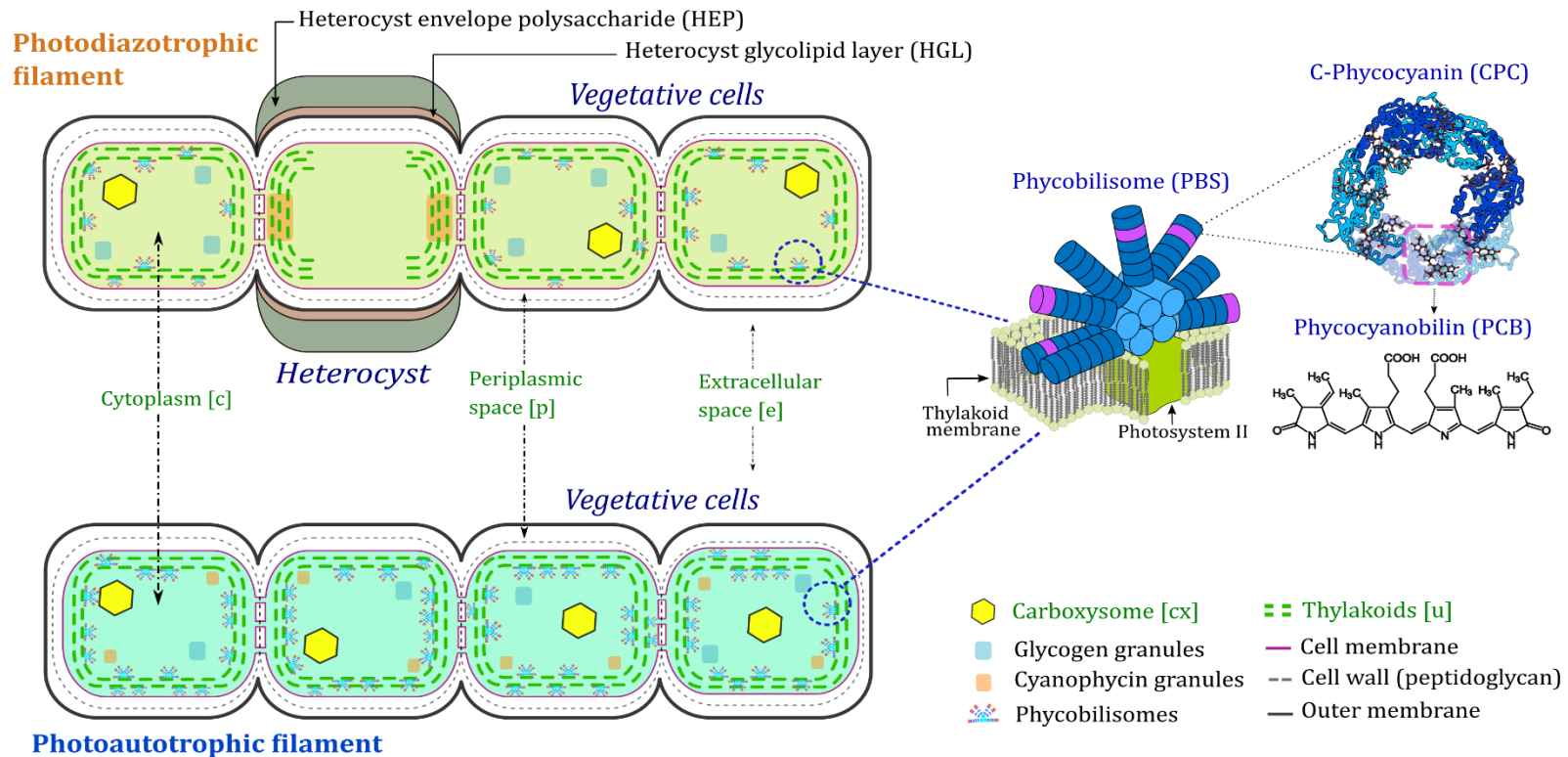


Figure 5.1. Photodiazotrophic and photoautotrophic filaments of *Anabaena*.

In photodiazotrophic filaments, some vegetative cells differentiate into heterocysts to perform N_2 -fixation. These cells degrade carboxysomes, glycogen granules, photosystem II (PSII) complexes, and phycobilisomes, giving rise to external glycolipid (HGL) and envelope polysaccharide (HEP) layers that prevent the entrance of oxygen. Heterocysts also contain polar granules of cyanophycin regulating the N-transit through the filament. Photoautotrophic filaments accumulate excess nitrogen in the form of cyanophycin granules in the cytoplasm. *Anabaena* have an uninterrupted outer membrane that creates a continuous periplasmic space for the exchange of metabolites within the filament.

Table 5.1. Properties of *DN1004* compared to reference GSMMs.

Cyanobacterium	<i>Synechocystis</i> <i>sp.</i> PCC 6803	<i>Cyanothece sp.</i> ATCC 51142	<i>Trichodesmium</i> <i>erythraeum</i> IMS 101	<i>Anabaena sp.</i> PCC 7120 *	<i>Anabaena sp.</i> UTEX 2576
Genome size	3.57 Mb	5.46 Mb	7.75 Mb	7.21 Mb	7.21 Mb
Morphology	Unicellular	Unicellular	Filamentous	Filamentous	Filamentous
Genes in model	678	773	647	869	1004
Total proteins (CDS)	3575	5159	6500	6694	6694
Percent of genes covered	18.9%	15.0%	10.0%	13.0%	15%
Reactions	863	946	973	897	1073
Metabolites	790	811	988	777	858
Compartments	3	5	2	6	5
N ₂ fixation	No	Yes	Yes	Yes	Yes
N ₂ -fixation cell type	-	diazocyte	diazocyte	heterocyst	heterocyst
Spectral decomposition reactions	No	No	No	No	Yes
Phycobiliprotein assembly reactions	No	No	No	No	Yes
Experimental biomass equation	No	No	Yes	No	Yes
Reference	[204]	[208]	[213]	[382]	This work

* Considers only the portion of the single-cell model

Table 5.1 compares the properties of different cyanobacterial GSMMs. The key features of *i*DN1004 are the following. *i*DN1004 describes biochemical and transport reactions encoded by 15% of the protein coding regions (total 6694) of *Anabaena* sequence ID 103690 [408]. The representation of photosynthetic reactions in *Anabaena* filaments was updated considering spectral decomposition reactions that describe the portion of the visible-spectrum light (red, indigo/blue, violet/blue and red/orange radiations) captured by the photosystems and the phycobilisomes. PBPs assembly reactions were defined considering the amino-acid sequences of α and β subunits of c-phycocyanin (CPC), allophycocyanin (APC), and phycoerythrocyanin (PEC), as well as their chromophore content [416]. Cyanophycin biosynthesis was modelled as the conformation of a tetra-peptide with two units of aspartate and two units of arginine, simulating the polymer growth from a cyanophycin primer catalyzed by cyanophycin synthase (EC 6.3.2.29). For the first time, cyanophycin degradation was modelled considering the enzymatic reactions of cyanophycinase (EC 3.4.15.6) and β -isoaspartyl aminopeptidase (EC 3.4.19.5). *Anabaena*-specific biomass equations represent important differences at the global chemical composition level between photoauto- and photodiazotrophic cultures. After including pigment biosynthesis, photosynthesis, cyanophycin, and PBPs synthesis reactions, *i*DN1004 provides a more biologically accurate representation of the cyanobacterial metabolism, compared to the first published model [382].

Besides metabolic reactions, *i*DN1004 includes exchange and sink reactions describing uptake of nutrients from the medium and metabolic sinks. In order to provide a clear sequence of biochemical events inside the cell, the model lists nutrient uptake

reactions first, followed by central metabolic reactions and sink reactions. The biomass equations are presented at the end as consequence of the biological events leading to cellular growth and biomass generation. A proper level of metabolite connectivity was assured after minimizing the number of metabolic sinks. Most nutrient uptake reactions were defined based on the type of transporter (ABC, TRAP, symporter, antiporter, or porin) identified by PATRIC from the genome annotation. Figure 5.2 presents an overview of the *Anabaena* model in terms of the biochemical reactions describing the filament metabolism. Out of 931 metabolic reactions, the most abundant subsystems are 172 equations describing the synthesis of amino acids, 158 reactions associated with lipid metabolism, and 141 reactions related to carbohydrate metabolism. Appendix B is a summary of the complete GSMM. COBRA toolbox functions [363] confirmed mass and charge balance of the metabolic reactions throughout the metabolic network. The model /DN1004 is also compatible with the BiGG database, which has a large collection of high-quality genome-scale metabolic models [374].

5.5.2 Construction of biomass equations from composition data

The biomass reaction is a modeling reaction that accounts for all known biomass constituents (e.g., amino acids, carbohydrates, lipids, nucleotides, and pigments) within the cell. Experimental data are included in terms of fractional abundance per gram of biomass (g_{DW}). Two biomass equations (i.e., photoautotrophic and photodiazotrophic) were generated for *Anabaena* filaments.

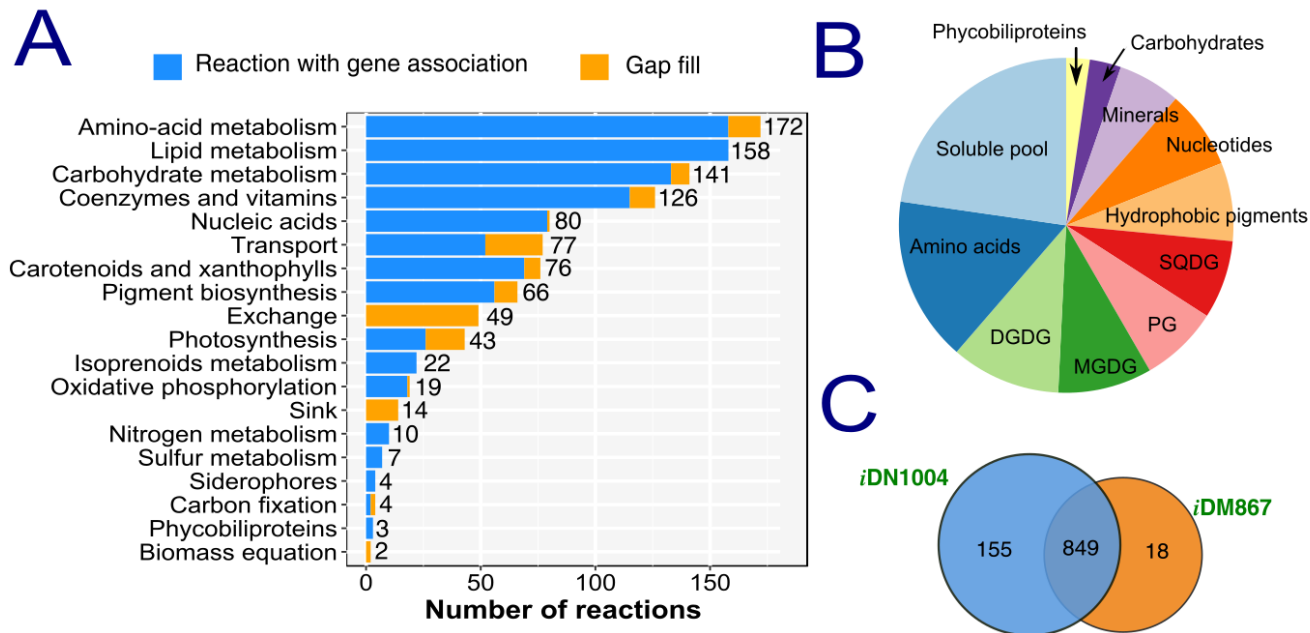


Figure 5.2. General properties of the *Anabaena* GSMM, iDN1004.

A: The bar plot presents the type and number of reactions included in the model. Blue regions in the bars represent the portion of reactions of each kind with gene association. Gold regions correspond to gap fills (i.e., reactions considered in the model to improve network connectivity and production of essential metabolites). Most reactions in the model are associated with a set of genes, except for biomass, sink and exchange, which are used for modelling purposes. The model contains 931 metabolic reactions, which do not account for sink (14 reactions), transport (77 reactions), exchange (49 reactions), nor biomass equations (2 reactions). B: The pie bar summarizes the types of metabolites defining biomass-forming reactions. Biomass equations contain 30 vitamins, coenzymes and polyamines (Soluble pool), 21 amino acids (20 proteinogenic AA + cyanophycin), 10 DGDG, 10 MGDG, 10 PG, 10 SQDG, 12 hydrophobic pigments, 8 nucleotides, 14 minerals (inorganic ions), 4 carbohydrates (i.e., glucose, glycogen, peptidoglycan, and lipopolysaccharide Lipid A IV), and 3 PBPs (CPC, APC, PEC). C: iDN1004 compared with iDM867 (a previous *Anabaena* GSMM) [382] in terms of number of genes involved in the model conception.

These equations became objective functions in the FBA analysis of *Δ*DN1004, aiming to estimate total amino-acid production fluxes in BG11 and BG11_o media. Global biomass composition from the exponential phase (1 to 10 days old) were preferred to define representative biomass equations because of higher reproducibility and stability in this stage of cellular growth [348]. Figure 5.3 summarizes the differences in global chemical composition between photoautotrophic and photodiazotrophic *Anabaena* cultures in exponential phase.

Global composition data from Figure 5.3 correspond to cultures in exponential phase. Additionally, global biomass composition for cultures in stationary phase (>10 days) was measured to identify the main differences under N-limitation. A two-way ANOVA statistical analysis was used to process three independent replicates of the chemical composition data for cultures of different age and in different growth media. For this analysis, nitrogen source (NaNO₃ or N₂) and culture phase (exponential or stationary) were selected as independent variables (factors), using biomass composition fractions (in g g_{dw}⁻¹) as response variables. Hence, 21 response variables were considered in the analysis (i.e., the fractions of total protein, total carbohydrate, total lipid, 10 types of FAME, three PBPs (APC, CPC and PEC), chlorophyll A, total carotenoids [grouping carotenes and xanthophylls], cyanophycin, DNA, and RNA). This statistical analysis identified the main differences between cultures in BG11 and BG11_o media at the chemical composition level. The final biomass equations were constructed mostly from chemical composition data of cells in the exponential phase, but some data from cultures in stationary phase were also included when the biomass fraction of a given response variable was not statistically different for filaments in stationary phase.

Photoautotrophic

Photodiazotrophic

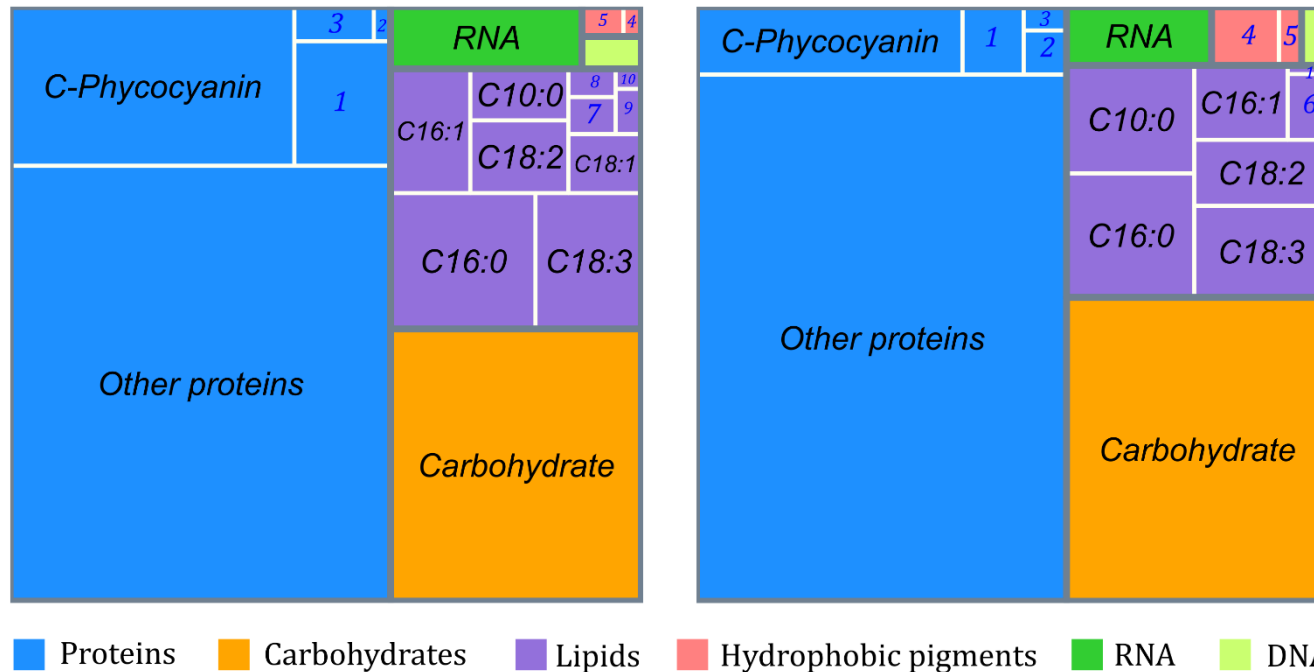


Figure 5.3. Whole-cell biomass composition of *Anabaena*

The size of each rectangle is proportional to the fraction of each component. Different colors and gray lines identify and separate the main composition categories. White lines divide subcategories within the main composition groups. Blue numbers represent the following subcategories: **1.** Allophycocyanin (APC), **2.** Phycoerythrocyanin (PEC), **3.** Cyanophycin, **4.** ChlA, **5.** CaroT, **6.** C18:1, **7.** C6:0, **8.** C14:0, **9.** C12:0, **10.** C18:0. The plot shows that the main differences in composition between photoautotrophic and photodiazotrophic cultures are the fractions of PBPs (e.g., CPC, APC, PEC), cyanophycin and hydrophobic pigments. The type of growth medium also affects lipid profiles.

Subsection 5.5.3 contains additional interpretations of the Two-way ANOVA statistical analysis.

The main differences at the chemical composition level ($p\text{-value} < 0.05$) between photoautotrophic and photodiazotrophic cultures were the fractions of DNA ($p\text{-value} = 0.0014$), RNA ($p\text{-value} = 0.0003$), chlorophyll A ($p\text{-value} = 8.13 \times 10^{-8}$), CPC ($p\text{-value} = 3.02 \times 10^{-6}$), APC ($p\text{-value} = 3.16 \times 10^{-7}$), PEC ($p\text{-value} = 0.030$), and cyanophycin ($p\text{-value} = 1.62 \times 10^{-5}$). Significant differences were also identified for fractions of fatty acid methyl esters derived from palmitoleic (C16:1, $p\text{-value} = 0.0002$), oleic (C18:1, $p\text{-value} = 0.0003$), and γ -linolenic (C18:3, $p\text{-value} = 0.01$) acids. *Anabaena* filaments presented a higher growth rate in BG11 medium with NaNO_3 , which can explain the higher content of nucleic acids. Moreover, growing the cells in the presence of NaNO_3 also stimulated a higher accumulation of nitrogen reserves in the form of CPC, APC, PEC, and cyanophycin. High availability of a ready-to-use nitrogen source as the nitrate ion, for which multiple transporters are encoded in the *Anabaena* genome [408], can explain higher fractions of nitrogen storage compounds. Higher fractions of ChlA were observed in photodiazotrophic cells and this correlates with the lower production of phycobilisomes (PBSs) in filaments requiring N_2 -fixation. While the molar PCB to ChlA ratio was 6.73 ± 0.86 in BG11 medium, it was only 0.38 ± 0.17 in BG11_o medium. The activity levels of fatty acid desaturases ($\Delta 9\text{FAD}$, $\Delta 12\text{FAD}$, and $\Delta 15\text{FAD}$) can explain the main changes on the lipid profiles of *Anabaena* filaments using different nitrogen sources. In cyanobacteria, fatty acid desaturases (FAD) introduce double bonds in C16:0 and C18:0 hydrocarbon chains [418], leading to changes in the lipid profile depending on the gene regulation responses. A recent study with the microalgae *Auxenochlorella pyrenoidosa*

demonstrated that high levels of NO_3 downregulate the activity of FAD enzymes, leading to lower content of monounsaturated (MUFA) and polyunsaturated (PUFA) fatty acids in microalgal cultures using NaNO_3 as nitrogen source [419]. However, nitrogen starvation also reduced the production of PUFA in the algae *Scenedesmus rubescens* and *Ettlia oleoabundans*, indicating downregulation of FAD genes expression [420, 421]. Although higher fractions of C16:1 and C18:3 lipids were observed in nitrogen-rich medium (BG11), consistent with studies in *Chlorella sorokiniana* and *Ettlia oleoabundans* [421, 422], further research is necessary to explain reduced accumulation of C18:1 lipids in photodiazotrophic *Anabaena* filaments. In this organism, explaining the regulation of FAD enzymes goes beyond a genetic on-off switch mechanism because diazotrophic cyanobacteria do not exhibit total nitrogen starvation [17, 423].

The next step in the construction of the biomass equations was to explain in more detail the composition of proteins, carbohydrates, lipids, carotenoids, and nucleic acids, using the metabolites listed in *DN1004*. The amino-acid composition of the protein fraction was calculated from the *Anabaena* proteome obtained from UniProt [411]. To do this, the cellular abundance of each proteinogenic amino acid was determined by combining protein amino-acid sequences with the TPM values (transcripts per kilobase million) of respective messenger RNA transcripts reported for photoautotrophic and photodiazotrophic *Anabaena* cells [424]. Following this strategy, a representative composition of the bulk protein in *Anabaena* ("Other proteins" field in Figure) was estimated using the amino-acid sequences of 5951 proteins, which represent 96.8% of the total proteins included in the *Anabaena* proteome (6148) [408]. The primary structure of proteins P07121 (*CpcA*) and P07120 (*CpcB*) served to estimate the amino-acid

composition of α and β subunits forming the CPC trimer. Likewise, the primary structures of P35796 (*PecA*), P35797 (*PecB*), P80555 (*ApcA1*), P80556 (*ApcD*), and P80557 (*ApcB*), were used to estimate the amino-acid composition of α and β subunits of PEC and APC. The biomass equations of *MDN1004* divide the total carbohydrate fraction in terms of four representative carbohydrates (i.e., glycogen, glucose, peptidoglycan, and lipopolysaccharide). While fractions of peptidoglycan, glycogen and lipopolysaccharides were adjusted from reference studies [346–348], the glucose equivalent represents the fraction of other carbohydrates from the biomass not described by the biomass equations. This fraction was calculated by subtracting reference fractions of glycogen, peptidoglycan, and lipopolysaccharide from the total measured carbohydrate content. A detailed lipid composition in terms of fractions of phosphoglycerides was assembled from the measured FAME fractions. In cyanobacteria, monogalactosyldiacylglycerols (MGDG), digalactosyldiacylglycerols (DGDG), sulfoquinovosyldiacylglycerols (SQDG), and phosphatidylglycerols (PG) are the main components of cell membranes and thylakoids, with negligible content of phosphatidylcholine, phosphatidylethanolamine, and phosphatidylserine [30]. Using MGDG (34%), DGDG (22.5%), SQDG (19.5%), and PG (24%) contents reported for *Nostoc* sp. PCC 7120 [425], the lipid composition was modelled assuming that each phosphoglyceride contained two fatty acid molecules of the same kind. From a literature review, it was determined that β -carotene, echinenone, myxoxanthophylls, canthaxanthin, and zeaxanthin are the main carotenoids produced by cyanobacteria of the genera *Nostoc* and *Anabaena* [426–429]. *Anabaena* myxoxanthophylls are the carotenoid glucoside pigments (3R,2'S)-Myxol 2'-alpha-L-fucoside and (3S,2'S)-4-Ketomyxol 2'-alpha-L-fucoside. The biosynthesis of these

pigments in *DN1004* was modelled considering γ -carotene as their most immediate precursor [427, 430, 431]. The nucleotide abundance of DNA was calculated from the genome sequence [408] to obtain the fractions of deoxyribonucleotides (dGTP, dCTP, dATP and dTTP). On the other hand, fractions of ribonucleotides (GTP, CTP, ATP and UTP), describing the RNA composition, were calculated from the nucleotide sequences of ribosomal RNA (rRNA), transfer (tRNA) and messenger RNA (mRNA) listed in the genome annotation. A global RNA composition was calculated considering 90% of rRNA, 5% tRNA, and 5% mRNA [348] .

The experimental information summarized in Figure 5.3 represents ~97.5% of the dry weight composition data used to determine *Anabaena* biomass equations. Fractions of inorganic ions and the soluble pool were not measured, but determined from reference values for *Synechocystis* sp. PCC 6803 (henceforth *Synechocystis*), *Anabaena cylindrica*, and *Escherichia coli* [204, 348, 432]. The fractions of these subgroups accounted for the remaining ~2.5% of the data used to construct the equations. As an improvement on the composition of the cyanobacterial soluble pool, the biomass equations of *DN1004* incorporate concentrations of the full set of vitamin B complex not considered in previous studies [204, 382]. The concentrations of thiamin (vitamin B1), riboflavin (vitamin B2), niacin (vitamin B3), pantothenate (vitamin B5), pyridoxal phosphate (vitamin B6), biotin (vitamin B7), folic acid (vitamin B9), and cobalamin (vitamin B12) were derived from studies on *Anabaena cylindrica*, *Arthrospira platensis* and *Arthrospira maxima* [13, 432]. Other vitamin contents considered in the biomass equations include phylloquinone (vitamin K1) and vitamin E (α -tocopherol) [433, 434].

The final step in specifying biomass equations was the incorporation of the ATP required for biosynthesis and maintenance. The ATP cost needs to be included because energy is required to generate biomass and perform metabolic functions like motility, maintenance of osmotic equilibrium, synthesis of macromolecules, and control of transmembrane gradients [369]. While the ATP cost required for biosynthesis was modelled after mixotrophic and autotrophic cells of *Synechocystis*, the maintenance ATP cost was derived from values reported for heterotrophic and autotrophic cells of the same model cyanobacterium [370, 371]. The total ATP required for biomass synthesis in *ΔDN1004* ($54 \text{ mmol g}_{\text{DW}}^{-1}$) was in agreement with the numbers presented in reference reconstructions for *Synechocystis* [204, 208] and *Nostoc* sp. PCC 7120 ($53.35 \text{ mmol g}_{\text{DW}}^{-1}$) [382]. The total ATP cost was similar in photoautotrophic and photodiazotrophic filaments of *Anabaena* because the nitrogen fixation reactions included additional ATP requirements for the heterocysts. Photoautotrophic and photodiazotrophic biomass equations describe the formation of *Anabaena* biomass from 132 metabolites. The molecular weights of photoautotrophic and photodiazotrophic biomass were exactly $1000 \text{ mg mmol}^{-1}$, which is consistent with the standard defined for GSMMs [368].

5.5.3 Statistical analysis of biomass composition data

Cellular composition changes over time and depends on the N-source of the growth medium. We collected global composition data of photoautotrophic and photodiazotrophic *Anabaena* cultures in exponential and stationary phase to identify the main differences. Two-way ANOVA is a statistical analysis commonly used to analyze the effect of two independent variables on a variable of interest. This analysis is equivalent

to a 2²-factorial analysis, where two factors, each one with two levels, determine the treatments of an experimental design. Table 5.2 summarizes the factors and treatments of factorial analysis for the biomass composition variables, as well as the number of biological replicates in each case. This factorial analysis revealed factors and interactions having an important effect on the values of 21 biomass composition variables: fractions of total protein, total carbohydrate, total lipid, 10 types of FAME, three PBPs (APC, CPC and PEC), ChlA, Carot (carotenes and xanthophylls), cyanophycin, DNA, and RNA.

Table 5.2. Two-Way ANOVA factors for biomass composition analysis

Culture type	N-source (Medium)	Culture phase	Biological replicates
Photoautotrophic	NaNO ₃ (BG11)	Exponential (3 to 6 days old)	3
Photoautotrophic	NaNO ₃ (BG11)	Stationary (12 to 20 days old)	3
Photodiazotrophic	N ₂ (BG11 _o)	Exponential (3 to 6 days old)	3
Photodiazotrophic	N ₂ (BG11 _o)	Stationary (12 to 20 days old)	5

Although the scientific community has been calling to limit statistical significance analyses [435], the use of p-values was useful to determine the most important differences in biomass composition for *Anabaena* cultures in BG11 and BG11_o media. Figure shows standardized effects of two factors (N-source and culture phase) and the interaction of both independent variables on the calculated fractions of the 21-biomass composition variables involved in our study. In this type of study, a plot of standardized effects for each response variable represents the effect of the independent variables is associated with the size of the horizontal bars. A threshold value usually determined by the confidence level (95% in this case) sets the limit between compatibility regions for

which statistically important effects are observed. With a significance level $\alpha = 0.05$, each bar surpassing the standardized effect threshold (vertical blue dashed line in Figure 5.4) indicates significant differences among biomass composition variables. In practical terms, this plot summarizes the main biomass composition differences to be considered in the construction of biomass equations for photoautotrophic and photodiazotrophic *Anabaena* cultures. The analysis of Figure 5.4 provided the following outcomes for each row:

- a) The growth phase affected the protein and carbohydrate fractions of *Anabaena* cultures, but the N-source did not. While the average protein fraction was higher in the exponential phase, the carbohydrate fraction increased for cultures in stationary phase. Besides, the N-source and the culture phase did not have a significant effect on the average of the total fraction of lipids.
- b) The N-source had a significant effect on the fractions of nucleic acids, but the growth phase did not present significant changes on DNA or RNA fractions. The content of nucleic acids was higher for photoautotrophic cultures. While the ChlA content of *Anabaena* filaments was significantly different for cultures using N_2 or $NaNO_3$ as N-sources, neither of the factors affected the average content of CarOT. Interestingly, the cells exhibited more ChlA content in BG11_o.
- c) The N-source affected the content of cyanobacterial nitrogen reserves. Fractions of C-phycocyanin, allophycocyanin, phycoerythrocyanin, and cyanophycin were strongly affected by the N-source. Photoautotrophic cultures growing with $NaNO_3$ presented a higher mean content of native nitrogen reserves compared to filaments depending on N_2 -fixation.

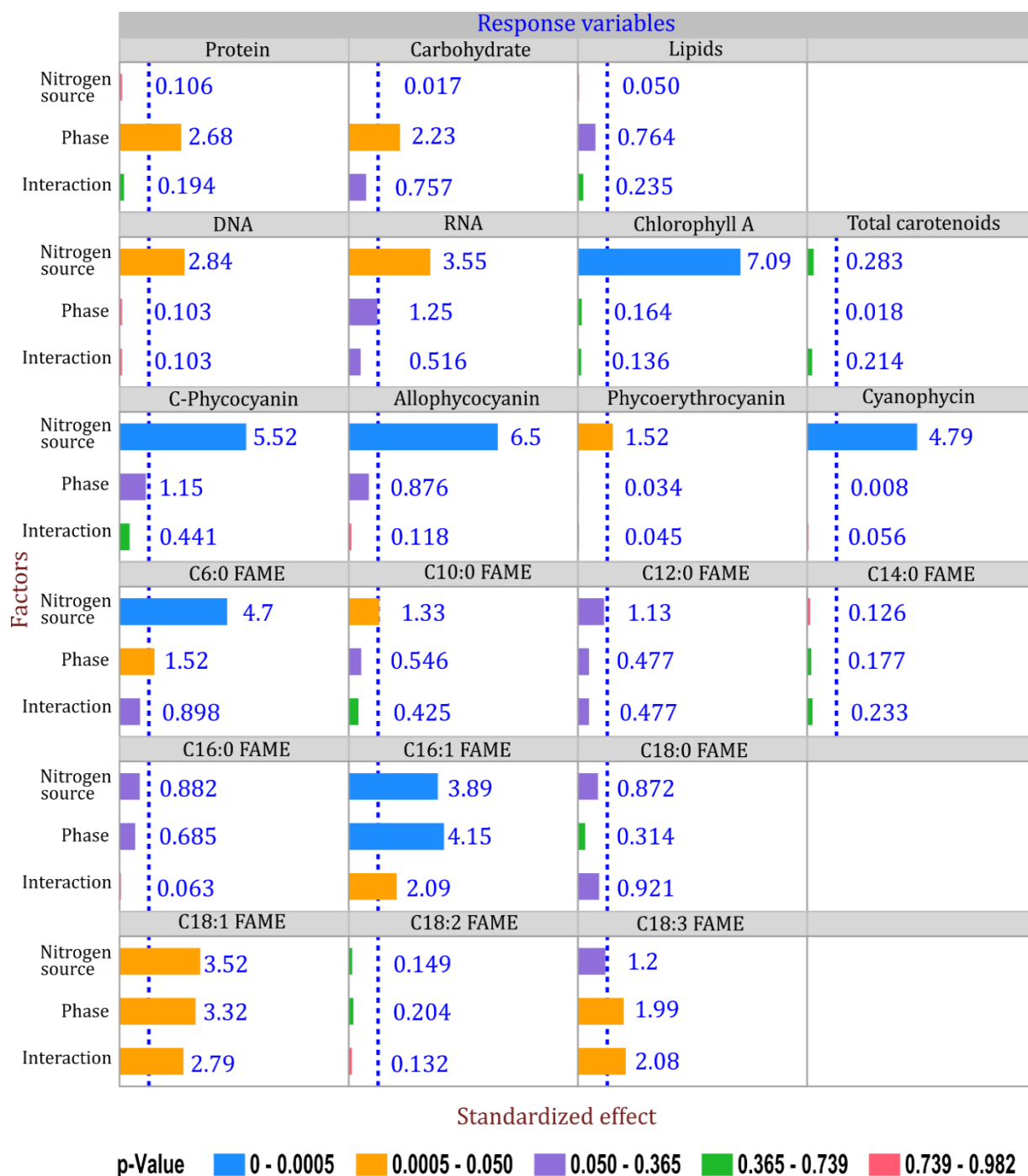


Figure 5.4. Stacked chart of standardized effects for composition data

This plot summarizes the results of the two-way ANOVA analysis. The standardized effects of N-source, growth phase, and the interaction of both factors on the mass fraction of cellular components were analyzed considering a confidence level of 95%. The size of bars represents the effect (logarithmic worth) of associated p-values. Blue and gold bars surpass the threshold logarithmic worth value of 1.30 (p-value ≤ 0.05), representing significant effects. Standardized effects calculated as $-\text{Log}(\text{p-value})$.

- d) We only observed a strong effect of the N-source on the measured fraction of FAME derived from hexanoic (C6:0) and decanoic (C10:0) acids. Cells growing in BG11 medium with NaNO_3 presented a significant increase in the production of C6:0 lipids, but the N_2 -fixing cells growing in BG11_o medium had higher content of C10:0 lipids. No significant differences were observed for the fractions of C12:0 nor C14:0 fatty acid methyl esters.
- e) We observed a significant impact of the N-source and the culture phase on the average content of FAME derived from palmitoleic acid (C16:1). The production of this monounsaturated (MUFA) fatty acid was significantly higher in stationary-phase cells growing with NaNO_3 .
- f) The type of medium (N-source) and the growth phase also had important effects on the average fraction of FAME produced from oleic acid moieties (C18:1). However, only the growth phase affected the content of FAME produced from lipids containing γ -linolenic acid (C18:3). No significant effects on the composition of linoleic acid (C18:2) lipids were observed after changing the N-source or the culture phase. Cultures growing with NaNO_3 presented higher fractions of C18:1. Moreover, the fractions of C18:3 FAME decreased during the stationary phase.

5.5.4 Experimentally determined metabolic constraints

Resolving a GSMM through FBA relies heavily on defining adequate minimum and maximum limits for the metabolic fluxes through reactions of interest. These constraints restrict the flow of metabolites through the metabolic network, making it possible to calculate theoretical flux values for the entire network, even without detailed kinetic

parameters [362, 364]. Physiological growth experiments as well as target metabolomics analysis were carried out to determine the metabolic constraints associated with light availability, N-source uptake, and biomass composition of *Anabaena* under culture conditions. These results are summarized in Table 5.3. Although the experimental growth rate parameters were not used as model constraints, they were used to iterate the CO₂ and bicarbonate flux values needed for the observed biomass production rates in photoauto- and photodiazotrophic cultures.

Table 5.3. Growth rate parameters and model constraints

Average values and standard deviations of experimental growth rates and model constraints were calculated from at least 3 independent measurements.

Parameter	Photoautotrophic (BG11)	Photodiazotrophic (BG11 _o)	Type of variable
μ_{\max} (day ⁻¹)	0.471 ± 0.161	0.429 ± 0.080	Experimental growth rate
$y_{\infty} = \ln(\text{OD}_{730\max}/\text{OD}_{730o})$	2.318 ± 0.169	2.579 ± 0.108	
Growth rate (day ⁻¹)	0.680 ± 0.232	0.619 ± 0.116	
Growth rate (h ⁻¹)	0.028 ± 0.010	0.026 ± 0.005	
Min. NO ₃ metabolic flux	0.013 ± 0.004	-	Model constraints
Max. NO ₃ metabolic flux	0.244 ± 0.023	-	
Min. N ₂ metabolic flux	-	0.010 ± 0.001	
Max. N ₂ metabolic flux	-	0.126 ± 0.017	
Min. CPC metabolic flux	5.84E-6 ± 4.1e-7	5.11E-6 ± 1.7E-7	
Max. CPC metabolic flux	1.47E-4 ± 1.03e-5	1.03E-4 ± 2.74E-6	
Max. Photon metabolic flux	87.09 ± 9.32	102.53 ± 10.97	

Metabolic fluxes given in mmol g_{DW}⁻¹ h⁻¹

The experimental growth rates and generation times in exponential phase were calculated from the μ_{\max} parameter in the saturation growth model (see Table 5.3 and Figure 5.5). Growth kinetics of photoautotrophic cultures in BG11 medium and photodiazotrophic cultures in BG11_o medium was determined from at least four biological replicates. After fitting optical density values to the saturation growth model, the average

growth rates were $0.028 \pm 0.010 \text{ h}^{-1}$ under photoautotrophy and $0.026 \pm 0.005 \text{ h}^{-1}$ under photodiazotrophy. These numbers are consistent with the average growth rate of 0.0158 h^{-1} reported for photodiazotrophic cultures of *Anabaena* at lower PPFD [382] and the mean growth rate of 0.085 h^{-1} for autotrophic cultures of *Synechocystis* [204, 370], which can grow up to three times faster than filamentous cyanobacteria [328]. Based on the fitted saturation model, the exponential phase lasted from day 0 through day 10, followed by the stationary phase.

Uptake rates of NaNO_3 and N_2 were determined to constrain *DN1004*. Ultimately, these rates were transformed into NO_3 and N_2 metabolic fluxes entering the filaments. The minimum and maximum values of these fluxes were estimated from first order kinetic models describing NO_3 consumption and N_2 fixation (see Figure 5.6). For cultures in BG11 medium, NO_3 concentration was analyzed over the course of growth (28 days). For photodiazotrophic filaments (BG11_o), the N_2 fixation rate was estimated by measuring the change in the total nitrogen content over time (20 days).

The minimum flux of NO_3 was calculated using the first order reaction constant for NO_3 consumption ($0.0504 \pm 0.005 \text{ day}^{-1}$) and the total nitrate consumed per gram of biomass produced at the end of the exponential phase ($522 \pm 104 \text{ mg NO}_3 \text{ g}_{\text{DW}}^{-1}$ after 11.5 days). The maximum NO_3 flux was calculated differently to account for the high concentration of NaNO_3 in the liquid. The maximum flux of NO_3 allowed into *Anabaena* filaments in BG11 medium was three times the number calculated from the NO_3 consumption constant and the NO_3 consumed per gram of biomass in the early exponential phase ($3292 \pm 155 \text{ mg NO}_3 \text{ g}_{\text{DW}}^{-1}$ after 1.25 days).

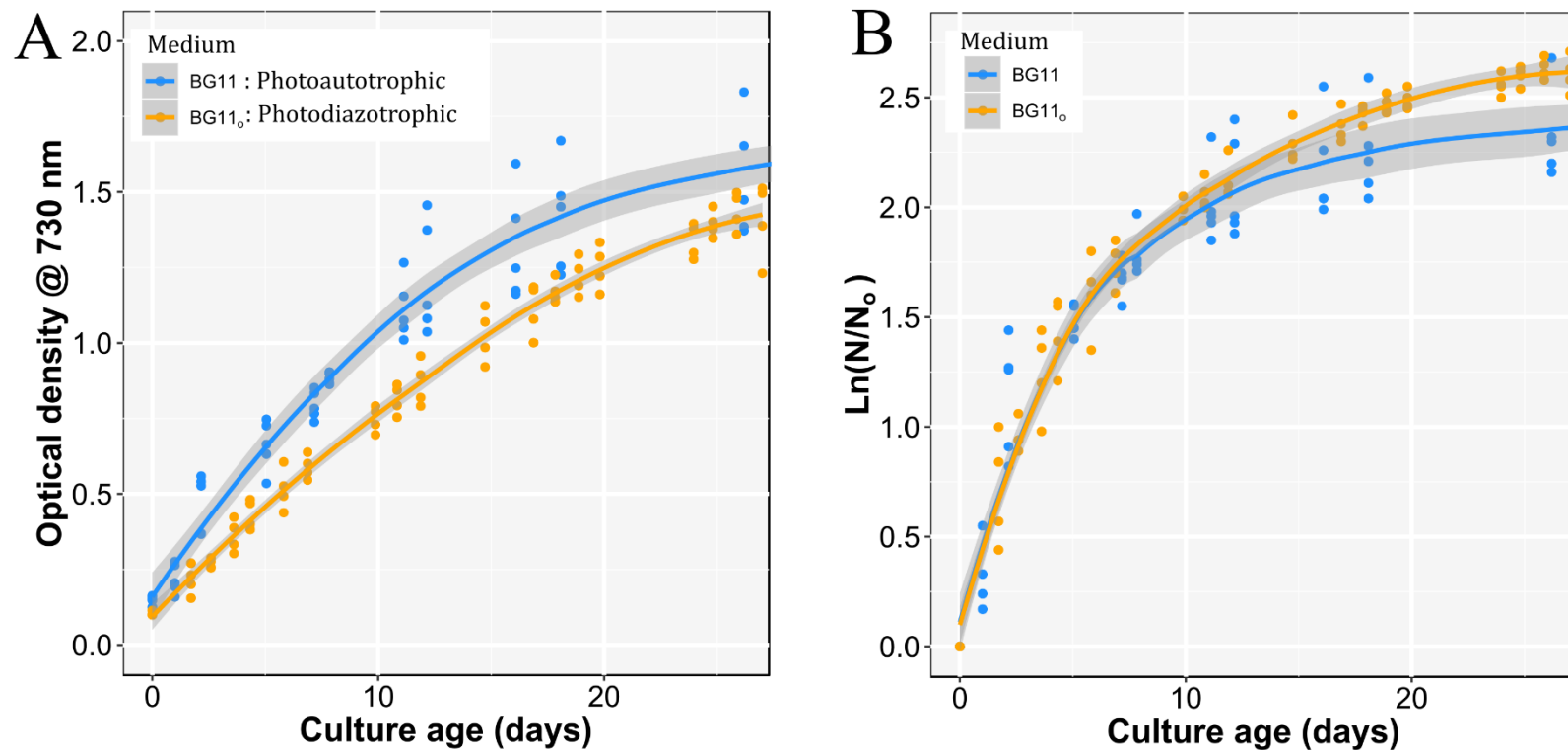


Figure 5.5. Growth kinetics of *Anabaena* cultures.

Dots represent experimental measurements of biological replicates (five replicates in BG11 and four in BG11₀), solid lines represent fitting to saturation model, and shaded area indicates the 95% confidence interval of the mean. A: Growth kinetics based on OD₇₃₀ observations. B: Transformation of optical density data to saturation model, where $N = \text{OD}_{730}$ and $N_0 = \text{OD}_{730}$ at $t = 0$ days. Non-linear regression tool from JMP Pro 14 software was used to fit the experimental data to Equation 3-1, where μ_{max} represents the intrinsic rate of natural increase and y_{∞} represents the maximum ratio between the actual and the initial optical densities at 730 nm (OD₇₃₀).

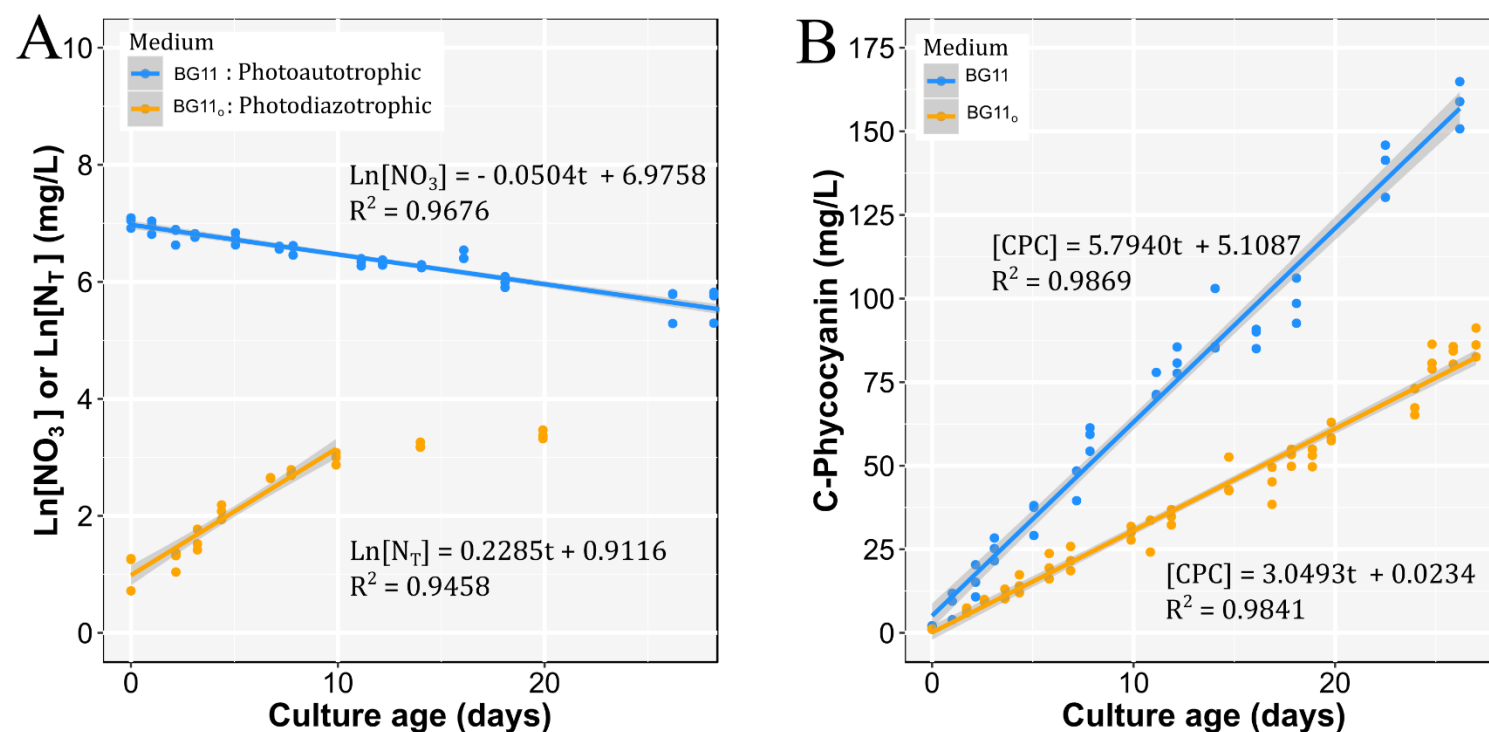


Figure 5.6. NO_3 consumption, N_2 -fixation and CPC production rates

A: Nitrate $[\text{NO}_3]$ consumption (for cultures in BG11) and nitrogen fixation (cultures in BG11_o). The natural log transformation of NO_3 and total nitrogen concentration $[\text{N}_T]$ measurements was used to fit these data to first-order kinetic models, providing consumption and fixation reaction constants. The full set of NO_3 consumption data was considered for the analysis, but only data from the exponential phase were used to analyze N_2 -fixation kinetics. B: A zero-order kinetic model reveals constant production rates of CPC in photoautotrophic (BG11) and photodiazotrophic (BG11_o) filaments. The shaded area represents the 95% confidence interval of the average values for each line.

The minimum flux of N_2 into photodiazotrophic filaments in BG11_o was estimated using the first order nitrogen fixation constant ($0.2285 \pm 0.0248 \text{ day}^{-1}$) and the total nitrogen fixed per gram of biomass produced by the end of the exponential phase ($30 \pm 2 \text{ mg N}_T \text{ g}_{DW}^{-1}$ after 11 days). The maximum flux of atmospheric nitrogen allowed into *Anabaena* in BG11_o medium was ten times the number calculated from the N_2 fixation constant and the total nitrogen fixed per gram of biomass in the early exponential phase ($37 \pm 6 \text{ mg N}_T \text{ g}_{DW}^{-1}$ after 4 days). This was done to account for an almost unlimited supply of N_2 from the atmosphere. Table 5.3 contains the minimum and maximum values of calculated metabolic fluxes of NO_3 and N_2 .

CPC concentration data were used to calculate pigment production rates in *Anabaena* cultures and further constrain *i*DN1004. A constant production of CPC was observed in photoautotrophic and photodiazotrophic filaments. By constraining the production of CPC, the main PBP in *Anabaena*, *i*DN1004 calculated metabolic fluxes through different metabolic reactions needed to meet the requirements of the biomass equation. This outcome was useful to identify the most active internal metabolic routes. Using this approach, experimental data on biomass generation, nutrient uptake and metabolite production were combined to predict the fluxes through amino acid producing reactions. CPC concentration data were monitored during the growth evaluation period (28 days) and fitted to a zero-order kinetic model. Using biomass concentration estimates from the early and late exponential phase, the CPC production constant was transformed into minimum and maximum metabolic fluxes. As presented in Figure 5.6, the CPC production constants for *Anabaena* cultures in BG11 and BG11_o media were $5.794 \pm 0.409 \text{ mg L}^{-1} \text{ day}^{-1}$ and $3.0493 \pm 0.081 \text{ mg L}^{-1} \text{ day}^{-1}$ respectively. The upper limit for the

CPC metabolic flux was calculated using biomass concentration data of cultures in the early exponential phase, when the metabolic activity was higher. Furthermore, the lower limit for the CPC metabolic flux was estimated with data from late exponential phase, when metabolism starts to slow down before entering the stationary phase. In photoautotrophic cultures, the biomass concentration was $45.85 \pm 2.7 \text{ mg}_{\text{DW}} \text{ L}^{-1}$ on day one, yielding a maximum CPC metabolic flux of $1.47 \times 10^{-4} \text{ mmol g}_{\text{DW}}^{-1} \text{ h}^{-1}$. On the other hand, the biomass concentration was $1152 \pm 67 \text{ mg}_{\text{DW}} \text{ L}^{-1}$ after 12.16 days, resulting in a minimum CPC metabolic flux of $5.84 \times 10^{-6} \text{ mmol g}_{\text{DW}}^{-1} \text{ h}^{-1}$. In photodiazotrophic cultures, the biomass concentration was $34.28 \pm 2.0 \text{ mg}_{\text{DW}} \text{ L}^{-1}$ after 1.72 days, yielding a maximum CPC metabolic flux of $1.03 \times 10^{-4} \text{ mmol g}_{\text{DW}}^{-1} \text{ h}^{-1}$. Conversely, the biomass concentration was $692 \pm 39 \text{ mg}_{\text{DW}} \text{ L}^{-1}$ after 11.88 days, resulting on a minimum CPC metabolic flux of $5.11 \times 10^{-6} \text{ mmol g}_{\text{DW}}^{-1} \text{ h}^{-1}$. The slowest production of CPC in photodiazotrophic cultures was consistent with the N-limiting condition proper of these cells. Table 5.3 summarizes calculated CPC metabolic fluxes for *Anabaena* cultures.

Light source and availability affect the metabolic activity of autotrophic cultures of cyanobacteria. Hence, maximum photon fluxes entering the cells were also calculated from experimental conditions. The PPFD in the incubator was $100 \pm 10 \mu\text{mol m}^{-2} \text{ s}^{-1}$. The light intensity was checked with a lux meter and converted to photon flux density using a factor of $0.0135 \mu\text{mol m}^{-2} \text{ s}^{-1} \text{ lux}^{-1}$ (white fluorescent lamps). PPFD values were transformed into photon metabolic fluxes by estimating the mass and surface area of the cells. These flux values were used as the maximum available light for cultures in BG11 and BG11_o. The surface area of heterocysts and vegetative cells was estimated from cell diameter measurements and mass per cell estimates resulting from empirical relations

for biomass and cell density (see subsections 3.4 and 3.10). A reference OD_{730} of 0.66 was used to approximate biomass ($\sim 350 \text{ mg L}^{-1}$) and cell densities ($\sim 3.3 \times 10^9 \text{ cells L}^{-1}$) of cultures in mid-exponential phase. While the maximum photon flux for photoautotrophic cultures was calculated assuming 100% of vegetative cells, the maximum photon flux for photodiazotrophic cultures was estimated considering 15% heterocysts and 85% vegetative cells. The percent of heterocysts resulted from flow cytometry runs. The resulting upper limits for the photon uptake reactions (maximum light-availability) were $87.1 \pm 9.3 \text{ mmol g}_{\text{DW}}^{-1} \text{ h}^{-1}$ (photoautotrophic) and $102.5 \pm 11.0 \text{ mmol g}_{\text{DW}}^{-1} \text{ h}^{-1}$ (photodiazotrophic).

5.5.5 Phycocyanobilin (PCB) production rate and nutrient requirements

Using experimentally determined growth constraints, as well as *Anabaena* growth specific biomass equations, the FBA algorithm calculated the metabolic fluxes through the reactions listed in fDN1004 . This strategy was useful to find a set of fluxes satisfying the constraints imposed by our observations of NO_3 uptake, N_2 fixation, CPC production, and maximum theoretical light availability. In other words, rates of NO_3 , N_2 , and light uptake, as well as product biosynthesis, were used to estimate intracellular metabolic fluxes. The flux distribution estimated demands of inorganic carbon (C_i : combined flux of CO_2 and $[\text{HCO}_3^-]$) and photons needed to sustain cellular growth. The chemical composition measurements incorporated in the biomass equations provided a way to quantify the differences in intracellular metabolic fluxes when *Anabaena* filaments grew with different nitrogen sources. fDN1004 was oriented towards the analysis of metabolic potentials of these cyanobacteria to guide the selection of pathways and branching

metabolites to produce native and non-native nitrogen-compounds (e.g., secondary metabolites). PCB was selected as the reference metabolite to compare the model predictions with the experimental observations because it is the most abundant chromophore in *Anabaena* phycobiliproteins [337, 416]. Moreover, the commercialization of the blue pigment CPC has become one of the most successful large-scale applications of cyanobacterial biomass [17, 114, 297].

The enzyme phycocyanobilin:ferredoxin oxidoreductase (EC 1.3.7.5) catalyzes the conversion of biliverdin to PCB [436]. This reaction was included in *DN1004* as part of the porphyrin and chlorophyll metabolism subsystem (see reaction “PHYCYFX” in Table B.1). Observed and simulated fluxes through the PCB production reaction were compared to assess the accuracy of the metabolic flux calculated by the FBA algorithm. FBA predicted metabolic fluxes of $2.92 \times 10^{-4} \text{ mmol g}_{\text{DW}}^{-1} \text{ h}^{-1}$ and $1.04 \times 10^{-4} \text{ mmol g}_{\text{DW}}^{-1} \text{ h}^{-1}$ through this reaction for photoautotrophic and photodiazotrophic filaments, respectively. These results are consistent with the experimental observations of CPC production rates in BG11 and BG11_o media (see Figure 5.6), in which the blue pigment is produced more slowly in diazotrophic filaments. In the experiments, CPC accounted for 76.87% mole of the phycobiliproteins in photoautotrophic cultures and 73.97% mole in photodiazotrophic cultures. Moreover, PCB accounted for 99.64% of the chromophores in the PBPs of photoautotrophic cultures and 96.83% in the PBPs of photodiazotrophic cultures. Total PCB production rates were calculated from CPC production rates using these fractions as correction factors, considering that each subunit of CPC contains three molecules of PCB chromophore [416]. Starting from CPC production rates (Figure 5.6) and biomass concentration relations (Figure 5.5 and Figure 3.1), the experimental metabolic flux

through the PCB biosynthesis reaction was $2.89 \times 10^{-4} \pm 2.04 \times 10^{-5} \text{ mmol g}_{\text{DW}}^{-1} \text{ h}^{-1}$ for photoautotrophic cultures on day two. Similarly, the observed metabolic flux through the PCB biosynthesis reaction was $1.02 \times 10^{-4} \pm 2.72 \times 10^{-6} \text{ mmol g}_{\text{DW}}^{-1} \text{ h}^{-1}$ for photodiazotrophic cultures after 4.5 days. These results suggest that FBA-predicted fluxes accurately represent the synthesis of PCB in photoautotrophic and photodiazotrophic *Anabaena* cultures in exponential phase.

Based on stoichiometry, FBA calculated the flux of nitrogen source (NO_3 or N_2) required to meet the biomass objective function. At observed growth rates, the theoretical NO_3 flux required for photoautotrophic filaments was $0.237\text{-mmol g}_{\text{DW}}^{-1} \text{ h}^{-1}$. Meanwhile, the required flux of N_2 into photodiazotrophic filaments was $0.103\text{-mmol g}_{\text{DW}}^{-1} \text{ h}^{-1}$. As presented in Table 5.3, these flux values fall into the constraint limits calculated from experimental data. Since the flux values are closer to the upper limits of their respective metabolic flux constraints, they should represent the condition of highly metabolically active cells, such as *Anabaena* filaments at the beginning of the exponential phase.

The experimentally determined growth rate parameters were used in combination with iDN1004 and FBA to estimate the inorganic carbon (C_i) fixation potential of *Anabaena* cultures. To do this, the combined flux of CO_2 and HCO_3^- uptake reactions (“EX_co2_e” and “EX_hco3_e” in Table B.1) was iterated until the flux values through the photoauto- and photodiazotrophic biomass objective equations were similar to the average observed growth rates (i.e., 0.0283 h^{-1} and 0.0258 h^{-1}). As a result, the total estimated C_i fixation fluxes of photoautotrophic and photodiazotrophic cultures of *Anabaena* were 1.187 and $1.083 \text{ mmol g}_{\text{DW}}^{-1} \text{ h}^{-1}$, respectively. These C_i uptake fluxes are consistent with the $3.7 \text{ mmol g}_{\text{DW}}^{-1} \text{ h}^{-1}$ C_i uptake flux reported for *Synechocystis*, which grows at a faster rate of

0.085 h⁻¹ [204, 370]. After determining the C_i fixation potential of *Anabaena* filaments, it was desired to calculate the portions of the C_i flux entering the cells in the form of CO₂ and HCO₃⁻. This was done to provide a more realistic quantitative description of the cyanobacterial carbon concentration mechanism (CCM) in *DN1004*. Photoauto- and photodiazotrophic *Anabaena* cultures grew in liquid media with initial sodium carbonate (Na₂CO₃) concentration of 1.88x10⁻⁴ M and pH 8.0. Considering the first base dissociation constant (K_{b1}=1.72x10⁻⁴ [437]) of the carbonate ion (CO₃²⁻) at 25°C, the initial concentration of HCO₃⁻ from the liquid media was estimated at 1.13x10⁻⁴ M. The concentration of dissolved CO₂ in the liquid media (1.33x10⁻⁵ M) was calculated using Henry's constant (0.032 mol L⁻¹ bar⁻¹ [438]) with an average concentration of 410 ppm of CO₂ in the atmosphere at 28 °C (partial pressure of 4.15x10⁻⁴ bar). After also accounting for the formation of carbonic acid (H₂CO₃) and HCO₃⁻ from dissolved CO₂ [439], a CO₂ concentration to HCO₃⁻ concentration ratio of 0.12 was determined for BG11 and BG11_o media at the beginning of the growth experiments. A similar procedure was used to estimate the dissolved CO₂ to HCO₃⁻ ratio in the liquid media at the end of the growth experiments. Considering only 12% of the initial Na₂CO₃ left (2.26x10⁻⁵ M) and pH 10, a ratio of CO₂ concentration to HCO₃⁻ concentration of 0.98 was calculated for the end of the growth experiments. These different ratios were used to define that, in average, 70% of the C_i flux entered the cells in the form HCO₃⁻ and 30% in the form of dissolved CO₂. Although these fractions are not exact, they are consistent with the fact that cyanobacterial CCMs have higher affinities for HCO₃⁻ than CO₂ [440, 441]. In other words, while atmospheric CO₂ represented a constant supply of C_i for *Anabaena* cultures over time, thermodynamics suggested that most of the C_i used for cyanobacterial growth was

obtained from the Na_2CO_3 in BG11 and BG11_o media, at least during the early stages of cellular growth.

Specific photon flux requirements for photoauto- and photodiazotrophic cultures of *Anabaena* were obtained from FBA predictions. Total photon flux values of $11.79 \text{ mmol g}_{\text{DW}}^{-1} \text{ h}^{-1}$ (photoautotrophic) and $9.36 \text{ mmol g}_{\text{DW}}^{-1} \text{ h}^{-1}$ (photodiazotrophic) were obtained through the reaction listed as “PRISM_fluorescent_warm_18W” in *i*DN1004 (see Table B.1). However, not all these photons can excite the photosystems in cyanobacteria and the spectral decomposition reactions were useful to quantify the portions of visible light that promoted photosynthesis. CPC-producing cyanobacteria can use blue, red and orange radiations to start photosynthesis. While blue and red light excite the chlorophyll A in photosystems I and II, orange radiations excite the phycobilisomes attached to photosystem II [50, 328]. This condition was represented in *i*DN1004 by letting only five components of the fluorescent light spectral decomposition reach the thylakoid compartment [u]. These effective radiation reactions are listed in Table B.1 as “Photon437u” (406 to 454 nm, indigo/blue), “Photon438u” (378 to 482 nm, violet/blue), “Photon646u” (608 to 666 nm, orange/red), “Photon673u” (659 to 684 nm, red), and “Photon680u” (662 to 691 nm, red). The FBA-predicted combined flux values through these reactions entering the thylakoids were $7.27 \text{ mmol g}_{\text{DW}}^{-1} \text{ h}^{-1}$ (photoautotrophic) and $5.77 \text{ mmol g}_{\text{DW}}^{-1} \text{ h}^{-1}$ (photodiazotrophic). Considering the PPFD flux values calculated from cell diameter, mass and surface area, photoauto- and photodiazotrophic filaments received maximum photon fluxes of $87.1 \pm 9.3 \text{ mmol g}_{\text{DW}}^{-1} \text{ h}^{-1}$ and $102.5 \pm 11.0 \text{ mmol g}_{\text{DW}}^{-1} \text{ h}^{-1}$, respectively. After comparing these maximum photon flux values with the corresponding combined flux of effective radiations reaching the thylakoids, average

photosynthetic efficiencies were calculated for photoautotrophic (8.35%) and photodiazotrophic (5.63%) *Anabaena* filaments. These values are consistent with the maximum photosynthetic efficiency of 10% reported for cyanobacteria [32, 442]. Table 5.4 summarizes the metabolic fluxes through the reactions involved in PCB synthesis, C_i fixation and light requirements. Experimental and simulated values were compared when possible. Small differences between these numbers suggest that other metabolic fluxes predicted by the model provide a good estimate of the metabolic activity of *Anabaena*.

Table 5.4. Comparison of experimental and simulated metabolic flux values.

Variable	Photoautotrophic cultures (BG11)			Photodiazotrophic cultures (BG11 _o)		
	Experimental	Simulation	Abs Error	Experimental	Simulation	Abs Error
Growth rate (h^{-1})	2.831E-2	2.830E-2	0.05%	2.577E-2	2.580E-2	0.11%
PCB production flux	2.891E-4	2.918E-4	0.94%	1.025E-4	1.041E-4	1.56%
Total C_i uptake flux	-	1.187	-	-	1.083	-
HCO_3^- flux		0.831			0.758	
CO_2 flux		0.356			0.325	
Total photon flux	-	11.790	-	-	9.365	-
Effective photon flux	-	7.269	-	-	5.774	-
Max PPFD flux	87.09	-	-	102.53	-	-
Photosynthetic efficiency	-	8.35%	-	-	5.63%	-

Flux units are $\text{mmol g}_{\text{DW}}^{-1} \text{h}^{-1}$

5.5.6 Prediction of amino-acid production flux values with FBA

After confirming the accuracy of the FBA analysis to predict PCB production fluxes (see Table 5.4), iDN1004 was used to calculate the combined fluxes through amino-acid

producing reactions. The size of these combined fluxes was analyzed to determine the amino acids with the highest potential to become branching points for the introduction of biosynthetic pathways in *Anabaena*, aiming to obtain higher yields of secondary metabolites and high-value nitrogen compounds. The reactions considered to calculate the combined production flux of each amino acid within the network are also presented in data set 9. While positive fluxes describe forward reactions (happening from left to right); negative fluxes describe reverse reactions (going from right to left). The general sequence of metabolic events is the following. Initially, CO_2 , HCO_3^- , phosphates, and metallic ions enter the cell coming from the growth medium (extracellular). While ABC transporters, TRAP systems, symporters, and antiporters bring extracellular metabolites directly into the cytoplasm, passive diffusion of nutrients occurs first into the periplasm, and from there into the cytoplasm. The spectral decomposition reaction of light from white fluorescent lamps indicates the type and wavelengths of photons available for the light phase of photosynthesis. These reactions occur in the thylakoids, where only red, blue and orange radiations excite photosystems I and II. While chlorophyll A is directly excited by blue and red radiations, light-harvesting complexes (i.e., phycobilisomes) capture orange radiations as part of the chromatic acclimation mechanism [328]. Oxygen diffuses out of the cell as a product of the water-splitting reaction in photosystem II (only vegetative cells). The ATP and NADPH generated through photosynthesis fuel the CO_2 fixation reactions of the Calvin cycle. Carbon fixation proceeds in the carboxysome and sugars are synthesized from 3-phosphoglycerate. Flux values through the Calvin cycle reactions are among the highest in the system because they sustain the autotrophic metabolic networks of *Anabaena* in non-diazotrophic and diazotrophic media. Glucose, the main

product of photosynthesis, goes through the glycolytic pathway to produce phosphoenolpyruvate (*pep*) and pyruvate (*pyr*). The glycolytic and the pentose phosphate pathways connect the products of CO₂ fixation reactions with the citric acid cycle reactions (TCA cycle), where 2-oxoglutarate or α-ketoglutarate (*akg*) is produced. *Pep*, *pyr* and *akg* become the most important precursors of amino acids, providing the carbon skeleton. *Anabaena* can use multiple sources of nitrogen to transform these skeletons into amino acids and other metabolites. In this model, photoautotrophic filaments consume NO₃ from the medium, but photodiazotrophic filaments fix N₂. The network further transforms amino acids and products of the central carbon metabolism into nucleotides, pigments, cofactors, vitamins, lipids, cyanophycin, peptidoglycan, lipopolysaccharides, and waste compounds (metabolic sinks). The cell uses amino acids, PCB, and phycoviolobilin (PVB) to assemble CPC, APC, and PEC. At the end, the metabolic fluxes through the biomass equations describe the FBA predicted growth rates of photoautotrophic and photodiazotrophic cultures.

Figure 5.7 shows the reactions and metabolic fluxes describing the biosynthesis of eight amino acids with the highest combined production flux values as predicted by FBA on *DN1004*: glutamate (*glu-L*), aspartate (*asp-L*), threonine (*thr-L*), glycine (*gly*), valine (*val-L*), glutamine (*gln-L*), alanine (*ala-L*), and serine (*ser-L*). Given that FBA provides one possible solution among multiple alternatives describing the metabolic map [362, 364], Figure 5.7 only represents one of the intracellular routes that leads to the production of cyanobacterial amino acids.

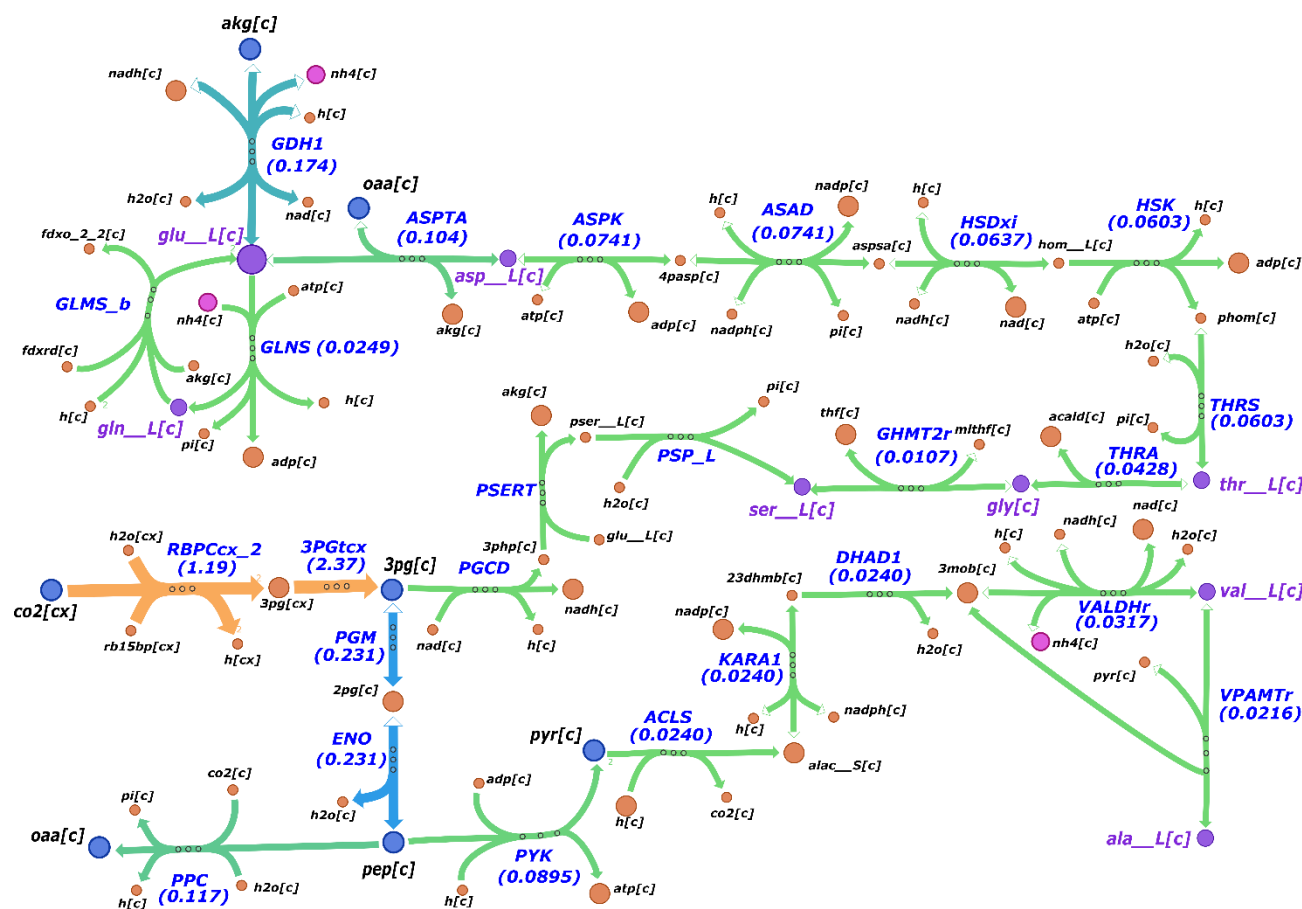


Figure 5.7. Amino acid production sub-network of *Anabaena*.

Network summarizes flux partitioning through 25 amino acid production reactions. Blue numbers next to each reaction name indicate FBA-calculated fluxes in $\text{mmol g}_{\text{DW}}^{-1} \text{h}^{-1}$. Dark blue circles represent essential precursor metabolites pyruvate (*pyr*), phosphoenolpyruvate (*pep*), 2-oxoglutarate (*akg*), oxaloacetate (*oaa*), 3-phosphoglycerate (*3pg*), and carbon dioxide (*co2*). Gold arrows indicate very high fluxes ($> 1 \text{ mmol g}_{\text{DW}}^{-1} \text{h}^{-1}$), and green arrows represent moderate fluxes ($< 0.15 \text{ mmol g}_{\text{DW}}^{-1} \text{h}^{-1}$), with blue flux arrows showing relatively high fluxes. Glutamate (*glu-L*) biosynthesis from *akg* represents the most important amino-acid biosynthesis reaction, feeding the synthesis of glutamine (*gln-L*) and aspartate (*asp-L*). Threonine (*thr-L*), glycine (*gly*), and serine (*ser-L*) can be produced from aspartate or *3pg*, the highly abundant product of carbon fixation. These three amino acids represent key branching points for secondary metabolite synthesis in autotrophic organisms. Valine and alanine are also important branching point amino acids derived from pyruvate. These fluxes resulted after using the photoautotrophic biomass equation for filaments growing in BG11 medium with NO_3

Figure 5.7 represents 25 reactions through the pathways that produce the most abundant proteinogenic amino acids, according to FBA. The name of each reaction is presented in blue letters with numbers in parenthesis showing the FBA-predicted value of the corresponding metabolic flux. The reactions without flux value represent alternative routes involved in amino-acid production. The production steps of the eight amino acids presented in the subnetwork are depicted with purple circles. The incorporation of ammonium (NH_4^+) coming from metabolized nitrogen sources is represented by pink circles. Important carbon compounds involved in the amino-acid biosynthesis process are shown as blue circles. The remaining metabolites participating in these reactions are presented as orange circles, and their size does not necessarily represent abundance. The fluxes are color coded to show the relative abundance of each reaction within the amino-acid subnetwork: orange arrows indicate flux values higher than $1 \text{ mmol g}_{\text{DW}}^{-1} \text{ h}^{-1}$, blue arrows represent flux values between 0.15 and $1 \text{ mmol g}_{\text{DW}}^{-1} \text{ h}^{-1}$, and green arrows represent reactions with flux values under $0.15 \text{ mmol g}_{\text{DW}}^{-1} \text{ h}^{-1}$. While filled arrowheads represent the default direction of each reaction, blank arrowheads indicate reversibility. In *Anabaena* cells, the synthesis reactions of glutamate (*glu-L*) and glutamine (*gln-L*) represent essential steps to produce other amino acids because they are part of the glutamine synthetase-glutamate synthase (GS/GOGAT) cycle for nitrogen assimilation. In Figure 5.7 (blue reaction on top left corner), these essential steps are represented by the *glu-L* producing reaction “GDH1”, and the *gln-L* cycle composed by “GLNS” and “GLMS_b”. In reality, this cycle is more complex in cyanobacteria and it is subject to strong regulation associated with nitrogen control [443]. The *glu-L* production reaction carries the largest flux among the amino-acids and directly relates to the large combined

production flux of glutamate, which is necessary to synthesize other metabolites. From the FBA predicted fluxes for “GDH1”, “GLNS”, and “ASPTA”, it was calculated that ~72% of the total *glu-L* flux ($0.174 \text{ mmol g}_{\text{DW}}^{-1} \text{ h}^{-1}$) is needed to produce *asp-L* ($0.104 \text{ mmol g}_{\text{DW}}^{-1} \text{ h}^{-1}$), and *gln-L* ($0.0249 \text{ mmol g}_{\text{DW}}^{-1} \text{ h}^{-1}$). This result indicates that *glu-L*, *gln-L* and *asp-L* represent the most important amino acids available for secondary metabolite biosynthesis in *Anabaena*. Figure also suggest that 58% of the *asp-L* flux ($0.0603 \text{ mmol g}_{\text{DW}}^{-1} \text{ h}^{-1}$) is ultimately used to produce *thr-L*, *gly*, and *ser-L* (“THRS”, “THRA”, and “GHMT2r” reactions). Interestingly, these three amino acids can also be synthesized from 3-phosphoglycerate (*3pg*), a highly abundant product of the Ribulose-bisphosphate carboxylase reaction (“RBPCcx_2”, orange reaction to the left). Given that these amino acids are produced from major metabolic routes, active in cyanobacteria during autotrophic growth with a constant supply of nitrogen source, *Anabaena* cultures should produce significant amounts of *thr-L*, *gly*, and *ser-L*, which are precursors of valuable secondary metabolites. The significant values of the metabolic fluxes through *val-L* and *ala-L* producing reactions (“VALDHr” and “VPAMTr”) can be related to the relatively high abundance of *pyr*, an essential precursor derived from *pep*, which is derived from *3pg* or oxaloacetate (*oaa*) within the central carbon fixation metabolism of cyanobacteria. According to Figure 5.7, about 27% of the *pyr* production flux (“PYK”, $0.0895 \text{ mmol g}_{\text{DW}}^{-1} \text{ h}^{-1}$) is employed to produce *val-L* (flux from “DHAD1”, $0.0240 \text{ mmol g}_{\text{DW}}^{-1} \text{ h}^{-1}$). An additional 24% of the of the *pyr* production is employed to produce *ala-L* (“VPAMTr”, $0.0216 \text{ mmol g}_{\text{DW}}^{-1} \text{ h}^{-1}$). Alternative *ala-L* producing reactions in *Anabaena* also require *pyr* and *ser-L*, which supports the importance of *3pg* derived *ser-L* as building

block for other downstream metabolites. A similar behavior of the FBA predicted fluxes was observed for photoautotrophic and photodiazotrophic simulations.

Based on the analysis of Figure 5.7, *glu-L* is by far the most abundant amino acid in the *Anabaena* network. Apart from being a central metabolite to synthesize the remaining proteinogenic amino acids, *glu-L* is needed to produce Heme, a precursor of PCB. The enzyme glutamyl-transfer ribonucleate synthetase (E.C 6.1.1.17) catalyzes the first step in the production of heme from glutamate [444] and this reaction was included in *i*DN1004 (see reaction “GLUTRS” in Table B.1). Although PCB flux values were used to verify the prediction accuracy of *i*DN1004, it was found that the heme synthesis flux only accounted for up to 1.47% of the combined *glu-L* production flux ($0.0028\text{-mmol g}_{\text{DW}}^{-1} \text{ h}^{-1}$ for photoautotrophic cultures). Since *glu-L* participates in more than 46 reactions of the *Anabaena* metabolic network and it is also essential to produce the chromophores of PBPs, disrupting the native cyanobacterial metabolism of glutamate could be catastrophic. Therefore, the production of native and non-native cyanobacterial metabolites from amino acids in *Anabaena* should start from *asp-L*, *thr-L*, *gly*, *val-L*, *ala-L* and *ser-L*. Glutamine was excluded from this list because of its intricate relation with *glu-L* in the Nitrogen assimilation mechanism, especially in the GS/GOGAT cycle.

5.5.7 Evaluation of amino acid production flux with FVA

The individual metabolic fluxes predicted by the FBA algorithm are not unique because the cells have multiple pathways to produce a given metabolite [364]. Therefore, it was important to calculate the feasible flux space of the amino acid producing reactions using FVA. Since FVA provides a range of metabolic fluxes leading to the similar biomass

generation rates [365], this analysis was useful to confirm the early conclusions of the FBA calculations. In this analysis, the flux through each of the 70 amino acid producing reactions of *Δ*DN1004 (See Table C.1) was maximized and then minimized, keeping the same constraints of the original FBA problem, and satisfying at least 95% of the originally predicted growth rates. This algorithm produced 140 different flux distributions for each growth condition (photoautotrophic and photodiazotrophic). Combined production flux values (i.e., the sum of production fluxes) for each amino acid were calculated using the FVA results. Since FVA can predict very large flux values for cyclic and redundant reactions [43, 44], only biologically feasible results were considered (e.g., lower than the C_i uptake fluxes). The FBA-predicted combined flux was also considered to analyze the combined flux distribution for each amino acid. Depending on the number of reactions involved in the production of a given amino acid, the sample size of combined amino-acid production fluxes ranged from 39 data points for *glu-L* to only 2 for asparagine (*asn-L*).

Figure 5.8 presents an abundance-based ranking of combined amino-acid production fluxes after grouping the fluxes through the 70 reactions describing amino acid biosynthesis in *Δ*DN1004. This figure illustrates the relative importance of each amino acid production flux in photoautotrophic and photodiazotrophic cells. The ranking of amino acids is almost identical for both kinds of filaments, except for the predicted relative importance of tyrosine (*tyr-L*) and phenylalanine (*phe-L*), which changed after switching the N-source. Figure 5.8 suggests eight Pareto amino acids representing more than 87.5% of the total amino-acid production fluxes. These results are consistent with the information discussed in Figure 5.7. However, the most important difference is related to the combined flux of *ser-L* producing reactions.

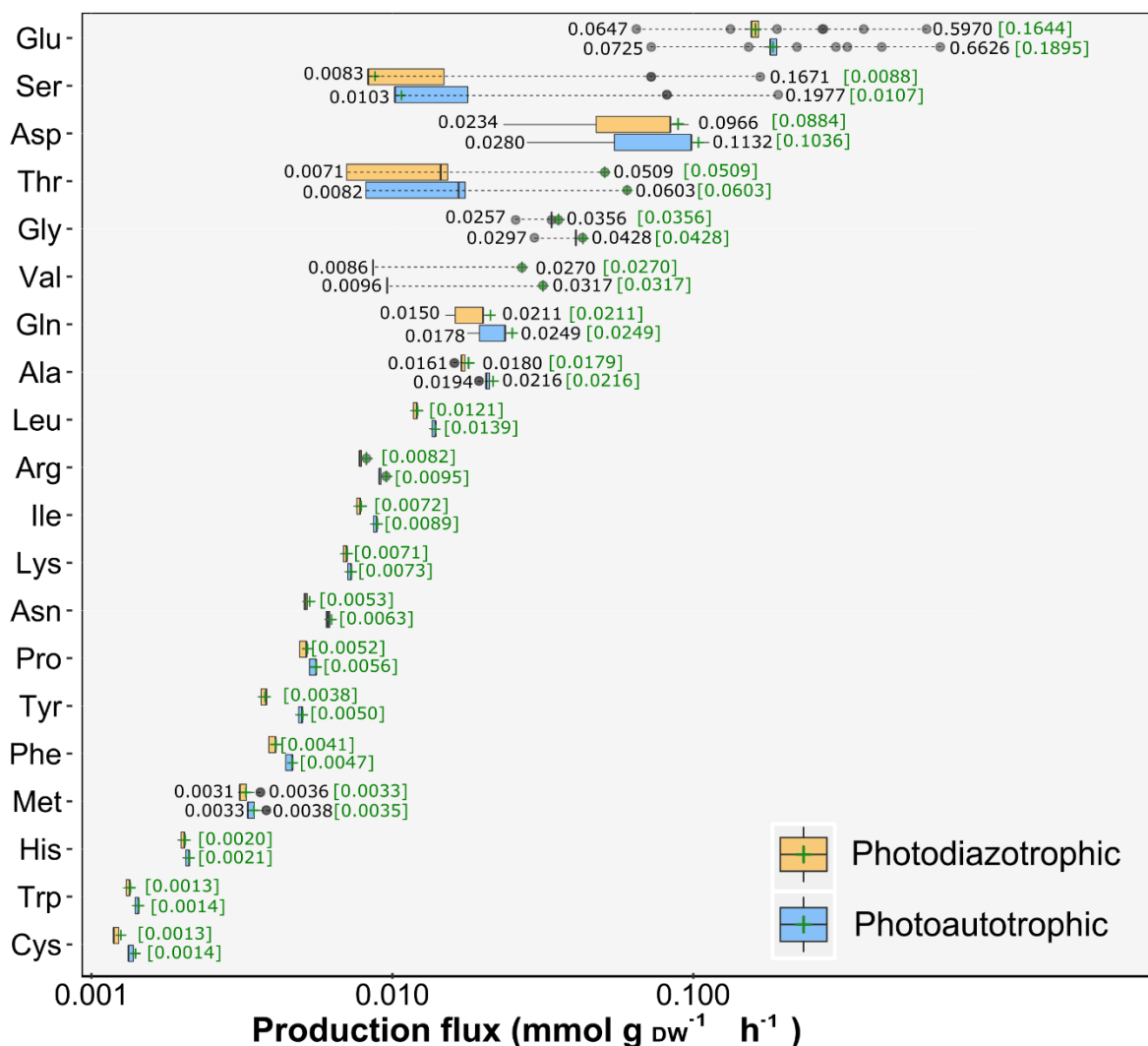


Figure 5.8. Amino acid production ranking predicted by FBA and FVA.

Figure compares combined amino-acid production fluxes for photoautotrophic (blue) and photodiazotrophic (gold) cultures of *Anabaena*. The flux values are organized based on the maximum predicted combined flux. These horizontal boxplot-type bars represent the range of feasible fluxes through the amino-acid producing reactions. The black numbers on the extremes of each boxplot represent the minimum and maximum combined production flux, respectively. The boxes represent the limits of the 25% and 75% quartiles of the combined flux distribution. The combined flux value predicted using only FBA data is represented with green crosses and numbers between brackets. The horizontal blue dashed lined separates this plot in two regions. The upper region groups eight amino acids representing 87.5% of the total predicted amino-acid production (The Pareto fluxes), while the lower region encompasses the amino acids providing the remaining 12.5% of the production fluxes. We suggest selecting amino-acid branching points from the list of Pareto fluxes to maximize the yields of nitrogen-compounds obtained through metabolic engineering, especially those derived from aspartate, glycine, serine, and threonine.

In the initial FBA prediction, serine production flux was only $0.0108 \text{ mmol g}_{\text{DW}}^{-1} \text{ h}^{-1}$, but FVA suggested that this combined flux could be as high as $0.1977 \text{ mmol g}_{\text{DW}}^{-1} \text{ h}^{-1}$ (photoautotrophic) or $0.1671 \text{ mmol g}_{\text{DW}}^{-1} \text{ h}^{-1}$ (photodiazotrophic). Again, this variation can be explained by the ability to produce *ser-L* from *3pg*, an abundant product of the carbon fixation reactions. This variation also explains the wide solution space of *thr-L* biosynthesis reactions. As previously stated, *glu-L* and *gln-L* are essential for the synthesis of multiple metabolites and using them as amino-acid branching point for metabolic engineering efforts could be difficult. We suggest using the remaining six Pareto amino acids as branching points to produce native and non-native secondary metabolites (i.e., *asp-L*, *ser-L*, *gly*, *thr-L*, *val-L*, and *ala-L*). Interestingly, three amino acid directly connected to the carbon fixation reactions (*ser-L*, *gly*, and *thr-L*) emerged as important non-obvious players in the secondary metabolism of *Anabaena*, and possibly other autotrophic cyanobacterial cultures.

5.5.8 Secondary metabolites from Pareto amino acids

Cyanobacteria can utilize some biosynthetic pathways to produce valuable nitrogen compounds from *asp-L*, *ser-L*, *val-L*, and *gly*. Based on FBA and FVA predictions, *i*DN1004 suggests evaluating these amino-acid branching points to conduct metabolic engineering in *Anabaena*. Since *asp-L* is a pivotal compound inside the cyanobacterial network, it can also be precursor of other amino acids like arginine, asparagine, lysine, and methionine. However, *asp-L* also has a central role in the synthesis of the cyanobacterial polymer reserve cyanophycin [278, 384]. Cyanophycin is a precursor of PASP, which finds industrial application as a biodegradable replacement

of polyacrylates [34, 165]. Besides cyanophycin, *asp-L* is implicated in the production of schizokinen, which is a hydroxamate-type siderophore derived from lysine and ornithine [394]. The probable high abundance of *ser-L* production flux in the *Anabaena* metabolic network becomes clear after analyzing its production pathway, which starts with the production of 3-phosphonooxypyruvate (*3php*) through the “PGCD” reaction (see Figure). The enzyme phosphoglycerate dehydrogenase (EC 1.1.1.95) catalyzes the transformation of *3pg* into *3php*. Because *3pg* is the first product of the main CO₂ fixation reaction catalysed by RuBisCo (EC 4.1.1.39) in the Calvin cycle [445], an abundant pool of *ser-L* is reasonable in photosynthetic cells. Although *ser-L* is a non-essential amino acid with low commercial interest, plant and animal cells produce the sphingolipid sphingosine from serine and palmitoyl-CoA [446]. After introducing the sphingolipid production pathway in *Anabaena*, this organism could become a photosynthetic source of sphingosine, which is a valuable ceramide widely used in skin and hair care products [447]. Cyanobacteria synthesize *val-L* from pyruvate, the main product of glycolysis. Because glucose is the main product of photosynthesis, a significant pool of pyruvate is expected in a photosynthetic organism [122]. Recently, Miao *et al.* selected the *val-L* biosynthesis pathway to enhance the photosynthetic production of isobutanol in *Synechocystis* [448, 449]. In addition, Videau *et al.* recently presented *Anabaena* as a heterologous producer of lyngbyatoxin A [118], an emerging drug that is produced from *val-L* and tryptophan through the nonribosomal peptide synthetase system (NRPS) of *Moorea producens* [399]. One of the most important uses of *ser-L* inside the cyanobacterial metabolic network is *gly* production. Therefore, a probably abundant production flux of *gly* is also related to the abundant *3pg* in autotrophic cells. *Gly*, *ser-L*

and sedoheptulose-7-phosphate (a product of the pentose phosphate pathway) are the main precursors of the cyanobacterial sunscreen shinorine, which has been incorporated in commercial cosmetic products like Helionori[™] and Helioguard 365[™] [400, 450]. Although the cyanobacterium *Anabaena variabilis* [451], is a native producer of shinorine, the production of this natural UV-protectant could also be possible through metabolic engineering in *Anabaena*.

5.6 Chapter conclusion

Cyanobacteria metabolism is loaded with several pathways for production of valuable chemicals. The *Anabaena* model, *i*DN1004, was created as a detailed genome-scale metabolic model to gain reliable understanding of the metabolic network using experimental measurements of biomass generation, nutrient and light uptake, and phycocyanobilin (PCB) production under photoauto- and photodiazotrophic conditions. *Anabaena* specific biomass equations were developed to enhance the prediction potential of *i*DN1004, which also describes unique cyanobacterial processes (e.g., spectral-decomposition reactions in the phycobilisomes, assembly of phycobiliproteins, and synthesis of cyanophycin). From a biotechnological standpoint, *i*DN1004 is a highly comprehensive *Anabaena* GSMM describing the photosynthetic chemical production potential of these cyanobacteria, including specialty chemicals. From *i*DN1004, *Anabaena* is proposed as a platform to synthesize non-native secondary metabolites using amino acids as branching points. Using FBA and FVA, metabolic flux distributions were predicted to estimate combined amino acid production fluxes used in the synthesis of more complex nitrogen-containing compounds. It was found that *glu-L*, *asp-L*, *ser-L*,

thr-L, *val-L*, *gly*, *gln-L*, and *ala-L* constitute the list of Pareto metabolic branching points, grouping more than 87.5% of the total amino acids available to produce secondary metabolites. FBA simulations also suggested that photoautotrophic cultures of *Anabaena* have higher C_i potential and photosynthetic efficiency than photodiazotrophic cultures. Considering the ranking of amino acids produced by *Anabaena* to generate their biomass, iDN1004 was used to identify schizokinen, sphingosine, lyngbyatoxin A, and shinorine as high-value amino-acid derived metabolites to be synthesized with theoretically higher yields. In addition, the availability of these amino acids in the culture medium might benefit the production of these secondary metabolites. Overall, the high-quality metabolic model iDN1004 revealed hidden potential biotechnological applications of *Anabaena* sp. UTEX 2576.

CHAPTER 6. NITROGEN METABOLISM AND IRON AVAILABILITY AFFECT PIGMENT BIOSYNTHESIS AND NUTRIENT CONSUMPTION IN *ANABAENA*

6.1 Preamble

Developing microbial biofactories is challenging because the metabolic network that sustains life is extremely complex. Even for well-known microorganisms, strain and growth medium optimization are meaningful research topics in constant evolution. Developing a GSMM of *Anabaena* is only one of multiple strategies used to analyze intimate relationships among metabolic processes in cyanobacteria. This chapter describes a complementary study about the impact of nutrient availability on pigment production and cultivation of *Anabaena*. Multiple synthetic biology strategies have been evaluated to enhance photosynthetic chemical production in cyanobacteria (See section 2.6). However, most of these studies have been completed through genetic engineering or by altering the Carbon source, ignoring the effects of other components of the growth medium. The last part of this dissertation intends to expand the current knowledge about nutrient utilization by cyanobacteria beyond Carbon and Nitrogen metabolism. This work was inspired by a renewed interest on studying the interface between biology and inorganic chemistry to advance biotechnological and environmental applications with cyanobacteria. The results of this study can be used to revamp *DN1004*.

6.2 Introduction to inorganic interactions in cyanobacteria

Chemical production by cyanobacteria has gained interest for carbon dioxide (CO₂) bio-sequestration applications. In this regard, most CO₂ transformation studies

have focused on the production of biofuels and commodities derived from the cyanobacterial central carbon metabolism [122]. Nevertheless, recent evidence indicates that feasible large-scale cyanobacterial biotechnology should involve the synthesis of valuable bio-active compounds like antioxidants, vitamins, and secondary metabolites [452, 453]. From this perspective, the biotechnological importance of *Anabaena* is enhanced when considering their photosynthetic capacity and their ability to use different inorganic and organic Nitrogen sources (N-sources).

Although CO₂ fixation is the most attractive feature of cyanobacterial metabolism, their global metabolic network is also affected by the N-source and Iron (Fe) concentration in the growth medium, especially for N₂-fixing species like *Anabaena* sp. [20, 325, 454, 455]. While the N-source is used for synthesizing proteins, nucleic acids, co-factors, and secondary metabolites [327], Fe is essential for the synthesis of DNA and iron-sulfur proteins [18]. Given that Iron-sulfur proteins are involved in photosynthesis and N-assimilation, cyanobacterial cells demand at least 10 times more Fe than non-photosynthetic bacteria like *Escherichia coli* [456, 457]. In addition, Fe requirements of diazotrophic species like *Anabaena* sp. UTEX 2576 are even higher compared to other non-N₂-fixing cyanobacteria [19].

Fe is essential for bacterial metabolism and is also the most important transition metal added to the widely used BG-11 growth medium [326]. However, excessive illumination conditions trigger Fe-catalyzed formation of reactive oxygen species (ROS) like superoxide (O₂⁻) and Hydrogen peroxide (H₂O₂) during photosynthesis [456, 458, 459]. Therefore, Fe plays a contradictory role in cyanobacterial metabolism, both as nutrient and catalyzer of damaging oxidative reactions. To deal with this paradox,

cyanobacteria have evolved Fe homeostasis mechanisms mediated by ferric uptake regulator proteins (FUR) [18]. Although the FUR proteins are mainly responsible for maintaining the intracellular Fe balance in cyanobacterial cells, they are also crucial for keeping the balance of other essential metals like Manganese (Mn), Zinc (Zn), and Nickel (Ni) [18, 460–462]. The consumption of other important elements like Phosphorous (P), Calcium (Ca), Magnesium (Mg), Boron (B), Molybdenum (Mo), Copper (Cu), and Cobalt (Co) is not under the direct influence of FUR proteins [18, 325, 454, 463]. However, the question on how Fe availability affects the consumption of these nutrients remains under study.

Cyanobacteria can grow in BG-11 mineral medium without any source of organic Carbon (C) because they are autotrophic organisms, capable of oxygenic photosynthesis. This is a highly sophisticated physical, chemical and biological process that uses visible light radiations, polypeptides, light-sensitive organic pigments, and metal ions to obtain energy (light phase) and fixate CO₂ from the environment to form sugars (dark phase). The light phase of photosynthesis is facilitated by light sensitive pigment-protein complexes that catalyze electron transfer reactions to produce chemical energy in the form of ATP and NADPH. In cyanobacteria, such pigment-protein complexes are photosystem II (PSII, EC 1.10.3.9), photosystem I (PSI, EC 1.97.1.12) and phycobilisomes (PBSs), which are abundant in the thylakoid membranes. In PSII, a Mn-Ca based cluster (Mn₄CaO₅) works in tandem with light-excited Chlorophyll A P680, Pheophytin A, Plastoquinone (PQ-9) and β-Carotene to draw electrons from water. In the process, PQ-9 is reduced to Plastoquinol (PQH₂) and water molecules are converted into protons (H⁺) and molecular Oxygen (O₂) [464, 465]. Electrons from PQH₂ are then

transferred to plastocyanin (PC), a Cu containing protein, by the action of Cytochrome *b₆f*. Electron flow through PSII also produces O_2^- , and this side reaction has been attributed to the PSII-associated protein Cytochrome b559, which promotes the oxidation of PQH₂ to PQ and the reduction of O₂ to O_2^- [466]. Eventually, O_2^- is partitioned into ordinary O₂ and H₂O₂ by the action of Superoxide dismutase, SOD (EC 1.15.1.1) [467, 468]. H₂O₂ can also be produced when the O₂-evolving activity of the Mn₄CaO₅ cluster of PSII is disrupted during photoinhibition [456]. In PSI, light-excited Chlorophyll A P700, phylloquinone (vitamin K₁), β -Carotene, and ferredoxins (Iron-Sulphur proteins), work together to transfer the electrons from PC to NADP⁺, producing NADPH [469]. In a parallel transport reaction, the H⁺ gradient generated across the thylakoid membranes fuels the production of ATP by ATP-synthase [12]. In order to take advantage of a wider portion of the visible light spectrum for photosynthesis, cyanobacteria have developed PBSs. These are light-harvesting protein complexes, responsible for the cyanobacterial chromatic acclimation mechanism [470]. In *Anabaena sp.*, these complexes are composed of multiple disc-shaped stacked subunits of phycobiliproteins (PBPs), forming considerably large antenna-like structures of five inner cylinders and eight peripheral rods connected to PSII [471]. While the typical molecular mass of the cyanobacterial PSII dimer is ~700 kDa, the approximate mass of the PBSs in *Anabaena sp.* is ~6000 kDa [464, 471, 472]. The distinctive PBP subunits of this organism are C-Phycocyanin (CPC, ~35.8 kDa), Phycoerythrocyanin (PEC, ~35.7 kDa) and Allophycocyanin (APC, ~34.7 kDa) [416].

Although the main photosynthetic pigment in cyanobacteria is chlorophyll A (ChlA), a Mg-containing compound, other auxiliary photosynthetic pigments are carotenoids and phycobilins [11, 12]. The carotenoids are a group of isoprenoid compounds formed by

different types of Carotenes (e.g., α -Carotene, β -Carotene, γ -Carotene, Lycopene, Torulene) and their oxygenated derivatives, the xanthophylls (e.g., Echinenone, Myxoxanthophyll, Canthaxanthin, Zeaxanthin) [427, 430, 431]. These compounds play multiple roles in photosynthetic organisms, participating in light-harvesting and defense mechanisms like energy dissipation under excess illumination, non-photochemical quenching, and photooxidation and lipid peroxidation protection [473, 474]. Although β -Carotene is the most common carotenoid in the photosystems of *Anabaena* sp. and other cyanobacteria [427, 428, 430, 431, 464, 469], Echinenone, Hydroxyechinenone, Canthaxanthin, and Zeaxanthin can be produced as a result of non-photochemical quenching, when β -Carotene ketolase (EC 1.14.99.63) oxidizes β -Carotene to counteract the damaging effect of ROS during oxidative stress, Fe surplus and deficit, and growth on urea [329, 427, 474–476]. The phycobilins are the chromophore molecules linked to the PBPs in cyanobacterial phycobilisomes. Chemically, these pigments are open-chain tetrapyrroles biosynthesized from Fe-Heme and Biliverdin [46, 50]. Therefore the synthesis of phycobilins is directly related with ChlA production and Fe metabolism [19]. In *Anabaena* sp., the most important phycobilin pigments are phyphycocyanobilin (PCB) and phycoviolobilin (PVB), which are present in CPC, APC and PEC proteins. It has been demonstrated that Fe limitation leads to increased expression of *FurA*, the master transcriptional regulator of Fe metabolism [477]. Consequently, the expression of Heme biosynthesis and degradation genes in wild-type *Anabaena* sp. is also up-regulated under Fe starvation [19].

Considering these biochemical relationships, quantifying the impact of different N-sources and the Fe availability on the autotrophic metabolism of *Anabaena* sp. is crucial.

Specifically, it is important to determine the impact of these nutrients on the growth kinetics and the bioproduction of valuable metabolites of biotechnological interest like CPC, APC, PEC and β -Carotene (Pro-Vitamin A), which have been used in nutraceutical and cosmetic products as natural colorants, dietary supplements and anti-oxidant ingredients [298, 341, 478]. In addition, having a clearer understanding of the intricate relationship between N and Fe metabolism in photosynthetic microorganisms can provide useful insights to optimize culture media for research purposes, improve current large-scale operations and design next generation wastewater bioremediation operations using cyanobacteria [107, 453, 479]. The main objective of this study is to quantify the effect of three different N-sources - i.e., dinitrogen (N_2), sodium nitrate ($NaNO_3$) and urea (CH_4N_2O) – and Fe availability on the production of β -Carotene, ChlA and PBPs, as well as the effect on nutrient consumption, on the model filamentous cyanobacterium *Anabaena* sp. UTEX 2576. Moreover, this work also presents a novel approach for efficient quantification of P and metallic elements in the widely used mineral medium BG-11. To our knowledge, this is the first study providing a systemic analysis on the reproduction of *Anabaena* sp., taking into consideration the balance between nutrient demands and oxidative stress. This information advances our understanding on nutrient utilization preferences of *Anabaena* sp. beyond C, N and Fe substrates.

6.3 Methodology

Standard cultivation conditions and biomass characterization methods for *Anabaena* have been covered in Chapter 3. However, the experiments described in this chapter relied on the introduction of a new N-source (i.e., urea) and the modification of

the Fe concentration in the growth media. The election of urea as a third N-source for cyanobacteria was a result of the manual curation of *DN1004*, the *Anabaena* GSMM (See sections 4 and 5). In this process, it was realized that wild type *Anabaena* is one of few cyanobacterial strains with the full set of genes needed for transport and catabolism of urea [332]. Preliminary experiments were conducted in a medium with 9 mM urea, supplying comparable molar N-levels to the standard BG-11 medium [361]. However, such levels of urea led to inconsistent growth kinetics and rapid cellular death. The BG11u medium was defined after lowering the urea concentration to 3 mM and including compulsory pH buffering with TES-NaOH (See subsection 3.3). Cultivation of *Anabaena* with urea is not a trivial task, given the epigenetic challenges at metabolic level arising from the utilization of this nutrient [329]. After this process of growth medium development, *Anabaena* cultures were routinely cultivated in BG11_o, BG11 and BG11_u media. To evaluate the impact of Fe-availability, each medium was prepared with initial Fe concentration of 0.3 ppm, 1.2 ppm and 5.0 ppm. Soluble Fe was supplied in the form of Ammonium ferric citrate (Fe^{3+} as $\text{C}_6\text{H}_8\text{FeNO}_7$).

Other modifications of the growth media involved changes in P and Zn concentrations. Additionally, a new mineral (NiSO_4) was introduced in the micronutrient cocktail. The nominal initial concentration of P (supplied as $\text{K}_2\text{HPO}_4 \cdot 2\text{H}_2\text{O}$) was 20% higher than the standard BG-11 concentration to sustain possible increased demand of phosphate for the biosynthesis of nucleic acids, ADP and ATP. Considering that Zn is needed for essential cyanobacterial processes like DNA protection during oxidative stress, gene regulation and carbonic anhydrase activity [462, 480], the initial nominal availability of Zn (as $\text{ZnSO}_4 \cdot 7\text{H}_2\text{O}$) was two times higher than in standard BG-11.

Although the standard BG-11 formulation does not contain Ni, 1.5 μM $\text{NiSO}_4 \cdot 6\text{H}_2\text{O}$ (0.01 ppm of Ni) was added to the growth media to ensure a basal level of urease activity in each culture [330].

This part of the project required the implementation of efficient methods for quality control of cyanobacterial medium and reliable determination of β -Carotene. Fast and reliable methods for NO_3 , N_T and urea quantification were implemented to validate the concentrations of N-sources in fresh media. Here, a commercial Cadmium reduction test was preferred for NO_3 and N_T quantification, instead of the lengthy sulfanilic acid method. Urea concentration was determined using a modified version of the O-Phthalaldehyde method [359] (see subsection 3.11). Measurements of Total Organic Carbon (TOC) were also introduced as part of the medium characterization routine (see subsection 3.12). Determination of B, Na, Mg, P, K, Ca, Mn, Fe, Co, Ni, Cu, Zn and Mo concentrations was accomplished by developing a mineral medium analysis method with ICP-OES (see subsection 3.13). Quantification of β -Carotene was accomplished through MS-TOF analysis of cold methanol extracts (see subsection 3.5.3).

Given the special circumstances during the Covid-19 crisis in March and April of 2020, most analysis presented in this chapter are derived from data for only two independent biological replicates for each medium type and Fe-level combination.

6.4 Results

This section discusses the impact of N and Fe availability on the bioproduction potential of *Anabaena* sp. This section presents the effect of N-source type and initial

Fe concentration on cellular growth, pigment production, and nutrient consumption kinetics.

6.4.1 Effect of N and Fe availability on the growth of *Anabaena*

Figure 6.1 summarizes the evolution of optical density at 730 nm (OD_{730}), cell density and biomass concentration with different media and Fe-levels during the 14-day growth experiment. Normalized OD_{730} data (i.e., $\ln(N/N_0)$) were adjusted to a saturation growth model to determine average growth rates and generation times. Sustained growth of *Anabaena* sp. was accomplished in BG11_o, BG11 and BG11_u media with different initial Fe concentrations. However, the type of N-source had the most significant effect on the growth rates, generation times and biomass production over 14 days as presented in Table 6.1 and Figure 6.2. The chemical properties of fresh media are presented in Table 6.2 and Table 6.3. In average, growth rates in BG11 medium were at least 57% higher than in BG11_o and BG11_u media. Remarkably, the average biomass generation of BG11 cultures was more than two times the biomass generation of BG11_o cultures over two weeks. Although Fe concentration did not significantly impact the growth kinetics in BG11_o nor BG11 media, Fe-starvation (0.3 ppm) significantly reduced the growth rate of cultures in BG11_u by at least 46%. Reduction in growth rates was accompanied by increase in generation time and lower biomass generation over 14 days. While cell cultures in BG11_o and BG11_u media exhibited comparable growth rates, the biomass generation was lowest for diazotrophic filaments in BG11_o. Even when *Anabaena* sp. cells can successfully metabolize each N-source, the differences in growth rate and final biomass concentration suggest that dissimilar cellular stress phenomena occur in each growth medium.

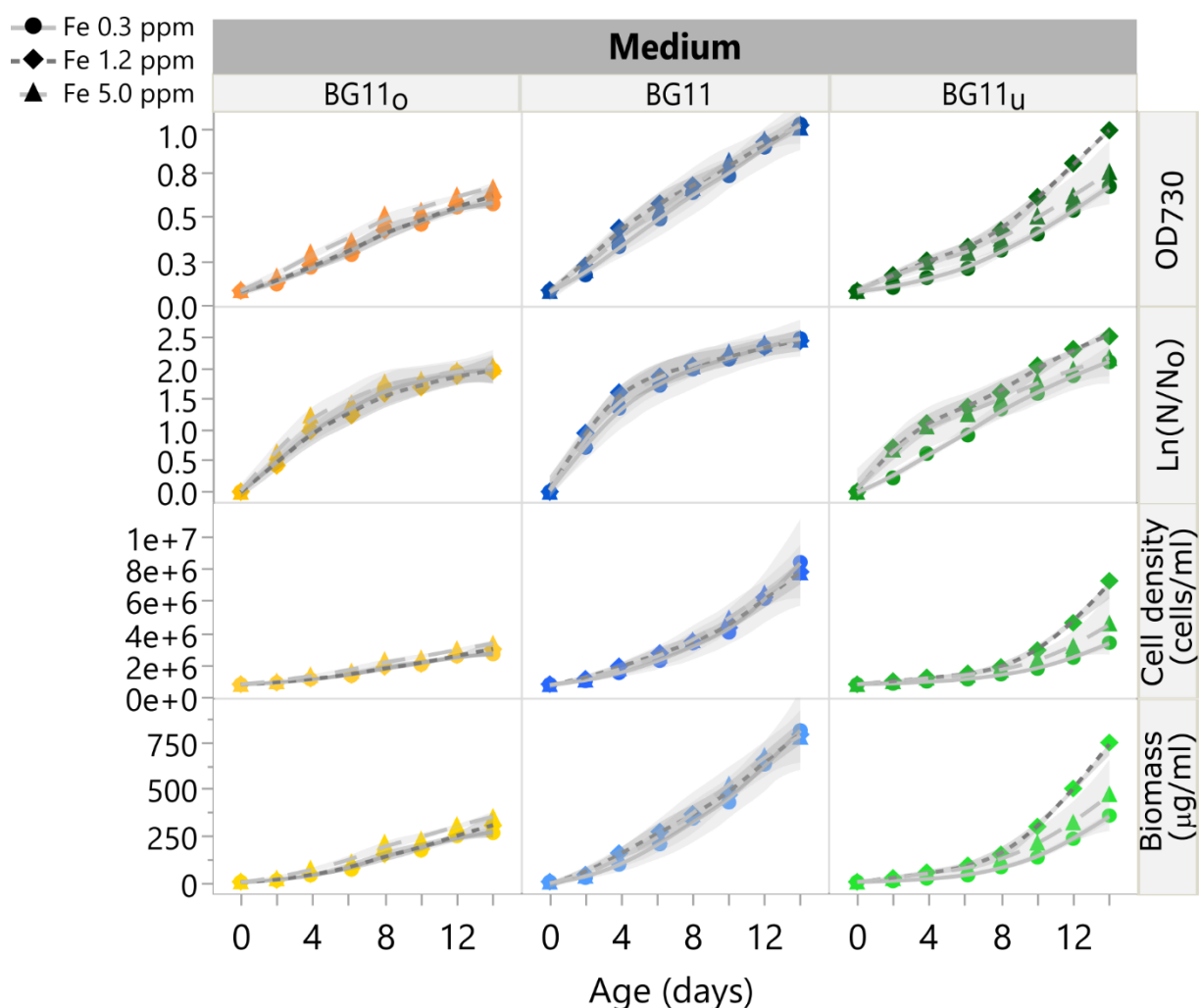


Figure 6.1. Growth kinetics of *Anabaena* sp. in BG11_o, BG11 and BG11_u

Fe concentration did not significantly affect cellular growth in BG11_o nor BG11, but higher biomass generation in BG11_u cultures was observed with initial Fe supply of 1.2 ppm. Overall, cell growth was lowest and slowest in BG11_o medium, while BG11_u cultures exhibited longer exponential phase. Highest biomass generation was observed in BG11 cultures. Absorbance at 730 nm was used as an indicator of change in cellular density over time (first row). In the second row, OD₇₃₀ readings were normalized to have a clearer view of exponential (steep region) and stationary phases (flat region). The term $\ln(N/N_0)$ represents the natural logarithm of OD₇₃₀ over initial OD₇₃₀. Starting nominal OD₇₃₀ (at day 0) was 0.1 for all cultures. Mathematical expressions were used to estimate cell density (third row) and biomass concentration (fourth row) from OD₇₃₀ data. Markers represent average values and shaded areas represent confidence fit intervals using a significance level $\alpha=0.05$. Optical densities were measured in triplicate. The data were taken from two biological replicates for each combination of medium and Fe concentration.

Table 6.1. Growth and biomass generation of *Anabaena* in different media

Values represent the average and standard errors from two independent biological replicates. Biomass data correspond to the biomass generated over 14 days of growth. Two-way ANOVA was used to analyze statistically significant differences with a significance level $\alpha=0.05$. Medium and Fe-level used as independent predictors. Medium levels not connected by same group letter are significantly different. Fe-levels not connected by same number of stars within medium type are significantly different. Medium p-Value = 0.0441. Fe-level p-Value = 0.3591. Interaction p-Value = 0.8901.

Medium/ Fe-level	Growth rate (h ⁻¹)	Generation time (h)	Biomass-14 days (µg ml ⁻¹)	Group
a.BG11 _o	0.021 ± 0.003	50.82 ± 6.26	309.85 ± 27.08	A
Fe 0.3 ppm	0.019 ± 0.006	55.94 ± 18.93	267.88 ± 31.03	*
Fe 1.2 ppm	0.02 ± 0.007	54.27 ± 19.17	307.98 ± 73.89	*
Fe 5.0 ppm	0.025 ± 0.009	42.25 ± 15.09	353.69 ± 29.91	*
b.BG11	0.034 ± 0.012	33.49 ± 12.52	797.15 ± 74.06	B
Fe 0.3 ppm	0.03 ± 0.014	36.51 ± 16.24	816.32 ± 231.13	*
Fe 1.2 ppm	0.036 ± 0.012	29.06 ± 9.42	794.34 ± 63.49	*
Fe 5.0 ppm	0.034 ± 0.019	34.89 ± 19.22	780.8 ± 155.49	*
c.BG11 _u	0.018 ± 0.008	64.49 ± 25.47	465.52 ± 84.19	A
Fe 0.3 ppm	0.011 ± 0.001	88.15 ± 11.28	360.57 ± 25.47	*
Fe 1.2 ppm	0.021 ± 0.006	48.56 ± 12.98	562.01 ± 188.77	**
Fe 5.0 ppm	0.022 ± 0.013	56.77 ± 34.66	473.98 ± 222.82	**

While cultures in BG11 and BG11_u exhibited more intense green color than BG11_o cultures, the production speed of essential proteins like PBPs was slower for cultures in BG11_u (See Figure 6.3). Dissimilar pigmentation of cells may be related to chromatic acclimation mechanisms in the PBSs, up-regulation of PEC biosynthesis under diazotrophic metabolism (e.g., obligated N₂ fixation) or oxidation of carotenoids by ROS.

6.4.2 Effect of N and Fe availability on the accumulation of PBPs

Diazotrophic cells accumulate up to two-times more PBPs than non-diazotrophic cell, while higher Fe levels reduce the average content of CPC and APC.

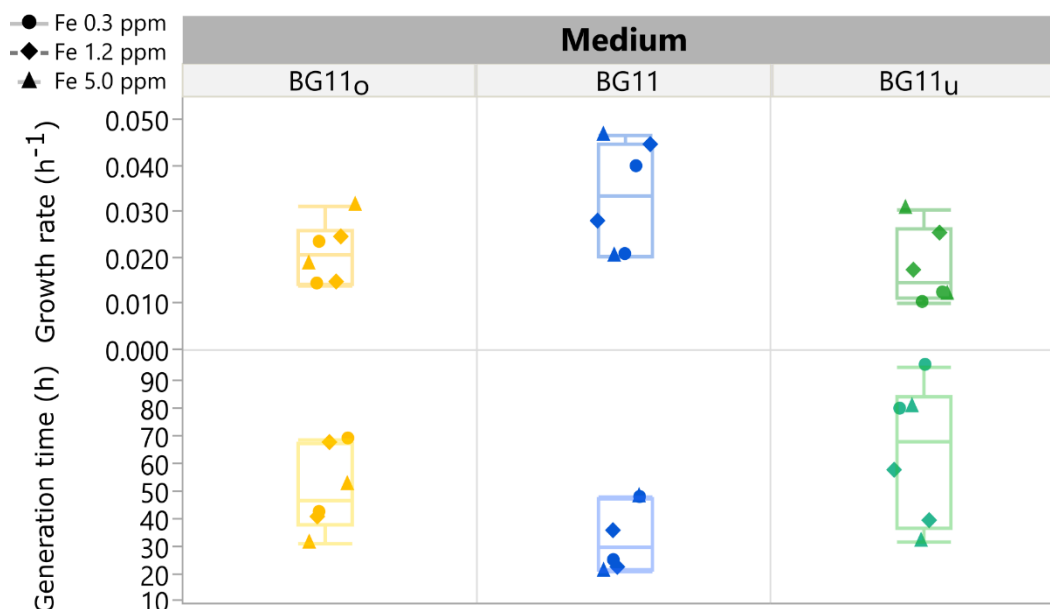


Figure 6.2. Growth constants of *Anabaena* sp. in different media.

Varying Fe concentrations did not affect growth rates significantly in BG11_o and BG11, but the N-source impacts growth speed. Fastest growth rates and shortest generation times correspond to cultures in BG11 medium. Cultures in BG11_o and BG11_u presented comparable growth rates but low initial Fe concentration in BG11_u limited growth speed.

Table 6.2. Properties of fresh mineral media

The properties of fresh media were evaluated and compared against nominal (design) concentrations. No traces of elemental Nitrogen were detected in BG11_o medium, but satisfactory initial levels of NaNO₃ and urea were observed in BG11 and BG11_u media. Total organic carbon (TOC) values indicate concentration of organic compounds in fresh media. Initial TOC values of BG11_o and BG11 media were negative, indicating negligible traces of organic compounds in these mineral media. TOC values of fresh BG11_u media are attributed to urea and TES-NaOH buffer.

Medium	Fe level (ppm)	N source	Nominal conc. (mM)	Nominal conc. (ppm)	Measured conc. (ppm)	TOC (ppm)	pH
BG11 _o	0.3	N ₂	0	0	0	-1.8 ± 0.7	8.04 ± 0.01
BG11 _o	1.2	N ₂	0	0	0	-0.8 ± 0.4	8.01 ± 0.08
BG11 _o	5.0	N ₂	0	0	0	-1.2 ± 0.6	8.01 ± 0.06
BG11	0.3	NaNO ₃	17.7	1500	1786 ± 214	-11 ± 2.2	7.98 ± 0.05
BG11	1.2	NaNO ₃	17.7	1500	1756 ± 171	-19 ± 2.8	7.98 ± 0.03
BG11	5.0	NaNO ₃	17.7	1500	1794 ± 77	-20 ± 3.3	8.03 ± 0.01
BG11 _u	0.3	Urea	3.0	180	194 ± 10	625 ± 6.3	7.95 ± 0.06
BG11 _u	1.2	Urea	3.0	180	188 ± 9	616 ± 6.0	7.92 ± 0.03
BG11 _u	5.0	Urea	3.0	180	202 ± 11	647 ± 7.9	7.97 ± 0.03

Table 6.3. Concentration of mineral elements in growth media

Levels of P, Ni, and Zn (in parenthesis) were deliberately higher than in standard BG-11 medium. Actual levels of Na and K were affected by pH adjustment.

Initial concentration in BG11 _o	Element	Nominal conc. (ppm)	Conc. in low Fe (ppm)	Conc. in medium Fe (ppm)	Conc. in high Fe (ppm)
	B	0.50	0.53 ± 0.04	0.51 ± 0.05	0.44 ± 0.05
	Na	8.87	32.63 ± 0.39	32 ± 0.79	31.8 ± 0.77
	Mg	7.40	6.97 ± 0.57	6.85 ± 0.58	6.87 ± 0.63
	P	7.11 (8.50)	8.64 ± 0.9	8.73 ± 0.83	8.89 ± 1.31
	K	17.96	15.32 ± 0.45	13.65 ± 0.88	14.39 ± 0.92
	Ca	9.81	10.51 ± 1.46	10.01 ± 0.83	10.36 ± 1.47
	Mn	0.50	0.49 ± 0.07	0.51 ± 0.06	0.45 ± 0.04
	Fe	1.28	0.21 ± 0.07	1.09 ± 0.17	5.45 ± 0.52
	Co	0.01	0.009 ± 0.001	0.011 ± 0.001	0.008 ± 0.001
	Ni	0.00 (0.01)	0.012 ± 0.003	0.01 ± 0.003	0.011 ± 0.004
	Cu	0.02	0.017 ± 0.003	0.017 ± 0.003	0.023 ± 0.003
	Zn	0.05 (0.10)	0.096 ± 0.007	0.099 ± 0.016	0.084 ± 0.009
Initial concentration in BG11	Mo	0.15	0.17 ± 0.01	0.16 ± 0.01	0.19 ± 0.04
	B	0.50	0.499 ± 0.02	0.561 ± 0.02	0.51 ± 0.07
	Na	414.62	516.236 ± 25.73	441.286 ± 0.49	452.196 ± 0.68
	Mg	7.40	8.164 ± 0.55	8.081 ± 0.87	8.278 ± 0.76
	P	7.11 (8.50)	8.288 ± 0.31	8.513 ± 1.07	8.751 ± 1.03
	K	17.96	23.239 ± 1.07	21.396 ± 1.1	21.367 ± 1.16
	Ca	9.81	10.199 ± 0.3	10.059 ± 0.69	9.549 ± 0.57
	Mn	0.50	0.456 ± 0.04	0.467 ± 0.03	0.436 ± 0.04
	Fe	1.28	0.375 ± 0.06	0.964 ± 0.24	5.294 ± 0.75
	Co	0.01	0.008 ± 0.001	0.01 ± 0.001	0.008 ± 0.001
	Ni	0.00 (0.01)	0.007 ± 0.003	0.008 ± 0.002	0.009 ± 0.004
	Cu	0.02	0.018 ± 0.002	0.017 ± 0.003	0.019 ± 0.005
	Zn	0.05 (0.10)	0.089 ± 0.001	0.083 ± 0.003	0.097 ± 0.014
	Mo	0.15	0.122 ± 0.01	0.139 ± 0.01	0.135 ± 0.01
Initial concentration in BG11 _u	B	0.50	0.507 ± 0.04	0.531 ± 0.07	0.472 ± 0.07
	Na	8.87	147.728 ± 19.71	144.611 ± 7.08	145.66 ± 9.28
	Mg	7.40	7.43 ± 0.33	7.365 ± 0.42	7.205 ± 0.27
	P	7.11 (8.50)	8.766 ± 1.03	8.541 ± 0.86	8.603 ± 1.08
	K	17.96	16.826 ± 0.91	16.636 ± 0.75	17.247 ± 1.01
	Ca	9.81	8.296 ± 1.29	6.775 ± 0.55	7.559 ± 1.56
	Mn	0.50	0.495 ± 0.05	0.478 ± 0.03	0.404 ± 0.04
	Fe	1.28	0.226 ± 0.07	1.127 ± 0.12	5.683 ± 0.6
	Co	0.01	0.007 ± 0.001	0.008 ± 0.001	0.005 ± 0.001
	Ni	0.00 (0.01)	0.011 ± 0.005	0.011 ± 0.002	0.007 ± 0.004
	Cu	0.02	0.015 ± 0.001	0.019 ± 0.001	0.019 ± 0.001
	Zn	0.05 (0.10)	0.087 ± 0.006	0.088 ± 0.001	0.075 ± 0.003
	Mo	0.15	0.133 ± 0.01	0.145 ± 0.01	0.137 ± 0.01

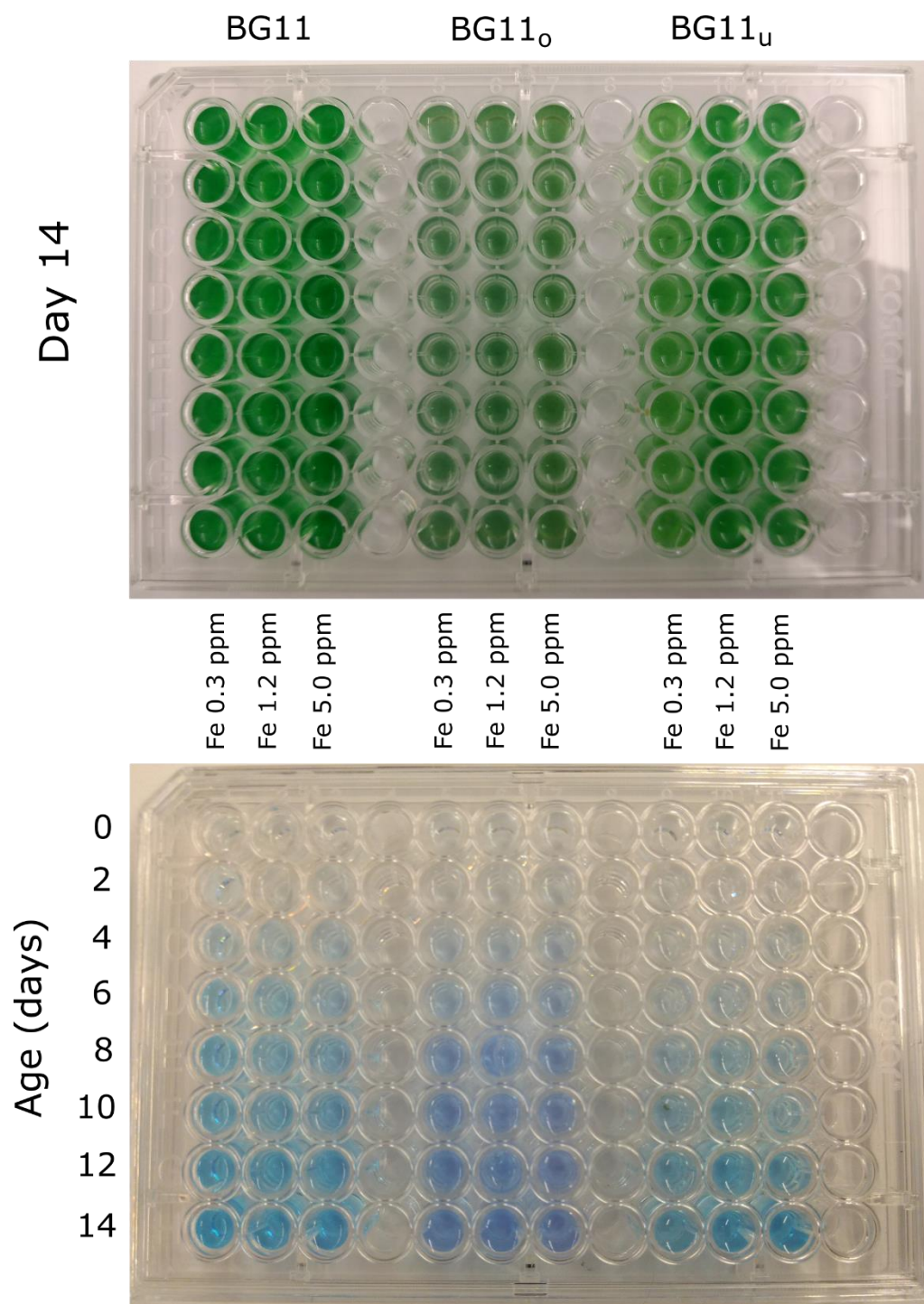


Figure 6.3. Pigmentation of *Anabaena* sp. cultures.

Top: Culture appearance at day 14. Bottom: Progressive accumulation of PBPs. The differences in cellular pigmentation are evident between diazotrophic (BG11_o) and non-diazotrophic cultures (BG11 and BG11_u). Production of PBPs is faster for cells grown in BG11 and BG11_o media. Fe levels have a more significant effect on the production of PBPs in BG11_u.

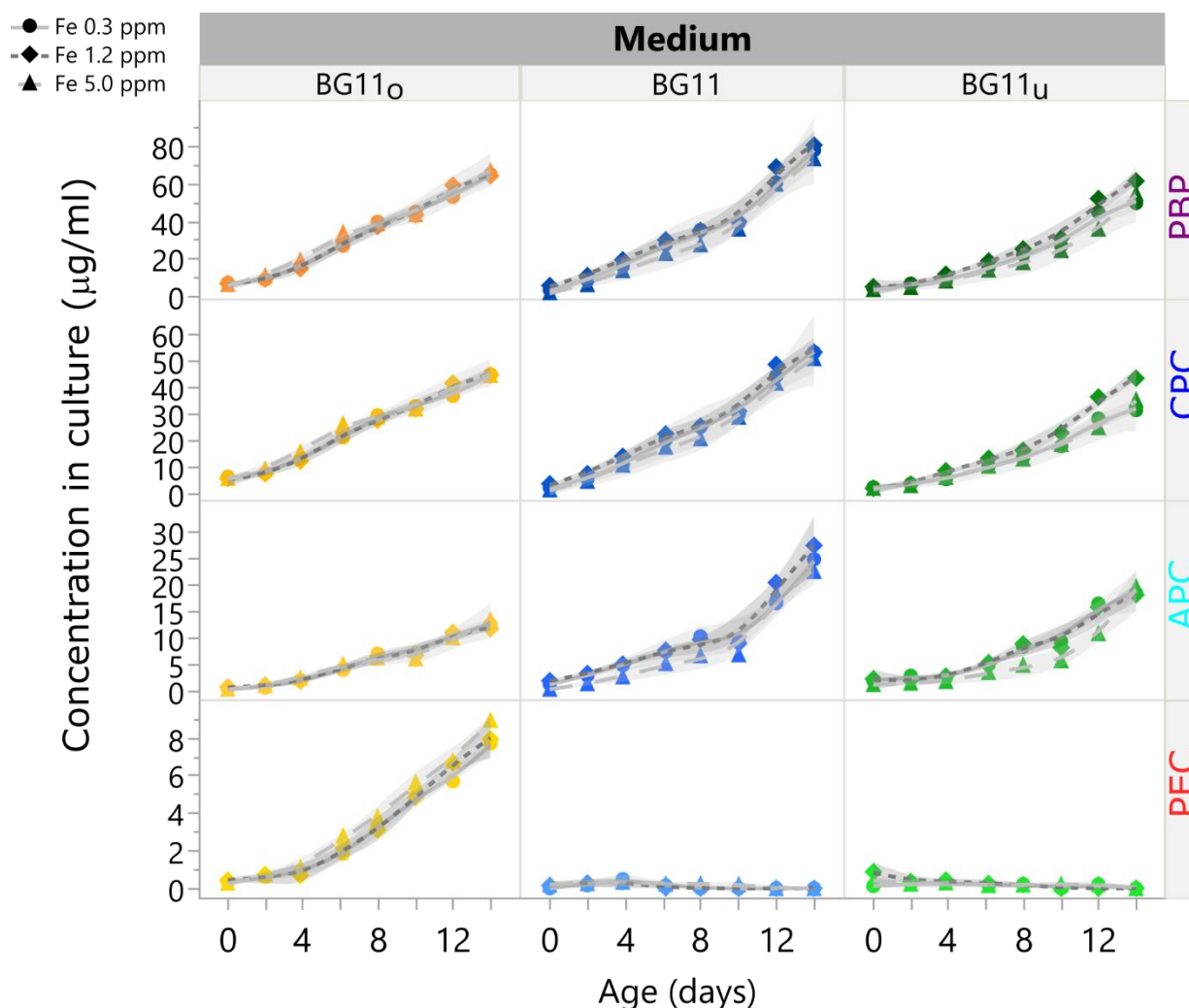


Figure 6.4. Concentration of PBPs in media with different N-sources.

While Phycoerythrocyanin (PEC) production was significantly higher in BG11_o cultures, C-phycoerythrocyanin (CPC) and Allophycocyanin (APC) production profiles were more pronounced in BG11 cultures. *Anabaena* sp. cells in BG11 and BG11_u produced comparable profiles of PBPs, but pigment-protein production was slower in BG11_u cultures. Markers represent the average of two biological replicates and shaded areas represent confidence fit intervals using a significance level $\alpha=0.05$.

The concentration of CPC, APC, PEC, and total PBPs of the cultures was determined and compared with the cell density to determine average abundance of these pigment-protein complexes per cell over time. Direct measurements of the concentration of PBPs for each medium type and Fe-level treatment are summarized in Figure 6.4.

Furthermore, Figure 6.5 presents the cellular abundance profiles of CPC, APC, PEC, and total PBPs over time. Remarkably, the cellular abundances of all PBPs were higher for diazotrophic cultures in BG11_o, which produced up to 2.5 times more PBPs per cell than cultures in BG11. Diazotrophic cells also produced at least 47% more PBPs per cell than BG11_u cultures after day 8. In BG11_o medium, increasing Fe-levels had a negative effect on the average accumulation of CPC and APC in the long run (i.e., after day 8). Accumulation of PEC in BG11_o was not significantly impacted by the Fe-level. Over 14 days, the biomass production and cellular density of *Anabaena* sp. cultures in BG11_o were the lowest (Figure 6.1), but the total concentration of PBPs in this type of medium was comparable to BG11 and BG11_u cultures (first row of Figure 6.4). This suggests that diazotrophic cells maintained similar levels of PBP biosynthesis despite the imposed N-limiting conditions. Since PBSs act as special N-reserves of cyanobacteria [328], this also suggests that the heterocysts supplied sufficient levels of N₂-fixation to sustain the base N-demand required for the diazotrophic metabolism.

Although cultures in BG11 medium presented the highest accumulation of PBPs amongst growth media, they also exhibited the lowest abundance of PBPs per cell. Since the growth speeds were fastest in media with NaNO₃, lower average intrinsic content of PBPs may have resulted from lower generation times dictating shorter periods of cellular division, as suggested by Table 6.1. Interestingly, higher Fe levels reduced the average cellular abundance levels of CPC and APC in BG11 during the early stages of growth (up to day 10). These results agree with semi-quantitative reverse transcription-PCR data suggesting downregulation of tetrapyrrole and phycobilin biosynthesis (i.e., the PCB chromophore) in wild-type *Anabaena* sp. at low levels of *FurA* transcription factor in Fe-

replete conditions [19]. As cells reproduced over time, Fe became scarcer on a per-cell basis, leading to upregulation of PCB production at later stages of cell growth. The observed abundance of PEC in BG11 cultures was the lowest during the entire duration of the experiment.

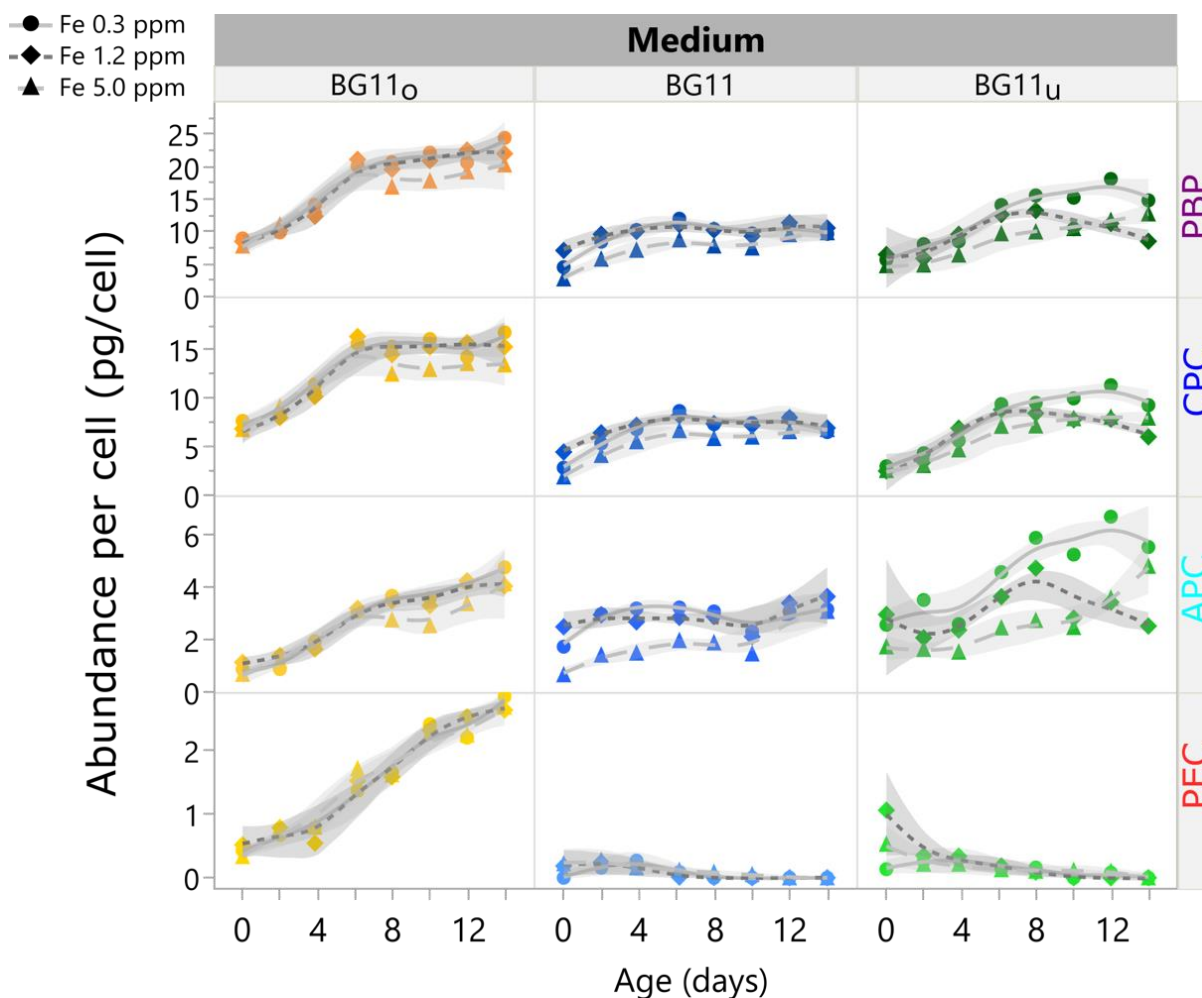


Figure 6.5. Abundance of phycobiliproteins (PBPs) per cell over time.

Cells in BG11_o medium presented higher abundances per cell of PBPs, and specially PEC, compared to the cultures in BG11 and BG11_u. High Fe levels (5.0 ppm) led to a statistically significant reduction on the abundance of CPC and APC accumulation in BG11 and BG11_u media. The most pronounced reduction in the APC content per cell with increasing Fe was observed for BG11_u cultures. The PEC content in BG11 and BG11_u was consistently reduced over time, as non-diazotrophic filaments of *Anabaena* sp. lowered the production of PEC. The highest abundance of APC was registered for low Fe cultures in BG11_u, specifically at the end of the experiments. Markers represent the average of two biological replicates and shaded areas represent confidence fit intervals using a significance level $\alpha=0.05$.

Similar observations on the abundance of PBPs per cell and the effect of high Fe levels were registered for cells growing with NaNO_3 and urea. However, the upregulation effect of PCB (the only chromophore in CPC and APC) under Fe-depleted conditions (initial Fe level of 0.3 ppm) was more pronounced for the accumulation of APC in urea. These results also agree with RNA-Seq experiments presenting transcription levels of genes encoding the subunits α and β of APC (alr0021 and alr0022) in *Anabaena* sp. It has been shown that the transcript abundance of these genes in medium with NH_4^+ is two times the transcription level in diazotrophic cells [424]. NH_4^+ is a product of intracellular and extracellular degradation of urea [332, 481]. After comparing the starting concentrations of elemental N in BG11 and BG11_u media (~18 mM vs 6 mM), the initial elemental N-availability in BG11 medium was 3 times the initial N-availability in BG11_u. Despite this, the cellular abundance levels of PBPs in these media were similar. This suggests that excess N in the growth medium does not necessarily increase the accumulation of this element as a N reserve in the PBSs. Instead, the assembly of PBSs may be significantly influenced by the generation time (Table 6.1). Moreover, it was observed that the production of PEC is minimized in non-diazotrophic cultures, regardless of the Fe-level.

6.4.3 Effect of N and Fe availability on hydrophobic pigments

Diazotrophic cultures present at least 30% higher relative abundance of ChlA than non-diazotrophic cultures but β -carotene is more abundant in cells grown with NaNO_3 .

Two different methods of solvent extraction were routinely used to measure the concentration of ChlA and carotenoids in liquid cultures of *Anabaena* sp. In the first

approach, solvent extraction with cold acetone 90% v/v was used to have an indicator of the concentration of ChlA and total carotenoids (CaroT) every other day. Since acetone is a less effective solvent for extracting these hydrophobic pigments [428, 430, 478], measured concentrations of these compounds are significantly lower than the actual abundances. However, these data were used as an indicator of the relative abundance of hydrophobic pigments in different growth media. ChlA and CaroT concentration profiles after cold acetone extraction are presented in Figure 6.6. After considering the cell density, relative cellular abundance data for ChlA and CaroT are summarized in Figure 6.7. Cultures in BG11 and BG11_u media exhibited similar profiles, with maximum values of ChlA and CaroT abundance in the exponential phase (between 4 and 8 days). In contrast, ChlA and CaroT abundance profiles of diazotrophic cultures in BG11_o continued to grow until the end of the evaluation period. This was also the case for the ChlA and CaroT concentration profiles from Figure 6.6. Although increasing Fe levels had a small effect on promoting higher abundance of ChlA and CaroT in BG11_o medium, the Fe-availability did not significantly affect the cellular abundance of these pigments in BG11 nor BG11_u. Using the maximum values of cellular abundance data from Figure 6.7, cultures in BG11_o accumulated up to 35% more ChlA than cells grown in BG11 and 30% more ChlA than BG11_u cultures.

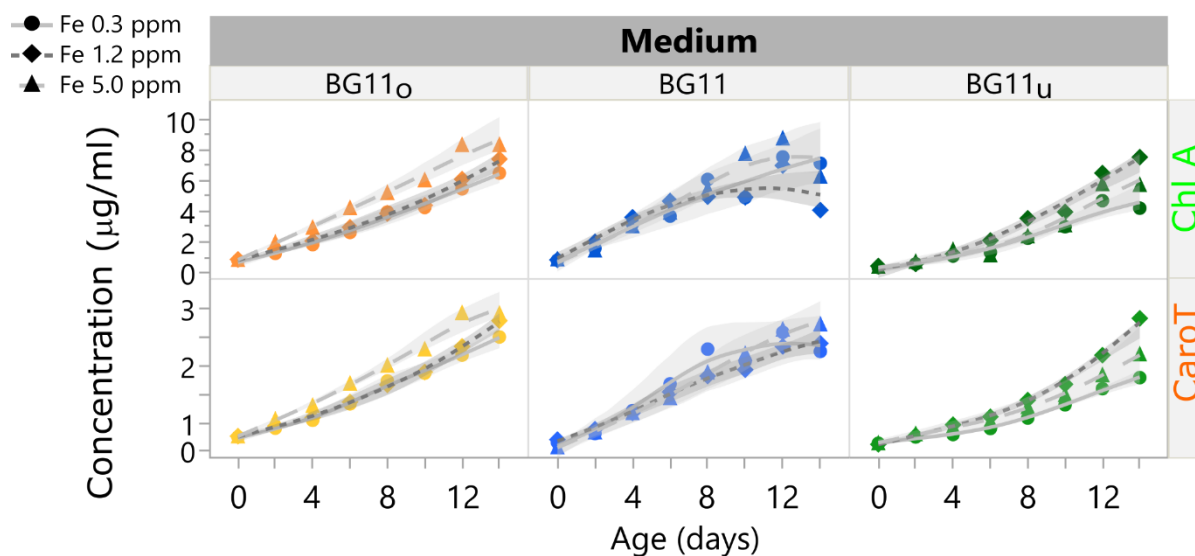


Figure 6.6. Concentration of Chl A and Carot in different growth media.

Anabaena sp. cells in all media presented steady increase in concentration of hydrophobic pigments (Chl A and Carot). Markers represent the average of two biological replicates and shaded areas represent confidence fit intervals using a significance level $\alpha=0.05$.

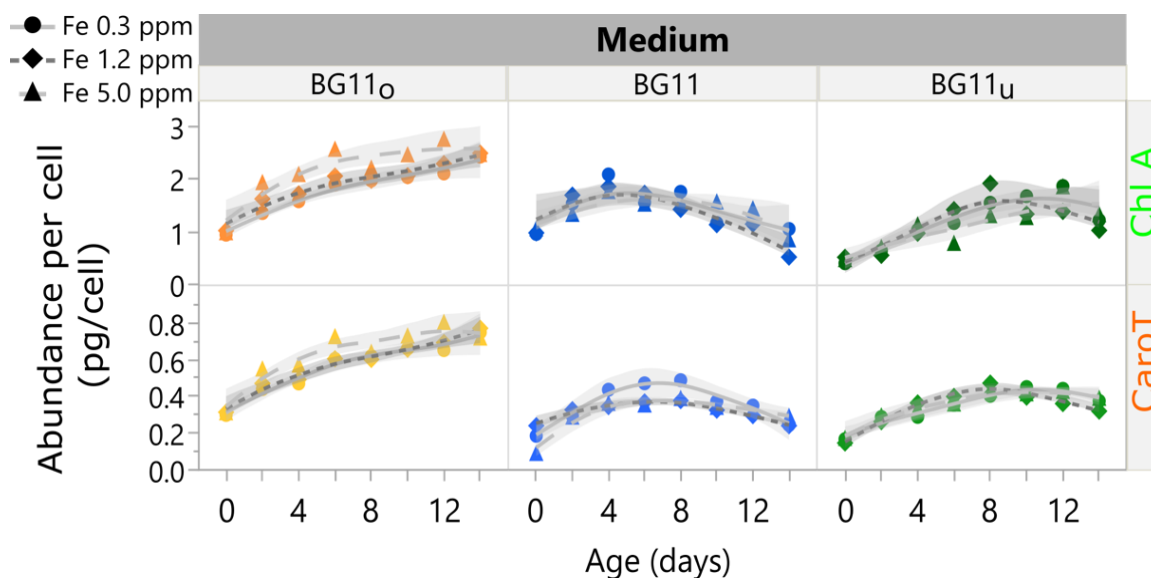


Figure 6.7. Relative abundance of Chl A and Carot per cell.

Chl A and Carot were more abundant in diazotrophic cultures, showing steady increase in the accumulation of hydrophobic pigments until the end of the experiment. Non-diazotrophic cultures in BG11 and BG11_U media presented maximum values of Chl A and Carot abundance per cell during the exponential phase. Markers represent the average of two biological replicates and shaded areas represent confidence fit intervals using a significance level $\alpha=0.05$.

A second strategy, using cold methanol extraction, was followed for accurate quantification of β -Carotene using TOF-MS (See subsection 3.5.3). The ion abundance intensity of the β -Carotene peak (molecular ion, $[\text{C}_{40}\text{H}_{56}]^+$, $m/z = 536.4382$) was compared with the peak intensities of Echinenone (protonated molecule, $[\text{C}_{40}\text{H}_{54}\text{O} + \text{H}]^+$, $m/z = 551.4253$), Pheophytin A (protonated molecule, $[\text{C}_{55}\text{H}_{74}\text{N}_4\text{O}_5 + \text{H}]^+$, $m/z = 871.5737$) and ChlA (protonated molecule, $[\text{C}_{55}\text{H}_{74}\text{MgN}_4\text{O}_5 + \text{H}]^+$, $m/z = 893.5431$). The β -carotene abundance per cell and the ratios of relative abundance (as peak intensity ratios) were used to analyze the oxidation of carotenoids in *Anabaena* sp.

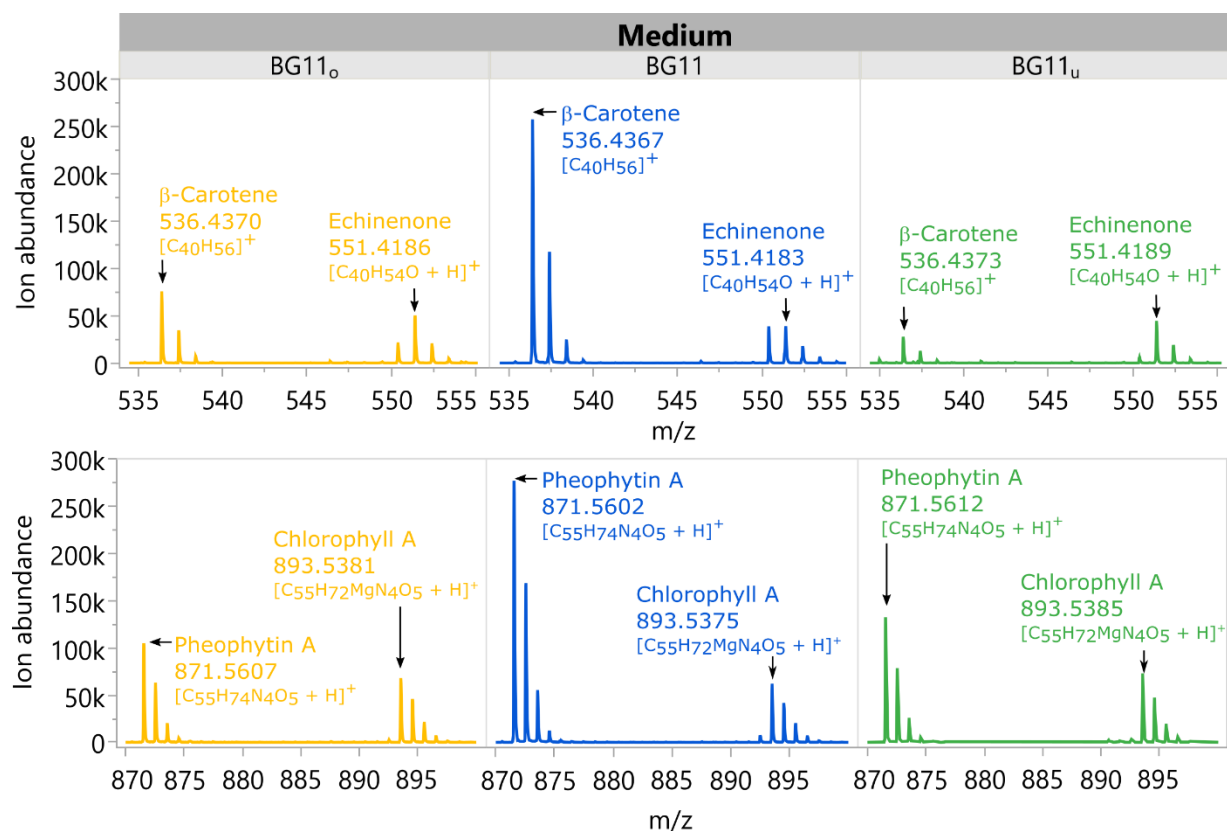


Figure 6.8. MS-TOF analysis of methanol extracts.

Mass spectrometry was used to identify β -Carotene, Echinenone, Pheophytin A and ChlA in methanol extracts of *Anabaena* based on their representative masses. Peak heights indicate abundance of the corresponding ions. Extracts with similar levels of ChlA are compared.

Methanol extraction was performed only for samples on days 6, 10 and 14. A statistical analysis of the data indicated that Fe-levels did not have a significant impact on the β -carotene abundance per cell. Therefore, the abundance and oxidation of β -carotene were analyzed as a function of time and medium type. TOF-MS results from Figure 6.8 correspond to Methanol extractions on day 10, where the ChIA signals for cultures in all media were similar.

Figure 6.9 summarizes the cellular abundance of β -Carotene in different growth media and compares the Echinenone to β -Carotene ratio using peak intensities. Cellular content of β -Carotene was higher in younger cultures grown in BG11_o and BG11 media. Cells grown in BG11_u exhibited low abundance of β -Carotene during the entire duration of the growth experiments. Echinenone is the most abundant product of β -Carotene oxidation in *Anabaena* sp., mediated by β -Carotene ketolase (EC 1.14.99.63) [427, 430, 431]. Therefore, the signal ratios of Echinenone to β -Carotene were used as an indicator of β -Carotene oxidation in different growth media. It was observed that cells grown in BG11 medium presented the lowest levels of β -Carotene oxidation, which probably increased over time as a result of continuous illumination. The oxidation levels of β -Carotene were significantly higher in cells grown in BG11_o and BG11_u. Given that the cellular abundance of Carot was highest for BG11_o cultures (second row in Figure 6.7), this suggests that the conversion of β -Carotene into other carotenoids was amplified during diazotrophic growth. Oxidation of β -Carotene was highest in cells grown in BG11_u medium. This is consistent with previous reports describing the growth on urea as a stressful condition for cyanobacteria, triggering peroxidation and cellular death [329]. Although the Echinenone to β -Carotene signal ratio decreased over time, this does not

necessarily mean a reduction of oxidation levels. Instead, it is possible that other carotenes and xanthophylls are produced by *Anabaena* sp. in BG11_u medium as a result of metabolic stress. This is partially exemplified in Figure 6.8, where a new peak of significant height ($m/z = 535.0288$) was observed only in methanolic extractions from cells in BG11_u. Further analysis is necessary to identify this peak, but it might correspond to Torulene, which participates in the synthesis of myxoxanthophylls [482, 483].

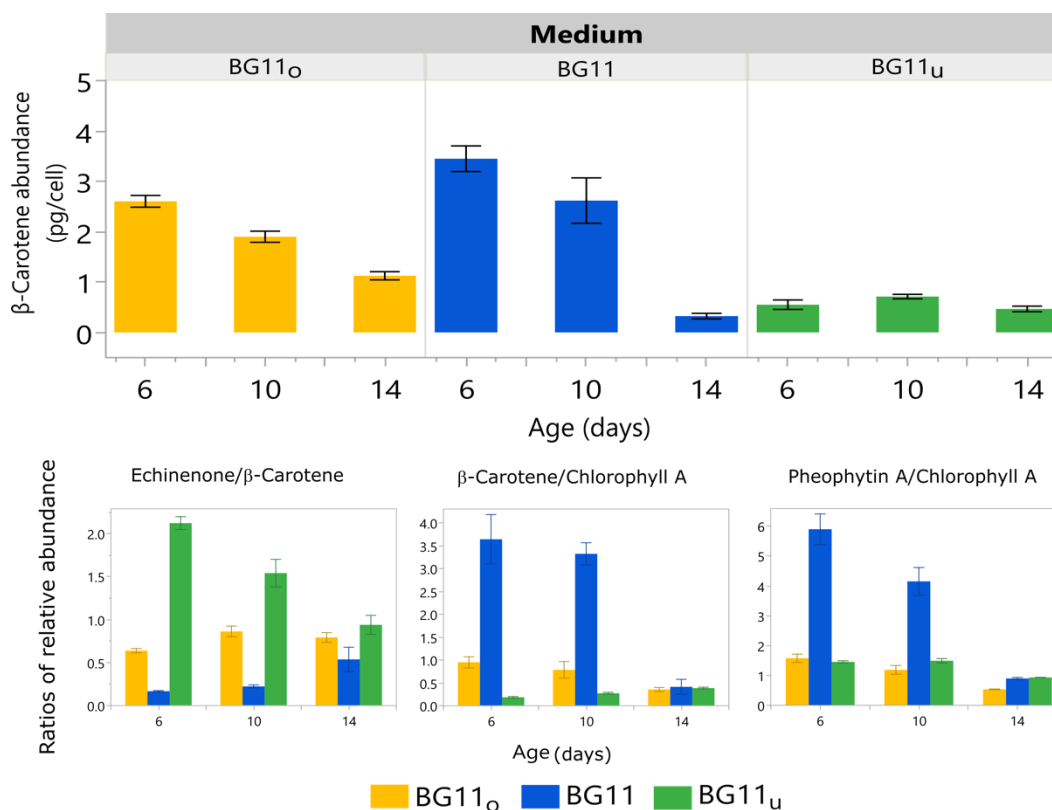


Figure 6.9. Cellular abundance and oxidation of β-Carotene.

Cellular abundance of β-Carotene is reduced over time for BG11_o and BG11 cultures and is lowest for cells grown in BG11_u medium (except for day 14). The Echinenone to β-Carotene ratio is used as an indicator of β-Carotene oxidation, suggesting that cultures in BG11_u are exposed to higher carotene-oxidation levels. The β-Carotene to ChlA ratio indicates the abundance of non-oxidized carotenoid relative to the abundance of the main photosynthetic pigment. The Pheophytin A to ChlA ratio is used as an indicator of PSII integrity. Bars represent the mean of three measurements per sample and each error bar is constructed using one standard error from the mean. Data represent results for six biological replicates per medium type.

Figure 6.9 also presents ratios of relative abundance of β -Carotene to ChlA and Pheophytin A to ChlA. Although ChlA is the main photosynthetic pigment in PSI and PSII, β -Carotene plays an essential role for light-harvesting and defense [12, 456, 473, 474]. Therefore, the β -Carotene to ChlA ratio was interpreted as an indicator of photodamage protection in the photosystems. Results suggest that the photodamage protection level was highest for cells in BG11 medium, specially at the beginning of the growth experiments. Cells grown in BG11_u medium presented the lowest β -Carotene to ChlA ratios, which can be explained by increased oxidative stress with urea [329]. Since Pheophytin A is exclusively present in PSII [464, 484], the Pheophytin A to ChlA ratio was used as an indicator of PSII integrity. This ratio was highest for younger cultures in BG11 and lowest for older cells in BG11_o. These differences can be explained after considering that *Anabaena* sp. degrades PSII when vegetative cells differentiate into heterocysts to accomplish N₂-fixation [327, 328]. Overall, these results indicate that β -Carotene oxidation is minimized when *Anabaena* sp. uses NaNO₃ as their N-source. Although these cells can grow with urea, this N-source promotes oxidation of β -Carotene.

6.4.4 Effect of N and Fe availability on nutrient consumption

CO₂ consumption rates were 20% higher for non-diazotrophic cultures and P-demands were at least 70% higher in cells grown in BG11_u and BG11_o media.

Mineral medium for cyanobacteria is mainly composed of a Nitrogen substrate, phosphates, inorganic carbon and mineral salts that supply essential metallic micronutrients. Although C and N-sources are the most important nutrients, all the components of the growth medium are used to sustain autotrophic metabolism and cell

reproduction. In the end, cyanobacteria are sophisticated microbial photosynthetic bio-factories with simple nutrient requirements, most of which are inorganic compounds. Despite this highly simplified description of the cyanobacterial metabolism, lack and availability of some nutrients have important implications for biomass generation and biotechnological applications of *Anabaena* sp. Table 6.4 summarizes the consumption rates of N-sources and CO₂ equivalents in different growth media. These results are not presented for different Fe-levels because changes in the initial Fe-availability did not affect N or C-demands significantly. While the consumption of N-sources was represented by apparent first-order rate constants, the consumption of CO₂ equivalents is represented by apparent zero-order rate constants. Considering the implications of the Carbon concentrating mechanism (CCM) in cyanobacteria, CO₂ equivalents mainly refer to bicarbonate (HCO₃⁻) ions, either supplied by the growth medium or obtained through CO₂ fixation [453]. Additional details are presented in Figure 6.10 and Figure 6.12. Remarkably, Table 6.4 indicates that cells grown in BG11 and BG11_u media (i.e., non-diazotrophic cells) presented CO₂ consumption rates ~20% higher than diazotrophic cultures in BG11_o. Since urea degradation in the aqueous medium supplies NH₄⁺ and HCO₃⁻, higher levels of CO₂ consumption can be associated with high urease (EC 3.5.1.5) activity levels in BG11_u medium (See Figure 6.11).

Table 6.4. Rate constants for N and C-source consumption.

N-source consumption rates represent the average and standard deviation of first-order rate constants. TOC formation rates represent the zero-order rate constant. Eq. CO₂ consumption rate was calculated by multiplying TOC formation rate by 3.67. Numbers represent averages and standard errors for consumption/ fixation rates considering at least four biological replicates per medium type.

Medium	BG11 _o	BG11	BG11 _u
N ₂ fixation rate (day ⁻¹)	0.21 ± 0.013	-	-
NO ₃ consumption rate (day ⁻¹)	-	0.06 ± 0.004	-
Urea consumption rate (day ⁻¹)	-	-	0.08 ± 0.012
TOC formation rate (mg L ⁻¹ day ⁻¹)	14.5 ± 1.1	17.2 ± 0.7	18 ± 1.3
Eq. CO ₂ consumption rate (mg L ⁻¹ day ⁻¹)	53.1 ± 3.9	63.1 ± 2.7	66 ± 4.9

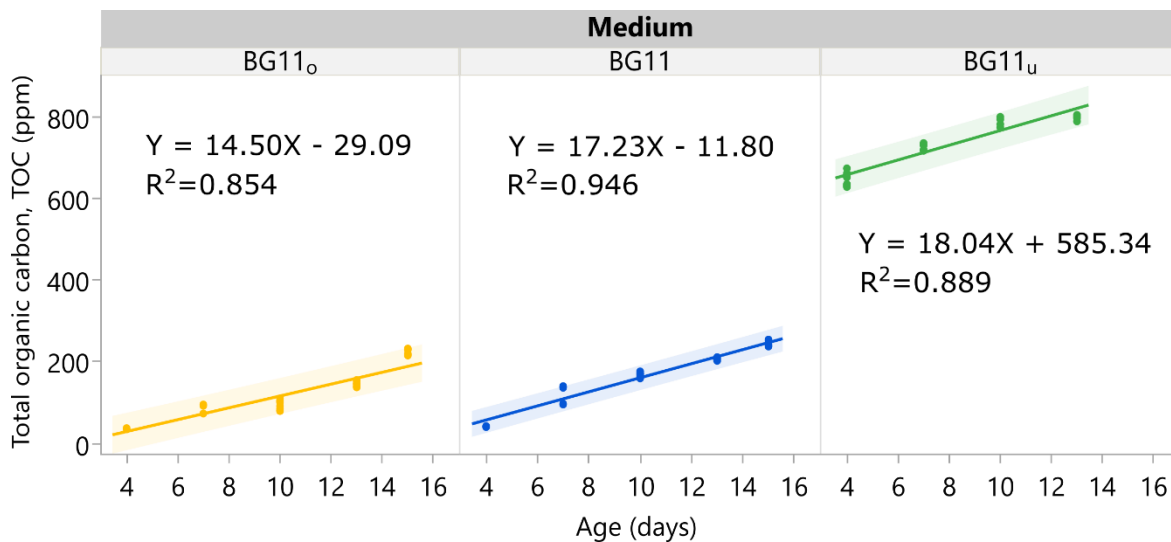


Figure 6.10. TOC formation profiles.

BG11u medium presented higher initial content of organic carbon due to the TES buffer. TOC profiles were fitted to a linear model to determine zero-order CO₂ fixation rates in each medium. Data represent 4 biological replicates per medium type. Shaded areas represent confidence fit intervals using a significance level $\alpha=0.05$.

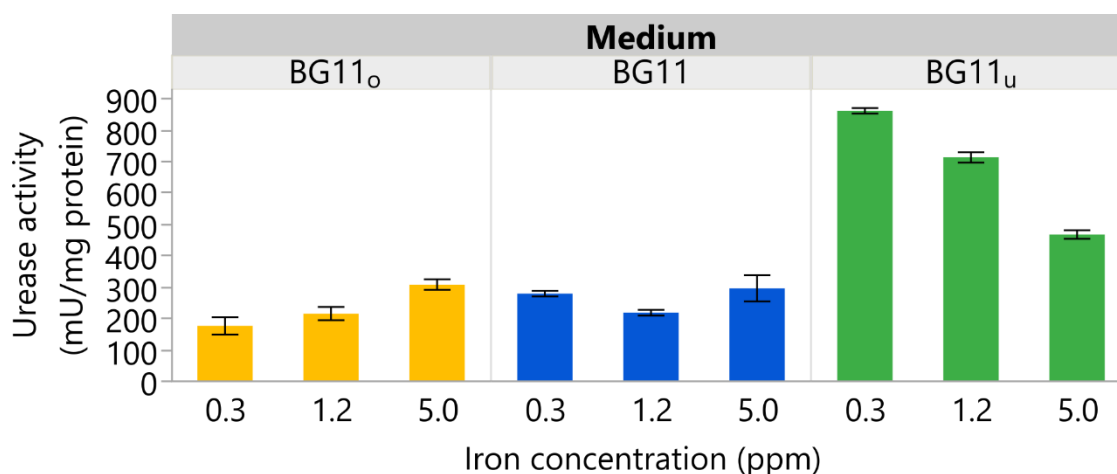


Figure 6.11. *Anabaena* sp. urease activity in different media.

The urease activity of *Anabaena* sp. was highest in BG11_u medium, where Fe-levels affected the activity of the enzyme. Bars represent the mean of two biological replicates. Error bars were constructed one standard error from the mean.

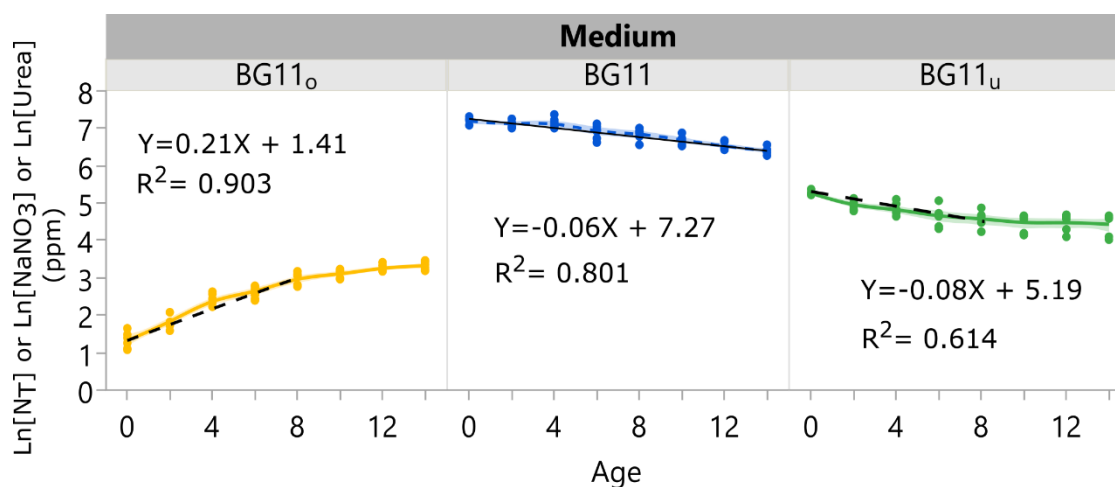


Figure 6.12. Consumption profiles of N-sources.

Consumption profiles of N₂, NaNO₃ and urea were adjusted to a first order kinetic model. Data represent the mean of six biological replicates per medium type. Rate constants for N₂-fixation (BG11_o) and urea consumption (BG11_u) were calculated with data from the exponential phase (up to day 8). NO₃ consumption was constant for two weeks in BG11. Data are consistent with the findings from section 5.5.4.

ICP-OES was used to monitor changes in the concentration of mineral elements in liquid media during cellular growth. For most elements, concentration profiles were converted into consumption profiles after subtracting the element concentration at a given time from their initial concentration in fresh media. This was important to analyze excess levels of mineral nutrients in the growth media. Figure 6.13 presents Fe consumption profiles in BG11_o, BG11 and BG11_u. Regardless of the initial Fe concentration in the growth media, this element was almost immediately consumed at the beginning of the growth experiments. Fe is extremely valuable for cyanobacteria and these profiles indicate that the starting population of *Anabaena* sp. cells in each culture immediately incorporated this nutrient, activating Fe accumulation mechanisms involving siderophores and bacterioferritins [393, 455, 457]. Given that no extra Fe-source was added to the cultures during the growth experiments, the Fe reserves had to be distributed from mother to daughter cells during reproduction.

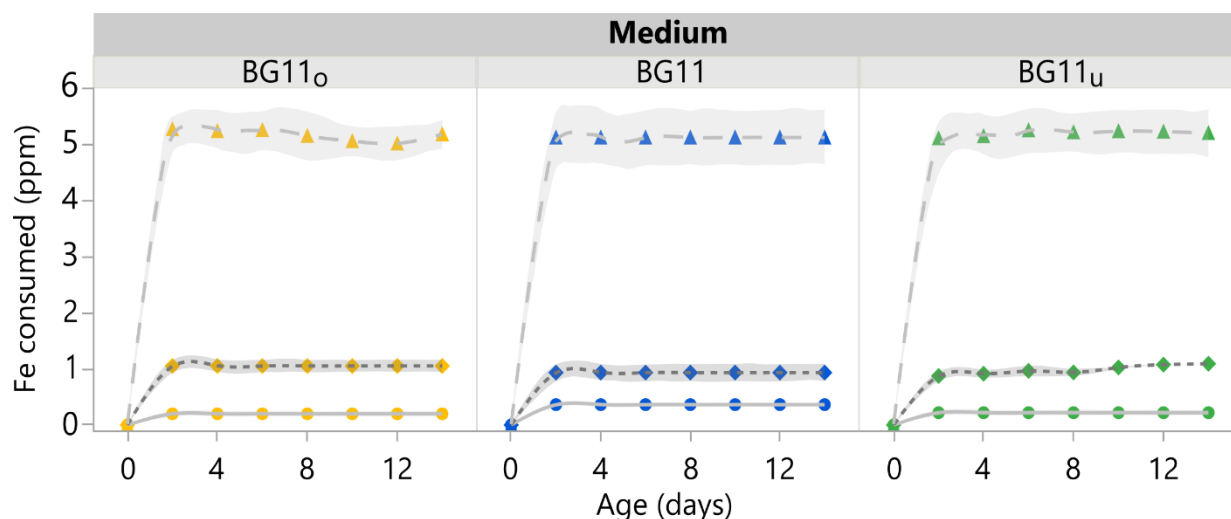


Figure 6.13. Fe consumption profiles in growth media.

Fe was immediately consumed by *Anabaena* sp. cells, regardless of the concentration level supplied in fresh media.

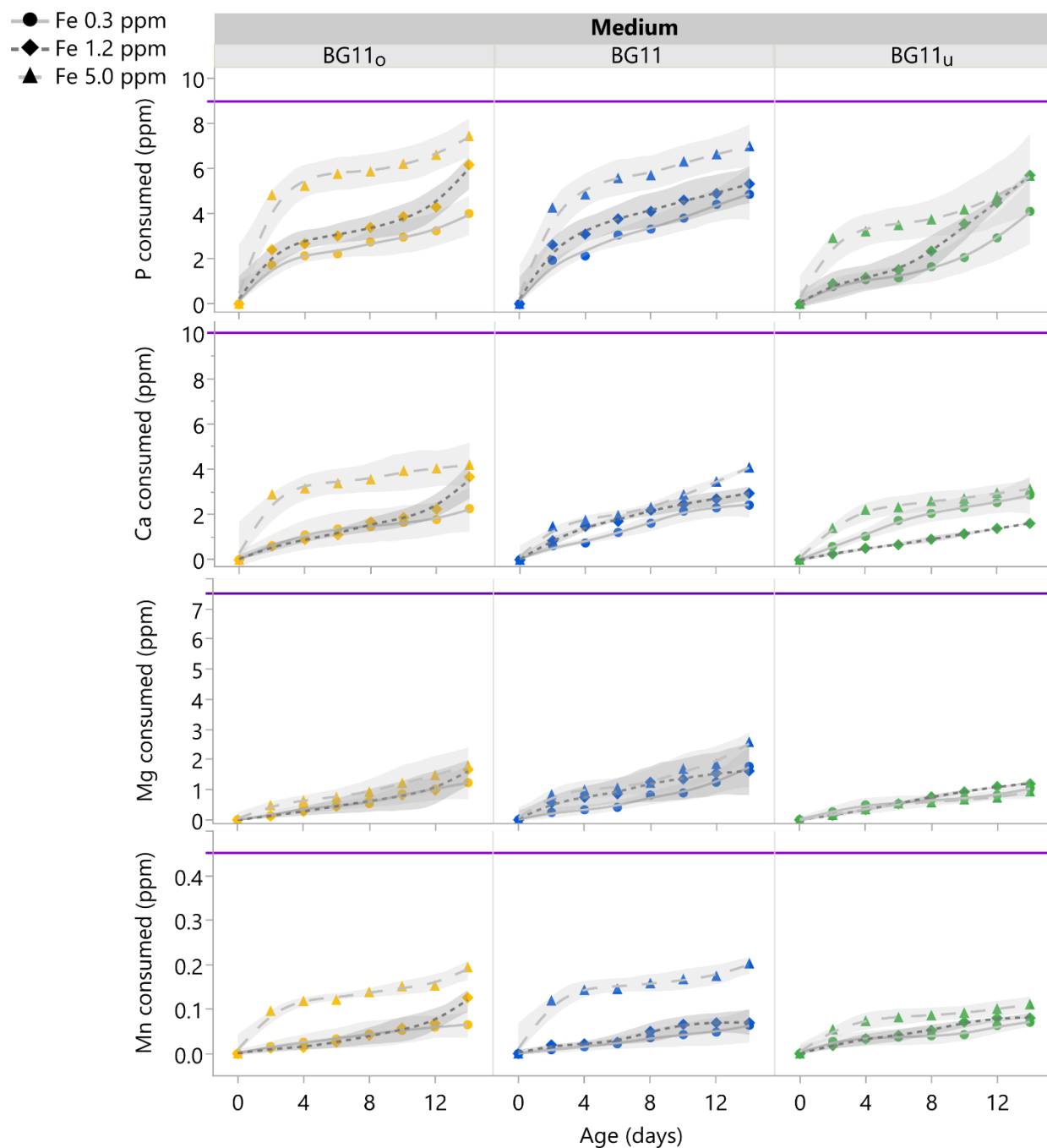


Figure 6.14. Consumption profiles of P, Ca, Mg and Mn.

P, Ca, Mg and Mn were consumed over time. Consumption profiles were affected by starting Fe-levels in the growth medium. Purple lines represent the initial concentration of each element. P was closest to exhaustion at the end of growth experiments, especially in BG11_o cultures. Markers represent mean values for two biological replicates. Shaded areas represent confidence fit intervals using a significance level $\alpha=0.05$.

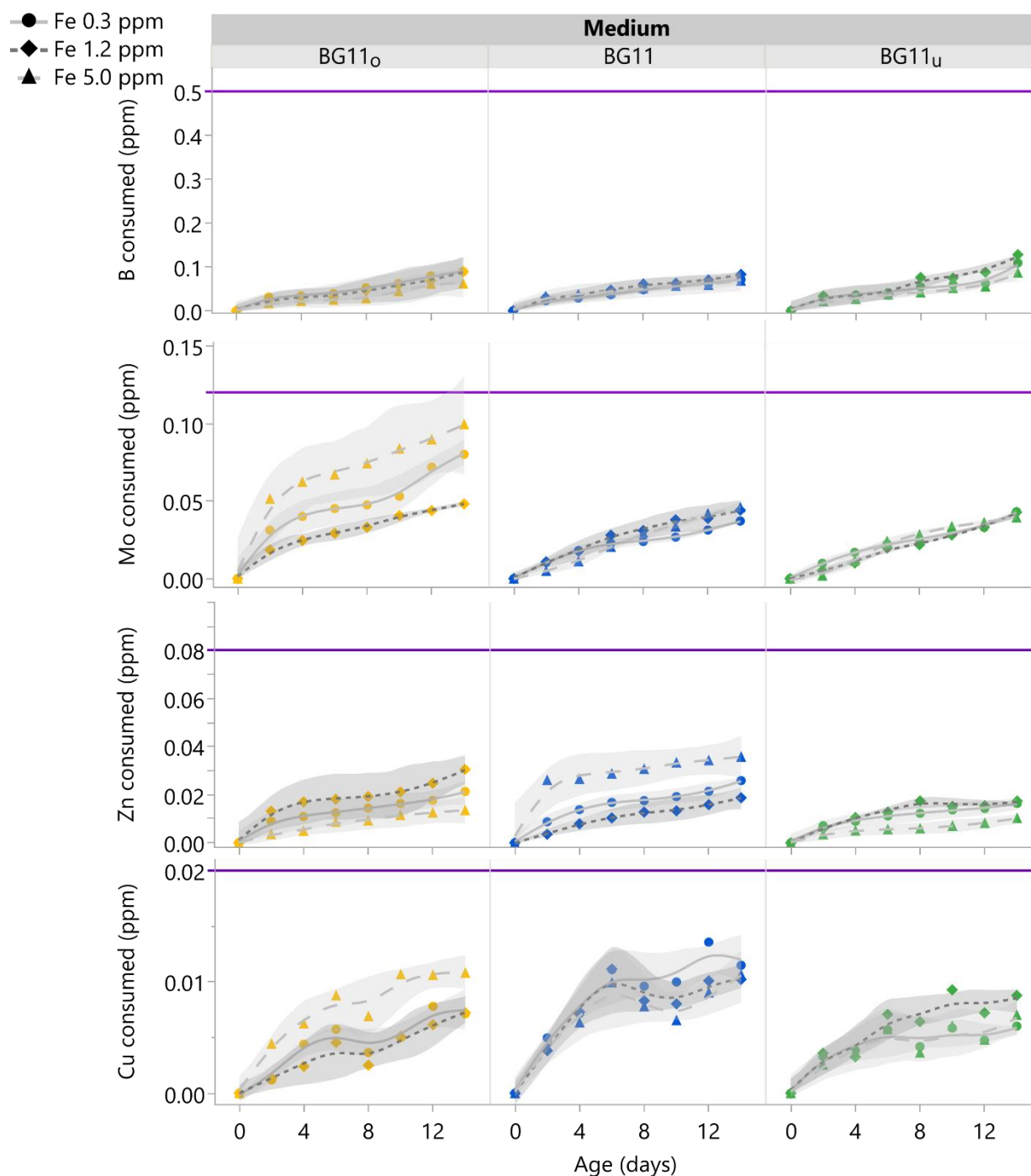


Figure 6.15. Consumption profiles of B, Mo, Zn and Cu.

B, Mo, Zn and Cu were consumed over time. Consumption profiles were affected by starting Fe-levels in the growth medium. Purple lines represent the initial concentration of each element. Mo was closest to exhaustion at the end of growth experiments, especially in BG11_o cultures. Markers represent mean values for two biological replicates. Shaded areas represent confidence fit intervals using a significance level $\alpha=0.05$.

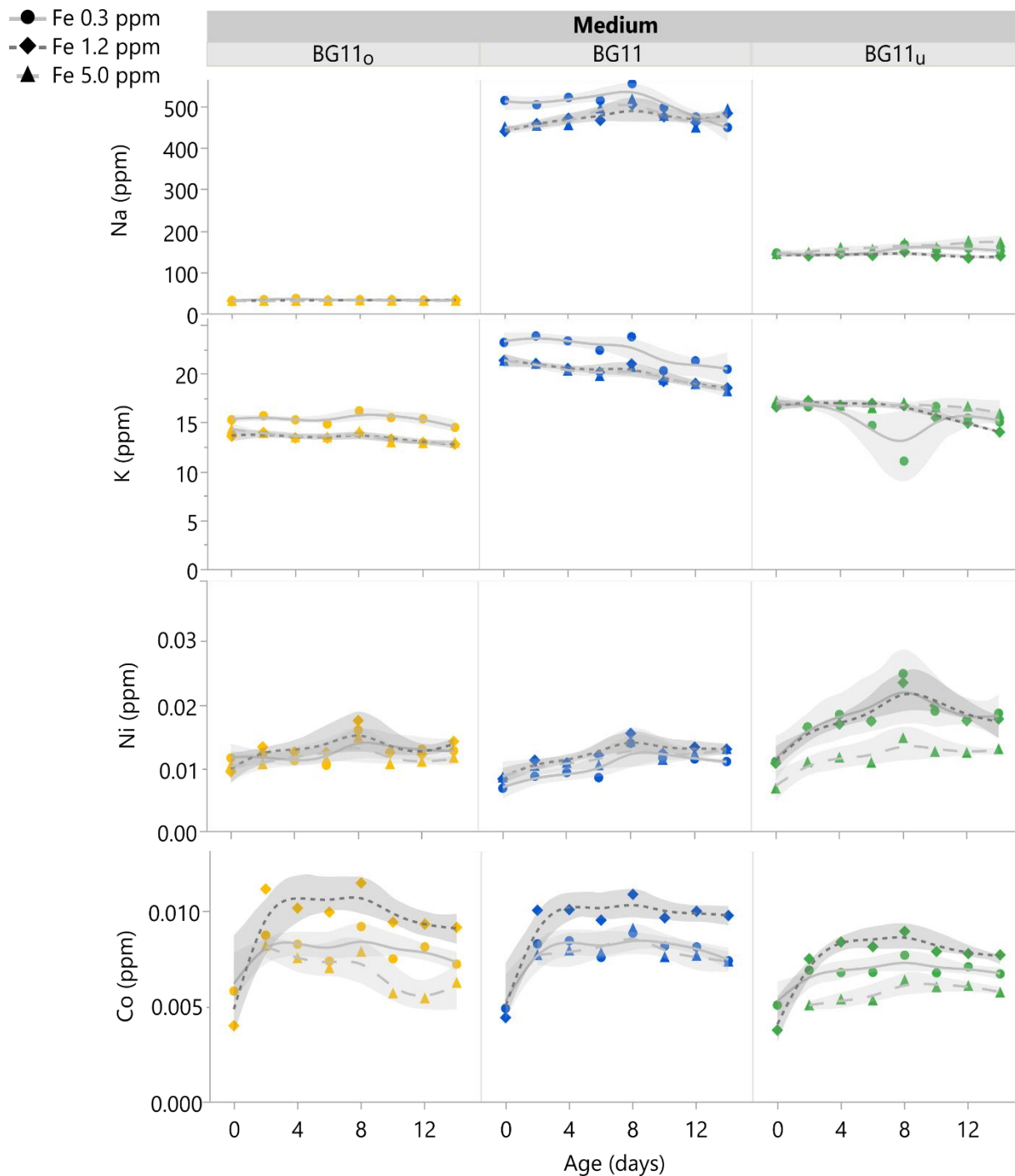


Figure 6.16. Concentration profiles of Na, K, Ni and Co.

Na, K, Ni and Co were not apparently consumed over time. Co levels were too low to ensure reliable quantification. Markers represent mean values for two biological replicates. Shaded areas represent confidence fit intervals using a significance level $\alpha=0.05$.

Figure 6.14 and Figure 6.15 present consumption profiles of P, Ca, Mg, Mn, B, Mo, Zn, and Cu, suggesting that all these elements were supplied in excess. However, the amount of P supplied in the growth media was close to exhaustion after 14 days, especially for cultures in BG11_o and BG11 media with high starting Fe-levels. The consumption of Mo in BG11_o cultures was also close to exhaustion after 14 days, especially under low and high starting Fe-levels. This is because Mo is an essential component of Nitrogenase (EC 1.18.6.1) [325, 327]. Figure 6.16 presents concentration profiles of Na, K, Ni, and Co. These profiles were not converted to consumption data because they did not present significant variations over time in the growth medium. Moreover, the Co-level in the growth media was so low that it approached the lower detection limit of the method. These consumption profiles suggest that it is possible to adjust the concentrations of micronutrients and minimize excess of ingredients depending on the duration of each growth experiment. This is important for large-scale continuous operations, where raw material use needs to be optimized.

After considering the number of cells produced at a given time, the consumption profiles of P, Ca, Mg, and Mn per cell are presented in Figure 6.17. Similar consumption profiles for B, Mo, Zn, and Cu are summarized in Figure 6.18. These figures show that the demands for mineral nutrients per cell produced were higher during the exponential phase of culture growth (e.g., up to day 8). The implications of changing P, Ca and Mn demands will be further discussed using consumption data for day 4 as a reference.

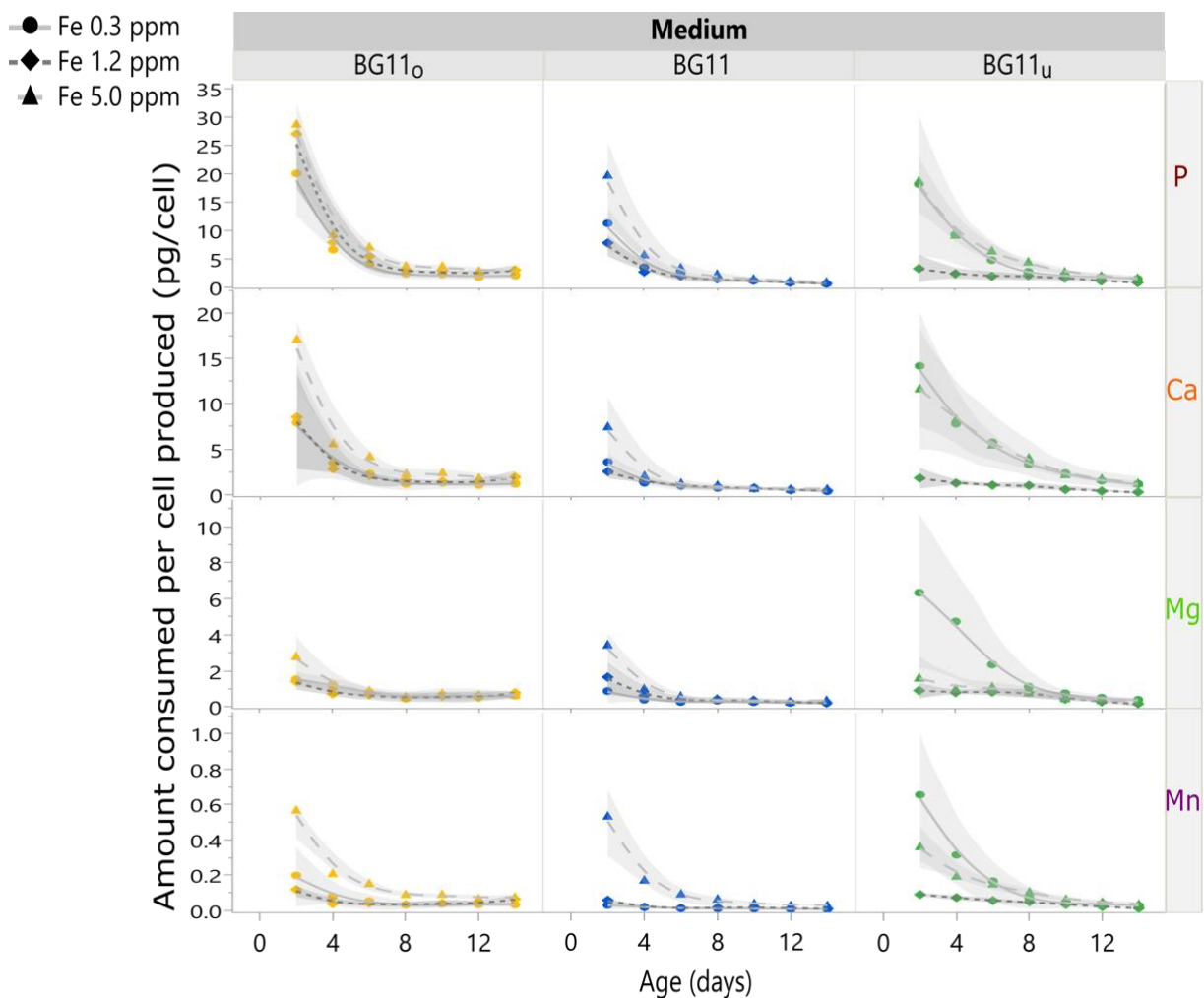


Figure 6.17. Consumption profiles of P, Ca, Mg and Mn per cell.

The demand of these nutrient elements per cell is pronounced during the early stages of cellular growth. High initial Fe-levels maximize the demand of P and Ca in all growth media. Low initial Fe-levels increased Mg and Mn consumption in BG11_u medium. High starting Fe-levels also maximized the consumption of Mn in BG11_o and BG11 media, probably as a defense strategy against Fe-promoted oxidation. Markers represent the average of two biological replicates and gray shaded areas represent confidence fit intervals with a significance level $\alpha=0.05$.

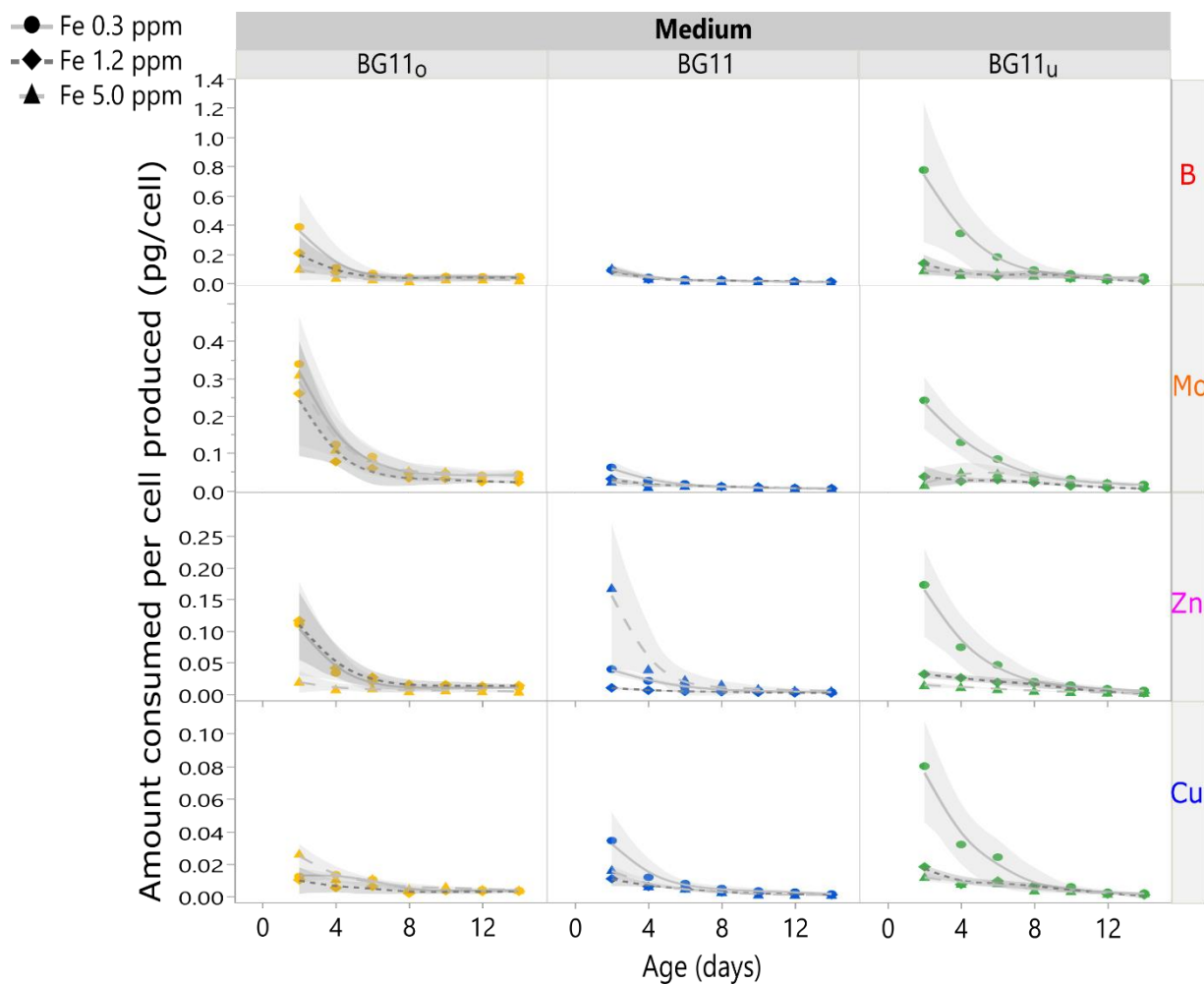


Figure 6.18. Consumption profiles of B, Mo, Zn and Cu per cell.

The demand of these nutrient elements per cell is pronounced during the early stages of cellular growth. High initial Fe-levels maximize the demand of Zn in BG11. Low initial Fe-levels increased B, Mo, Zn and Cu consumption in BG11_u medium. Markers represent the average of two biological replicates and gray shaded areas represent confidence fit intervals with a significance level $\alpha=0.05$.

Compared to BG11 cultures, the average P-demand per cell in BG11_o medium was almost doubled. Similarly, the average P-demand of cells grown in BG11_u medium was at least 72% higher than in BG11. For all types of media, the maximum Fe-level (5.0 ppm) also promoted the significantly higher P-consumptions. At day 4, the P-consumption per cell in BG11_u cultures was almost 4 times higher with Fe 0.3 ppm and Fe 5.0 ppm compared to Fe 1.2 ppm. Since P is necessary for the synthesis of ADP and ATP, higher P-demands may be interpreted as a sign of intense metabolic activity. In the case of BG11_o cultures, increased P-consumption can be attributed to N₂-fixation because heterocysts require at least 16 moles of ATP to fixate one molecule of N₂ [327]. This process does not occur in non-diazotrophic cultures. In BG11_u cultures with high and low initial Fe-levels, intense metabolic activity can be related to increased activity of defense mechanisms against peroxidation [329]. Compared to BG11 cultures, higher Ca-demands per cell were observed for cells grown in BG11_o (2.5 times more) and BG11_u media (3.7 times more). High Ca-demands in BG11_o cultures are reasonable because Ca²⁺ ions are important for signal transduction in the differentiation of heterocysts for N₂-fixation [485]. In BG11_u cultures, high Ca-demands with low and high Fe-levels can be explained because Ca²⁺ ions are messengers for cell regulation processes triggered during cellular stress [486].

Elevated consumption of Mn was observed during the first 8 days of growth in BG11_o and BG11 media with Fe 5.0 ppm. High Mn-demands were also evident for BG11_u cultures with low (0.3 ppm) and high (5.0 ppm) Fe-levels. On the other hand, the lowest Mn-demands were observed for BG11 cultures with medium (1.2 ppm) and low (0.3 ppm) starting Fe-levels. Comparing the data for day 4, the average Mn-demand of BG11_u

cultures was almost three times the Mn required by BG11 cultures. For BG11_o cultures, the mean Mn-demand was at least 55% higher than in BG11 medium. Mn is an essential micronutrient in cyanobacterial growth media because it is present in the Mn₄CaO₅ cluster of PSII, which is responsible for O₂ evolution and electron transfer from water [464, 465]. Remarkably, Mn is also involved in the defense mechanisms of *Anabaena* sp. against oxidative stress, as this element is present in Mn-catalase (EC 1.11.1.6) and Mn-superoxide dismutase (E.C. 1.15.1.1) [487, 488]. These enzymes are responsible for the degradation of ROS (i.e., O₂⁻ and H₂O₂), which are produced during photosynthesis [466–468]. Therefore, high Mn demand may be related to increased oxidative stress. Low levels of Mn consumption per cell in BG11 with Fe 1.2 and Fe 0.3 ppm, indicate reduced oxidative stress when NaNO₃ is used as N-source. High Mn-requirements in BG11_u medium become evidence of increased levels of oxidative stress.

6.4.5 Ranking of Mineral element utilization

C and N-sources are the most important nutrients for cyanobacterial growth. However, it is possible to determine an extended nutrient hierarchy based on the amount of element required per cell produced during the exponential phase. The consumption profiles presented in Figure 6.14 and Figure 6.15 were expressed in terms of the cells produced instead of time. These profiles were used to estimate element requirements per cell in the exponential phase. A regression method was used to fit element consumption data to cell density change over time. A reference cell density change of 1x10⁶ cells/ml was typical during the first 6 days of growth in all cultures (See Figure 6.1). Regression equations are summarized in Table D.1. Element demands, as well as the effect of

starting Fe concentration in each growth media, are summarized in Figure 6.19. Considering the vast differences in mineral element demands, a logarithmic scale was used to present all nutrient requirements on the same plot.

Excluding C and N-sources, the most important mineral elements in cyanobacterial growth medium are P, Ca, and Mg. This is not surprising because these elements participate in essential metabolic processes. While P is incorporated in the phosphate groups of ATP, NADPH, DNA, RNA and membrane lipids, Ca plays a pivotal role in cell signaling [328, 486]. Although Mg is necessary for the biosynthesis of ChlA, this versatile element is also involved in nucleic acid stabilization, DNA replication, ribosomal stabilization, and regulation of RuBisCo (Ribulose-1,5-bisphosphate carboxylase/oxygenase, EC 4.1.1.39) [456, 489]. The effect of varying Fe-levels on the consumption of P, Ca, and Mg is not similar for all types of media, but P and Ca requirements per cell increased for BG11_o and BG11 cultures with higher Fe-levels. While Mg consumption was not evidently affected by Fe-levels in BG11_o, the requirements of this element were affected in BG11 and BG11_u media (non-diazotrophic metabolism). These data demonstrate that the mineral nutrient consumption is affected by N and Fe metabolism in *Anabaena* sp., probably as a result of changing cellular processes during diazotrophic and non-diazotrophic metabolism. Remarkably, the demand for P during the exponential phase was consistently higher for diazotrophic cultures in BG11_o.

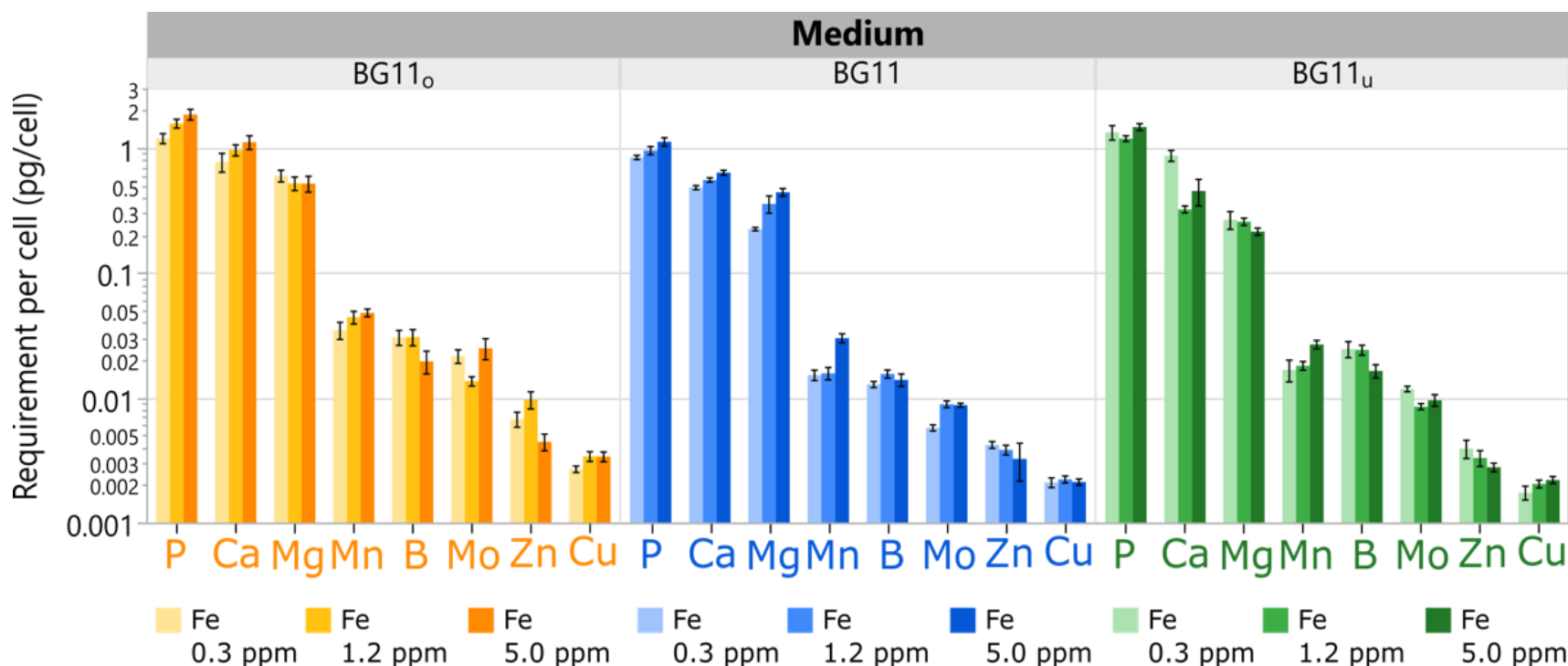


Figure 6.19. Ranking of mineral element demands per cell.

Element demand are calculated based on the cellular production in the exponential phase. P, Ca and Mg are the most important inorganic nutrients, excluding C and N-sources. These elements participate in ATP biosynthesis, cellular signaling and ChlA production. Mn is essential for photosynthesis and oxidative stress defense. B and Mo are more important for diazotrophic cells in BG11_o. Zn and Cu are involved in gene regulation and electron transfer through PSI, respectively. Each bar represents estimated requirements using the derivative of nutrient consumption expressions (Appendix D). Error bars represent the confidence fit interval of estimated demands with a significance level $\alpha=0.05$. Actual sizes of the error bars may differ due to the logarithmic scale on the Y-axis. Data represent results for two biological replicates.

A second group of mineral elements is composed by Mn, B and Mo. As previously discussed, Mn plays an important role in photosynthesis and defense during oxidative stress [487, 488]. Considering that increased Fe-availability amplifies the presence of ROS in *Anabaena* sp. [19, 456, 458], higher Mn requirements with increasing Fe-levels across all growth media are justified. B is utilized for bacterial quorum sensing, a process that confers communal response during changing environmental conditions [490]. In N₂-fixing bacteria like *Anabaena* sp., this element is also involved in heterocyst stabilization and Nitrogenase activity [463]. Interestingly, B requirements were negatively affected by increasing Fe-levels in BG11_o and BG11 cultures. Mo is incorporated in molybdoenzymes involved in N assimilation processes. Therefore, a basal consumption of this element is necessary for metabolizing N₂, nitrates and urea in photosynthetic organisms [491, 492]. Since Mo demands are higher for Nitrogenase activity, increased Mo consumption is expected for N₂-fixing organisms [325]. Figure 6.19 successfully captures the amplified importance of B and Mo in BG11_o cultures.

Zn and Cu appear at the end of the nutrient consumption ranking. While Zn participates in gene regulation and carbonic anhydrase activation, Cu participates electron transport through PSI as PC [462, 469, 480]. Interestingly, the Zn requirements per cell were reduced with increasing Fe-levels in all growth media. This effect can be associated with Fe and Zn homeostasis processes involving the Zn uptake regulator (*Zur*), which is essential for cellular defense during oxidative stress conditions [480]. Figure 6.19 also shows that Zn consumption was lowest with urea (BG11_u medium), which is the N-source that triggers oxidative stress in cyanobacteria [329].

6.5 Discussion

The results presented above demonstrate a systemic approach to analyze the effect of different N-sources and Fe-levels on the growth of *Anabaena* sp. These data also suggest underlying differences in oxidative stress, affecting pigment production and nutrient consumption in different culture media. The selection of N-sources was based on the capacity of *Anabaena* sp. to metabolize N₂, NaNO₃ and urea, which are abundant in the environment [325]. The starting Fe-levels were selected after considering reported Fe³⁺ concentrations allowing cellular growth under Fe-depleted (0.3 ppm) and Fe-surplus (5.0 ppm) conditions [493]. Although *Anabaena* sp. can slowly grow in liquid media with Fe 20 to 50 ppm, these organisms are normally grown in mineral medium with Fe 1.2 ppm [326, 493, 494]. Maximum growth rates for *Anabaena* sp. have been reported in culture media with Fe 2.8 ppm [493]. Given that the growth rate drops above this concentration, it is implied that the damaging effects of Fe begin to outweigh the beneficial effects. In this study, maximum growth rates were observed for cultures in BG11 medium. This study suggests that maximum growth rates for *Anabaena* sp. occur in the Fe-range between 1.2 and 5.0 ppm, in agreement with previously reported results [493].

The abundance of PBPs per cell was higher in BG11_o and BG11_u cultures than in BG11 cultures. Cells in BG11_o and BG11_u also presented slower growth rates than BG11 cultures. Increased PBPs abundance was attributed to higher doubling times allowing the formation of more PBSs before another replication event. In average, cells also developed around 47% more PBPs in BG11_o than in BG11_u medium. The composition of PBPs was also affected by the N-source. In average, the PBPs composition of BG11_o cultures was 9% w/w PEC, 74% w/w CPC and 17% w/w APC. In BG11 medium, this composition

changed to 72% w/w CPC and 28% w/w APC, exhibiting almost complete inhibition of PEC. In BG11_u medium, the average PBP composition was 1% w/w PEC, 65% w/w CPC and 34% w/w APC. These differences in composition are responsible for the changes in cell pigmentation. While CPC remained the most important PBP in *Anabaena* sp. regardless of the N-source, PEC gained importance in diazotrophic cells (BG11_o medium) and APC abundance increased in cells grown with urea (BG11_u). Although the abundance of PBPs per cell was higher for diazotrophic cultures, the lower biomass generation potential of these cells would limit a large-scale operation. Cultivation of diazotrophic *Anabaena* sp. would be more appropriate for production PEC.

A consistent reduction in the average abundance of CPC and APC was observed when *Anabaena* sp. cultures were grown with higher Fe-levels. These changes are consistent with a study suggesting that Fe-starvation triggers the expression of the *FurA* redox-sensing regulator in *Anabaena* sp. High *FurA* levels increase the transcript abundance of Heme oxygenases I and II (EC 1.14.99.3), promoting the synthesis of PCB, which is the blue pigment of CPC and APC proteins [19]. Since urea is a common contaminant of agro-industrial wastewater, the production of CPC and APC could be combined with a bioremediation operation using *Anabaena* sp.

The cellular abundance of ChlA, Carot and β -Carotene was principally affected by the N-source in the growth medium. In average, the abundance of ChlA per cell was 36% higher in BG11_o than in BG11 medium. Remarkably, mean ChlA abundance was also 94% higher in BG11_o than in BG11_u medium. Increased presence of ChlA in diazotrophic cells has been previously attributed to the chlorophyll regulator (*ChlR*), which is an activator of ChlA biosynthesis in anoxic environments [495–497]. In *Anabaena* sp.,

oxygen-free conditions occur in the heterocysts (N_2 -fixing cells), which are exclusively differentiated in BG11_o medium [327, 328]. Although the cellular abundance of Carot was also higher for BG11_o cultures, the mean abundance of β -Carotene was lower in BG11_o than in BG11 cultures. This suggests that the carotenoid composition of *Anabaena* sp. is different between diazotrophic and non-diazotrophic cells. Since carotenoid composition analysis of *Anabaena* sp. have been mostly performed with cells grown in regular BG-11 medium with NaNO_3 [427, 430, 431], further analysis would be required to determine differences in the carotenoid composition of diazotrophic cells. One important finding of this study is that the cellular abundance of β -Carotene is dramatically reduced when *Anabaena* sp. metabolize urea as N-source. Given that urea metabolism triggers oxidative stress in cyanobacteria [329, 330], the carotenoid composition of *Anabaena* sp. in BG11_u medium may be richer in xanthophylls (i.e., oxidized carotenes). Evidence of this oxidation process is supported with MS-TOF data, which also suggest lower levels of photosystem II stability and photodamage protection in BG11 medium. This analysis suggests that production of β -Carotene (Pro-Vitamin A) by *Anabaena* sp. might be more effective in mineral growth medium with NaNO_3 .

The composition of growth media needs to be properly assessed to guarantee cellular reproduction of microorganisms. This is relevant because nutrient consumption varies under changing environmental conditions. Although growth requirements for *Anabaena* sp. cultures are simpler than those of other organisms with biotechnological interest, it is important to learn about nutrient demands in these model cyanobacteria. The consumption rates of CO_2 , N_2 , NaNO_3 , and urea were mostly affected by the type of N-source in the growth medium. These rate constants can be used to determine or

validate metabolic constraints for mathematical modeling purposes. In average, CO₂ consumption rates of non-diazotrophic cultures (BG11 and BG11_u) of *Anabaena* sp. were 19% to 24% higher than in diazotrophic cultures (BG11_o). These differences can be explained by higher growth rates in BG11 and higher activity levels of urease in BG11_u.

Besides C and N-sources, cyanobacterial growth media contained other mineral elements (e.g., B, Na, Mg, P, K, Ca, Mn, Fe, Co, Ni, Cu, Zn and Mo). Concentration and consumption profiles of these elements in *Anabaena* sp. cultures were assessed with a multielement ICP-OES detection method. The election of Fe-availability as a factor impacting pigment production and nutrient consumption in *Anabaena* sp. was supported by the vital role of this element in cyanobacteria and its involvement in the dynamic behavior of the master global regulator *FurA* [18–20, 456, 457, 459]. The mineral demands of P, Ca, Mg, Mn, B, Mo, Zn, and Cu were higher during the early exponential phase. While Fe was almost immediately exhausted, Na, K, Ni, and Co concentration profiles in the growth medium presented nonapparent variations. This can be explained because Na⁺ and K⁺ are continuously exchanged in and out of the cell for homeostatic reasons [328]. Although Ni is needed for urease activity, the Ni requirements in urea-consuming cyanobacteria are extremely low [329, 330]. Urease activity was affected by the presence of urea and Fe-levels, but not by Ni-consumption. While Co is necessary for the biosynthesis of Vitamin B12 (Cobalamin) in cyanobacteria, the requirements of these element are also extremely low [498].

A ranking of mineral element demands was prepared considering nutrient requirements per cell produced during the exponential phase. Based on these mineral consumption levels, three groups of elements were identified. Excluding C, N and Fe, the

group of elements with highest demand was integrated by P, Ca and Mg. These elements are involved in essential processes like energy management, cell signaling, DNA replication, photosynthesis and CO₂ fixation [328, 456, 486, 489]. A second group was integrated by Mn, B and Mo, which participate in oxidative stress defense, quorum-sensing, and N-metabolism [325, 456, 458, 490]. The lowest element demands were observed for Zn and Cu, which are involved in DNA protection and electron transport [462, 469, 480]. The relative importance of each of these elements may be related to their abundance in standard BG-11 [326]. However, the element demands presented here are not necessarily proportional to the concentrations of these minerals in the growth media.

6.6 Chapter conclusion

After considering the effect of the N-source and starting Fe-levels on pigment production and nutrient consumption, it becomes clear that oxidative stress plays a significant role on the definition of biotechnological applications for *Anabaena* sp. These oxidative stress events in cyanobacteria can be manipulated to maximize the efficiency of a desired outcome. While low oxidative stress in BG11 medium could enhance the bioproduction potential of commercially important pigments (i.e., APC, CPC and β -Carotene), high oxidative stress would be desired for cyanobacteria-mediated bioremediation of wastewater with high loads of urea and phosphates. Combined operations of bioproduction and bioremediation could be achieved after establishing an optimal level of oxidative stress.

The information presented in this chapter demonstrates the significant effect of minerals and micronutrients on the metabolism of *Anabaena* sp. By having a deep

understanding of biological and inorganic interactions in cyanobacteria, it is possible to optimize growth media for a specific biotechnological or bioremediation application. Although the composition of growth media is usually taken for granted, controlling the concentration of nutrients is extremely important for the development of sustainable microbial biofactories. Therefore, the development of efficient chemical analysis methods for mineral media represents a significant step forward for standardization of cyanobacteria cultivation at larger scale. Pigments and vitamins are some of the most valuable biotechnological products of cyanobacteria and their biosynthesis is also influenced by the presence of metallic elements and Nitrogen sources. Epigenetic interactions between cyanobacteria and metals represent a highly under-explored research field that could complement Synthetic Biology efforts. The results presented in this chapter leave open multiple and extensive topics of discussion. However, they demonstrate the importance of having a systemic interpretation of the cyanobacterial metabolism.

CONCLUSIONS AND RECOMMENDATIONS

In the previous chapters, the metabolic network of model cyanobacteria *Anabaena* sp. UTEX 2576 has been rigorously studied to explain the effects of nutrient utilization on production of biomass. This research project relied on three major objectives. The first macro-objective was to have a global understanding of the importance of cyanobacterial cultivation for chemical production and biotechnological applications. This was accomplished by elaborating a complete literature review, as presented in Chapter 2. The second macro-objective was to analyze the photosynthetic metabolic network of *Anabaena* using Systems Biology and Bioinformatic tools. This was accomplished by generating the Genome-Scale metabolic reconstruction model (GSMM), iDN1004, which is presented in Chapter 5. The third macro-objective was to analyze the importance of growth medium formulation on metabolic response and reproduction. This was completed by analyzing nutrient consumption and pigment production in *Anabaena*, using reliable and efficient chemical characterization methods. Answers to specific objectives within each macro-objective will be provided in the next conclusions. Recommendations for future work will be mentioned alongside each of these final comments.

- a) Large-scale cultivation of unicellular cyanobacteria is challenging because smaller cells require more energy for separation operations. Therefore, a filamentous strain of cyanobacteria was selected for analyzing its potential as a photoautotrophic bio-factory of chemicals. Size was not the only important factor for strain selection, as the robust metabolism of wild-type *Anabaena* offered a plethora of biochemical pathways for specialty chemical production.

The study of other filamentous cyanobacterial species like *Moorea producens* and *Plectonema* sp. UTEX 1541 is highly recommended.

- b) Synthetic biology, and more specifically Metabolic engineering, have been used to enhance commodity chemical production in cyanobacteria. Although it is possible to alter the cyanobacterial metabolism using genetic engineering techniques, this brings up a lot of questions regarding the feasibility of developing large-scale applications with genetically modified cyanobacteria. Therefore, this research project was oriented towards the study of stress biology and growth optimization of the wild type. It is recommended to use metabolic engineering for metabolizing contaminant nitrogenated compounds like cyanates and triazines (herbicides) or for producing secondary metabolites with medical applications.
- c) There are still multiple limitations for implementing industrial processes with cyanobacteria. However, the recent emergence of multiple cyanobacterial start-ups has proven that it is possible to develop sustainable chemical operations utilizing photosynthetic organisms. Developing this next generation of chemical plants requires the optimization of cyanobacterial biomass generation. Such prominent goal can be achieved by having a detailed understanding of the biological, chemical and physical phenomena that control photosynthetic reproduction.
- d) Genome-scale metabolic models are powerful tools to study metabolic networks of microbial organisms. Besides providing a quantitative method for systemic assessment of metabolism, GSMMs are fueled by the discoveries of

scientists and engineers over many decades. In other words, GSMMs are a result of collaborative science and organization. However, the development of a GSMM is a highly demanding process that has not even been completed for widely studied organisms like *E. Coli* or *S. cerevisiae*. Therefore, the iDN1004 model presented in Chapter 5 is only a starting point to enhance simulation of *Anabaena* metabolic networks. Additional genes and metabolic reactions can be integrated as new data becomes available. To the authors knowledge, this is the most updated GSMM of the *Anabaena* metabolism so far.

- e) iDN1004 may be revamped and reutilized for the analysis of other biotechnological applications. Moreover, new data on nutrient consumption, metabolite production, substrate utilization, epigenetics, and gene regulation can be used to increase the accuracy of the metabolic model. One important outcome of this work was defining photoautotrophic and diazotrophic biomass equations for *Anabaena*, which were not available for the scientific community. Future work could involve the introduction of other nutrient constraints (e.g., Phosphates and metals), upgrading the biomass equations with more chemical composition data, or developing a specific biomass equation for growth with urea and other nitrogenated organic compounds.
- f) The amino acid production sub-network was analyzed to assess the potential of *Anabaena* to produce secondary metabolites. From this evaluation, schizokinen, sphingosine, lyngbyatoxin A, and shinorine were identified as possible candidates for efficient production of bioactive compounds in cyanobacteria. However, checking these results will require the implementation

of metabolic engineering strategies in *Anabaena* and direct measurement of amino-acid flux by Metabolic Flux Analysis (MFA). One significant outcome of *DN1004* analysis through FBA and FVA was the elucidation of serine, threonine, valine, glycine and alanine as significant amino acid branching points within the metabolic network. This was remarkable because the amino acid metabolism in cyanobacteria is dominated by glutamate, glutamine and aspartate, which usually mask the importance of other amino acids as metabolic precursors. Checking the actual metabolic flux values of the Pareto amino acids is highly recommended.

- g) Quality control in cyanobacterial mineral medium was overlooked at the beginning of this research project. Because of this, it was difficult to maintain consistent growth of *Anabaena*. This changed after implementing reliable chemical analysis techniques to check the concentration of the ingredients in the growth medium. The introduction of ICP-OES in routine cyanobacterial cultivation increased the success rate of long-term culture preservation because standard conditions of the growth media were ensured. It is highly recommended to continue using this method for quality control of mineral medium at small and large-scale.
- h) Elucidating the relationship between Nitrogen and Iron metabolism in cyanobacteria is a relatively recent research topic. Most studies have focused on analyzing changes on RNA transcripts levels under different conditions of Fe and N availability. Moreover, the intimate relationship between N and Fe regulators in diazotrophic cyanobacteria is becoming clearer. However, Fe

availability also affects the dynamics of consumption of other metallic ions and minerals in the growth medium. In Chapter 6, a detailed analysis of nutrient consumption and pigment production was presented. Fe-levels played a central role in these experiments. The effects of different N-substrates and Fe-levels on biomass production were analyzed, using a holistic approach. This work presents new data on pigment production and nutrient consumption kinetics, which can be directly used to design biotechnological and environmental applications with cyanobacteria.

- i) Biological sequestration of CO₂ is still one of the major goals of cyanobacterial biotechnology. However, CO₂-fixation by these organisms should be understood as a cumulative effect of the utilization of multiple nutrients. In this regard, non-diazotrophic cultures have higher CO₂-fixation potential than diazotrophic systems. The data presented in Chapter 6 presents only the introduction to an under-explored topic in cyanobacterial research. Hopefully, it will be possible to elucidate more relationships involving mineral consumption. This is significant because understanding the cyanobacterial metabolism opens the door for developing new bioremediation processes, aiming to reduce eutrophication and heavy metal pollution in water bodies.

This is the end of this document. The author truthfully thanks his audience for taking the time to read this dissertation. Hopefully, the results of this research journey will provide multiple insights to continue developing cyanobacteria as sustainable platforms for high-value chemical production and bioremediation.

APPENDIX A. PUBLISHING AGREEMENTS

Re: Publishing agreement documents [200215-005344]

Monday, February 17, 2020 6:58 PM

Subject	Re: Publishing agreement documents [200215-005344]
Link to Outlook Item	Click here
From	Researcher Support
To	Daniel A Norena Caro
Sent	2/17/2020, 6:55:28 PM

Dear Mr. Daniel Norena-Caro,

Article reference: JCOU_758

title: Cyanobacteria as photoautotrophic biofactories of high-value chemicals

I can confirm that that authors can use their articles, in full or in part, for a wide range of scholarly, non-commercial purposes one of which is inclusion in a thesis or dissertation. See the following link for further information on this

<https://www.elsevier.com/about/our-business/policies/copyright/personal-use>

As you will be able to see from the above link, our policy is to allow authors to use their work in their thesis or dissertation (provided that this is not to be published commercially).

Therefore, I can confirm that you can make it publicly available on your university web site/repository for non- commercial use.

If you require further clarification please contact permissionshelpdesk@elsevier.com who will be able to help.

<https://service.elsevier.com/app/contact/supporthub/permissions-helpdesk/>

Should you need further assistance, please do not hesitate to contact me.

Kind regards,

Jasper Jules Mabilangan

Researcher Support

ELSEVIER

Find out some simple ways to [share your research data](#), including features that are directly available when you submit your research article to an Elsevier journal.

For assistance, please visit our [Customer Support site](#) where you can search for solutions on a range of topics and find answers to frequently asked questions.

APPENDIX B. GENOME-SCALE METABOLIC MODEL

Table B.1 presents a condensed version of the list of reactions in *Anabaena* GSMM *i*DN1004. The names of reactions mentioned in Chapter 5 are highlighted. Reduced versions of biomass equations are presented in subsection B.2. Table B.2 presents the list of metabolites.

B.1 List of *i*DN1004 Reactions

Table B.1 List of Reactions in *i*DN1004

Reaction abbreviations correspond to standard names used in the BiGG Database [374]. Lower and upper bounds correspond to default values based on the reaction thermodynamics. Actual bound values were modified after determining constraints experimentally.

Abbreviation	Reaction	Subsystem	Compartment	Lower bound	Upper bound
EX_co2_e	co2[e] <=>	Exchange	Extracellular	-1000	0
CO2tex	co2[e] <=> co2[p]	Transport	Cytoplasm	-1000	1000
CO2tpp	co2[p] <=> co2[c]	Transport	Periplasm	-1000	1000
CO2tcx	co2[c] --> co2[cx]	Transport	Carboxysome	0	1000
EX_hco3_e	hco3[e] <=>	Exchange	Extracellular	-1000	0
HCO3abc	hco3[e] + atp[c] + h2o[c] --> hco3[c] + adp[c] + h[c] + pi[c]	Transport	Cytoplasm	0	1000
HCO3_Nat	hco3[e] + na1[e] --> hco3[c] + na1[c]	Transport	Cytoplasm	0	1000
HCO3_h_ti	hco3[e] + h[e] --> hco3[c] + h[c]	Transport	Cytoplasm	0	1000
HCO3tcx	hco3[c] --> hco3[cx]	Transport	Carboxysome	0	1000
HCO3E	hco3[c] + h[c] <=> h2o[c] + co2[c]	Transport	Cytoplasm	0	1000
HCO3E_cx	hco3[cx] + h[cx] <=> h2o[cx] + co2[cx]	Transport	Carboxysome	0	1000

EX_h_e	$h[e] \rightleftharpoons$	Exchange	Extracellular	-1000	1000
Ht	$h[e] \rightleftharpoons h[c]$	Transport	Cytoplasm	-1000	1000
Htcx	$h[c] \rightleftharpoons h[cx]$	Transport	Carboxysome	-1000	1000
EX_na1_e	$na1[e] \rightleftharpoons$	Exchange	Extracellular	-1000	1000
NAt3_1	$na1[e] + h[c] \rightleftharpoons na1[c] + h[e]$	Transport	Cytoplasm	-1000	1000
EX_k_e	$k[e] \rightleftharpoons$	Exchange	Extracellular	-1000	1000
NaKt	$3 na1[c] + 2 k[e] + atp[c] + h2o[c] \rightarrow 3 na1[e] + 2 k[c] + adp[c] + h[c] + pi[c]$	Transport	Cytoplasm	0	1000
Kt3r	$k[c] + h[e] \rightleftharpoons h[c] + k[e]$	Transport	Cytoplasm	0	1000
Kt1	$k[e] \rightleftharpoons k[c]$	Transport	Cytoplasm	-1000	1000
EX_photon_e	$photon[e] \rightleftharpoons$	Exchange	Extracellular	-1000	0
PHOt_e	$photon[e] \rightleftharpoons photon[c]$	Transport	Cytoplasm	-1000	1000
PRISM_solar_litho	$photon[c] \rightarrow 4.26984e-05 photon298[c] + 0.0882531 photon437[c] + 0.187391 photon438[c] + 0.114958 photon450[c] + 0.185664 photon646[c] + 0.0836165 photon673[c] + 0.0944049 photon680[c] + 0.19581 photon490[c]$	Light decomposition	Cytoplasm	0	0
PRISM_solar_exo	$photon[c] \rightarrow 0.00912663 photon298[c] + 0.107054 photon437[c] + 0.224062 photon438[c] + 0.133592 photon450[c] + 0.171752 photon646[c] + 0.0728979 photon673[c] + 0.0843155 photon680[c] + 0.20968 photon490[c]$	Light decomposition	Cytoplasm	0	0
PRISM_incandescent_60W	$photon[c] \rightarrow 1.65225e-05 photon298[c] + 0.00999388 photon437[c] + 0.0246023 photon438[c] + 0.0162762 photon450[c] + 0.229913 photon646[c] + 0.127541 photon673[c] + 0.152917 photon680[c] + 0.053691 photon490[c]$	Light decomposition	Cytoplasm	0	0
PRISM_fluorescent_warm_18W	$photon[c] \rightarrow 0.0226083 photon298[c] + 0.152956 photon437[c] + 0.231224 photon438[c] + 0.152106 photon450[c] + 0.159332 photon646[c] + 0.0351273 photon673[c] + 0.037872 photon680[c] + 0.11038 photon490[c]$	Light decomposition	Cytoplasm	0	1000
PRISM_fluorescent_cool_215W	$photon[c] \rightarrow 9.86916e-05 photon298[c] + 0.0979155 photon437[c] + 0.15074 photon438[c] + 0.107797 photon450[c] + 0.194659 photon646[c] + 0.0307226 photon673[c] + 0.0313578 photon680[c] + 0.11138 photon490[c]$	Light decomposition	Cytoplasm	0	0

PRISM_metal_halide	photon[c] --> 0.12093 photon437[c] + 0.191655 photon438[c] + 0.134004 photon450[c] + 0.119049 photon646[c] + 0.0401929 photon673[c] + 0.0452113 photon680[c] + 0.119084 photon490[c]	Light decomposition	Cytoplasm	0	0
PRISM_high_pressure_sodium	photon[c] --> 0.0151965 photon437[c] + 0.0328055 photon438[c] + 0.02772 photon450[c] + 0.242893 photon646[c] + 0.0514568 photon673[c] + 0.0536969 photon680[c] + 0.058194 photon490[c]	Light decomposition	Cytoplasm	0	0
PRISM_growth_room	photon[c] --> 4.11266e-05 photon298[c] + 0.0754123 photon437[c] + 0.117406 photon438[c] + 0.0830332 photon450[c] + 0.20333 photon646[c] + 0.0570026 photon673[c] + 0.0643077 photon680[c] + 0.094128 photon490[c]	Light decomposition	Cytoplasm	0	0
PRISM_white_LED	photon[c] --> 0.000222204 photon298[c] + 0.00711767 photon437[c] + 0.0459156 photon438[c] + 0.0273521 photon450[c] + 0.256809 photon646[c] + 0.0703213 photon673[c] + 0.0753153 photon680[c] + 0.15185 photon490[c]	Light decomposition	Cytoplasm	0	0
PRISM_red_LED_array_653nm	photon[c] --> 0.870291 photon646[c] + 0.274325 photon673[c] + 0.195494 photon680[c]	Light decomposition	Cytoplasm	0	0
PRISM_red_LED_674nm	photon[c] --> 0.265728 photon646[c] + 0.660147 photon673[c] + 0.725321 photon680[c]	Light decomposition	Cytoplasm	0	0
PRISM_design_growth	photon[c] --> 0.220794 photon646[c] + 0.638343 photon673[c] + 0.733622 photon680[c]	Light decomposition	Cytoplasm	0	0
Photon437u	photon437[c] <=> photon437[u]	Thylakoid light	Thylakoid	-1000	1000
Photon438u	photon438[c] <=> photon438[u]	Thylakoid light	Thylakoid	-1000	1000
Photon646u	photon646[c] <=> photon646[u]	Thylakoid light	Thylakoid	-1000	1000
Photon673u	photon673[c] <=> photon673[u]	Thylakoid light	Thylakoid	-1000	1000
Photon680u	photon680[c] <=> photon680[u]	Thylakoid light	Thylakoid	-1000	1000
DM_photon298_c	photon298[c] <=>	Sink	Cytoplasm	0	1000
DM_photon437_c	photon437[c] <=>	Sink	Cytoplasm	0	1000
DM_photon438_c	photon438[c] <=>	Sink	Cytoplasm	0	1000
DM_photon450_c	photon450[c] <=>	Sink	Cytoplasm	0	1000
DM_photon490_c	photon490[c] <=>	Sink	Cytoplasm	0	1000
DM_photon646_c	photon646[c] <=>	Sink	Cytoplasm	0	1000
DM_photon673_c	photon673[c] <=>	Sink	Cytoplasm	0	1000
DM_photon680_c	photon680[c] <=>	Sink	Cytoplasm	0	1000

EX_pi_e	$\text{pi}[e] \rightleftharpoons$	Exchange	Extracellular	-1000	1000
Piabc	$\text{pi}[e] + \text{atp}[c] + \text{h2o}[c] \rightleftharpoons 2 \text{pi}[c] + \text{adp}[c] + \text{h}[c]$	Transport	Cytoplasm	0	1000
Plt2r	$\text{pi}[e] + \text{h}[e] \rightleftharpoons \text{pi}[c] + \text{h}[c]$	Transport	Cytoplasm	-1000	1000
EX_h2o_e	$\text{h2o}[e] \rightleftharpoons$	Exchange	Extracellular	-1000	0
H2Otex	$\text{h2o}[e] \rightleftharpoons \text{h2o}[p]$	Transport	Periplasm	-1000	1000
H2Otp	$\text{h2o}[p] \rightleftharpoons \text{h2o}[c]$	Transport	Cytoplasm	-1000	1000
H2Otcx	$\text{h2o}[c] \rightleftharpoons \text{h2o}[cx]$	Transport	Carboxysome	-1000	1000
H2Otu_syn	$\text{h2o}[c] \rightleftharpoons \text{h2o}[u]$	Transport	Thylakoid	-1000	1000
EX_o2_e	$\text{o2}[e] \rightleftharpoons$	Exchange	Extracellular	-1000	1000
O2tex	$\text{o2}[p] \rightleftharpoons \text{o2}[e]$	Transport	Periplasm	-1000	1000
O2tp	$\text{o2}[c] \rightleftharpoons \text{o2}[p]$	Transport	Cytoplasm	-1000	1000
O2tu	$\text{o2}[u] \rightleftharpoons \text{o2}[c]$	Transport	Thylakoid	-1000	1000
O2tcx	$\text{o2}[c] \rightleftharpoons \text{o2}[cx]$	Transport	Carboxysome	-1000	1000
EX_ca2_e	$\text{ca2}[e] \rightleftharpoons$	Exchange	Extracellular	-1000	1000
CAt4	$\text{ca2}[e] + \text{h}[c] \rightleftharpoons \text{ca2}[c] + \text{h}[e]$	Transport	Cytoplasm	-1000	1000
EX_cu2_e	$\text{cu2}[e] \rightleftharpoons$	Exchange	Extracellular	-1000	1000
Cuabc	$\text{cu2}[e] + \text{atp}[c] + \text{h2o}[c] \rightleftharpoons \text{cu2}[c] + \text{adp}[c] + \text{h}[c] + \text{pi}[c]$	Transport	Cytoplasm	-1000	1000
EX_mn2_e	$\text{mn2}[e] \rightleftharpoons$	Exchange	Extracellular	-1000	1000
Mnabc	$\text{mn2}[e] + \text{atp}[c] + \text{h2o}[c] \rightleftharpoons \text{mn2}[c] + \text{adp}[c] + \text{h}[c] + \text{pi}[c]$	Transport	Cytoplasm	-1000	1000
EX_mobd_e	$\text{mobd}[e] \rightleftharpoons$	Exchange	Extracellular	-1000	1000
MOBDabc	$\text{mobd}[e] + \text{atp}[c] + \text{h2o}[c] \rightleftharpoons \text{mobd}[c] + \text{adp}[c] + \text{h}[c] + \text{pi}[c]$	Transport	Cytoplasm	-1000	1000
EX_zn2_e	$\text{zn2}[e] \rightleftharpoons$	Exchange	Extracellular	-1000	1000
ZNabc	$\text{zn2}[e] + \text{atp}[c] + \text{h2o}[c] \rightleftharpoons \text{zn2}[c] + \text{adp}[c] + \text{h}[c] + \text{pi}[c]$	Transport	Cytoplasm	-1000	1000
EX_ni2_e	$\text{ni2}[e] \rightleftharpoons$	Exchange	Extracellular	-1000	1000
Niabc	$\text{ni2}[e] + \text{atp}[c] + \text{h2o}[c] \rightleftharpoons \text{ni2}[c] + \text{adp}[c] + \text{h}[c] + \text{pi}[c]$	Transport	Cytoplasm	-1000	1000
Ex_bh4o4_e	$\text{bh4o4}[e] \rightleftharpoons$	Exchange	Extracellular	-1000	1000
Bh4o4t	$\text{bh4o4}[e] \rightleftharpoons \text{bh4o4}[c]$	Transport	Cytoplasm	-1000	1000
EX_succ_e	$\text{succ}[e] \rightleftharpoons$	Exchange	Extracellular	0	0
SUCCt	$\text{succ}[e] \rightleftharpoons \text{succ}[c]$	Transport	Cytoplasm	-1000	1000
EX_fum_e	$\text{fum}[e] \rightleftharpoons$	Exchange	Extracellular	0	0

FUMtr	fum[e] <=> fum[c]	Transport	Cytoplasm	-1000	1000
EX_mal__L_e	mal__L[e] <=>	Exchange	Extracellular	0	0
MALt	mal__L[e] <=> mal__L[c]	Transport	Cytoplasm	-1000	1000
EX_pyr_e	pyr[e] <=>	Exchange	Extracellular	0	0
PYRt	pyr[e] <=> pyr[c]	Transport	Cytoplasm	-1000	1000
EX_cit_e	cit[e] <=>	Exchange	Extracellular	-1000	0
CITt	cit[e] <=> cit[c]	Transport	Cytoplasm	0	1000
EX_ile__L_e	ile__L[e] <=>	Exchange	Extracellular	0	0
ILEt2r	ile__L[e] + h[e] <=> ile__L[c] + h[c]	Transport	Cytoplasm	-1000	1000
ILEabc	ile__L[e] + atp[c] + h2o[c] <=> ile__L[c] + adp[c] + h[c] + pi[c]	Transport	Cytoplasm	0	1000
EX_leu__L_e	leu__L[e] <=>	Exchange	Extracellular	0	0
LEUt2r	leu__L[e] + h[e] <=> leu__L[c] + h[c]	Transport	Cytoplasm	-1000	1000
LEUabc	leu__L[e] + atp[c] + h2o[c] <=> leu__L[c] + adp[c] + h[c] + pi[c]	Transport	Cytoplasm	0	1000
EX_val__L_e	val__L[e] <=>	Exchange	Extracellular	0	0
VALt2r	val__L[e] + h[e] <=> val__L[c] + h[c]	Transport	Cytoplasm	-1000	1000
VALabc	val__L[e] + atp[c] + h2o[c] <=> val__L[c] + adp[c] + h[c] + pi[c]	Transport	Cytoplasm	0	1000
EX_met__L_e	met__L[e] <=>	Exchange	Extracellular	-1000	0
METabc	met__L[e] + atp[c] + h2o[c] <=> met__L[c] + adp[c] + h[c] + pi[c]	Transport	Cytoplasm	0	1000
EX_gln__L_e	gln__L[e] <=>	Exchange	Extracellular	-1000	0
GLNabc	gln__L[e] + atp[c] + h2o[c] <=> gln__L[c] + adp[c] + h[c] + pi[c]	Transport	Cytoplasm	0	1000
GLNt	gln__L[e] <=> gln__L[c]	Transport	Extracellular	0	1000
EX_glu__L_e	glu__L[e] <=>	Exchange	Extracellular	-1000	0
GLUt4	glu__L[e] + na1[e] <=> glu__L[c] + na1[c]	Transport	Cytoplasm	0	1000
EX_arg__L_e	arg__L[e] <=>	Exchange	Extracellular	-1000	0
ARGabc	arg__L[e] + atp[c] + h2o[c] <=> arg__L[c] + adp[c] + h[c] + pi[c]	Transport	Cytoplasm	0	1000
EX_lys__L_e	lys__L[e] <=>	Exchange	Extracellular	-1000	0
LYSabc	lys__L[e] + atp[c] + h2o[c] <=> lys__L[c] + adp[c] + h[c] + pi[c]	Transport	Cytoplasm	0	1000
EX_his__L_e	his__L[e] <=>	Exchange	Extracellular	-1000	0
HISabc	his__L[e] + atp[c] + h2o[c] <=> his__L[c] + adp[c] + h[c] + pi[c]	Transport	Cytoplasm	0	1000
PSII_438	4 h[c] + 2 pq[u] + 2 h2o[u] + 4 photon438[u] --> 4 h[u] + 2 pqh2[u] + o2[u]	Photosynthesis	Thylakoid	0	1000

PSII_437	4 h[c] + 2 pq[u] + 2 h2o[u] + 4 photon437[u] --> 4 h[u] + 2 pqh2[u] + o2[u]	Photosynthesis	Thylakoid	0	1000
PSII_673	4 h[c] + 2 pq[u] + 2 h2o[u] + 4 photon673[u] --> 4 h[u] + 2 pqh2[u] + o2[u]	Photosynthesis	Thylakoid	0	1000
PSII_680	4 h[c] + 2 pq[u] + 2 h2o[u] + 4 photon680[u] --> 4 h[u] + 2 pqh2[u] + o2[u]	Photosynthesis	Thylakoid	0	1000
PSII_646	4 h[c] + 2 pq[u] + 2 h2o[u] + 4 photon646[u] --> 4 h[u] + 2 pqh2[u] + o2[u]	Photosynthesis	Thylakoid	0	1000
CYTBDu	2 pqh2[u] + o2[u] --> 2 pq[u] + 2 h2o[u]	Photosynthesis	Thylakoid	0	1000
CBFCu	2 h[c] + pqh2[u] + 2 pcox[u] --> 4 h[u] + pq[u] + 2 pcrd[u]	Photosynthesis	Thylakoid	0	1000
CBFC2u	2 h[c] + pqh2[u] + 2 ficytc6[u] --> 4 h[u] + pq[u] + 2 focytc6[u]	Photosynthesis	Thylakoid	0	1000
PSI_438	2 pcrd[u] + fdxo_2_2[c] + 2 photon438[u] --> 2 pcox[u] + fdxrd[c]	Photosynthesis	Thylakoid	0	1000
PSI_437	2 pcrd[u] + fdxo_2_2[c] + 2 photon437[u] --> 2 pcox[u] + fdxrd[c]	Photosynthesis	Thylakoid	0	1000
PSI_673	2 pcrd[u] + fdxo_2_2[c] + 2 photon673[u] --> 2 pcox[u] + fdxrd[c]	Photosynthesis	Thylakoid	0	1000
PSI_680	2 pcrd[u] + fdxo_2_2[c] + 2 photon680[u] --> 2 pcox[u] + fdxrd[c]	Photosynthesis	Thylakoid	0	1000
PSI_2_438	2 focytc6[u] + fdxo_2_2[c] + 2 photon438[c] --> 2 ficytc6[u] + fdxrd[c]	Photosynthesis	Thylakoid	0	1000
PSI_2_437	2 focytc6[u] + fdxo_2_2[c] + 2 photon437[c] --> 2 ficytc6[u] + fdxrd[c]	Photosynthesis	Thylakoid	0	1000
PSI_2_673	2 focytc6[u] + fdxo_2_2[c] + 2 photon673[c] --> 2 ficytc6[u] + fdxrd[c]	Photosynthesis	Thylakoid	0	1000
PSI_2_680	2 focytc6[u] + fdxo_2_2[c] + 2 photon680[c] --> 2 ficytc6[u] + fdxrd[c]	Photosynthesis	Thylakoid	0	1000
FQR_1	2 h[c] + pq[u] + fdxrd[c] --> pqh2[u] + fdxo_2_2[c]	Photosynthesis	Thylakoid	0	1000
FNOR_2	fdxrd[c] + nadp[c] + h[c] <=> fdxo_2_2[c] + nadph[c]	Photosynthesis	Cytoplasm	0	1000
MEHLER_2	fdxrd[c] + 2 h[c] + o2[c] --> fdxo_2_2[c] + h2o2[c]	Photosynthesis	Cytoplasm	0	1000
FTR_2	2 h[c] + trdox[c] + fdxrd[c] <=> trdrd[c] + fdxo_2_2[c]	Photosynthesis	Cytoplasm	-1000	1000
CAT	2 h2o2[c] <=> 2 h2o[c] + o2[c]	Photosynthesis	Cytoplasm	0	1000
MEHLER	2 h[c] + o2[c] + 2 nadph[c] --> 2 h2o[c] + 2 nadp[c]	Photosynthesis	Cytoplasm	0	1000
SUCDu_syn	pq[u] + succ[c] --> fum[c] + pqh2[u]	Photosynthesis	Cytoplasm	0	1000
CYO1b_syn	8 h[c] + 4 focytc6[u] + o2[u] --> 4 h[u] + 4 ficytc6[u] + 2 h2o[u]	Photosynthesis	Thylakoid	0	1000
CYO1b2_syn	8 h[c] + 4 pcrd[u] + o2[u] --> 4 h[u] + 4 pcox[u] + 2 h2o[u]	Photosynthesis	Thylakoid	0	1000
ATPSu	14 h[u] + 3 adp[c] + 3 pi[c] --> 11 h[c] + 3 atp[c] + 3 h2o[c]	Photosynthesis	Cytoplasm	0	1000
RBPCcx_2	h2o[cx] + co2[cx] + rb15bp[cx] --> 2 h[cx] + 2 3pg[cx]	Carbon fixation in photosynthetic organisms	Carboxysome	0	1000
RBChcx	o2[cx] + rb15bp[cx] <=> 2pglyc[cx] + 3pg[cx] + 2 h[cx]	Carbon fixation in photosynthetic organisms	Carboxysome	0	1000
3PGtcx	3pg[cx] <=> 3pg[c]	Carbon fixation in photosynthetic organisms	Carboxysome	0	1000
2PGLYCtcx	2pglyc[cx] <=> 2pglyc[c]	Carbon fixation in photosynthetic organisms	Carboxysome	0	1000

PGK	$\text{atp}[c] + 3\text{pg}[c] \rightleftharpoons \text{adp}[c] + 13\text{dpg}[c]$	Glycolysis / Gluconeogenesis	Cytoplasm	-1000	1000
GAPD	$\text{nadh}[c] + \text{h}[c] + 13\text{dpg}[c] \rightleftharpoons \text{nad}[c] + \text{pi}[c] + \text{g3p}[c]$	Glycolysis / Gluconeogenesis	Cytoplasm	-1000	1000
GAPDi_nadp	$\text{nadph}[c] + \text{h}[c] + 13\text{dpg}[c] \rightleftharpoons \text{nadp}[c] + \text{pi}[c] + \text{g3p}[c]$	Glycolysis / Gluconeogenesis	Cytoplasm	-1000	1000
TPI	$\text{g3p}[c] \rightleftharpoons \text{dhap}[c]$	Glycolysis / Gluconeogenesis	Cytoplasm	-1000	1000
FBA	$\text{dhap}[c] + \text{g3p}[c] \rightleftharpoons \text{fdp}[c]$	Glycolysis / Gluconeogenesis	Cytoplasm	-1000	1000
MGSA	$\text{dhap}[c] \rightleftharpoons \text{mthgl}[c] + \text{pi}[c]$	Glycolysis / Gluconeogenesis	Cytoplasm	0	1000
FBP	$\text{h2o}[c] + \text{fdp}[c] \rightleftharpoons \text{pi}[c] + \text{f6p}[c]$	Glycolysis / Gluconeogenesis	Cytoplasm	-1000	1000
ALKP	$\text{dhap}[c] + \text{h2o}[c] \rightleftharpoons \text{dha}[c] + \text{pi}[c]$	Glycolysis / Gluconeogenesis	Cytoplasm	-1000	1000
TKT2	$\text{f6p}[c] + \text{g3p}[c] \rightleftharpoons \text{xu5p_D}[c] + \text{e4p}[c]$	Pentose phosphate pathway	Cytoplasm	-1000	1000
FBA3	$\text{dhap}[c] + \text{e4p}[c] \rightleftharpoons \text{s17bp}[c]$	Pentose phosphate pathway	Cytoplasm	-1000	1000
RPE	$\text{xu5p_D}[c] \rightleftharpoons \text{ru5p_D}[c]$	Pentose phosphate pathway	Cytoplasm	-1000	1000
SBP	$\text{h2o}[c] + \text{s17bp}[c] \rightleftharpoons \text{pi}[c] + \text{s7p}[c]$	Pentose phosphate pathway	Cytoplasm	-1000	1000
PKETF	$\text{pi}[c] + \text{f6p}[c] \rightleftharpoons \text{h2o}[c] + \text{actp}[c] + \text{e4p}[c]$	Pentose phosphate pathway	Cytoplasm	-1000	1000
PKETX	$\text{pi}[c] + \text{xu5p_D}[c] \rightleftharpoons \text{h2o}[c] + \text{g3p}[c] + \text{actp}[c]$	Pentose phosphate pathway	Cytoplasm	-1000	1000
TKT1	$\text{g3p}[c] + \text{s7p}[c] \rightleftharpoons \text{r5p}[c] + \text{xu5p_D}[c]$	Pentose phosphate pathway	Cytoplasm	-1000	1000
RPI	$\text{r5p}[c] \rightleftharpoons \text{ru5p_D}[c]$	Pentose phosphate pathway	Cytoplasm	-1000	1000
PRPPS	$\text{atp}[c] + \text{r5p}[c] \rightleftharpoons \text{amp}[c] + \text{h}[c] + \text{prpp}[c]$	Pentose phosphate pathway	Cytoplasm	-1000	1000
RBK	$\text{adp}[c] + \text{h}[c] + \text{r5p}[c] \rightleftharpoons \text{atp}[c] + \text{rib_D}[c]$	Pentose phosphate pathway	Cytoplasm	-1000	1000
TALA	$\text{f6p}[c] + \text{e4p}[c] \rightleftharpoons \text{g3p}[c] + \text{s7p}[c]$	Pentose phosphate pathway	Cytoplasm	-1000	1000
DRPA	$\text{acald}[c] + \text{g3p}[c] \rightleftharpoons 2\text{dr5p}[c]$	Pentose phosphate pathway	Cytoplasm	-1000	1000
DRBK	$\text{adp}[c] + \text{h}[c] + 2\text{dr5p}[c] \rightleftharpoons \text{atp}[c] + \text{drib}[c]$	Pentose phosphate pathway	Cytoplasm	-1000	1000
PRUK	$\text{atp}[c] + \text{ru5p_D}[c] \rightleftharpoons \text{adp}[c] + \text{h}[c] + \text{rb15bp}[c]$	Pentose phosphate pathway	Cytoplasm	-1000	1000
RB15BPtcx	$\text{rb15bp}[c] \rightleftharpoons \text{rb15bp}[cx]$	Transport	Carboxysome	0	1000
PFK	$\text{adp}[c] + \text{h}[c] + \text{fdp}[c] \rightleftharpoons \text{atp}[c] + \text{f6p}[c]$	Glycolysis / Gluconeogenesis	Cytoplasm	-1000	1000

PFK_adp	$\text{adp}[c] + \text{f6p}[c] \rightleftharpoons \text{amp}[c] + 2 \text{h}[c] + \text{fdp}[c]$	Glycolysis / Gluconeogenesis	Cytoplasm	-1000	1000
G6PI3	$\text{f6p}[c] \rightleftharpoons \text{g6p_B}[c]$	Glycolysis / Gluconeogenesis	Cytoplasm	-1000	1000
G6PI	$\text{g6p_B}[c] \rightleftharpoons \text{g6p}[c]$	Glycolysis / Gluconeogenesis	Cytoplasm	-1000	1000
PGMT	$\text{g6p}[c] \rightleftharpoons \text{g1p}[c]$	Glycolysis / Gluconeogenesis	Cytoplasm	-1000	1000
G1PP	$\text{g1p}[c] + \text{h2o}[c] \rightleftharpoons \text{glc_D}[c] + \text{pi}[c]$	Glycolysis / Gluconeogenesis	Cytoplasm	-1000	1000
GLGC	$\text{atp}[c] + \text{g1p}[c] \rightleftharpoons \text{adpglc}[c] + \text{ppi}[c]$	Glycolysis and sugar metabolism	Cytoplasm	0	1000
GGPS	$\text{adpglc}[c] + \text{glyc3p}[c] \rightleftharpoons \text{adp}[c] + \text{glcglycp}[c]$	Glycolysis and sugar metabolism	Cytoplasm	0	1000
GGPP	$\text{h2o}[c] + \text{glcglycp}[c] \rightleftharpoons \text{pi}[c] + \text{glcglyc}[c]$	Glycolysis and sugar metabolism	Cytoplasm	0	1000
AMYS	$\text{adpglc}[c] \rightleftharpoons \text{adp}[c] + \text{amylose}[c]$	Glycolysis and sugar metabolism	Cytoplasm	0	1000
GLCS3	$\text{adpglc}[c] + \text{amylose}[c] \rightleftharpoons 14\text{glucan}[c] + \text{adp}[c]$	Glycolysis and sugar metabolism	Cytoplasm	0	1000
GLCBAN3	$14\text{glucan}[c] + \text{adpglc}[c] \rightleftharpoons \text{adp}[c] + \text{glycogen}[c]$	Glycolysis and sugar metabolism	Cytoplasm	0	1000
GLCDBAN3	$\text{glycogen}[c] + \text{h2o}[c] \rightleftharpoons 14\text{glucan}[c] + \text{glc_D}[c]$	Glycolysis and sugar metabolism	Cytoplasm	0	1000
GLCP2_1	$14\text{glucan}[c] + \text{pi}[c] \rightleftharpoons \text{g1p}[c] + \text{amylose}[c]$	Glycolysis and sugar metabolism	Cytoplasm	0	1000
MALTS	$\text{glc_D}[c] + \text{amylose}[c] \rightleftharpoons \text{malt}[c]$	Glycolysis and sugar metabolism	Cytoplasm	0	1000
MALT	$\text{h2o}[c] + \text{malt}[c] \rightleftharpoons 2 \text{glc_D}[c]$	Glycolysis and sugar metabolism	Cytoplasm	0	1000
TREGS	$\text{h2o}[c] + 14\text{glucan}[c] \rightleftharpoons \text{tre}[c]$	Glycolysis and sugar metabolism	Cytoplasm	0	1000
TREH	$\text{h2o}[c] + \text{tre}[c] \rightleftharpoons 2 \text{glc_D}[c]$	Glycolysis and sugar metabolism	Cytoplasm	0	1000
DEXT	$14\text{glucan}[c] \rightleftharpoons \text{dextrin}[c]$	Glycolysis and sugar metabolism	Cytoplasm	0	1000
MLTG6	$2 \text{h2o}[c] + \text{dextrin}[c] \rightleftharpoons 2 \text{glc_D}[c]$	Glycolysis and sugar metabolism	Cytoplasm	0	1000
MAN6PI	$\text{f6p}[c] \rightleftharpoons \text{man6p}[c]$	Glycolysis and sugar metabolism	Cytoplasm	-1000	1000
PMANM	$\text{man6p}[c] \rightleftharpoons \text{man1p}[c]$	Glycolysis and sugar metabolism	Cytoplasm	-1000	1000
MAN1PT2	$\text{gdp}[c] + \text{man1p}[c] \rightleftharpoons \text{gdpmann}[c] + \text{pi}[c]$	Glycolysis and sugar metabolism	Cytoplasm	0	1000
MAN1PT	$\text{gtp}[c] + \text{man1p}[c] \rightleftharpoons \text{gdpmann}[c] + \text{ppi}[c]$	Glycolysis and sugar metabolism	Cytoplasm	0	1000
GMAND	$\text{gdpmann}[c] \rightleftharpoons \text{gdpddman}[c] + \text{h2o}[c]$	Glycolysis and sugar metabolism	Cytoplasm	-1000	1000

GFUCS	gdpddman[c] + nadph[c] + h[c] <=> nadp[c] + gdpfuc[c]	Glycolysis and sugar metabolism	Cytoplasm	-1000	1000
HEX7	atp[c] + fru[c] <=> adp[c] + f6p[c] + h[c]	Glycolysis and sugar metabolism	Cytoplasm	-1000	1000
SBTD_D2	fru[c] + h[c] + nadh[c] <=> nad[c] + sbt__D[c]	Glycolysis and sugar metabolism	Cytoplasm	-1000	1000
G1PTMT	dttp[c] + g1p[c] <=> ppi[c] + dtdpglc[c]	Glycolysis and sugar metabolism	Cytoplasm	0	1000
TDPGDH_1	dtdpglc[c] <=> dtdp4d6dg[c] + h2o[c]	Glycolysis and sugar metabolism	Cytoplasm	0	1000
TDPDRE_1	dtdp4d6dg[c] <=> dtdprham[c]	Glycolysis and sugar metabolism	Cytoplasm	-1000	1000
TDPDRR_2	h[c] + nadph[c] + dtdprham[c] <=> dtdprmn[c] + nadp[c]	Glycolysis and sugar metabolism	Cytoplasm	0	1000
MI1PS	g6p[c] <=> mi1p__D[c]	Glycolysis and sugar metabolism	Cytoplasm	0	1000
MI1PP	h2o[c] + mi1p__D[c] <=> inost[c] + pi[c]	Glycolysis and sugar metabolism	Cytoplasm	0	1000
G1PCTYT	ctp[c] + g1p[c] <=> ppi[c] + cdpglc[c]	Glycolysis and sugar metabolism	Cytoplasm	-1000	1000
HEX1	atp[c] + glc__D[c] <=> adp[c] + h[c] + g6p[c]	Glycolysis / Gluconeogenesis	Cytoplasm	-1000	1000
G1Dx	glc__D[c] + nad[c] <=> h[c] + nadh[c] + g15lac[c]	Pentose phosphate pathway	Cytoplasm	-1000	1000
G1Dx_nadp	glc__D[c] + nadp[c] <=> h[c] + nadph[c] + g15lac[c]	Pentose phosphate pathway	Cytoplasm	-1000	1000
DGLACHa	h2o[c] + g15lac[c] <=> glcn[c] + h[c]	Pentose phosphate pathway	Cytoplasm	0	1000
GLUK_PP	pi[c] + glc__D[c] <=> h2o[c] + g6p[c]	Glycolysis and sugar metabolism	Cytoplasm	0	1000
G6PBDH	nadp[c] + g6p_B[c] <=> nadph[c] + h[c] + 6pgl[c]	Pentose phosphate pathway	Cytoplasm	-1000	1000
G6PDH2r	g6p[c] + nadp[c] <=> 6pgl[c] + h[c] + nadph[c]	Pentose phosphate pathway	Cytoplasm	-1000	1000
PGL	h2o[c] + 6pgl[c] <=> h[c] + 6pgc[c]	Pentose phosphate pathway	Cytoplasm	-1000	1000
GND	nadp[c] + 6pgc[c] <=> nadph[c] + co2[c] + ru5p__D[c]	Pentose phosphate pathway	Cytoplasm	0	1000
GNK	atp[c] + glcn[c] <=> 6pgc[c] + adp[c] + h[c]	Pentose phosphate pathway	Cytoplasm	-1000	1000
2DGLCNry	h[c] + nadph[c] + 2dhglcn[c] <=> glcn[c] + nadp[c]	Pentose phosphate pathway	Cytoplasm	-1000	1000
DPGM	h[c] + 13dpg[c] <=> 23dpg[c]	Glycolysis / Gluconeogenesis	Cytoplasm	-1000	1000
DPGase	23dpg[c] + h2o[c] <=> 2pg[c] + pi[c] + 2 h[c]	Glycolysis / Gluconeogenesis	Cytoplasm	0	1000
PGM	3pg[c] <=> 2pg[c]	Glycolysis / Gluconeogenesis	Cytoplasm	-1000	1000

ENO	2pg[c] <=> h2o[c] + pep[c]	Glycolysis / Gluconeogenesis	Cytoplasm	-1000	1000
PYK	adp[c] + pep[c] + h[c] --> atp[c] + pyr[c]	Glycolysis / Gluconeogenesis	Cytoplasm	0	1000
PPC	h2o[c] + co2[c] + pep[c] --> pi[c] + oaa[c] + h[c]	Pyruvate metabolism	Cytoplasm	0	1000
EDA	2ddg6p[c] <=> g3p[c] + pyr[c]	Pyruvate metabolism	Cytoplasm	-1000	1000
PORb	coa[c] + pyr[c] + fdxo_2_2[c] --> co2[c] + accoa[c] + fdxrd[c] + h[c]	Citrate cycle (TCA cycle)	Cytoplasm	0	1000
CS	h2o[c] + accoa[c] + oaa[c] --> coa[c] + h[c] + cit[c]	Citrate cycle (TCA cycle)	Cytoplasm	0	1000
PDH	coa[c] + nad[c] + pyr[c] <=> accoa[c] + co2[c] + nadh[c]	Pyruvate metabolism	Cytoplasm	0	1000
HCITS	accoa[c] + akc[c] + h2o[c] <=> coa[c] + h[c] + hci[c]	Pyruvate metabolism	Cytoplasm	-1000	1000
ACONTa	cit[c] --> h2o[c] + acon[c][c]	Citrate cycle (TCA cycle)	Cytoplasm	0	1000
ACONTb	h2o[c] + acon[c][c] --> icit[c]	Citrate cycle (TCA cycle)	Cytoplasm	0	1000
r0422	nadp[c] + icit[c] <=> nadph[c] + h[c] + HC01434[c]	Citrate cycle (TCA cycle)	Cytoplasm	-1000	1000
r0082	h[c] + HC01434[c] --> co2[c] + akc[c]	Citrate cycle (TCA cycle)	Cytoplasm	0	1000
OXGDC	akc[c] + h[c] --> co2[c] + succal[c]	Citrate cycle (TCA cycle)	Cytoplasm	0	1000
SSALx	h2o[c] + nad[c] + succal[c] --> nadh[c] + succ[c] + 2 h[c]	Citrate cycle (TCA cycle)	Cytoplasm	0	1000
SSALy	h2o[c] + nadp[c] + succal[c] --> nadph[c] + succ[c] + 2 h[c]	Citrate cycle (TCA cycle)	Cytoplasm	0	1000
MCITL2	micit[c] <=> pyr[c] + succ[c]	Citrate cycle (TCA cycle)	Cytoplasm	-1000	1000
MICITDr	2mcacn[c] + h2o[c] <=> micit[c]	Citrate cycle (TCA cycle)	Cytoplasm	-1000	1000
NADH5	h[c] + nadh[c] + q8[c] --> nad[c] + q8h2[c]	Oxidative phosphorylation	Cytoplasm	0	1000
NADH10	h[c] + nadh[c] + mqn8[c] --> nad[c] + mql8[c]	Oxidative phosphorylation	Cytoplasm	0	1000
NADH17pp	4 h[c] + nadh[c] + mqn8[c] --> nad[c] + 3 h[p] + mql8[c]	Oxidative phosphorylation	Periplasm	0	1000
NADH17u	4 h[c] + nadh[c] + mqn8[c] --> nad[c] + 3 h[u] + mql8[c]	Oxidative phosphorylation	Thylakoid	0	1000
NADH16pp	4 h[c] + nadh[c] + q8[c] --> nad[c] + 3 h[p] + q8h2[c]	Oxidative phosphorylation	Periplasm	0	1000
NADH16u	4 h[c] + nadh[c] + q8[c] --> nad[c] + 3 h[u] + q8h2[c]	Oxidative phosphorylation	Thylakoid	0	1000
FRD2	succ[c] + mqn8[c] --> fum[c] + mql8[c]	Citrate cycle (TCA cycle)	Cytoplasm	0	1000
SUCDi	succ[c] + q8[c] --> fum[c] + q8h2[c]	Citrate cycle (TCA cycle)	Cytoplasm	0	1000
CBFC2_q8_pp	2 h[c] + q8h2[c] + 2 ficytc6[p] --> 4 h[p] + q8[c] + 2 focytc6[p]	Oxidative phosphorylation	Periplasm	0	1000

CBFC2_mqn8_pp	2 h[c] + mql8[c] + 2 ficytc6[p] --> 4 h[p] + mqn8[c] + 2 focytc6[p]	Oxidative phosphorylation	Periplasm	0	1000
CBFC_q8_pp	2 h[c] + q8h2[c] + 2 pcox[p] --> 4 h[p] + q8[c] + 2 pcrd[p]	Oxidative phosphorylation	Periplasm	0	1000
CBFC_mqn8_pp	2 h[c] + mql8[c] + 2 pcox[p] --> 4 h[p] + mqn8[c] + 2 pcrd[p]	Oxidative phosphorylation	Periplasm	0	1000
CYO1bpp_syn	8 h[c] + 4 focytc6[p] + o2[c] --> 4 h[p] + 4 ficytc6[p] + 2 h2o[c]	Oxidative phosphorylation	Periplasm	0	1000
CYO1b2pp_syn	8 h[c] + 4 pcrd[p] + o2[c] --> 4 h[p] + 4 pcox[p] + 2 h2o[c]	Oxidative phosphorylation	Periplasm	0	1000
CYTBD2pp	4 h[c] + 2 mql8[c] + o2[c] --> 2 mqn8[p] + 2 h2o[c] + 4 h[p]	Oxidative phosphorylation	Cytoplasm	0	1000
CYTBDpp	4 h[c] + 2 q8h2[c] + o2[c] --> 2 q8[c] + 2 h2o[c] + 4 h[p]	Oxidative phosphorylation	Cytoplasm	0	1000
ATPS4rpp_1	14 h[p] + 3 adp[c] + 3 pi[c] --> 11 h[c] + 3 atp[c] + 3 h2o[c]	Oxidative phosphorylation	Periplasm	0	1000
PPA	h2o[c] + ppi[c] --> 2 pi[c] + h[c]	Oxidative phosphorylation	Cytoplasm	0	1000
PPK2	atp[c] + ppi[c] + h[c] <=> adp[c] + ppp[i]	Oxidative phosphorylation	Cytoplasm	-1000	1000
PPK	atp[c] + pi[c] --> adp[c] + ppi[c]	Oxidative phosphorylation	Cytoplasm	0	1000
FUM	h2o[c] + fum[c] --> mal__L[c]	Citrate cycle (TCA cycle)	Cytoplasm	0	1000
MDH	nad[c] + mal__L[c] --> nadh[c] + oaa[c] + h[c]	Citrate cycle (TCA cycle)	Cytoplasm	0	1000
MDHy	nadp[c] + mal__L[c] --> nadph[c] + oaa[c] + h[c]	Citrate cycle (TCA cycle)	Cytoplasm	0	1000
SUCOAS	atp[c] + coa[c] + succ[c] <=> adp[c] + pi[c] + succoa[c]	Citrate cycle (TCA cycle)	Cytoplasm	-1000	1000
PGLYCP	2pglyc[c] + h2o[c] <=> glyclt[c] + pi[c]	Glycine, serine and threonine metabolism	Cytoplasm	0	1000
GLYCLTDx	glyclt[c] + nad[c] <=> glx[c] + h[c] + nadh[c]	Glycine, serine and threonine metabolism	Cytoplasm	0	1000
GLYCTO1	glyclt[c] + o2[c] <=> glx[c] + h2o2[c]	Glycine, serine and threonine metabolism	Cytoplasm	0	1000
GLXO3r	glx[c] + h2o[c] + o2[c] <=> h[c] + h2o2[c] + oxa[c]	Glycine, serine and threonine metabolism	Cytoplasm	0	1000
OXADC	h[c] + oxa[c] <=> co2[c] + for[c]	Glycine, serine and threonine metabolism	Cytoplasm	0	1000
GLXCL	2 glx[c] + h[c] <=> 2h3oppa[c] + co2[c]	Glycine, serine and threonine metabolism	Cytoplasm	0	1000
TRSARr	2h3oppa[c] + h[c] + nadh[c] <=> glyc__R[c] + nad[c]	Glycine, serine and threonine metabolism	Cytoplasm	-1000	1000
GLYCK	atp[c] + glyc__R[c] <=> 3pg[c] + adp[c] + h[c]	Glycine, serine and threonine metabolism	Cytoplasm	0	1000
GLYALDDr	glyc__R[c] + 2 h[c] + nadh[c] <=> glyald[c] + h2o[c] + nad[c]	Glycerolipid metabolism	Cytoplasm	-1000	1000
ALCD19	nadh[c] + h[c] + glyald[c] <=> nad[c] + gly[c]	Glycerolipid metabolism	Cytoplasm	-1000	1000

ALCD19y	glyald[c] + h[c] + nadph[c] <=> glyc[c] + nadp[c]	Glycerolipid metabolism	Cytoplasm	-1000	1000
EX_urea_e	urea[e] <=>	Exchange	Extracellular	-1000	1000
UREAabc	urea[e] + atp[c] + h2o[c] <=> urea[c] + adp[c] + h[c] + pi[c]	Transport	Cytoplasm	0	1000
EX_ptrc_e	ptrc[e] <=>	Exchange	Extracellular	-1000	1000
PTRCabc	ptrc[e] + atp[c] + h2o[c] <=> ptrc[c] + adp[c] + h[c] + pi[c]	Transport	Cytoplasm	0	1000
EX_spm�_e	spmd[e] <=>	Exchange	Extracellular	-1000	1000
SPMDabc	atp[c] + h2o[c] + spmd[e] <=> adp[c] + h[c] + pi[c] + spmd[c]	Transport	Cytoplasm	0	1000
EX_nh4_e	nh4[e] <=>	Exchange	Extracellular	-1000	0
NH4tex	nh4[e] <=> nh4[p]	Transport	Periplasm	-1000	1000
NH4tpp	nh4[p] <=> nh4[c]	Transport	Cytoplasm	-1000	1000
EX_n2_e	n2[e] <=>	Exchange	Extracellular	-1000	0
N2tex	n2[e] <=> n2[p]	Transport	Periplasm	-1000	1000
N2trpp	n2[p] <=> n2[c]	Transport	Cytoplasm	-1000	1000
NIT1b_2	16 h2o[c] + 16 atp[c] + n2[c] + 4 fdxrd[c] --> 16 adp[c] + 16 pi[c] + 2 nh4[c] + 6 h[c] + 4 fdxo_2_2[c] + h2[c]	Nitrogen metabolism	Cytoplasm	0	1000
EX_h2_e	h2[e] <=>	Exchange	Extracellular	0	1000
H2tex	h2[e] <=> h2[p]	Transport	Periplasm	-1000	1000
H2tpp	h2[p] <=> h2[c]	Transport	Cytoplasm	-1000	1000
EX_no3_e	no3[e] <=>	Exchange	Extracellular	-1000	1000
NO3abc	h2o[c] + atp[c] + no3[e] --> adp[c] + pi[c] + h[c] + no3[c]	Transport	Cytoplasm	0	1000
NAR_syn_2	2 h[c] + no3[c] + fdxrd[c] --> h2o[c] + no2[c] + fdxo_2_2[c]	Nitrogen metabolism	Cytoplasm	0	1000
NOR_b	8 h[c] + no2[c] + 3 fdxrd[c] --> 2 h2o[c] + nh4[c] + 3 fdxo_2_2[c]	Nitrogen metabolism	Cytoplasm	0	1000
EX_cynt_e	cynt[e] <=>	Exchange	Extracellular	-1000	1000
CYNTt_c	cynt[e] <=> cynt[c]	Transport	Extracellular	0	1000
CYNL	cynt[c] + h[c] + hco3[c] <=> cbm[c] + co2[c]	Nitrogen metabolism	Cytoplasm	0	1000
CBMD	cbm[c] + 2 h[c] <=> co2[c] + nh4[c]	Nitrogen metabolism	Cytoplasm	0	1000
GDH1	h2o[c] + nad[c] + glu__L[c] <=> nadh[c] + nh4[c] + akc[c] + h[c]	Nitrogen metabolism	Cytoplasm	-1000	1000
GDH2_nadp	h2o[c] + nadp[c] + glu__L[c] <=> nadph[c] + nh4[c] + akc[c] + h[c]	Nitrogen metabolism	Cytoplasm	-1000	1000
GLNS	atp[c] + nh4[c] + glu__L[c] --> adp[c] + pi[c] + gln__L[c] + h[c]	Nitrogen metabolism	Cytoplasm	0	1000
GLUN	h2o[c] + gln__L[c] --> nh4[c] + glu__L[c]	Nitrogen metabolism	Cytoplasm	0	1000

GLMS_b	$\text{akg}[c] + \text{gln_L}[c] + 2 \text{ h}[c] + \text{fdxrd}[c] \rightleftharpoons 2 \text{ glu_L}[c] + \text{fdxo_2_2}[c]$	Nitrogen metabolism	Cytoplasm	0	1000
ASPTA	$\text{glu_L}[c] + \text{oaa}[c] \rightleftharpoons \text{akg}[c] + \text{asp_L}[c]$	Arginine biosynthesis	Cytoplasm	-1000	1000
ACGS	$\text{accoa}[c] + \text{glu_L}[c] \rightarrow \text{coa}[c] + \text{h}[c] + \text{acglu}[c]$	Arginine biosynthesis	Cytoplasm	0	1000
ACGK	$\text{atp}[c] + \text{acglu}[c] \rightleftharpoons \text{adp}[c] + \text{acg5p}[c]$	Arginine biosynthesis	Cytoplasm	0	1000
AGPR	$\text{nadph}[c] + \text{h}[c] + \text{acg5p}[c] \rightleftharpoons \text{nadp}[c] + \text{pi}[c] + \text{acg5sa}[c]$	Arginine biosynthesis	Cytoplasm	0	1000
ACOTA	$\text{glu_L}[c] + \text{acg5sa}[c] \rightleftharpoons \text{akg}[c] + \text{acorn}[c]$	Arginine biosynthesis	Cytoplasm	0	1000
ORNTAC	$\text{glu_L}[c] + \text{acorn}[c] \rightleftharpoons \text{orn}[c] + \text{acglu}[c]$	Arginine biosynthesis	Cytoplasm	0	1000
ACODA	$\text{h2o}[c] + \text{acorn}[c] \rightleftharpoons \text{ac}[c] + \text{orn}[c]$	Arginine biosynthesis	Cytoplasm	0	1000
CPSc	$\text{h2o}[c] + 2 \text{ atp}[c] + \text{co2}[c] + \text{nh4}[c] \rightleftharpoons 2 \text{ adp}[c] + \text{pi}[c] + 3 \text{ h}[c] + \text{cbp}[c]$	Arginine biosynthesis	Cytoplasm	0	1000
CBPS	$\text{h2o}[c] + 2 \text{ atp}[c] + \text{gln_L}[c] + \text{hco3}[c] \rightleftharpoons 2 \text{ adp}[c] + \text{pi}[c] + \text{glu_L}[c] + 2 \text{ h}[c] + \text{cbp}[c]$	Arginine biosynthesis	Cytoplasm	0	1000
OCBT	$\text{orn}[c] + \text{cbp}[c] \rightleftharpoons \text{pi}[c] + \text{h}[c] + \text{citr_L}[c]$	Arginine biosynthesis	Cytoplasm	-1000	1000
AOTC	$\text{cbp}[c] + \text{acorn}[c] \rightleftharpoons \text{pi}[c] + \text{h}[c] + \text{accitr_L}[c]$	Arginine biosynthesis	Cytoplasm	-1000	1000
ARGSS_1	$\text{atp}[c] + \text{asp_L}[c] + \text{citr_L}[c] \rightarrow \text{ppi}[c] + \text{amp}[c] + 2 \text{ h}[c] + \text{argsuc}[c]$	Arginine biosynthesis	Cytoplasm	0	1000
ARGSL	$\text{argsuc}[c] \rightleftharpoons \text{arg_L}[c] + \text{fum}[c]$	Arginine biosynthesis	Cytoplasm	-1000	1000
ARGDr	$\text{arg_L}[c] + \text{h2o}[c] \rightleftharpoons \text{citr_L}[c] + \text{nh4}[c]$	Arginine and proline metabolism	Cytoplasm	0	1000
LARGOX	$\text{arg_L}[c] + \text{h2o}[c] + \text{o2}[c] \rightleftharpoons \text{h2o2}[c] + \text{nh4}[c] + 5\text{g2op}[c]$	Arginine and proline metabolism	Cytoplasm	0	1000
GOPP	$\text{h2o2}[c] + 5\text{g2op}[c] \rightleftharpoons \text{co2}[c] + \text{h2o}[c] + 4\text{gudbutn}[c]$	Arginine and proline metabolism	Cytoplasm	0	1000
GUDBUTNAH	$\text{h2o}[c] + 4\text{gudbutn}[c] \rightleftharpoons 4\text{abut}[c] + \text{urea}[c]$	Arginine and proline metabolism	Cytoplasm	0	1000
AMID	$\text{h2o}[c] + 4\text{gudbd}[c] \rightleftharpoons \text{nh4}[c] + 4\text{gudbutn}[c]$	Arginine and proline metabolism	Cytoplasm	-1000	1000
ABTA	$\text{akg}[c] + 4\text{abut}[c] \rightleftharpoons \text{glu_L}[c] + \text{sucsa}[c]$	Butanoate metabolism	Cytoplasm	-1000	1000
ARGN	$\text{arg_L}[c] + \text{h2o}[c] \rightleftharpoons \text{orn}[c] + \text{urea}[c]$	Arginine and proline metabolism	Cytoplasm	-1000	1000
ARGDC	$\text{arg_L}[c] + \text{h}[c] \rightarrow \text{co2}[c] + \text{agm}[c]$	Arginine and proline metabolism	Cytoplasm	0	1000
AGMT	$\text{h2o}[c] + \text{agm}[c] \rightarrow \text{urea}[c] + \text{ptrc}[c]$	Arginine and proline metabolism	Cytoplasm	0	1000
UREA	$\text{h2o}[c] + 2 \text{ h}[c] + \text{urea}[c] \rightarrow \text{co2}[c] + 2 \text{ nh4}[c]$	Arginine and proline metabolism	Cytoplasm	0	1000
SPMS	$\text{ametam}[c] + \text{ptrc}[c] \rightleftharpoons 5\text{mta}[c] + \text{h}[c] + \text{spmd}[c]$	Arginine and proline metabolism	Cytoplasm	0	1000
SPMSy	$\text{ametam}[c] + \text{spmd}[c] \rightleftharpoons 5\text{mta}[c] + \text{h}[c] + \text{spm}[c]$	Arginine and proline metabolism	Cytoplasm	0	1000
GLU5K	$\text{atp}[c] + \text{glu_L}[c] \rightleftharpoons \text{adp}[c] + \text{glu5p}[c]$	Arginine and proline metabolism	Cytoplasm	0	1000

G5SD	$\text{nadph}[c] + \text{h}[c] + \text{glu5p}[c] \rightleftharpoons \text{nadp}[c] + \text{pi}[c] + \text{glu5sa}[c]$	Arginine and proline metabolism	Cytoplasm	0	1000
PUTA3	$\text{nadh}[c] + \text{glu_L}[c] + 2 \text{h}[c] \rightleftharpoons \text{h2o}[c] + \text{nad}[c] + \text{glu5sa}[c]$	Arginine and proline metabolism	Cytoplasm	-1000	1000
G5SADs	$\text{glu5sa}[c] \rightarrow \text{h2o}[c] + \text{h}[c] + 1\text{pyr5c}[c]$	Arginine and proline metabolism	Cytoplasm	0	1000
ORNTA	$\text{akg}[c] + \text{orn}[c] \rightleftharpoons \text{glu_L}[c] + \text{glu5sa}[c]$	Arginine and proline metabolism	Cytoplasm	-1000	1000
ORNDC	$\text{orn}[c] + \text{h}[c] \rightarrow \text{co2}[c] + \text{ptrc}[c]$	Arginine and proline metabolism	Cytoplasm	0	1000
P5CRx	$\text{nadh}[c] + 2 \text{h}[c] + 1\text{pyr5c}[c] \rightleftharpoons \text{nad}[c] + \text{pro_L}[c]$	Arginine and proline metabolism	Cytoplasm	0	1000
P5CR	$\text{nadph}[c] + 2 \text{h}[c] + 1\text{pyr5c}[c] \rightleftharpoons \text{nadp}[c] + \text{pro_L}[c]$	Arginine and proline metabolism	Cytoplasm	0	1000
ASNN	$\text{h2o}[c] + \text{asn_L}[c] \rightarrow \text{nh4}[c] + \text{asp_L}[c]$	Alanine, aspartate and glutamate metabolism	Cytoplasm	0	1000
ASNS1	$\text{amp}[c] + \text{ppi}[c] + \text{asn_L}[c] + \text{glu_L}[c] + 2 \text{h}[c] \rightleftharpoons \text{atp}[c] + \text{asp_L}[c] + \text{gln_L}[c] + \text{h2o}[c]$	Alanine, aspartate and glutamate metabolism	Cytoplasm	-1000	1000
ASPO1	$\text{h2o}[c] + \text{o2}[c] + \text{asp_L}[c] \rightarrow \text{nh4}[c] + \text{h2o2}[c] + \text{oaa}[c]$	Alanine, aspartate and glutamate metabolism	Cytoplasm	0	1000
NACASPAH	$\text{h2o}[c] + \text{Nacasp}[c] \rightleftharpoons \text{ac}[c] + \text{asp_L}[c]$	Alanine, aspartate and glutamate metabolism	Cytoplasm	-1000	1000
ASPK	$\text{atp}[c] + \text{asp_L}[c] \rightleftharpoons \text{adp}[c] + 4\text{pasp}[c]$	Glycine, serine and threonine metabolism	Cytoplasm	-1000	1000
ASAD	$\text{nadph}[c] + \text{h}[c] + 4\text{pasp}[c] \rightleftharpoons \text{nadp}[c] + \text{pi}[c] + \text{aspsa}[c]$	Glycine, serine and threonine metabolism	Cytoplasm	-1000	1000
DABAAT2	$\text{aspsa}[c] + \text{glu_L}[c] \rightleftharpoons \text{akg}[c] + \text{h}[c] + 24\text{dab}[c]$	Glycine, serine and threonine metabolism	Cytoplasm	-1000	1000
DABAC	$24\text{dab}[c] \rightleftharpoons \text{co2}[c] + 13\text{dampp}[c]$	Glycine, serine and threonine metabolism	Cytoplasm	0	1000
HSDxi	$\text{nadh}[c] + \text{h}[c] + \text{aspsa}[c] \rightleftharpoons \text{nad}[c] + \text{hom_L}[c]$	Glycine, serine and threonine metabolism	Cytoplasm	-1000	1000
HSDy	$\text{nadph}[c] + \text{h}[c] + \text{aspsa}[c] \rightleftharpoons \text{nadp}[c] + \text{hom_L}[c]$	Glycine, serine and threonine metabolism	Cytoplasm	-1000	1000
HSK	$\text{atp}[c] + \text{hom_L}[c] \rightarrow \text{adp}[c] + \text{h}[c] + \text{phom}[c]$	Glycine, serine and threonine metabolism	Cytoplasm	0	1000
THRS	$\text{h2o}[c] + \text{phom}[c] \rightleftharpoons \text{pi}[c] + \text{thr_L}[c]$	Glycine, serine and threonine metabolism	Cytoplasm	-1000	1000
THRD_L	$\text{thr_L}[c] \rightarrow \text{nh4}[c] + 2\text{obut}[c]$	Glycine, serine and threonine metabolism	Cytoplasm	0	1000
THRA	$\text{thr_L}[c] \rightleftharpoons \text{gly}[c] + \text{acald}[c]$	Glycine, serine and threonine metabolism	Cytoplasm	-1000	1000
GLYTA	$\text{glu_L}[c] + \text{glx}[c] \rightleftharpoons \text{akg}[c] + \text{gly}[c]$	Glycine, serine and threonine metabolism	Cytoplasm	0	1000
GOR1	$\text{glx}[c] + \text{h}[c] + \text{nadh}[c] + \text{nh4}[c] \rightleftharpoons \text{gly}[c] + \text{h2o}[c] + \text{nad}[c]$	Glycine, serine and threonine metabolism	Cytoplasm	0	1000

SPT_syn	glx[c] + ser__L[c] <=> gly[c] + hpyr[c]	Glycine, serine and threonine metabolism	Cytoplasm	-1000	1000
H4THDPS	aspsa[c] + pyr[c] <=> 4hthdp[c] + h2o[c] + h[c]	Lysine biosynthesis	Cytoplasm	-1000	1000
H4THDPR_2	4hthdp[c] + nadh[c] + h[c] <=> thdp[c] + nad[c] + h2o[c]	Lysine biosynthesis	Cytoplasm	-1000	1000
H4THDPR	4hthdp[c] + nadph[c] + h[c] <=> thdp[c] + nadp[c] + h2o[c]	Lysine biosynthesis	Cytoplasm	-1000	1000
LDAPAT	h2o[c] + glu__L[c] + h[c] + thdp[c] <=> akgl[c] + 26dap_LL[c]	Lysine biosynthesis	Cytoplasm	-1000	1000
DAPE	26dap_LL[c] <=> 26dap__M[c]	Lysine biosynthesis	Cytoplasm	-1000	1000
DAPDC	h[c] + 26dap__M[c] --> co2[c] + lys__L[c]	Lysine biosynthesis	Cytoplasm	0	1000
PGCD	nad[c] + 3pg[c] <=> nadh[c] + h[c] + 3php[c]	Glycine, serine and threonine metabolism	Cytoplasm	0	1000
PSERT	glu__L[c] + 3php[c] <=> akgl[c] + pser__L[c]	Glycine, serine and threonine metabolism	Cytoplasm	0	1000
PSP_L	h2o[c] + pser__L[c] <=> pi[c] + ser__L[c]	Glycine, serine and threonine metabolism	Cytoplasm	0	1000
SERD_L	ser__L[c] --> nh4[c] + pyr[c]	Glycine, serine and threonine metabolism	Cytoplasm	0	1000
SPTc	pyr[c] + ser__L[c] <=> ala__L[c] + hpyr[c]	Glycine, serine and threonine metabolism	Cytoplasm	-1000	1000
HPYRRy	h[c] + hpyr[c] + nadph[c] <=> glyc__R[c] + nadp[c]	Glycine, serine and threonine metabolism	Cytoplasm	0	1000
HPYRRx	h[c] + hpyr[c] + nadh[c] <=> glyc__R[c] + nad[c]	Glycine, serine and threonine metabolism	Cytoplasm	0	1000
GLYAT	accoa[c] + gly[c] --> coa[c] + 2aobut[c]	Glycine, serine and threonine metabolism	Cytoplasm	0	1000
AOBUTDs	2aobut[c] + h[c] --> aact[c] + co2[c]	Glycine, serine and threonine metabolism	Cytoplasm	0	1000
APPLDHr	aact[c] + nadh[c] + h[c] <=> nad[c] + appl[c]	Glycine, serine and threonine metabolism	Cytoplasm	-1000	1000
AACTOOR	aact[c] + h2o[c] + o2[c] <=> h2o2[c] + mthgxl[c] + nh4[c]	Glycine, serine and threonine metabolism	Cytoplasm	0	1000
EX_so4_e	so4[e] <=>	Exchange	Extracellular	-1000	0
SO4t2	so4[e] + h[e] <=> so4[c] + h[c]	Transport	Cytoplasm	-1000	1000
SULabc	so4[e] + atp[c] + h2o[c] <=> so4[c] + adp[c] + h[c] + pi[c]	Transport	Cytoplasm	0	1000
EX_tsul_e	tsul[e] <=>	Exchange	Extracellular	-1000	0

TSULt2	tsul[e] + h[e] <=> tsul[c] + h[c]	Transport	Cytoplasm	-1000	1000
TSULabc	tsul[e] + atp[c] + h2o[c] <=> tsul[c] + adp[c] + h[c] + pi[c]	Transport	Cytoplasm	0	1000
SADT	atp[c] + so4[c] <=> ppi[c] + aps[c]	Sulfur metabolism	Cytoplasm	-1000	1000
BPNT2	pi[c] + aps[c] <=> h2o[c] + paps[c]	Sulfur metabolism	Cytoplasm	-1000	1000
PAPSR	paps[c] + trdrd[c] <=> pap[c] + h[c] + so3[c] + trdox[c]	Sulfur metabolism	Cytoplasm	-1000	1000
ADSK	aps[c] + atp[c] <=> adp[c] + h[c] + paps[c]	Sulfur metabolism	Cytoplasm	0	1000
TRDR	nadph[c] + h[c] + trdox[c] <=> nadp[c] + trdrd[c]	Sulfur metabolism	Cytoplasm	-1000	1000
SULR3_b	6 h[c] + so3[c] + 3 fdxrd[c] <=> 3 h2o[c] + h2s[c] + 3 fdxo_2_2[c]	Sulfur metabolism	Cytoplasm	-1000	1000
MCPCST	pyr[c] + tsul[c] <=> so3[c] + mercppyr[c]	Sulfur metabolism	Cytoplasm	-1000	1000
GHMT2r	ser__L[c] + thf[c] <=> h2o[c] + gly[c] + mlthf[c]	Glycine, serine and threonine metabolism	Cytoplasm	-1000	1000
SERAT	accoa[c] + ser__L[c] --> coa[c] + acser[c]	Cysteine and methionine metabolism	Cytoplasm	0	1000
CYSS_2	h2s[c] + acser[c] --> ac[c] + cys__L[c]	Cysteine and methionine metabolism	Cytoplasm	0	1000
ASPTA4	glu__L[c] + mercppyr[c] <=> akc[c] + cys__L[c]	Cysteine and methionine metabolism	Cytoplasm	-1000	1000
HSERTA	accoa[c] + hom__L[c] --> coa[c] + achms[c]	Cysteine and methionine metabolism	Cytoplasm	0	1000
AHSERL2	h2s[c] + achms[c] <=> ac[c] + hcys__L[c]	Cysteine and methionine metabolism	Cytoplasm	-1000	1000
AHAL_c	tsul[c] + achms[c] + trdrd[c] <=> ac[c] + h[c] + so3[c] + hcys__L[c] + trdox[c]	Cysteine and methionine metabolism	Cytoplasm	-1000	1000
METS_1	hcys__L[c] + 5mthf[c] <=> met__L[c] + thf[c]	Cysteine and methionine metabolism	Cytoplasm	-1000	1000
CYSTS	hcys__L[c] + ser__L[c] <=> cyst__L[c] + h2o[c]	Cysteine and methionine metabolism	Cytoplasm	-1000	1000
CYSTL	cyst__L[c] + h2o[c] <=> hcys__L[c] + nh4[c] + pyr[c]	Cysteine and methionine metabolism	Cytoplasm	0	1000
MTAP	5mta[c] + pi[c] <=> ade[c] + 5mdr1p[c]	Cysteine and methionine metabolism	Cytoplasm	0	1000
MTRI	5mdr1p[c] <=> 5mdru1p[c]	Cysteine and methionine metabolism	Cytoplasm	-1000	1000
MDRPD	5mdru1p[c] <=> h2o[c] + dkmpp[c]	Cysteine and methionine metabolism	Cytoplasm	0	1000
ENOPH	h2o[c] + dkmpp[c] <=> pi[c] + dhmtpp[c]	Cysteine and methionine metabolism			
ARD1	o2[c] + dhmtpp[c] <=> for[c] + h[c] + co[c] + mtp[c]	Cysteine and methionine metabolism	Cytoplasm	-1000	1000

ACDO	$\text{o2[c]} + \text{dhmtp[c]} \rightleftharpoons \text{for[c]} + 2 \text{ h[c]} + 2 \text{ kmb[c]}$	Cysteine and methionine metabolism	Cytoplasm	-1000	1000
UNK3	$\text{glu_L[c]} + 2 \text{ kmb[c]} \rightleftharpoons \text{akg[c]} + \text{met_L[c]}$	Cysteine and methionine metabolism	Cytoplasm	-1000	1000
AGTi	$\text{ala_L[c]} + \text{glx[c]} \rightleftharpoons \text{pyr[c]} + \text{gly[c]}$	Alanine, aspartate and glutamate metabolism	Cytoplasm	0	1000
GLYO1	$\text{gly[c]} + \text{h2o[c]} + \text{o2[c]} \rightleftharpoons \text{glx[c]} + \text{h2o2[c]} + \text{nh4[c]}$	Glycine, serine and threonine metabolism	Cytoplasm	0	1000
GLUDC	$\text{glu_L[c]} + \text{h[c]} \rightarrow \text{co2[c]} + 4 \text{ abut[c]}$	Alanine, aspartate and glutamate metabolism	Cytoplasm	0	1000
ALAD_L	$\text{h2o[c]} + \text{nad[c]} + \text{ala_L[c]} \rightarrow \text{nadh[c]} + \text{nh4[c]} + \text{pyr[c]} + \text{h[c]}$	Alanine, aspartate and glutamate metabolism	Cytoplasm	0	1000
P5CD	$2 \text{ h2o[c]} + \text{nad[c]} + 1 \text{ pyr5[c]} \rightleftharpoons \text{nadh[c]} + \text{glu_L[c]} + \text{h[c]}$	Alanine, aspartate and glutamate metabolism	Cytoplasm	-1000	1000
ACHBS	$\text{pyr[c]} + \text{h[c]} + 2 \text{ obut[c]} \rightarrow \text{co2[c]} + 2 \text{ ahbut[c]}$	Valine, leucine and isoleucine biosynthesis	Cytoplasm	0	1000
KARI_1	$2 \text{ ahbut[c]} \rightleftharpoons 3 \text{ hmop[c]}$	Valine, leucine and isoleucine biosynthesis	Cytoplasm	-1000	1000
KARI_23dhmp_1	$\text{nadph[c]} + \text{h[c]} + 3 \text{ hmop[c]} \rightleftharpoons \text{nadp[c]} + 23 \text{ dhmp[c]}$	Valine, leucine and isoleucine biosynthesis	Cytoplasm	-1000	1000
DHAD2	$23 \text{ dhmp[c]} \rightarrow \text{h2o[c]} + 3 \text{ mop[c]}$	Valine, leucine and isoleucine biosynthesis	Cytoplasm	0	1000
ILEDH_nad	$\text{nadh[c]} + \text{nh4[c]} + \text{h[c]} + 3 \text{ mop[c]} \rightleftharpoons \text{h2o[c]} + \text{nad[c]} + \text{ile_L[c]}$	Valine, leucine and isoleucine biosynthesis	Cytoplasm	-1000	1000
ACLS	$2 \text{ pyr[c]} + \text{h[c]} \rightarrow \text{co2[c]} + \text{alac_S[c]}$	Valine, leucine and isoleucine biosynthesis	Cytoplasm	0	1000
ACLSa	$\text{pyr[c]} + \text{thmpp[c]} \rightleftharpoons \text{co2[c]} + 2 \text{ ahethmpp[c]}$	Valine, leucine and isoleucine biosynthesis	Cytoplasm	0	1000
ACLSb	$\text{h[c]} + \text{pyr[c]} + 2 \text{ ahethmpp[c]} \rightleftharpoons \text{alac_S[c]} + \text{thmpp[c]}$	Valine, leucine and isoleucine biosynthesis	Cytoplasm	0	1000
ACHBSb	$2 \text{ obut[c]} + 2 \text{ ahethmpp[c]} + \text{h[c]} \rightleftharpoons 2 \text{ ahbut[c]} + \text{thmpp[c]}$	Valine, leucine and isoleucine biosynthesis	Cytoplasm	0	1000
KARI_3hmoa_1	$\text{alac_S[c]} \rightleftharpoons 3 \text{ hmoa[c]}$	Valine, leucine and isoleucine biosynthesis	Cytoplasm	-1000	1000
KARI_23dhmb_1	$\text{nadph[c]} + \text{h[c]} + 3 \text{ hmoa[c]} \rightleftharpoons \text{nadp[c]} + 23 \text{ dhmb[c]}$	Valine, leucine and isoleucine biosynthesis	Cytoplasm	-1000	1000

DHAD1	23dhmb[c] --> h2o[c] + 3mob[c]	Valine, leucine and isoleucine biosynthesis	Cytoplasm	0	1000
VALDHr	nadh[c] + nh4[c] + h[c] + 3mob[c] <=> h2o[c] + nad[c] + val__L[c]	Valine, leucine and isoleucine biosynthesis	Cytoplasm	-1000	1000
VPAMTr	ala__L[c] + 3mob[c] <=> pyr[c] + val__L[c]	Valine, leucine and isoleucine biosynthesis	Cytoplasm	-1000	1000
IPPS	h2o[c] + accoa[c] + 3mob[c] --> coa[c] + h[c] + 3c3hmp[c]	Valine, leucine and isoleucine biosynthesis	Cytoplasm	0	1000
IPPMib	3c3hmp[c] <=> h2o[c] + 2ippm[c]	Valine, leucine and isoleucine biosynthesis	Cytoplasm	-1000	1000
IPPMla	h2o[c] + 2ippm[c] <=> 3c2hmp[c]	Valine, leucine and isoleucine biosynthesis	Cytoplasm	-1000	1000
IPMD	nad[c] + 3c2hmp[c] <=> nadh[c] + h[c] + 3c4mop[c]	Valine, leucine and isoleucine biosynthesis	Cytoplasm	-1000	1000
OMCDC	h[c] + 3c4mop[c] --> co2[c] + 4mop[c]	Valine, leucine and isoleucine biosynthesis	Cytoplasm	0	1000
LLEUDr	nadh[c] + nh4[c] + h[c] + 4mop[c] <=> h2o[c] + nad[c] + leu__L[c]	Valine, leucine and isoleucine biosynthesis	Cytoplasm	-1000	1000
MMS	accoa[c] + h2o[c] + pyr[c] <=> coa[c] + h[c] + 2mm__R[c]	Valine, leucine and isoleucine biosynthesis	Cytoplasm	0	1000
MMHL	2mm__R[c] <=> h2o[c] + 2mm[c]	Valine, leucine and isoleucine biosynthesis	Cytoplasm	-1000	1000
MMHTASE	h2o[c] + 2mm[c] <=> e3mmal[c]	Valine, leucine and isoleucine biosynthesis	Cytoplasm	-1000	1000
MM3OR1	nad[c] + e3mmal[c] <=> 2obut[c] + co2[c] + nadh[c]	Valine, leucine and isoleucine biosynthesis	Cytoplasm	0	1000
ACCAH	1acpc[c] + h2o[c] <=> 2obut[c] + nh4[c]	Valine, leucine and isoleucine biosynthesis	Cytoplasm	-1000	1000
DDPA	h2o[c] + pep[c] + e4p[c] --> pi[c] + 2dda7p[c]	Phenylalanine, tyrosine and tryptophan biosynthesis	Cytoplasm	0	1000
DHQS	2dda7p[c] --> pi[c] + 3dhq[c]	Phenylalanine, tyrosine and tryptophan biosynthesis	Cytoplasm	0	1000
DHQTi	3dhq[c] --> h2o[c] + 3dhsk[c]	Phenylalanine, tyrosine and tryptophan biosynthesis	Cytoplasm	0	1000
SHK3Dr	nadph[c] + h[c] + 3dhsk[c] <=> nadp[c] + skm[c]	Phenylalanine, tyrosine and tryptophan biosynthesis	Cytoplasm	-1000	1000
SHKK	atp[c] + skm[c] --> adp[c] + h[c] + skm5p[c]	Phenylalanine, tyrosine and tryptophan biosynthesis	Cytoplasm	0	1000
PSCVT	pep[c] + skm5p[c] <=> pi[c] + 3psme[c]	Phenylalanine, tyrosine and tryptophan biosynthesis	Cytoplasm	-1000	1000

CHORS	3psme[c] --> pi[c] + chor[c]	Phenylalanine, tyrosine and tryptophan biosynthesis	Cytoplasm	0	1000
CHORM	chor[c] --> pphn[c]	Phenylalanine, tyrosine and tryptophan biosynthesis	Cytoplasm	0	1000
PPNDH	h[c] + pphn[c] --> h2o[c] + co2[c] + phpyr[c]	Phenylalanine, tyrosine and tryptophan biosynthesis	Cytoplasm	0	1000
PPND	nad[c] + pphn[c] --> nadh[c] + co2[c] + 34hpp[c]	Phenylalanine, tyrosine and tryptophan biosynthesis	Cytoplasm	0	1000
PPND2	nadp[c] + pphn[c] --> nadph[c] + co2[c] + 34hpp[c]	Phenylalanine, tyrosine and tryptophan biosynthesis	Cytoplasm	0	1000
PPHTA	asp__L[c] + pphn[c] <=> oaa[c] + Largn[c]	Phenylalanine, tyrosine and tryptophan biosynthesis	Cytoplasm	-1000	1000
ARODH_2	nad[c] + Largn[c] --> nadh[c] + co2[c] + tyr__L[c]	Phenylalanine, tyrosine and tryptophan biosynthesis	Cytoplasm	0	1000
ARODH	nadp[c] + Largn[c] --> nadph[c] + co2[c] + tyr__L[c]	Phenylalanine, tyrosine and tryptophan biosynthesis	Cytoplasm	0	1000
AROH	h[c] + Largn[c] --> h2o[c] + co2[c] + phe__L[c]	Phenylalanine, tyrosine and tryptophan biosynthesis	Cytoplasm	0	1000
PHETA1	akg[c] + phe__L[c] <=> glu__L[c] + phpyr[c]	Phenylalanine metabolism	Cytoplasm	-1000	1000
TYRTA	glu__L[c] + 34hpp[c] <=> akg[c] + tyr__L[c]	Phenylalanine, tyrosine and tryptophan biosynthesis	Cytoplasm	-1000	1000
ANS2	nh4[c] + chor[c] --> h2o[c] + pyr[c] + h[c] + anth[c]	Phenylalanine, tyrosine and tryptophan biosynthesis	Cytoplasm	0	1000
ANS	gln__L[c] + chor[c] --> pyr[c] + glu__L[c] + h[c] + anth[c]	Phenylalanine, tyrosine and tryptophan biosynthesis	Cytoplasm	0	1000
ACS3	atp[c] + coa[c] + ac[c] <=> adp[c] + pi[c] + accoa[c]	Glycolysis / Gluconeogenesis	Cytoplasm	-1000	1000
ACS	atp[c] + coa[c] + ac[c] --> ppi[c] + amp[c] + accoa[c] + h[c]	Glycolysis / Gluconeogenesis	Cytoplasm	0	1000

PFOR	coa[c] + pyr[c] + fldox[c] --> co2[c] + accoa[c] + h[c] + fldrd[c]	Glycolysis / Gluconeogenesis	Cytoplasm	0	1000
ALDD2x	h2o[c] + nad[c] + acald[c] <=> nadh[c] + ac[c] + 2 h[c]	Glycolysis / Gluconeogenesis	Cytoplasm	-1000	1000
ALCD2x	nad[c] + etoh[c] <=> nadh[c] + h[c] + acald[c]	Glycolysis / Gluconeogenesis	Cytoplasm	-1000	1000
ALCD1	meoh[c] + nad[c] <=> fald[c] + h[c] + nadh[c]	Glycolysis / Gluconeogenesis	Cytoplasm	-1000	1000
ANPRT	anth[c] + prpp[c] --> ppi[c] + h[c] + pran[c]	Phenylalanine, tyrosine and tryptophan biosynthesis	Cytoplasm	0	1000
PRAli	pran[c] <=> 2cpr5p[c]	Phenylalanine, tyrosine and tryptophan biosynthesis	Cytoplasm	-1000	1000
IGPS	h[c] + 2cpr5p[c] --> h2o[c] + co2[c] + 3ig3p[c]	Phenylalanine, tyrosine and tryptophan biosynthesis	Cytoplasm	0	1000
TRPS3	3ig3p[c] <=> g3p[c] + indole[c]	Phenylalanine, tyrosine and tryptophan biosynthesis	Cytoplasm	-1000	1000
TRPS2	ser__L[c] + indole[c] <=> h2o[c] + trp__L[c]	Phenylalanine, tyrosine and tryptophan biosynthesis	Cytoplasm	-1000	1000
ATPPRT	atp[c] + prpp[c] --> ppi[c] + h[c] + prbatp[c]	Histidine metabolism	Cytoplasm	0	1000
PRATPP	h2o[c] + prbatp[c] --> ppi[c] + 2 h[c] + prbamp[c]	Histidine metabolism	Cytoplasm	0	1000
PRAMPC	h2o[c] + prbamp[c] <=> prfp[c]	Histidine metabolism	Cytoplasm	-1000	1000
PRMICI	h[c] + prfp[c] --> prlp[c]	Histidine metabolism	Cytoplasm	0	1000
IG3PS_1	gln__L[c] + prlp[c] --> glu__L[c] + 2 h[c] + eig3p[c] + aicar[c]	Histidine metabolism	Cytoplasm	0	1000
IGPDH	eig3p[c] --> h2o[c] + imacp[c]	Histidine metabolism	Cytoplasm	0	1000
HSTPT	glu__L[c] + imacp[c] <=> akc[c] + hisp[c]	Histidine metabolism	Cytoplasm	-1000	1000
HISTP	h2o[c] + hisp[c] <=> pi[c] + histd[c]	Histidine metabolism	Cytoplasm	-1000	1000
HISTDa	nad[c] + histd[c] <=> nadh[c] + h[c] + histda[c]	Histidine metabolism	Cytoplasm	-1000	1000
HISTDb	h2o[c] + nad[c] + histda[c] <=> nadh[c] + 2 h[c] + his__L[c]	Histidine metabolism	Cytoplasm	-1000	1000
ASP1DC	asp__L[c] + h[c] --> co2[c] + ala_B[c]	beta-Alanine metabolism	Cytoplasm	0	1000
CYPHYP	asp__L[c] + arg__L[c] --> precyanphy[c] + h2o[c]	Cyanophycin metabolism	Cytoplasm	0	1000
CYPHYS	2 atp[c] + precyanphy[c] + asp__L[c] + arg__L[c] --> 2 adp[c] + 2 pi[c] + cyanphy[c] + 2 h[c]	Cyanophycin metabolism	Cytoplasm	0	1000
CYPHYC_2	h2o[c] + cyanphy[c] --> 2 asp__L_arg__L[c]	Cyanophycin metabolism	Cytoplasm	0	1000

CYPH_BIA	asp__L_arg__L[c] + h2o[c] --> asp__L[c] + arg__L[c]	Cyanophycin metabolism	Cytoplasm	0	1000
GLUCYS	atp[c] + cys__L[c] + glu__L[c] <=> adp[c] + glucys[c] + h[c] + pi[c]	Glutathione metabolism	Cytoplasm	0	1000
GTHS	atp[c] + glucys[c] + gly[c] <=> adp[c] + gthrd[c] + h[c] + pi[c]	Glutathione metabolism	Cytoplasm	0	1000
GTHOr	2 gthrd[c] + nadp[c] <=> gthox[c] + h[c] + nadph[c]	Glutathione metabolism	Cytoplasm	-1000	1000
GTHPi	2 gthrd[c] + h2o2[c] <=> gthox[c] + 2 h2o[c]	Glutathione metabolism	Cytoplasm	0	1000
GTHRDH_syn	gthrd[c] + h2o[c] <=> cgly[c] + glu__L[c]	Glutathione metabolism	Cytoplasm	0	1000
AMPTASECG	cgly[c] + h2o[c] <=> cys__L[c] + gly[c]	Glutathione metabolism	Cytoplasm	0	1000
OPAH	atp[c] + 2 h2o[c] + 5oxpro[c] <=> adp[c] + glu__L[c] + h[c] + pi[c]	Glutathione metabolism	Cytoplasm	-1000	1000
LGTHL	gthrd[c] + mthgxl[c] <=> lgt__S[c]	Glutathione metabolism	Cytoplasm	-1000	1000
GLYOX	h2o[c] + lgt__S[c] <=> gthrd[c] + h[c] + lac__D[c]	Glutathione metabolism	Cytoplasm	0	1000
SFGTHi	Sfglutth[c] + h2o[c] <=> for[c] + gthrd[c] + h[c]	Glutathione metabolism	Cytoplasm	-1000	1000
FALDH2	hmgth[c] + nad[c] <=> Sfglutth[c] + h[c] + nadh[c]	Glutathione metabolism	Cytoplasm	-1000	1000
FALGTHLs	fald[c] + gthrd[c] <=> hmgth[c]	Glutathione metabolism	Cytoplasm	0	1000
13DAMPPOX_2	13dampp[c] + o2[c] + nadph[c] + h[c] <=> h2o[c] + nhapp[c] + nadp[c]	Schizokinen siderophore biosynthesis	Cytoplasm	-1000	1000
ACNHAPP	nhapp[c] + accoa[c] <=> coa[c] + nachapp[c]	Schizokinen siderophore biosynthesis	Cytoplasm	-1000	1000
LNACHAPP	atp[c] + nachapp[c] + cit[c] <=> h[c] + amp[c] + ppi[c] + ncachapp[c]	Schizokinen siderophore biosynthesis	Cytoplasm	0	1000
SCHIZS	atp[c] + nachapp[c] + ncachapp[c] <=> amp[c] + ppi[c] + schiz[c]	Schizokinen siderophore biosynthesis	Cytoplasm	0	1000
GTPDHF	h2o[c] + gtp[c] --> fapn3p[c]	Folate and molybdopterin biosynthesis	Cytoplasm	0	1000
FAP3PDH	h2o[c] + fapn3p[c] <=> for[c] + h[c] + 25dap3p[c]	Folate and molybdopterin biosynthesis	Cytoplasm	-1000	1000
DAPN3PM	25dap3p[c] <=> 25dattop[c]	Folate and molybdopterin biosynthesis	Cytoplasm	-1000	1000
DHP3PDH	25dattop[c] --> h2o[c] + ahdt[c]	Folate and molybdopterin biosynthesis	Cytoplasm	-1000	1000
AKP1	3 h2o[c] + ahdt[c] --> 3 pi[c] + 3 h[c] + dhnpt[c]	Folate and molybdopterin biosynthesis	Cytoplasm	0	1000
DHNPA2r	dhnpt[c] <=> gcald[c] + 6hnhpt[c]	Folate and molybdopterin biosynthesis	Cytoplasm	0	1000
GCALDDy	gcald[c] + h2o[c] + nadp[c] <=> glyclt[c] + 2 h[c] + nadph[c]	Glycine, serine and threonine metabolism	Cytoplasm	0	1000
HPPK2	atp[c] + 6hnhpt[c] --> amp[c] + h[c] + 6hnhptpp[c]	Folate and molybdopterin biosynthesis	Cytoplasm	0	1000
ADCS	gln__L[c] + chor[c] <=> glu__L[c] + 4adcho[c]	Folate and molybdopterin biosynthesis	Cytoplasm	0	1000

ADCL	4adcho[c] --> pyr[c] + h[c] + 4abz[c]	Folate and molybdopterin biosynthesis	Cytoplasm	0	1000
FOLD3_1	4abz[c] + 6hnhptpp[c] --> ppi[c] + h[c] + dhpt[c]	Folate and molybdopterin biosynthesis	Cytoplasm	0	1000
DHPS	4abz[c] + 6hnhpt[c] --> h2o[c] + dhpt[c]	Folate and molybdopterin biosynthesis	Cytoplasm	0	1000
DHFS	atp[c] + glu__L[c] + dhpt[c] --> adp[c] + pi[c] + h[c] + dhf[c]	Folate and molybdopterin biosynthesis	Cytoplasm	0	1000
FOLR2	nadph[c] + fol[c] <=> dhf[c] + nadp[c]	Folate and molybdopterin biosynthesis	Cytoplasm	-1000	1000
THFOR2	h[c] + 2 nadph[c] + fol[c] <=> 2 nadp[c] + thf[c]	Folate and molybdopterin biosynthesis	Cytoplasm	-1000	1000
DHFR	nadph[c] + h[c] + dhf[c] <=> nadp[c] + thf[c]	Folate and molybdopterin biosynthesis	Cytoplasm	-1000	1000
THFGLUS	atp[c] + glu__L[c] + thf[c] <=> adp[c] + h[c] + pi[c] + thfglu[c]	Folate and molybdopterin biosynthesis	Cytoplasm	0	1000
DNTPPA	ahdt[c] + h2o[c] <=> dhmp[c] + 2 h[c] + ppi[c]	Folate and molybdopterin biosynthesis	Cytoplasm	0	1000
DNMPPA	dhmp[c] + h2o[c] <=> dhnp[c] + pi[c]	Folate and molybdopterin biosynthesis	Cytoplasm	0	1000
PTHPS	ahdt[c] <=> ppi[c] + 6pthp[c]	Folate and molybdopterin biosynthesis	Cytoplasm	-1000	1000
CPH4S	ahdt[c] + h2o[c] <=> acald[c] + cph4[c] + h[c] + ppi[c]	Folate and molybdopterin biosynthesis	Cytoplasm	-1000	1000
CDGS	cph4[c] + h[c] <=> cdg[c] + nh4[c]	Folate and molybdopterin biosynthesis	Cytoplasm	-1000	1000
CCGS	atp[c] + cdg[c] + nh4[c] <=> adp[c] + h[c] + h2o[c] + pi[c] + preq0[c]	Folate and molybdopterin biosynthesis	Cytoplasm	0	1000
CDGR	3 h[c] + 2 nadph[c] + preq0[c] <=> 2 nadp[c] + preq1[c]	Folate and molybdopterin biosynthesis	Cytoplasm	0	1000
GTPC	amet[c] + gtp[c] <=> dad_5[c] + met__L[c] + 38ch2gtp[c]	Folate and molybdopterin biosynthesis	Cytoplasm	0	1000
CPMPS_1	h2o[c] + 38ch2gtp[c] <=> cpmp[c] + ppi[c]	Folate and molybdopterin biosynthesis	Cytoplasm	0	1000
MPTS	cpmp[c] + 2 moadcosh[c] <=> 3 h[c] + 2 moadcoo[c] + mpt[c]	Folate and molybdopterin biosynthesis	Cytoplasm	0	1000
MPTSS	atp[c] + h[c] + moadcoo[c] <=> moadamp[c] + ppi[c] + h[c]	Folate and molybdopterin biosynthesis	Cytoplasm	0	1000
MOADSUX_1	moadamp[c] + nadh[c] + sufse[c] <=> amp[c] + moadcosh[c] + nad[c] + sufse[c]	Folate and molybdopterin biosynthesis	Cytoplasm	-1000	1000
GLYCL	nad[c] + gly[c] + thf[c] --> nadh[c] + co2[c] + nh4[c] + mlthf[c]	One carbon pool by folate	Cytoplasm	0	1000
MTHFD	nadp[c] + mlthf[c] <=> nadph[c] + methf[c]	One carbon pool by folate	Cytoplasm	-1000	1000
THFAT	h2o[c] + methf[c] <=> h[c] + 5fthf[c]	One carbon pool by folate	Cytoplasm	0	1000

MTHFC	$\text{h2o}[c] + \text{methf}[c] \rightleftharpoons \text{h}[c] + 10\text{fthf}[c]$	One carbon pool by folate	Cytoplasm	0	1000
FTHFCL	$\text{atp}[c] + 5\text{fthf}[c] \rightarrow \text{adp}[c] + \text{pi}[c] + \text{methf}[c]$	One carbon pool by folate	Cytoplasm	0	1000
FTHFD	$\text{h2o}[c] + 10\text{fthf}[c] \rightarrow \text{for}[c] + \text{h}[c] + \text{thf}[c]$	One carbon pool by folate	Cytoplasm	0	1000
FDH	$\text{nad}[c] + \text{for}[c] \rightarrow \text{nadh}[c] + \text{co2}[c]$	One carbon pool by folate	Cytoplasm	0	1000
MTHFR3_1	$\text{nadp}[c] + 5\text{mthf}[c] \rightleftharpoons \text{nadph}[c] + \text{h}[c] + \text{mlthf}[c]$	One carbon pool by folate	Cytoplasm	-1000	1000
MTHFR2_1	$\text{nad}[c] + 5\text{mthf}[c] \rightleftharpoons \text{nadh}[c] + \text{h}[c] + \text{mlthf}[c]$	One carbon pool by folate	Cytoplasm	-1000	1000
GLUPRT	$\text{h2o}[c] + \text{gln_L}[c] + \text{prpp}[c] \rightarrow \text{ppi}[c] + \text{glu_L}[c] + \text{h}[c] + \text{pram}[c]$	Purine metabolism	Cytoplasm	0	1000
PRAGSr	$\text{atp}[c] + \text{gly}[c] + \text{pram}[c] \rightarrow \text{adp}[c] + \text{pi}[c] + \text{h}[c] + \text{gar}[c]$	Purine metabolism	Cytoplasm	0	1000
PRAGFt	$\text{h2o}[c] + \text{methf}[c] + \text{gar}[c] \rightarrow 2 \text{h}[c] + \text{thf}[c] + \text{fgam}[c]$	One carbon pool by folate	Cytoplasm	0	1000
GARFT	$10\text{fthf}[c] + \text{gar}[c] \rightleftharpoons \text{h}[c] + \text{thf}[c] + \text{fgam}[c]$	Purine metabolism	Cytoplasm	-1000	1000
PRFGS	$\text{h2o}[c] + \text{atp}[c] + \text{gln_L}[c] + \text{fgam}[c] \rightarrow \text{adp}[c] + \text{pi}[c] + \text{glu_L}[c] + \text{h}[c] + \text{fpram}[c]$	Purine metabolism	Cytoplasm	0	1000
PRAIS_1	$\text{atp}[c] + \text{fpram}[c] \rightarrow \text{adp}[c] + \text{pi}[c] + \text{h}[c] + \text{air}[c]$	Purine metabolism	Cytoplasm	0	1000
AIRC2	$\text{atp}[c] + \text{hco3}[c] + \text{air}[c] \rightarrow \text{adp}[c] + \text{pi}[c] + \text{h}[c] + 5\text{caiz}[c]$	Purine metabolism	Cytoplasm	0	1000
AIRC3	$5\text{caiz}[c] \rightleftharpoons 5\text{aizc}[c]$	Purine metabolism	Cytoplasm	-1000	1000
PRASCSi	$\text{atp}[c] + \text{asp_L}[c] + 5\text{aizc}[c] \rightarrow \text{adp}[c] + \text{pi}[c] + \text{h}[c] + 25\text{aics}[c]$	Purine metabolism	Cytoplasm	0	1000
ADSL2r	$25\text{aics}[c] \rightleftharpoons \text{h}[c] + \text{fum}[c] + \text{aicar}[c]$	Purine metabolism	Cytoplasm	-1000	1000
AICART	$10\text{fthf}[c] + \text{aicar}[c] \rightarrow \text{thf}[c] + \text{fprica}[c]$	Purine metabolism	Cytoplasm	0	1000
IMPC	$\text{fprica}[c] \rightleftharpoons \text{h2o}[c] + \text{imp}[c]$	Purine metabolism	Cytoplasm	-1000	1000
NTD11	$\text{h2o}[c] + \text{imp}[c] \rightleftharpoons \text{ins}[c] + \text{pi}[c]$	Purine metabolism	Cytoplasm	-1000	1000
NTPP9	$\text{h2o}[c] + \text{itp}[c] \rightleftharpoons \text{h}[c] + \text{imp}[c] + \text{ppi}[c]$	Purine metabolism	Cytoplasm	-1000	1000
IMPD	$\text{h2o}[c] + \text{nad}[c] + \text{imp}[c] \rightarrow \text{nadh}[c] + \text{h}[c] + \text{xmp}[c]$	Purine metabolism	Cytoplasm	0	1000
NTPP11	$\text{h2o}[c] + \text{xtp}[c] \rightleftharpoons \text{h}[c] + \text{ppi}[c] + \text{xmp}[c]$	Purine metabolism	Cytoplasm	-1000	1000
GMPS	$\text{atp}[c] + \text{nh4}[c] + \text{xmp}[c] \rightarrow 1 \text{ppi}[c] + \text{amp}[c] + 3 \text{h}[c] + \text{gmp}[c]$	Purine metabolism	Cytoplasm	0	1000
GK1	$\text{atp}[c] + \text{h}[c] + \text{gmp}[c] \rightleftharpoons \text{adp}[c] + \text{gdp}[c]$	Purine metabolism	Cytoplasm	-1000	1000
NDPK1	$\text{atp}[c] + \text{gdp}[c] \rightleftharpoons \text{adp}[c] + \text{gtp}[c]$	Purine metabolism	Cytoplasm	-1000	1000
GTPHR	$\text{gtp}[c] + \text{h2o}[c] \rightleftharpoons \text{gdp}[c] + \text{pi}[c] + \text{h}[c]$	Purine metabolism	Cytoplasm	0	1000
NTPP2	$\text{gtp}[c] + \text{h2o}[c] \rightleftharpoons \text{gmp}[c] + 2 \text{h}[c] + \text{ppi}[c]$	Purine metabolism	Cytoplasm	0	1000

GUACYC	$\text{gtp}[\text{c}] \rightleftharpoons 35\text{cgmp}[\text{c}] + \text{ppi}[\text{c}] + \text{h}[\text{c}]$	Purine metabolism	Cytoplasm	-1000	1000
ADNCYC	$\text{atp}[\text{c}] \rightleftharpoons \text{camp}[\text{c}] + \text{ppi}[\text{c}] + \text{h}[\text{c}]$	Purine metabolism	Cytoplasm	-1000	1000
PPGPPDP	$\text{h2o}[\text{c}] + \text{ppgpp}[\text{c}] \rightleftharpoons \text{gdp}[\text{c}] + \text{ppi}[\text{c}]$	Purine metabolism	Cytoplasm	-1000	1000
GTPDPDP	$\text{gdp}[\text{c}] + \text{h2o}[\text{c}] \rightleftharpoons \text{pi}[\text{c}] + \text{ppgpp}[\text{c}]$	Purine metabolism	Cytoplasm	-1000	1000
RNDR2	$\text{gdp}[\text{c}] + \text{trdrd}[\text{c}] \rightleftharpoons \text{h2o}[\text{c}] + \text{dgd}[\text{c}] + \text{trdox}[\text{c}]$	Purine metabolism	Cytoplasm	-1000	1000
NDPK5	$\text{atp}[\text{c}] + \text{dgd}[\text{c}] \rightleftharpoons \text{adp}[\text{c}] + \text{dgt}[\text{c}]$	Purine metabolism	Cytoplasm	-1000	1000
DGK1	$\text{atp}[\text{c}] + \text{h}[\text{c}] + \text{dgmp}[\text{c}] \rightleftharpoons \text{adp}[\text{c}] + \text{dgd}[\text{c}]$	Purine metabolism	Cytoplasm	-1000	1000
NTD8	$\text{h2o}[\text{c}] + \text{dgmp}[\text{c}] \rightleftharpoons \text{pi}[\text{c}] + \text{dgsn}[\text{c}]$	Purine metabolism	Cytoplasm	-1000	1000
NTD9	$\text{h2o}[\text{c}] + \text{gmp}[\text{c}] \rightleftharpoons \text{pi}[\text{c}] + \text{gsn}[\text{c}]$	Purine metabolism	Cytoplasm	-1000	1000
GNNUC	$\text{h2o}[\text{c}] + \text{gsn}[\text{c}] \rightleftharpoons \text{rib_D}[\text{c}] + \text{gua}[\text{c}]$	Purine metabolism	Cytoplasm	-1000	1000
GUAPRT	$\text{prpp}[\text{c}] + \text{gua}[\text{c}] \rightarrow \text{ppi}[\text{c}] + \text{h}[\text{c}] + \text{gmp}[\text{c}]$	Purine metabolism	Cytoplasm	0	1000
ADSS	$\text{gtp}[\text{c}] + \text{asp_L}[\text{c}] + \text{imp}[\text{c}] \rightarrow \text{pi}[\text{c}] + \text{gdp}[\text{c}] + 2 \text{h}[\text{c}] + \text{dcamp}[\text{c}]$	Purine metabolism	Cytoplasm	0	1000
ADSL1r	$\text{dcamp}[\text{c}] \rightleftharpoons \text{amp}[\text{c}] + \text{fum}[\text{c}]$	Purine metabolism	Cytoplasm	-1000	1000
NTD7	$\text{h2o}[\text{c}] + \text{amp}[\text{c}] \rightleftharpoons \text{pi}[\text{c}] + \text{adn}[\text{c}]$	Purine metabolism	Cytoplasm	-1000	1000
ADNK1	$\text{atp}[\text{c}] + \text{adn}[\text{c}] \rightarrow \text{adp}[\text{c}] + \text{amp}[\text{c}] + \text{h}[\text{c}]$	Purine metabolism	Cytoplasm	0	1000
ADNUC	$\text{h2o}[\text{c}] + \text{adn}[\text{c}] \rightleftharpoons \text{rib_D}[\text{c}] + \text{ade}[\text{c}]$	Purine metabolism	Cytoplasm	-1000	1000
ADPT	$\text{prpp}[\text{c}] + \text{ade}[\text{c}] \rightarrow \text{ppi}[\text{c}] + \text{amp}[\text{c}] + \text{h}[\text{c}]$	Purine metabolism	Cytoplasm	0	1000
ADK1	$\text{atp}[\text{c}] + \text{amp}[\text{c}] + \text{h}[\text{c}] \rightleftharpoons 2 \text{adp}[\text{c}]$	Purine metabolism	Cytoplasm	-1000	1000
NTPP6	$\text{atp}[\text{c}] + \text{h2o}[\text{c}] \rightleftharpoons \text{amp}[\text{c}] + 2 \text{h}[\text{c}] + \text{ppi}[\text{c}]$	Purine metabolism	Cytoplasm	0	1000
RNDR1	$\text{adp}[\text{c}] + \text{trdrd}[\text{c}] \rightleftharpoons \text{h2o}[\text{c}] + \text{dadp}[\text{c}] + \text{trdox}[\text{c}]$	Purine metabolism	Cytoplasm	-1000	1000
NDPK8	$\text{atp}[\text{c}] + \text{dadp}[\text{c}] \rightleftharpoons \text{adp}[\text{c}] + \text{datp}[\text{c}]$	Purine metabolism	Cytoplasm	-1000	1000
DADK	$\text{atp}[\text{c}] + \text{h}[\text{c}] + \text{damp}[\text{c}] \rightleftharpoons \text{adp}[\text{c}] + \text{dadp}[\text{c}]$	Purine metabolism	Cytoplasm	-1000	1000
NTD6	$\text{h2o}[\text{c}] + \text{damp}[\text{c}] \rightleftharpoons \text{pi}[\text{c}] + \text{dad_2}[\text{c}]$	Purine metabolism	Cytoplasm	-1000	1000
ADA	$\text{adn}[\text{c}] + \text{h}[\text{c}] + \text{h2o}[\text{c}] \rightleftharpoons \text{ins}[\text{c}] + \text{nh4}[\text{c}]$	Purine metabolism	Cytoplasm	0	1000
DADA	$\text{dad_2}[\text{c}] + \text{h}[\text{c}] + \text{h2o}[\text{c}] \rightleftharpoons \text{din}[\text{c}] + \text{nh4}[\text{c}]$	Purine metabolism	Cytoplasm	0	1000
INSH	$\text{h2o}[\text{c}] + \text{ins}[\text{c}] \rightleftharpoons \text{hxan}[\text{c}] + \text{rib_D}[\text{c}]$	Purine metabolism	Cytoplasm	0	1000
ATPATF1	$\text{adp}[\text{c}] + \text{atp}[\text{c}] \rightleftharpoons \text{ap4a}[\text{c}] + \text{pi}[\text{c}] + \text{h}[\text{c}]$	Purine metabolism	Cytoplasm	-1000	1000
ASPCT	$\text{asp_L}[\text{c}] + \text{cbp}[\text{c}] \rightleftharpoons \text{pi}[\text{c}] + \text{h}[\text{c}] + \text{cbasp}[\text{c}]$	Pyrimidine metabolism	Cytoplasm	-1000	1000
DHORTS	$\text{h}[\text{c}] + \text{cbasp}[\text{c}] \rightleftharpoons \text{h2o}[\text{c}] + \text{dhor_S}[\text{c}]$	Pyrimidine metabolism	Cytoplasm	-1000	1000
DHORD_NAD	$\text{nad}[\text{c}] + \text{dhor_S}[\text{c}] \rightleftharpoons \text{nadh}[\text{c}] + \text{h}[\text{c}] + \text{orot}[\text{c}]$	Pyrimidine metabolism	Cytoplasm	-1000	1000

DHORDfum	dhor__S[c] + fum[c] <=> orot[c] + succ[c]	Pyrimidine metabolism	Cytoplasm	-1000	1000
ORPT	prpp[c] + orot[c] --> ppi[c] + h[c] + orot5p[c]	Pyrimidine metabolism	Cytoplasm	0	1000
OMPDc	h[c] + orot5p[c] --> co2[c] + ump[c]	Pyrimidine metabolism	Cytoplasm	0	1000
UMPK	atp[c] + h[c] + ump[c] <=> adp[c] + udp[c]	Pyrimidine metabolism	Cytoplasm	-1000	1000
NDPK2	atp[c] + udp[c] <=> adp[c] + utp[c]	Pyrimidine metabolism	Cytoplasm	-1000	1000
NTPP8	utp[c] + h2o[c] <=> ump[c] + 2 h[c] + ppi[c]	Pyrimidine metabolism	Cytoplasm	0	1000
UPPRT	ppi[c] + ump[c] + h[c] <=> prpp[c] + ura[c]	Pyrimidine metabolism	Cytoplasm	-1000	1000
CTPS1	atp[c] + nh4[c] + utp[c] <=> adp[c] + pi[c] + ctp[c] + 2 h[c]	Pyrimidine metabolism	Cytoplasm	-1000	1000
CTPS2	h2o[c] + atp[c] + gln__L[c] + utp[c] --> adp[c] + pi[c] + glu__L[c] + ctp[c] + 2 h[c]	Pyrimidine metabolism	Cytoplasm	0	1000
DCTPD2	h2o[c] + ctp[c] + h[c] --> nh4[c] + utp[c]	Pyrimidine metabolism	Cytoplasm	0	1000
NDPK3	atp[c] + cdp[c] <=> adp[c] + ctp[c]	Pyrimidine metabolism	Cytoplasm	-1000	1000
CYTK1	atp[c] + cmp[c] + h[c] <=> adp[c] + cdp[c]	Pyrimidine metabolism	Cytoplasm	-1000	1000
NTPP4	ctp[c] + h2o[c] <=> cmp[c] + 2 h[c] + ppi[c]	Pyrimidine metabolism	Cytoplasm	0	1000
RNDR3	cdp[c] + trdrd[c] <=> h2o[c] + dcdp[c] + trdox[c]	Pyrimidine metabolism	Cytoplasm	-1000	1000
CMPN	h2o[c] + cmp[c] <=> r5p[c] + csu[c]	Pyrimidine metabolism	Cytoplasm	-1000	1000
NTD4	h2o[c] + cmp[c] <=> pi[c] + cytd[c]	Pyrimidine metabolism	Cytoplasm	-1000	1000
NDPK7	atp[c] + dcdp[c] <=> adp[c] + dctp[c]	Pyrimidine metabolism	Cytoplasm	-1000	1000
CYTK2	atp[c] + h[c] + dcmp[c] <=> adp[c] + dcdp[c]	Pyrimidine metabolism	Cytoplasm	-1000	1000
NTD3	h2o[c] + dcmp[c] <=> pi[c] + dcyt[c]	Pyrimidine metabolism	Cytoplasm	-1000	1000
DCYTD	h2o[c] + h[c] + dcyt[c] --> nh4[c] + duri[c]	Pyrimidine metabolism	Cytoplasm	0	1000
DCTPD	h2o[c] + h[c] + dctp[c] --> nh4[c] + dudp[c]	Pyrimidine metabolism	Cytoplasm	0	1000
NDPK6	atp[c] + dudp[c] <=> adp[c] + dudp[c]	Pyrimidine metabolism	Cytoplasm	-1000	1000
URIDK2r	atp[c] + h[c] + dudp[c] <=> adp[c] + dudp[c]	Pyrimidine metabolism	Cytoplasm	-1000	1000
RNDR4	udp[c] + trdrd[c] <=> h2o[c] + dudp[c] + trdox[c]	Pyrimidine metabolism	Cytoplasm	-1000	1000
TMDS3	nadph[c] + h[c] + mlthf[c] + dump[c] --> nadp[c] + thf[c] + dtmp[c]	Pyrimidine metabolism	Cytoplasm	0	1000
DUTPDP	h2o[c] + dudp[c] --> ppi[c] + 2 h[c] + dump[c]	Pyrimidine metabolism	Cytoplasm	0	1000
DTMPK	atp[c] + h[c] + dtmp[c] <=> adp[c] + dtdp[c]	Pyrimidine metabolism	Cytoplasm	-1000	1000
NDPK4	atp[c] + dtdp[c] <=> adp[c] + dtdp[c]	Pyrimidine metabolism	Cytoplasm	-1000	1000
CSND	h2o[c] + h[c] + csu[c] --> nh4[c] + ura[c]	Pyrimidine metabolism	Cytoplasm	0	1000

NTD5	$\text{h2o[c]} + \text{dtmp[c]} \rightleftharpoons \text{pi[c]} + \text{thymd[c]}$	Pyrimidine metabolism	Cytoplasm	-1000	1000
ASPO6	$\text{o2[c]} + \text{asp_L[c]} \rightarrow \text{h2o2[c]} + \text{h[c]} + \text{iasp[c]}$	Nicotinate and nicotinamide metabolism	Cytoplasm	0	1000
QULNS	$\text{dhap[c]} + \text{iasp[c]} \rightleftharpoons 2 \text{h2o[c]} + \text{pi[c]} + \text{quln[c]}$	Nicotinate and nicotinamide metabolism	Cytoplasm	-1000	1000
NNDPR	$\text{h[c]} + \text{prpp[c]} + \text{quln[c]} \rightarrow \text{co2[c]} + \text{ppi[c]} + \text{nicrnt[c]}$	Nicotinate and nicotinamide metabolism	Cytoplasm	0	1000
NAMNPP_2	$\text{h[c]} + \text{ppi[c]} + \text{pi[c]} + \text{nicrnt[c]} + \text{adp[c]} \rightleftharpoons \text{prpp[c]} + \text{nac[c]} + \text{h2o[c]} + \text{atp[c]}$	Nicotinate and nicotinamide metabolism	Cytoplasm	-1000	1000
NT5C	$\text{h2o[c]} + \text{nicrnt[c]} \rightleftharpoons \text{pi[c]} + \text{nicrns[c]}$	Nicotinate and nicotinamide metabolism	Cytoplasm	-1000	1000
NNATr	$\text{atp[c]} + \text{nicrnt[c]} \rightleftharpoons \text{ppi[c]} + \text{dnad[c]}$	Nicotinate and nicotinamide metabolism	Cytoplasm	-1000	1000
NADS1	$\text{atp[c]} + \text{nh4[c]} + \text{dnad[c]} \rightarrow \text{nad[c]} + \text{ppi[c]} + \text{amp[c]} + 2 \text{h[c]}$	Nicotinate and nicotinamide metabolism	Cytoplasm	0	1000
NMNAT	$\text{atp[c]} + \text{nmn[c]} \rightleftharpoons \text{nad[c]} + \text{ppi[c]}$	Nicotinate and nicotinamide metabolism	Cytoplasm	-1000	1000
NMNDA	$\text{h2o[c]} + \text{nmn[c]} \rightarrow \text{nh4[c]} + \text{nicrnt[c]}$	Nicotinate and nicotinamide metabolism	Cytoplasm	0	1000
NMNHYD	$\text{h2o[c]} + \text{nmn[c]} \rightleftharpoons \text{pi[c]} + \text{rnam[c]}$	Nicotinate and nicotinamide metabolism	Cytoplasm	-1000	1000
RNMK	$\text{atp[c]} + \text{rnam[c]} \rightarrow \text{adp[c]} + \text{h[c]} + \text{nmn[c]}$	Nicotinate and nicotinamide metabolism	Cytoplasm	0	1000
RNAMRH	$\text{h2o[c]} + \text{rnam[c]} \rightarrow \text{h[c]} + \text{rib_D[c]} + \text{ncam[c]}$	Nicotinate and nicotinamide metabolism	Cytoplasm	0	1000
NADN	$\text{h2o[c]} + \text{nad[c]} \rightleftharpoons \text{adprib[c]} + \text{h[c]} + \text{ncam[c]}$	Nicotinate and nicotinamide metabolism	Cytoplasm	0	1000
ADPRDP	$\text{adprib[c]} + \text{h2o[c]} \rightleftharpoons \text{amp[c]} + 2 \text{h[c]} + \text{r5p[c]}$	Nicotinate and nicotinamide metabolism	Cytoplasm	-1000	1000
NADK	$\text{atp[c]} + \text{nad[c]} \rightarrow \text{nadp[c]} + \text{adp[c]} + \text{h[c]}$	Nicotinate and nicotinamide metabolism	Cytoplasm	0	1000
NADTRHD	$\text{nad[c]} + \text{nadph[c]} \rightleftharpoons \text{nadh[c]} + \text{nadp[c]}$	Nicotinate and nicotinamide metabolism	Cytoplasm	-1000	1000
NADS2	$\text{h2o[c]} + \text{atp[c]} + \text{gln_L[c]} + \text{dnad[c]} \rightarrow \text{nad[c]} + \text{ppi[c]} + \text{amp[c]} + \text{glu_L[c]} + 2 \text{h[c]}$	Nicotinate and nicotinamide metabolism	Cytoplasm	0	1000
NNAM	$\text{h2o[c]} + \text{ncam[c]} \rightarrow \text{nh4[c]} + \text{nac[c]}$	Nicotinate and nicotinamide metabolism	Cytoplasm	0	1000
DXPS	$\text{pyr[c]} + \text{h[c]} + \text{g3p[c]} \rightarrow \text{co2[c]} + \text{dxy15p[c]}$	Terpenoid backbone biosynthesis	Cytoplasm	0	1000
DXPRli	$\text{nadph[c]} + \text{h[c]} + \text{dxy15p[c]} \rightleftharpoons \text{nadp[c]} + 2 \text{me4p[c]}$	Terpenoid backbone biosynthesis	Cytoplasm	-1000	1000
MEPCT	$\text{ctp[c]} + 2 \text{me4p[c]} \rightleftharpoons \text{ppi[c]} + 4 \text{c2me[c]}$	Terpenoid backbone biosynthesis	Cytoplasm	-1000	1000
CDPMEK	$\text{atp[c]} + 4 \text{c2me[c]} \rightarrow \text{adp[c]} + \text{h[c]} + 2 \text{p4c2me[c]}$	Terpenoid backbone biosynthesis	Cytoplasm	0	1000

MECDPS	2p4c2me[c] <=> cmp[c] + 2mecdp[c]	Terpenoid backbone biosynthesis	Cytoplasm	-1000	1000
MECDPDHf_2	2 h[c] + 2mecdp[c] + fdxrd[c] --> h2o[c] + h2mb4p[c] + fdxo_2_2[c]	Terpenoid backbone biosynthesis	Cytoplasm	0	1000
IDS	nadph[c] + h[c] + h2mb4p[c] --> h2o[c] + nadp[c] + ipdp[c]	Terpenoid backbone biosynthesis	Cytoplasm	0	1000
IPDPS	nadh[c] + h[c] + h2mb4p[c] --> h2o[c] + nad[c] + ipdp[c]	Terpenoid backbone biosynthesis	Cytoplasm	0	1000
DMPPS	nadh[c] + h[c] + h2mb4p[c] --> h2o[c] + nad[c] + dmpp[c]	Terpenoid backbone biosynthesis	Cytoplasm	0	1000
IPDDI	ipdp[c] <=> dmpp[c]	Terpenoid backbone biosynthesis	Cytoplasm	-1000	1000
DMATT	ipdp[c] + dmpp[c] --> ppi[c] + h[c] + grdp[c]	Terpenoid backbone biosynthesis	Cytoplasm	0	1000
GRTT	ipdp[c] + grdp[c] --> ppi[c] + h[c] + frdp[c]	Terpenoid backbone biosynthesis	Cytoplasm	0	1000
FRTT	ipdp[c] + frdp[c] --> ppi[c] + h[c] + ggdp[c]	Terpenoid backbone biosynthesis	Cytoplasm	0	1000
GGDPR	3 nadph[c] + 3 h[c] + ggdp[c] --> 3 nadp[c] + phdp[c]	Terpenoid backbone biosynthesis	Cytoplasm	0	1000
OCTDPS	5 ipdp[c] + frdp[c] --> 5 ppi[c] + 5 h[c] + octdp[c]	Terpenoid backbone biosynthesis	Cytoplasm	0	1000
NPDPS_2	ipdp[c] + octdp[c] --> ppi[c] + h[c] + npdp[c]	Terpenoid backbone biosynthesis	Cytoplasm	0	1000
GLUTRS	atp[c] + glu__L[c] + trnaglu[c] <=> ppi[c] + amp[c] + h[c] + glutrna[c]	Porphyrin and chlorophyll metabolism	Cytoplasm	-1000	1000
GLUTRR	nadph[c] + h[c] + glutrna[c] <=> nadp[c] + glu1sa[c] + trnaglu[c]	Porphyrin and chlorophyll metabolism	Cytoplasm	-1000	1000
G1SAT	glu1sa[c] <=> 5aop[c]	Porphyrin and chlorophyll metabolism	Cytoplasm	-1000	1000
PPBNGS	2 5aop[c] --> 2 h2o[c] + h[c] + ppbng[c]	Porphyrin and chlorophyll metabolism	Cytoplasm	0	1000
HMBS	h2o[c] + 4 ppbng[c] --> 4 nh4[c] + hmbil[c]	Porphyrin and chlorophyll metabolism	Cytoplasm	0	1000
UPP3S	hmbil[c] <=> h2o[c] + uppg3[c]	Porphyrin and chlorophyll metabolism	Cytoplasm	-1000	1000
UPPDC1	4 h[c] + uppg3[c] --> 4 co2[c] + cpppg3[c]	Porphyrin and chlorophyll metabolism	Cytoplasm	0	1000
CPPPGO	o2[c] + 2 h[c] + cpppg3[c] --> 2 h2o[c] + 2 co2[c] + pppg9[c]	Porphyrin and chlorophyll metabolism	Cytoplasm	0	1000
CPPPGO2	2 amet[c] + cpppg3[c] --> 2 co2[c] + 2 met__L[c] + pppg9[c] + 2 dad_5[c]	Porphyrin and chlorophyll metabolism	Cytoplasm	0	1000
PPPGO	3 o2[c] + 2 pppg9[c] <=> 6 h2o[c] + 2 ppp9[c]	Porphyrin and chlorophyll metabolism	Cytoplasm	-1000	1000
FCLT	ppp9[c] + fe2[c] <=> pheme[c] + 2 h[c]	Porphyrin and chlorophyll metabolism	Cytoplasm	-1000	1000

HEMEOS	$\text{frdp}[c] + \text{h2o}[c] + \text{pHEME}[c] \rightleftharpoons \text{hemeO}[c] + \text{ppi}[c] + \text{h}[c]$	Porphyrin and chlorophyll metabolism	Cytoplasm	-1000	1000
EX_fe2_e	$\text{fe2}[e] \rightleftharpoons$	Exchange	Extracellular	-1000	1000
FE2t	$\text{fe2}[e] \rightleftharpoons \text{fe2}[c]$	Transport	Cytoplasm	-1000	1000
EX_fe3_e	$\text{fe3}[e] \rightleftharpoons$	Exchange	Extracellular	-1000	0
FE3tex	$\text{fe3}[e] \rightleftharpoons \text{fe3}[p]$	Transport	Cytoplasm	0	1000
FE3abcpp	$\text{fe3}[p] + \text{atp}[c] + \text{h2o}[c] \rightleftharpoons \text{fe3}[c] + \text{adp}[c] + \text{h}[c] + \text{pi}[c]$	Transport	Cytoplasm	0	1000
FERIRDQ8	$2 \text{fe3}[c] + \text{q8h2}[c] \rightleftharpoons 2 \text{fe2}[c] + 2 \text{h}[c] + \text{q8}[c]$	Oxidative phosphorylation	Cytoplasm	-1000	1000
EX_mg2_e	$\text{mg2}[e] \rightleftharpoons$	Exchange	Extracellular	-1000	1000
MGt5	$\text{mg2}[e] \rightleftharpoons \text{mg2}[c]$	Transport	Cytoplasm	-1000	1000
MPML	$\text{h2o}[c] + \text{atp}[c] + \text{mg2}[c] + \text{ppp9}[c] \rightleftharpoons \text{adp}[c] + \text{pi}[c] + 3 \text{h}[c] + \text{mPPP9}[c]$	Porphyrin and chlorophyll metabolism	Cytoplasm	-1000	1000
MPOMT	$\text{amet}[c] + \text{mPPP9}[c] \rightleftharpoons \text{ahcys}[c] + \text{mPPP9om}[c]$	Porphyrin and chlorophyll metabolism	Cytoplasm	-1000	1000
MPOMC1	$\text{nadph}[c] + \text{o2}[c] + \text{h}[c] + \text{mPPP9om}[c] \rightarrow \text{h2o}[c] + \text{nadp}[c] + \text{hmPPP9}[c]$	Porphyrin and chlorophyll metabolism	Cytoplasm	0	1000
MPOMMM	$\text{nadph}[c] + \text{o2}[c] + \text{h}[c] + \text{hmPPP9}[c] \rightarrow 2 \text{h2o}[c] + \text{nadp}[c] + \text{omPPP9}[c]$	Porphyrin and chlorophyll metabolism	Cytoplasm	0	1000
MPOMOR	$\text{nadph}[c] + \text{o2}[c] + \text{h}[c] + \text{omPPP9}[c] \rightleftharpoons 2 \text{h2o}[c] + \text{nadp}[c] + \text{dvpchlld}[c]$	Porphyrin and chlorophyll metabolism	Cytoplasm	-1000	1000
DVOCHR_2	$\text{nadph}[c] + \text{h}[c] + \text{dvpchlld}[c] \rightleftharpoons \text{nadp}[c] + \text{dvchlda}[c]$	Porphyrin and chlorophyll metabolism	Cytoplasm	-1000	1000
DVOCHR	$\text{nadph}[c] + \text{h}[c] + \text{dvpchlld}[c] \rightleftharpoons \text{nadp}[c] + \text{pchlld}[c]$	Porphyrin and chlorophyll metabolism	Cytoplasm	-1000	1000
DPOR_2	$\text{h2o}[c] + \text{atp}[c] + \text{fdxrd}[c] + \text{pchlld}[c] \rightleftharpoons \text{adp}[c] + \text{fdxo_2_2}[c] + \text{pi}[c] + \text{chlld}[c]$	Porphyrin and chlorophyll metabolism	Cytoplasm	-1000	1000
CHPHYS	$\text{h}[c] + \text{chlld}[c] + \text{phdp}[c] \rightleftharpoons \text{ppi}[c] + \text{cholphy}[c]$	Porphyrin and chlorophyll metabolism	Cytoplasm	-1000	1000
HOXG	$3 \text{o2}[c] + \text{pHEME}[c] + 3 \text{nadph}[c] + 5 \text{h}[c] \rightleftharpoons \text{biliverd}[c] + \text{co}[c] + \text{fe2}[c] + 3 \text{h2o}[c] + 3 \text{nadp}[c]$	Porphyrin and chlorophyll metabolism	Cytoplasm	-1000	1000
PHYCYFX	$4 \text{h}[c] + \text{biliverd}[c] + 2 \text{fdxrd}[c] \rightleftharpoons \text{phycy}[c] + 2 \text{fdxo_2_2}[c]$	Porphyrin and chlorophyll metabolism	Cytoplasm	0	1000
PHYCYI	$\text{phycy}[c] \rightarrow \text{phyvi}[c]$	Porphyrin and chlorophyll metabolism	Cytoplasm	0	1000
BILIRED2	$\text{nadh}[c] + \text{h}[c] + \text{biliverd}[c] \rightleftharpoons \text{nad}[c] + \text{bilirub}[c]$	Porphyrin and chlorophyll metabolism	Cytoplasm	-1000	1000

BILIRED	nadp[c] + bilirub[c] <=> nadph[c] + h[c] + biliverd[c]	Porphyrin and chlorophyll metabolism	Cytoplasm	-1000	1000
CPP3O_1	6 nadp[c] + cpppg3[c] <=> 6 nadph[c] + cpp3[c]	Porphyrin and chlorophyll metabolism	Cytoplasm	-1000	1000
UPP3MT	2 amet[c] + uppg3[c] <=> 2 ahcys[c] + h[c] + dsc[c]	Porphyrin and chlorophyll metabolism	Cytoplasm	-1000	1000
SHCHD2	nad[c] + dsc[c] <=> nadh[c] + 2 h[c] + scl[c]	Porphyrin and chlorophyll metabolism	Cytoplasm	-1000	1000
SHCHF	scl[c] + fe2[c] <=> 2 h[c] + sheme[c]	Porphyrin and chlorophyll metabolism	Cytoplasm	-1000	1000
EX_cobalt2_e	cobalt2[e] <=>	Exchange	Extracellular	-1000	1000
COabc	cobalt2[e] + atp[c] + h2o[c] --> cobalt2[c] + adp[c] + h[c] + pi[c]	Transport	Cytoplasm	-1000	1000
SHCHCC_2	cobalt2[c] + scl[c] <=> 2 h[c] + copre2[c]	Porphyrin and chlorophyll metabolism	Cytoplasm	-1000	1000
CPC2MTf	amet[c] + 7 h[c] + copre2[c] <=> ahcys[c] + cofac3[c]	Porphyrin and chlorophyll metabolism	Cytoplasm	-1000	1000
CPC3DH	cofac3[c] + fdxrd[c] <=> 5 h[c] + copre3[c] + fdxo_2_2[c]	Porphyrin and chlorophyll metabolism	Cytoplasm	-1000	1000
CPC3MT	amet[c] + copre3[c] <=> ahcys[c] + copre4[c]	Porphyrin and chlorophyll metabolism	Cytoplasm	-1000	1000
CODSCL4MT	amet[c] + copre4[c] --> ahcys[c] + h[c] + codscl5a[c]	Porphyrin and chlorophyll metabolism	Cytoplasm	0	1000
CODSCL5DA	h2o[c] + codscl5a[c] <=> acald[c] + codscl5b[c]	Porphyrin and chlorophyll metabolism	Cytoplasm	-1000	1000
CODSCL5BMT	amet[c] + codscl5b[c] <=> ahcys[c] + h[c] + copre6[c]	Porphyrin and chlorophyll metabolism	Cytoplasm	-1000	1000
CPC6R	nadph[c] + h[c] + copre6[c] <=> nadp[c] + codhpre6[c]	Porphyrin and chlorophyll metabolism	Cytoplasm	-1000	1000
CODSCL6BMT	amet[c] + codhpre6[c] --> ahcys[c] + h[c] + codscl7[c]	Porphyrin and chlorophyll metabolism	Cytoplasm	0	1000
CODSCL7MTDC	amet[c] + codscl7[c] --> ahcys[c] + codscl8x[c] + co2[c]	Porphyrin and chlorophyll metabolism	Cytoplasm	0	1000
CODSCL8XI	2 h[c] + codscl8x[c] --> cobya[c]	Porphyrin and chlorophyll metabolism	Cytoplasm	0	1000
COBNAD	2 h2o[c] + 2 atp[c] + 2 glu__L[c] + cobya[c] --> 2 adp[c] + 2 pi[c] + 2 glu__L[c] + 2 h[c] + cob2nda[c]	Porphyrin and chlorophyll metabolism	Cytoplasm	0	1000
PC20M	amet[c] + dsc[c] <=> ahcys[c] + h[c] + pre3a[c]	Porphyrin and chlorophyll metabolism	Cytoplasm	-1000	1000
PRE3BS	nadh[c] + o2[c] + 2 h[c] + pre3a[c] --> h2o[c] + nad[c] + pre3b[c]	Porphyrin and chlorophyll metabolism	Cytoplasm	0	1000
PC17M_1	amet[c] + pre3b[c] <=> ahcys[c] + 2 h[c] + pre4[c]	Porphyrin and chlorophyll metabolism	Cytoplasm	-1000	1000
PC11M	amet[c] + pre4[c] <=> ahcys[c] + h[c] + pre5[c]	Porphyrin and chlorophyll metabolism	Cytoplasm	-1000	1000
R05219	h2o[c] + amet[c] + pre5[c] <=> ahcys[c] + ac[c] + 2 h[c] + pre6a[c]	Porphyrin and chlorophyll metabolism	Cytoplasm	-1000	1000

PC6AR	nadph[c] + h[c] + pre6a[c] <=> nadp[c] + pre6b[c]	Porphyrin and chlorophyll metabolism	Cytoplasm	-1000	1000
PC6YM	2 amet[c] + pre6b[c] --> co2[c] + 2 ahcys[c] + 2 h[c] + pre8[c]	Porphyrin and chlorophyll metabolism	Cytoplasm	0	1000
PC8XM	3 h[c] + pre8[c] <=> hgbyr[c]	Porphyrin and chlorophyll metabolism	Cytoplasm	-1000	1000
R05224	2 h2o[c] + 2 atp[c] + 2 gln__L[c] + hgbyr[c] --> 2 adp[c] + 2 pi[c] + 2 glu__L[c] + 2 h[c] + hgbam[c]	Porphyrin and chlorophyll metabolism	Cytoplasm	0	1000
COCHL	h2o[c] + atp[c] + cobalt2[c] + hgbam[c] <=> adp[c] + pi[c] + 2 h[c] + cob2nda[c]	Porphyrin and chlorophyll metabolism	Cytoplasm	-1000	1000
CYRDAR	nadh[c] + 2 cob2nda[c] <=> nad[c] + h[c] + 2 co1dam[c]	Porphyrin and chlorophyll metabolism	Cytoplasm	-1000	1000
CYRDAAT	atp[c] + h[c] + co1dam[c] <=> pppi[c] + adcobdam[c]	Porphyrin and chlorophyll metabolism	Cytoplasm	-1000	1000
ADCYRS	4 h2o[c] + 4 atp[c] + 4 gln__L[c] + adcobdam[c] --> 4 adp[c] + 4 pi[c] + 4 glu__L[c] + 4 h[c] + adcobhex[c]	Porphyrin and chlorophyll metabolism	Cytoplasm	0	1000
ADCPs1	atp[c] + appl[c] + adcobhex[c] --> adp[c] + pi[c] + h[c] + adocbi[c]	Porphyrin and chlorophyll metabolism	Cytoplasm	0	1000
ADOCBIK	atp[c] + adocbi[c] --> adp[c] + h[c] + adocbip[c]	Porphyrin and chlorophyll metabolism	Cytoplasm	0	1000
ADOCBIK_gtp	gtp[c] + adocbi[c] --> gdp[c] + h[c] + adocbip[c]	Porphyrin and chlorophyll metabolism	Cytoplasm	0	1000
CBIAT	pppi[c] + adocbi[c] <=> atp[c] + h[c] + cbi[c]	Porphyrin and chlorophyll metabolism	Cytoplasm	-1000	1000
LTHRK	atp[c] + thr__L[c] --> adp[c] + h[c] + thrp[c]	Porphyrin and chlorophyll metabolism	Cytoplasm	0	1000
THRPDC	h[c] + thrp[c] --> co2[c] + applp[c]	Porphyrin and chlorophyll metabolism	Cytoplasm	0	1000
ADCPs2	atp[c] + applp[c] + adcobhex[c] --> adp[c] + pi[c] + h[c] + adocbip[c]	Porphyrin and chlorophyll metabolism	Cytoplasm	0	1000
ACBIPGT	gtp[c] + adocbip[c] <=> ppi[c] + h[c] + agdpcbi[c]	Porphyrin and chlorophyll metabolism	Cytoplasm	-1000	1000
NNDMBRT	nicrnt[c] + dmbzid[c] <=> h[c] + nac[c] + 5prdmzbz[c]	Porphyrin and chlorophyll metabolism	Cytoplasm	-1000	1000
RZ5PP	h2o[c] + 5prdmzbz[c] <=> pi[c] + rdmbzi[c]	Porphyrin and chlorophyll metabolism	Cytoplasm	-1000	1000
ADOCBLS	rdmbzi[c] + agdpcbi[c] <=> h[c] + gmp[c] + adocbl[c]	Porphyrin and chlorophyll metabolism	Cytoplasm	-1000	1000
EX_adocbl_e	adocbl[e] <=>	Exchange	Extracellular	-1000	0
ADOCBLabc	adocbl[e] + atp[c] + h2o[c] --> adocbl[c] + adp[c] + h[c] + pi[c]	Transport	Cytoplasm	0	1000
34HPPOR	o2[c] + 34hpp[c] --> co2[c] + hgentis[c]	Ubiquinone and other terpenoid-quinone biosynthesis	Cytoplasm	0	1000
HGPHT	hgentis[c] + phdp[c] --> co2[c] + ppi[c] + 2m6phol[c]	Ubiquinone and other terpenoid-quinone biosynthesis	Cytoplasm	0	1000

HGGGT	ggdp[c] + hgentis[c] --> co2[c] + ppi[c] + 2m6ggol[c]	Ubiquinone and other terpenoid-quinone biosynthesis	Cytoplasm	0	1000
MPBQ	amet[c] + 2m6phol[c] --> ahcys[c] + h[c] + 23dmphol[c]	Ubiquinone and other terpenoid-quinone biosynthesis	Cytoplasm	0	1000
TOCOPHS1	23dmphol[c] --> gtocophe[c]	Ubiquinone and other terpenoid-quinone biosynthesis	Cytoplasm	0	1000
TOCOPHS2	2m6phol[c] --> dtocophe[c]	Ubiquinone and other terpenoid-quinone biosynthesis	Cytoplasm	0	1000
TOCOPHOM2	amet[c] + dtocophe[c] --> ahcys[c] + h[c] + bvite[c]	Ubiquinone and other terpenoid-quinone biosynthesis	Cytoplasm	0	1000
TOCOPHOM1	amet[c] + gtocophe[c] --> ahcys[c] + h[c] + avite1[c]	Ubiquinone and other terpenoid-quinone biosynthesis	Cytoplasm	0	1000
TMTB_1	amet[c] + bvite[c] <=> ahcys[c] + h[c] + avite1[c]	Ubiquinone and other terpenoid-quinone biosynthesis	Cytoplasm	-1000	1000
GGMBQ	amet[c] + 2m6ggol[c] --> ahcys[c] + h[c] + 23dmggol[c]	Ubiquinone and other terpenoid-quinone biosynthesis	Cytoplasm	0	1000
TOCOTRS1	23dmggol[c] --> gtocotri[c]	Ubiquinone and other terpenoid-quinone biosynthesis	Cytoplasm	0	1000
TOCOTRS2	2m6ggol[c] --> dtocotri[c]	Ubiquinone and other terpenoid-quinone biosynthesis	Cytoplasm	0	1000
TOCOTROM2	amet[c] + dtocotri[c] --> ahcys[c] + h[c] + btocotri[c]	Ubiquinone and other terpenoid-quinone biosynthesis	Cytoplasm	0	1000
TOCOTROM1	amet[c] + gtocotri[c] --> ahcys[c] + h[c] + atocotri[c]	Ubiquinone and other terpenoid-quinone biosynthesis	Cytoplasm	0	1000
CHRPL	chor[c] --> pyr[c] + 4hbz[c]	Ubiquinone and other terpenoid-quinone biosynthesis	Cytoplasm	0	1000
HBZOPT	4hbz[c] + octdp[c] --> ppi[c] + h[c] + 3ophb[c]	Ubiquinone and other terpenoid-quinone biosynthesis	Cytoplasm	0	1000
OPHBDC	h[c] + 3ophb[c] --> co2[c] + 2oph[c]	Ubiquinone and other terpenoid-quinone biosynthesis	Cytoplasm	0	1000
OPHHXy	nadph[c] + o2[c] + h[c] + 2oph[c] <=> h2o[c] + nadp[c] + 2ohph[c]	Ubiquinone and other terpenoid-quinone biosynthesis	Cytoplasm	-1000	1000

OHPHM	amet[c] + 2ohph[c] <=> ahcys[c] + h[c] + 2omph[c]	Ubiquinone and other terpenoid-quinone biosynthesis	Cytoplasm	-1000	1000
OMPHHX2	o2[c] + 2omph[c] --> h2o[c] + 2ombz[c]	Ubiquinone and other terpenoid-quinone biosynthesis	Cytoplasm	0	1000
URFGTT	amet[c] + 2ombz[c] --> ahcys[c] + h[c] + 2ommb[c]	Ubiquinone and other terpenoid-quinone biosynthesis	Cytoplasm	0	1000
O3MMBQOR	nadph[c] + o2[c] + h[c] + 2ommb[c] --> h2o[c] + nadp[c] + 2omhmb[c]	Ubiquinone and other terpenoid-quinone biosynthesis	Cytoplasm	0	1000
P6HPMp	amet[c] + 2omhmb[c] <=> ahcys[c] + h[c] + q8[p]	Ubiquinone and other terpenoid-quinone biosynthesis	Cytoplasm	-1000	1000
P6HPM	amet[c] + 2omhmb[c] <=> ahcys[c] + h[c] + q8[c]	Ubiquinone and other terpenoid-quinone biosynthesis	Cytoplasm	-1000	1000
ICHORS	chor[c] <=> ichor[c]	Ubiquinone and other terpenoid-quinone biosynthesis	Cytoplasm	-1000	1000
SEPHCHCS	akg[c] + h[c] + ichor[c] --> co2[c] + 2sephchc[c]	Ubiquinone and other terpenoid-quinone biosynthesis	Cytoplasm	0	1000
SHCHCS3	2sephchc[c] --> pyr[c] + 2shchc[c]	Ubiquinone and other terpenoid-quinone biosynthesis	Cytoplasm	0	1000
SUCBZS	2shchc[c] --> h2o[c] + sucbz[c]	Ubiquinone and other terpenoid-quinone biosynthesis	Cytoplasm	0	1000
SUCBZL	atp[c] + coa[c] + sucbz[c] --> ppi[c] + amp[c] + h[c] + sbzcoa[c]	Ubiquinone and other terpenoid-quinone biosynthesis	Cytoplasm	0	1000
DHNCOAS	h[c] + sbzcoa[c] --> h2o[c] + 14dhncoa[c]	Ubiquinone and other terpenoid-quinone biosynthesis	Cytoplasm	0	1000
DHNCOAT	h2o[c] + 14dhncoa[c] --> coa[c] + h[c] + dhna[c]	Ubiquinone and other terpenoid-quinone biosynthesis	Cytoplasm	0	1000
DHNAPHT_2	fdxo_2_2[c] + dhna[c] + phdp[c] --> co2[c] + ppi[c] + 2 h[c] + dmtphllqne[c] + fdxrd[c]	Ubiquinone and other terpenoid-quinone biosynthesis	Cytoplasm	0	1000
DHNAOT_2	fdxo_2_2[c] + dhna[c] + octdp[c] --> co2[c] + ppi[c] + 2dmmq8[c] + 2 h[c] + fdxrd[c]	Ubiquinone and other terpenoid-quinone biosynthesis	Cytoplasm	0	1000
DMTPHT	amet[c] + dmtphllqne[c] --> ahcys[c] + h[c] + phllqne[c]	Ubiquinone and other terpenoid-quinone biosynthesis	Cytoplasm	0	1000

AMMQT8_2p	amet[c] + 2dmmq8[c] --> ahcys[c] + h[c] + mqn8[p]	Ubiquinone and other terpenoid-quinone biosynthesis	Cytoplasm	0	1000
AMMQT8_2	amet[c] + 2dmmq8[c] --> ahcys[c] + h[c] + mqn8[c]	Ubiquinone and other terpenoid-quinone biosynthesis	Cytoplasm	0	1000
NADHVKR	nadh[c] + h[c] + phllqne[c] <=> nad[c] + phllqn[c]	Ubiquinone and other terpenoid-quinone biosynthesis	Cytoplasm	-1000	1000
NADHQR3p	nadh[c] + h[c] + mqn8[p] <=> nad[c] + mql8[p]	Ubiquinone and other terpenoid-quinone biosynthesis	Cytoplasm	-1000	1000
NADHQR3	nadh[c] + h[c] + mqn8[c] <=> nad[c] + mql8[c]	Ubiquinone and other terpenoid-quinone biosynthesis	Cytoplasm	-1000	1000
NADPHQR3p	nadph[c] + h[c] + mqn8[p] <=> nadp[c] + mql8[p]	Ubiquinone and other terpenoid-quinone biosynthesis	Cytoplasm	-1000	1000
NADPHQR3	nadph[c] + h[c] + mqn8[c] <=> nadp[c] + mql8[c]	Ubiquinone and other terpenoid-quinone biosynthesis	Cytoplasm	-1000	1000
NADPHQR2p	nadph[c] + h[c] + q8[p] <=> nadp[c] + q8h2[p]	Ubiquinone and other terpenoid-quinone biosynthesis	Cytoplasm	-1000	1000
NADPHQR2	nadph[c] + h[c] + q8[c] <=> nadp[c] + q8h2[c]	Ubiquinone and other terpenoid-quinone biosynthesis	Cytoplasm	-1000	1000
HNPHT	hgentis[c] + npdp[c] --> co2[c] + ppi[c] + 2m6npol[c]	Ubiquinone and other terpenoid-quinone biosynthesis	Cytoplasm	0	1000
2MNPTQ9	amet[c] + 2m6npol[c] --> ahcys[c] + h[c] + pqh2[c]	Ubiquinone and other terpenoid-quinone biosynthesis	Cytoplasm	0	1000
PQH2tu	pqh2[c] <=> pqh2[u]	Ubiquinone and other terpenoid-quinone biosynthesis	Thylakoid	-1000	1000
METAT	h2o[c] + atp[c] + met__L[c] <=> pi[c] + ppi[c] + amet[c] + h[c]	Cysteine and methionine metabolism	Cytoplasm	-1000	1000
ADMDC	amet[c] + h[c] <=> ametam[c] + co2[c]	Cysteine and methionine metabolism	Cytoplasm	0	1000
AHCi	h2o[c] + ahcys[c] <=> hcys__L[c] + adn[c]	Cysteine and methionine metabolism	Cytoplasm	-1000	1000
LDH_D	nadh[c] + pyr[c] + h[c] <=> nad[c] + lac__D[c]	Pyruvate metabolism	Cytoplasm	-1000	1000
PPS	h2o[c] + atp[c] + pyr[c] --> pi[c] + amp[c] + pep[c] + 3 h[c]	Pyruvate metabolism	Cytoplasm	0	1000
ME2	nadp[c] + mal__L[c] --> nadph[c] + co2[c] + pyr[c]	Pyruvate metabolism	Cytoplasm	0	1000
ACYP_2	h2o[c] + actp[c] --> pi[c] + ac[c] + h[c]	Pyruvate metabolism	Cytoplasm	0	1000

PTAr	accoa[c] + pi[c] <=> actp[c] + coa[c]	Pyruvate metabolism	Cytoplasm	0	1000
ACOAM	atp[c] + ac[c] --> ppi[c] + acadl[c]	Pyruvate metabolism	Cytoplasm	0	1000
ACKr	ac[c] + atp[c] <=> actp[c] + adp[c]	Pyruvate metabolism	Cytoplasm	0	1000
AACLAM	coa[c] + acadl[c] --> amp[c] + accoa[c] + h[c]	Pyruvate metabolism	Cytoplasm	0	1000
KARA1	nadph[c] + h[c] + alac__S[c] <=> nadp[c] + 23dhmb[c]	Pantothenate and CoA biosynthesis	Cytoplasm	-1000	1000
MOHMT	h2o[c] + 3mob[c] + mlthf[c] <=> thf[c] + 2dhp[c]	Pantothenate and CoA biosynthesis	Cytoplasm	-1000	1000
DPR	nadph[c] + h[c] + 2dhp[c] <=> nadp[c] + pant__R[c]	Pantothenate and CoA biosynthesis	Cytoplasm	-1000	1000
PBAL	atp[c] + ala_B[c] + pant__R[c] --> ppi[c] + amp[c] + 2 h[c] + pnto__R[c]	Pantothenate and CoA biosynthesis	Cytoplasm	0	1000
PNTK	atp[c] + pnto__R[c] --> adp[c] + h[c] + 4ppan[c]	Pantothenate and CoA biosynthesis	Cytoplasm	0	1000
PPNCL2	ctp[c] + cys__L[c] + 4ppan[c] --> ppi[c] + cmp[c] + 2 h[c] + 4ppcys[c]	Pantothenate and CoA biosynthesis	Cytoplasm	0	1000
PPNCL3	atp[c] + cys__L[c] + 4ppan[c] --> ppi[c] + amp[c] + 2 h[c] + 4ppcys[c]	Pantothenate and CoA biosynthesis	Cytoplasm	0	1000
PPCDC	h[c] + 4ppcys[c] --> co2[c] + pan4p[c]	Pantothenate and CoA biosynthesis	Cytoplasm	0	1000
PTPATi	atp[c] + pan4p[c] <=> ppi[c] + dpcoa[c]	Pantothenate and CoA biosynthesis	Cytoplasm	-1000	1000
DPCOAK	atp[c] + dpcoa[c] --> adp[c] + coa[c] + h[c]	Pantothenate and CoA biosynthesis	Cytoplasm	0	1000
ACPS1_1	coa[c] + apoACP[c] <=> pap[c] + ACP[c] + h[c]	Pantothenate and CoA biosynthesis	Cytoplasm	-1000	1000
GTPCII2	3 h2o[c] + gtp[c] --> ppi[c] + for[c] + 3 h[c] + 25drapp[c]	Riboflavin metabolism	Cytoplasm	0	1000
DHPPDA2	h2o[c] + h[c] + 25drapp[c] --> nh4[c] + 5apru[c]	Riboflavin metabolism	Cytoplasm	0	1000
APRAUR	nadph[c] + h[c] + 5apru[c] <=> nadp[c] + 5aprbu[c]	Riboflavin metabolism	Cytoplasm	-1000	1000
PMDPHT	h2o[c] + 5aprbu[c] <=> pi[c] + 4r5au[c]	Riboflavin metabolism	Cytoplasm	-1000	1000
DMHDRFS_1	34hpp[c] + 4r5au[c] + 2 amet[c] + h2o[c] <=> 2 dad_5[c] + 2 met__L[c] + nh4[c] + oxa[c] + ddhrb[c]	Riboflavin metabolism	Cytoplasm	-1000	1000
DB4PS	ru5p__D[c] --> for[c] + h[c] + db4p[c]	Riboflavin metabolism	Cytoplasm	0	1000
RBFSa	4r5au[c] + db4p[c] <=> 2 h2o[c] + pi[c] + h[c] + dmlz[c]	Riboflavin metabolism	Cytoplasm	-1000	1000
RIBFSc	h[c] + 2 dmlz[c] --> ribflv[c] + 4r5au[c]	Riboflavin metabolism	Cytoplasm	0	1000
RBFK	atp[c] + ribflv[c] --> adp[c] + fmn[c] + h[c]	Riboflavin metabolism	Cytoplasm	0	1000
FMNRx2	nadph[c] + fmn[c] + 2 h[c] <=> nadp[c] + fmnh2[c]	Riboflavin metabolism	Cytoplasm	-1000	1000
FMNAT	atp[c] + fmn[c] <=> ppi[c] + fad[c]	Riboflavin metabolism	Cytoplasm	-1000	1000

FADRx2	nadph[c] + fad[c] + 2 h[c] <=> nadp[c] + fadh2[c]	Riboflavin metabolism	Cytoplasm	-1000	1000
DMBZIDS2	fmnh2[c] + o2[c] + nadh[c] + h[c] <=> h2o[c] + e4p[c] + dmbzid[c] + dialurate[c] + nad[c]	Riboflavin metabolism	Cytoplasm	0	1000
EX_ribflv_e	ribflv[e] <=>	Exchange	Extracellular	-1000	0
RIBFLVt3	ribflv[e] + atp[c] + h2o[c] --> ribflv[c] + adp[c] + h[c] + pi[c]	Transport	Cytoplasm	0	1000
E4PD	e4p[c] + h2o[c] + nad[c] <=> 4per[c] + 2 h[c] + nadh[c]	Vitamin B6 metabolism	Cytoplasm	0	1000
PERD	4per[c] + nad[c] <=> h[c] + nadh[c] + ohpb[c]	Vitamin B6 metabolism	Cytoplasm	0	1000
OHPBAT	glu__L[c] + ohpb[c] <=> akgl[c] + phthr[c]	Vitamin B6 metabolism	Cytoplasm	-1000	1000
HTHRPDH	nad[c] + phthr[c] <=> h[c] + nadh[c] + 2a3pp[c]	Vitamin B6 metabolism	Cytoplasm	0	1000
4HTHRS	h2o[c] + phthr[c] <=> 4hthr[c] + pi[c]	Vitamin B6 metabolism	Cytoplasm	-1000	1000
AOXPBDC	h[c] + 2a3pp[c] <=> co2[c] + 3a2oxpp[c]	Vitamin B6 metabolism	Cytoplasm	0	1000
PDX5PS2	dxy15p[c] + 3a2oxpp[c] <=> h[c] + 2 h2o[c] + pdx5p[c] + pi[c]	Vitamin B6 metabolism	Cytoplasm	-1000	1000
PDX5POi	o2[c] + pdx5p[c] <=> h2o2[c] + pydx5p[c]	Vitamin B6 metabolism	Cytoplasm	-1000	1000
PYAM5PO	h2o[c] + o2[c] + pyam5p[c] <=> h2o2[c] + nh4[c] + pydx5p[c]	Vitamin B6 metabolism	Cytoplasm	-1000	1000
PSPPS	2 frdp[c] --> ppi[c] + h[c] + psqldp[c]	Sesquiterpenoid and triterpenoid biosynthesis	Cytoplasm	0	1000
SS	nadph[c] + psqldp[c] --> nadp[c] + ppi[c] + sql[c]	Sesquiterpenoid and triterpenoid biosynthesis	Cytoplasm	0	1000
AFNSES	frdp[c] --> ppi[c] + h[c] + afnse[c]	Sesquiterpenoid and triterpenoid biosynthesis	Cytoplasm	0	1000
EASELNS	frdp[c] --> ppi[c] + h[c] + 5easeln[c]	Sesquiterpenoid and triterpenoid biosynthesis	Cytoplasm	0	1000
SQLC	sql[c] --> dptne[c]	Sesquiterpenoid and triterpenoid biosynthesis	Cytoplasm	0	1000
SQLC2	h2o[c] + sql[c] --> dpterol[c]	Sesquiterpenoid and triterpenoid biosynthesis	Cytoplasm	0	1000
PHYTES	2 ggdp[c] --> ppi[c] + h[c] + prephytedp[c]	Carotenoid biosynthesis	Cytoplasm	0	1000
PHYTES3	prephytedp[c] --> ppi[c] + h[c] + cisphytoe[c]	Carotenoid biosynthesis	Cytoplasm	0	1000
PHYTES2	prephytedp[c] --> ppi[c] + h[c] + phytoe[c]	Carotenoid biosynthesis	Cytoplasm	0	1000
CPDS1	cisphytoe[c] + pq[u] <=> pqh2[u] + cphytfl[c]	Carotenoid biosynthesis	Cytoplasm	-1000	1000
CPDS2	pq[u] + cphytfl[c] <=> pqh2[u] + tczcaro[c]	Carotenoid biosynthesis	Cytoplasm	-1000	1000
ZISO	tczcaro[c] <=> dczcaro[c]	Carotenoid biosynthesis	Cytoplasm	-1000	1000
ZCARDS1_k1	phllqne[c] + dczcaro[c] <=> phllqnl[c] + tcneuspn[c]	Carotenoid biosynthesis	Cytoplasm	-1000	1000
ZCARDS1_mqn8	dczcaro[c] + mqn8[p] <=> mql8[p] + tcneuspn[c]	Carotenoid biosynthesis	Cytoplasm	-1000	1000
ZCARDS1_q8	dczcaro[c] + q8[p] <=> q8h2[p] + tcneuspn[c]	Carotenoid biosynthesis	Cytoplasm	-1000	1000

ZCARDS1	pq[u] + dczcaro[c] <=> tcneuspn[c] + pqh2[u]	Carotenoid biosynthesis	Cytoplasm	-1000	1000
ZCARDS2_k1	phllqne[c] + tcneuspn[c] <=> phllqnl[c] + ttclcyo[c]	Carotenoid biosynthesis	Cytoplasm	-1000	1000
ZCARDS2_mqn8	mqn8[p] + tcneuspn[c] <=> ttclcyo[c] + mq18[p]	Carotenoid biosynthesis	Cytoplasm	-1000	1000
ZCARDS2_q8	q8[p] + tcneuspn[c] <=> ttclcyo[c] + q8h2[p]	Carotenoid biosynthesis	Cytoplasm	-1000	1000
ZCARDS2	pq[u] + tcneuspn[c] <=> ttclcyo[c] + pqh2[u]	Carotenoid biosynthesis	Cytoplasm	-1000	1000
PLYCOI	ttclcyo[c] <=> lycop[c]	Carotenoid biosynthesis	Cytoplasm	-1000	1000
TPDS1	phytoe[c] + pq[u] <=> phytfl[c] + pqh2[u]	Carotenoid biosynthesis	Cytoplasm	-1000	1000
TPDS2	phytfl[c] + pq[u] <=> zcarote[c] + pqh2[u]	Carotenoid biosynthesis	Cytoplasm	-1000	1000
ZDS_1	o2[c] + zcarote[c] + pqh2[u] <=> 2 h2o[c] + neuspn[c] + pq[u]	Carotenoid biosynthesis	Cytoplasm	-1000	1000
NOR_1	o2[c] + neuspn[c] + pqh2[u] <=> 2 h2o[c] + lycop[c] + pq[u]	Carotenoid biosynthesis	Cytoplasm	-1000	1000
LYCOPC	lycop[c] <=> gcarote[c]	Carotenoid biosynthesis	Cytoplasm	-1000	1000
GCATENEC	gcarote[c] <=> caro[c]	Carotenoid biosynthesis	Cytoplasm	-1000	1000
BCAROE	caro[c] + o2[c] --> h2o[c] + echin[c]	Carotenoid biosynthesis	Cytoplasm	0	1000
BCAROE2	echin[c] + o2[c] --> h2o[c] + cantxan[c]	Carotenoid biosynthesis	Cytoplasm	0	1000
BCAROHX	caro[c] + nadph[c] + o2[c] + h[c] --> bcriptox[c] + h2o[c] + nadp[c]	Carotenoid biosynthesis	Cytoplasm	0	1000
BCAROHX2	bcriptox[c] + nadph[c] + o2[c] + h[c] --> zeax[c] + h2o[c] + nadp[c]	Carotenoid biosynthesis	Cytoplasm	0	1000
LYCOPH	h2o[c] + gcarote[c] <=> 1hgcarote[c]	Carotenoid biosynthesis	Cytoplasm	0	1000
PXANTS	1hgcarote[c] + o2[c] <=> h2o[c] + pxanth[c]	Carotenoid biosynthesis	Cytoplasm	0	1000
PXANTOX	pxanth[c] + nadph[c] + o2[c] + h[c] <=> myxl[c] + nadp[c] + h2o[c]	Carotenoid biosynthesis	Cytoplasm	0	1000
MXFUCS	gdpfuc[c] + myxl[c] <=> gdp[c] + myxlfuc[c]	Carotenoid biosynthesis	Cytoplasm	0	1000
KMXFUCS	myxlfuc[c] + 2 o2[c] + 2 nadph[c] + 2 h[c] <=> 3 h2o[c] + 2 nadp[c] + kmyxlfuc[c]	Carotenoid biosynthesis	Cytoplasm	0	1000
AMPMS3	amet[c] + air[c] <=> for[c] + met__L[c] + 3 h[c] + co[c] + 4ampm[c] + dad_5[c]	Thiamine metabolism	Cytoplasm	-1000	1000
PMPK	atp[c] + h[c] + 4ampm[c] --> adp[c] + 2mahmp[c]	Thiamine metabolism	Cytoplasm	0	1000
THZPSN	atp[c] + tyr__L[c] + cys__L[c] + dxyl5p[c] --> h2o[c] + co2[c] + ppi[c] + amp[c] + ala__L[c] + 2 h[c] + 4mpetz[c] + 4hba[c]	Thiamine metabolism	Cytoplasm	0	1000
TMPPP	4mpetz[c] + 2mahmp[c] --> ppi[c] + thmmp[c]	Thiamine metabolism	Cytoplasm	0	1000
TMPK	atp[c] + h[c] + thmmp[c] <=> adp[c] + thmpp[c]	Thiamine metabolism	Cytoplasm	-1000	1000
THMP	h2o[c] + thmmp[c] <=> pi[c] + thm[c]	Thiamine metabolism	Cytoplasm	-1000	1000
TMN	h2o[c] + thm[c] <=> 4ahmmp[c] + 4mhetz[c] + h[c]	Thiamine metabolism	Cytoplasm	0	1000

HETZK	4mhetz[c] + atp[c] <=> 4mpetz[c] + adp[c] + h[c]	Thiamine metabolism	Cytoplasm	0	1000
HMPK1	4ahmmp[c] + atp[c] <=> 4ampm[c] + adp[c] + h[c]	Thiamine metabolism	Cytoplasm	0	1000
ACCOAC	atp[c] + accoa[c] + hco3[c] <=> adp[c] + pi[c] + h[c] + malcoa[c]	Fatty acid biosynthesis	Cytoplasm	-1000	1000
MCOATA	malcoa[c] + ACP[c] <=> coa[c] + malACP[c]	Fatty acid biosynthesis	Cytoplasm	-1000	1000
KAS15	accoa[c] + h[c] + malACP[c] --> coa[c] + co2[c] + actACP[c]	Fatty acid biosynthesis	Cytoplasm	0	1000
ACOATA	accoa[c] + ACP[c] <=> coa[c] + acACP[c]	Fatty acid biosynthesis	Cytoplasm	-1000	1000
KAS14	malACP[c] + acACP[c] + h[c] --> co2[c] + actACP[c] + ACP[c]	Fatty acid biosynthesis	Cytoplasm	0	1000
3OAR40_2	nadph[c] + h[c] + actACP[c] <=> nadp[c] + 3hbutACP[c]	Fatty acid biosynthesis	Cytoplasm	-1000	1000
3HAD40_2	3hbutACP[c] <=> h2o[c] + but2eACP[c]	Fatty acid biosynthesis	Cytoplasm	-1000	1000
EAR40x	nadh[c] + h[c] + but2eACP[c] --> nad[c] + butACP[c]	Fatty acid biosynthesis	Cytoplasm	0	1000
3OAS60	butACP[c] + h[c] + malACP[c] --> co2[c] + 3ohexACP[c] + ACP[c]	Fatty acid biosynthesis	Cytoplasm	0	1000
3OAR60	nadph[c] + h[c] + 3ohexACP[c] <=> nadp[c] + 3hhexACP[c]	Fatty acid biosynthesis	Cytoplasm	-1000	1000
3HAD60	3hhexACP[c] <=> h2o[c] + thex2eACP[c]	Fatty acid biosynthesis	Cytoplasm	-1000	1000
EAR60x	nadh[c] + h[c] + thex2eACP[c] --> nad[c] + hexACP[c]	Fatty acid biosynthesis	Cytoplasm	0	1000
3OAS80	hexACP[c] + h[c] + malACP[c] --> co2[c] + 3ooctACP[c] + ACP[c]	Fatty acid biosynthesis	Cytoplasm	0	1000
3OAR80	nadph[c] + h[c] + 3ooctACP[c] <=> nadp[c] + 3hoctACP[c]	Fatty acid biosynthesis	Cytoplasm	-1000	1000
3HAD80	3hoctACP[c] <=> h2o[c] + toct2eACP[c]	Fatty acid biosynthesis	Cytoplasm	-1000	1000
EAR80x	nadh[c] + h[c] + toct2eACP[c] --> nad[c] + ocACP[c]	Fatty acid biosynthesis	Cytoplasm	0	1000
3OAS100	ocACP[c] + h[c] + malACP[c] --> co2[c] + 3odecACP[c] + ACP[c]	Fatty acid biosynthesis	Cytoplasm	0	1000
3OAR100	nadph[c] + h[c] + 3odecACP[c] <=> nadp[c] + 3hdecACP[c]	Fatty acid biosynthesis	Cytoplasm	-1000	1000
3HAD100	3hdecACP[c] <=> h2o[c] + tdec2eACP[c]	Fatty acid biosynthesis	Cytoplasm	-1000	1000
EAR100x	nadh[c] + h[c] + tdec2eACP[c] --> nad[c] + dcaACP[c]	Fatty acid biosynthesis	Cytoplasm	0	1000
3OAS120	dcaACP[c] + h[c] + malACP[c] --> co2[c] + 3oddecACP[c] + ACP[c]	Fatty acid biosynthesis	Cytoplasm	0	1000
3OAR120	nadph[c] + h[c] + 3oddecACP[c] <=> nadp[c] + 3hddecACP[c]	Fatty acid biosynthesis	Cytoplasm	-1000	1000
3HAD120	3hddecACP[c] <=> h2o[c] + tddec2eACP[c]	Fatty acid biosynthesis	Cytoplasm	-1000	1000
EAR120x	nadh[c] + h[c] + tddec2eACP[c] --> nad[c] + ddcaACP[c]	Fatty acid biosynthesis	Cytoplasm	0	1000
3OAS140	ddcaACP[c] + h[c] + malACP[c] --> co2[c] + 3omrsACP[c] + ACP[c]	Fatty acid biosynthesis	Cytoplasm	0	1000
3OAR140	nadph[c] + h[c] + 3omrsACP[c] <=> nadp[c] + 3hmrsACP[c]	Fatty acid biosynthesis	Cytoplasm	-1000	1000
3HAD140	3hmrsACP[c] <=> h2o[c] + tmrs2eACP[c]	Fatty acid biosynthesis	Cytoplasm	-1000	1000
EAR140x	nadh[c] + h[c] + tmrs2eACP[c] --> nad[c] + myrsACP[c]	Fatty acid biosynthesis	Cytoplasm	0	1000

3OAS160	myrsACP[c] + h[c] + malACP[c] --> co2[c] + 3opalmACP[c] + ACP[c]	Fatty acid biosynthesis	Cytoplasm	0	1000
3OAR160	nadph[c] + h[c] + 3opalmACP[c] <=> nadp[c] + 3hpalmACP[c]	Fatty acid biosynthesis	Cytoplasm	-1000	1000
3HAD160	3hpalmACP[c] <=> h2o[c] + tpalm2eACP[c]	Fatty acid biosynthesis	Cytoplasm	-1000	1000
EAR160x	nadh[c] + h[c] + tpalm2eACP[c] --> nad[c] + palmACP[c]	Fatty acid biosynthesis	Cytoplasm	0	1000
3OAS180	palmACP[c] + h[c] + malACP[c] --> co2[c] + 3ooctdACP[c] + ACP[c]	Fatty acid biosynthesis	Cytoplasm	0	1000
3OAR180	nadph[c] + h[c] + 3ooctdACP[c] <=> nadp[c] + 3hoctaACP[c]	Fatty acid biosynthesis	Cytoplasm	-1000	1000
3HAD180	3hoctaACP[c] <=> h2o[c] + toctd2eACP[c]	Fatty acid biosynthesis	Cytoplasm	-1000	1000
EAR180x	nadh[c] + h[c] + toctd2eACP[c] --> nad[c] + ocdcaACP[c]	Fatty acid biosynthesis	Cytoplasm	0	1000
DESAT16a	h[c] + palmACP[c] + nadph[c] + o2[c] <=> 2 h2o[c] + nadp[c] + hdeACP[c]	Fatty acid biosynthesis	Cytoplasm	-1000	1000
DESAT18a_1	h[c] + ocdcaACP[c] + nadph[c] + o2[c] <=> 2 h2o[c] + nadp[c] + octe_9_ACP[c]	Fatty acid biosynthesis	Cytoplasm	-1000	1000
DESAT18a_2	h[c] + octe_9_ACP[c] + nadph[c] + o2[c] <=> 2 h2o[c] + nadp[c] + octe_9_12_ACP[c]	Fatty acid biosynthesis	Cytoplasm	-1000	1000
DESAT18a_3	h[c] + octe_9_12_ACP[c] + nadph[c] + o2[c] <=> 2 h2o[c] + nadp[c] + octe_9_12_15_ACP[c]	Fatty acid biosynthesis	Cytoplasm	-1000	1000
EX_glyc_e	glyc[e] <=>	Exchange	Extracellular	-1000	1000
GLYCt	glyc[e] <=> glyc[c]	Transport	Cytoplasm	0	0
MALCOAM	amet[c] + malACP[c] <=> ahcys[c] + malmeACP[c]	Biotin metabolism	Cytoplasm	0	1000
MALACPD	h[c] + malACP[c] + malmeACP[c] <=> ACP[c] + co2[c] + skgmeACP[c]	Biotin metabolism	Cytoplasm	-1000	1000
KGLACPR	h[c] + nadph[c] + skgmeACP[c] <=> nadp[c] + 3hgmeACP[c]	Biotin metabolism	Cytoplasm	-1000	1000
HGLACPHL	3hgmeACP[c] <=> egmeACP[c] + h2o[c]	Biotin metabolism	Cytoplasm	-1000	1000
EGLACPR	egmeACP[c] + h[c] + nadph[c] <=> nadp[c] + glmeACP[c]	Biotin metabolism	Cytoplasm	-1000	1000
KPIMD	h[c] + malACP[c] + glmeACP[c] <=> ACP[c] + co2[c] + skpmeACP[c]	Biotin metabolism	Cytoplasm	-1000	1000
KPIMR	h[c] + nadph[c] + skpmeACP[c] <=> nadp[c] + 3hpmeACP[c]	Biotin metabolism	Cytoplasm	-1000	1000
HPIMHL	3hpmeACP[c] <=> epmeACP[c] + h2o[c]	Biotin metabolism	Cytoplasm	-1000	1000
EPMEACPR	epmeACP[c] + h[c] + nadph[c] <=> nadp[c] + pmeACP[c]	Biotin metabolism	Cytoplasm	-1000	1000
PMEACPE	h2o[c] + pmeACP[c] <=> meoh[c] + pimACP[c]	Biotin metabolism	Cytoplasm	0	1000
AOXSr2	ala__L[c] + pimACP[c] <=> 8aonn[c] + ACP[c] + co2[c]	Biotin metabolism	Cytoplasm	-1000	1000
AMAOTr	8aonn[c] + amet[c] <=> amob[c] + dann[c]	Biotin metabolism	Cytoplasm	0	1000

DBTS	atp[c] + co2[c] + dann[c] <=> adp[c] + dtbt[c] + 3 h[c] + pi[c]	Biotin metabolism	Cytoplasm	-1000	1000
BTS6	amet[c] + cys__L[c] + dtbt[c] <=> ala__L[c] + btn[c] + dad_5[c] + h[c] + met__L[c]	Biotin metabolism	Cytoplasm	0	1000
BACCL	atp[c] + btn[c] <=> ppi[c] + btamp[c]	Biotin metabolism	Cytoplasm	-1000	1000
BTNPL2	btamp[c] + accp[c] <=> amp[c] + h[c] + btnCCP[c]	Biotin metabolism	Cytoplasm	-1000	1000
GLYCDx	nad[c] + glyc[c] <=> nadh[c] + h[c] + dha[c]	Glycerolipid metabolism	Cytoplasm	-1000	1000
GLYK	atp[c] + glyc[c] --> adp[c] + h[c] + glyc3p[c]	Glycerolipid metabolism	Cytoplasm	0	1000
G3PD1ir	nad[c] + glyc3p[c] <=> nadh[c] + h[c] + dhap[c]	Glycerophospholipid metabolism	Cytoplasm	-1000	1000
G3PD2	nadp[c] + glyc3p[c] <=> nadph[c] + h[c] + dhap[c]	Glycerophospholipid metabolism	Cytoplasm	-1000	1000
G3PAT160	glyc3p[c] + palmACP[c] <=> ACP[c] + 1hdecg3p[c]	Glycerophospholipid metabolism	Cytoplasm	-1000	1000
AGPAT160	palmACP[c] + 1hdecg3p[c] <=> ACP[c] + pa160[c]	Glycerophospholipid metabolism	Cytoplasm	-1000	1000
DASYN160	ctp[c] + pa160[c] --> ppi[c] + cdpdhdecg[c]	Glycerophospholipid metabolism	Cytoplasm	0	1000
PGSA160	glyc3p[c] + cdpdhdecg[c] --> cmp[c] + h[c] + pgp160[c]	Glycerophospholipid metabolism	Cytoplasm	0	1000
PGPP160	h2o[c] + pgp160[c] --> pi[c] + pg160[c]	Glycerophospholipid metabolism	Cytoplasm	0	1000
PAPA160	h2o[c] + pa160[c] <=> pi[c] + 12dgr160[c]	Glycerolipid metabolism	Cytoplasm	-1000	1000
DAGK160	12dgr160[c] + atp[c] <=> adp[c] + h[c] + pa160[c]	Glycerolipid metabolism	Cytoplasm	0	1000
GALUi	utp[c] + g1p[c] <=> ppi[c] + udpg[c]	Pentose and glucuronate interconversions	Cytoplasm	-1000	1000
UDPG4E	udpg[c] <=> udpgal[c]	Galactolipids metabolism	Cytoplasm	-1000	1000
SPS	f6p[c] + udpg[c] <=> suc6p[c] + udp[c]	Glycogen and sucrose metabolism	Cytoplasm	0	1000
SPP	h2o[c] + suc6p[c] <=> pi[c] + sucr[c]	Glycogen and sucrose metabolism	Cytoplasm	0	1000
SUCRS	udpg[c] + fru[c] <=> udp[c] + sucr[c]	Glycogen and sucrose metabolism	Cytoplasm	0	1000
SUCRS_2	adp[c] + sucr[c] <=> fru[c] + adpglc[c]	Glycogen and sucrose metabolism	Cytoplasm	0	1000
SUCR	h2o[c] + sucr[c] <=> fru[c] + glc__D[c]	Glycogen and sucrose metabolism	Cytoplasm	0	1000
UDPGD	h2o[c] + 2 nad[c] + udpg[c] <=> 3 h[c] + 2 nadh[c] + udpglc[c]	Glycolysis and sugar metabolism	Cytoplasm	-1000	1000
UDPGLDC	h[c] + udpglc[c] <=> co2[c] + udpxyl[c]	Glycolysis and sugar metabolism	Cytoplasm	0	1000
CELLSYN	glc__D[c] + udpg[c] <=> h2o[c] + udp[c] + b14glucan[c]	Glycolysis and sugar metabolism	Cytoplasm	-1000	1000

MGDG160	udpgal[c] + 12dgr160[c] <=> udp[c] + mgdg160[c]	Galactolipids metabolism	Cytoplasm	-1000	1000
DGDG160	udpgal[c] + mgdg160[c] <=> udp[c] + dgdg160[c]	Galactolipids metabolism	Cytoplasm	-1000	1000
SQD1	udpg[c] + so3[c] --> h2o[c] + udpsq[c]	Amino sugar and nucleotide sugar metabolism	Cytoplasm	0	1000
SQDGS160_1	udpsq[c] + 12dgr160[c] <=> udp[c] + sqdg160[c]	Sulfolipids metabolism	Cytoplasm	-1000	1000
G3PAT161	glyc3p[c] + hdeACP[c] <=> ACP[c] + 1hdec9eg3p[c]	Glycerophospholipid metabolism	Cytoplasm	-1000	1000
AGPAT161	hdeACP[c] + 1hdec9eg3p[c] <=> ACP[c] + pa161[c]	Glycerophospholipid metabolism	Cytoplasm	-1000	1000
DASYN161	ctp[c] + pa161[c] --> ppi[c] + cdpdhdec9eg[c]	Glycerophospholipid metabolism	Cytoplasm	0	1000
PGSA161	glyc3p[c] + cdpdhdec9eg[c] --> cmp[c] + h[c] + pgp161[c]	Glycerophospholipid metabolism	Cytoplasm	0	1000
PGPP161	h2o[c] + pgp161[c] --> pi[c] + pg161[c]	Glycerophospholipid metabolism	Cytoplasm	0	1000
PAPA161	h2o[c] + pa161[c] <=> pi[c] + 12dgr161[c]	Glycerolipid metabolism	Cytoplasm	-1000	1000
DAGK161	12dgr161[c] + atp[c] <=> adp[c] + h[c] + pa161[c]	Glycerolipid metabolism	Cytoplasm	0	1000
MGDG161	udpgal[c] + 12dgr161[c] <=> udp[c] + mgdg161[c]	Galactolipids metabolism	Cytoplasm	-1000	1000
DGDG161	udpgal[c] + mgdg161[c] <=> udp[c] + dgdg161[c]	Galactolipids metabolism	Cytoplasm	-1000	1000
SQDGS161	udpsq[c] + 12dgr161[c] <=> udp[c] + sqdg161[c]	Sulfolipids metabolism	Cytoplasm	-1000	1000
G3PAT180	glyc3p[c] + ocdcaACP[c] <=> ACP[c] + 1odecg3p[c]	Glycerophospholipid metabolism	Cytoplasm	-1000	1000
AGPAT180	ocdcaACP[c] + 1odecg3p[c] <=> ACP[c] + pa180[c]	Glycerophospholipid metabolism	Cytoplasm	-1000	1000
DASYN180	ctp[c] + pa180[c] --> ppi[c] + cdpdodecg[c]	Glycerophospholipid metabolism	Cytoplasm	0	1000
PGSA180	glyc3p[c] + cdpdodecg[c] --> cmp[c] + h[c] + pgp180[c]	Glycerophospholipid metabolism	Cytoplasm	0	1000
PGPP180	h2o[c] + pgp180[c] --> pi[c] + pg180[c]	Glycerophospholipid metabolism	Cytoplasm	0	1000
PAPA180	h2o[c] + pa180[c] <=> pi[c] + 12dgr180[c]	Glycerolipid metabolism	Cytoplasm	-1000	1000
DAGK180	12dgr180[c] + atp[c] <=> adp[c] + h[c] + pa180[c]	Glycerolipid metabolism	Cytoplasm	0	1000
MGDG180	udpgal[c] + 12dgr180[c] <=> udp[c] + mgdg180[c]	Galactolipids metabolism	Cytoplasm	-1000	1000
DGDG180	udpgal[c] + mgdg180[c] <=> udp[c] + dgdg180[c]	Galactolipids metabolism	Cytoplasm	-1000	1000
SQDGS180	udpsq[c] + 12dgr180[c] <=> udp[c] + sqdg180[c]	Sulfolipids metabolism	Cytoplasm	-1000	1000
G3PAT181_9	glyc3p[c] + octe_9_ACP[c] <=> ACP[c] + 1odec9eg3p[c]	Glycerophospholipid metabolism	Cytoplasm	-1000	1000
AGPAT181_9	octe_9_ACP[c] + 1odec9eg3p[c] <=> ACP[c] + pa181_9[c]	Glycerophospholipid metabolism	Cytoplasm	-1000	1000

DASYN181_9	ctp[c] + pa181_9[c] --> ppi[c] + cdpdodec9eg[c]	Glycerophospholipid metabolism	Cytoplasm	0	1000
PGSA181_9	glyc3p[c] + cdpdodec9eg[c] --> cmp[c] + h[c] + pgp181_9[c]	Glycerophospholipid metabolism	Cytoplasm	0	1000
PGPP181_9	h2o[c] + pgp181_9[c] --> pi[c] + pg181_9[c]	Glycerophospholipid metabolism	Cytoplasm	0	1000
PAPA181_9	h2o[c] + pa181_9[c] <=> pi[c] + 12dgr181_9[c]	Glycerolipid metabolism	Cytoplasm	-1000	1000
DAGK181_9	12dgr181_9[c] + atp[c] <=> adp[c] + h[c] + pa181_9[c]	Glycerolipid metabolism	Cytoplasm	0	1000
MGDG181_9	udpgal[c] + 12dgr181_9[c] <=> udp[c] + mgdg181_9[c]	Galactolipids metabolism	Cytoplasm	-1000	1000
DGDG181_9	udpgal[c] + mgdg181_9[c] <=> udp[c] + dgdg181_9[c]	Galactolipids metabolism	Cytoplasm	-1000	1000
SQDGS181_9	udpsq[c] + 12dgr181_9[c] <=> udp[c] + sqdg181_9[c]	Sulfolipids metabolism	Cytoplasm	-1000	1000
G3PAT182_9_12	glyc3p[c] + octe_9_12_ACP[c] <=> ACP[c] + 1odec912eg3p[c]	Glycerophospholipid metabolism	Cytoplasm	-1000	1000
AGPAT182_9_12	octe_9_12_ACP[c] + 1odec912eg3p[c] <=> ACP[c] + pa182_9_12[c]	Glycerophospholipid metabolism	Cytoplasm	-1000	1000
DASYN182_9_12	ctp[c] + pa182_9_12[c] --> ppi[c] + cdpdodec912eg[c]	Glycerophospholipid metabolism	Cytoplasm	0	1000
PGSA182_9_12	glyc3p[c] + cdpdodec912eg[c] --> cmp[c] + h[c] + pgp182_9_12[c]	Glycerophospholipid metabolism	Cytoplasm	0	1000
PGPP182_9_12	h2o[c] + pgp182_9_12[c] --> pi[c] + pg182_9_12[c]	Glycerophospholipid metabolism	Cytoplasm	0	1000
PAPA182_9_12	h2o[c] + pa182_9_12[c] <=> pi[c] + 12dgr182_9_12[c]	Glycerolipid metabolism	Cytoplasm	-1000	1000
DAGK182_9_12	12dgr182_9_12[c] + atp[c] <=> adp[c] + h[c] + pa182_9_12[c]	Glycerolipid metabolism	Cytoplasm	0	1000
MGDG182_9_12	udpgal[c] + 12dgr182_9_12[c] <=> udp[c] + mgdg182_9_12[c]	Galactolipids metabolism	Cytoplasm	-1000	1000
DGDG182_9_12	udpgal[c] + mgdg182_9_12[c] <=> udp[c] + dgdg182_9_12[c]	Galactolipids metabolism	Cytoplasm	-1000	1000
SQDGS182_9_12	udpsq[c] + 12dgr182_9_12[c] <=> udp[c] + sqdg182_9_12[c]	Sulfolipids metabolism	Cytoplasm	-1000	1000
G3PAT183_9_12_15	glyc3p[c] + octe_9_12_15_ACP[c] <=> ACP[c] + 1odec91215eg3p[c]	Glycerophospholipid metabolism	Cytoplasm	-1000	1000
AGPAT183_9_12_15	octe_9_12_15_ACP[c] + 1odec91215eg3p[c] <=> ACP[c] + pa183_9_12_15[c]	Glycerophospholipid metabolism	Cytoplasm	-1000	1000
DASYN183_9_12_15	ctp[c] + pa183_9_12_15[c] --> ppi[c] + cdpdodec91215eg[c]	Glycerophospholipid metabolism	Cytoplasm	0	1000
PGSA183_9_12_15	glyc3p[c] + cdpdodec91215eg[c] --> cmp[c] + h[c] + pgp183_9_12_15[c]	Glycerophospholipid metabolism	Cytoplasm	0	1000
PGPP183_9_12_15	h2o[c] + pgp183_9_12_15[c] --> pi[c] + pg183_9_12_15[c]	Glycerophospholipid metabolism	Cytoplasm	0	1000
PAPA183_9_12_15	h2o[c] + pa183_9_12_15[c] <=> pi[c] + 12dgr183_9_12_15[c]	Glycerolipid metabolism	Cytoplasm	-1000	1000
DAGK183_9_12_15	12dgr183_9_12_15[c] + atp[c] <=> adp[c] + h[c] + pa183_9_12_15[c]	Glycerolipid metabolism	Cytoplasm	0	1000

MGDG183_9_12_15	udpgal[c] + 12dgr183_9_12_15[c] <=> udp[c] + mgdg183_9_12_15[c]	Galactolipids metabolism	Cytoplasm	-1000	1000
DGDG183_9_12_15	udpgal[c] + mgdg183_9_12_15[c] <=> udp[c] + dgdg183_9_12_15[c]	Galactolipids metabolism	Cytoplasm	-1000	1000
SQDGS183_9_12_15	udpsq[c] + 12dgr183_9_12_15[c] <=> udp[c] + sqdg183_9_12_15[c]	Sulfolipids metabolism	Cytoplasm	-1000	1000
G3PAT140	glyc3p[c] + myrsACP[c] <=> ACP[c] + 1tdecg3p[c]	Glycerophospholipid metabolism	Cytoplasm	-1000	1000
AGPAT140	myrsACP[c] + 1tdecg3p[c] <=> ACP[c] + pa140[c]	Glycerophospholipid metabolism	Cytoplasm	-1000	1000
DASYN140	ctp[c] + pa140[c] --> ppi[c] + cdpdtdecg[c]	Glycerophospholipid metabolism	Cytoplasm	0	1000
PGSA140	glyc3p[c] + cdpdtdecg[c] --> cmp[c] + h[c] + pgp140[c]	Glycerophospholipid metabolism	Cytoplasm	0	1000
PGPP140	h2o[c] + pgp140[c] --> pi[c] + pg140[c]	Glycerophospholipid metabolism	Cytoplasm	0	1000
PAPA140	h2o[c] + pa140[c] <=> pi[c] + 12dgr140[c]	Glycerolipid metabolism	Cytoplasm	-1000	1000
DAGK140	12dgr140[c] + atp[c] <=> adp[c] + h[c] + pa140[c]	Glycerolipid metabolism	Cytoplasm	0	1000
MGDG140	udpgal[c] + 12dgr140[c] <=> udp[c] + mgdg140[c]	Galactolipids metabolism	Cytoplasm	-1000	1000
DGDG140	udpgal[c] + mgdg140[c] <=> udp[c] + dgdg140[c]	Galactolipids metabolism	Cytoplasm	-1000	1000
SQDGS140	udpsq[c] + 12dgr140[c] <=> udp[c] + sqdg140[c]	Sulfolipids metabolism	Cytoplasm	-1000	1000
G3PAT120	glyc3p[c] + ddcaACP[c] <=> ACP[c] + 1ddecg3p[c]	Glycerophospholipid metabolism	Cytoplasm	-1000	1000
AGPAT120	ddcaACP[c] + 1ddecg3p[c] <=> ACP[c] + pa120[c]	Glycerophospholipid metabolism	Cytoplasm	-1000	1000
DASYN120	ctp[c] + pa120[c] --> ppi[c] + cdpdddecg[c]	Glycerophospholipid metabolism	Cytoplasm	0	1000
PGSA120	glyc3p[c] + cdpdddecg[c] --> cmp[c] + h[c] + pgp120[c]	Glycerophospholipid metabolism	Cytoplasm	0	1000
PGPP120	h2o[c] + pgp120[c] --> pi[c] + pg120[c]	Glycerophospholipid metabolism	Cytoplasm	0	1000
PAPA120	h2o[c] + pa120[c] <=> pi[c] + 12dgr120[c]	Glycerolipid metabolism	Cytoplasm	-1000	1000
DAGK120	12dgr120[c] + atp[c] <=> adp[c] + h[c] + pa120[c]	Glycerolipid metabolism	Cytoplasm	0	1000
MGDG120	udpgal[c] + 12dgr120[c] <=> udp[c] + mgdg120[c]	Galactolipids metabolism	Cytoplasm	-1000	1000
DGDG120	udpgal[c] + mgdg120[c] <=> udp[c] + dgdg120[c]	Galactolipids metabolism	Cytoplasm	-1000	1000
SQDGS120	udpsq[c] + 12dgr120[c] <=> udp[c] + sqdg120[c]	Sulfolipids metabolism	Cytoplasm	-1000	1000
G3PAT100	glyc3p[c] + dcaACP[c] <=> ACP[c] + 1decg3p[c]	Glycerophospholipid metabolism	Cytoplasm	-1000	1000
AGPAT100	dcaACP[c] + 1decg3p[c] <=> ACP[c] + pa100[c]	Glycerophospholipid metabolism	Cytoplasm	-1000	1000
DASYN100	ctp[c] + pa100[c] --> ppi[c] + cdpddecg[c]	Glycerophospholipid metabolism	Cytoplasm	0	1000
PGSA100	glyc3p[c] + cdpddecg[c] --> cmp[c] + h[c] + pgp100[c]	Glycerophospholipid metabolism	Cytoplasm	0	1000

PGPP100	$\text{h2o[c]} + \text{pgp100[c]} \rightarrow \text{pi[c]} + \text{pg100[c]}$	Glycerophospholipid metabolism	Cytoplasm	0	1000
PAPA100	$\text{h2o[c]} + \text{pa100[c]} \rightleftharpoons \text{pi[c]} + \text{12dgr100[c]}$	Glycerolipid metabolism	Cytoplasm	-1000	1000
DAGK100	$\text{12dgr100[c]} + \text{atp[c]} \rightleftharpoons \text{adp[c]} + \text{h[c]} + \text{pa100[c]}$	Glycerolipid metabolism	Cytoplasm	0	1000
MGDG100	$\text{udpgal[c]} + \text{12dgr100[c]} \rightleftharpoons \text{udp[c]} + \text{mgdg100[c]}$	Galactolipids metabolism	Cytoplasm	-1000	1000
DGDG100	$\text{udpgal[c]} + \text{mgdg100[c]} \rightleftharpoons \text{udp[c]} + \text{dgdg100[c]}$	Galactolipids metabolism	Cytoplasm	-1000	1000
SQDGS100	$\text{udpsq[c]} + \text{12dgr100[c]} \rightleftharpoons \text{udp[c]} + \text{sqdg100[c]}$	Sulfolipids metabolism	Cytoplasm	-1000	1000
G3PAT80	$\text{glyc3p[c]} + \text{ocACP[c]} \rightleftharpoons \text{ACP[c]} + \text{1ocg3p[c]}$	Glycerophospholipid metabolism	Cytoplasm	-1000	1000
AGPAT80	$\text{ocACP[c]} + \text{1ocg3p[c]} \rightleftharpoons \text{ACP[c]} + \text{pa80[c]}$	Glycerophospholipid metabolism	Cytoplasm	-1000	1000
DASYN80	$\text{ctp[c]} + \text{pa80[c]} \rightarrow \text{ppi[c]} + \text{cdpdocg[c]}$	Glycerophospholipid metabolism	Cytoplasm	0	1000
PGSA80	$\text{glyc3p[c]} + \text{cdpdocg[c]} \rightarrow \text{cmp[c]} + \text{h[c]} + \text{pgp80[c]}$	Glycerophospholipid metabolism	Cytoplasm	0	1000
PGPP80	$\text{h2o[c]} + \text{pgp80[c]} \rightarrow \text{pi[c]} + \text{pg80[c]}$	Glycerophospholipid metabolism	Cytoplasm	0	1000
PAPA80	$\text{h2o[c]} + \text{pa80[c]} \rightleftharpoons \text{pi[c]} + \text{12dgr80[c]}$	Glycerolipid metabolism	Cytoplasm	-1000	1000
DAGK80	$\text{12dgr80[c]} + \text{atp[c]} \rightleftharpoons \text{adp[c]} + \text{h[c]} + \text{pa80[c]}$	Glycerolipid metabolism	Cytoplasm	0	1000
MGDG80	$\text{udpgal[c]} + \text{12dgr80[c]} \rightleftharpoons \text{udp[c]} + \text{mgdg80[c]}$	Galactolipids metabolism	Cytoplasm	-1000	1000
DGDG80	$\text{udpgal[c]} + \text{mgdg80[c]} \rightleftharpoons \text{udp[c]} + \text{dgdg80[c]}$	Galactolipids metabolism	Cytoplasm	-1000	1000
SQDGS80	$\text{udpsq[c]} + \text{12dgr80[c]} \rightleftharpoons \text{udp[c]} + \text{sqdg80[c]}$	Sulfolipids metabolism	Cytoplasm	-1000	1000
G3PAT60	$\text{glyc3p[c]} + \text{hexACP[c]} \rightleftharpoons \text{ACP[c]} + \text{1hexg3p[c]}$	Glycerophospholipid metabolism	Cytoplasm	-1000	1000
AGPAT60	$\text{hexACP[c]} + \text{1hexg3p[c]} \rightleftharpoons \text{ACP[c]} + \text{pa60[c]}$	Glycerophospholipid metabolism	Cytoplasm	-1000	1000
DASYN60	$\text{ctp[c]} + \text{pa60[c]} \rightarrow \text{ppi[c]} + \text{cdpdhexg[c]}$	Glycerophospholipid metabolism	Cytoplasm	0	1000
PGSA60	$\text{glyc3p[c]} + \text{cdpdhexg[c]} \rightarrow \text{cmp[c]} + \text{h[c]} + \text{pgp60[c]}$	Glycerophospholipid metabolism	Cytoplasm	0	1000
PGPP60	$\text{h2o[c]} + \text{pgp60[c]} \rightarrow \text{pi[c]} + \text{pg60[c]}$	Glycerophospholipid metabolism	Cytoplasm	0	1000
PAPA60	$\text{h2o[c]} + \text{pa60[c]} \rightleftharpoons \text{pi[c]} + \text{12dgr60[c]}$	Glycerolipid metabolism	Cytoplasm	-1000	1000
DAGK60	$\text{12dgr60[c]} + \text{atp[c]} \rightleftharpoons \text{adp[c]} + \text{h[c]} + \text{pa60[c]}$	Glycerolipid metabolism	Cytoplasm	0	1000
MGDG60	$\text{udpgal[c]} + \text{12dgr60[c]} \rightleftharpoons \text{udp[c]} + \text{mgdg60[c]}$	Galactolipids metabolism	Cytoplasm	-1000	1000
DGDG60	$\text{udpgal[c]} + \text{mgdg60[c]} \rightleftharpoons \text{udp[c]} + \text{dgdg60[c]}$	Galactolipids metabolism	Cytoplasm	-1000	1000
SQDGS60	$\text{udpsq[c]} + \text{12dgr60[c]} \rightleftharpoons \text{udp[c]} + \text{sqdg60[c]}$	Sulfolipids metabolism	Cytoplasm	-1000	1000
GF6PTA	$\text{gln_L[c]} + \text{f6p[c]} \rightleftharpoons \text{glu_L[c]} + \text{gam6p[c]}$	Alanine, aspartate and glutamate metabolism	Cytoplasm	-1000	1000

G6PDA	gam6p[c] + h2o[c] <=> f6p[c] + nh4[c]	Amino sugar and nucleotide sugar metabolism	Cytoplasm	0	1000
AGDC	acgam6p[c] + h2o[c] <=> ac[c] + gam6p[c]	Amino sugar and nucleotide sugar metabolism	Cytoplasm	-1000	1000
ACM6PH	acgam6p[c] + lac__D[c] <=> acmum6p[c] + h2o[c]	Amino sugar and nucleotide sugar metabolism	Cytoplasm	-1000	1000
PGAMT	gam6p[c] <=> gam1p[c]	Amino sugar and nucleotide sugar metabolism	Cytoplasm	-1000	1000
G1PACT	accoa[c] + gam1p[c] --> coa[c] + h[c] + acgam1p[c]	Amino sugar and nucleotide sugar metabolism	Cytoplasm	0	1000
UAGDP	utp[c] + acgam1p[c] <=> ppi[c] + uacgam[c]	Amino sugar and nucleotide sugar metabolism	Cytoplasm	-1000	1000
UAG2E	uacgam[c] <=> uacmam[c]	Amino sugar and nucleotide sugar metabolism	Cytoplasm	-1000	1000
UAG2EMA	h2o[c] + uacgam[c] <=> acmana[c] + udp[c]	Amino sugar and nucleotide sugar metabolism	Cytoplasm	-1000	1000
ACGAM2E	acgam[c] <=> acmana[c]	Amino sugar and nucleotide sugar metabolism	Cytoplasm	-1000	1000
UAGCVT	uacgam[c] + pep[c] <=> pi[c] + uaccg[c]	Amino sugar and nucleotide sugar metabolism	Cytoplasm	-1000	1000
UAPGR	nadph[c] + h[c] + uaccg[c] --> nadp[c] + uamr[c]	Amino sugar and nucleotide sugar metabolism	Cytoplasm	0	1000
GLUR	glu__L[c] <=> glu__D[c]	D-Glutamine and D-glutamate metabolism	Cytoplasm	-1000	1000
UAMAS	atp[c] + ala__L[c] + uamr[c] --> adp[c] + pi[c] + h[c] + uama[c]	D-Glutamine and D-glutamate metabolism	Cytoplasm	0	1000
UAMAGS	atp[c] + glu__D[c] + uama[c] --> adp[c] + pi[c] + h[c] + uamag[c]	D-Glutamine and D-glutamate metabolism	Cytoplasm	0	1000
UAGAAT	uacgam[c] + 3hmrsACP[c] --> u3aga[c] + ACP[c]	Lipopolysaccharide biosynthesis	Cytoplasm	0	1000
UHGADA	h2o[c] + u3aga[c] <=> ac[c] + u3hga[c]	Lipopolysaccharide biosynthesis	Cytoplasm	-1000	1000
U23GAAT	u3hga[c] + 3hmrsACP[c] --> u23ga[c] + ACP[c] + h[c]	Lipopolysaccharide biosynthesis	Cytoplasm	0	1000
USHD	h2o[c] + u23ga[c] --> 2 h[c] + ump[c] + lipidX[c]	Lipopolysaccharide biosynthesis	Cytoplasm	0	1000
LPADSS	u23ga[c] + lipidX[c] <=> udp[c] + lipidAds[c]	Lipopolysaccharide biosynthesis	Cytoplasm	-1000	1000

TDSK	atp[c] + lipidAds[c] --> adp[c] + h[c] + lipidA[c]	Lipopolysaccharide biosynthesis	Cytoplasm	0	1000
ALAR	ala__L[c] <=> ala__D[c]	D-Alanine metabolism	Cytoplasm	-1000	1000
ALAALAR	atp[c] + 2 ala__D[c] --> adp[c] + pi[c] + h[c] + alaala[c]	D-Alanine metabolism	Cytoplasm	0	1000
UAAGDS	atp[c] + 26dap__M[c] + uamag[c] --> adp[c] + pi[c] + h[c] + ugmd[c]	Lysine biosynthesis	Cytoplasm	0	1000
UGMDDS	atp[c] + alaala[c] + ugmd[c] --> adp[c] + pi[c] + h[c] + ugmda[c]	Lysine biosynthesis	Cytoplasm	0	1000
UDCPDPS	8 ipdp[c] + frdp[c] --> 8 ppi[c] + 8 h[c] + udcpp[c]	Peptidoglycan biosynthesis	Cytoplasm	0	1000
UDCPDP	h2o[c] + udcpp[c] --> pi[c] + 2 h[c] + udcpp[c]	Peptidoglycan biosynthesis	Cytoplasm	0	1000
PAPPT3	udcpp[c] + ugmda[c] --> ump[c] + uagmda[c]	Peptidoglycan biosynthesis	Cytoplasm	0	1000
UAGPT3	uacgam[c] + uagmda[c] <=> udp[c] + uaagmda[c]	Peptidoglycan biosynthesis	Cytoplasm	-1000	1000
PPTGS_Ana	uaagmda[c] <=> udcpp[c] + peptido_ana[c]	Peptidoglycan biosynthesis	Cytoplasm	-1000	1000
SCHIZt	schiz[c] <=> schiz[e]	Transport	Extracellular	-1000	1000
EX_schiz_e	schiz[e] <=>	Exchange	Extracellular	0	1000
DM_amob_c	amob[c] <=>	Sink	Cytoplasm	0	1000
DM_etoh_c	etoh[c] <=>	Sink	Cytoplasm	0	1000
DM_dad_5_c	dad_5[c] <=>	Sink	Cytoplasm	0	1000
DM_co_c	co[c] <=>	Sink	Cytoplasm	0	1000
DM_4hba_c	4hba[c] <=>	Sink	Cytoplasm	0	1000
DM_dialurate_c	dialurate[c] <=>	Sink	Cytoplasm	0	1000
PECPBPS	39 h[c] + 49 ala__L[c] + 18 arg__L[c] + 22 asn__L[c] + 20 asp__L[c] + 7 cys__L[c] + 13 glu__L[c] + 11 gln__L[c] + 27 gly[c] + 4 his__L[c] + 16 ile__L[c] + 28 leu__L[c] + 13 lys__L[c] + 6 met__L[c] + 10 phe__L[c] + 8 pro__L[c] + 28 ser__L[c] + 13 thr__L[c] + 2 trp__L[c] + 16 tyr__L[c] + 23 val__L[c] + 2 phycy[c] + phyvi[c] <=> pecpbp[c] + 333 h2o[c]	Phycobiliproteins	Cytoplasm	-1000	1000
CPCPBPS	41 h[c] + 51 ala__L[c] + 20 arg__L[c] + 18 asn__L[c] + 19 asp__L[c] + 4 cys__L[c] + 16 glu__L[c] + 15 gln__L[c] + 27 gly[c] + 3 his__L[c] + 19 ile__L[c] + 29 leu__L[c] + 12 lys__L[c] + 5 met__L[c] + 8 phe__L[c] + 10 pro__L[c] + 22 ser__L[c] + 22 thr__L[c] + trp__L[c] + 14 tyr__L[c] + 21 val__L[c] + 3 phycy[c] <=> cpcpbp[c] + 335 h2o[c]	Phycobiliproteins	Cytoplasm	-1000	1000

APCPBPS	42 h[c] + 45 ala__L[c] + 19 arg__L[c] + 9 asn__L[c] + 20 asp__L[c] + 2 cys__L[c] + 18 glu__L[c] + 12 gln__L[c] + 28 gly[c] + 20 ile__L[c] + 31 leu__L[c] + 14 lys__L[c] + 7 met__L[c] + 4 phe__L[c] + 8 pro__L[c] + 20 ser__L[c] + 20 thr__L[c] + 20 tyr__L[c] + 26 val__L[c] + 2 phycy[c] <=> apcpbp[c] + 322 h2o[c]	Phycobiliproteins	Cytoplasm	-1000	1000
BOF_ANA_T	biomass_ana[c] <=> biomass_ana[e]	Transport	Cytoplasm	-1000	1000
DM_BOF_ANA	biomass_ana[e] <=>	Exchange	Extracellular	-1000	1000

B.2 Biomass equations for *Anabaena* sp. UTEX 2576

BOF_ANA_AUTO: Photoautotrophic biomass equation

0.343545571378618 ala__L[c] + 0.251585205023803 arg__L[c] + 0.161756832847017 asn__L[c] + 0.184719160175941 asp__L[c] + 0.0351879588535387 cys__L[c] + 0.282487290254007 glu__L[c] + 0.20618761787305 gln__L[c] + 0.26909068712621 gly[c] + 0.0659140486345752 his__L[c] + 0.242358896751124 ile__L[c] + 0.382587601380897 leu__L[c] + 0.211587552051987 lys__L[c] + 0.0980995860884037 met__L[c] + 0.137922918976174 phe__L[c] + 0.161777862296098 pro__L[c] + 0.248188294076941 ser__L[c] + 0.223924116421026 thr__L[c] + 0.0477269816304533 trp__L[c] + 0.119881515630401 tyr__L[c] + 0.275164331238067 val__L[c] + 0.00579899682604259 cyanphy[c] + 0.00453383150196182 datp[c] + 0.00318395641259673 dctp[c] + 0.00318442074456638 dgtp[c] + 0.0045294235579181 dttp[c] + 0.0194264344704913 ctp[c] + 0.0260469595905486 gtp[c] + 0.0182090321453034 utp[c] + 3.66611080635934E-05 pecpbbp[c] + 0.00285363017217725 cpcpbbp[c] + 0.000822095099355652 apcpbbp[c] + 0.00152531301762978 cholphy[a] + 0.00241876055914424 caro[c] + 0.000114076735760436 zeax[c] + 0.00175204140622158 echin[c] + 0.000563210670916585 avite1[c] + 2.55134255843932E-05 bvite[c] + 2.55134255843932E-05 gtocophe[c] + 0.000408034009524621 dtocophe[c] + 0.000164515117290348 cantxan[c] + 0.000499632619312097 phllqne[c] + 0.000412089921440229 kmyxlfuc[c] + 0.00038582823799093 myxlfuc[c] + 0.00576245345786342 mgdg60[c] + 0.013067449039366 mgdg100[c] + 0.000403587578124703 mgdg120[c] + 0.00333039785032683 mgdg140[c] + 0.0207291405893151 mgdg160[c] + 0.0114155215588366 mgdg161[c] + 0.000650058696358575 mgdg180[c] + 0.00441935133472286 mgdg181_9[c] + 0.00885568891760284 mgdg182_9_12[c] + 0.0133903276624423 mgdg183_9_12_15[c] + 0.00381338831770373 dgdg60[c] + 0.00864757657016868 dgdg100[c] + 0.000267080014935465 dgdg120[c] + 0.00220393975389275 dgdg140[c] + 0.013717813625282 dgdg160[c] + 0.00755438926687714 dgdg161[c] + 0.000430185902001998 dgdg180[c] + 0.00292457073621366 dgdg181_9[c] + 0.00586038237194305 dgdg182_9_12[c] + 0.00886124624720446 dgdg183_9_12_15[c] + 0.0033049365420099 sqdg60[c] + 0.00749456636081286 sqdg100[c] + 0.000231469346277403 sqdg120[c] + 0.00191008112004039 sqdg140[c] + 0.0118887718085778 sqdg160[c] + 0.00654713736462685 sqdg161[c] + 0.000372827781735065 sqdg180[c] + 0.00253462797138517 sqdg181_9[c] + 0.00507899805568398 sqdg182_9_12[c] + 0.0076797467475772 sqdg183_9_12_15[c] + 0.00406761420555065 pg60[c] + 0.00922408167484659 pg100[c] + 0.000284885349264496 pg120[c] + 0.00235086907081894 pg140[c] + 0.0146323345336342 pg160[c] + 0.00805801521800228 pg161[c] + 0.000458864962135465 pg180[c] + 0.0031195421186279 pg181_9[c] + 0.00625107453007259 pg182_9_12[c] + 0.00945199599701809 pg183_9_12_15[c] + 0.180724350841235 glc__D[c] + 0.0675484456351028 glycogen[c] + 0.0233737543428871 lipidA[c] + 0.078026731399405 peptido_ana[c] + 0.000214926258600788 10fthf[c] + 0.000215371822978115 5mthf[c] + 0.000268462958797713 accoa[c] + 9.1659435664868E-07 adocbl[c] + 0.000216391413108053 amet[c] + 7.12051719824053E-07 btn[c] + 0.000213921507968711 chor[c] + 0.00016103361853518 coa[c] + 0.000215291427819844 fad[c] + 0.000032843101393284 fol[c] + 0.000215137408743943 gthrd[c] + 0.000215349764281768 hemeO[c] + 3.00399259107229E-05 malcoa[c] + 0.000214894113496053 mlthf[c] + 0.000612331935428076 nac[c] + 0.00172152362350439 nad[c] + 4.30382889943805E-05 nadh[c] + 0.000107338135659093 nadp[c] + 0.00032201677832255 nadph[c] + 0.000387934128153945 pnto__R[c] + 0.000241798625667692 pHEME[c] + 0.000386577738616482 ptrc[c] + 2.73740396698289E-05 pydx5p[c] + 2.97874489127873E-05 ribflv[c] + 0.000193288810486435 spm[c] + 0.000773155579499096 spmd[c] + 9.44202617543905E-05 succoa[c] + 0.000214868463558524 thf[c] + 0.0000212418998997 thm[c] + 5.33222601422945E-05 udcpd[c] + 0.235572283876166 k[c] + 0.0109791264990248 nh4[c] + 0.152694982094824 mg2[c] + 0.0757203780428822 ca2[c] + 0.0102626511023355 fe2[c] + 0.00659808050293102 fe3[c] + 0.00292776706640663 cu2[c] + 0.00292776472155156 mn2[c] + 0.00292765723807457 mobd[c] + 0.00292776731480374 cobalt2[c] + 0.000240952731861566 zn2[c] + 0.00365970883300828 so4[c] + 0.00365970883300828 pi[c] + 0.0979513621699711 na1[c] + 54.0254881147118 atp[c] + 50.0527371090162 h2o[c] --> 54.0024311377245 adp[c] + 54.0024311377245 h[c] + 54.0024311377245 pi[c] + 0.102171035410607 ppi[c] + biomass_ana[c]

BOF_ANA_DIAZO: Photodiazotrophic biomass equation

0.387233097346666 ala_L[c] + 0.284639965500961 arg_L[c] + 0.180676981018473 asn_L[c] + 0.215325214437279 asp_L[c] + 0.0419644093150285 cys_L[c] + 0.32701562206501 glu_L[c] + 0.219972930778798 gln_L[c] + 0.317705787722262 gly[c] + 0.0751751780758606 his_L[c] + 0.275919833758181 ile_L[c] + 0.425479435719102 leu_L[c] + 0.255569237784526 lys_L[c] + 0.105492535056774 met_L[c] + 0.147737528729876 phe_L[c] + 0.187181760244793 pro_L[c] + 0.255548199696005 ser_L[c] + 0.25778253486385 thr_L[c] + 0.0505647875482449 trp_L[c] + 0.123855285896274 tyr_L[c] + 0.320467991370355 val_L[c] + 0.00246761284046439 cyanphy[c] + 0.0034386432740462 datp[c] + 0.00241484278767187 dctp[c] + 0.00241519495603183 dgtp[c] + 0.0034353001089701 dttp[c] + 0.0139084752680253 ctp[c] + 0.0186484809563325 gtp[c] + 0.0130368685840076 utp[c] + 0.000127970448363211 pecpbp[c] + 0.00105400004072789 cpcpbp[c] + 0.000243001897194655 apcpbp[c] + 0.0106460093638088 cholphy[a] + 0.00297013498598748 caro[c] + 0.000140081374606669 zeax[c] + 0.00215143225229311 echin[c] + 0.000550877784895961 avite1[c] + 2.49547462376118E-05 bvite[c] + 2.49547462376118E-05 gtocophe[c] + 0.000399099099033995 dtocophe[c] + 0.000202017559671461 cantxan[c] + 0.000488691931458769 phllqne[c] + 0.000506028878474641 kmyxfuc[c] + 0.000473780649310823 myxfuc[c] + 0.000430346162280911 mgdg60[c] + 0.0155835200970487 mgdg100[c] + 0.000481296320014625 mgdg120[c] + 0.003971649070556 mgdg140[c] + 0.0247204315084753 mgdg160[c] + 0.0091793817258235 mgdg161[c] + 0.000775224202401528 mgdg180[c] + 0.0031344596435818 mgdg181_9[c] + 0.0105608069183923 mgdg182_9_12[c] + 0.0159685673619325 mgdg183_9_12_15[c] + 0.000284787901509427 dgdg60[c] + 0.0103126235936351 dgdg100[c] + 0.000318504917656737 dgdg120[c] + 0.00262829717904441 dgdg140[c] + 0.016359109086491 dgdg160[c] + 0.00607459084797144 dgdg161[c] + 0.000513016016295128 dgdg180[c] + 0.00207427476413501 dgdg181_9[c] + 0.00698876928423019 dgdg182_9_12[c] + 0.0105674342836318 dgdg183_9_12_15[c] + 0.00024681618130817 sqdg60[c] + 0.00893760711448379 sqdg100[c] + 0.000276037595302506 sqdg120[c] + 0.00227785755517182 sqdg140[c] + 0.0141778945416255 sqdg160[c] + 0.00526464540157524 sqdg161[c] + 0.000444613880789111 sqdg180[c] + 0.00179770479558368 sqdg181_9[c] + 0.00605693337966616 sqdg182_9_12[c] + 0.00915844304581424 sqdg183_9_12_15[c] + 0.000303773761610055 pg60[c] + 0.0110001318332108 pg100[c] + 0.000339738578833853 pg120[c] + 0.0028035169909807 pg140[c] + 0.0174497163589237 pg160[c] + 0.00647956357116953 pg161[c] + 0.000547217084048137 pg180[c] + 0.00221255974841068 pg181_9[c] + 0.0074546872365122 pg182_9_12[c] + 0.0112719299025406 pg183_9_12_15[c] + 0.313999908347771 glc_D[c] + 0.0663438601123801 glycogen[c] + 0.0229569322261323 lipidA[c] + 0.0780186774113636 peptido_ana[c] + 0.000210219918350081 10fthf[c] + 0.000210655725996997 5mthf[c] + 0.000262584300521897 accoa[c] + 8.96523263696378E-07 adocbl[c] + 0.00021165298968763 amet[c] + 6.96459592126813E-07 btn[c] + 0.000209237169209922 chor[c] + 0.00015750739049044 coa[c] + 0.0002105770912889 fad[c] + 3.21239207261493E-05 fol[c] + 0.000210426444840341 gthrd[c] + 0.000210634150330184 hemeO[c] + 2.93821276809379E-05 malcoa[c] + 0.000210188477141655 mlthf[c] + 0.000598923418231247 nac[c] + 0.00168382662000845 nad[c] + 4.20958595623768E-05 nadh[c] + 0.000104987702577639 nadp[c] + 0.00031496542715174 nadph[c] + 0.000379439354114514 pnto_R[c] + 0.000236503848696493 pheme[c] + 0.000378112666069634 ptrc[c] + 2.67746175910131E-05 pydx5p[c] + 2.91351792892578E-05 ribflv[c] + 0.000189056275501059 spm[c] + 0.000756225432166032 spmd[c] + 9.23526973661674E-05 succoa[c] + 0.000210163388872738 thf[c] + 2.06616237765133E-05 thm[c] + 5.21546378108022E-05 udcpdp[c] + 0.230413848007161 k[c] + 0.0107387114594836 nh4[c] + 0.14935134905067 mg2[c] + 0.0740622937059472 ca2[c] + 0.0100379250578013 fe2[c] + 0.00645359926527066 fe3[c] + 0.00286365638919562 cu2[c] + 0.00286365409568693 mn2[c] + 0.00286354896582563 mobd[c] + 0.00286365663215346 cobalt2[c] + 0.00023567647782048 zn2[c] + 0.00357957048649452 so4[c] + 0.00357957048649452 pi[c] + 0.0958064756335687 na1[c] + 54.0189389222421 atp[c] + 49.5471228207962 h2o[c] --> 54.0024311377245 adp[c] + 54.0024311377245 h[c] + 54.0024311377245 pi[c] + 0.0738055904525844 ppi[c] + biomass_ana[c]

B.3 List of iDN1004 Metabolites

Table B.2 List of metabolites in iDN1004

Metabolites were named according to the BiGG standard. Formulas and charges are presented alongside the compartments where these compounds participate within the metabolic network

Abbreviation	Description	Formula	Charge	Compartment
10fthf[c]	10-Formyltetrahydrofolate	C20H21N7O7	-2	Cytoplasm
12dgr100[c]	1,2-Diacyl-sn-glycerol-didecanoyl	C23H44O5	0	Cytoplasm
12dgr120[c]	1,2-Diacyl-sn-glycerol (didodecanoyl, n-C12:0)	C27H52O5	0	Cytoplasm
12dgr140[c]	1,2-Diacyl-sn-glycerol (ditetradecanoyl, n-C14:0)	C31H60O5	0	Cytoplasm
12dgr160[c]	1,2-Diacyl-sn-glycerol (dihexadecanoyl, n-C16:0)	C35H68O5	0	Cytoplasm
12dgr161[c]	1,2-Diacyl-sn-glycerol (dihexadec-9-enoyl, n-C16:1)	C35H64O5	0	Cytoplasm
12dgr180[c]	1,2-Diacyl-sn-glycerol (dioctadecanoyl, n-C18:0)	C39H76O5	0	Cytoplasm
12dgr181_9[c]	1,2-Diacyl-sn-glycerol (dioctadec-9-enoyl, n-C18 1)	C39H72O5	0	Cytoplasm
12dgr182_9_12[c]	1,2-Diacyl-sn-glycerol (dioctadec-9-12-dienoyl, n-C18 2)	C39H68O5	0	Cytoplasm
12dgr183_9_12_15[c]	1,2-Diacyl-sn-glycerol (dioctadec-9-12-15-trienoyl, n-C18 3)	C39H64O5	0	Cytoplasm
12dgr60[c]	1,2-Diacyl-sn-glycerol-dihexanoyl	C15H28O5	0	Cytoplasm
12dgr80[c]	1,2-Diacyl-sn-glycerol-dioctanoyl	C19H36O5	0	Cytoplasm
13dampp[c]	1 3 Diaminopropane C3H12N2	C3H10N2	0	Cytoplasm
13dpg[c]	3-Phospho-D-glyceroyl phosphate	C3H4O10P2	-4	Cytoplasm
14dhncoa[c]	1,4-dihydroxy-2-naphthoyl-CoA	C32H38N7O19P3S	-4	Cytoplasm
14glucan[c]	1,4-alpha-D-glucan	C12H20O10	0	Cytoplasm
1acpc[c]	1-Aminocyclopropane-1-carboxylate	C4H7NO2	0	Cytoplasm
1ddecg3p[c]	1-dodecanoyl-sn-glycerol 3-phosphate	C15H29O7P	-2	Cytoplasm
1decg3p[c]	1-decanoyl-sn-glycerol-3-phosphate	C13H25O7P	-2	Cytoplasm
1hdec9eg3p[c]	1-hexadec-9-enoyl-sn-glycerol 3-phosphate	C19H35O7P	-2	Cytoplasm
1hdecg3p[c]	1-hexadecanoyl-sn-glycerol 3-phosphate	C19H37O7P	-2	Cytoplasm
1hexg3p[c]	1-hexanoyl-sn-glycerol-3-phosphate	C9H17O7P	-2	Cytoplasm

1hgcarote[c]	1'-Hydroxy-gamma-carotene	C40H58O	0	Cytoplasm
1ocg3p[c]	1-octanoyl-sn-glycerol-3-phosphate	C11H21O7P	-2	Cytoplasm
1odec91215eg3p[c]	1-octadec-9-12-15-trienoyl-sn-glycerol 3-phosphate	C21H35O7P	-2	Cytoplasm
1odec912eg3p[c]	1-octadec-9-12-dienoyl-sn-glycerol 3-phosphate	C21H37O7P	-2	Cytoplasm
1odec9eg3p[c]	1-octadec-9-enoyl-sn-glycerol 3-phosphate	C21H39O7P	-2	Cytoplasm
1odecg3p[c]	1-octadecanoyl-sn-glycerol 3-phosphate	C21H41O7P	-2	Cytoplasm
1pyr5c[c]	1-Pyrroline-5-carboxylate	C5H6NO2	-1	Cytoplasm
1tdecg3p[c]	1-tetradecanoyl-sn-glycerol 3-phosphate	C17H33O7P	-2	Cytoplasm
23dhmb[c]	(R)-2,3-Dihydroxy-3-methylbutanoate	C5H9O4	-1	Cytoplasm
23dhmp[c]	(R)-2,3-Dihydroxy-3-methylpentanoate	C6H11O4	-1	Cytoplasm
23dmggol[c]	2,3-dimethyl-6-geranylgeranyl-1,4-benzoquinol	C28H42O2	0	Cytoplasm
23dmphol[c]	2,3-Dimethyl-5-phytylquinol	C28H48O2	0	Cytoplasm
23dpg[c]	2 3 Disphospho D glycerate C3H3O10P2	C3H5O10P2	-3	Cytoplasm
24dab[c]	L-2,4-Diaminobutanoate	C4H10N2O2	0	Cytoplasm
25aics[c]	(S)-2-[5-Amino-1-(5-phospho-D-ribosyl)imidazole-4-carboxamido]succinate	C13H16N4O12P	-3	Cytoplasm
25dap3p[c]	2,5-Diaminopyrimidine nucleoside triphosphate	C9H15N5O14P3	-3	Cytoplasm
25dattop[c]	2,5-Diamino-6-(5-triphosphoryl-3,4-trihydroxy-2-oxopentyl)- amino-4-oxopyrimidine	C9H15N5O14P3	-3	Cytoplasm
25drapp[c]	2,5-Diamino-6-(ribosylamino)-4-(3H)-pyrimidinone 5'-phosphate	C9H14N5O8P	-2	Cytoplasm
26dap__M[c]	Meso-2,6-Diaminoheptanedioate	C7H14N2O4	0	Cytoplasm
26dap_LL[c]	LL-2,6-Diaminoheptanedioate	C7H14N2O4	0	Cytoplasm
2a3pp[c]	2-Amino-3-phosphonopropanoate	C4H6NO7P	-2	Cytoplasm
2ahbut[c]	(S)-2-Aceto-2-hydroxybutanoate	C6H9O4	-1	Cytoplasm
2ahethmpp[c]	2-(alpha-Hydroxyethyl)thiamine diphosphate	C14H20N4O8P2S	-2	Cytoplasm
2aobut[c]	L-2-Amino-3-oxobutanoate	C4H7NO3	0	Cytoplasm
2cpr5p[c]	1-(2-Carboxyphenylamino)-1-deoxy-D-ribulose 5-phosphate	C12H13NO9P	-3	Cytoplasm
2dda7p[c]	2-Dehydro-3-deoxy-D-arabino-heptonate 7-phosphate	C7H10O10P	-3	Cytoplasm
2ddg6p[c]	2-Dehydro-3-deoxy-D-gluconate 6-phosphate	C6H8O9P	-3	Cytoplasm
2dhglcn[c]	2-Dehydro-D-gluconate	C6H9O7	-1	Cytoplasm
2dhp[c]	2-Dehydropantoate	C6H9O4	-1	Cytoplasm
2dmmq8[c]	2-Demethylmenaquinone 8	C50H70O2	0	Cytoplasm

2dr5p[c]	2-Deoxy-D-ribose 5-phosphate	C5H9O7P	-2	Cytoplasm
2h3oppan[c]	2-Hydroxy-3-oxopropanoate	C3H3O4	-1	Cytoplasm
2ippm[c]	2-Isopropylmaleate	C7H8O4	-2	Cytoplasm
2kmb[c]	2-keto-4-methylthiobutyrate	C5H7O3S	-1	Cytoplasm
2m6ggol[c]	2-methyl-6-geranylgeranyl-1,4-benzoquinol	C27H40O2	0	Cytoplasm
2m6npol[c]	2-Methyl-6-solanyl-1,4-benzoquinol	C52H80O2	0	Cytoplasm
2m6phol[c]	2-Methyl-6-phytylquinol	C27H46O2	0	Cytoplasm
2mahmp[c]	2-Methyl-4-amino-5-hydroxymethylpyrimidine diphosphate	C6H9N3O7P2	-2	Cytoplasm
2mcacn[c]	Cis-2-Methylaconitate	C7H5O6	-3	Cytoplasm
2me4p[c]	2-C-methyl-D-erythritol 4-phosphate	C5H11O7P	-2	Cytoplasm
2mecdp[c]	2-C-methyl-D-erythritol 2,4-cyclodiphosphate	C5H10O9P2	-2	Cytoplasm
2mm[c]	2-Methylmaleate	C5H4O4	-2	Cytoplasm
2mm__R[c]	(R)-2-Methylmalate	C5H6O5	-2	Cytoplasm
2obut[c]	2-Oxobutanoate	C4H5O3	-1	Cytoplasm
2ohph[c]	2-Octaprenyl-6-hydroxyphenol	C46H70O2	0	Cytoplasm
2ombz[c]	2-Octaprenyl-6-methoxy-1,4-benzoquinone	C47H70O3	0	Cytoplasm
2omhmb[c]	2-Octaprenyl-3-methyl-5-hydroxy-6-methoxy-1,4-benzoquinone	C48H72O4	0	Cytoplasm
2ommb[c]	2-Octaprenyl-3-methyl-6-methoxy-1,4-benzoquinone	C48H72O3	0	Cytoplasm
2omph[c]	2-Octaprenyl-6-methoxyphenol	C47H72O2	0	Cytoplasm
2oph[c]	2-Octaprenylphenol	C46H70O	0	Cytoplasm
2p4c2me[c]	2-phospho-4-(cytidine 5'-diphospho)-2-C-methyl-D-erythritol	C14H22N3O17P3	-4	Cytoplasm
2pg[c]	D-Glycerate 2-phosphate	C3H4O7P	-3	Cytoplasm
2pglyc[c]	2-Phosphoglycolate	C2H2O6P	-3	Cytoplasm
2pglyc[cx]	2-Phosphoglycolate	C2H2O6P	-3	Carboxysome
2sephchc[c]	2-succinyl-5-enolpyruvyl-6-hydroxy-3-cyclohexene-1-carboxylate	C14H13O9	-3	Cytoplasm
2shchc[c]	2-Succinyl-6-hydroxy-2,4-cyclohexadiene-1-carboxylate	C11H10O6	-2	Cytoplasm
34hpp[c]	3-(4-Hydroxyphenyl)pyruvate	C9H7O4	-1	Cytoplasm
35cgmp[c]	3',5'-Cyclic GMP	C10H11N5O7P	-1	Cytoplasm
38ch2gtp[c]	(8S)-3',8-cyclo-7,8-dihydroguanosine 5'-triphosphate	C10H12N5O14P3	-4	Cytoplasm
3a2oxpp[c]	3-Amino-2-oxopropyl phosphate	C3H7NO5P	-1	Cytoplasm
3c2hmp[c]	3-Carboxy-2-hydroxy-4-methylpentanoate	C7H10O5	-2	Cytoplasm

3c3hmp[c]	3-Carboxy-3-hydroxy-4-methylpentanoate	C7H10O5	-2	Cytoplasm
3c4mop[c]	3-Carboxy-4-methyl-2-oxopentanoate	C7H8O5	-2	Cytoplasm
3dhq[c]	3-Dehydroquininate	C7H9O6	-1	Cytoplasm
3dhsk[c]	3-Dehydroshikimate	C7H7O5	-1	Cytoplasm
3hbutACP[c]	(R)-3-Hydroxybutanoyl-[acyl-carrier protein]	C15H27N2O9PRS	-1	Cytoplasm
3hdecACP[c]	(R)-3-Hydroxydodecanoyl-[acyl-carrier protein]	C23H43N2O9PRS	-1	Cytoplasm
3hdecACP[c]	(R)-3-Hydroxydecanoyl-[acyl-carrier protein]	C21H39N2O9PRS	-1	Cytoplasm
3hgmeACP[c]	3-Hydroxyglutaryl-ACP methyl ester	C17H29N2O11PRS	-1	Cytoplasm
3hhexACP[c]	(R)-3-Hydroxyhexanoyl-[acyl-carrier protein]	C17H31N2O9PRS	-1	Cytoplasm
3hmoa[c]	3-Hydroxy-3-methyl-2-oxobutanoic acid	C5H7O4	-1	Cytoplasm
3hmop[c]	(R)-3-Hydroxy-3-methyl-2-oxopentanoate	C6H9O4	-1	Cytoplasm
3hmrsACP[c]	(R)-3-Hydroxytetradecanoyl-[acyl-carrier protein]	C25H47N2O9PRS	-1	Cytoplasm
3hoctaACP[c]	(R)-3-Hydroxyoctadecanoyl-[acyl-carrier protein]	C29H55N2O9PRS	-1	Cytoplasm
3hoctACP[c]	(R)-3-Hydroxyoctanoyl-[acyl-carrier protein]	C19H35N2O9PRS	-1	Cytoplasm
3hpalmACP[c]	R-3-hydroxypalmitoyl-[acyl-carrier protein]	C27H51N2O9PRS	-1	Cytoplasm
3hpmeACP[c]	3-Hydroxypimeloyl-[acyl-carrier protein] methyl ester	C19H33N2O11PRS	-1	Cytoplasm
3ig3p[c]	C'-(3-Indolyl)-glycerol 3-phosphate	C11H12NO6P	-2	Cytoplasm
3mob[c]	3-Methyl-2-oxobutanoate	C5H7O3	-1	Cytoplasm
3mop[c]	(S)-3-Methyl-2-oxopentanoate	C6H9O3	-1	Cytoplasm
3oddecACP[c]	3-Oxododecanoyl-[acyl-carrier protein]	C23H41N2O9PRS	-1	Cytoplasm
3odecACP[c]	3-Oxodecanoyl-[acyl-carrier protein]	C21H37N2O9PRS	-1	Cytoplasm
3ohexACP[c]	3-Oxohexanoyl-[acyl-carrier protein]	C17H29N2O9PRS	-1	Cytoplasm
3omrsACP[c]	3-Oxotetradecanoyl-[acyl-carrier protein]	C25H45N2O9PRS	-1	Cytoplasm
3ooctACP[c]	3-Oxoctanoyl-[acyl-carrier protein]	C19H33N2O9PRS	-1	Cytoplasm
3ooctdACP[c]	3-Oxoctadecanoyl-[acyl-carrier protein]	C29H53N2O9PRS	-1	Cytoplasm
3opalmACP[c]	3-Oxohexadecanoyl-[acyl-carrier protein]	C27H49N2O9PRS	-1	Cytoplasm
3ophb[c]	3-Octaprenyl-4-hydroxybenzoate	C47H69O3	-1	Cytoplasm
3pg[c]	3-Phospho-D-glycerate	C3H4O7P	-3	Cytoplasm
3pg[cx]	3-Phospho-D-glycerate	C3H4O7P	-3	Carboxysome
3php[c]	3-Phosphohydroxypyruvate	C3H2O7P	-3	Cytoplasm
3psme[c]	5-O-(1-Carboxyvinyl)-3-phosphoshikimate	C10H9O10P	-4	Cytoplasm

4abut[c]	4-Aminobutanoate	C4H9NO2	0	Cytoplasm
4abz[c]	4-Aminobenzoate	C7H6NO2	-1	Cytoplasm
4adcho[c]	4-amino-4-deoxychorismate	C10H10NO5	-1	Cytoplasm
4ahmmp[c]	4-Amino-5-hydroxymethyl-2-methylpyrimidine	C6H9N3O	0	Cytoplasm
4ampm[c]	4-Amino-2-methyl-5-phosphomethylpyrimidine	C6H8N3O4P	-2	Cytoplasm
4c2me[c]	4-(cytidine 5'-diphospho)-2-C-methyl-D-erythritol	C14H23N3O14P2	-2	Cytoplasm
4gudbd[c]	4 Guanidinobutanamide C5H13N4O	C5H13N4O	1	Cytoplasm
4gudbutn[c]	4 Guanidinobutanoate C5H11N3O2	C5H11N3O2	0	Cytoplasm
4hba[c]	4-Hydroxy-benzyl alcohol	C7H8O2	0	Cytoplasm
4hbz[c]	4-Hydroxybenzoate	C7H5O3	-1	Cytoplasm
4hthdp[c]	(2S,4S)-4-Hydroxy-2,3,4,5-tetrahydrodipicolinate	C7H7NO5	-2	Cytoplasm
4hthr[c]	4-Hydroxy-L-threonine	C4H9NO4	0	Cytoplasm
4mhetz[c]	4-Methyl-5-(2-hydroxyethyl)-thiazole	C6H9NOS	0	Cytoplasm
4mop[c]	4-Methyl-2-oxopentanoate	C6H9O3	-1	Cytoplasm
4mpetz[c]	4-Methyl-5-(2-phosphoethyl)-thiazole	C6H8NO4PS	-2	Cytoplasm
4pasp[c]	4-Phospho-L-aspartate	C4H6NO7P	-2	Cytoplasm
4per[c]	4-Phospho-D-erythronate	C4H6O8P	-3	Cytoplasm
4ppan[c]	D-4'-Phosphopantothenate	C9H15NO8P	-3	Cytoplasm
4ppcys[c]	N-((R)-4-Phosphopantothenoyl)-L-cysteine	C12H20N2O9PS	-3	Cytoplasm
4r5au[c]	4-(1-D-Ribitylamino)-5-aminouracil	C9H16N4O6	0	Cytoplasm
5aizc[c]	5-amino-1-(5-phospho-D-ribosyl)imidazole-4-carboxylate	C9H12N3O9P	-2	Cytoplasm
5aop[c]	5-Amino-4-oxopentanoate	C5H9NO3	0	Cytoplasm
5aprbu[c]	5-Amino-6-(5'-phosphoribitylamino)uracil	C9H15N4O9P	-2	Cytoplasm
5apru[c]	5-Amino-6-(5'-phosphoribosylamino)uracil	C9H13N4O9P	-2	Cytoplasm
5caiz[c]	5-phosphoribosyl-5-carboxyaminoimidazole	C9H12N3O9P	-2	Cytoplasm
5easeln[c]	5-epi-alpha-selinene	C15H24	0	Cytoplasm
5fthf[c]	5-Formyltetrahydrofolate	C20H21N7O7	-2	Cytoplasm
5g2op[c]	5-Guanidino-2-oxopentanoate	C6H11N3O3	0	Cytoplasm
5mdr1p[c]	5-Methylthio-5-deoxy-D-ribose 1-phosphate	C6H11O7PS	-2	Cytoplasm
5mdru1p[c]	5-Methylthio-5-deoxy-D-ribose 1-phosphate	C6H11O7PS	-2	Cytoplasm
5mta[c]	5-Methylthioadenosine	C11H15N5O3S	0	Cytoplasm

5mthf[c]	5-Methyltetrahydrofolate	C20H23N7O6	-2	Cytoplasm
5oxpro[c]	5-Oxoproline	C5H6NO3	-1	Cytoplasm
5prdmzb[c]	N1-(5-Phospho-alpha-D-ribosyl)-5,6-dimethylbenzimidazole	C14H17N2O7P	-2	Cytoplasm
6hmhpt[c]	6-hydroxymethyl dihydropterin	C7H9N5O2	0	Cytoplasm
6hmhptpp[c]	6-hydroxymethyl-dihydropterin pyrophosphate	C7H9N5O8P2	-2	Cytoplasm
6pgc[c]	6-Phospho-D-gluconate	C6H10O10P	-3	Cytoplasm
6pgl[c]	6-phospho-D-glucono-1,5-lactone	C6H9O9P	-2	Cytoplasm
6pthp[c]	6-Pyruvoyl-5,6,7,8-tetrahydropterin	C9H11N5O3	0	Cytoplasm
8aonn[c]	8-Amino-7-oxononanoate	C9H17NO3	0	Cytoplasm
aact[c]	Aminoacetone	C3H8NO	1	Cytoplasm
ac[c]	Acetate	C2H3O2	-1	Cytoplasm
acACP[c]	Acetyl-ACP	C13H23N2O8PRS	-1	Cytoplasm
acadl[c]	Acetyl adenylate	C12H15N5O8P	-1	Cytoplasm
acald[c]	Acetaldehyde	C2H4O	0	Cytoplasm
accitr__L[c]	N-Acetyl-L-citrulline	C8H14N3O4	-1	Cytoplasm
accoa[c]	Acetyl-CoA	C23H34N7O17P3S	-4	Cytoplasm
accp[c]	Apo-carboxylase	C7H13N3O2R2	0	Cytoplasm
acg5p[c]	N-Acetyl-L-glutamyl 5-phosphate	C7H9NO8P	-3	Cytoplasm
acg5sa[c]	N-Acetyl-L-glutamate 5-semialdehyde	C7H10NO4	-1	Cytoplasm
acgam[c]	N-Acetyl-D-glucosamine	C8H15NO6	0	Cytoplasm
acgam1p[c]	N-Acetyl-D-glucosamine 1-phosphate	C8H14NO9P	-2	Cytoplasm
acgam6p[c]	N-Acetyl-D-glucosamine 6-phosphate	C8H14NO9P	-2	Cytoplasm
acglu[c]	N-Acetyl-L-glutamate	C7H9NO5	-2	Cytoplasm
achms[c]	O Acetyl L homoserine C6H11NO4	C6H11NO4	0	Cytoplasm
acmana[c]	N-Acetyl-D-mannosamine	C8H15NO6	0	Cytoplasm
acmum6p[c]	N-acetylmuramate 6-phosphate	C11H17NO11P	-3	Cytoplasm
acon[c][c]	Aconitate	C6H3O6	-3	Cytoplasm
acorn[c]	N2-Acetyl-L-ornithine	C7H14N2O3	0	Cytoplasm
ACP[c]	Acyl carrier protein	C11H21N2O7PRS	-1	Cytoplasm
acser[c]	O-Acetyl-L-serine	C5H9NO4	0	Cytoplasm
actACP[c]	Acetoacetyl-ACP	C15H25N2O9PRS	-1	Cytoplasm

actp[c]	Acetyl phosphate	C2H3O5P	-2	Cytoplasm
adcobdam[c]	Adenosyl cobyrate diamide	C55H71CoN11O15	-1	Cytoplasm
adcobhex[c]	Adenosyl-cobyric acid	C55H79CoN15O11	3	Cytoplasm
ade[c]	Adenine	C5H5N5	0	Cytoplasm
adn[c]	Adenosine	C10H13N5O4	0	Cytoplasm
adocbi[c]	Adenosyl cobinamide	C58H87CoN16O11	4	Cytoplasm
adocbip[c]	Adenosyl cobinamide phosphate	C58H86CoN16O14P	2	Cytoplasm
adocbl[c]	Adenosylcobalamin	C72H102CoN18O17P	2	Cytoplasm
adocbl[e]	Adenosylcobalamin	C72H102CoN18O17P	2	Extracellular
adp[c]	ADP C10H12N5O10P2	C10H13N5O10P2	-2	Cytoplasm
adpglc[c]	ADPGlucose C16H23N5O15P2	C16H23N5O15P2	-2	Cytoplasm
adprib[c]	ADPribose C15H21N5O14P2	C15H21N5O14P2	-2	Cytoplasm
afnse[c]	alpha-Farnesene	C15H24	0	Cytoplasm
agdpcci[c]	Adenosine-GDP-cobinamide	C68H97CoN21O21P2	1	Cytoplasm
agm[c]	Agmatine	C5H16N4	2	Cytoplasm
ahcys[c]	S-Adenosyl-L-homocysteine	C14H20N6O5S	0	Cytoplasm
ahdt[c]	2-Amino-4-hydroxy-6-(erythro-1,2,3-trihydroxypropyl) dihydropteridine triphosphate	C9H13N5O13P3	-3	Cytoplasm
aicar[c]	5-Amino-1-(5-Phospho-D-ribosyl)imidazole-4-carboxamide	C9H13N4O8P	-2	Cytoplasm
air[c]	5-amino-1-(5-phospho-D-ribosyl)imidazole	C8H13N3O7P	-1	Cytoplasm
akg[c]	2-Oxoglutarate	C5H4O5	-2	Cytoplasm
ala__D[c]	D-Alanine	C3H7NO2	0	Cytoplasm
ala__L[c]	L-Alanine	C3H7NO2	0	Cytoplasm
ala_B[c]	Beta-Alanine	C3H7NO2	0	Cytoplasm
alaala[c]	D-Alanyl-D-alanine	C6H12N2O3	0	Cytoplasm
alac__S[c]	(S)-2-Acetolactate	C5H7O4	-1	Cytoplasm
amet[c]	S-Adenosyl-L-methionine	C15H23N6O5S	1	Cytoplasm
ametam[c]	S-Adenosylmethioninamine	C14H24N6O3S	2	Cytoplasm
amob[c]	S-Adenosyl-4-methylthio-2-oxobutanoate	C15H19N5O6S	0	Cytoplasm
amp[c]	AMP C10H12N5O7P	C10H12N5O7P	-2	Cytoplasm
amylose[c]	Amylose	C6H10O5	0	Cytoplasm
anth[c]	Anthranilate	C7H6NO2	-1	Cytoplasm

ap4a[c]	P1,P4-Bis(5'-adenosyl) tetraphosphate	C20H24N10O19P4	-4	Cytoplasm
apcpbp[c]	Allophycocyanin Anabaena sp. UTEX 2576	C1594H2572N423O493S9	33	Cytoplasm
apoACP[c]	Apoprotein [acyl carrier protein]	HOR	0	Cytoplasm
appl[c]	1-Aminopropan-2-ol	C3H10NO	1	Cytoplasm
applp[c]	D-1-Aminopropan-2-ol O-phosphate	C3H9NO4P	-1	Cytoplasm
aps[c]	Adenosine 5'-phosphosulfate	C10H12N5O10PS	-2	Cytoplasm
arg__L[c]	L-Arginine	C6H15N4O2	1	Cytoplasm
arg__L[e]	L-Arginine	C6H15N4O2	1	Extracellular
argsuc[c]	N(omega)-(L-Arginino)succinate	C10H17N4O6	-1	Cytoplasm
asn__L[c]	L-Asparagine	C4H8N2O3	0	Cytoplasm
asp__L[c]	L-Aspartate	C4H6NO4	-1	Cytoplasm
asp__L_arg__L[c]	L-aspartate-L-arginine dimer	C10H19N5O5	0	Cytoplasm
aspsa[c]	L-Aspartate 4-semialdehyde	C4H7NO3	0	Cytoplasm
atocotri[c]	Alpha-Tocotrienol	C29H44O2	0	Cytoplasm
atp[c]	ATP C10H12N5O13P3	C10H13N5O13P3	-3	Cytoplasm
avite1[c]	Alpha-Tocopherol	C29H50O2	0	Cytoplasm
b14glucan[c]	Cellulose (beta-1,4-glucan)	C12H20O10	0	Cytoplasm
bcryptox[c]	Beta-Cryptoxanthin	C40H56O	0	Cytoplasm
bh4o4[c]	Tetrahydroxyborate	BH4O4	-1	Cytoplasm
bh4o4[e]	Tetrahydroxyborate	BH4O4	-1	Extracellular
bilirub[c]	Bilirubin cytosol	C33H34N4O6	-2	Cytoplasm
biliverd[c]	Biliverdin cytosol	C33H32N4O6	-2	Cytoplasm
biomass_ana[c]	Biomass Anabaena sp. UTEX 2576	n.d		Cytoplasm
biomass_ana[e]	Biomass Anabaena sp. UTEX 2576	n.d		Extracellular
btamp[c]	Biotinyl 5 AMP C20H27N7O9PS	C20H27N7O9PS	-1	Cytoplasm
btn[c]	Biotin	C10H15N2O3S	-1	Cytoplasm
btnCCP[c]	Holo-[carboxylase]	C17H27N5O4SR2	0	Cytoplasm
btocotri[c]	Beta-Tocotrienol	C28H42O2	0	Cytoplasm
but2eACP[c]	But-2-enoyl-[acyl-carrier protein]	C15H25N2O8PRS	-1	Cytoplasm
butACP[c]	Butyryl acyl carrier protein	C15H27N2O8PRS	-1	Cytoplasm
bvite[c]	Beta-Tocopherol	C28H48O2	0	Cytoplasm

ca2[c]	Calcium	Ca	2	Cytoplasm
ca2[e]	Calcium	Ca	2	Extracellular
camp[c]	CAMP C10H11N5O6P	C10H11N5O6P	-1	Cytoplasm
cantxan[c]	Canthaxanthin	C40H52O2	0	Cytoplasm
caro[c]	Beta-Carotene	C40H56	0	Cytoplasm
cbasp[c]	N-Carbamoyl-L-aspartate	C5H6N2O5	-2	Cytoplasm
cbi[c]	Cobinamide	C48H75CoN11O8	3	Cytoplasm
cbm[c]	Carbamate	CH2NO2	-1	Cytoplasm
cbp[c]	Carbamoyl phosphate	CH2NO5P	-2	Cytoplasm
cdg[c]	7-deaza-7-carboxyguanine	C7H5N4O3	-1	Cytoplasm
cdp[c]	CDP C9H12N3O11P2	C9H13N3O11P2	-2	Cytoplasm
cdpdddecg[c]	CDP-1,2-didodecanoylglycerol	C36H63N3O15P2	-2	Cytoplasm
cdpddecg[c]	CDP-1,2-didecanoylglycerol	C32H55N3O15P2	-2	Cytoplasm
cdpdhdec9eg[c]	CDP-1,2-dihexadec-9-enoylglycerol	C44H75N3O15P2	-2	Cytoplasm
cdpdhdecg[c]	CDP-1,2-dihexadecanoylglycerol	C44H79N3O15P2	-2	Cytoplasm
cdpdhexg[c]	CDP-1,2-dihexanoylglycerol	C24H39N3O15P2	-2	Cytoplasm
cdpdocg[c]	CDP-1,2-dioctanoylglycerol	C28H47N3O15P2	-2	Cytoplasm
cdpdodec91215eg[c]	CDP-1,2-dioctadec-9-12-15-trienoylglycerol	C48H75N3O15P2	-2	Cytoplasm
cdpdodec912eg[c]	CDP-1,2-dioctadec-9-12-dienoylglycerol	C48H79N3O15P2	-2	Cytoplasm
cdpdodec9eg[c]	CDP-1,2-dioctadec-9-enoylglycerol	C48H83N3O15P2	-2	Cytoplasm
cdpdodecg[c]	CDP-1,2-dioctadecanoylglycerol	C48H87N3O15P2	-2	Cytoplasm
cdpdtdecg[c]	CDP-1,2-ditetradecanoylglycerol	C40H71N3O15P2	-2	Cytoplasm
cdpglc[c]	CDP-glucose	C15H23N3O16P2	-2	Cytoplasm
cgly[c]	Cys Gly C5H10N2O3S	C5H10N2O3S	0	Cytoplasm
chlId[c]	Chlorophyllide a	C35H32MgN4O5	-2	Cytoplasm
cholphy[a]	Chlorophyll a	C55H72MgN4O5	0	Cytoplasm
chor[c]	Chorismate	C10H8O6	-2	Cytoplasm
cisphytoe[c]	15-cis-Phytoene	C40H64	0	Cytoplasm
cit[c]	Citrate	C6H5O7	-3	Cytoplasm
cit[e]	Citrate	C6H5O7	-3	Extracellular

citr__L[c]	L-Citrulline	C6H13N3O3	0	Cytoplasm
cmp[c]	CMP C9H12N3O8P	C9H12N3O8P	-2	Cytoplasm
co[c]	Carbon monoxide	CO	0	Cytoplasm
co1dam[c]	Cob(II)yrinate a,c diamide	C45H59CoN6O12	-2	Cytoplasm
co2[c]	CO2 CO2	CO2	0	Cytoplasm
co2[cx]	CO2 CO2	CO2	0	Carboxysome
co2[e]	CO2 CO2	CO2	0	Extracellular
co2[p]	CO2 CO2	CO2	0	Periplasm
coa[c]	Coenzyme A	C21H32N7O16P3S	-4	Cytoplasm
cob2nda[c]	Cob-II-yrinate-a-c-diamide	C45H59CoN6O12	-1	Cytoplasm
cobalt2[c]	Co2+	Co	2	Cytoplasm
cobalt2[e]	Co2+	Co	2	Extracellular
coby[a]	Cobyrinate	C45H55CoN4O14	-3	Cytoplasm
codhpre6[c]	Cobalt-dihydro-precorrin 6	C44H48CoN4O16	-6	Cytoplasm
codscl5a[c]	Cobalt-precorrin-5a	C45H46CoN4O16	-6	Cytoplasm
codscl5b[c]	Cobalt-precorrin-5b	C43H44CoN4O16	-6	Cytoplasm
codscl7[c]	Cobalt-precorrin-7	C45H50CoN4O16	-6	Cytoplasm
codscl8x[c]	Cobalt-precorrin-8x	C45H53CoN4O14	-5	Cytoplasm
cofac3[c]	Cobalt-factor III	C43H46CoN4O16	0	Cytoplasm
copre2[c]	Cobalt-precorrin-2	C42H36CoN4O16	-8	Cytoplasm
copre3[c]	Cobalt-precorrin 3	C43H41CoN4O16	-7	Cytoplasm
copre4[c]	Cobalt-precorrin 4	C44H44CoN4O16	-6	Cytoplasm
copre6[c]	Cobalt-precorrin 6	C44H46CoN4O16	-6	Cytoplasm
cpcbp[c]	C-Phycocyanin Anabaena sp. UTEX 2576	C1662H2648N460O516S9	32	Cytoplasm
cph4[c]	6-carboxy-5,6,7,8-tetrahydropterin	C7H8N5O3	-1	Cytoplasm
cphytfl[c]	15,9'-dicis-Phytofluene	C40H62	0	Cytoplasm
cpmp[c]	Cyclic pyranopterin monophosphate	C10H13N5O8P	-1	Cytoplasm
cpp3[c]	Coproporphyrin III	C36H34N4O8	2	Cytoplasm
cpppg3[c]	Coproporphyrinogen III	C36H40N4O8	-4	Cytoplasm
csn[c]	Cytosine	C4H5N3O	0	Cytoplasm
ctp[c]	CTP C9H12N3O14P3	C9H13N3O14P3	-3	Cytoplasm

cu2[c]	Copper	Cu	2	Cytoplasm
cu2[e]	Copper	Cu	2	Extracellular
cyanphy[c]	Cyanophycin (multi-Larginyl-poli [L--aspartic acid]) polimer (n+2)	C20H36N10O9	0	Cytoplasm
cynt[c]	Cyanate	CNO	-1	Cytoplasm
cynt[e]	Cyanate	CNO	-1	Extracellular
cys__L[c]	L-Cysteine	C3H7NO2S	0	Cytoplasm
cyst__L[c]	L-Cystathionine	C7H14N2O4S	0	Cytoplasm
cytd[c]	Cytidine	C9H13N3O5	0	Cytoplasm
dad_2[c]	Deoxyadenosine	C10H13N5O3	0	Cytoplasm
dad_5[c]	5'-Deoxyadenosine	C10H13N5O3	0	Cytoplasm
dadp[c]	DADP C10H12N5O9P2	C10H13N5O9P2	-2	Cytoplasm
damp[c]	DAMP C10H12N5O6P	C10H12N5O6P	-2	Cytoplasm
dann[c]	7,8-Diaminononanoate	C9H21N2O2	1	Cytoplasm
datp[c]	DATP C10H12N5O12P3	C10H13N5O12P3	-3	Cytoplasm
db4p[c]	3,4-dihydroxy-2-butanone 4-phosphate	C4H7O6P	-2	Cytoplasm
dcaACP[c]	Decanoyl-ACP (n-C10:0ACP)	C21H39N2O8PRS	-1	Cytoplasm
dcamp[c]	N6-(1,2-Dicarboxyethyl)-AMP	C14H14N5O11P	-4	Cytoplasm
dcdp[c]	DCDP C9H12N3O10P2	C9H13N3O10P2	-2	Cytoplasm
dcmp[c]	DCMP C9H12N3O7P	C9H12N3O7P	-2	Cytoplasm
dctp[c]	DCTP C9H12N3O13P3	C9H13N3O13P3	-3	Cytoplasm
dcyt[c]	Deoxycytidine	C9H13N3O4	0	Cytoplasm
dczcaro[c]	9,9-dicis-zeta-Carotene	C40H60	0	Cytoplasm
ddcaACP[c]	Dodecanoyl-ACP (n-C12:0ACP)	C23H43N2O8PRS	-1	Cytoplasm
ddhrb[c]	7,8-didemethyl-8-hydroxy-5-deazariboflavin	C16H19N3O7	2	Cytoplasm
dextrin[c]	Dextrin C12H20O10	C12H20O10	0	Cytoplasm
dgdg100[c]	Digalactosyl-diacylglycerol(n-C10-0)	C35H64O15	0	Cytoplasm
dgdg120[c]	Digalactosyl-diacylglycerol(n-C12-0)	C39H72O15	0	Cytoplasm
dgdg140[c]	Digalactosyl-diacylglycerol(n-C14-0)	C43H80O15	0	Cytoplasm
dgdg160[c]	Digalactosyl-diacylglycerol(n-C16)	C47H88O15	0	Cytoplasm
dgdg161[c]	Digalactosyl-diacylglycerol(n-C16 1)	C47H84O15	0	Cytoplasm
dgdg180[c]	Digalactosyl-diacylglycerol(n-C18 0)	C51H96O15	0	Cytoplasm

dgdg181_9[c]	Digalactosyl-diacylglycerol(n-C18 1)	C51H92O15	0	Cytoplasm
dgdg182_9_12[c]	Digalactosyl-diacylglycerol(n-C18 2)	C51H88O15	0	Cytoplasm
dgdg183_9_12_15[c]	Digalactosyl-diacylglycerol(n-C18 3)	C51H84O15	0	Cytoplasm
dgdg60[c]	Digalactosyl-diacylglycerol(n-C6-0)	C27H48O15	0	Cytoplasm
dgdg80[c]	Digalactosyl-diacylglycerol(n-C8-0)	C31H56O15	0	Cytoplasm
dgdp[c]	DGDP C10H12N5O10P2	C10H13N5O10P2	-2	Cytoplasm
dgmp[c]	DGMP C10H12N5O7P	C10H12N5O7P	-2	Cytoplasm
dgsn[c]	Deoxyguanosine	C10H13N5O4	0	Cytoplasm
dgtp[c]	DGTP C10H12N5O13P3	C10H13N5O13P3	-3	Cytoplasm
dha[c]	Dihydroxyacetone	C3H6O3	0	Cytoplasm
dhap[c]	Dihydroxyacetone phosphate	C3H5O6P	-2	Cytoplasm
dhf[c]	7,8-Dihydrofolate	C19H19N7O6	-2	Cytoplasm
dhmtp[c]	1,2-Dihydroxy-5-(methylthio)pent-1-en-3-one	C6H10O3S	0	Cytoplasm
dhna[c]	1,4-Dihydroxy-2-naphthoate	C11H7O4	-1	Cytoplasm
dhnpt[c]	Dihydroneopterin	C9H13N5O4	0	Cytoplasm
dhor__S[c]	(S)-Dihydroorotate	C5H5N2O4	-1	Cytoplasm
dhppm[c]	Dihydroneopterin monophosphate	C9H12N5O7P	-2	Cytoplasm
dhpt[c]	Dihydropteroate	C14H13N6O3	-1	Cytoplasm
dialurate[c]	Dialurate	C4H4N2O3	0	Cytoplasm
din[c]	Deoxyinosine	C10H12N4O4	0	Cytoplasm
dkmpp[c]	2,3-diketo-5-methylthio-1-phosphopentane	C6H9O6PS	-2	Cytoplasm
dmbzid[c]	5,6-Dimethylbenzimidazole	C9H10N2	0	Cytoplasm
dmlz[c]	6,7-Dimethyl-8-(1-D-ribityl)lumazine	C13H17N4O6	-1	Cytoplasm
dmpp[c]	Dimethylallyl diphosphate	C5H10O7P2	-2	Cytoplasm
dmtphlqne[c]	Demethylphyloquinone	C30H44O2	0	Cytoplasm
dnad[c]	Deamino-NAD+	C21H24N6O15P2	-2	Cytoplasm
dpcoa[c]	Dephospho-CoA	C21H33N7O13P2S	-2	Cytoplasm
dptrol[c]	Diplopterol	C30H52O	0	Cytoplasm
dptne[c]	Diploptene	C30H50	0	Cytoplasm
drib[c]	Deoxyribose C5H10O4	C5H10O4	0	Cytoplasm

dscI[c]	Dihydrosirohydrochlorin	C42H41N4O16	-7	Cytoplasm
dtbt[c]	Dethiobiotin	C10H17N2O3	-1	Cytoplasm
ddp[c]	DDP C10H13N2O11P2	C10H14N2O11P2	-2	Cytoplasm
ddp4d6dg[c]	DDP-4-dehydro-6-deoxy-D-glucose	C16H22N2O15P2	-2	Cytoplasm
ddpglc[c]	DDPglucose	C16H24N2O16P2	-2	Cytoplasm
ddprham[c]	DDP-4-dehydro-beta-L-rhamnose	C16H22N2O15P2	-2	Cytoplasm
ddprmn[c]	DDP-L-rhamnose	C16H24N2O15P2	-2	Cytoplasm
dtmp[c]	DTMP C10H13N2O8P	C10H13N2O8P	-2	Cytoplasm
dtocophe[c]	Delta-Tocopherol	C27H46O2	0	Cytoplasm
dtocotri[c]	Delta-Tocotrienol	C27H40O2	0	Cytoplasm
dttp[c]	DTTP C10H13N2O14P3	C10H14N2O14P3	-3	Cytoplasm
dudp[c]	DUDP C9H11N2O11P2	C9H12N2O11P2	-2	Cytoplasm
dump[c]	DUMP C9H11N2O8P	C9H11N2O8P	-2	Cytoplasm
duri[c]	Deoxyuridine	C9H12N2O5	0	Cytoplasm
duTP[c]	DUTP C9H11N2O14P3	C9H12N2O14P3	-3	Cytoplasm
dvchlda[c]	Divinyl chlorophyllide a	C35H31MgN4O5	-1	Cytoplasm
dvpchlld[c]	Divinylprotochlorophyllide	C35H29N4O5Mg	-1	Cytoplasm
dxyl5p[c]	1-deoxy-D-xylulose 5-phosphate	C5H9O7P	-2	Cytoplasm
e3mmal[c]	D-erythro-3-Methylmalate	C5H6O5	-2	Cytoplasm
e4p[c]	D-Erythrose 4-phosphate	C4H7O7P	-2	Cytoplasm
echin[c]	Echinenone	C40H54O	0	Cytoplasm
egmeACP[c]	Enoylglutaryl-[acyl-carrier protein] methyl ester	C17H27N2O10PRS	-1	Cytoplasm
eig3p[c]	D-erythro-1-(Imidazol-4-yl)glycerol 3-phosphate	C6H9N2O6P	-2	Cytoplasm
epmeACP[c]	Enoylpimeloyl-[acyl-carrier protein] methyl ester	C19H31N2O10PRS	-1	Cytoplasm
etoh[c]	Ethanol	C2H6O	0	Cytoplasm
f6p[c]	D-Fructose 6-phosphate	C6H11O9P	-2	Cytoplasm
fad[c]	Flavin adenine dinucleotide oxidized	C27H30N9O15P2	-3	Cytoplasm
fadh2[c]	Flavin adenine dinucleotide reduced	C27H33N9O15P2	-2	Cytoplasm
fald[c]	Formaldehyde	CH2O	0	Cytoplasm
fapn3p[c]	Formamidopyrimidine nucleoside triphosphate	C10H15N5O15P3	-3	Cytoplasm
fdp[c]	D-Fructose 1,6-bisphosphate	C6H10O12P2	-4	Cytoplasm

fdxo_2_2[c]	Oxidized ferredoxin	Fe2R4S6	6	Cytoplasm
fdxrd[c]	Reduced ferredoxin	Fe2R4S6	4	Cytoplasm
fe2[c]	Fe2+ mitochondria	Fe	2	Cytoplasm
fe2[e]	Fe2+ mitochondria	Fe	2	Extracellular
fe3[c]	Iron (Fe3+)	Fe	3	Cytoplasm
fe3[e]	Iron (Fe3+)	Fe	3	Extracellular
fe3[p]	Iron (Fe3+)	Fe	3	Periplasm
fgam[c]	N2-Formyl-N1-(5-phospho-D-ribosyl)glycinamide	C8H13N2O9P	-2	Cytoplasm
ficyc6[p]	Ferricytochrome c6	C33H30FeN4O4	3	Periplasm
ficyc6[u]	Ferricytochrome c6	C33H30FeN4O4	3	Thylakoid
fldox[c]	Flavodoxin (oxidized) - obsolete	R	0	Cytoplasm
fldrd[c]	Flavodoxin (reduced) - obsolete	R	-2	Cytoplasm
fmn[c]	FMN C17H19N4O9P	C17H18N4O9P	-3	Cytoplasm
fmnh2[c]	Reduced FMN	C17H21N4O9P	-2	Cytoplasm
focyc6[p]	Ferrocycytochrome c6	C33H30FeN4O4	2	Periplasm
focyc6[u]	Ferrocycytochrome c6	C33H30FeN4O4	2	Thylakoid
fol[c]	Folate	C19H18N7O6	-1	Cytoplasm
for[c]	Formate	CHO2	-1	Cytoplasm
fpram[c]	2-(Formamido)-N1-(5-phospho-D-ribosyl)acetamidine	C8H15N3O8P	-1	Cytoplasm
fprica[c]	5-Formamido-1-(5-phospho-D-ribosyl)imidazole-4-carboxamide	C10H13N4O9P	-2	Cytoplasm
frdp[c]	Farnesyl diphosphate	C15H26O7P2	-2	Cytoplasm
fru[c]	D-Fructose	C6H12O6	0	Cytoplasm
fum[c]	Fumarate	C4H2O4	-2	Cytoplasm
fum[e]	Fumarate	C4H2O4	-2	Extracellular
g15lac[c]	D Glucono 1 5 lactone C6H10O6	C6H10O6	0	Cytoplasm
g1p[c]	D-Glucose 1-phosphate	C6H11O9P	-2	Cytoplasm
g3p[c]	Glyceraldehyde 3-phosphate	C3H5O6P	-2	Cytoplasm
g6p[c]	D-Glucose 6-phosphate	C6H11O9P	-2	Cytoplasm
g6p_B[c]	Beta D glucose 6 phosphate C6H11O9P	C6H11O9P	-2	Cytoplasm
gam1p[c]	D-Glucosamine 1-phosphate	C6H13NO8P	-1	Cytoplasm
gam6p[c]	D-Glucosamine 6-phosphate	C6H13NO8P	-1	Cytoplasm

gar[c]	N1-(5-Phospho-D-ribosyl)glycinamide	C7H14N2O8P	-1	Cytoplasm
gcald[c]	Glycolaldehyde	C2H4O2	0	Cytoplasm
gcarote[c]	Gamma-Carotene	C40H56	0	Cytoplasm
gdp[c]	GDP C10H12N5O11P2	C10H13N5O11P2	-2	Cytoplasm
gdppdman[c]	GDP-4-dehydro-6-deoxy-D-mannose	C16H21N5O15P2	-2	Cytoplasm
gdpfuc[c]	GDP-L-fucose	C16H23N5O15P2	-2	Cytoplasm
gdpmann[c]	GDP-D-mannose	C16H23N5O16P2	-2	Cytoplasm
gdptp[c]	Guanosine 3'-diphosphate 5'-triphosphate	C10H11N5O20P5	-7	Cytoplasm
ggdp[c]	Geranylgeranyl diphosphate C20H33O7P2	C20H34O7P2	-2	Cytoplasm
glc__D[c]	D-Glucose	C6H12O6	0	Cytoplasm
glcglyc[c]	2-(beta-D-Glucosyl)-sn-glycerol	C9H18O8	0	Cytoplasm
glcglycp[c]	2-(beta-D-Glucosyl)-sn-glycerol 3-phosphate	C9H17O11P	-2	Cytoplasm
glcn[c]	D-Gluconate	C6H11O7	-1	Cytoplasm
glmeACP[c]	Glutaryl-[acp] methyl ester	C17H29N2O10PRS	-1	Cytoplasm
gln__L[c]	L-Glutamine	C5H10N2O3	0	Cytoplasm
gln__L[e]	L-Glutamine	C5H10N2O3	0	Extracellular
glu__D[c]	D-Glutamate	C5H8NO4	-1	Cytoplasm
glu__L[c]	L-Glutamate	C5H8NO4	-1	Cytoplasm
glu__L[e]	L-Glutamate	C5H8NO4	-1	Extracellular
glu1sa[c]	L-Glutamate 1-semialdehyde	C5H9NO3	0	Cytoplasm
glu5p[c]	L-Glutamate 5-phosphate	C5H8NO7P	-2	Cytoplasm
glu5sa[c]	L-Glutamate 5-semialdehyde	C5H9NO3	0	Cytoplasm
glucys[c]	Gamma-L-Glutamyl-L-cysteine	C8H13N2O5S	-1	Cytoplasm
glutrna[c]	L-Glutamyl-tRNA(Glu)	C15H19N6O6R	0	Cytoplasm
glx[c]	Glyoxylate	C2HO3	-1	Cytoplasm
gly[c]	Glycine	C2H5NO2	0	Cytoplasm
glyald[c]	D-Glyceraldehyde	C3H6O3	0	Cytoplasm
glyc[c]	Glycerol	C3H8O3	0	Cytoplasm
glyc[e]	Glycerol	C3H8O3	0	Extracellular
glyc__R[c]	(R)-Glycerate	C3H5O4	-1	Cytoplasm
glyc3p[c]	Glycerol 3-phosphate	C3H7O6P	-2	Cytoplasm

glyclt[c]	Glycolate C2H3O3	C2H3O3	-1	Cytoplasm
glycogen[c]	Glycogen C6H10O5	C18H30O15	0	Cytoplasm
gmp[c]	GMP C10H12N5O8P	C10H12N5O8P	-2	Cytoplasm
grdp[c]	Geranyl diphosphate	C10H18O7P2	-2	Cytoplasm
gsn[c]	Guanosine	C10H13N5O5	0	Cytoplasm
gthox[c]	Oxidized glutathione	C20H30N6O12S2	-2	Cytoplasm
gthrd[c]	Reduced glutathione	C10H16N3O6S	-1	Cytoplasm
gtocophe[c]	Gamma-Tocopherol	C28H48O2	0	Cytoplasm
gtocotri[c]	Gamma-Tocotrienol	C28H42O2	0	Cytoplasm
gtp[c]	GTP C10H12N5O14P3	C10H13N5O14P3	-3	Cytoplasm
gua[c]	Guanine	C5H5N5O	0	Cytoplasm
h[c]	H+	H	1	Cytoplasm
h[cx]	H+	H	1	Carboxysome
h[e]	H+	H	1	Extracellular
h[p]	H+	H	1	Periplasm
h[u]	H+	H	1	Thylakoid
h2[c]	Hydrogen	H2	0	Cytoplasm
h2[e]	Hydrogen	H2	0	Extracellular
h2[p]	Hydrogen	H2	0	Periplasm
h2mb4p[c]	1-hydroxy-2-methyl-2-(E)-butenyl 4-diphosphate	C5H10O8P2	-2	Cytoplasm
h2o[c]	H2O H2O	H2O	0	Cytoplasm
h2o[cx]	H2O H2O	H2O	0	Carboxysome
h2o[e]	H2O H2O	H2O	0	Extracellular
h2o[p]	H2O H2O	H2O	0	Periplasm
h2o[u]	H2O H2O	H2O	0	Thylakoid
h2o2[c]	Hydrogen peroxide	H2O2	0	Cytoplasm
h2s[c]	Hydrogen sulfide	HS	-1	Cytoplasm
HC01434[c]	Oxalatosuccinate(3-)	C6H3O7	-3	Cytoplasm
hct[c]	2 Hydroxybutane 1 2 4 tricarboxylate C7H7O7	C7H7O7	-3	Cytoplasm
hco3[c]	Bicarbonate	CHO3	-1	Cytoplasm
hco3[cx]	Bicarbonate	CHO3	-1	Carboxysome

hco3[e]	Bicarbonate	CHO3	-1	Extracellular
hcys__L[c]	L-Homocysteine	C4H9NO2S	0	Cytoplasm
hdeACP[c]	Cis-hexadec-9-enoyl-[acyl-carrier protein] (n-C16:1)	C27H49N2O8PRS	-1	Cytoplasm
hemeO[c]	Heme O C49H56FeN4O5	C49H56FeN4O5	-2	Cytoplasm
hexACP[c]	Hexanoyl acyl carrier protein	C17H31N2O8PRS	-1	Cytoplasm
hgbam[c]	Hydrogenobyrate a,c diamide	C45H60N6O12	-2	Cytoplasm
hgbyr[c]	Hydrogenobyrate	C45H56N4O14	-4	Cytoplasm
hgentis[c]	Homogentisate C8H7O4	C8H7O4	-1	Cytoplasm
his__L[c]	L-Histidine	C6H9N3O2	0	Cytoplasm
his__L[e]	L-Histidine	C6H9N3O2	0	Extracellular
hisp[c]	L-Histidinol phosphate	C6H11N3O4P	-1	Cytoplasm
histd[c]	L-Histidinol	C6H12N3O	1	Cytoplasm
histda[c]	L-histidinal	C6H10N3O	1	Cytoplasm
hmbil[c]	Hydroxymethylbilane	C40H38N4O17	-8	Cytoplasm
hmgth[c]	Hydroxymethylglutathione	C11H18N3O7S	-1	Cytoplasm
hmppp9[c]	13(1)-Hydroxy-magnesium-protoporphyrin IX 13-monomethyl ester	C35H33N4O5Mg	-1	Cytoplasm
hom__L[c]	L-Homoserine	C4H9NO3	0	Cytoplasm
hpyr[c]	Hydroxypyruvate	C3H3O4	-1	Cytoplasm
hxan[c]	Hypoxanthine	C5H4N4O	0	Cytoplasm
iasp[c]	Iminoaspartate	C4H3NO4	-2	Cytoplasm
ichor[c]	Isochorismate	C10H8O6	-2	Cytoplasm
icit[c]	Isocitrate	C6H5O7	-3	Cytoplasm
ile__L[c]	L-Isoleucine	C6H13NO2	0	Cytoplasm
ile__L[e]	L-Isoleucine	C6H13NO2	0	Extracellular
imacp[c]	3-(Imidazol-4-yl)-2-oxopropyl phosphate	C6H7N2O5P	-2	Cytoplasm
imp[c]	IMP C10H11N4O8P	C10H11N4O8P	-2	Cytoplasm
indole[c]	Indole	C8H7N	0	Cytoplasm
inost[c]	Myo-Inositol	C6H12O6	0	Cytoplasm
ins[c]	Inosine	C10H12N4O5	0	Cytoplasm
ipdp[c]	Isopentenyl diphosphate	C5H10O7P2	-2	Cytoplasm
itp[c]	ITP C10H11N4O14P3	C10H11N4O14P3	-4	Cytoplasm

k[c]	Potassium	K	1	Cytoplasm
k[e]	Potassium	K	1	Extracellular
kmyxlfuc[c]	ketomyxolfucoside	C46H64O8	0	Cytoplasm
lac__D[c]	D-Lactate	C3H5O3	-1	Cytoplasm
Largn[c]	L-Arogenate	C10H12NO5	-1	Cytoplasm
leu__L[c]	L-Leucine	C6H13NO2	0	Cytoplasm
leu__L[e]	L-Leucine	C6H13NO2	0	Extracellular
lgt__S[c]	(R)-S-Lactoylglutathione	C13H20N3O8S	-1	Cytoplasm
lipidA[c]	2,3,2'3'-Tetrakis(beta-hydroxymyristoyl)-D-glucosaminyl-1,6-beta-D-glucosamine 1,4'-bisphosphate	C68H126N2O23P2	-4	Cytoplasm
lipidAds[c]	Lipid A Disaccharide	C68H127N2O20P	-2	Cytoplasm
lipidX[c]	2,3-Bis(3-hydroxytetradecanoyl)-beta-D-glucosaminyl 1-phosphate	C34H64NO12P	-2	Cytoplasm
lycop[c]	Lycopene	C40H56	0	Cytoplasm
lys__L[c]	L-Lysine	C6H15N2O2	1	Cytoplasm
lys__L[e]	L-Lysine	C6H15N2O2	1	Extracellular
mal__L[c]	L-Malate	C4H4O5	-2	Cytoplasm
mal__L[e]	L-Malate	C4H4O5	-2	Extracellular
malACP[c]	Malonyl acyl carrier protein	C14H22N2O10PRS	-2	Cytoplasm
malcoa[c]	Malonyl CoA C24H33N7O19P3S	C24H33N7O19P3S	-5	Cytoplasm
malmeACP[c]	Malonyl-[acp] methyl ester	C15H25N2O10PRS	-1	Cytoplasm
malt[c]	Maltose C12H22O11	C12H22O11	0	Cytoplasm
man1p[c]	D-Mannose 1-phosphate	C6H11O9P	-2	Cytoplasm
man6p[c]	D-Mannose 6-phosphate	C6H11O9P	-2	Cytoplasm
meoh[c]	Methanol	CH4O	0	Cytoplasm
mercppyr[c]	Mercaptopyruvate	C3H3O3S	-1	Cytoplasm
met__L[c]	L-Methionine	C5H11NO2S	0	Cytoplasm
met__L[e]	L-Methionine	C5H11NO2S	0	Extracellular
methf[c]	5,10-Methenyltetrahydrofolate	C20H20N7O6	-1	Cytoplasm
mg2[c]	Magnesium	Mg	2	Cytoplasm
mg2[e]	Magnesium	Mg	2	Extracellular
mgdg100[c]	1,2-Diacyl-3-beta-D-galactosyl-sn-glycerol-(n-C10-0)	C29H54O10	0	Cytoplasm

mgdg120[c]	1,2-Diacyl-3-beta-D-galactosyl-sn-glycerol-(n-C12-0)	C33H62O10	0	Cytoplasm
mgdg140[c]	1,2-Diacyl-3-beta-D-galactosyl-sn-glycerol-(n-C14-0)	C37H70O10	0	Cytoplasm
mgdg160[c]	1,2-Diacyl-3-beta-D-galactosyl-sn-glycerol (n-C16)	C41H78O10	0	Cytoplasm
mgdg161[c]	1,2-Diacyl-3-beta-D-galactosyl-sn-glycerol (n-C16 1)	C41H74O10	0	Cytoplasm
mgdg180[c]	1,2-Diacyl-3-beta-D-galactosyl-sn-glycerol (n-C18 0)	C45H86O10	0	Cytoplasm
mgdg181_9[c]	1,2-Diacyl-3-beta-D-galactosyl-sn-glycerol (n-C18 1)	C45H82O10	0	Cytoplasm
mgdg182_9_12[c]	1,2-Diacyl-3-beta-D-galactosyl-sn-glycerol (n-C18 2)	C45H78O10	0	Cytoplasm
mgdg183_9_12_15[c]	1,2-Diacyl-3-beta-D-galactosyl-sn-glycerol (n-C18 3)	C45H74O10	0	Cytoplasm
mgdg60[c]	1,2-Diacyl-3-beta-D-galactosyl-sn-glycerol-(n-C6-0)	C21H38O10	0	Cytoplasm
mgdg80[c]	1,2-Diacyl-3-beta-D-galactosyl-sn-glycerol-(n-C8-0)	C25H46O10	0	Cytoplasm
mi1p__D[c]	1D-myo-Inositol 1-phosphate	C6H11O9P	-2	Cytoplasm
micit[c]	Methylisocitrate	C7H7O7	-3	Cytoplasm
mlthf[c]	5,10-Methylenetetrahydrofolate	C20H21N7O6	-2	Cytoplasm
mn2[c]	Manganese	Mn	2	Cytoplasm
mn2[e]	Manganese	Mn	2	Extracellular
moamp[c]	MoaD Protein with bound AMP	C11H12N5O8PR	-1	Cytoplasm
moacoo[c]	MoaD Protein with carboxylate	CO2R	-1	Cytoplasm
moacosh[c]	MoaD Protein with thiocarboxylate	CHOSR	0	Cytoplasm
mobd[c]	Molybdate	MoO4	-2	Cytoplasm
mobd[e]	Molybdate	MoO4	-2	Extracellular
mppp9[c]	Magnesium protoporphyrin	C34H30N4O4Mg	-2	Cytoplasm
mppp9om[c]	Magnesium protoporphyrin monomethyl ester	C35H33N4O4Mg	-1	Cytoplasm
mpt[c]	Molybdopterin	C10H12N5O6PS2	-2	Cytoplasm
mql8[c]	Menaquinol 8	C51H74O2	0	Cytoplasm
mql8[p]	Menaquinol 8	C51H74O2	0	Periplasm
mqn8[c]	Menaquinone 8	C51H72O2	0	Cytoplasm
mqn8[p]	Menaquinone 8	C51H72O2	0	Periplasm
mthgx[c]	Methylglyoxal	C3H4O2	0	Cytoplasm
mtp[c]	3-methylthiopropionate	C4H8O2S	0	Cytoplasm
myrACP[c]	Myristoyl-ACP (n-C14:0ACP)	C25H47N2O8PRS	-1	Cytoplasm

myxl[c]	myxol	C40H56O3	0	Cytoplasm
myxlfuc[c]	myxolfucoside	C46H66O7	0	Cytoplasm
n2[c]	Nitrogen	N2	0	Cytoplasm
n2[e]	Nitrogen	N2	0	Extracellular
n2[p]	Nitrogen	N2	0	Periplasm
na1[c]	Sodium	Na	1	Cytoplasm
na1[e]	Sodium	Na	1	Extracellular
na[c]	Nicotinate	C6H4NO2	-1	Cytoplasm
Nacasp[c]	N-Acetyl-L-aspartate	C6H7NO5	-2	Cytoplasm
nachapp[c]		C5H12N2O2	0	Cytoplasm
nad[c]	Nicotinamide adenine dinucleotide	C21H26N7O14P2	-1	Cytoplasm
nadh[c]	Nicotinamide adenine dinucleotide - reduced	C21H27N7O14P2	-2	Cytoplasm
nadp[c]	Nicotinamide adenine dinucleotide phosphate	C21H25N7O17P3	-3	Cytoplasm
nadph[c]	Nicotinamide adenine dinucleotide phosphate - reduced	C21H26N7O17P3	-4	Cytoplasm
ncachapp[c]		C11H16N2O8	-2	Cytoplasm
ncam[c]	Nicotinamide	C6H6N2O	0	Cytoplasm
neuspn[c]	Neurosporene	C40H58	0	Cytoplasm
nh4[c]	Ammonium	H4N	1	Cytoplasm
nh4[e]	Ammonium	H4N	1	Extracellular
nh4[p]	Ammonium	H4N	1	Periplasm
nhapp[c]		C3H10N2O	0	Cytoplasm
ni2[c]	Nickel	Ni	2	Cytoplasm
ni2[e]	Nickel	Ni	2	Extracellular
nicrns[c]	Nicotinate D-ribonucleoside	C11H13NO6	0	Cytoplasm
nicrnt[c]	Nicotinate D-ribonucleotide	C11H12NO9P	-2	Cytoplasm
nmn[c]	NMN C11H14N2O8P	C11H14N2O8P	-1	Cytoplasm
no2[c]	Nitrite	NO2	-1	Cytoplasm
no3[c]	Nitrate	NO3	-1	Cytoplasm
no3[e]	Nitrate	NO3	-1	Extracellular
npdp[c]	All-trans-Nonaprenyl diphosphate	C45H74O7P2	-2	Cytoplasm
o2[c]	O2 O2	O2	0	Cytoplasm

o2[cx]	O2 O2	O2	0	Carboxysome
o2[e]	O2 O2	O2	0	Extracellular
o2[p]	O2 O2	O2	0	Periplasm
o2[u]	O2 O2	O2	0	Thylakoid
oaa[c]	Oxaloacetate	C4H2O5	-2	Cytoplasm
ocACP[c]	Octanoyl-ACP (n-C8:0ACP)	C19H35N2O8PRS	-1	Cytoplasm
ocdcaACP[c]	Octadecanoyl-ACP (n-C18:0ACP)	C29H55N2O8PRS	-1	Cytoplasm
octdp[c]	All-trans-Octaprenyl diphosphate	C40H66O7P2	-2	Cytoplasm
octe_9_12_15_AC P[c]	A-linoleoyl-ACP (n-C18 3ACP)	C29H49N2O8PRS	-1	Cytoplasm
octe_9_12_ACP[c]	Linoleoyl-ACP (n-C18 2ACP)	C29H51N2O8PRS	-1	Cytoplasm
octe_9_ACP[c]	Cis-octadec-9-enoyl-[acyl-carrier protein] (n-C18 1)	C29H53N2O8PRS	-1	Cytoplasm
ohpb[c]	2-Oxo-3-hydroxy-4-phosphobutanoate	C4H4O8P	-3	Cytoplasm
omppp9[c]	13(1)-Oxo-magnesium-protoporphyrin IX 13-monomethyl ester	C35H31N4O5Mg	-1	Cytoplasm
orn[c]	Ornithine	C5H13N2O2	1	Cytoplasm
orot[c]	Orotate C5H3N2O4	C5H3N2O4	-1	Cytoplasm
orot5p[c]	Orotidine 5'-phosphate	C10H10N2O11P	-3	Cytoplasm
oxa[c]	Oxalate	C2O4	-2	Cytoplasm
pa100[c]	1,2-didecanoyl-sn-glycerol-3-phosphate	C23H43O8P	-2	Cytoplasm
pa120[c]	1,2-didodecanoyl-sn-glycerol 3-phosphate	C27H51O8P	-2	Cytoplasm
pa140[c]	1,2-ditetradecanoyl-sn-glycerol 3-phosphate	C31H59O8P	-2	Cytoplasm
pa160[c]	1,2-dihexadecanoyl-sn-glycerol 3-phosphate	C35H67O8P	-2	Cytoplasm
pa161[c]	1,2-dihexadec-9-enoyl-sn-glycerol 3-phosphate	C35H63O8P	-2	Cytoplasm
pa180[c]	1,2-dioctadecanoyl-sn-glycerol 3-phosphate	C39H75O8P	-2	Cytoplasm
pa181_9[c]	1,2-dioctadec-9-enoyl-sn-glycerol 3-phosphate	C39H71O8P	-2	Cytoplasm
pa182_9_12[c]	1,2-dioctadec-9-12-dienoyl-sn-glycerol 3-phosphate	C39H67O8P	-2	Cytoplasm
pa183_9_12_15[c]	1,2-dioctadec-9-12-15-trienoyl-sn-glycerol 3-phosphate	C39H63O8P	-2	Cytoplasm
pa60[c]	1,2-dihexanoyl-sn-glycerol-3-phosphate	C15H27O8P	-2	Cytoplasm
pa80[c]	1,2-dioctanoyl-sn-glycerol-3-phosphate	C19H35O8P	-2	Cytoplasm
palmACP[c]	Palmitoyl-ACP (n-C16:0ACP)	C27H51N2O8PRS	-1	Cytoplasm
pan4p[c]	Pantetheine 4'-phosphate	C11H21N2O7PS	-2	Cytoplasm

pant__R[c]	(R)-Pantoate	C6H11O4	-1	Cytoplasm
pap[c]	Adenosine 3',5'-bisphosphate	C10H11N5O10P2	-4	Cytoplasm
paps[c]	3'-Phosphoadenylyl sulfate	C10H11N5O13P2S	-4	Cytoplasm
pchlId[c]	Protochlorophyllide	C35H31N4O5Mg	-1	Cytoplasm
pcox[p]	Plastocyanin(Cu2+)	CuR	2	Periplasm
pcox[u]	Plastocyanin(Cu2+)	CuR	2	Thylakoid
pcrd[p]	Plastocyanin(Cu+)	CuR	1	Periplasm
pcrd[u]	Plastocyanin(Cu+)	CuR	1	Thylakoid
pdx5p[c]	Pyridoxine 5'-phosphate	C8H10NO6P	-2	Cytoplasm
pecbp[c]	Phycoerythrocyanin Anabaena sp. UTEX 2576	C1660H2605N456O509S13	31	Cytoplasm
pep[c]	Phosphoenolpyruvate	C3H2O6P	-3	Cytoplasm
peptido_ana[c]	Peptidoglycan subunit of Anabaena sp. UTEX 2576 (Based on Synechocystis sp. PCC6803)	C40H62N8O21	-2	Cytoplasm
pg100[c]	Phosphatidylglycerol-didecanoyl	C26H50O10P	-1	Cytoplasm
pg120[c]	Phosphatidylglycerol (didodecanoyl, n-C12:0)	C30H58O10P	-1	Cytoplasm
pg140[c]	Phosphatidylglycerol (ditetradecanoyl, n-C14:0)	C34H66O10P	-1	Cytoplasm
pg160[c]	Phosphatidylglycerol (dihexadecanoyl, n-C16:0)	C38H74O10P	-1	Cytoplasm
pg161[c]	Phosphatidylglycerol (dihexadec-9-enoyl, n-C16:1)	C38H70O10P	-1	Cytoplasm
pg180[c]	Phosphatidylglycerol (dioctadecanoyl, n-C18:0)	C42H82O10P	-1	Cytoplasm
pg181_9[c]	Phosphatidylglycerol (dioctadec-9-enoyl, n-C18 1)	C42H78O10P	-1	Cytoplasm
pg182_9_12[c]	Phosphatidylglycerol (dioctadec-9-12-dienoyl, n-C18 2)	C42H74O10P	-1	Cytoplasm
pg183_9_12_15[c]	Phosphatidylglycerol (dioctadec-9-12-15-trienoyl, n-C18 3)	C42H70O10P	-1	Cytoplasm
pg60[c]	Phosphatidylglycerol-dihexanoyl	C18H34O10P	-1	Cytoplasm
pg80[c]	Phosphatidylglycerol-dioctanoyl	C22H42O10P	-1	Cytoplasm
pgp100[c]	Phosphatidylglycerophosphate-didecanoyl	C26H49O13P2	-3	Cytoplasm
pgp120[c]	Phosphatidylglycerophosphate (didodecanoyl, n-C12:0)	C30H57O13P2	-3	Cytoplasm
pgp140[c]	Phosphatidylglycerophosphate (ditetradecanoyl, n-C14:0)	C34H65O13P2	-3	Cytoplasm
pgp160[c]	Phosphatidylglycerophosphate (dihexadecanoyl, n-C16:0)	C38H73O13P2	-3	Cytoplasm
pgp161[c]	Phosphatidylglycerophosphate (dihexadec-9-enoyl, n-C16:1)	C38H69O13P2	-3	Cytoplasm
pgp180[c]	Phosphatidylglycerophosphate (dioctadecanoyl, n-C18:0)	C42H81O13P2	-3	Cytoplasm
pgp181_9[c]	Phosphatidylglycerophosphate (dioctadec-9-enoyl, n-C18 1)	C42H77O13P2	-3	Cytoplasm

pgp182_9_12[c]	Phosphatidylglycerophosphate (dioctadec-9-12-dienoyl, n-C18 2)	C42H73O13P2	-3	Cytoplasm
pgp183_9_12_15[c]	Phosphatidylglycerophosphate (dioctadec-9-12-15-trienoyl, n-C18 3)	C42H69O13P2	-3	Cytoplasm
pgp60[c]	Phosphatidylglycerophosphate-dihexanoyl	C18H33O13P2	-3	Cytoplasm
pgp80[c]	Phosphatidylglycerophosphate-dioctanoyl	C22H41O13P2	-3	Cytoplasm
phdp[c]	Phytol diphosphate	C20H40O7P2	-2	Cytoplasm
phe__L[c]	L-Phenylalanine	C9H11NO2	0	Cytoplasm
pheme[c]	Protoheme C34H30FeN4O4	C34H30FeN4O4	-2	Cytoplasm
phllqne[c]	Phylloquinone	C31H46O2	0	Cytoplasm
phllqn[c]	Phylloquinol	C31H48O2	0	Cytoplasm
phom[c]	O-Phospho-L-homoserine	C4H8NO6P	-2	Cytoplasm
photon[c]	Photon	Z	0	Cytoplasm
photon[e]	Photon	Z	0	Extracellular
photon298[c]	Photon (281 to 306 nm, UVB)	Z	0	Cytoplasm
photon437[c]	Photon (406 to 454 nm, indigo/blue)	Z	0	Cytoplasm
photon437[u]	Photon (406 to 454 nm, indigo/blue)	Z	0	Thylakoid
photon438[c]	Photon (378 to 482 nm, violet/blue)	Z	0	Cytoplasm
photon438[u]	Photon (378 to 482 nm, violet/blue)	Z	0	Thylakoid
photon450[c]	Photon (417 to 472 nm, indigo/blue)	Z	0	Cytoplasm
photon490[c]	Photon (451 to 526 nm, blue/green)	Z	0	Cytoplasm
photon646[c]	Photon (608 to 666 nm, orange/red)	Z	0	Cytoplasm
photon646[u]	Photon (608 to 666 nm, orange/red)	Z	0	Thylakoid
photon673[c]	Photon (659 to 684 nm, red)	Z	0	Cytoplasm
photon673[u]	Photon (659 to 684 nm, red)	Z	0	Thylakoid
photon680[c]	Photon (662 to 691 nm, red)	Z	0	Cytoplasm
photon680[u]	Photon (662 to 691 nm, red)	Z	0	Thylakoid
phpyr[c]	Phenylpyruvate	C9H7O3	-1	Cytoplasm
phthr[c]	O-Phospho-4-hydroxy-L-threonine	C4H8NO7P	-2	Cytoplasm
phycy[c]	(3Z)-Phycocyanobilin	C33H36N4O6	-2	Cytoplasm
phytfl[c]	All-trans-Phytofluene	C40H62	0	Cytoplasm
phytoe[c]	Phytoene	C40H64	0	Cytoplasm

phyvi[c]	(15Z)-Phycoviolobilin	C33H36N4O6	-2	Cytoplasm
pi[c]	Phosphate	HO4P	-2	Cytoplasm
pi[e]	Phosphate	HO4P	-2	Extracellular
pimACP[c]	Pimeloyl-[acyl-carrier protein]	C18H31N2O10PRS	-1	Cytoplasm
pmeACP[c]	Pimeloyl-[acyl-carrier protein] methyl ester	C19H33N2O10PRS	-1	Cytoplasm
pnto__R[c]	(R)-Pantothenate	C9H16NO5	-1	Cytoplasm
ppbng[c]	Porphobilinogen	C10H13N2O4	-1	Cytoplasm
ppgpp[c]	Guanosine 3',5'-bis(diphosphate)	C10H12N5O17P4	-5	Cytoplasm
pphn[c]	Prephenate	C10H8O6	-2	Cytoplasm
ppi[c]	Diphosphate	HO7P2	-3	Cytoplasm
ppp9[c]	Protoporphyrin	C34H32N4O4	-2	Cytoplasm
pppg9[c]	Protoporphyrinogen IX	C34H38N4O4	-2	Cytoplasm
pppi[c]	Inorganic triphosphate	H2O10P3	-3	Cytoplasm
pq[u]	Plastoquinone	C53H80O2	0	Thylakoid
pqh2[c]	Plastoquinol	C53H82O2	0	Cytoplasm
pqh2[u]	Plastoquinol	C53H82O2	0	Thylakoid
pram[c]	5-Phospho-beta-D-ribosylamine	C5H11NO7P	-1	Cytoplasm
pran[c]	N-(5-Phospho-D-ribosyl)anthranilate	C12H13NO9P	-3	Cytoplasm
prbamp[c]	1-(5-Phosphoribosyl)-AMP	C15H19N5O14P2	-4	Cytoplasm
prbatp[c]	1-(5-Phosphoribosyl)-ATP	C15H20N5O20P4	-5	Cytoplasm
pre3a[c]	Precorrin 3 A	C43H43N4O16	-7	Cytoplasm
pre3b[c]	Precorrin 3B	C43H44N4O17	-6	Cytoplasm
pre4[c]	Precorrin 4	C44H45N4O17	-7	Cytoplasm
pre5[c]	Precorrin 5	C45H47N4O17	-7	Cytoplasm
pre6a[c]	Precorrin 6A	C44H47N4O16	-7	Cytoplasm
pre6b[c]	Precorrin 6B	C44H49N4O16	-7	Cytoplasm
pre8[c]	Precorrin 8	C45H53N4O14	-7	Cytoplasm
precyanphy[c]	Cyanophycin (multi-Larginyl-poli [L--aspartic acid]) polimer (n)	C10H19N5O5	0	Cytoplasm
prephytedp[c]	Prephytoene diphosphate	C40H66O7P2	-2	Cytoplasm
preq0[c]	7-cyano-7-carbaguanine	C7H5N5O	0	Cytoplasm
preq1[c]	7-aminomethyl-7-deazaguanine	C7H10N5O	1	Cytoplasm

prfp[c]	1-(5-Phosphoribosyl)-5-[(5-phosphoribosylamino)methylideneamino]imidazole-4-carboxamide	C15H21N5O15P2	-4	Cytoplasm
prlp[c]	5-[(5-phospho-1-deoxyribulos-1-ylamino)methylideneamino]-1-(5-phosphoribosyl)imidazole-4-carboxamide	C15H22N5O15P2	-3	Cytoplasm
pro__L[c]	L-Proline	C5H9NO2	0	Cytoplasm
prpp[c]	5-Phospho-alpha-D-ribose 1-diphosphate	C5H9O14P3	-4	Cytoplasm
pser__L[c]	O-Phospho-L-serine	C3H6NO6P	-2	Cytoplasm
psqldp[c]	Presqualene diphosphate	C30H50O7P2	-2	Cytoplasm
ptrc[c]	Putrescine	C4H14N2	2	Cytoplasm
ptrc[e]	Putrescine	C4H14N2	2	Extracellular
pxanth[c]	0	C40H56O2	0	Cytoplasm
pyam5p[c]	Pyridoxamine 5'-phosphate	C8H12N2O5P	-1	Cytoplasm
pydx5p[c]	Pyridoxal 5'-phosphate	C8H8NO6P	-2	Cytoplasm
pyr[c]	Pyruvate	C3H3O3	-1	Cytoplasm
pyr[e]	Pyruvate	C3H3O3	-1	Extracellular
q8[c]	Ubiquinone-8	C49H74O4	0	Cytoplasm
q8[p]	Ubiquinone-8	C49H74O4	0	Periplasm
q8h2[c]	Ubiquinol-8	C49H76O4	0	Cytoplasm
q8h2[p]	Ubiquinol-8	C49H76O4	0	Periplasm
quln[c]	Quinolate	C7H3NO4	-2	Cytoplasm
r5p[c]	Alpha-D-Ribose 5-phosphate	C5H9O8P	-2	Cytoplasm
rb15bp[c]	D-Ribulose 1,5-bisphosphate	C5H8O11P2	-4	Cytoplasm
rb15bp[cx]	D-Ribulose 1,5-bisphosphate	C5H8O11P2	-4	Carboxysome
rdmbzi[c]	N1-(alpha-D-ribosyl)-5,6-dimethylbenzimidazole	C14H18N2O4	0	Cytoplasm
rib__D[c]	D-Ribose	C5H10O5	0	Cytoplasm
ribflv[c]	Riboflavin C17H20N4O6	C17H19N4O6	-1	Cytoplasm
ribflv[e]	Riboflavin C17H20N4O6	C17H19N4O6	-1	Extracellular
rnam[c]	N Ribosylnicotinamide C11H15N2O5	C11H15N2O5	1	Cytoplasm
ru5p__D[c]	D-Ribulose 5-phosphate	C5H9O8P	-2	Cytoplasm
s17bp[c]	Sedoheptulose 1,7-bisphosphate	C7H12O13P2	-4	Cytoplasm
s7p[c]	Sedoheptulose 7-phosphate	C7H13O10P	-2	Cytoplasm
sbt__D[c]	D-Sorbitol	C6H14O6	0	Cytoplasm

sbzcoa[c]	O-Succinylbenzoyl-CoA	C32H39N7O20P3S	-5	Cytoplasm
schiz[c]	Schizokinen	C16H28N4O9	0	Cytoplasm
schiz[e]	Schizokinen	C16H28N4O9	0	Extracellular
scl[c]	Sirohydrochlorin	C42H38N4O16	-8	Cytoplasm
ser__L[c]	L-Serine	C3H7NO3	0	Cytoplasm
Sfglutth[c]	S-Formylglutathione	C11H16N3O7S	-1	Cytoplasm
sheme[c]	Siroheme C42H36FeN4O16	C42H36FeN4O16	-8	Cytoplasm
skgmeACP[c]	3-Ketoglutaryl-ACP methyl ester	C17H27N2O11PRS	-1	Cytoplasm
skm[c]	Shikimate	C7H9O5	-1	Cytoplasm
skm5p[c]	Shikimate 5-phosphate	C7H8O8P	-3	Cytoplasm
skpmeACP[c]	3-Ketopimeloyl-[acp] methyl ester	C19H31N2O11PRS	-1	Cytoplasm
so3[c]	Sulfite	HO3S	-1	Cytoplasm
so4[c]	Sulfate	O4S	-2	Cytoplasm
so4[e]	Sulfate	O4S	-2	Extracellular
spmd[c]	Spermidine	C7H22N3	3	Cytoplasm
spmd[e]	Spermidine	C7H22N3	3	Extracellular
spm[c]	Spermine	C10H30N4	4	Cytoplasm
sqdg100[c]	Sulfoquinovosyldiacylglycerol(n-C10-0)	C29H53O12S	-1	Cytoplasm
sqdg120[c]	Sulfoquinovosyldiacylglycerol(n-C12-0)	C33H61O12S	-1	Cytoplasm
sqdg140[c]	Sulfoquinovosyldiacylglycerol(n-C14-0)	C37H69O12S	-1	Cytoplasm
sqdg160[c]	Sulfoquinovosyldiacylglycerol (n-C16 0)	C41H77O12S	-1	Cytoplasm
sqdg161[c]	Sulfoquinovosyldiacylglycerol (n-C16 1)	C41H73O12S	-1	Cytoplasm
sqdg180[c]	Sulfoquinovosyldiacylglycerol (n-C18 0)	C45H85O12S	-1	Cytoplasm
sqdg181_9[c]	Sulfoquinovosyldiacylglycerol (n-C18 1)	C45H81O12S	-1	Cytoplasm
sqdg182_9_12[c]	Sulfoquinovosyldiacylglycerol (n-C18 2)	C45H77O12S	-1	Cytoplasm
sqdg183_9_12_15[c]	Sulfoquinovosyldiacylglycerol (n-C18 3)	C45H73O12S	-1	Cytoplasm
sqdg60[c]	Sulfoquinovosyldiacylglycerol(n-C6-0)[c]	C21H37O12S	-1	Cytoplasm
sqdg80[c]	Sulfoquinovosyldiacylglycerol(n-C8-0)	C25H45O12S	-1	Cytoplasm
sql[c]	Squalene C30H50	C30H50	0	Cytoplasm
suc6p[c]	Sucrose 6-phosphate	C12H21O14P	-2	Cytoplasm

sucbz[c]	O-Succinylbenzoate	C11H8O5	-2	Cytoplasm
succ[c]	Succinate	C4H4O4	-2	Cytoplasm
succ[e]	Succinate	C4H4O4	-2	Extracellular
succoa[c]	Succinyl-CoA	C25H35N7O19P3S	-5	Cytoplasm
sucr[c]	Sucrose C12H22O11	C12H22O11	0	Cytoplasm
sucsal[c]	Succinic semialdehyde	C4H5O3	-1	Cytoplasm
sufse[c]	SufSE sulfur acceptor complex	HSR	0	Cytoplasm
sufsesh[c]	SufSE with bound sulfur	HS2R	0	Cytoplasm
tcneusp[c]	7,9,9'-tricyclic-Neurosporene	C40H58	0	Cytoplasm
tczcaro[c]	9,15,9-tricyclic-zeta-Carotene	C40H60	0	Cytoplasm
tddec2eACP[c]	Trans-Dodec-2-enoyl-[acyl-carrier protein]	C23H41N2O8PRS	-1	Cytoplasm
tdec2eACP[c]	Trans-Dec-2-enoyl-[acyl-carrier protein]	C21H37N2O8PRS	-1	Cytoplasm
thdp[c]	2,3,4,5-Tetrahydrodipicolinate	C7H7NO4	-2	Cytoplasm
thex2eACP[c]	Trans-Hex-2-enoyl-[acyl-carrier protein]	C17H29N2O8PRS	-1	Cytoplasm
thf[c]	5,6,7,8-Tetrahydrofolate	C19H21N7O6	-2	Cytoplasm
thfglu[c]	Tetrahydrofolyl Glu 2 C24H27N8O9	C24H27N8O9	-3	Cytoplasm
thm[c]	Thiamin	C12H17N4OS	1	Cytoplasm
thmmp[c]	Thiamin monophosphate	C12H16N4O4PS	-1	Cytoplasm
thmpp[c]	Thiamine diphosphate	C12H17N4O7P2S	-1	Cytoplasm
thr__L[c]	L-Threonine	C4H9NO3	0	Cytoplasm
thrp[c]	L-Threonine O-3-phosphate	C4H8NO6P	-2	Cytoplasm
thymd[c]	Thymidine C10H14N2O5	C10H14N2O5	0	Cytoplasm
tmrs2eACP[c]	Trans-Tetradec-2-enoyl-[acyl-carrier protein]	C25H45N2O8PRS	-1	Cytoplasm
toct2eACP[c]	Trans-Oct-2-enoyl-[acyl-carrier protein]	C19H33N2O8PRS	-1	Cytoplasm
toctd2eACP[c]	Trans-octadec-2-enoyl-[acyl-carrier protein]	C29H53N2O8PRS	-1	Cytoplasm
tpalm2eACP[c]	Trans-Hexadec-2-enoyl-[acyl-carrier protein]	C27H49N2O8PRS	-1	Cytoplasm
trdox[c]	Oxidized thioredoxin	C6H7NO2R2S2	0	Cytoplasm
trdrd[c]	Reduced thioredoxin	C6H9NO2R2S2	0	Cytoplasm
tre[c]	Trehalose	C12H22O11	0	Cytoplasm
trnaglu[c]	TRNA (Glu)	C10H12N5O3R	0	Cytoplasm
trp__L[c]	L-Tryptophan	C11H12N2O2	0	Cytoplasm

tsul[c]	Thiosulfate	HO3S2	-1	Cytoplasm
tsul[e]	Thiosulfate	HO3S2	-1	Extracellular
ttclyco[c]	7,9,7,9-tetrakis-Lycopene	C40H56	0	Cytoplasm
tyr__L[c]	L-Tyrosine	C9H11NO3	0	Cytoplasm
u23ga[c]	UDP-2,3-bis(3-hydroxytetradecanoyl)glucosamine	C43H75N3O20P2	-2	Cytoplasm
u3aga[c]	UDP-3-O-(3-hydroxytetradecanoyl)-N-acetylglucosamine	C31H51N3O19P2	-2	Cytoplasm
u3hga[c]	UDP-3-O-(3-hydroxytetradecanoyl)-D-glucosamine	C29H50N3O18P2	-1	Cytoplasm
uaagmda[c]	Undecaprenyl-diphospho-N-acetylmuramoyl-(N-acetylglucosamine)-L-ala-D-glu-meso-2,6-diaminopimeloyl-D-ala-D-ala	C95H152N8O28P2	-4	Cytoplasm
uaccg[c]	UDP-N-acetyl-3-O-(1-carboxyvinyl)-D-glucosamine	C20H26N3O19P2	-3	Cytoplasm
uacgam[c]	UDP-N-acetyl-D-glucosamine	C17H25N3O17P2	-2	Cytoplasm
uacmam[c]	UDP-N-acetyl-D-mannosamine	C17H25N3O17P2	-2	Cytoplasm
uagmda[c]	Undecaprenyl-diphospho-N-acetylmuramoyl-L-alanyl-D-glutamyl-meso-2,6-diaminopimeloyl-D-alanyl-D-alanine	C87H139N7O23P2	-4	Cytoplasm
uama[c]	UDP-N-acetylmuramoyl-L-alanine	C23H33N4O20P2	-3	Cytoplasm
uamag[c]	UDP-N-acetylmuramoyl-L-alanyl-D-glutamate	C28H39N5O23P2	-4	Cytoplasm
uamr[c]	UDP-N-acetylmuramate	C20H28N3O19P2	-3	Cytoplasm
udcpdp[c]	Undecaprenyl diphosphate	C55H90O7P2	-2	Cytoplasm
udcpp[c]	Undecaprenyl phosphate	C55H89O4P	-2	Cytoplasm
udp[c]	UDP C9H11N2O12P2	C9H12N2O12P2	-2	Cytoplasm
udpg[c]	UDPglucose	C15H22N2O17P2	-2	Cytoplasm
udpgal[c]	UDPgaltose	C15H22N2O17P2	-2	Cytoplasm
udpglcur[c]	UDP-D-glucuronate	C15H19N2O18P2	-3	Cytoplasm
udpsq[c]	UDP-6-sulfoquinovose	C15H21N2O19P2S	-3	Cytoplasm
udpxyl[c]	UDP-D-xylose	C14H20N2O16P2	-2	Cytoplasm
ugmd[c]	UDP-N-acetylmuramoyl-L-alanyl-D-gamma-glutamyl-meso-2,6-diaminopimelate	C35H51N7O26P2	-4	Cytoplasm
ugmda[c]	UDP-N-acetylmuramoyl-L-alanyl-D-glutamyl-meso-2,6-diaminopimeloyl-D-alanyl-D-alanine	C41H61N9O28P2	-4	Cytoplasm
ump[c]	UMP C9H11N2O9P	C9H11N2O9P	-2	Cytoplasm
uppg3[c]	Uroporphyrinogen III	C40H36N4O16	-8	Cytoplasm
ura[c]	Uracil	C4H4N2O2	0	Cytoplasm
urea[c]	Urea CH4N2O	CH4N2O	0	Cytoplasm
urea[e]	Urea CH4N2O	CH4N2O	0	Extracellular

utp[c]	UTP C ₉ H ₁₁ N ₂ O ₁₅ P ₃	C ₉ H ₁₂ N ₂ O ₁₅ P ₃	-3	Cytoplasm
val__L[c]	L-Valine	C ₅ H ₁₁ NO ₂	0	Cytoplasm
val__L[e]	L-Valine	C ₅ H ₁₁ NO ₂	0	Extracellular
xmp[c]	Xanthosine 5'-phosphate	C ₁₀ H ₁₁ N ₄ O ₉ P	-2	Cytoplasm
xtp[c]	XTP	C ₁₀ H ₁₁ N ₄ O ₁₅ P ₃	-4	Cytoplasm
xu5p__D[c]	D-Xylulose 5-phosphate	C ₅ H ₉ O ₈ P	-2	Cytoplasm
zcarote[c]	Zeta-Carotene	C ₄₀ H ₆₀	0	Cytoplasm
zeax[c]	Zeaxanthin	C ₄₀ H ₅₆ O ₂	0	Cytoplasm
zn2[c]	Zinc	Zn	2	Cytoplasm
zn2[e]	Zinc	Zn	2	Extracellular

APPENDIX C. MATLAB CODE

C.1 FBA Algorithm called from MATLAB CobraToolbox

```
%iDN1004 Script (November 7th, 2019) - Daniel N. Caro
%Genome scale metabolic model of Anabaena sp. UTEX 2576
%a.k.a. Nostoc sp. PCC7120

clc
clear

%initCobraToolbox

%Changes default solver to Gurobi
changeCobraSolver ('gurobi', 'all', 1)

%Transforms model from Excel file to matlab model
model = readCbModel('Data_set_1_iDN1004.xls');

%Load model from mat iDN776.mat file
%load Dataset_2_iDN776_PAuto.mat or Dataset_3_iDN776_PDiazo.mat

%Prints the stoichiometric matrix for the model

%To extract the S matrix from the model
mat = full(model.S);

%Saves matrix as csv
%csvwrite('stoiqiDN1004.csv',mat)

%Identify metabolic Dead ends

outputMets = detectDeadEnds(model);
DeadEnds = model.mets(outputMets);

answer = questdlg('What is the nitrogen source?', ...
    'Growth conditions', ...
    'NaNO3 (Photoautotrophic)', 'N2 (Photodiazotrophic)', 'Abort');
% Handle response
switch answer
    case 'NaNO3 (Photoautotrophic)'
        %Change objective function (Non-diazotrophic)
        model = changeObjective(model,'BOF_ANA_AUTO',1);
```

```

fprintf('The Objective reaction is: \n')
%Print Objective function
printRxnFormula(model,'BOF_ANA_AUTO');

%Change reaction limits for cultures in BG11 (Photoautotrophic)

%Photon flux based on experimental PPFD
model = changeRxnBounds(model, 'EX_photon_e', -87.09, 'l');
%Citrate flux from BG11 medium
model = changeRxnBounds(model, 'EX_cit_e', -0.01, 'l');
%Pyruvate from BG11 medium blocked
model = changeRxnBounds(model, 'EX_pyr_e', 0, 'b');
%L-Methionine flux from BG11 medium blocked
model = changeRxnBounds(model, 'EX_met__L_e', 0, 'b');
%L-Glutamate flux from BG11 medium blocked
model = changeRxnBounds(model, 'EX_gln__L_e', 0, 'b');
%L-Glutamine flux from BG11 medium blocked
model = changeRxnBounds(model, 'EX_glu__L_e', 0, 'b');
%L-Arginine flux from BG11 medium blocked
model = changeRxnBounds(model, 'EX_arg__L_e', 0, 'b');
%L-Lysine flux from BG11 medium blocked
model = changeRxnBounds(model, 'EX_lys__L_e', 0, 'b');
%L-Histidine flux from BG11 medium blocked
model = changeRxnBounds(model, 'EX_his__L_e', 0, 'b');
%Urea flux from medium blocked, but excretion allowed
model = changeRxnBounds(model, 'EX_urea_e', 0, 'l');
%Putrescine flux from medium blocked, but excretion allowed
model = changeRxnBounds(model, 'EX_ptrc_e', 0, 'l');
%Spermidine flux from medium blocked, but excretion allowed
model = changeRxnBounds(model, 'EX_spm_d_e', 0, 'l');
%Cyanate flux from medium blocked
model = changeRxnBounds(model, 'EX_cynt_e', 0, 'b');
%Ammonium ion flux/uptake from medium
model = changeRxnBounds(model, 'EX_nh4_e', 0, 'l');
%model = changeRxnBounds(model, 'EX_nh4_e', 0, 'u');
%Diazotrophy is blocked in BG11 medium (No N2 uptake)
model = changeRxnBounds(model, 'EX_n2_e', 0, 'b');
%Nitrate ion flux/uptake from medium
model = changeRxnBounds(model, 'EX_no3_e', -0.2438, 'l');
model = changeRxnBounds(model, 'EX_no3_e', -0.0129, 'u');
%Biosynthesis of phycocyanobilin pigment
%model = changeRxnBounds(model, 'PHYCYFX', 2.27E-5, 'l');
%model = changeRxnBounds(model, 'PHYCYFX', 5.70E-4, 'u');
%Biosynthesis of c-phycocyanin phycobiliprotein
model = changeRxnBounds(model, 'CPCPBPS', 5.84E-6, 'l');
model = changeRxnBounds(model, 'CPCPBPS', 1.47E-4, 'u');

```



```

%Uptake of Vitamin B12/ Calomide from medium blocked
model = changeRxnBounds(model, 'EX_adocbl_e', 0, 'l');
%Uptake of Vitamin B2/ Riboflavin from medium blocked
model = changeRxnBounds(model, 'EX_ribflv_e', 0, 'l');
%Uptake of Glycerol from medium blocked
model = changeRxnBounds(model, 'EX_glyc_e', 0, 'b');
%Constrained HCO3 and CO2 uptake reaction
%HCO3 uptake is 70% of total Ci required
%CO2 uptake is 30% of total Ci required
model = changeRxnBounds(model, 'EX_co2_e', -0.3561, 'b');
model = changeRxnBounds(model, 'EX_hco3_e', -0.8309, 'b');
%Constrained secretion of Schizokinen
model = changeRxnBounds(model, 'SCHIZt', 0.000491, 'l');
%Fe 2+ availability constraint (Only Fe 3+ in medium)
model = changeRxnBounds(model, 'EX_fe2_e', 0, 'b');

```

```

%Run FBA
FBAolution = optimizeCbModel (model, 'max','one');
obj_f_value = FBAolution.f;%Objective function

['Reaction ID', 'Objective', 'Flux'];...
model.rxns, num2cell(model.c), num2cell(FBAolution.x)]

```

```

case 'N2 (Photodiazotrophic)'

```

```

%Change objective function (Diazotrophic)
model = changeObjective(model,'BOF_ANA_DIAZO',1);

```

```

fprintf ('The Objective reaction is: \n')
%Print Objective function
printRxnFormula(model,'BOF_ANA_DIAZO');

```

```

%Change reaction limits for cultures in BG11o (Diazotrophic)

```

```

%Photon flux based on experimental PPFD
model = changeRxnBounds(model, 'EX_photon_e', -102.53, 'l');
%Citrate flux from BG11o medium
model = changeRxnBounds(model, 'EX_cit_e', -0.01, 'l');
%Pyruvate from BG11o medium blocked
model = changeRxnBounds(model, 'EX_pyr_e', 0, 'b');
%L-Methionine flux from BG11o medium blocked
model = changeRxnBounds(model, 'EX_met__L_e', 0, 'b');
%L-Glutamine flux from BG11 medium blocked

```

```

model = changeRxnBounds(model, 'EX_glu__L_e', 0, 'b');
%L-Glutamine flux from BG11o medium blocked
model = changeRxnBounds(model, 'EX_gln__L_e', 0, 'b');
%L-Arginine flux from BG11o medium blocked
model = changeRxnBounds(model, 'EX_arg__L_e', 0, 'b');
%L-Lysine flux from BG11o medium blocked
model = changeRxnBounds(model, 'EX_lys__L_e', 0, 'b');
%L-Histidine flux from BG11o medium blocked
model = changeRxnBounds(model, 'EX_his__L_e', 0, 'b');
%Urea flux from medium blocked, but excretion allowed
model = changeRxnBounds(model, 'EX_urea_e', 0, 'l');
%Putrescine flux from medium blocked, but excretion allowed
model = changeRxnBounds(model, 'EX_ptrc_e', 0, 'l');
%Spermidine flux from medium blocked, but excretion allowed
model = changeRxnBounds(model, 'EX_spmd_e', 0, 'l');
%Cyanate flux from medium blocked
model = changeRxnBounds(model, 'EX_cynt_e', 0, 'b');
%Ammonium ion flux/uptake from medium
model = changeRxnBounds(model, 'EX_nh4_e', 0, 'l');
%model = changeRxnBounds(model, 'EX_nh4_e', 0, 'u');
%Diazotrophy is allowed in BG11o medium (N2 uptake)
model = changeRxnBounds(model, 'EX_n2_e', -0.1255, 'l');
model = changeRxnBounds(model, 'EX_n2_e', -0.0104, 'u');
%BG11o medium lacks Nitrate, no nitrate uptake
model = changeRxnBounds(model, 'EX_no3_e', 0, 'b');
%Biosynthesis of phycocyanobilin pigment
%model = changeRxnBounds(model, 'PHYCYFX', 2.01E-5, 'l');
%model = changeRxnBounds(model, 'PHYCYFX', 4.05E-4, 'u');
%Biosynthesis of c-phycocyanin phycobiliprotein
model = changeRxnBounds(model, 'CPCPBPS', 5.11E-6, 'l');
model = changeRxnBounds(model, 'CPCPBPS', 1.03E-4, 'u');
%Uptake of Vitamin B12/ Calomide from medium blocked
model = changeRxnBounds(model, 'EX_adocbl_e', 0, 'l');
%Uptake of Vitamin B2/ Riboflavin from medium blocked
model = changeRxnBounds(model, 'EX_ribflv_e', 0, 'l');
%Uptake of Glycerol from medium blocked
model = changeRxnBounds(model, 'EX_glyc_e', 0, 'b');
%Constrained CO2 uptake reaction
%HCO3 uptake is 70% of total Ci required
%CO2 uptake is 30% of total Ci required
model = changeRxnBounds(model, 'EX_co2_e', -0.3249, 'l');
model = changeRxnBounds(model, 'EX_hco3_e', -0.7581, 'l');
%Constrained secretion of Schizokinen
model = changeRxnBounds(model, 'SCHIZt', 0.0004373, 'l');
%Fe 2+ availability constraint (Only Fe 3+ in medium)
model = changeRxnBounds(model, 'EX_fe2_e', 0, 'b');

```

```

%Run FBA
FBAsolution = optimizeCbModel (model, 'max','one');

%printFluxVector(model,FBAsolution.x,true)
obj_f_value = FBAsolution.f;%Objective function

['Reaction ID', 'Objective', 'Flux'];...
model.rxns, num2cell(model.c), num2cell(FBAsolution.x)]

case 'Abort'
    disp('Operation aborted')

end

%Check Stoichiometry matrix sparsity
S = model.S;
[nMets, nRxns] = size(S);
nElem = numel(S);
nNz = nnz(S);
sparsityRatio = (1-nNz/nElem)*100;
compSparsityRatio = 100 - sparsityRatio;

colDensityAv = 0;

for j=1:nRxns
    colDensityAv = colDensityAv + nnz(S(:,j));
end

colDensityAv = colDensityAv/ nRxns;

colDensityRel = (colDensityAv/nMets)*100;

spyc(S, colormap(advancedColormap('cobratoolbox')));
set(gca, 'fontsize',14);

%Check Mass and charge balance of reactions

[~,imBalancedMass,imBalancedCharge,imBalancedBool,~]
checkMassChargeBalance(model,1);

writeCbModel(model)
=

```

C.2 FVA Algorithm called from MATLAB CobraToolbox

%iDN1004 Script FVA (November 13th, 2019) - Daniel N. Caro

%Genome scale metabolic model of Anabaena sp. UTEX 2576

%a.k.a. Nostoc sp. PCC7120

clc

clear

%initCobraToolbox

%Changes default solver to Gurobi

changeCobraSolver ('gurobi', 'all', 1)

rxnlist

{'GDH1';'GDH2_nadp';'GLUN';'GLMS_b';'CBPS';'ABTA';'ORNTA';'P5CD';'ANS';'GTHRD
H_syn';'OPAH';'ADCS';'GLUPRT';'PRFGS';'CTPS2';'NADS2';'COBNAD';'R05224';'ADC
YRS';'GLUR';'GLNS';'ASNN';'NACASPAH';'ASPK';'PPHTA';'ASPCT';'PSP_L';'CYSTS';'V
ALDHR';'GLYTA';'GOR1';'AGTi';'THZPSN';'AOXSr2';'ALAR';'THRS';'LLEUDr';'ILEDH_na
d';'ARGSL';'ARGN';'CYPH_BIA';'DAPDC';'P5CRx';'P5CR';'ARODH_2';'ARODH';'TYRTA'
';'AROH';'METS_1';'UNK3';'GTPC';'CPPPGO2';'METAT';'DMHDRFS_1';'AMPMS3';'CYS
S_2';'ASPTA4';'HISTDb';'AMPTASECG';'ASNS1';'ASPTA';'BTS6';'GF6PTA';'GHMT2r';'P
HETA1';'SPT_syn';'SPTc';'THRA';'TRPS2';'VPAMTr'};

for i=1:70;

load('Data_set_2_iDN1004_PAUTO.mat');

modelfva1= model;

load('Data_set_3_iDN1004_PDIAZO.mat');

modelfva2= model;

modelfva1 = changeObjective(modelfva1,'BOF_ANA_AUTO',0);

modelfva1 = changeObjective(modelfva1,rxnlist(i),1);

modelfva2 = changeObjective(modelfva2,'BOF_ANA_DIAZO',0);

modelfva2 = changeObjective(modelfva2,rxnlist(i),1);

%Change growth constraint to at least gamma=95% of FBA solution

%Change gamma as needed when solution is not feasible

modelfva1 = changeRxnBounds(modelfva1, 'BOF_ANA_AUTO', 0.026885, 'l');

modelfva2 = changeRxnBounds(modelfva2, 'BOF_ANA_DIAZO', 0.02451, 'l');

%Run FBA (Min/Max reaction)

FVAAsolution1 = optimizeCbModel (modelfva1, 'max','one');

```

FVAsolution2 = optimizeCbModel (modelfva1, 'min','one');
FVAsolution3 = optimizeCbModel (modelfva2, 'max','one');
FVAsolution4 = optimizeCbModel (modelfva2, 'min','one');

```

```

PAdataMax(:,i)=FVAsolution1.x;
PAdataMin(:,i)=FVAsolution2.x;
PDdataMax(:,i)=FVAsolution3.x;
PDdataMin(:,i)=FVAsolution4.x;

```

```
end
```

Table C.1 List of reactions for FVA

Reaction	Genes	AA1	AA2	AA3	AA4
'THZPSN'	all3519	Ala			
'AOXSr2'	all0374	Ala			
'ALAR'	alr2458	Ala			
'BTS6'	alr1921	Ala	Met		
'ARGSL'	alr3887	Arg			
'ARGN'	alr2310	Arg			
'CYPH_BIA'	all3922	Arg			
'ASNN'	alr4171	Asp			
'NACASPAH'	alr3912	Asp			
'ASPK'	alr3644 or alr1245	Asp			
'PPHTA'	alr2398	Asp			
'ASPCT'	all1681	Asp			
'CYSS_2'	all1169 or all2521 or alr4552 or alr7586	Cys			
'ASPTA4'	alr4853 or alr1039	Cys			
'GLNS'	alr2328	Gln			
'GDH1'	alr4255	Glu			
'GDH2_nadp'	alr4255	Glu			
'GLUN'	all2934 or all4774	Glu			
'GLMS_b'	alr4344	Glu			
'CBPS'	alr3809 and alr1155	Glu			
'ABTA'	alr2398	Glu			
'ORNTA'	alr2398	Glu			
'P5CD'	alr0540	Glu			
'ANS'	alr3233 or all0414 or (all0328 and all0269)	Glu			
'GTHRDH_syn'	alr2051	Glu			
'OPAH'	all4970	Glu			
'ADCS'	alr3443	Glu			
'GLUPRT'	(all3651 or all0409 or alr1153)	Glu			
'PRFGS'	(all3652 and alr2475 and asr2474)	Glu			
'CTPS2'	alr5000 or alr4798	Glu			
'NADS2'	alr2485	Glu			

Table 8-3 Continued

Reaction	Genes	AA1	AA2	AA3	AA4
'COBNAD'	alr3934	Glu			
'R05224'	alr3934	Glu			
'ADCYRS'	alr2377	Glu			
'GLUR'	(alr0094 or alr2048 or alr4841)	Glu			
'ASNS1'		Glu	Gln	Asp	Asn
'ASPTA'	alr4853 or alr1039	Glu	Asp		
'GF6PTA'	alr3464	Glu	Gln		
'PHETA1'	(alr4853 or all4966 or alr2092)	Glu	Phe		
'GLYTA'	alr1004 or alr2765	Gly			
'GOR1'	alr2355	Gly			
'AGTi'	alr1004	Gly			
'AMPTASECG'	alr0237 or all0594	Gly	Cys		
'GHMT2r'	alr4806	Gly	Ser		
'THRA'	alr3296	Gly	Thr		
'HISTDb'	alr3056 and all1591	His			
'ILEDH_nad'	all0426	Ile			
'LLEUDr'	all0426	Leu			
'DAPDC'	all2997	Lys			
'METS_1'	alr0308	Met			
'UNK3'		Met			
'GTPC'	all3865 and alr3382	Met			
'CPPPGO2'	alr3126	Met			
'METAT'	all3244 or alr4124	Met			
'DMHDRFS_1'	alr3573 and alr4129	Met			
'AMPMS3'	all0982	Met			
'AROH'	alr4334	Phe			
'P5CRx'	alr0488	Pro			
'P5CR'	alr0488	Pro			
'PSP_L'	alr0346 and all1758	Ser			
'CYSTS'	alr4416	Ser			
'SPT_syn'	alr1004	Ser	Gly		
'SPTc'	alr1004	Ser	Ala		
'TRPS2'	(all0410 or all3794) and (alr4811 or all0411)	Ser	Trp		
'THRS'	all2072 or alr3293	Thr			
'ARODH_2'	all1141	Tyr			
'ARODH'	all1141	Tyr			
'TYRTA'	(alr1039 or alr4853 or all4966 or alr2092)	Tyr			
'VALDHr'	all0426	Val			
'VPAMTr'	alr2811	Val	Ala		

APPENDIX D. REGRESSION EQUATIONS FOR MINERAL CONSUMPTION

Table D.1 Regression equations for mineral consumption

Element	Medium	Fe level (ppm)	Nutrient consumption expression	R ²
P (µg/ml)	BG11	0.3	$(0.66 \pm 0.19) + (1.71 \times 10^{-3} \pm 1.16 \times 10^{-4}) * \sqrt{CD}$	0.94
		1.2	$(0.78 \pm 0.42) + (1.94 \times 10^{-3} \pm 2.51 \times 10^{-4}) * \sqrt{CD}$	0.81
		5.0	$(1.81 \pm 0.51) + (2.28 \times 10^{-3} \pm 3.02 \times 10^{-4}) * \sqrt{CD}$	0.80
	BG11 _o	0.3	$(0.43 \pm 0.36) + (2.42 \times 10^{-3} \pm 3.87 \times 10^{-4}) * \sqrt{CD}$	0.74
		1.2	$(0.60 \pm 0.43) + (3.19 \times 10^{-3} \pm 4.48 \times 10^{-4}) * \sqrt{CD}$	0.78
		5.0	$(1.67 \pm 0.69) + (3.77 \times 10^{-3} \pm 6.42 \times 10^{-4}) * \sqrt{CD}$	0.71
	BG11 _u	0.3	$(0.65 \pm 0.36) + (1.35 \times 10^{-6} \pm 3.12 \times 10^{-7}) * CD$	0.57
		1.2	$(-0.23 \pm 0.25) + (2.42 \times 10^{-3} \pm 2.21 \times 10^{-4}) * \sqrt{CD}$	0.92
		5.0	$(0.79 \pm 0.36) + (2.99 \times 10^{-3} \pm 3.26 \times 10^{-4}) * \sqrt{CD}$	0.86
Ca (µg/ml)	BG11	0.3	$(0.07 \pm 0.10) + (9.77 \times 10^{-4} \pm 6.45 \times 10^{-5}) * \sqrt{CD}$	0.94
		1.2	$(0.18 \pm 0.13) + (1.13 \times 10^{-3} \pm 7.85 \times 10^{-5}) * \sqrt{CD}$	0.94
		5.0	$(0.40 \pm 0.17) + (1.29 \times 10^{-3} \pm 1.02 \times 10^{-4}) * \sqrt{CD}$	0.92
	BG11 _o	0.3	$(0.02 \pm 0.43) + (1.57 \times 10^{-3} \pm 4.66 \times 10^{-4}) * \sqrt{CD}$	0.45
		1.2	$(-0.11 \pm 0.33) + (1.95 \times 10^{-3} \pm 3.45 \times 10^{-4}) * \sqrt{CD}$	0.70
		5.0	$(0.99 \pm 0.53) + (2.26 \times 10^{-3} \pm 4.91 \times 10^{-4}) * \sqrt{CD}$	0.60
	BG11 _u	0.3	$(0.36 \pm 0.27) + (1.76 \times 10^{-3} \pm 3.05 \times 10^{-4}) * \sqrt{CD}$	0.71
		1.2	$(0.08 \pm 0.08) + (6.55 \times 10^{-4} \pm 7.25 \times 10^{-5}) * \sqrt{CD}$	0.88
		5.0	$(1.33 \pm 0.42) + (9.18 \times 10^{-4} \pm 3.80 \times 10^{-4}) * \sqrt{CD}$	0.29
Mg (µg/ml)	BG11	0.3	$(0.12 \pm 0.05) + (2.27 \times 10^{-7} \pm 1.22 \times 10^{-8}) * CD$	0.96
		1.2	$(-0.04 \pm 0.33) + (7.24 \times 10^{-4} \pm 1.98 \times 10^{-4}) * \sqrt{CD}$	0.49
		5.0	$(0.003 \pm 0.18) + (7.24 \times 10^{-4} \pm 1.98 \times 10^{-4}) * \sqrt{CD}$	0.83
	BG11 _o	0.3	$(0.05 \pm 0.13) + (6.08 \times 10^{-7} \pm 1.13 \times 10^{-7}) * CD$	0.62
		1.2	$(-0.25 \pm 0.22) + (1.06 \times 10^{-3} \pm 2.27 \times 10^{-4}) * \sqrt{CD}$	0.61
		5.0	$(-0.09 \pm 0.29) + (1.05 \times 10^{-3} \pm 2.67 \times 10^{-4}) * \sqrt{CD}$	0.53
	BG11 _u	0.3	$(0.18 \pm 0.14) + (5.41 \times 10^{-4} \pm 1.52 \times 10^{-4}) * \sqrt{CD}$	0.47
		1.2	$(0.05 \pm 0.07) + (5.21 \times 10^{-4} \pm 6.03 \times 10^{-5}) * \sqrt{CD}$	0.87
		5.0	$(0.10 \pm 0.06) + (4.34 \times 10^{-4} \pm 5.02 \times 10^{-5}) * \sqrt{CD}$	0.84
Mn (µg/ml)	BG11	0.3	$(-0.012 \pm 0.008) + (3.08 \times 10^{-5} \pm 5.14 \times 10^{-6}) * \sqrt{CD}$	0.72
		1.2	$(-0.005 \pm 0.010) + (3.18 \times 10^{-5} \pm 6.27 \times 10^{-6}) * \sqrt{CD}$	0.65
		5.0	$(-0.005 \pm 0.010) + (3.18 \times 10^{-5} \pm 6.27 \times 10^{-6}) * \sqrt{CD}$	0.78
	BG11 _o	0.3	$(0.006 \pm 0.011) + (3.52 \times 10^{-8} \pm 9.57 \times 10^{-9}) * CD$	0.49
		1.2	$(0.002 \pm 0.011) + (4.47 \times 10^{-8} \pm 9.09 \times 10^{-9}) * CD$	0.63
		5.0	$(0.029 \pm 0.013) + (9.72 \times 10^{-5} \pm 1.20 \times 10^{-5}) * \sqrt{CD}$	0.82
	BG11 _u	0.3	$(0.015 \pm 0.010) + (3.39 \times 10^{-5} \pm 1.16 \times 10^{-5}) * \sqrt{CD}$	0.38
		1.2	$(0.007 \pm 0.006) + (3.66 \times 10^{-5} \pm 5.04 \times 10^{-6}) * \sqrt{CD}$	0.83
		5.0	$(0.025 \pm 0.008) + (5.42 \times 10^{-5} \pm 7.28 \times 10^{-6}) * \sqrt{CD}$	0.80
B (µg/ml)	BG11	0.3	$(0.006 \pm 0.004) + (2.59 \times 10^{-5} \pm 2.53 \times 10^{-6}) * \sqrt{CD}$	0.88
		1.2	$(0.003 \pm 0.007) + (3.16 \times 10^{-5} \pm 4.14 \times 10^{-6}) * \sqrt{CD}$	0.80
		5.0	$(0.003 \pm 0.01) + (2.82 \times 10^{-5} \pm 5.54 \times 10^{-6}) * \sqrt{CD}$	0.65
	BG11 _o	0.3	$(-0.001 \pm 0.01) + (6.17 \times 10^{-5} \pm 1.47 \times 10^{-5}) * \sqrt{CD}$	0.56
		1.2	$(-0.007 \pm 0.02) + (6.20 \times 10^{-5} \pm 1.59 \times 10^{-5}) * \sqrt{CD}$	0.52
		5.0	$(-0.005 \pm 0.02) + (3.97 \times 10^{-5} \pm 1.42 \times 10^{-5}) * \sqrt{CD}$	0.36
	BG11 _u	0.3	$(0.01 \pm 0.01) + (4.98 \times 10^{-5} \pm 1.26 \times 10^{-5}) * \sqrt{CD}$	0.53
		1.2	$(0.006 \pm 0.009) + (4.89 \times 10^{-5} \pm 7.82 \times 10^{-6}) * \sqrt{CD}$	0.78
		5.0	$(0.01 \pm 0.008) + (3.32 \times 10^{-5} \pm 7.06 \times 10^{-6}) * \sqrt{CD}$	0.61

Table D.1 Continued

Element	Medium	Fe level (ppm)	Nutrient consumption expression	R ²
Mo (µg/ml)	BG11	0.3	$(0.006 \pm 0.002) + (1.16 \times 10^{-5} \pm 1.14 \times 10^{-6}) * \sqrt{CD}$	0.88
		1.2	$(0.0003 \pm 0.003) + (1.80 \times 10^{-5} \pm 1.94 \times 10^{-6}) * \sqrt{CD}$	0.86
		5.0	$(-0.002 \pm 0.002) + (1.77 \times 10^{-5} \pm 1.10 \times 10^{-6}) * \sqrt{CD}$	0.95
	BG11 _o	0.3	$(0.011 \pm 0.009) + (4.36 \times 10^{-5} \pm 9.45 \times 10^{-6}) * \sqrt{CD}$	0.60
		1.2	$(0.007 \pm 0.004) + (2.75 \times 10^{-5} \pm 4.05 \times 10^{-6}) * \sqrt{CD}$	0.77
		5.0	$(0.018 \pm 0.018) + (5.05 \times 10^{-5} \pm 1.68 \times 10^{-5}) * \sqrt{CD}$	0.39
	BG11 _u	0.3	$(0.005 \pm 0.002) + (2.38 \times 10^{-5} \pm 2.13 \times 10^{-6}) * \sqrt{CD}$	0.90
		1.2	$(0.001 \pm 0.002) + (1.72 \times 10^{-5} \pm 1.65 \times 10^{-6}) * \sqrt{CD}$	0.91
		5.0	$(0.004 \pm 0.004) + (1.94 \times 10^{-5} \pm 3.58 \times 10^{-6}) * \sqrt{CD}$	0.68
Zn (µg/ml)	BG11	0.3	$(0.004 \pm 0.001) + (8.50 \times 10^{-6} \pm 9.21 \times 10^{-7}) * \sqrt{CD}$	0.86
		1.2	$(-0.001 \pm 0.002) + (7.75 \times 10^{-6} \pm 1.19 \times 10^{-6}) * \sqrt{CD}$	0.75
		5.0	$(0.018 \pm 0.006) + (6.56 \times 10^{-6} \pm 3.82 \times 10^{-6}) * \sqrt{CD}$	0.17
	BG11 _o	0.3	$(0.002 \pm 0.003) + (1.36 \times 10^{-5} \pm 3.24 \times 10^{-6}) * \sqrt{CD}$	0.56
		1.2	$(0.002 \pm 0.005) + (1.95 \times 10^{-5} \pm 5.31 \times 10^{-6}) * \sqrt{CD}$	0.49
		5.0	$(-0.001 \pm 0.003) + (8.99 \times 10^{-6} \pm 2.38 \times 10^{-6}) * \sqrt{CD}$	0.50
	BG11 _u	0.3	$(0.005 \pm 0.002) + (7.94 \times 10^{-6} \pm 2.28 \times 10^{-6}) * \sqrt{CD}$	0.46
		1.2	$(0.005 \pm 0.002) + (6.67 \times 10^{-6} \pm 1.67 \times 10^{-6}) * \sqrt{CD}$	0.59
		5.0	$(0.001 \pm 0.001) + (5.63 \times 10^{-6} \pm 7.76 \times 10^{-7}) * \sqrt{CD}$	0.79
Cu (µg/ml)	BG11	0.3	$(0.003 \pm 0.001) + (4.25 \times 10^{-6} \pm 6.49 \times 10^{-7}) * \sqrt{CD}$	0.75
		1.2	$(0.001 \pm 0.001) + (4.50 \times 10^{-6} \pm 5.06 \times 10^{-7}) * \sqrt{CD}$	0.85
		5.0	$(0.001 \pm 0.001) + (4.29 \times 10^{-6} \pm 4.23 \times 10^{-7}) * \sqrt{CD}$	0.88
	BG11 _o	0.3	$(0.00 \pm 0.00) + (5.42 \times 10^{-6} \pm 5.61 \times 10^{-7}) * \sqrt{CD}$	0.87
		1.2	$(0.0001 \pm 0.000) + (3.44 \times 10^{-9} \pm 5.33 \times 10^{-10}) * CD$	0.75
		5.0	$(0.00 \pm 0.001) + (6.85 \times 10^{-6} \pm 1.06 \times 10^{-7}) * \sqrt{CD}$	0.75
	BG11 _u	0.3	$(0.002 \pm 0.001) + (3.52 \times 10^{-6} \pm 7.70 \times 10^{-7}) * \sqrt{CD}$	0.60
		1.2	$(0.001 \pm 0.001) + (4.14 \times 10^{-6} \pm 5.06 \times 10^{-7}) * \sqrt{CD}$	0.86
		5.0	$(0.000 \pm 0.001) + (4.45 \times 10^{-6} \pm 5.01 \times 10^{-7}) * \sqrt{CD}$	0.85

LIST OF REFERENCES

1. Heidorn T, Camsund D, Huang H-H, et al (2011) Synthetic Biology in Cyanobacteria. In: *Methods in Enzymology*. Elsevier, pp 539–579
2. Durall C, Lindblad P (2015) Mechanisms of carbon fixation and engineering for increased carbon fixation in cyanobacteria. *Algal Res* 11:263–270. <https://doi.org/10.1016/j.algal.2015.07.002>
3. Sciuto K, Moro I (2015) Cyanobacteria: the bright and dark sides of a charming group. *Biodivers Conserv* 24:711–738. <https://doi.org/10.1007/s10531-015-0898-4>
4. Gonzalez-Esquer CR, Newnham SE, Kerfeld CA (2016) Bacterial microcompartments as metabolic modules for plant synthetic biology. *Plant J* 87:66–75. <https://doi.org/10.1111/tpj.13166>
5. Kupriyanova EV, Sinetova MA, Cho SM, et al (2013) CO₂-concentrating mechanism in cyanobacterial photosynthesis: organization, physiological role, and evolutionary origin. *Photosynth Res* 117:133–146. <https://doi.org/10.1007/s11120-013-9860-z>
6. Antal TK, Kovalenko IB, Rubin AB, Tyystjärvi E (2013) Photosynthesis-related quantities for education and modeling. *Photosynth Res* 117:1–30. <https://doi.org/10.1007/s11120-013-9945-8>
7. Rosgaard L, de Porcellinis AJ, Jacobsen JH, et al (2012) Bioengineering of carbon fixation, biofuels, and biochemicals in cyanobacteria and plants. *J Biotechnol* 162:134–147. <https://doi.org/10.1016/j.jbiotec.2012.05.006>
8. Zhou J, Zhu T, Cai Z, Li Y (2016) From cyanochemicals to cyanofactories: a review and perspective. *Microb Cell Factories* 15:. <https://doi.org/10.1186/s12934-015-0405-3>
9. US Department of Commerce ESRL Global Monitoring Division - Global Greenhouse Gas Reference Network. <https://www.esrl.noaa.gov/gmd/ccgg/trends/global.html>. Accessed 16 Feb 2020
10. Friend AD, Geider RJ, Behrenfeld MJ, Still CJ (2009) Photosynthesis in Global-Scale Models. In: Laisk A, Nedbal L, Govindjee (eds) *Photosynthesis in silico*. Springer Netherlands, pp 465–497
11. Oren A (2014) Cyanobacteria: biology, ecology and evolution. In: Sharma NK, Rai AK, Stal LJ (eds) *Cyanobacteria*. John Wiley & Sons, Ltd, pp 1–20
12. Shevela D, Pishchalnikov RY, Eichacker LA, Govindjee (2013) Oxygenic Photosynthesis in Cyanobacteria. In: Srivastava AK, Rai AN, Neilan BA (eds) *Stress Biology of Cyanobacteria*. CRC Press/ Taylor & Francis Group, Boca Raton, FL, pp 3–40

13. Becker EW (1994) *Microalgae: Biotechnology and Microbiology*. Cambridge University Press
14. Flores E, Herrero A (2005) *Nitrogen assimilation and nitrogen control in cyanobacteria*. Portland Press Limited
15. Herrero A, Muro-Pastor AM, Flores E (2001) Nitrogen control in cyanobacteria. *J Bacteriol* 183:411–425
16. Ohashi Y, Shi W, Takatani N, et al (2011) Regulation of nitrate assimilation in cyanobacteria. *J Exp Bot* 62:1411–1424. <https://doi.org/10.1093/jxb/erq427>
17. Heimann K, Cirés S (2015) N₂-Fixing Cyanobacteria: Ecology and Biotechnological Applications. In: *Handbook of Marine Microalgae*. Elsevier, pp 501–515
18. Fillat MF (2014) The FUR (ferric uptake regulator) superfamily: Diversity and versatility of key transcriptional regulators. *Arch Biochem Biophys* 546:41–52. <https://doi.org/10.1016/j.abb.2014.01.029>
19. González A, Bes MT, Valladares A, et al (2012) FurA is the master regulator of iron homeostasis and modulates the expression of tetrapyrrole biosynthesis genes in *Anabaena* sp. PCC 7120. *Environ Microbiol* 14:3175–3187. <https://doi.org/10.1111/j.1462-2920.2012.02897.x>
20. López-Gomollón S, Hernández JA, Pellicer S, et al (2007) Cross-talk Between Iron and Nitrogen Regulatory Networks in *Anabaena* (Nostoc) sp. PCC 7120: Identification of Overlapping Genes in FurA and NtcA Regulons. *J Mol Biol* 374:267–281. <https://doi.org/10.1016/j.jmb.2007.09.010>
21. Raven JA, Giordano M, Beardall J, Maberly SC (2012) Algal evolution in relation to atmospheric CO₂: carboxylases, carbon-concentrating mechanisms and carbon oxidation cycles. *Phil Trans R Soc B* 367:493–507. <https://doi.org/10.1098/rstb.2011.0212>
22. Vats SK, Kumar S, Ahuja PS (2011) CO₂ sequestration in plants: lesson from divergent strategies. *Photosynthetica* 49:481–496. <https://doi.org/10.1007/s11099-011-0078-z>
23. Cohen Y, Gurevitz M (2006) *The Prokaryotes - Chapter 2.2 The Cyanobacteria-Ecology-Physiology and Molecular genetics*. Springer US, New York, NY
24. Waterbury J (2006) *The Prokaryotes - Chapter 2.1 The Cyanobacteria - Isolation, Purification and Identification*. Springer US, New York, NY
25. Durai P, Batool M, Choi S (2015) Structure and Effects of Cyanobacterial Lipopolysaccharides. *Mar Drugs* 13:4217–4230. <https://doi.org/10.3390/md13074217>

26. Hoiczky E, Hansel A (2000) Cyanobacterial Cell Walls: News from an Unusual Prokaryotic Envelope. J Bacteriol 182:1191–1199. <https://doi.org/10.1128/JB.182.5.1191-1199.2000>
27. Huang F, Hedman E, Funk C, et al (2004) Isolation of Outer Membrane of *Synechocystis* sp. PCC 6803 and Its Proteomic Characterization. Mol Cell Proteomics 3:586–595. <https://doi.org/10.1074/mcp.M300137-MCP200>
28. Moslavac S, Bredemeier R, Mirus O, et al (2005) Proteomic Analysis of the Outer Membrane of *Anabaena* sp. Strain PCC 7120. J Proteome Res 4:1330–1338. <https://doi.org/10.1021/pr050044c>
29. Nicolaisen K, Mariscal V, Bredemeier R, et al (2009) The outer membrane of a heterocyst-forming cyanobacterium is a permeability barrier for uptake of metabolites that are exchanged between cells. Mol Microbiol 74:58–70. <https://doi.org/10.1111/j.1365-2958.2009.06850.x>
30. van Eerden FJ, de Jong DH, de Vries AH, et al (2015) Characterization of thylakoid lipid membranes from cyanobacteria and higher plants by molecular dynamics simulations. Biochim Biophys Acta BBA - Biomembr 1848:1319–1330. <https://doi.org/10.1016/j.bbamem.2015.02.025>
31. Purves WK, Orians GH, Sadava D, Heller HC (2003) Life: The Science of Biology: Volume III: Plants and Animals. Macmillan
32. Ducat DC, Way JC, Silver PA (2011) Engineering cyanobacteria to generate high-value products. Trends Biotechnol 29:95–103. <https://doi.org/10.1016/j.tibtech.2010.12.003>
33. Hess WR (2011) Cyanobacterial genomics for ecology and biotechnology. Curr Opin Microbiol 14:608–614. <https://doi.org/10.1016/j.mib.2011.07.024>
34. Khlystov NA, Chan WY, Kunjapur AM, et al (2017) Material properties of the cyanobacterial reserve polymer multi-L-arginyl-poly-L-aspartate (cyanophycin). Polymer 109:238–245. <https://doi.org/10.1016/j.polymer.2016.11.058>
35. Singh AK, Sharma L, Mallick N, Mala J (2016) Progress and challenges in producing polyhydroxyalkanoate biopolymers from cyanobacteria. J Appl Phycol. <https://doi.org/10.1007/s10811-016-1006-1>
36. Singh SP, Montgomery BL (2011) Determining cell shape: adaptive regulation of cyanobacterial cellular differentiation and morphology. Trends Microbiol 19:278–285. <https://doi.org/10.1016/j.tim.2011.03.001>
37. Ting CS (2014) The Architecture of Cyanobacteria, Archetypes of Microbial Innovation. In: Hohmann-Marriott MF (ed) The Structural Basis of Biological Energy Generation. Springer Netherlands, pp 249–275

38. Sandh G, Xu L, Bergman B (2012) Diazocyte development in the marine diazotrophic cyanobacterium *Trichodesmium*. *Microbiology* 158:345–352. <https://doi.org/10.1099/mic.0.051268-0>
39. Nürnberg DJ, Mariscal V, Parker J, et al (2014) Branching and intercellular communication in the Section V cyanobacterium *Mastigocladus laminosus*, a complex multicellular prokaryote. *Mol Microbiol* 91:935–949. <https://doi.org/10.1111/mmi.12506>
40. Long BM, Rae BD, Rolland V, et al (2016) Cyanobacterial CO₂-concentrating mechanism components: function and prospects for plant metabolic engineering. *Curr Opin Plant Biol* 31:1–8. <https://doi.org/10.1016/j.pbi.2016.03.002>
41. Vermaas VF (2001) Photosynthesis and respiration in cyanobacteria. *Encycl. Life Sci.*
42. Fromme P, Grotjohann I (2006) Structural Analysis of Cyanobacterial Photosystem I. In: Golbeck JH (ed) *Photosystem I*. Springer Netherlands, pp 47–69
43. Komárek J (2014) Modern classification of cyanobacteria. In: Sharma NK, Rai AK, Stal LJ (eds) *Cyanobacteria*. John Wiley & Sons, Ltd, pp 21–39
44. Koller M, Muhr A, Braunegg G (2014) Microalgae as versatile cellular factories for valued products. *Algal Res* 6:52–63. <https://doi.org/10.1016/j.algal.2014.09.002>
45. Trampe E, Kühl M (2016) Chlorophyll f distribution and dynamics in cyanobacterial beachrock biofilms. *J Phycol* 52:990–996. <https://doi.org/10.1111/jpy.12450>
46. Chakdar H, Pabbi S (2016) Cyanobacterial Phycobilins: Production, Purification, and Regulation. In: Shukla P (ed) *Frontier Discoveries and Innovations in Interdisciplinary Microbiology*. Springer India, New Delhi, pp 45–69
47. Kühl M, Chen M, Larkum AW (2007) Biology of the chlorophyll d-containing cyanobacterium *Acaryochloris marina*. In: *Algae and Cyanobacteria in Extreme Environments*. Springer, pp 101–123
48. Pinevich A, Velichko N, Ivanikova N (2012) Cyanobacteria of the Genus *Prochlorothrix*†. *Front Microbiol* 3:. <https://doi.org/10.3389/fmicb.2012.00173>
49. Kühl M, Larkum AW (2001) The microenvironment and photosynthetic performance of *Prochloron* sp. in symbiosis with didemnid ascidians. In: *Symbiosis*. Springer, pp 273–290
50. Bermejo R (2014) Phycocyanins. In: Sharma NK, Rai AK, Stal LJ (eds) *Cyanobacteria*. John Wiley & Sons, Ltd, pp 209–225
51. Yokono M, Akimoto S, Koyama K, et al (2008) Energy transfer processes in *Gloeobacter violaceus* PCC 7421 that possesses phycobilisomes with a unique

- morphology. *Biochim Biophys Acta BBA - Bioenerg* 1777:55–65. <https://doi.org/10.1016/j.bbabi.2007.11.001>
52. Jablonsky J, Bauwe H, Wolkenhauer O (2011) Modeling the Calvin-Benson cycle. *BMC Syst Biol* 5:185
 53. Blankenship RE (2002) Carbon Metabolism. In: *Molecular Mechanisms of Photosynthesis*. Blackwell Science Ltd, pp 171–203
 54. Kimber MS (2014) Carboxysomes – Sequestering RubisCO for Efficient Carbon Fixation. In: Hohmann-Marriott MF (ed) *The Structural Basis of Biological Energy Generation*. Springer Netherlands, Dordrecht, pp 133–148
 55. Erb TJ, Zarzycki J (2016) Biochemical and synthetic biology approaches to improve photosynthetic CO₂-fixation. *Curr Opin Chem Biol* 34:72–79. <https://doi.org/10.1016/j.cbpa.2016.06.026>
 56. Bar-Even A, Noor E, Lewis NE, Milo R (2010) Design and analysis of synthetic carbon fixation pathways. *Proc Natl Acad Sci* 107:8889–8894. <https://doi.org/10.1073/pnas.0907176107>
 57. Bertrand J-C, Bonin P, Caumette P, et al (2015) Biogeochemical Cycles. In: Bertrand J-C, Caumette P, Lebaron P, et al (eds) *Environmental Microbiology: Fundamentals and Applications*. Springer Netherlands, Dordrecht, pp 511–617
 58. Fair JR, Steinmeyer MA, Penney WR, Crocker SM Perry's Chemical Engineers' Handbook. Gas Absorption and Gas-Liquid System Design, Seventh Edition
 59. Sander R (1999) Compilation of Henry's law constants for inorganic and organic species of potential importance in environmental chemistry. Max-Planck Institute of Chemistry, Air Chemistry Department Mainz, Germany
 60. Price GD, Badger MR, Woodger FJ, Long BM (2007) Advances in understanding the cyanobacterial CO₂-concentrating-mechanism (CCM): functional components, Ci transporters, diversity, genetic regulation and prospects for engineering into plants. *J Exp Bot* 59:1441–1461. <https://doi.org/10.1093/jxb/erm112>
 61. Marion GM, Millero FJ, Camões MF, et al (2011) pH of seawater. *Mar Chem* 126:89–96. <https://doi.org/10.1016/j.marchem.2011.04.002>
 62. Gonçalves AL, Rodrigues CM, Pires JCM, Simões M (2016) The effect of increasing CO₂ concentrations on its capture, biomass production and wastewater bioremediation by microalgae and cyanobacteria. *Algal Res* 14:127–136. <https://doi.org/10.1016/j.algal.2016.01.008>
 63. Singh RN, Sharma S (2012) Development of suitable photobioreactor for algae production – A review. *Renew Sustain Energy Rev* 16:2347–2353. <https://doi.org/10.1016/j.rser.2012.01.026>

64. Jacob-Lopes E, Gimenes Scoparo CH, Queiroz MI, Franco TT (2010) Biotransformations of carbon dioxide in photobioreactors. *Energy Convers Manag* 51:894–900. <https://doi.org/10.1016/j.enconman.2009.11.027>
65. Zhang K, Miyachi S, Kurano N (2001) Evaluation of a vertical flat-plate photobioreactor for outdoor biomass production and carbon dioxide bio-fixation: effects of reactor dimensions, irradiation and cell concentration on the biomass productivity and irradiation utilization efficiency. *Appl Microbiol Biotechnol* 55:428–433
66. Martínez L, Redondas V, García A-I, Morán A (2011) Optimization of growth operational conditions for CO₂ biofixation by native *Synechocystis* sp. *J Chem Technol Biotechnol* 86:681–690. <https://doi.org/10.1002/jctb.2568>
67. González López CV, Acién Fernández FG, Fernández Sevilla JM, et al (2009) Utilization of the cyanobacteria *Anabaena* sp. ATCC 33047 in CO₂ removal processes. *Bioresour Technol* 100:5904–5910. <https://doi.org/10.1016/j.biortech.2009.04.070>
68. Kumar A, Yuan X, Sahu AK, et al (2010) A hollow fiber membrane photo-bioreactor for CO₂ sequestration from combustion gas coupled with wastewater treatment: a process engineering approach. *J Chem Technol Biotechnol* 85:387–394. <https://doi.org/10.1002/jctb.2332>
69. Chiang C-L, Lee C-M, Chen P-C (2011) Utilization of the cyanobacteria *Anabaena* sp. CH1 in biological carbon dioxide mitigation processes. *Bioresour Technol* 102:5400–5405. <https://doi.org/10.1016/j.biortech.2010.10.089>
70. Nayak BK, Das D (2013) Improvement of carbon dioxide biofixation in a photobioreactor using *Anabaena* sp. PCC 7120. *Process Biochem* 48:1126–1132. <https://doi.org/10.1016/j.procbio.2013.05.015>
71. Kajiwara S, Yamada H, Ohkuni N, Ohtaguchi K (1997) Design of the bioreactor for carbon dioxide fixation by *Synechococcus* PCC7942. *Energy Convers Manag* 38:S529–S532. [https://doi.org/10.1016/S0196-8904\(96\)00322-6](https://doi.org/10.1016/S0196-8904(96)00322-6)
72. Jin H-F, Lim B-R, Lee K (2006) Influence of Nitrate Feeding on Carbon Dioxide Fixation by Microalgae. *J Environ Sci Health Part A* 41:2813–2824. <https://doi.org/10.1080/10934520600967928>
73. Sydney EB, Sturm W, de Carvalho JC, et al (2010) Potential carbon dioxide fixation by industrially important microalgae. *Bioresour Technol* 101:5892–5896. <https://doi.org/10.1016/j.biortech.2010.02.088>
74. Sobczuk TM, Camacho FG, Rubio FC, et al (2000) Carbon dioxide uptake efficiency by outdoor microalgal cultures in tubular airlift photobioreactors. *Biotechnol Bioeng* 67:465–475. [https://doi.org/10.1002/\(SICI\)1097-0290\(20000220\)67:4<465::AID-BIT10>3.0.CO;2-9](https://doi.org/10.1002/(SICI)1097-0290(20000220)67:4<465::AID-BIT10>3.0.CO;2-9)

75. Fan L-H, Zhang Y-T, Cheng L-H, et al (2007) Optimization of Carbon Dioxide Fixation by *Chlorella vulgaris* Cultivated in a Membrane-Photobioreactor. *Chem Eng Technol* 30:1094–1099. <https://doi.org/10.1002/ceat.200700141>
76. Hulatt CJ, Thomas DN (2011) Productivity, carbon dioxide uptake and net energy return of microalgal bubble column photobioreactors. *Bioresour Technol* 102:5775–5787. <https://doi.org/10.1016/j.biortech.2011.02.025>
77. Martínez García L (2012) Eliminación de CO₂ con microalgas autóctonas
78. Ho S-H, Chen W-M, Chang J-S (2010) *Scenedesmus obliquus* CNW-N as a potential candidate for CO₂ mitigation and biodiesel production. *Bioresour Technol* 101:8725–8730. <https://doi.org/10.1016/j.biortech.2010.06.112>
79. Tang D, Han W, Li P, et al (2011) CO₂ biofixation and fatty acid composition of *Scenedesmus obliquus* and *Chlorella pyrenoidosa* in response to different CO₂ levels. *Bioresour Technol* 102:3071–3076. <https://doi.org/10.1016/j.biortech.2010.10.047>
80. Leakey ADB, Bernacchi CJ, Dohleman FG, et al (2004) Will photosynthesis of maize (*Zea mays*) in the US Corn Belt increase in future [CO₂] rich atmospheres? An analysis of diurnal courses of CO₂ uptake under free-air concentration enrichment (FACE). *Glob Change Biol* 10:951–962. <https://doi.org/10.1111/j.1529-8817.2003.00767.x>
81. Yordanov I, Tsonev T, Velikova V, et al Changes in CO₂ assimilation, transpiration and stomatal resistance of different wheat cultivars experiencing drought under field conditions. 14
82. Chen TM, Brown RH, Black CC (1970) CO₂ Compensation Concentration, Rate of Photosynthesis, and Carbonic Anhydrase Activity of Plants. *Weed Sci* 18:399–403
83. Fader GM, Koller HR (1983) Relationships between Carbon Assimilation, Partitioning, and Export in Leaves of Two Soybean Cultivars. *Plant Physiol* 73:297–303
84. Lal A, Ku MSB, Edwards GE (1996) Analysis of inhibition of photosynthesis due to water stress in the C₃ species *Hordeum vulgare* and *Vicia faba*: Electron transport, CO₂ fixation and carboxylation capacity. *Photosynth Res* 49:57–69. <https://doi.org/10.1007/BF00029428>
85. Poór P, Gémes K, Horváth F, et al (2011) Salicylic acid treatment via the rooting medium interferes with stomatal response, CO₂ fixation rate and carbohydrate metabolism in tomato, and decreases harmful effects of subsequent salt stress. *Plant Biol* 13:105–114. <https://doi.org/10.1111/j.1438-8677.2010.00344.x>
86. Pearcy RW, Osteryoung K, Calkin HW (1985) Photosynthetic Responses to Dynamic Light Environments by Hawaiian Trees : Time Course of CO₂ Uptake and

Carbon Gain during Sunflecks. *Plant Physiol* 79:896–902.
<https://doi.org/10.1104/pp.79.3.896>

87. Kanno K, Makino A (2010) Increased grain yield and biomass allocation in rice under cool night temperature. *Soil Sci Plant Nutr* 56:412–417.
<https://doi.org/10.1111/j.1747-0765.2010.00473.x>
88. Rae BD, Long BM, Badger MR, Price GD (2013) Functions, Compositions, and Evolution of the Two Types of Carboxysomes: Polyhedral Microcompartments That Facilitate CO₂ Fixation in Cyanobacteria and Some Proteobacteria. *Microbiol Mol Biol Rev* 77:357–379. <https://doi.org/10.1128/MMBR.00061-12>
89. Menon BB, Heinhorst S, Shively JM, Cannon GC (2010) The Carboxysome Shell Is Permeable to Protons. *J Bacteriol* 192:5881–5886.
<https://doi.org/10.1128/JB.00903-10>
90. Hopkinson BM, Young JN, Tansik AL, Binder BJ (2014) The minimal CO₂ concentrating mechanism of *Prochlorococcus* MED4 is effective and efficient. *Plant Physiol* pp.114.247049. <https://doi.org/10.1104/pp.114.247049>
91. Mangan NM, Flamholz A, Hood RD, et al (2016) pH determines the energetic efficiency of the cyanobacterial CO₂ concentrating mechanism. *Proc Natl Acad Sci* 113:E5354–E5362. <https://doi.org/10.1073/pnas.1525145113>
92. Cameron JC, Wilson SC, Bernstein SL, Kerfeld CA (2013) Biogenesis of a Bacterial Organelle: The Carboxysome Assembly Pathway. *Cell* 155:1131–1140.
<https://doi.org/10.1016/j.cell.2013.10.044>
93. Pena KL, Castel SE, de Araujo C, et al (2010) Structural basis of the oxidative activation of the carboxysomal -carbonic anhydrase, CcmM. *Proc Natl Acad Sci* 107:2455–2460. <https://doi.org/10.1073/pnas.0910866107>
94. Badger MR, Price GD, Long BM, Woodger FJ (2006) The environmental plasticity and ecological genomics of the cyanobacterial CO₂ concentrating mechanism. *J Exp Bot* 57:249–265. <https://doi.org/10.1093/jxb/eri286>
95. Burnap R, Hagemann M, Kaplan A (2015) Regulation of CO₂ Concentrating Mechanism in Cyanobacteria. *Life* 5:348–371. <https://doi.org/10.3390/life5010348>
96. Burnap RL, Nambudiri R, Holland S (2013) Regulation of the carbon-concentrating mechanism in the cyanobacterium *Synechocystis* sp. PCC6803 in response to changing light intensity and inorganic carbon availability. *Photosynth Res* 118:115–124. <https://doi.org/10.1007/s11120-013-9912-4>
97. Nishimura T, Takahashi Y, Yamaguchi O, et al (2008) Mechanism of low CO₂-induced activation of the cmp bicarbonate transporter operon by a LysR family protein in the cyanobacterium *Synechococcus elongatus* strain PCC 7942. *Mol Microbiol* 68:98–109. <https://doi.org/10.1111/j.1365-2958.2008.06137.x>

98. Omata T, Gohta S, Takahashi Y, et al (2001) Involvement of a CbbR Homolog in Low CO₂-Induced Activation of the Bicarbonate Transporter Operon in Cyanobacteria. *J Bacteriol* 183:1891–1898. <https://doi.org/10.1128/JB.183.6.1891-1898.2001>
99. Takahashi Y, Yamaguchi O, Omata T (2004) Roles of CmpR, a LysR family transcriptional regulator, in acclimation of the cyanobacterium *Synechococcus* sp. strain PCC 7942 to low-CO₂ and high-light conditions. *Mol Microbiol* 52:837–845. <https://doi.org/10.1111/j.1365-2958.2004.04021.x>
100. Daley SME, Kappell AD, Carrick MJ, Burnap RL (2012) Regulation of the Cyanobacterial CO₂-Concentrating Mechanism Involves Internal Sensing of NADP⁺ and α -Ketogutarate Levels by Transcription Factor CcmR. *PLoS ONE* 7:. <https://doi.org/10.1371/journal.pone.0041286>
101. Wang H-L, Postier BL, Burnap RL (2004) Alterations in Global Patterns of Gene Expression in *Synechocystis* sp. PCC 6803 in Response to Inorganic Carbon Limitation and the Inactivation of *ndhR*, a LysR Family Regulator. *J Biol Chem* 279:5739–5751. <https://doi.org/10.1074/jbc.M311336200>
102. Woodger FJ, Bryant DA, Price GD (2007) Transcriptional Regulation of the CO₂-Concentrating Mechanism in a Euryhaline, Coastal Marine Cyanobacterium, *Synechococcus* sp. Strain PCC 7002: Role of *NdhR/CcmR*. *J Bacteriol* 189:3335–3347. <https://doi.org/10.1128/JB.01745-06>
103. Lieman-Hurwitz J, Haimovich M, Shalev-Malul G, et al (2009) A cyanobacterial AbrB-like protein affects the apparent photosynthetic affinity for CO₂ by modulating low-CO₂-induced gene expression. *Environ Microbiol* 11:927–936. <https://doi.org/10.1111/j.1462-2920.2008.01818.x>
104. Kopf M, Klähn S, Scholz I, et al (2014) Comparative Analysis of the Primary Transcriptome of *Synechocystis* sp. PCC 6803. *DNA Res Int J Rapid Publ Rep Genes Genomes* 21:527–539. <https://doi.org/10.1093/dnares/dsu018>
105. Kopf M, Hess WR (2015) Regulatory RNAs in photosynthetic cyanobacteria. *FEMS Microbiol Rev* 39:301–315. <https://doi.org/10.1093/femsre/fuv017>
106. Richmond A (2004) *Handbook of microalgal culture: biotechnology and applied phycology*. Blackwell Science, Oxford, OX, UK ; Ames, Iowa, USA
107. Markou G, Georgakakis D (2011) Cultivation of filamentous cyanobacteria (blue-green algae) in agro-industrial wastes and wastewaters: A review. *Appl Energy* 88:3389–3401. <https://doi.org/10.1016/j.apenergy.2010.12.042>
108. Luque I, Forchhammer K (2008) Nitrogen Assimilation and C/N Balance Sensing. In: Herrero A, Flores E (eds) *The Cyanobacteria: Molecular Biology, Genomics, and Evolution*. Horizon Scientific Press, pp 341–349

109. Berman-Frank I, Lundgren P, Falkowski P (2003) Nitrogen fixation and photosynthetic oxygen evolution in cyanobacteria. *Res Microbiol* 154:157–164. [https://doi.org/10.1016/S0923-2508\(03\)00029-9](https://doi.org/10.1016/S0923-2508(03)00029-9)
110. Fowler D, Coyle M, Skiba U, et al (2013) The global nitrogen cycle in the twenty-first century. *Phil Trans R Soc B* 368:20130164. <https://doi.org/10.1098/rstb.2013.0164>
111. Hutchins DA, Fu F-X, Zhang Y, et al (2007) CO₂ control of *Trichodesmium* N₂ fixation, photosynthesis, growth rates, and elemental ratios: Implications for past, present, and future ocean biogeochemistry. *Limnol Oceanogr* 52:1293–1304. <https://doi.org/10.4319/lo.2007.52.4.1293>
112. Flores E, Herrero A, Wolk CP, Maldener I (2006) Is the periplasm continuous in filamentous multicellular cyanobacteria? *Trends Microbiol* 14:439–443. <https://doi.org/10.1016/j.tim.2006.08.007>
113. Andersen RA (2005) *Algal culturing techniques*. Elsevier/Academic Press, Burlington, Mass
114. Saha S, Murray P (2018) Exploitation of Microalgae Species for Nutraceutical Purposes: Cultivation Aspects. *Fermentation* 4:46. <https://doi.org/10.3390/fermentation4020046>
115. Herrero A, Picossi S, Flores E (2013) Gene Expression during Heterocyst Differentiation. In: *Advances in Botanical Research*. Elsevier, pp 281–329
116. Li B, Gao M-H, Zhang X-C, Chu X-M (2006) Molecular immune mechanism of C-phycocyanin from *Spirulina platensis* induces apoptosis in HeLa cells in vitro. *Biotechnol Appl Biochem* 43:155–164. <https://doi.org/10.1042/BA20050142>
117. Yang F, Li B, Chu X-M, et al (2014) Molecular mechanism of inhibitory effects of C-phycocyanin combined with all-trans-retinoic acid on the growth of HeLa cells in vitro. *Tumor Biol* 35:5619–5628. <https://doi.org/10.1007/s13277-014-1744-0>
118. Videau P, Wells KN, Singh AJ, et al (2016) Assessment of *Anabaena* sp. Strain PCC 7120 as a Heterologous Expression Host for Cyanobacterial Natural Products: Production of Lyngbyatoxin A. *ACS Synth Biol* 5:978–988. <https://doi.org/10.1021/acssynbio.6b00038>
119. Jiang W, Zhou W, Uchida H, et al (2014) A New Lyngbyatoxin from the Hawaiian Cyanobacterium *Moorea producens*. *Mar Drugs* 12:2748–2759. <https://doi.org/10.3390/md12052748>
120. Mochly-Rosen D, Das K, Grimes KV (2012) Protein kinase C, an elusive therapeutic target? *Nat Rev Drug Discov* 11:937–957. <https://doi.org/10.1038/nrd3871>

121. Clares ME, Moreno J, Guerrero MG, García-González M (2014) Assessment of the CO₂ fixation capacity of *Anabaena* sp. ATCC 33047 outdoor cultures in vertical flat-panel reactors. *J Biotechnol* 187:51–55. <https://doi.org/10.1016/j.jbiotec.2014.07.014>
122. Angermayr SA, Gorchs Rovira A, Hellingwerf KJ (2015) Metabolic engineering of cyanobacteria for the synthesis of commodity products. *Trends Biotechnol* 33:352–361. <https://doi.org/10.1016/j.tibtech.2015.03.009>
123. Singh N, Chanan R (2013) Third Generation Green Energy: Cyanobacteria, Key to Production of Sustainable Energy Through Metabolic Engineering. In: Salar RK, Gahlawat SK, Siwach P, Duhan JS (eds) *Biotechnology: Prospects and Applications*. Springer India, New Delhi, pp 143–152
124. Singh V, Mani I, Chaudhary DK, Dhar PK (2014) Metabolic Engineering of Biosynthetic Pathway for Production of Renewable Biofuels. *Appl Biochem Biotechnol* 172:1158–1171. <https://doi.org/10.1007/s12010-013-0606-3>
125. Baroukh C, Muñoz-Tamayo R, Steyer J-P, Bernard O (2015) A state of the art of metabolic networks of unicellular microalgae and cyanobacteria for biofuel production. *Metab Eng* 30:49–60. <https://doi.org/10.1016/j.ymben.2015.03.019>
126. Lindberg P, Park S, Melis A (2010) Engineering a platform for photosynthetic isoprene production in cyanobacteria, using *Synechocystis* as the model organism. *Metab Eng* 12:70–79. <https://doi.org/10.1016/j.ymben.2009.10.001>
127. Pattanaik B, Lindberg P (2015) Terpenoids and Their Biosynthesis in Cyanobacteria. *Life* 5:269–293. <https://doi.org/10.3390/life5010269>
128. Xue Y, He Q (2015) Cyanobacteria as Cell Factories to Produce Plant Secondary Metabolites. *Front Bioeng Biotechnol* 3:. <https://doi.org/10.3389/fbioe.2015.00057>
129. Oliver JWK, Atsumi S (2014) Metabolic design for cyanobacterial chemical synthesis. *Photosynth Res* 120:249–261. <https://doi.org/10.1007/s11120-014-9997-4>
130. Hays SG, Ducat DC (2015) Engineering cyanobacteria as photosynthetic feedstock factories. *Photosynth Res* 123:285–295. <https://doi.org/10.1007/s11120-014-9980-0>
131. Iglesias AA, Preiss J (1992) Bacterial glycogen and plant starch biosynthesis. *Biochem Educ* 20:196–203. [https://doi.org/10.1016/0307-4412\(92\)90191-N](https://doi.org/10.1016/0307-4412(92)90191-N)
132. Pereira S, Zille A, Micheletti E, et al (2009) Complexity of cyanobacterial exopolysaccharides: composition, structures, inducing factors and putative genes involved in their biosynthesis and assembly. *FEMS Microbiol Rev* 33:917–941. <https://doi.org/10.1111/j.1574-6976.2009.00183.x>

133. Quintana N, Van der Kooy F, Van de Rhee MD, et al (2011) Renewable energy from Cyanobacteria: energy production optimization by metabolic pathway engineering. *Appl Microbiol Biotechnol* 91:471–490. <https://doi.org/10.1007/s00253-011-3394-0>
134. Berg JM, Tymoczko JL, Stryer L (2002) Glycolysis Is an Energy-Conversion Pathway in Many Organisms
135. Berg JM, Tymoczko JL, Stryer L (2002) 20.3 the Pentose Phosphate Pathway Generates NADPH and Synthesizes Five-Carbon Sugars
136. Berg JM, Tymoczko JL, Stryer L (2002) The Citric Acid Cycle
137. Zhang S, Bryant DA (2011) The Tricarboxylic Acid Cycle in Cyanobacteria. *Science* 334:1551–1553. <https://doi.org/10.1126/science.1213272>
138. Stepansky A, Leustek T (2006) Histidine biosynthesis in plants. *Amino Acids* 30:127–142. <https://doi.org/10.1007/s00726-005-0247-0>
139. Berg JM, Tymoczko JL, Stryer L (2002) Oxidative Phosphorylation
140. Renger G, Ludwig B (2011) Mechanism of Photosynthetic Production and Respiratory Reduction of Molecular Dioxygen: A Biophysical and Biochemical Comparison. In: Peschek GA, Obinger C, Renger G (eds) *Bioenergetic Processes of Cyanobacteria*. Springer Netherlands, pp 337–394
141. Sato N, Wada H (2009) Lipid Biosynthesis and its Regulation in Cyanobacteria. In: Wada H, Murata N (eds) *Lipids in Photosynthesis*. Springer Netherlands, pp 157–177
142. Lane CE, Benton MG (2015) Detection of the enzymatically-active polyhydroxyalkanoate synthase subunit gene, phaC, in cyanobacteria via colony PCR. *Mol Cell Probes* 29:454–460. <https://doi.org/10.1016/j.mcp.2015.07.001>
143. Kaewbai-ngam A, Incharoensakdi A, Monshupanee T (2016) Increased accumulation of polyhydroxybutyrate in divergent cyanobacteria under nutrient-deprived photoautotrophy: An efficient conversion of solar energy and carbon dioxide to polyhydroxybutyrate by *Calothrix scytonemicola* TISTR 8095. *Bioresour Technol* 212:342–347. <https://doi.org/10.1016/j.biortech.2016.04.035>
144. Wang B, Pugh S, Nielsen DR, et al (2013) Engineering cyanobacteria for photosynthetic production of 3-hydroxybutyrate directly from CO₂. *Metab Eng* 16:68–77. <https://doi.org/10.1016/j.ymben.2013.01.001>
145. Drosig B (2015) Photo-autotrophic Production of Poly(hydroxyalkanoates) in Cyanobacteria. *Chem Biochem Eng Q* 29:145–156. <https://doi.org/10.15255/CABEQ.2014.2254>

146. Taton A, Lis E, Adin DM, et al (2012) Gene Transfer in *Leptolyngbya* sp. Strain BL0902, a Cyanobacterium Suitable for Production of Biomass and Bioproducts. PLoS ONE 7:e30901. <https://doi.org/10.1371/journal.pone.0030901>
147. Samek D, Mišurcova L, Machu L, et al (2013) Influencing of Amino Acid Composition of Green Freshwater Algae and Cyanobacterium by Methods of Cultivation. Turk J Biochem 38:360–368. <https://doi.org/10.5505/tjb.2013.42104>
148. Kanehisa M, Goto S (2000) KEGG: kyoto encyclopedia of genes and genomes. Nucleic Acids Res 28:27–30. <https://doi.org/10.1093/nar/28.1.27>
149. KEGG PATHWAY Database. <http://www.genome.jp/kegg/pathway.html>. Accessed 2 Apr 2018
150. Lepiniec L, Vidal J, Chollet R, et al (1994) Phosphoenolpyruvate carboxylase: structure, regulation and evolution. Plant Sci 99:111–124
151. Riccardi G, de Rossi E, Milano A (1989) Amino acid biosynthesis and its regulation in cyanobacteria. Plant Sci 64:135–151. [https://doi.org/10.1016/0168-9452\(89\)90018-6](https://doi.org/10.1016/0168-9452(89)90018-6)
152. Ahlgren G, Gustafsson I-B, Boberg M (1992) Fatty Acid Content and Chemical Composition of Freshwater Microalgae1. J Phycol 28:37–50. <https://doi.org/10.1111/j.0022-3646.1992.00037.x>
153. Colman B, Norman EG (1997) Serine synthesis in cyanobacteria by a nonphotorespiratory pathway. Physiol Plant 100:133–136. <https://doi.org/10.1111/j.1399-3054.1997.tb03463.x>
154. Rédei GP (2008) Glycine Biosynthesis. Encycl Genet Genomics Proteomics Inform 808
155. Guédon E, Martin-Verstraete I (2006) Cysteine metabolism and its regulation in bacteria. In: Amino Acid Biosynthesis~ Pathways, Regulation and Metabolic Engineering. Springer, pp 195–218
156. Schneegurt MA, Arieli B, McKeehen JD, et al (1995) Compositional and toxicological evaluation of the diazotrophic Cyanobacterium, *Cyanothece* sp. strain ATCC 51142. Aquaculture 134:339–349. [https://doi.org/10.1016/0044-8486\(95\)00054-6](https://doi.org/10.1016/0044-8486(95)00054-6)
157. Pushparaj B, Pelosi E, Carlozzi P, Torzillo G (1995) Yield and biochemical composition of a marine cyanobacterium (*Nodularia* sp.) in outdoor culture. Aquat Microb Ecol 9:13–16
158. Kulis-Horn RK, Persicke M, Kalinowski J (2014) Histidine biosynthesis, its regulation and biotechnological application in *Corynebacterium glutamicum*. Microb Biotechnol 7:5–25. <https://doi.org/10.1111/1751-7915.12055>

159. Shylajanaciyar M, Dineshbabu G, Rajalakshmi R, et al (2015) Analysis and Elucidation of Phosphoenolpyruvate Carboxylase in Cyanobacteria. *Protein J* 34:73–81. <https://doi.org/10.1007/s10930-015-9598-x>
160. Durall C, Rukminasari N, Lindblad P (2016) Enhanced growth at low light intensity in the cyanobacterium *Synechocystis* PCC 6803 by overexpressing phosphoenolpyruvate carboxylase. *Algal Res* 16:275–281. <https://doi.org/10.1016/j.algal.2016.03.027>
161. Ahmed S, Kumar A, Mishra VK, Ghosh A (2016) Platform Chemicals and Pharmaceutical Industries. In: Platform Chemical Biorefinery. Elsevier, pp 285–306
162. Trautmann A, Watzer B, Wilde A, et al (2016) Effect of phosphate availability on cyanophycin accumulation in *Synechocystis* sp. PCC 6803 and the production strain BW86. *Algal Res* 20:189–196. <https://doi.org/10.1016/j.algal.2016.10.009>
163. Merritt MV, Sid SS, Mesh L, Allen MM (1994) Variations in the amino acid composition of cyanophycin in the cyanobacterium *Synechocystis* sp. PCC 6308 as a function of growth conditions. *Arch Microbiol* 162:158–166. <https://doi.org/10.1007/BF00314469>
164. Burnat M, Herrero A, Flores E (2014) Compartmentalized cyanophycin metabolism in the diazotrophic filaments of a heterocyst-forming cyanobacterium. *Proc Natl Acad Sci* 111:3823–3828. <https://doi.org/10.1073/pnas.1318564111>
165. Aravind J, Saranya T, Sudha G, Kanmani P (2016) A Mini Review on Cyanophycin: Production, Analysis and Its Applications. In: Prashanthi M, Sundaram R (eds) Integrated Waste Management in India. Springer International Publishing, pp 49–58
166. Li H, Sherman D, Bao S, Sherman L (2001) Pattern of cyanophycin accumulation in nitrogen-fixing and non-nitrogen-fixing cyanobacteria. *Arch Microbiol* 176:9–18. <https://doi.org/10.1007/s002030100281>
167. Bouvier F, Rahier A, Camara B (2005) Biogenesis, molecular regulation and function of plant isoprenoids. *Prog Lipid Res* 44:357–429. <https://doi.org/10.1016/j.plipres.2005.09.003>
168. Gao X, Gao F, Liu D, et al (2016) Engineering the methylerythritol phosphate pathway in cyanobacteria for photosynthetic isoprene production from CO₂. *Energy Env Sci* 9:1400–1411. <https://doi.org/10.1039/C5EE03102H>
169. Tanaka R, Takabayashi A, Ito H, Tanaka A (2012) Chlorophyll metabolism in photosynthetic organisms. In: Kadish KM, Smith KM, Guillard R (eds) Handbook of Porphyrin Science (Volumes 16 – 20): With Applications to Chemistry, Physics, Materials Science, Engineering, Biology and Medicine. World Scientific, pp 213–242
170. Von Wettstein D, Gough S, Kannangara C (1995) Chlorophyll Biosynthesis. *Plant Cell* 7:1039–1057

171. Secondary metabolites - Knowledge Encyclopedia. http://www.biologyreference.com/knowledge/Secondary_metabolites.html. Accessed 21 Mar 2017
172. Mandal S, Rath J (2015) Secondary Metabolites of Cyanobacteria and Drug Development. In: Extremophilic Cyanobacteria For Novel Drug Development. Springer International Publishing, Cham, pp 23–43
173. Nagle DG, Paul VJ (1999) Production of Secondary Metabolites by Filamentous Tropical Marine Cyanobacteria: Ecological Functions of the Compounds. *J Phycol* 35:1412–1421. <https://doi.org/10.1046/j.1529-8817.1999.3561412.x>
174. Nunnery JK, Mevers E, Gerwick WH (2010) Biologically active secondary metabolites from marine cyanobacteria. *Curr Opin Biotechnol* 21:787–793. <https://doi.org/10.1016/j.copbio.2010.09.019>
175. Rajneesh, Singh SP, Pathak J, Sinha RP (2017) Cyanobacterial factories for the production of green energy and value-added products: An integrated approach for economic viability. *Renew Sustain Energy Rev* 69:578–595. <https://doi.org/10.1016/j.rser.2016.11.110>
176. Dittmann E, Gugger M, Sivonen K, Fewer DP (2015) Natural Product Biosynthetic Diversity and Comparative Genomics of the Cyanobacteria. *Trends Microbiol* 23:642–652. <https://doi.org/10.1016/j.tim.2015.07.008>
177. Méjean A, Ploux O (2013) A Genomic View of Secondary Metabolite Production in Cyanobacteria. In: *Advances in Botanical Research*. Elsevier, pp 189–234
178. Codd GA, Lindsay J, Young FM, et al (2005) Harmful Cyanobacteria. In: Huisman J, Matthijs HCP, Visser PM (eds) *Harmful Cyanobacteria*. Springer Netherlands, pp 1–23
179. Dittmann E, Fewer DP, Neilan BA (2013) Cyanobacterial toxins: biosynthetic routes and evolutionary roots. *FEMS Microbiol Rev* 37:23–43. <https://doi.org/10.1111/j.1574-6976.2012.12000.x>
180. Puyana M, Acosta A, Bernal-Sotelo K, et al (2014) Spatial scale of cyanobacterial blooms in Old Providence Island, Colombian Caribbean. *Univ Sci* 20:83. <https://doi.org/10.11144/Javeriana.SC20-1.sscb>
181. Palacio HM, Ramírez JJ, Echenique RO, et al (2015) Floristic composition of cyanobacteria in a neotropical, eutrophic reservoir. *Braz J Bot* 38:865–876. <https://doi.org/10.1007/s40415-015-0185-3>
182. Palacio HM, Palacio JA, Echenique RO, et al (2015) *Dolichospermum lemmermannii* (Cyanobacteria): una especie de ambiente templado en un embalse eutrófico neotropical. *Bol Soc Argent Botánica* 50:309–321

183. Burja AM, Banaigs B, Abou-Mansour E, et al (2001) Marine cyanobacteria—a prolific source of natural products. *Tetrahedron* 57:9347–9377
184. Barrios-Llerena ME, Burja AM, Wright PC (2007) Genetic analysis of polyketide synthase and peptide synthetase genes in cyanobacteria as a mining tool for secondary metabolites. *J Ind Microbiol Biotechnol* 34:443–456. <https://doi.org/10.1007/s10295-007-0216-6>
185. Tan LT (2012) Marine Cyanobacteria. In: *Studies in Natural Products Chemistry*. Elsevier, pp 67–110
186. Vijayakumar S, Menakha M (2015) Pharmaceutical applications of cyanobacteria—A review. *J Acute Med* 5:15–23. <https://doi.org/10.1016/j.jacme.2015.02.004>
187. Nagarajan M, Maruthanayagam V, Sundararaman M (2012) A review of pharmacological and toxicological potentials of marine cyanobacterial metabolites: Pharmacologic and toxic potentials of marine cyanotoxins. *J Appl Toxicol* 32:153–185. <https://doi.org/10.1002/jat.1717>
188. Arif JM, Farooqui A, Siddiqui MH, et al (2012) Novel Bioactive Peptides from Cyanobacteria. In: *Studies in Natural Products Chemistry*. Elsevier, pp 111–161
189. Sharma NK, Tiwari SP, Tripathi K, Rai AK (2011) Sustainability and cyanobacteria (blue-green algae): facts and challenges. *J Appl Phycol* 23:1059–1081. <https://doi.org/10.1007/s10811-010-9626-3>
190. Micallef ML, D'Agostino PM, Al-Sinawi B, et al (2015) Exploring cyanobacterial genomes for natural product biosynthesis pathways. *Mar Genomics* 21:1–12. <https://doi.org/10.1016/j.margen.2014.11.009>
191. Rastogi RP, Sinha RP, Moh SH, et al (2014) Ultraviolet radiation and cyanobacteria. *J Photochem Photobiol B* 141:154–169. <https://doi.org/10.1016/j.jphotobiol.2014.09.020>
192. Rastogi RP, Sonani RR, Madamwar D (2015) Cyanobacterial Sunscreen Scytonemin: Role in Photoprotection and Biomedical Research. *Appl Biochem Biotechnol* 176:1551–1563. <https://doi.org/10.1007/s12010-015-1676-1>
193. Klisch M (2008) Mycosporine-Like Amino Acids and Marine Toxins - The Common and the Different. *Mar Drugs* 6:147–163. <https://doi.org/10.3390/md20080008>
194. Sivonen K, Leikoski N, Fewer DP, Jokela J (2010) Cyanobactins—ribosomal cyclic peptides produced by cyanobacteria. *Appl Microbiol Biotechnol* 86:1213–1225. <https://doi.org/10.1007/s00253-010-2482-x>

195. Moss NA, Bertin MJ, Kleigrew K, et al (2016) Integrating mass spectrometry and genomics for cyanobacterial metabolite discovery. *J Ind Microbiol Biotechnol* 43:313–324. <https://doi.org/10.1007/s10295-015-1705-7>
196. Mandal S, Rath J (2015) Issues and Challenges of Drug Development from Cyanobacteria. In: *Extremophilic Cyanobacteria For Novel Drug Development*. Springer International Publishing, Cham, pp 79–89
197. Donia MS, Hathaway BJ, Sudek S, et al (2006) Natural combinatorial peptide libraries in cyanobacterial symbionts of marine ascidians. *Nat Chem Biol* 2:729–735. <https://doi.org/10.1038/nchembio829>
198. Si T, Zhao H (2016) A brief overview of synthetic biology research programs and roadmap studies in the United States. *Synth Syst Biotechnol* 1:258–264. <https://doi.org/10.1016/j.synbio.2016.08.003>
199. Dress L, Hessel A, Cai Y, et al (2011) 3.53 - Synthetic Biology: An Overview. In: Moo-Young M (ed) *Comprehensive Biotechnology (Second Edition)*. Academic Press, Burlington, pp 629–640
200. Berla BM, Saha R, Immethun CM, et al (2013) Synthetic biology of cyanobacteria: unique challenges and opportunities. *Front Microbiol* 4:. <https://doi.org/10.3389/fmicb.2013.00246>
201. Steuer R, Knoop H, Machne R (2012) Modelling cyanobacteria: from metabolism to integrative models of phototrophic growth. *J Exp Bot* 63:2259–2274. <https://doi.org/10.1093/jxb/ers018>
202. Santos F, Boele J, Teusink B (2011) A Practical Guide to Genome-Scale Metabolic Models and Their Analysis. In: *Methods in Enzymology*. Elsevier, pp 509–532
203. Erdrich P, Steuer R, Klamt S (2015) An algorithm for the reduction of genome-scale metabolic network models to meaningful core models. *BMC Syst Biol* 9:. <https://doi.org/10.1186/s12918-015-0191-x>
204. Nogales J, Gudmundsson S, Knight EM, et al (2012) Detailing the optimality of photosynthesis in cyanobacteria through systems biology analysis. *Proc Natl Acad Sci* 109:2678–2683. <https://doi.org/10.1073/pnas.1117907109>
205. Yu Y, You L, Liu D, et al (2013) Development of *Synechocystis* sp. PCC 6803 as a Phototrophic Cell Factory. *Mar Drugs* 11:2894–2916. <https://doi.org/10.3390/md11082894>
206. Fu P (2009) Genome-scale modeling of *Synechocystis* sp. PCC 6803 and prediction of pathway insertion. *J Chem Technol Biotechnol* 84:473–483. <https://doi.org/10.1002/jctb.2065>

207. Knoop H, Zilliges Y, Lockau W, Steuer R (2010) The Metabolic Network of *Synechocystis* sp. PCC 6803: Systemic Properties of Autotrophic Growth. *Plant Physiol* 154:410–422. <https://doi.org/10.1104/pp.110.157198>
208. Saha R, Versepunt AT, Berla BM, et al (2012) Reconstruction and Comparison of the Metabolic Potential of Cyanobacteria *Cyanothece* sp. ATCC 51142 and *Synechocystis* sp. PCC 6803. *PLoS ONE* 7:e48285. <https://doi.org/10.1371/journal.pone.0048285>
209. Montagud A, Navarro E, de Córdoba PF, et al (2010) Reconstruction and analysis of genome-scale metabolic model of a photosynthetic bacterium. *BMC Syst Biol* 4:156
210. Hendry JI, Prasanna CB, Joshi A, et al (2016) Metabolic model of *Synechococcus* sp. PCC 7002: Prediction of flux distribution and network modification for enhanced biofuel production. *Bioresour Technol* 213:190–197. <https://doi.org/10.1016/j.biortech.2016.02.128>
211. Triana J, Montagud A, Siurana M, et al (2014) Generation and Evaluation of a Genome-Scale Metabolic Network Model of *Synechococcus elongatus* PCC7942. *Metabolites* 4:680–698. <https://doi.org/10.3390/metabo4030680>
212. Klanchui A, Khannapho C, Phodee A, et al (2012) i AK692: A genome-scale metabolic model of *Spirulina platensis* C1. *BMC Syst Biol* 6:71
213. Gardner JJ, Boyle NR (2017) The use of genome-scale metabolic network reconstruction to predict fluxes and equilibrium composition of N-fixing versus C-fixing cells in a diazotrophic cyanobacterium, *Trichodesmium erythraeum*. *BMC Syst Biol* 11:. <https://doi.org/10.1186/s12918-016-0383-z>
214. Yoshikawa K, Aikawa S, Kojima Y, et al (2015) Construction of a Genome-Scale Metabolic Model of *Arthrospira platensis* NIES-39 and Metabolic Design for Cyanobacterial Bioproduction. *PLOS ONE* 10:e0144430. <https://doi.org/10.1371/journal.pone.0144430>
215. Case AE, Atsumi S (2016) Cyanobacterial chemical production. *J Biotechnol* 231:106–114. <https://doi.org/10.1016/j.jbiotec.2016.05.023>
216. Oliver NJ, Rabinovitch-Deere CA, Carroll AL, et al (2016) Cyanobacterial metabolic engineering for biofuel and chemical production. *Curr Opin Chem Biol* 35:43–50. <https://doi.org/10.1016/j.cbpa.2016.08.023>
217. Park J, Choi Y (2017) Cofactor engineering in cyanobacteria to overcome imbalance between NADPH and NADH: A mini review. *Front Chem Sci Eng* 11:66–71. <https://doi.org/10.1007/s11705-016-1591-1>
218. Gao X, Sun T, Pei G, et al (2016) Cyanobacterial chassis engineering for enhancing production of biofuels and chemicals. *Appl Microbiol Biotechnol* 100:3401–3413. <https://doi.org/10.1007/s00253-016-7374-2>

219. Sarma MK, Kaushik S, Goswami P (2016) Cyanobacteria: A metabolic power house for harvesting solar energy to produce bio-electricity and biofuels. *Biomass Bioenergy* 90:187–201. <https://doi.org/10.1016/j.biombioe.2016.03.043>
220. Wendt KE, Ungerer J, Cobb RE, et al (2016) CRISPR/Cas9 mediated targeted mutagenesis of the fast growing cyanobacterium *Synechococcus elongatus* UTEX 2973. *Microb Cell Factories* 15:. <https://doi.org/10.1186/s12934-016-0514-7>
221. Li H, Shen CR, Huang C-H, et al (2016) CRISPR-Cas9 for the genome engineering of cyanobacteria and succinate production. *Metab Eng* 38:293–302. <https://doi.org/10.1016/j.ymben.2016.09.006>
222. Ungerer J, Pakrasi HB (2016) Cpf1 Is A Versatile Tool for CRISPR Genome Editing Across Diverse Species of Cyanobacteria. *Sci Rep* 6:. <https://doi.org/10.1038/srep39681>
223. Genome List - Genome - NCBI. <https://www.ncbi.nlm.nih.gov/genome/browse#!/prokaryotes/cyanobacteria>. Accessed 9 Apr 2018
224. Genome List Genomes. [https://www.patricbrc.org/view/GenomeList/?keyword\(cyanobacteria\)#view_tab=genomes](https://www.patricbrc.org/view/GenomeList/?keyword(cyanobacteria)#view_tab=genomes). Accessed 9 Apr 2018
225. Nabout JC, da Silva Rocha B, Carneiro FM, Sant'Anna CL (2013) How many species of Cyanobacteria are there? Using a discovery curve to predict the species number. *Biodivers Conserv* 22:2907–2918. <https://doi.org/10.1007/s10531-013-0561-x>
226. Dexter J, Fu P (2009) Metabolic engineering of cyanobacteria for ethanol production. *Energy Environ Sci* 2:857. <https://doi.org/10.1039/b811937f>
227. Dexter J, Armshaw P, Sheahan C, Pembroke J t. (2015) The state of autotrophic ethanol production in Cyanobacteria. *J Appl Microbiol* 119:11–24. <https://doi.org/10.1111/jam.12821>
228. Gao Z, Zhao H, Li Z, et al (2012) Photosynthetic production of ethanol from carbon dioxide in genetically engineered cyanobacteria. *Energy Env Sci* 5:9857–9865. <https://doi.org/10.1039/C2EE22675H>
229. Kusakabe T, Tatsuke T, Tsuruno K, et al (2013) Engineering a synthetic pathway in cyanobacteria for isopropanol production directly from carbon dioxide and light. *Metab Eng* 20:101–108. <https://doi.org/10.1016/j.ymben.2013.09.007>
230. Lan EI, Liao JC (2011) Metabolic engineering of cyanobacteria for 1-butanol production from carbon dioxide. *Metab Eng* 13:353–363. <https://doi.org/10.1016/j.ymben.2011.04.004>

231. Hirokawa Y, Maki Y, Tatsuke T, Hanai T (2016) Cyanobacterial production of 1,3-propanediol directly from carbon dioxide using a synthetic metabolic pathway. *Metab Eng* 34:97–103. <https://doi.org/10.1016/j.ymben.2015.12.008>
232. Oliver JWK, Machado IMP, Yoneda H, Atsumi S (2013) Cyanobacterial conversion of carbon dioxide to 2,3-butanediol. *Proc Natl Acad Sci* 110:1249–1254. <https://doi.org/10.1073/pnas.1213024110>
233. Jacobsen JH, Frigaard N-U (2014) Engineering of photosynthetic mannitol biosynthesis from CO₂ in a cyanobacterium. *Metab Eng* 21:60–70. <https://doi.org/10.1016/j.ymben.2013.11.004>
234. Winkelhausen E, Velickova E, Amartei SA, Kuzmanova S (2010) Ethanol Production Using Immobilized *Saccharomyces cerevisiae* in Lyophilized Cellulose Gel. *Appl Biochem Biotechnol* 162:2214–2220. <https://doi.org/10.1007/s12010-010-8995-z>
235. Kim Y, Ingram LO, Shanmugam KT (2007) Construction of an *Escherichia coli* K-12 Mutant for Homoethanogenic Fermentation of Glucose or Xylose without Foreign Genes. *Appl Environ Microbiol* 73:1766–1771. <https://doi.org/10.1128/AEM.02456-06>
236. Ji H, Yu J, Zhang X, Tan T (2012) Characteristics of an Immobilized Yeast Cell System Using Very High Gravity for the Fermentation of Ethanol. *Appl Biochem Biotechnol* 168:21–28. <https://doi.org/10.1007/s12010-011-9280-5>
237. Inal M, Yiğitoğlu M (2011) Production of bioethanol by immobilized *Saccharomyces Cerevisiae* onto modified sodium alginate gel. *J Chem Technol Biotechnol* 86:1548–1554. <https://doi.org/10.1002/jctb.2678>
238. Tesfaw A, Assefa F (2014) Current Trends in Bioethanol Production by *Saccharomyces cerevisiae*: Substrate, Inhibitor Reduction, Growth Variables, Coculture, and Immobilization. In: *Int. Sch. Res. Not.* <https://www.hindawi.com/journals/isrn/2014/532852/>. Accessed 10 Apr 2018
239. Hanai T, Atsumi S, Liao JC (2007) Engineered Synthetic Pathway for Isopropanol Production in *Escherichia coli*. *Appl Environ Microbiol* 73:7814–7818. <https://doi.org/10.1128/AEM.01140-07>
240. Liang L, Liu R, Garst AD, et al (2017) CRISPR Enabled Trackable genome Engineering for isopropanol production in *Escherichia coli*. *Metab Eng* 41:1–10. <https://doi.org/10.1016/j.ymben.2017.02.009>
241. Inokuma K, Liao JC, Okamoto M, Hanai T (2010) Improvement of isopropanol production by metabolically engineered *Escherichia coli* using gas stripping. *J Biosci Bioeng* 110:696–701. <https://doi.org/10.1016/j.jbiosc.2010.07.010>

242. Chu H, Xin B, Liu P, et al (2015) Metabolic engineering of *Escherichia coli* for production of (2S,3S)-butane-2,3-diol from glucose. *Biotechnol Biofuels* 8:. <https://doi.org/10.1186/s13068-015-0324-x>
243. Liang K, Shen CR (2017) Engineering cofactor flexibility enhanced 2,3-butanediol production in *Escherichia coli*. *J Ind Microbiol Biotechnol* 44:1605–1612. <https://doi.org/10.1007/s10295-017-1986-0>
244. Xu Y, Chu H, Gao C, et al (2014) Systematic metabolic engineering of *Escherichia coli* for high-yield production of fuel bio-chemical 2,3-butanediol. *Metab Eng* 23:22–33. <https://doi.org/10.1016/j.ymben.2014.02.004>
245. Reshamwala SMS, Pagar SK, Velhal VS, et al (2014) Construction of an efficient *Escherichia coli* whole-cell biocatalyst for d-mannitol production. *J Biosci Bioeng* 118:628–631. <https://doi.org/10.1016/j.jbiosc.2014.05.004>
246. Lan EI, Wei CT (2016) Metabolic engineering of cyanobacteria for the photosynthetic production of succinate. *Metab Eng* 38:483–493. <https://doi.org/10.1016/j.ymben.2016.10.014>
247. Lee SJ, Lee D-Y, Kim TY, et al (2005) Metabolic Engineering of *Escherichia coli* for Enhanced Production of Succinic Acid, Based on Genome Comparison and In Silico Gene Knockout Simulation. *Appl Environ Microbiol* 71:7880–7887. <https://doi.org/10.1128/AEM.71.12.7880-7887.2005>
248. Zhu L-W, Xia S-T, Wei L-N, et al (2016) Enhancing succinic acid biosynthesis in *Escherichia coli* by engineering its global transcription factor, catabolite repressor/activator (Cra). *Sci Rep* 6:36526. <https://doi.org/10.1038/srep36526>
249. Lan EI, Chuang DS, Shen CR, et al (2015) Metabolic engineering of cyanobacteria for photosynthetic 3-hydroxypropionic acid production from CO₂ using *Synechococcus elongatus* PCC 7942. *Metab Eng* 31:163–170. <https://doi.org/10.1016/j.ymben.2015.08.002>
250. Kildegaard KR, Jensen NB, Schneider K, et al (2016) Engineering and systems-level analysis of *Saccharomyces cerevisiae* for production of 3-hydroxypropionic acid via malonyl-CoA reductase-dependent pathway. *Microb Cell Factories* 15:53. <https://doi.org/10.1186/s12934-016-0451-5>
251. Matsakas L, Hrůzová K, Rova U, Christakopoulos P (2018) Biological Production of 3-Hydroxypropionic Acid: An Update on the Current Status. *Fermentation* 4:13. <https://doi.org/10.3390/fermentation4010013>
252. Jung I-Y, Lee J-W, Min W-K, et al (2015) Simultaneous conversion of glucose and xylose to 3-hydroxypropionic acid in engineered *Escherichia coli* by modulation of sugar transport and glycerol synthesis. *Bioresour Technol* 198:709–716. <https://doi.org/10.1016/j.biortech.2015.09.079>

253. Song CW, Kim JW, Cho IJ, Lee SY (2016) Metabolic Engineering of *Escherichia coli* for the Production of 3-Hydroxypropionic Acid and Malonic Acid through β -Alanine Route. *ACS Synth Biol* 5:1256–1263. <https://doi.org/10.1021/acssynbio.6b00007>
254. Liu Q, Ouyang S-P, Chung A, et al (2007) Microbial production of *R*-3-hydroxybutyric acid by recombinant *E. coli* harboring genes of *phbA*, *phbB*, and *tesB*. *Appl Microbiol Biotechnol* 76:811–818. <https://doi.org/10.1007/s00253-007-1063-0>
255. Lee SY, Lee Y (2003) Metabolic Engineering of *Escherichia coli* for Production of Enantiomerically Pure (R)-(-)-Hydroxycarboxylic Acids. *Appl Environ Microbiol* 69:3421–3426. <https://doi.org/10.1128/AEM.69.6.3421-3426.2003>
256. Yao L, Qi F, Tan X, Lu X (2014) Improved production of fatty alcohols in cyanobacteria by metabolic engineering. *Biotechnol Biofuels* 7:94
257. Straka L, Rittmann BE (2018) Effect of culture density on biomass production and light utilization efficiency of *Synechocystis* sp. PCC 6803. *Biotechnol Bioeng* 115:507–511. <https://doi.org/10.1002/bit.26479>
258. Runguphan W, Keasling JD (2014) Metabolic engineering of *Saccharomyces cerevisiae* for production of fatty acid-derived biofuels and chemicals. *Metab Eng* 21:103–113. <https://doi.org/10.1016/j.ymben.2013.07.003>
259. Liu A, Tan X, Yao L, Lu X (2013) Fatty alcohol production in engineered *E. coli* expressing *Marinobacter* fatty acyl-CoA reductases. *Appl Microbiol Biotechnol* 97:7061–7071. <https://doi.org/10.1007/s00253-013-5027-2>
260. Lee HJ, Choi J, Lee S-M, et al (2017) Photosynthetic CO₂ Conversion to Fatty Acid Ethyl Esters (FAEEs) Using Engineered Cyanobacteria. *J Agric Food Chem* 65:1087–1092. <https://doi.org/10.1021/acs.jafc.7b00002>
261. Jong BW de, Shi S, Valle-Rodríguez JO, et al (2015) Metabolic pathway engineering for fatty acid ethyl ester production in *Saccharomyces cerevisiae* using stable chromosomal integration. *J Ind Microbiol Biotechnol* 42:477–486. <https://doi.org/10.1007/s10295-014-1540-2>
262. Steen EJ, Kang Y, Bokinsky G, et al (2010) Microbial production of fatty-acid-derived fuels and chemicals from plant biomass. *Nature* 463:559–562. <https://doi.org/10.1038/nature08721>
263. Kalscheuer R (2006) Microdiesel: *Escherichia coli* engineered for fuel production. *Microbiology* 152:2529–2536. <https://doi.org/10.1099/mic.0.29028-0>

264. Wang W, Liu X, Lu X (2013) Engineering cyanobacteria to improve photosynthetic production of alkanes. *Biotechnol Biofuels* 6:69
265. Fatma Z, Hartman H, Poolman MG, et al (2018) Model-assisted metabolic engineering of *Escherichia coli* for long chain alkane and alcohol production. *Metab Eng* 46:1–12. <https://doi.org/10.1016/j.ymben.2018.01.002>
266. Yang J, Nie Q, Liu H, et al (2016) A novel MVA-mediated pathway for isoprene production in engineered *E. coli*. *BMC Biotechnol* 16:. <https://doi.org/10.1186/s12896-016-0236-2>
267. Kim J-H, Wang C, Jang H-J, et al (2016) Isoprene production by *Escherichia coli* through the exogenous mevalonate pathway with reduced formation of fermentation byproducts. *Microb Cell Factories* 15:. <https://doi.org/10.1186/s12934-016-0612-6>
268. Halfmann C, Gu L, Gibbons W, Zhou R (2014) Genetically engineering cyanobacteria to convert CO₂, water, and light into the long-chain hydrocarbon farnesene. *Appl Microbiol Biotechnol* 98:9869–9877. <https://doi.org/10.1007/s00253-014-6118-4>
269. Wang C, Yoon S-H, Jang H-J, et al (2011) Metabolic engineering of *Escherichia coli* for α -farnesene production. *Metab Eng* 13:648–655. <https://doi.org/10.1016/j.ymben.2011.08.001>
270. Meadows AL, Hawkins KM, Tsegaye Y, et al (2016) Rewriting yeast central carbon metabolism for industrial isoprenoid production. *Nature* 537:694–697. <https://doi.org/10.1038/nature19769>
271. Kiyota H, Okuda Y, Ito M, et al (2014) Engineering of cyanobacteria for the photosynthetic production of limonene from CO₂. *J Biotechnol* 185:1–7. <https://doi.org/10.1016/j.jbiotec.2014.05.025>
272. Alonso-Gutierrez J, Chan R, Batth TS, et al (2013) Metabolic engineering of *Escherichia coli* for limonene and perillyl alcohol production. *Metab Eng* 19:33–41. <https://doi.org/10.1016/j.ymben.2013.05.004>
273. Osanai T, Numata K, Oikawa A, et al (2013) Increased Bioplastic Production with an RNA Polymerase Sigma Factor SigE during Nitrogen Starvation in *Synechocystis* sp. PCC 6803. *DNA Res* 20:525–535. <https://doi.org/10.1093/dnares/dst028>
274. Lau N-S, Foong CP, Kurihara Y, et al (2014) RNA-Seq Analysis Provides Insights for Understanding Photoautotrophic Polyhydroxyalkanoate Production in Recombinant *Synechocystis* Sp. *PLoS ONE* 9:e86368. <https://doi.org/10.1371/journal.pone.0086368>
275. Tsuge T, Yamamoto T, Yano K, et al (2009) Evaluating the Ability of Polyhydroxyalkanoate Synthase Mutants to Produce P(3HB-co-3HA) from Soybean Oil. *Macromol Biosci* 9:71–78. <https://doi.org/10.1002/mabi.200800118>

276. Saranya V, Shenbagarathai R (2011) Production and characterization of PHA from recombinant *E. coli* harbouring phaC1 gene of indigenous *Pseudomonas* sp. LDC-5 using molasses. *Braz J Microbiol* 42:1109–1118. <https://doi.org/10.1590/S1517-83822011000300032>
277. Rodríguez-Contreras A, Koller M, Miranda-de Sousa Dias M, et al (2015) Influence of glycerol on poly(3-hydroxybutyrate) production by *Cupriavidus necator* and *Burkholderia sacchari*. *Biochem Eng J* 94:50–57. <https://doi.org/10.1016/j.bej.2014.11.007>
278. Watzer B, Engelbrecht A, Hauf W, et al (2015) Metabolic pathway engineering using the central signal processor PII. *Microb Cell Factories* 14:. <https://doi.org/10.1186/s12934-015-0384-4>
279. Du J, Li L, Zhou S (2017) Enhanced cyanophycin production by *Escherichia coli* overexpressing the heterologous cphA gene from a deep sea metagenomic library. *J Biosci Bioeng* 123:239–244. <https://doi.org/10.1016/j.jbiosc.2016.08.008>
280. Saha BC, Racine FM (2011) Biotechnological production of mannitol and its applications. *Appl Microbiol Biotechnol* 89:879–891. <https://doi.org/10.1007/s00253-010-2979-3>
281. Werpy T, Petersen G, Aden A, et al (2004) Top value added chemicals from biomass. Volume 1-Results of screening for potential candidates from sugars and synthesis gas. DTIC Document
282. Zhang S, Liu Y, Bryant DA (2015) Metabolic engineering of *Synechococcus* sp. PCC 7002 to produce poly-3-hydroxybutyrate and poly-3-hydroxybutyrate-co-4-hydroxybutyrate. *Metab Eng* 32:174–183. <https://doi.org/10.1016/j.ymben.2015.10.001>
283. Tan X, Yao L, Gao Q, et al (2011) Photosynthesis driven conversion of carbon dioxide to fatty alcohols and hydrocarbons in cyanobacteria. *Metab Eng* 13:169–176. <https://doi.org/10.1016/j.ymben.2011.01.001>
284. Choi SY, Lee HJ, Choi J, et al (2016) Photosynthetic conversion of CO₂ to farnesyl diphosphate-derived phytochemicals (amorpha-4,11-diene and squalene) by engineered cyanobacteria. *Biotechnol Biofuels* 9:. <https://doi.org/10.1186/s13068-016-0617-8>
285. Miyake M, Takase K, Narato M, et al (2000) Polyhydroxybutyrate production from carbon dioxide by cyanobacteria. *Appl Biochem Biotechnol* 84:991–1002
286. Stal LJ (1992) Poly (hydroxyalkanoate) in cyanobacteria: an overview. *FEMS Microbiol Rev* 9:169–180

287. Wang Y, Yin J, Chen G-Q (2014) Polyhydroxyalkanoates, challenges and opportunities. *Curr Opin Biotechnol* 30:59–65. <https://doi.org/10.1016/j.copbio.2014.06.001>
288. Beck C, Knoop H, Axmann IM, Steuer R (2012) The diversity of cyanobacterial metabolism: genome analysis of multiple phototrophic microorganisms. *BMC Genomics* 13:56. <https://doi.org/10.1186/1471-2164-13-56>
289. Wiefel L, Bröker A, Steinbüchel A (2011) Synthesis of a citrulline-rich cyanophycin by use of *Pseudomonas putida* ATCC 4359. *Appl Microbiol Biotechnol* 90:1755–1762. <https://doi.org/10.1007/s00253-011-3224-4>
290. Meussen BJ, Weusthuis RA, Sanders JPM, Graaff LH de (2012) Production of cyanophycin in *Rhizopus oryzae* through the expression of a cyanophycin synthetase encoding gene. *Appl Microbiol Biotechnol* 93:1167–1174. <https://doi.org/10.1007/s00253-011-3604-9>
291. Steinle A, Steinbüchel A (2010) Establishment of a simple and effective isolation method for cyanophycin from recombinant *Saccharomyces cerevisiae*. *Appl Microbiol Biotechnol* 85:1393–1399. <https://doi.org/10.1007/s00253-009-2213-3>
292. Niederholtmeyer H, Wolfstadter BT, Savage DF, et al (2010) Engineering Cyanobacteria To Synthesize and Export Hydrophilic Products. *Appl Environ Microbiol* 76:3462–3466. <https://doi.org/10.1128/AEM.00202-10>
293. Möllers KB, Cannella D, Jørgensen H, Frigaard N-U (2014) Cyanobacterial biomass as carbohydrate and nutrient feedstock for bioethanol production by yeast fermentation. *Biotechnol Biofuels* 7:64
294. Richmond A (1992) Mass Culture of Cyanobacteria. In: Mann NH, Carr NG (eds) *Photosynthetic Prokaryotes*. Springer US, Boston, MA, pp 181–208
295. Takenaka H, Yamaguchi Y (2013) Commercial-scale culturing of cyanobacteria: an industrial experience. In: Sharma NK, Rai AK, Stal LJ (eds) *Cyanobacteria*. John Wiley & Sons, Ltd, Chichester, UK, pp 293–301
296. Welker M, Dittmann E, von Döhren H (2012) Cyanobacteria as a Source of Natural Products. In: *Methods in Enzymology*. Elsevier, pp 23–46
297. Abed RMM, Dobretsov S, Sudesh K (2009) Applications of cyanobacteria in biotechnology. *J Appl Microbiol* 106:1–12. <https://doi.org/10.1111/j.1365-2672.2008.03918.x>
298. Raja R, Hemaiswarya S, Carvalho IS, Ganesan V (2013) Therapeutic applications of cyanobacteria with emphasis on their economics. In: Sharma NK, Rai AK, Stal LJ (eds) *Cyanobacteria*. John Wiley & Sons, Ltd, Chichester, UK, pp 93–102

299. Troschl C, Meixner K, Drosch B, et al (2017) Cyanobacterial PHA Production—Review of Recent Advances and a Summary of Three Years' Working Experience Running a Pilot Plant. *Bioengineering* 4:26. <https://doi.org/10.3390/bioengineering4020026>
300. DIC Welcome to DIC Spirulina | DIC LIFETEC Co., Ltd. <http://www.dlt-spl.co.jp/business/en/spirulina/>. Accessed 9 Sep 2018
301. Cyanotech Spirulina – Cyanotech. <https://www.cyanotech.com/spirulina/>. Accessed 9 Sep 2018
302. Boonsom Boonsom Farm. <https://www.boonsomfarm.com/en/>. Accessed 10 Sep 2018
303. Parry Nutraceuticals organic spirulina | Parry Nutraceuticals | Parry Nutraceuticals. <http://www.parrynutraceuticals.com/products/organic-spirulina/>. Accessed 10 Sep 2018
304. IGV IGV PLANTTECH • Microalgae variety. <http://www.igv-gmbh.de/en/planttech/microalgae-variety/>. Accessed 10 Sep 2018
305. Algae Biotecnologia Algae Biotecnologia. <http://www.algae.com.br/site/en/>. Accessed 10 Sep 2018
306. Algaen Algaen Corporation | Tradition – Nutrition – Innovation. <http://algaen.com/>. Accessed 6 Sep 2018
307. Catarina Guedes A, Katkam NG, Varela J, Xavier Malcata F (2013) Photobioreactors for cyanobacterial culturing. In: Sharma NK, Rai AK, Stal LJ (eds) *Cyanobacteria*. John Wiley & Sons, Ltd, Chichester, UK, pp 270–292
308. Jacob-Lopes E, Mérida LGR, Zepka MIQ and LQ (2015) Microalgal Biorefineries. *Biomass Prod Uses*. <https://doi.org/10.5772/59969>
309. Huisman IH (2000) Membrane Separations: Microfiltration. In: Wilson ID (ed) *Encyclopedia of Separation Science*. Academic Press, Oxford, pp 1764–1777
310. Delattre C, Pierre G, Laroche C, Michaud P (2016) Production, extraction and characterization of microalgal and cyanobacterial exopolysaccharides. *Biotechnol Adv* 34:1159–1179. <https://doi.org/10.1016/j.biotechadv.2016.08.001>
311. Johnson T (2016) Enhancing the Industrial Potential of Filamentous Cyanobacteria. *Electron Theses Diss*
312. Borowitzka MA (2013) Patents on cyanobacteria and cyanobacterial products and uses. In: Sharma NK, Rai AK, Stal LJ (eds) *Cyanobacteria*. John Wiley & Sons, Ltd, Chichester, UK, pp 329–338

313. Jawaharraj K, Karpagam R, Ashokkumar B, et al (2015) Green renewable energy production from *Myxosarcina* sp.: media optimization and assessment of biodiesel fuel properties. *RSC Adv* 5:51149–51157. <https://doi.org/10.1039/C5RA09372D>
314. Algenol Biotech Algenol. In: Algenol. <http://algenol.com/>. Accessed 23 Aug 2018
315. AZoCleantech (2017) Large-Scale Farming of Cyanobacteria Could Provide a New Source of Biofuel. In: AZoCleantech.com. <https://www.azocleantech.com/news.aspx?newsID=24228>. Accessed 23 Aug 2018
316. HelioBioSys About HelioBioSys. In: HelioBioSys. <http://heliobiosys.com/about.html>. Accessed 11 Sep 2018
317. Phytonix Phytonix Corporation. <http://phytonix.com/>. Accessed 11 Sep 2018
318. Cyano Biotech GmbH Cyano Biotech GmbH. <http://www.cyano-biotech.com/content/home/index.php>. Accessed 11 Sep 2018
319. Photanol Scale up Photanol BV to build demonstration plant at AkzoNobel site in Delfzijl. In: Photanol. <https://www.photanol.com/single-post/2018/09/07/Press-release-7918>. Accessed 11 Sep 2018
320. Gupta VK, Tuohy MG, Xu F (2014) *Bioenergy Research: Advances and Applications*. Elsevier
321. Sharma NK, Stal LJ (2013) The economics of cyanobacteria-based biofuel production: challenges and opportunities. In: Sharma NK, Rai AK, Stal LJ (eds) *Cyanobacteria*. John Wiley & Sons, Ltd, Chichester, UK, pp 167–180
322. Yu J, Liberton M, Cliften PF, et al (2015) *Synechococcus elongatus* UTEX 2973, a fast growing cyanobacterial chassis for biosynthesis using light and CO₂. *Sci Rep* 5:8132. <https://doi.org/10.1038/srep08132>
323. Brinkhuis H, Schouten S, Collinson ME, et al (2006) Episodic fresh surface waters in the Eocene Arctic Ocean. *Nature* 441:606–609. <https://doi.org/10.1038/nature04692>
324. Abd-El-Karem Y, Elbers T, Reichelt R, Steinbüchel A (2011) Heterologous expression of *Anabaena* sp. PCC7120 cyanophycin metabolism genes *cphA1* and *cphB1* in *Sinorhizobium* (Ensifer) *meliloti* 1021. *Appl Microbiol Biotechnol* 89:1177–1192. <https://doi.org/10.1007/s00253-010-2891-x>
325. Glass JB, Wolfe-Simon F, Anbar AD (2009) Coevolution of metal availability and nitrogen assimilation in cyanobacteria and algae. *Geobiology* 7:100–123. <https://doi.org/10.1111/j.1472-4669.2009.00190.x>

326. Rippka R, Deruelles J, Waterbury JB, et al (1979) Generic Assignments, Strain Histories and Properties of Pure Cultures of Cyanobacteria. *Microbiology* 111:1–61. <https://doi.org/10.1099/00221287-111-1-1>
327. Herrero A, Flores E, Imperial J (2019) Nitrogen Assimilation in Bacteria. In: Reference Module in Life Sciences. Elsevier, p B9780128096338207000
328. Flores E, Herrero A (2014) Cell Biology of Cyanobacteria. Caister Academic Press
329. Sakamoto T, Delgaizo VB, Bryant DA (1998) Growth on Urea Can Trigger Death and Peroxidation of the Cyanobacterium *Synechococcus* sp. Strain PCC 7002. *APPL Env MICROBIOL* 64:6
330. Sakamoto T, Bryant DA (2001) Requirement of Nickel as an Essential Micronutrient for the Utilization of Urea in the Marine Cyanobacterium *Synechococcus* sp. PCC 7002. *Microbes Environ* 16:177–184. <https://doi.org/10.1264/jsme2.2001.177>
331. Krajewska B (2009) Ureases I. Functional, catalytic and kinetic properties: A review. *J Mol Catal B Enzym* 59:9–21. <https://doi.org/10.1016/j.molcatb.2009.01.003>
332. Veaudor T, Cassier-Chauvat C, Chauvat F (2019) Genomics of Urea Transport and Catabolism in Cyanobacteria: Biotechnological Implications. *Front Microbiol* 10:2052. <https://doi.org/10.3389/fmicb.2019.02052>
333. Lane C (2015) Bioplastic Production in Cyanobacteria and Consensus Degenerate PCR Probe Design. LSU Dr Diss
334. Azevedo R, Rodriguez E, Figueiredo D, et al (2012) Methodologies for the study of filamentous cyanobacteria by flow cytometry. *Fresenius Environ Bull* 21:679–684
335. Ermakova M, Allahverdiyeva Y (2015) Isolation of Heterocysts from *Anabaena* sp. PCC 7120. *BIO-Protoc* 5:. <https://doi.org/10.21769/BioProtoc.1456>
336. Ellis B, Haaland P, Hahne F, et al (2019) flowCore: flowCore: Basic structures for flow cytometry data. R package version 1.48.1.
337. Kaplan D, Calvert HE, Peters GA (1986) The *Azolla*-*Anabaena azollae* Relationship 1. *Plant Physiol* 80:884–890
338. Lichtenthaler HK, Buschmann C (2001) Chlorophylls and Carotenoids: Measurement and Characterization by UV-VIS Spectroscopy. *Curr Protoc Food Anal Chem* 1:F4.3.1-F4.3.8. <https://doi.org/10.1002/0471142913.faf0403s01>
339. Britton G (1985) General carotenoid methods. In: *Methods in Enzymology*. Elsevier, pp 113–149

340. Garcia-Pichel F, Castenholz RW (1991) Characterization and Biological Implications of Scytonemin, a Cyanobacterial Sheath Pigment1. *J Phycol* 27:395–409. <https://doi.org/10.1111/j.0022-3646.1991.00395.x>
341. Rivera SM, Christou P, Canela-Garayoa R (2014) Identification of carotenoids using mass spectrometry. *Mass Spectrom Rev* 33:353–372. <https://doi.org/10.1002/mas.21390>
342. Smith PK, Krohn RI, Hermanson GT, et al (1985) Measurement of protein using bicinchoninic acid. *Anal Biochem* 150:76–85
343. Allen MM (1988) [19] Inclusions: Cyanophycin. In: *Methods in Enzymology*. Academic Press, pp 207–213
344. Messineo L (1966) Modification of the Sakaguchi reaction: spectrophotometric determination of arginine in proteins without previous hydrolysis. *Arch Biochem Biophys* 117:534–540
345. Nielsen SS (2010) Phenol-Sulfuric Acid Method for Total Carbohydrates. In: Nielsen SS (ed) *Food Analysis Laboratory Manual*. Springer US, Boston, MA, pp 47–53
346. Yoo S-H, Spalding MH, Jane J (2002) Characterization of cyanobacterial glycogen isolated from the wild type and from a mutant lacking of branching enzyme. *Carbohydr Res* 337:2195–2203. [https://doi.org/10.1016/s0008-6215\(02\)00228-8](https://doi.org/10.1016/s0008-6215(02)00228-8)
347. Klanchui A, Dulsawat S, Chaloeamngam K, et al (2018) An Improved Genome-Scale Metabolic Model of *Arthrospira platensis* C1 (iAK888) and Its Application in Glycogen Overproduction. *Metabolites* 8:84. <https://doi.org/10.3390/metabo8040084>
348. Neidhardt FC, Ingraham JL, Schaechter M (1990) *Physiology of the Bacterial cell: A molecular approach*. Sinauer Associates Inc., Sunderland, Massachusetts
349. Bligh EG, Dyer WJ (1959) A rapid method of total lipid extraction and purification. *Can J Biochem Physiol* 37:7
350. Work VH, Radakovits R, Jinkerson RE, et al (2010) Increased Lipid Accumulation in the *Chlamydomonas reinhardtii* sta7-10 Starchless Isoamylase Mutant and Increased Carbohydrate Synthesis in Complemented Strains. *Eukaryot Cell* 9:1251–1261. <https://doi.org/10.1128/EC.00075-10>
351. Pendergrass SM (1998) Aerobic Bacteria by GC-FAME Method 0801. In: *NIOSH manual of analytical methods*, 4th edition. Atlanta, Georgia
352. Singh S, Verma E, Tiwari B, et al (2017) Modulation of fatty acids and hydrocarbons in *Anabaena* 7120 and its ntcA mutant under calcium: Modulation of fatty acids and hydrocarbons under calcium. *J Basic Microbiol* 57:171–183. <https://doi.org/10.1002/jobm.201600476>

353. Green MR, Sambrook J, Sambrook J (2012) Molecular cloning: a laboratory manual, 4th ed. Cold Spring Harbor Laboratory Press, Cold Spring Harbor, N.Y
354. Fischer ER, Hansen BT, Nair V, et al (2012) Scanning Electron Microscopy. Curr Protoc Microbiol CHAPTER:Unit2B.2. <https://doi.org/10.1002/9780471729259.mc02b02s25>
355. Liang FT, Xu Q, Sikdar R, et al (2010) BB0250 of *Borrelia burgdorferi* is a conserved and essential inner membrane protein required for cell division. J Bacteriol 192:6105–6115. <https://doi.org/10.1128/JB.00571-10>
356. Herrero A, Muro-Pastor AM, Valladares A, Flores E (2004) Cellular differentiation and the NtcA transcription factor in filamentous cyanobacteria. FEMS Microbiol Rev 28:469–487. <https://doi.org/10.1016/j.femsre.2004.04.003>
357. Odds FC (1981) Biochemical Tests for Identification of Medical Bacteria. J Clin Pathol 34:572. <https://doi.org/10.1136/jcp.34.5.572-a>
358. HACH Total Nitrogen Reagent Set, HR, TNT | Hach USA - Overview. <https://www.hach.com/total-nitrogen-reagent-set-hr-tnt/product?id=7640209860>. Accessed 25 Jul 2019
359. Jung D, Biggs H, Erikson J, Ledyard PU (1975) New Colorimetric Reaction for End-Point, Continuous-Flow, and Kinetic Measurement of Urea. Clin Chem 21:1136–1140. <https://doi.org/10.1093/clinchem/21.8.1136>
360. Environmental Monitoring Systems Laboratory (1996) DETERMINATION OF METALS AND TRACE ELEMENTS IN WATER AND WASTES BY INDUCTIVELY COUPLED PLASMA-ATOMIC EMISSION SPECTROMETRY. In: Methods for the Determination of Metals in Environmental Samples. Elsevier, pp 31–87
361. Rippka R, Deruelles J, Waterbury JB, et al (1979) Generic Assignments, Strain Histories and Properties of Pure Cultures of Cyanobacteria. Microbiology 111:1–61. <https://doi.org/10.1099/00221287-111-1-1>
362. Cuevas DA, Edirisinghe J, Henry CS, et al (2016) From DNA to FBA: How to Build Your Own Genome-Scale Metabolic Model. Front Microbiol 7:. <https://doi.org/10.3389/fmicb.2016.00907>
363. Thiele I, Palsson BØ (2010) A protocol for generating a high-quality genome-scale metabolic reconstruction. Nat Protoc 5:93–121. <https://doi.org/10.1038/nprot.2009.203>
364. Orth JD, Thiele I, Palsson BØ (2010) What is flux balance analysis? Nat Biotechnol 28:245–248. <https://doi.org/10.1038/nbt.1614>
365. Gudmundsson S, Thiele I (2010) Computationally efficient flux variability analysis. BMC Bioinformatics 11:489. <https://doi.org/10.1186/1471-2105-11-489>

366. Mahadevan R, Schilling CH (2003) The effects of alternate optimal solutions in constraint-based genome-scale metabolic models. *Metab Eng* 5:264–276. <https://doi.org/10.1016/j.ymben.2003.09.002>
367. Zuñiga C, Li C-T, Huelsman T, et al (2016) Genome-Scale Metabolic Model for the Green Alga *Chlorella vulgaris* UTEX 395 Accurately Predicts Phenotypes under Autotrophic, Heterotrophic, and Mixotrophic Growth Conditions¹. *Plant Physiol* 172:589–602. <https://doi.org/10.1104/pp.16.00593>
368. Chan SHJ, Cai J, Wang L, et al (2017) Standardizing biomass reactions and ensuring complete mass balance in genome-scale metabolic models. *Bioinformatics* 33:3603–3609. <https://doi.org/10.1093/bioinformatics/btx453>
369. Varma A, Palsson BO (1993) Metabolic capabilities of *Escherichia coli* II: Optimal growth patterns. *J Theor Biol* 165:503–522. <https://doi.org/10.1006/jtbi.1993.1203>
370. Shastri AA, Morgan JA (2005) Flux Balance Analysis of Photoautotrophic Metabolism. *Biotechnol Prog* 21:1617–1626. <https://doi.org/10.1021/bp050246d>
371. Yang C (2002) Metabolic Flux Analysis in *Synechocystis* Using Isotope Distribution from ¹³C-Labeled Glucose. *Metab Eng* 4:202–216. <https://doi.org/10.1006/mben.2002.0226>
372. Liu L, Agren R, Bordel S, Nielsen J (2010) Use of genome-scale metabolic models for understanding microbial physiology. *FEBS Lett* 584:2556–2564. <https://doi.org/10.1016/j.febslet.2010.04.052>
373. Noreña-Caro D, Benton MG (2018) Cyanobacteria as photoautotrophic biofactories of high-value chemicals. *J CO₂ Util* 28:335–366. <https://doi.org/10.1016/j.jcou.2018.10.008>
374. King ZA, Lu J, Dräger A, et al (2016) BiGG Models: A platform for integrating, standardizing and sharing genome-scale models. *Nucleic Acids Res* 44:D515–D522. <https://doi.org/10.1093/nar/gkv1049>
375. Home - Genome - NCBI. <https://www.ncbi.nlm.nih.gov/genome>. Accessed 12 Mar 2019
376. Enzyme Database - BRENDA. <https://www.brenda-enzymes.org/>. Accessed 12 Mar 2019
377. UniProt. <https://www.uniprot.org/>. Accessed 12 Mar 2019
378. KEGG: Kyoto Encyclopedia of Genes and Genomes. <https://www.genome.jp/kegg/>. Accessed 12 Mar 2019
379. PATRIC. <https://www.patricbrc.org/>. Accessed 12 Mar 2019

380. MetaCyc: Metabolic Pathways From all Domains of Life. <https://metacyc.org/>. Accessed 12 Mar 2019
381. Overbeek R, Olson R, Pusch GD, et al (2014) The SEED and the Rapid Annotation of microbial genomes using Subsystems Technology (RAST). *Nucleic Acids Res* 42:D206–D214. <https://doi.org/10.1093/nar/gkt1226>
382. Malatinszky D, Steuer R, Jones PR (2017) A Comprehensively Curated Genome-Scale Two-Cell Model for the Heterocystous Cyanobacterium *Anabaena* sp. PCC 7120. *Plant Physiol* 173:509–523. <https://doi.org/10.1104/pp.16.01487>
383. Zhang C-C, Zhou C-Z, Burnap RL, Peng L (2018) Carbon/Nitrogen Metabolic Balance: Lessons from Cyanobacteria. *Trends Plant Sci* 23:1116–1130. <https://doi.org/10.1016/j.tplants.2018.09.008>
384. Obst M, Steinbüchel A (2006) Cyanophycin—an ideal bacterial nitrogen storage material with unique chemical properties. In: *Inclusions in prokaryotes*. Springer, pp 167–193
385. Zilliges Y (2014) Glycogen: a Dynamic cellular sink and reservoir for carbon. In: *The Cell Biology of Cyanobacteria*. Caister Academic Press, pp 189–210
386. Mao X, Liu Z, Sun J, Lee SY (2017) Metabolic engineering for the microbial production of marine bioactive compounds. *Biotechnol Adv* 35:1004–1021. <https://doi.org/10.1016/j.biotechadv.2017.03.001>
387. Schluchter WM, Shen G, Alvey RM, et al (2010) Phycobiliprotein Biosynthesis in Cyanobacteria: Structure and Function of Enzymes Involved in Post-translational Modification. In: Hallenbeck PC (ed) *Recent Advances in Phototrophic Prokaryotes*. Springer New York, pp 211–228
388. Oborník M, Green BR (2005) Mosaic Origin of the Heme Biosynthesis Pathway in Photosynthetic Eukaryotes. *Mol Biol Evol* 22:2343–2353. <https://doi.org/10.1093/molbev/msi230>
389. Fujita Y, Tsujimoto R, Aoki R (2015) Evolutionary Aspects and Regulation of Tetrapyrrole Biosynthesis in Cyanobacteria under Aerobic and Anaerobic Environments. *Life* 5:1172–1203. <https://doi.org/10.3390/life5021172>
390. Nicolaisen K, Moslavac S, Samborski A, et al (2008) Alr0397 Is an Outer Membrane Transporter for the Siderophore Schizokinen in *Anabaena* sp. Strain PCC 7120. *J Bacteriol* 190:7500–7507. <https://doi.org/10.1128/JB.01062-08>
391. Goldman SJ, Lammers PJ, Berman MS, Sanders-Loehr J (1983) Siderophore-mediated iron uptake in different strains of *Anabaena* sp. *J Bacteriol* 156:1144–1150
392. Lynch D, O'Brien J, Welch T, et al (2001) Genetic Organization of the Region Encoding Regulation, Biosynthesis, and Transport of Rhizobactin 1021, a

- Siderophore Produced by *Sinorhizobium meliloti*. *J Bacteriol* 183:2576–2585. <https://doi.org/10.1128/JB.183.8.2576-2585.2001>
393. Årstøl E, Hohmann-Marriott MF (2019) Cyanobacterial Siderophores—Physiology, Structure, Biosynthesis, and Applications. *Mar Drugs* 17:281. <https://doi.org/10.3390/md17050281>
 394. Heemstra JR, Walsh CT, Sattely ES (2009) Enzymatic Tailoring of Ornithine in the Biosynthesis of the *Rhizobium* Cyclic Trihydroxamate Siderophore Vicibactin. *J Am Chem Soc* 131:15317–15329. <https://doi.org/10.1021/ja9056008>
 395. Ghosh M, Miller PA, Möllmann U, et al (2017) Targeted Antibiotic Delivery: Selective Siderophore Conjugation with Daptomycin Confers Potent Activity against Multidrug Resistant *Acinetobacter baumannii* Both in Vitro and in Vivo. *J Med Chem* 7
 396. Wilson BR, Bogdan AR, Miyazawa M, et al (2016) Siderophores in Iron Metabolism: From Mechanism to Therapy Potential. *Trends Mol Med* 22:1077–1090. <https://doi.org/10.1016/j.molmed.2016.10.005>
 397. Solter PF, Beasley VR (2013) Chapter 38 - Phycotoxins. In: Haschek WM, Rousseaux CG, Wallig MA (eds) *Haschek and Rousseaux's Handbook of Toxicologic Pathology* (Third Edition). Academic Press, Boston, pp 1155–1186
 398. Kim EJ, Lee JH, Choi H, et al (2012) Heterologous Production of 4-O-Demethylbarbamide, a Marine Cyanobacterial Natural Product. *Org Lett* 14:5824–5827. <https://doi.org/10.1021/ol302575h>
 399. Zhang L, Hoshino S, Awakawa T, et al (2016) Structural Diversification of Lyngbyatoxin A by Host-Dependent Heterologous Expression of the *tleABC* Biosynthetic Gene Cluster. *ChemBioChem* 17:1407–1411. <https://doi.org/10.1002/cbic.201600229>
 400. Balskus EP, Walsh CT (2010) The genetic and molecular basis for sunscreen biosynthesis in cyanobacteria. *Science* 329:1653–1656. <https://doi.org/10.1126/science.1193637>
 401. Soule T, Palmer K, Gao Q, et al (2009) A comparative genomics approach to understanding the biosynthesis of the sunscreen scytonemin in cyanobacteria. *BMC Genomics* 10:336. <https://doi.org/10.1186/1471-2164-10-336>
 402. Huang I-S, Zimba PV (2019) Cyanobacterial bioactive metabolites—A review of their chemistry and biology. *Harmful Algae* 83:42–94. <https://doi.org/10.1016/j.hal.2018.11.008>
 403. Rutherford SM, Gilani GS (2009) Amino Acid Analysis. In: Coligan JE, Dunn BM, Speicher DW, Wingfield PT (eds) *Current Protocols in Protein Science*. John Wiley & Sons, Inc., Hoboken, NJ, USA, pp 11.9.1–11.9.37

404. Tibocha-Bonilla JD, Zuñiga C, Godoy-Silva RD, Zengler K (2018) Advances in metabolic modeling of oleaginous microalgae. *Biotechnol Biofuels* 11:241. <https://doi.org/10.1186/s13068-018-1244-3>
405. Hendry JI, Gopalakrishnan S, Ungerer J, et al (2019) Genome-Scale Fluxome of *Synechococcus elongatus* UTEX 2973 Using Transient ¹³C-Labeling Data. *Plant Physiol* 179:761–769. <https://doi.org/10.1104/pp.18.01357>
406. Adebiyi AO, Jazmin LJ, Young JD (2015) ¹³C flux analysis of cyanobacterial metabolism. *Photosynth Res* 126:19–32. <https://doi.org/10.1007/s11120-014-0045-1>
407. Jazmin LJ, Xu Y, Cheah YE, et al (2017) Isotopically nonstationary ¹³C flux analysis of cyanobacterial isobutyraldehyde production. *Metab Eng* 42:9–18. <https://doi.org/10.1016/j.ymben.2017.05.001>
408. Kaneko T (2001) Complete Genomic Sequence of the Filamentous Nitrogen-fixing Cyanobacterium *Anabaena* sp. Strain PCC 7120. *DNA Res* 8:205–213. <https://doi.org/10.1093/dnares/8.5.205>
409. Wattam AR, Davis JJ, Assaf R, et al (2017) Improvements to PATRIC, the all-bacterial Bioinformatics Database and Analysis Resource Center. *Nucleic Acids Res* 45:D535–D542. <https://doi.org/10.1093/nar/gkw1017>
410. Caspi R, Altman T, Billington R, et al (2014) The MetaCyc database of metabolic pathways and enzymes and the BioCyc collection of Pathway/Genome Databases. *Nucleic Acids Res* 42:D459–D471. <https://doi.org/10.1093/nar/gkt1103>
411. The UniProt Consortium (2019) UniProt: a worldwide hub of protein knowledge. *Nucleic Acids Res* 47:D506–D515. <https://doi.org/10.1093/nar/gky1049>
412. Heirendt L, Arreckx S, Pfau T, et al (2019) Creation and analysis of biochemical constraint-based models using the COBRA Toolbox v.3.0. *Nat Protoc* 14:639. <https://doi.org/10.1038/s41596-018-0098-2>
413. Lieven C, Beber ME, Olivier BG, et al (2018) Memote: A community driven effort towards a standardized genome-scale metabolic model test suite. *bioRxiv* 350991. <https://doi.org/10.1101/350991>
414. Ebrahim A, Lerman JA, Palsson BO, Hyduke DR (2013) COBRApy: COntstraints-Based Reconstruction and Analysis for Python. *BMC Syst Biol* 7:74. <https://doi.org/10.1186/1752-0509-7-74>
415. King ZA, Dräger A, Ebrahim A, et al (2015) Escher: A Web Application for Building, Sharing, and Embedding Data-Rich Visualizations of Biological Pathways. *PLOS Comput Biol* 11:e1004321. <https://doi.org/10.1371/journal.pcbi.1004321>

416. Bryant DA, Glazer AN, Eiserling FA (1976) Characterization and structural properties of the major biliproteins of *Anabaena* sp. *Arch Microbiol* 110:61–75. <https://doi.org/10.1007/BF00416970>
417. Nicolaisen K, Mariscal V, Bredemeier R, et al (2009) The outer membrane of a heterocyst-forming cyanobacterium is a permeability barrier for uptake of metabolites that are exchanged between cells. *Mol Microbiol* 74:58–70. <https://doi.org/10.1111/j.1365-2958.2009.06850.x>
418. Chi X, Yang Q, Zhao F, et al (2008) Comparative Analysis of Fatty Acid Desaturases in Cyanobacterial Genomes. In: *Int. J. Genomics*. <https://www.hindawi.com/journals/ijg/2008/284508/>. Accessed 8 Jul 2019
419. Zhang Q, You Z, Miao X (2018) Variation of fatty acid desaturation in response to different nitrate levels in *Auxenochlorella pyrenoidosa*. *R Soc Open Sci* 5:. <https://doi.org/10.1098/rsos.181236>
420. Lin Q, Lin J (2011) Effects of nitrogen source and concentration on biomass and oil production of a *Scenedesmus rubescens* like microalga. *Bioresour Technol* 102:1615–1621. <https://doi.org/10.1016/j.biortech.2010.09.008>
421. Sturme MHJ, Gong Y, Heinrich JM, et al (2018) Transcriptome analysis reveals the genetic foundation for the dynamics of starch and lipid production in *Ettlia oleoabundans*. *Algal Res* 33:142–155. <https://doi.org/10.1016/j.algal.2018.05.004>
422. Negi S, Barry AN, Friedland N, et al (2016) Impact of nitrogen limitation on biomass, photosynthesis, and lipid accumulation in *Chlorella sorokiniana*. *J Appl Phycol* 28:803–812. <https://doi.org/10.1007/s10811-015-0652-z>
423. Herrero A, Muro-Pastor AM, Flores E (2001) Nitrogen Control in Cyanobacteria. *J Bacteriol* 183:411–425. <https://doi.org/10.1128/JB.183.2.411-425.2001>
424. Flaherty BL, Van Nieuwerburgh F, Head SR, Golden JW (2011) Directional RNA deep sequencing sheds new light on the transcriptional response of *Anabaena* sp. strain PCC 7120 to combined-nitrogen deprivation. *BMC Genomics* 12:. <https://doi.org/10.1186/1471-2164-12-332>
425. Wu F, Yang Z, Kuang T (2006) Impaired Photosynthesis in Phosphatidylglycerol-Deficient Mutant of Cyanobacterium *Anabaena* sp. PCC7120 with a Disrupted Gene Encoding a Putative Phosphatidylglycerophosphatase. *PLANT Physiol* 141:1274–1283. <https://doi.org/10.1104/pp.106.083451>
426. Deli J, Gonda S, Nagy LZs, et al (2014) Carotenoid composition of three bloom-forming algae species. *Food Res Int* 65:215–223. <https://doi.org/10.1016/j.foodres.2014.05.020>
427. Mochimaru M, Masukawa H, Takaichi S (2005) The cyanobacterium *Anabaena* sp. PCC 7120 has two distinct β -carotene ketolases: CrtO for echinenone and CrtW for

ketomyxol synthesis. FEBS Lett 579:6111–6114.
<https://doi.org/10.1016/j.febslet.2005.09.081>

428. Takaichi S, Maoka T, Mochimaru M (2009) Unique Carotenoids in the Terrestrial Cyanobacterium *Nostoc commune* NIES-24: 2-Hydroxymyxol 2'-Fucoside, Nostoxanthin and Canthaxanthin. *Curr Microbiol* 59:413–419. <https://doi.org/10.1007/s00284-009-9453-4>
429. Goodwin TW (1957) The Nature and Distribution of Carotenoids in some Blue-Green Algae. *J Gen Microbiol* 17:467–473. <https://doi.org/10.1099/00221287-17-2-467>
430. Takaichi S, Mochimaru M, Maoka T, Katoh H (2005) Myxol and 4-Ketomyxol 2'-Fucosides, not Rhamnosides, from *Anabaena* sp. PCC 7120 and *Nostoc punctiforme* PCC 73102, and Proposal for the Biosynthetic Pathway of Carotenoids. *Plant Cell Physiol* 46:497–504. <https://doi.org/10.1093/pcp/pci049>
431. Mochimaru M, Masukawa H, Maoka T, et al (2008) Substrate specificities and availability of fucosyltransferase and beta-carotene hydroxylase for myxol 2'-fucoside synthesis in *Anabaena* sp. strain PCC 7120 compared with *Synechocystis* sp. strain PCC 6803. *J Bacteriol* 190:6726–6733. <https://doi.org/10.1128/JB.01881-07>
432. Tarento TDC, McClure DD, Vasiljevski E, et al (2018) Microalgae as a source of vitamin K1. *Algal Res* 36:77–87. <https://doi.org/10.1016/j.algal.2018.10.008>
433. Assunção MFG, Amaral R, Martins CB, et al (2017) Screening microalgae as potential sources of antioxidants. *J Appl Phycol* 29:865–877. <https://doi.org/10.1007/s10811-016-0980-7>
434. Schledz M, Seidler A, Beyer P, Neuhaus G (2001) A novel phytyltransferase from *Synechocystis* sp. PCC 6803 involved in tocopherol biosynthesis. *FEBS Lett* 499:15–20. [https://doi.org/10.1016/S0014-5793\(01\)02508-X](https://doi.org/10.1016/S0014-5793(01)02508-X)
435. Amrhein V, Greenland S, McShane B (2019) Scientists rise up against statistical significance. *Nature* 567:305. <https://doi.org/10.1038/d41586-019-00857-9>
436. Frankenberg N, Mukougawa K, Kohchi T, Lagarias JC (2001) Functional Genomic Analysis of the HY2 Family of Ferredoxin-Dependent Bilin Reductases from Oxygenic Photosynthetic Organisms. *Plant Cell* 13:965–978. <https://doi.org/10.1105/tpc.13.4.965>
437. Brown TL (2012) *Chemistry: the central science*, 12th ed. Prentice Hall, Boston
438. National Institute of Standards and Technology (NIST) (2019) Carbon dioxide properties. <https://webbook.nist.gov/cgi/inchi?ID=C124389&Mask=10>. Accessed 21 Nov 2019

439. Wang X, Conway W, Burns R, et al (2010) Comprehensive Study of the Hydration and Dehydration Reactions of Carbon Dioxide in Aqueous Solution. *J Phys Chem A* 114:1734–1740. <https://doi.org/10.1021/jp909019u>
440. Ogawa T, Kaplan A (2003) Inorganic carbon acquisition systems in cyanobacteria. *Photosynth Res* 77:105–115. <https://doi.org/10.1023/A:1025865500026>
441. Kamennaya NA, Ahn S, Park H, et al (2015) Installing extra bicarbonate transporters in the cyanobacterium *Synechocystis* sp. PCC6803 enhances biomass production. *Metab Eng* 29:76–85. <https://doi.org/10.1016/j.ymben.2015.03.002>
442. Parmar A, Singh NK, Pandey A, et al (2011) Cyanobacteria and microalgae: A positive prospect for biofuels. *Bioresour Technol* 102:10163–10172. <https://doi.org/10.1016/j.biortech.2011.08.030>
443. Bolay P, Muro-Pastor M, Florencio F, Klähn S (2018) The Distinctive Regulation of Cyanobacterial Glutamine Synthetase. *Life* 8:52. <https://doi.org/10.3390/life8040052>
444. Ravel JM, Wang SF, Heinemeyer C, Shive W (1965) Glutamyl and glutaminyl ribonucleic acid synthetases of *Escherichia coli* w. Separation, properties, and stimulation of adenosine triphosphate-pyrophosphate exchange by acceptor ribonucleic acid. *J Biol Chem* 240:432–438
445. Bowes G, Ogren WL, Hageman RH (1971) Phosphoglycolate production catalyzed by ribulose diphosphate carboxylase. *Biochem Biophys Res Commun* 45:716–722. [https://doi.org/10.1016/0006-291x\(71\)90475-x](https://doi.org/10.1016/0006-291x(71)90475-x)
446. Engelking LR (2015) Chapter 59 - Sphingolipids. In: Engelking LR (ed) *Textbook of Veterinary Physiological Chemistry* (Third Edition). Academic Press, Boston, pp 378–383
447. Sajna KV, Gottumukkala LD, Sukumaran RK, Pandey A (2015) Chapter 18 - White Biotechnology in Cosmetics. In: Pandey A, Höfer R, Taherzadeh M, et al (eds) *Industrial Biorefineries & White Biotechnology*. Elsevier, Amsterdam, pp 607–652
448. Miao R, Liu X, Englund E, et al (2017) Isobutanol production in *Synechocystis* PCC 6803 using heterologous and endogenous alcohol dehydrogenases. *Metab Eng Commun* 5:45–53. <https://doi.org/10.1016/j.meteno.2017.07.003>
449. Miao R, Xie H, Lindblad P (2018) Enhancement of photosynthetic isobutanol production in engineered cells of *Synechocystis* PCC 6803. *Biotechnol Biofuels* 11:. <https://doi.org/10.1186/s13068-018-1268-8>
450. Cardozo KHM, Guaratini T, Barros MP, et al (2007) Metabolites from algae with economical impact. *Comp Biochem Physiol Part C Toxicol Pharmacol* 146:60–78. <https://doi.org/10.1016/j.cbpc.2006.05.007>

451. Katoch M, Mazmouz R, Chau R, et al (2016) Heterologous Production of Cyanobacterial Mycosporine-Like Amino Acids Mycosporine-Ornithine and Mycosporine-Lysine in *Escherichia coli*. *Appl Environ Microbiol* 82:6167–6173. <https://doi.org/10.1128/AEM.01632-16>
452. Martínez-Francés E, Escudero-Oñate C (2018) Cyanobacteria and Microalgae in the Production of Valuable Bioactive Compounds. *Microalgal Biotechnol*. <https://doi.org/10.5772/intechopen.74043>
453. Noreña-Caro D, Benton MG (2018) Cyanobacteria as photoautotrophic biofactories of high-value chemicals. *J CO2 Util* 28:335–366. <https://doi.org/10.1016/j.jcou.2018.10.008>
454. Tiwari S, Parihar P, Patel A, et al (2019) Metals in Cyanobacteria: Physiological and Molecular Regulation. In: *Cyanobacteria*. Elsevier, pp 261–276
455. Hutchins DA, Rueter JG, Fish W (1991) Siderophore production and nitrogenfixation are mutually exclusive strategies in *Anabaena* 712. *Limnol Oceanogr* 36:1–12. <https://doi.org/10.4319/lo.1991.36.1.0001>
456. Shcolnick S, Keren N (2006) Metal Homeostasis in Cyanobacteria and Chloroplasts. Balancing Benefits and Risks to the Photosynthetic Apparatus. *Plant Physiol* 141:805–810. <https://doi.org/10.1104/pp.106.079251>
457. Keren N, Aurora R, Pakrasi HB (2004) Critical Roles of Bacterioferritins in Iron Storage and Proliferation of Cyanobacteria. *Plant Physiol* 135:1666–1673. <https://doi.org/10.1104/pp.104.042770>
458. Touati D (2000) Iron and Oxidative Stress in Bacteria. *Arch Biochem Biophys* 373:1–6. <https://doi.org/10.1006/abbi.1999.1518>
459. González A, Bes MT, Peleato ML, Fillat MF (2016) Expanding the Role of FurA as Essential Global Regulator in Cyanobacteria. *PLOS ONE* 11:e0151384. <https://doi.org/10.1371/journal.pone.0151384>
460. Kaushik MS, Singh P, Tiwari B, Mishra AK (2016) Ferric Uptake Regulator (FUR) protein: properties and implications in cyanobacteria. *Ann Microbiol* 66:61–75. <https://doi.org/10.1007/s13213-015-1134-x>
461. Kaushik MS, Srivastava M, Verma E, Mishra AK (2015) Role of manganese in protection against oxidative stress under iron starvation in cyanobacterium *Anabaena* 7120. *J Basic Microbiol* 55:729–740. <https://doi.org/10.1002/jobm.201400742>
462. Blindauer CA (2008) Zinc-Handling in Cyanobacteria: An Update. *Chem Biodivers* 5:1990–2013. <https://doi.org/10.1002/cbdv.200890183>

463. Bonilla I, Garcia-González M, Mateo P (1990) Boron Requirement in Cyanobacteria: Its Possible Role in the Early Evolution of Photosynthetic Organisms. *Plant Physiol* 94:1554–1560. <https://doi.org/10.1104/pp.94.4.1554>
464. Umena Y, Kawakami K, Shen J-R, Kamiya N (2011) Crystal structure of oxygen-evolving photosystem II at a resolution of 1.9 Å. *Nature* 473:55–60. <https://doi.org/10.1038/nature09913>
465. Najafpour MM, Moghaddam AN, Shen J-R, Govindjee (2013) Water oxidation and Water-oxidizing complex in Cyanobacteria. In: *Stress Biology of Cyanobacteria*. CRC Press/ Taylor & Francis Group, pp 41–60
466. Bondarava N, Gross CM, Mubarakshina M, et al (2010) Putative function of cytochrome b559 as a plastoquinol oxidase. *Physiol Plant* 138:463–473. <https://doi.org/10.1111/j.1399-3054.2009.01312.x>
467. Raven JA, Evans MCW, Korb RE (1999) The role of trace metals in photosynthetic electron transport in O₂-evolving organisms. *Photosynth Res* 60:111–150. <https://doi.org/10.1023/A:1006282714942>
468. Smirnoff N, Arnaud D (2019) Hydrogen peroxide metabolism and functions in plants. *New Phytol* 221:1197–1214. <https://doi.org/10.1111/nph.15488>
469. Jordan P, Fromme P, Witt HT, et al (2001) Three-dimensional structure of cyanobacterial photosystem I at 2.5 Å resolution. *Nature* 411:909–917. <https://doi.org/10.1038/35082000>
470. Bussell A, Kehoe D (2014) Chromatic Acclimation: A Many-Coloured Mechanism For Maximizing Photosynthetic Light Harvesting Efficiency. In: *The Cell Biology of Cyanobacteria*. Caister Academic Press
471. Chang L, Liu X, Li Y, et al (2015) Structural organization of an intact phycobilisome and its association with photosystem II. *Cell Res* 25:726–737. <https://doi.org/10.1038/cr.2015.59>
472. Glauser M, Bryant DA, Frank G, et al (1992) Phycobilisome structure in the cyanobacteria *Mastigocladus laminosus* and *Anabaena* sp. PCC 7120. *Eur J Biochem* 205:907–915. <https://doi.org/10.1111/j.1432-1033.1992.tb16857.x>
473. Ramanan C, Berera R, Gundermann K, et al (2014) Exploring the mechanism(s) of energy dissipation in the light harvesting complex of the photosynthetic algae *Cyclotella meneghiniana*. *Biochim Biophys Acta BBA - Bioenerg* 1837:1507–1513. <https://doi.org/10.1016/j.bbabi.2014.02.016>
474. Tóth TN, Chukhutsina V, Domonkos I, et al (2015) Carotenoids are essential for the assembly of cyanobacterial photosynthetic complexes. *Biochim Biophys Acta BBA - Bioenerg* 1847:1153–1165. <https://doi.org/10.1016/j.bbabi.2015.05.020>

475. Latifi A, Ruiz M, Zhang C-C (2009) Oxidative stress in cyanobacteria. *FEMS Microbiol Rev* 33:258–278. <https://doi.org/10.1111/j.1574-6976.2008.00134.x>
476. Latifi A, Jeanjean R, Lemeille S, et al (2005) Iron starvation leads to oxidative stress in *Anabaena* sp. strain PCC 7120. *J Bacteriol* 187:6596–6598. <https://doi.org/10.1128/JB.187.18.6596-6598.2005>
477. Hernández JA, Bes MT, Fillat MF, et al (2002) Biochemical analysis of the recombinant Fur (ferric uptake regulator) protein from *Anabaena* PCC 7119: factors affecting its oligomerization state. *Biochem J* 366:315–322. <https://doi.org/10.1042/BJ20020135>
478. Amorim-Carrilho KT, Cepeda A, Fente C, Regal P (2014) Review of methods for analysis of carotenoids. *TrAC Trends Anal Chem* 56:49–73. <https://doi.org/10.1016/j.trac.2013.12.011>
479. Ahluwalia SS, Goyal D (2007) Microbial and plant derived biomass for removal of heavy metals from wastewater. *Bioresour Technol* 98:2243–2257. <https://doi.org/10.1016/j.biortech.2005.12.006>
480. Sein-Echaluce VC, González A, Napolitano M, et al (2015) Zur (FurB) is a key factor in the control of the oxidative stress response in *Anabaena* sp. PCC 7120. *Environ Microbiol* 17:2006–2017. <https://doi.org/10.1111/1462-2920.12628>
481. Valladares A, Montesinos ML, Herrero A, Flores E (2002) An ABC-type, high-affinity urea permease identified in cyanobacteria. *Mol Microbiol* 43:703–715. <https://doi.org/10.1046/j.1365-2958.2002.02778.x>
482. Graham JE, Bryant DA (2009) The Biosynthetic Pathway for Myxol-2' Fucoside (Myxoxanthophyll) in the Cyanobacterium *Synechococcus* sp. Strain PCC 7002. *J Bacteriol* 191:3292–3300. <https://doi.org/10.1128/JB.00050-09>
483. Ahrazem O, Gómez-Gómez L, Rodrigo MJ, et al (2016) Carotenoid Cleavage Oxygenases from Microbes and Photosynthetic Organisms: Features and Functions. *Int J Mol Sci* 17:. <https://doi.org/10.3390/ijms17111781>
484. Allakhverdiev SI, Tomo T, Shimada Y, et al (2010) Redox potential of pheophytin a in photosystem II of two cyanobacteria having the different special pair chlorophylls. *Proc Natl Acad Sci* 107:3924–3929. <https://doi.org/10.1073/pnas.0913460107>
485. Leganés F, Forchhammer K, Fernández-Piñas F (2009) Role of calcium in acclimation of the cyanobacterium *Synechococcus elongatus* PCC 7942 to nitrogen starvation. *Microbiol Read Engl* 155:25–34. <https://doi.org/10.1099/mic.0.022251-0>
486. Bachs O, Agell N (1995) Role of Calcium Ions in Cell Regulation. In: Bachs O, Agell N (eds) *Calcium and Calmodulin Function in the Cell Nucleus*. Springer, Berlin, Heidelberg, pp 1–9

487. Priya B, Premanandh J, Dhanalakshmi RT, et al (2007) Comparative analysis of cyanobacterial superoxide dismutases to discriminate canonical forms. *BMC Genomics* 8:435. <https://doi.org/10.1186/1471-2164-8-435>
488. Chakravarty D, Banerjee M, Bihani SC, Ballal A (2016) A Salt-Inducible Mn-Catalase (KatB) Protects Cyanobacterium from Oxidative Stress. *Plant Physiol* 170:761–773. <https://doi.org/10.1104/pp.15.01632>
489. Pohland A-C, Schneider D (2019) Mg²⁺ homeostasis and transport in cyanobacteria – at the crossroads of bacterial and chloroplast Mg²⁺ import. *Biol Chem* 400:1289–1301. <https://doi.org/10.1515/hsz-2018-0476>
490. Breydo L (2013) Boron, Biologically Active Compounds. In: Kretsinger RH, Uversky VN, Permyakov EA (eds) *Encyclopedia of Metalloproteins*. Springer, New York, NY, pp 295–299
491. Moraes MF, Reis AR, Moraes LAC, et al (2009) Effects of Molybdenum, Nickel, and Nitrogen Sources on the Mineral Nutrition and Growth of Rice Plants. *Commun Soil Sci Plant Anal* 40:3238–3251. <https://doi.org/10.1080/00103620903267590>
492. Cole JJ, Lane JM, Marino R, Howarth RW (1993) Molybdenum assimilation by cyanobacteria and phytoplankton in freshwater and salt water. *Limnol Oceanogr* 38:25–35. <https://doi.org/10.4319/lo.1993.38.1.0025>
493. Saxena RK, Pandey PK, Bisen PS (2002) Physiological and biochemical alterations in *Anabaena* 7120 under iron stress. *Indian J Exp Biol* 40:594–599
494. Stevanovic M, Lehmann C, Schleiff E (2013) The response of the TonB-dependent transport network in *Anabaena* sp. PCC 7120 to cell density and metal availability. *BioMetals* 26:549–560. <https://doi.org/10.1007/s10534-013-9644-0>
495. Pratte BS, Thiel T (2016) Homologous regulators, CnfR1 and CnfR2, activate expression of two distinct nitrogenase gene clusters in the filamentous cyanobacterium *Anabaena variabilis* ATCC 29413. *Mol Microbiol* 100:1096–1109. <https://doi.org/10.1111/mmi.13370>
496. Ludwig M, Pandelia M-E, Chew CY, et al (2014) ChlR protein of *Synechococcus* sp. PCC 7002 is a transcription activator that uses an oxygen-sensitive [4Fe-4S] cluster to control genes involved in pigment biosynthesis. *J Biol Chem* 289:16624–16639. <https://doi.org/10.1074/jbc.M114.561233>
497. Tsujimoto R, Kamiya N, Fujita Y (2014) Transcriptional regulators ChlR and CnfR are essential for diazotrophic growth in nonheterocystous cyanobacteria. *Proc Natl Acad Sci U S A* 111:6762–6767. <https://doi.org/10.1073/pnas.1323570111>
498. Helliwell KE, Lawrence AD, Holzer A, et al (2016) Cyanobacteria and Eukaryotic Algae Use Different Chemical Variants of Vitamin B12. *Curr Biol* 26:999–1008. <https://doi.org/10.1016/j.cub.2016.02.041>

VITA

Daniel Noreña Caro, born in Medellin, Colombia, graduated from INEM “Jose Felix de Restrepo”. He was awarded a full scholarship from the Medellin city government to pursue a degree in Process Engineering at Universidad EAFIT, from where he graduated in 2011. Between 2010 and 2014, he worked for a paper manufacturing facility, where he became interested in renewable materials, forestry and fibers. He became a full-time graduate student in 2014 to pursue a Master of Engineering in product design at Universidad EAFIT, where he worked on developing functionalized nanofiber filters by electrospinning. In 2015, he was awarded a Fulbright-Colciencias fellowship from the government of the Republic of Colombia and the U.S Department of State to pursue a doctoral degree in the United States. He joined the PhD program in Chemical Engineering at Louisiana State University Baton Rouge in 2015, from where he is a candidate for graduation in August of 2020. Upon completion of his studies, he will continue working on developing sustainable operations with microorganisms.